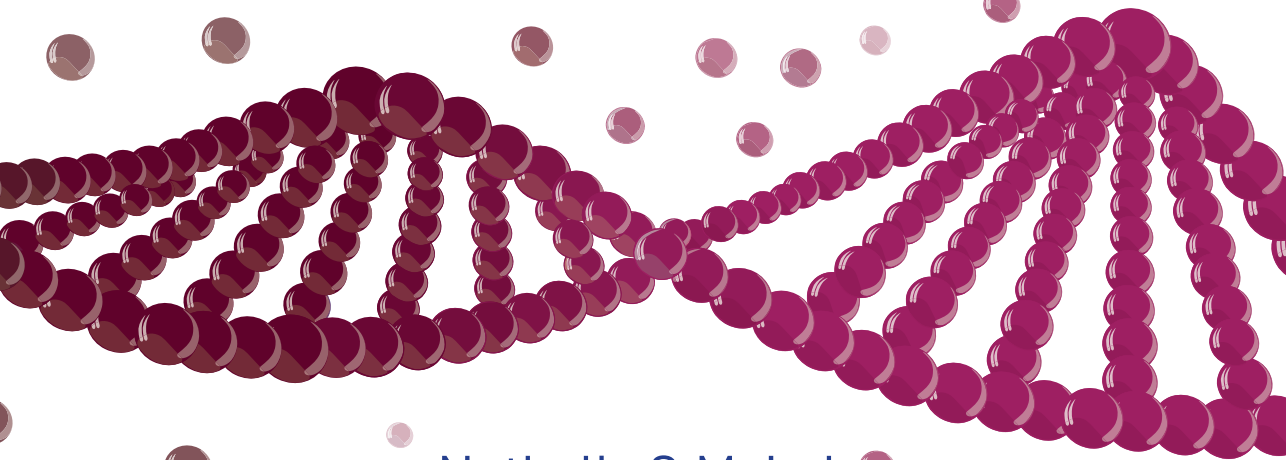


Liquid biopsies in pediatric rhabdomyosarcoma and beyond



Nathalie S.M. Lak

Liquid biopsies in pediatric rhabdomyosarcoma and beyond

Nathalie Saskia Marguerite Lak

Colofon

The research in this thesis was performed at the Princess Máxima Center for Pediatric Oncology (Utrecht, The Netherlands) and at the Department of Experimental Immunohematology of Sanquin Research (Amsterdam, The Netherlands).

The research was financially supported by KiKa (Children Cancer Free), grant number 312.

ISBN: 978-94-93353-58-9

DOI: 10.33540/2192

Cover image: Proefschrift-aio.nl | Guntra Laivacuma

Design and layout: Proefschrift-aio.nl | Annelies Lips

Printing: Proefschrift-aio.nl

Copyright © 2024 Nathalie S.M. Lak. All rights reserved. No parts of this thesis may be reproduced, sorted, or transmitted in any way or by any means without prior permission of the author, or when applicable, of the publishers of the publications.

Liquid biopsies in pediatric rhabdomyosarcoma and beyond

Vloeibare biopsieën bij het pediatrische rhabdomyosarcoom en daarbuiten
(met een samenvatting in het Nederlands)

Proefschrift

ter verkrijging van de graad van doctor aan de
Universiteit Utrecht
op gezag van de
rector magnificus, prof. dr. H.R.B.M. Kummeling,
ingevolge het besluit van het college voor promoties
in het openbaar te verdedigen op
dinsdag 19 maart 2024 des middags
te 4.15 uur

door

Nathalie Saskia Marguerite Lak

geboren op 17 april 1985
te Parijs, Frankrijk

Promotoren:

Prof. dr. M.M. van Noesel

Prof. dr. C.E. van der Schoot

Prof. dr. G.A.M. Tytgat

Copromotoren:

Dr. J. Stutterheim

Beoordelingscommissie:

Prof. dr. A. de Bruin

Prof. dr. E.E.S. Nieuwenhuis (voorzitter)

Prof. dr. ir. K. De Preter

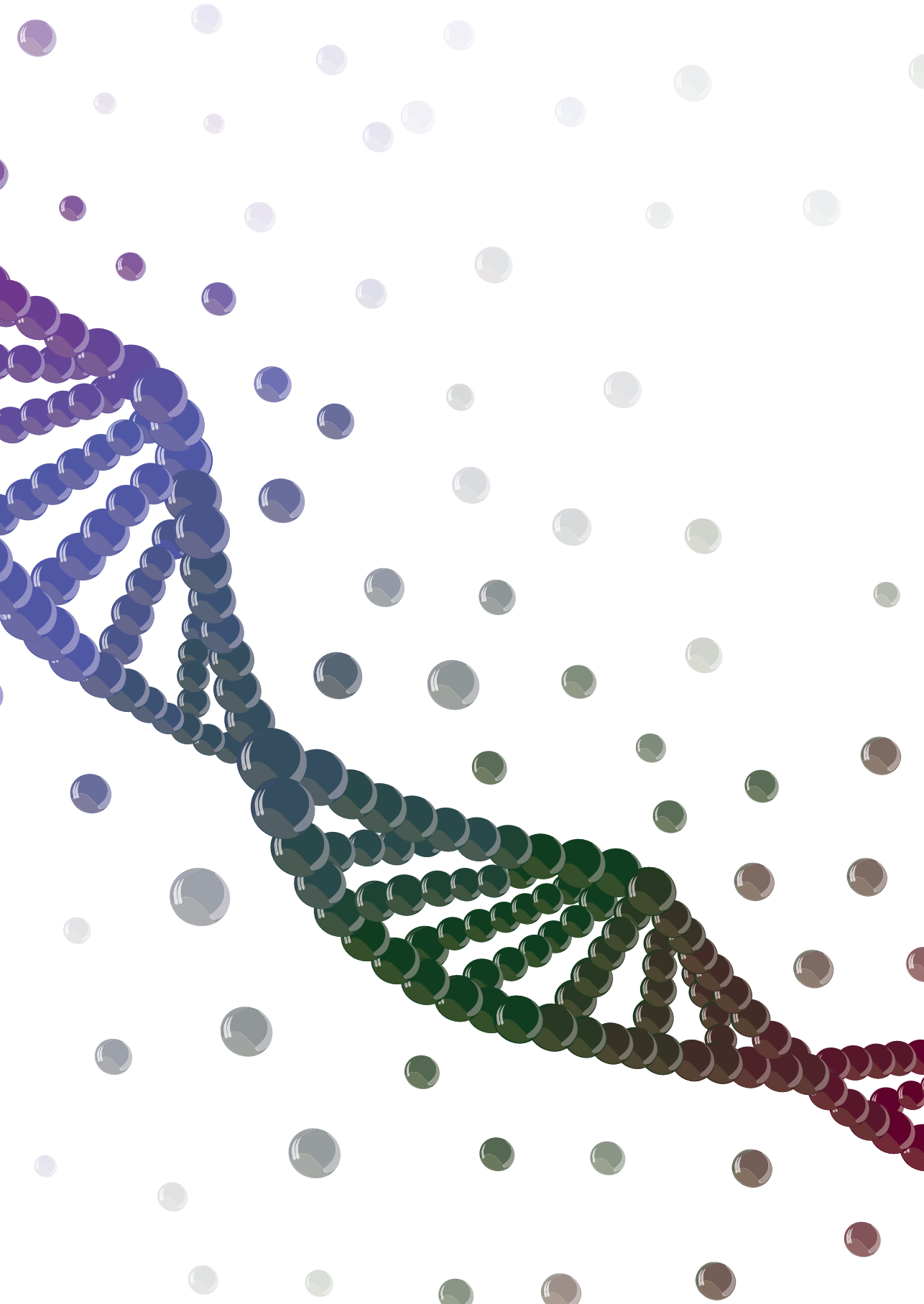
Prof. dr. H.J. Vormoor

Prof. dr. E. van der Wall

Dit proefschrift werd mogelijk gemaakt met financiële steun van KiKa (Stichting Kinderen Kankervrij).

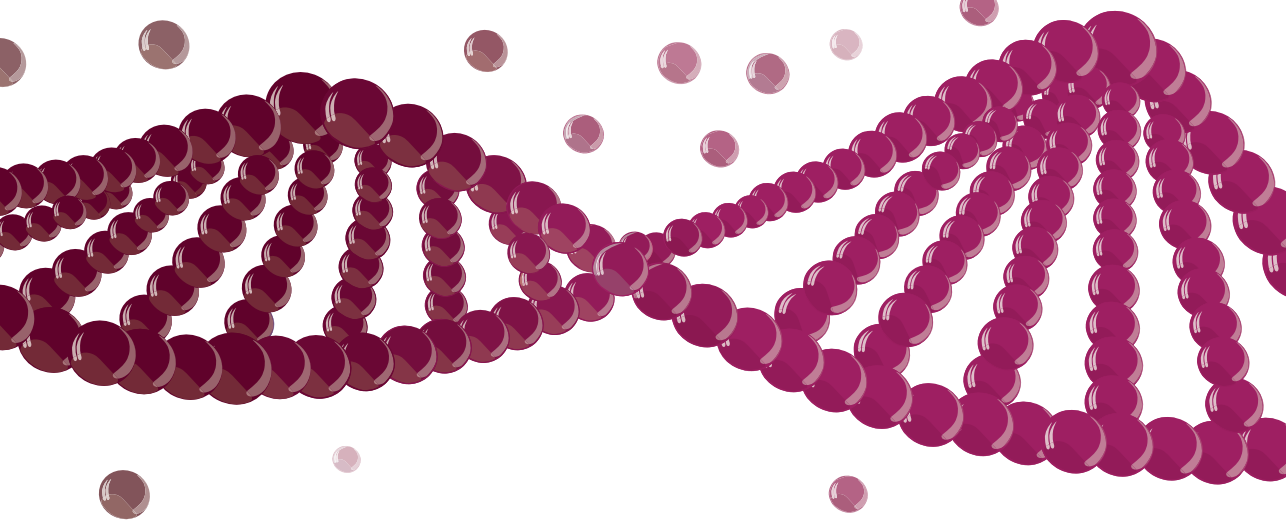
Content

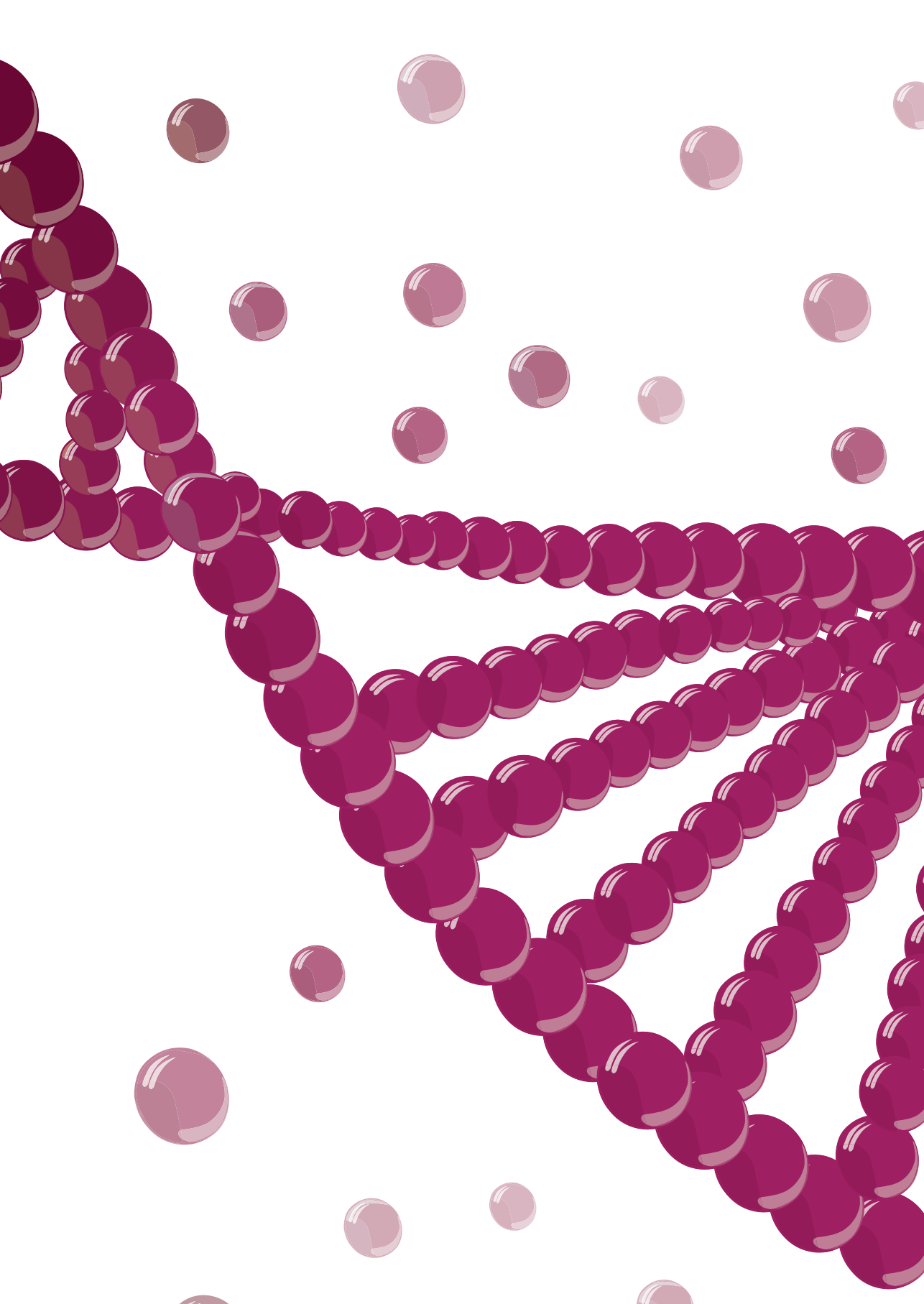
Chapter 1	Introduction and outline of this thesis	9
Part I: Liquid biopsies in pediatric rhabdomyosarcoma		
Chapter 2	Improving Risk Stratification for Pediatric Patients with Rhabdomyosarcoma by Molecular Detection of Disseminated Disease	29
Chapter 3	Novel Circulating Hypermethylated RASSF1A ddPCR for Liquid Biopsies in Patients With Pediatric Solid Tumors	71
Chapter 4	Cell-free DNA as a diagnostic and prognostic biomarker in pediatric rhabdomyosarcoma	95
Chapter 5	Molecular Characterization of Circulating Tumor DNA in Pediatric Rhabdomyosarcoma: A Feasibility Study	135
Chapter 6	Targeted Locus Amplification to develop robust patient-specific assays for liquid biopsies in pediatric solid tumors	189
Part II: Extracellular vesicles and cell-free RNA		
Chapter 7	Extracellular Vesicles: A New Source of Biomarkers in Pediatric Solid Tumors? A Systematic Review	221
Chapter 8	Cell-free RNA from plasma in patients with neuroblastoma: exploring the technical and clinical potentia	275
Chapter 9	Discussion and future directions	317
Appendices	English summary	334
	Nederlandse samenvatting	337
	Curriculum Vitae	341
	Acknowledgements	342



PART I

Liquid biopsies in pediatric rhabdomyosarcoma





Chapter 1

Introduction and outline of this thesis

Liquid biopsies in pediatric oncology

In the Netherlands, more than 550 children are diagnosed each year with a pediatric malignancy, of which 33% with a solid tumor.¹ Current patient stratification is based on radiological and nuclear imaging and tumor sampling techniques. The diagnosis and treatment stratification is based on tumor biopsy, imaging and often bone marrow biopsies for the presence of tumor dissemination.²⁻⁶ Once a patient is assigned to a treatment risk group, evaluation of therapy response is performed at standardized moments during treatment. Again, imaging and bone marrow punctures have a crucial role in this process. Liquid biopsies, e.g. novel techniques to sample tumor fragments in the blood or other liquids, are able to detect tumor potentially at a much higher sensitivity. This opens up a new area of diagnostic tools. It implies that the staging methods we currently use to investigate newly diagnosed or patients with relapse need to be revisited.

What can be the added value of liquid biopsies? Biopsy of the tumor itself allows for molecular analysis of the tissue. However, it represents only a fraction of the heterogeneous tumor and may not offer a comprehensive perspective of the complete genetic characteristics of the disease.⁷ Imaging of a tumor provides information on the localization and relationship to other anatomical structures. Also, it offers valuable information on imaging characteristics, cell density (diffusion restriction), cystic components and many more aspects. However, there are also important limitations. A tumor is only detected if it is large enough, which is approximately 1 cm³, corresponding to 10⁹ cells.⁸ The actual diagnosis is not always clear from the imaging and a complete understanding of the treatment response can seldomly be drawn exclusively from imaging of the tumor.^{9,10} In children, an important complicating factor is that imaging in patients up to 7 years often must be performed under anesthesia which has been under scrutiny during recent years for potential adverse effects on neurocognitive development.¹¹⁻¹³

Liquid biopsies include all sampling and molecular analysis of fluids present in the human body. In patients with cancer, these fluids can contain tumor cells or tumor-derived cell components.^{14,15} In this thesis, the focus lies on the liquid biopsies derived from peripheral blood and bone marrow. Blood circulates through the entire body and transports nutrients, but also cellular debris, ranging from metabolites, to nucleic acids (e.g. DNA and RNA) and circulating tumor cells (CTC).¹⁴⁻¹⁶ This molecular information can assist at the initial diagnostic work-up for treatment stratification or for response evaluation during treatment. Since material from both the primary tumor and metastatic lesions can circulate, liquid biopsies can

offer a comprehensive view on the genetic landscape of malignant disease.^{7,14} In many pediatric solid tumors, e.g. neuroblastoma and rhabdomyosarcoma, bone marrow represents a site for metastatic disease, and is sampled routinely to evaluate treatment response in patients that present with bone marrow metastases at primary diagnosis.^{2,17} Molecular analysis can be of added value to conventional morphological and immunohistochemical examination.^{2,17}

To enhance sensitivity of liquid biopsies, the choice of molecular targets is crucial. Pediatric tumors have a low mutational burden and have a distinct genetic profile compared to adult tumors. If pathogenic mutations are present, these are often limited to a single mutation.¹⁸ Some tumors contain a tumor-driving fusion gene. But in many patients, copy number alterations (CNAs) or aberrant methylation profiles can be the sole aberrations.¹⁸⁻²⁰

Cell-free DNA analysis

In a healthy state, cell-free DNA (cfDNA) is shed in peripheral blood plasma through apoptosis and necrosis from all cells in the body.²¹⁻²³ The majority of cfDNA originates from hematopoietic cells.^{24,25} Tumor-derived genetic aberrations can be detected in cfDNA and to differentiate between normal and tumor cell-derived cfDNA, several techniques are available.

A common approach is the polymerase chain reaction (PCR) assay for the analysis of cfDNA. Over the last decades real-time quantitative PCR (RT-qPCR) has been used frequently. In RT-qPCR a specific genetic target is amplified during several cycles of PCR using targeted primers. A specific fluorescing probe anneals to this amplified target and the readout is quantified per PCR cycle. In RT-qPCR a sample is analyzed in bulk, but this can hamper sensitivity since only a small fraction of cfDNA is tumor-derived. To increase sensitivity, digital PCR (dPCR) has been developed. The general principle behind dPCR is partitioning of a sample into thousands of units with the aim for each unit to contain at least one target molecule. The PCR reaction is conducted within each individual unit and every unit is evaluated for positivity for the fluorescence signal of the target, thereby reducing the background noise that is often affecting analysis of low abundant targets.²⁶⁻²⁸ This makes dPCR well-suited for detection of tumor-derived cfDNA from plasma, since these targets need to be uncovered in an abundance of normal cfDNA. The disadvantage of dPCR is that the total input of DNA that can be tested is limited. However, this low input is not a problem in case of cfDNA, as the total amount of DNA that can be isolated

from plasma is also relatively low. Several dPCR platforms are currently available.²⁸ The dPCR platform used in this thesis is droplet digital PCR (ddPCR). In ddPCR, a sample is partitioned into more than twenty thousands of droplets using a water/oil emulsion.²⁸

An increasingly popular approach to the analysis of cfDNA in pediatric oncology is the analysis of the complete base pair sequence of the DNA fragments to detect genetic alterations, such as mutations, insertions and deletions but also copy number aberrations (CNA). The sequence can be analyzed for the presence of CNA by shallow whole genome sequencing (shWGS). Whole exome sequencing (WES) and whole genome sequencing (WGS) are used to discover single nucleotide variations (SNVs) or structural variations.²⁹ If performed repeatedly during the course of the disease, it can be used to evaluate treatment response, clonal evolution and resistance mechanisms of the tumor itself.^{7,29,30} Furthermore, it can identify aberrations suited for use in targeted liquid biopsy assays, which might be more time and cost effective for frequent sampling during induction treatment. Lastly, tumor specific alterations potentially reveal targets for precision treatment. A limitation to sequencing platforms is the cost and the requirement for intricate bio-informatic pipelines. This can partly be avoided by the introduction of panel sequencing, where a limited number of genes is sequenced. However, this demands a careful choice of genes.

Epigenetic analysis of cfDNA is another approach that has shown its potential over the last decade. Within the genome, epigenetic modifications, e.g. methylation, histone modifications and positioning of nucleosomes on the DNA, play a pivotal role in silencing or activation of gene transcription.³¹ Methylation is binding of a methyl group to a CpG island, a region in the DNA with a C nucleotide followed by a G.³² The effect of methylation is dependent on where in the DNA it takes place.³³ Methylation of the promoter region of a gene can result in inhibition of transcription of this specific gene.³³ Hypo and hypermethylation of genes are dynamic processes, also essential for the development from embryo to adult.^{31,32} A specific methylation profile, e.g. the pattern of hypo- and hypermethylation of the CpG islands in the DNA of a cell, is unique for a specific cell type.³¹⁻³³ Changes in gene methylation play a role in the development of cancer. This can lead to activation of oncogenes or, on the contrary, silencing of tumor suppressor genes.^{31,32,34} A tumor also contains a specific methylation profile, which is different to healthy cells but comparable to similar tumors. Methylation profiling of tissue can thereby be used to differentiate between malignancy and cancer, and also assist in identifying tumor (sub)types. For central nervous tumors, methylation profiling is now implemented in clinical practice and essential for establishing a diagnosis.³⁵ In primary sarcoma



tumor material, methylation profile analysis was established as a classification tool for different sarcoma types.³⁶ Van Paemel et al. have adapted this approach for the methylation analysis of cfDNA from plasma: cell-free reduced representation bisulphite sequencing (cfRRBS).^{37,38} They have shown that cfRRBS on diagnostic cfDNA can classify pediatric solid tumors correctly.³⁸

Tumor suppressor genes are at the center of the 'two hit'-theory, which is often proposed as a pivotal mechanism in tumorigenesis.^{39,40} This entails that loss of both alleles of a tumor suppressor gene is necessary for a cell to acquire cancerous traits. Loss of each allele can be caused by an inactivating mutation or silencing through epigenetic modification.³⁹⁻⁴¹ An example is tumor suppressor gene RASSF1. At the beginning of this century, RASSF1 was identified as a protein that can associate to Ras and thereby affect the Ras pathway.⁴² The RASSF1 locus lies in the 3p21.3 region and has different transcript variants, of which RASSF1A is most studied for its role in cancer, together with RASSF1C.^{41,43,44} For RASSF1A, although inactivation through mutations has been described,⁴⁵ silencing through hypermethylation has been described most frequently in many tumors, adult as well as pediatric.^{41,43,46-50}

Finally, an upcoming technique for cfDNA is based on the difference in size of the cfDNA fragments and therefore called 'fragmentomics'. cfDNA originating from healthy cells is about 167 bp, which corresponds to the size of chromatin wrapped around a nucleosome.^{21,51} cfDNA fragments from malignant cells are shorter, around 90 to 150 bp. This difference in fragment length of cfDNA can be used as a method to enrich for tumor-derived cfDNA.^{23,52,53} This enrichment step can be used by itself to quantify tumor-derived cfDNA or as an enrichment step before further molecular analysis of tumor-specific genetic and/or epigenetic aberrations.

Circulating tumor cells: biology and analysis

Detection and analysis of CTC offer another application for liquid biopsy-based investigations. CTC have become detached from the surrounding tumor cells and extracellular matrix and have entered the blood stream. Whether this is an active or passive process, is still up for debate.⁵⁴ CTC face many challenges in the blood vessels, encountering immune cells and shear stress from the vessel walls.⁵⁵ Furthermore, detachment from surrounding cells and the extracellular matrix would induce anoikis and eventually apoptosis in normal cells.⁵⁶ Successful CTC use epithelial-to-mesenchymal transition (EMT) to evade these obstacles and eventually settle in their metastatic site, using a reversed process of mesenchymal-to-epithelial transition

(MET).^{56,57} Apart from increasing knowledge on the mechanisms behind EMT and MET, CTC also represent another biomarker for liquid biopsies. Various methods to enrich CTC from blood have been developed, using mechanical characteristics, e.g. cell size or density, or protein expression.^{56,58} They contain genetic and proteomic information on the tumor and the number of CTC can reflect disease stage.⁵⁹ However, an important limitation is that the number of CTC in a blood sample can vary greatly and is often very low.⁶⁰ When aiming to detect a CTC-derived signal, DNA-based techniques might not be sensitive enough. However, since expression of one gene can lead to multiple mRNA copies within a cell, detection of tumor-derived mRNA offers a sensitive alternative.⁶¹ In neuroblastoma, the use of an RNA-based approach to detect CTC in blood and disseminated tumor cells in bone marrow, has been shown to be sensitive and of clinical relevance.^{62–68}

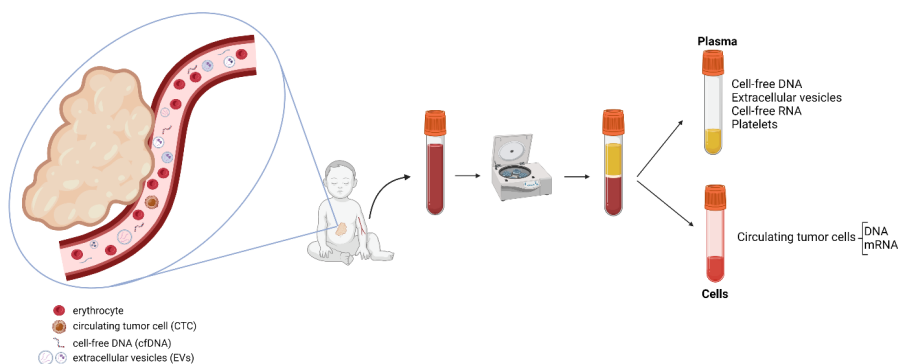


Figure 1. Illustration of the different particles present in peripheral blood (left) and preparation of peripheral blood by centrifugation (right).

Tumor-derived RNA can also circulate as cell-free RNA (cfRNA) in blood and form a potent biomarker. Due to the presence of RNases in blood, large cfRNA molecules are dependent on protection from degradation by association to other particles, e.g. protein aggregates or lipid-encased structures, e.g. extracellular vesicles (EV).^{16,69–71} During the last 20 years, EV have gained interest as biomarkers.⁷² They are shed by every cell in the body and contain cargo that is encapsulated in a lipid bilayer, which is thereby protected from degradation by plasmatic enzymes.^{69,70,73,74} EV cargo reflects their cell of origin, and can contain cfDNA, cfRNA or proteins.^{73,75} Different RNA subtypes have been described as cargo in EV, from microRNA (miRNA) to mRNA or even long non-coding RNA (lncRNA).^{16,75–77} EV are an extremely heterogeneous group of particles and many different approaches for their isolation from plasma and analysis of their content have been described.^{78–80} Tumor cells have been described

to be greatly active in shedding EV.⁸¹⁻⁸³ These tumor-derived EV represent a great source of biomarkers and this potential has been explored increasingly during the last decade.

Rhabdomyosarcoma: a genetic and clinical perspective

Twenty children are diagnosed with rhabdomyosarcoma every year in the Netherlands.¹ Rhabdomyosarcoma is considered a mesenchymal tumor of (muscle) stem cells that undergo aberrant differentiation and display muscle-like features.^{84,85} It can arise in any part of the body, also in sites without apparent presence of muscle.⁸⁴ The exact cell-of-origin of rhabdomyosarcoma has not been established yet. The most common rhabdomyosarcoma subtype has an embryonal morphology and often occurs in the head/neck area and genito-urinary tract.¹⁷ On a genetic level, embryonal rhabdomyosarcoma often harbor CNA and occasionally single nucleotide variations.^{86,87} In a subset of embryonal tumors, a recurring mutation in MYOD1, L122R, a transcription factor involved in muscle differentiation, has been reported.^{88,89} Patients with this mutation have poor clinical outcome. Furthermore, several mutations in the RAS/PI3KCA pathway have been described as well as in TP53.^{86,87,89}

Approximately 20% of patients with rhabdomyosarcoma have an alveolar morphology, resembling lung alveoli. This tumor frequently arises in the extremities and is associated with a higher frequency of metastatic disease at diagnosis, poor prognosis and typical translocations.¹⁷ Many alveolar tumors have a tumor-driving translocation between the PAX3 gene on chromosome 2, in 55% of cases, or the PAX7 gene on chromosome 1 and FOXO1 on chromosome 13, in 22%.⁹⁰⁻⁹² PAX3 and FOXO1 are both transcription factors, and the fusion gene of PAX3-FOXO1 results in an alternative transcription factor that leads to increased cell proliferation, cell survival and suppression of differentiation, all essential to tumorigenesis.⁹³ Tumors with the PAX3-FOXO1 translocation are considered the most aggressive, whereas clinical behavior of tumors with the PAX7-FOXO1 translocation tends more towards the embryonal subtype.^{89,94} Atypical fusions have also been identified, e.g. PAX3-NCOA1/2 or PAX3-FOXO4.⁹⁵

Patients with pediatric rhabdomyosarcoma can present at any age, but two peaks have been reported: between 2 and 6 years for the embryonal subtype, and between 10 and 18 years for the alveolar subtype.^{3,17} Several predisposition syndromes have

been associated with rhabdomyosarcoma, amongst them Li Fraumeni syndrome (germline mutation in TP53), Beckwith Wiedeman, Neurofibromatosis type 1 (germline mutation in NF1), DICER1 syndrome (germline DICER1 mutation).¹⁷ Survival depends on dissemination of the disease at initial diagnosis. Patients with localized disease have a 5 year overall survival of 75%.⁹⁶⁻⁹⁸ Fifteen percent of patients present with metastatic disease.⁹⁹ Common metastatic sites are the bone marrow, lungs and bones.¹⁷ Current investigations for metastatic disease consist of imaging (e.g. CT scan of the chest, MRI, FDG-PET scan) and bone marrow biopsy. Presence of metastasis in the bone marrow biopsy is assessed by morphology and immunohistochemistry. Overall survival of patients with metastatic disease is estimated between 30 and 50%, but patients with metastatic lesions in the bone marrow have a worse outcome.^{97,100,101} Of all patients, with both localized and metastatic disease, up to 1 in 3 will suffer from relapsed disease.¹⁰²⁻¹⁰⁴ Factors associated with poor outcome of relapsed disease are: metastatic recurrence, previous radiotherapy, large tumor size and unfavorable tumor site, nodal involvement and early relapse.¹⁰³

In the Netherlands, patients have been treated according to study protocols established by the European Paediatric Soft tissue Sarcoma Group (EpSSG). Between 2005 and 2017, patients were treated within the EpSSG RMS2005 protocol. Within this protocol, patients with localized disease were stratified according to patient and tumor characteristics into low, standard, high and very high risk groups (Table 1).^{102,105}

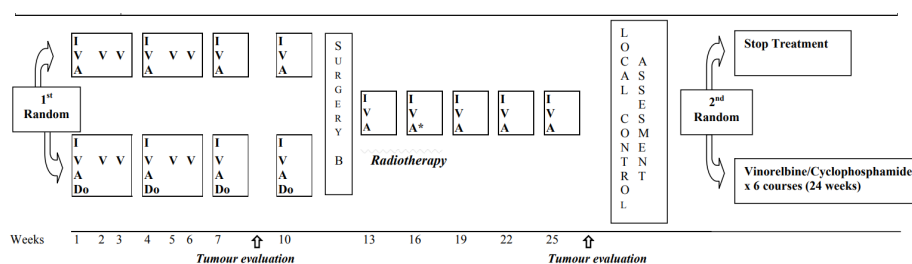


Figure 2. Treatment scheme for high risk group, as taken from the EpSSG RMS2005 protocol

I= Ifosfamide

V=Vincristin

A=Actinomycin D

Do=Doxorubicin

Table 1. Risk stratification for localized rhabdomyosarcoma from the EpSSG RMS2005 protocol.

Risk Group	Subgroups	Pathology	Post surgical Stage (IRS Group)	Site	Node Stage	Size & Age
Low Risk	A	Favourable	I	Any	N0	Favourable
Standard Risk	B	Favourable	I	Any	N0	Unfavourable
	C	Favourable	II, III	Favourable	N0	Any
	D	Favourable	II, III	Unfavourable	N0	Favourable
High Risk	E	Favourable	II, III	Unfavourable	N0	Unfavourable
	F	Favourable	II, III	Any	N1	Any
	G	Unfavourable	I, II, III	Any	N0	Any
Very High Risk	H	Unfavourable	I, II, III	Any	N1	Any

Pathology: favourable = all embryonal, spindle cells, botryoid RMS; unfavourable = all alveolar RMS (including the solid-alveolar variant)

Post surgical stage (according to the IRS grouping): Group I = primary complete resection (R0); Group II = microscopic residual (R1) or primary complete resection but N1; Group III = macroscopic residual (R2)

Site: Favourable = orbit, GU non bladder prostate (i.e. paratesticular and vagina/uterus) and non PM head & neck; unfavourable = all other sites (parameningeal, extremities, GU bladder-prostate and "other site")

Node stage: N0 = no clinical or pathological node involvement; N1 = clinical or pathological nodal involvement

Size & Age: favourable = tumour size (maximum dimension) <5cm and Age <10 years; unfavourable = all others (i.e. Size >5 cm or Age ≥10 years)

Except for patients with favorable characteristics and fully resectable disease, all patients were treated according to a 26 weeks regimen, consisting of 9 cycles of chemotherapy with response evaluation after 9 weeks (example shown in Figure 2). At this timepoint, a treatment plan for local control was determined, consisting of surgery and/or radiotherapy. Patients with high risk disease were randomized for maintenance chemotherapy after first line treatment. Introduction of maintenance therapy resulted in a significant increase of event-free survival (from 69.8% to 77.6%) and overall survival (from 73.7% to 86.5%).¹⁰⁵ Maintenance therapy is now standard of care in the current EpSSG treatment protocol (Frontline and relapsed rhabdomyosarcoma, FaR RMS) for this patient group.¹⁰⁶ In RMS2005, patients with high risk disease were randomized to assess whether addition of doxorubicin was of additional value to the first line chemotherapy regimen, which was not the case.¹⁰²

Metastatic patients were treated according to the MTS2008 protocol. Within this trial, patients received standard induction chemotherapy followed by 1 year maintenance chemotherapy. Concurrently, a subset of centers included patients with metastatic rhabdomyosarcoma in the BERNIE study. Within the BERNIE study, patients were treated according to MTS2008 but Bevacizumab, a VEGF inhibitor was added. First survival analyses of the BERNIE study showed no survival benefit for patients treated with Bevacizumab.¹⁰⁷ Recently, Schoot et al. published a pooled analysis of patients treated within the MTS2008 and BERNIE study.¹⁰⁰ In comparison to a previous pooled analysis of North American and European patients with metastatic rhabdomyosarcoma, both event-free survival (from 27% to 36%) and overall survival (from 34% to 49%) increased.^{97,100} Including this more mature survival data, bevacizumab still did not demonstrate any improvement of clinical outcome.¹⁰⁰

Liquid biopsies and rhabdomyosarcoma

Literature on the use of liquid biopsy in pediatric rhabdomyosarcoma is quite scarce and there is a distinction between RNA-based and DNA-based analysis. Previous studies in small cohorts reported that PCR-based detection of rhabdomyosarcoma-derived transcripts could be more sensitive than conventional morphology for detection of bone marrow metastasis and that presence of these transcripts in bone marrow was associated to poor clinical outcome. The first study dates from 1996 and subsequently 4 studies were published in the early 2000's on the use of RNA-markers for the detection of circulating and disseminated tumor cells in blood and bone marrow of patients with rhabdomyosarcoma. These studies often included two genes encoding transcription factors involved in muscle differentiation MYOG and MYOD1, and the transcripts of the PAX3/7-FOXO1 fusion genes.¹⁰⁸⁻¹¹¹ Overall, these 5 studies demonstrated that presence of rhabdomyosarcoma-specific transcripts in blood and/or BM at diagnosis was associated to poor clinical outcome and that detection of these transcripts in bone marrow could be of added value to conventional histology for the detection of BM metastasis.^{108,109,111} However, the number of patients analyzed in these studies were rather low, ranging from 5 to 48. Then, until this current thesis no more RNA-based liquid biopsy studies in pediatric rhabdomyosarcoma were published. However, interest in the analysis of cfDNA from plasma for patients with solid tumors gradually increased during the last decade. For pediatric rhabdomyosarcoma, reports on the analysis of cfDNA were still scarce previous to this thesis and focused on fusion gene-positive tumors. These reports were limited to single patient case reports or small cohorts.^{112,113} This thesis is the first to report on a large number of samples from patients with rhabdomyosarcoma and describes the analysis of liquid biopsies, both RNA- and DNA-based, from 99 patients.

Scope of this thesis

In **Part I** of this thesis, we investigated the potential of liquid biopsies for patients with rhabdomyosarcoma to improve current treatment stratification and response monitoring. We performed the first prospective collection of blood and bone marrow samples from Dutch patients treated for rhabdomyosarcoma. In **Chapter 2** we report on the development of a panel of markers to detect rhabdomyosarcoma-specific RNA in the cellular compartment of blood and bone marrow and analyzed if positivity of this panel was associated to clinical outcome.

In **Chapter 3** we describe a novel ddPCR assay for the detection of RASSF1A-M and validate this in cfDNA from patients with different types of pediatric solid tumors.

In **Chapter 4**, we explored the feasibility of different approaches for the analysis of cfDNA from plasma of patients with rhabdomyosarcoma. We used cfRRBS and CNA analysis, but also ddPCR for the detection of RASSF1A-M. For the RASSF1A-M assay, we studied whether presence of RASSF1A-M in plasma was associated to clinical outcome.

In **Chapter 5**, we investigated whether it was feasible to use genetic data from primary rhabdomyosarcoma tumors to design patient-specific ddPCR assays to assess tumor burden longitudinally.

For **Chapter 6**, we studied the potential of patient-specific ddPCR assays further in different types of pediatric solid tumors. The breakpoints in translocations or regions with CNAs are perfect for the design of patient-specific designs, since they are not present in normal (cf)DNA. So we sought collaboration with Cergentis, a company specialized in determining the exact sequence of specific targets, using targeted locus amplification (TLA).^{114,115}

In **Part II**, we explored novel cell-free markers from plasma. In **Chapter 7** we reviewed the literature on EV-derived biomarkers in different pediatric solid tumors. In **Chapter 8** we investigated the possibility to measure multiple cfrRNA targets in a multiplex ddPCR assay and studied whether these targets are associated to EV.

In **Chapter 9** we discuss our findings and future directions for the implementation of liquid biopsies in pediatric rhabdomyosarcoma and beyond.



References

1. Jaarverslag Zorg and Research Prinses Maxima Centrum 2021. https://www.prinsesmaximacentrum.nl/storage/configurations/prinsesmaximacentrumnl/files/hetmaxima_jaarverslag_cenr2021_low_res.pdf.
2. Matthay KK, Maris JM, Schleiermacher G, Nakagawara A, Mackall CL, Diller L, et al. Neuroblastoma. *Nat Rev Dis Primers* [Internet]. 2016;2:16078. Available from: <https://www.ncbi.nlm.nih.gov/pubmed/27830764>
3. Dasgupta R, Fuchs J, Rodeberg D. Rhabdomyosarcoma. *Semin Pediatr Surg* [Internet]. 2016;25(5):276–83. Available from: <https://www.ncbi.nlm.nih.gov/pubmed/27955730>
4. Grünewald TGP, Cidre-Aranaz F, Surdez D, Tomazou EM, de Álava E, Kovar H, et al. Ewing sarcoma. *Nat Rev Dis Primers*. 2018 Dec 5;4(1):5.
5. Cidre-Aranaz F, Watson S, Amatruda JF, Nakamura T, Delattre O, de Alava E, et al. Small round cell sarcomas. *Nat Rev Dis Primers*. 2022 Oct 6;8(1):66.
6. Jones DTW, Banito A, Grünewald TGP, Haber M, Jäger N, Kool M, et al. Molecular characteristics and therapeutic vulnerabilities across paediatric solid tumours. *Nat Rev Cancer*. 2019 Aug 12;19(8):420–38.
7. Chicard M, Colmet-Daage L, Clement N, Danzon A, Bohec M, Bernard V, et al. Whole-Exome Sequencing of Cell-Free DNA Reveals Temporo-spatial Heterogeneity and Identifies Treatment-Resistant Clones in Neuroblastoma. *Clin Cancer Res* [Internet]. 2018;24(4):939–49. Available from: <https://www.ncbi.nlm.nih.gov/pubmed/29191970>
8. Frangioni J v. New Technologies for Human Cancer Imaging. *Journal of Clinical Oncology*. 2008 Aug 20;26(24):4012–21.
9. Vaarwerk B, van der Lee JH, Breunis WB, Orbach D, Chisholm JC, Cozic N, et al. Prognostic relevance of early radiologic response to induction chemotherapy in pediatric rhabdomyosarcoma: A report from the International Society of Pediatric Oncology Malignant Mesenchymal Tumor 95 study. *Cancer* [Internet]. 2018;124(5):1016–24. Available from: <https://www.ncbi.nlm.nih.gov/pubmed/29211298>
10. van Ewijk R, Vaarwerk B, Breunis WB, Schoot RA, ter Horst SAJ, van Rijn RR, et al. The Value of Early Tumor Size Response to Chemotherapy in Pediatric Rhabdomyosarcoma. *Cancers (Basel)*. 2021 Jan 29;13(3):510.
11. Grabowski J, Goldin A, Arthur LG, Beres AL, Guner YS, Hu YY, et al. The effects of early anesthesia on neurodevelopment: A systematic review. *J Pediatr Surg*. 2021 May;56(5):851–61.
12. Wilder RT, Flick RP, Sprung J, Katusic SK, Barbaresi WJ, Mickelson C, et al. Early Exposure to Anesthesia and Learning Disabilities in a Population-based Birth Cohort. *Anesthesiology*. 2009 Apr 1;110(4):796–804.
13. Jevtovic-Todorovic V, Hartman RE, Izumi Y, Benshoff ND, Dikranian K, Zorumski CF, et al. Early Exposure to Common Anesthetic Agents Causes Widespread Neurodegeneration in the Developing Rat Brain and Persistent Learning Deficits. *The Journal of Neuroscience*. 2003 Feb 1;23(3):876–82.
14. Pantel K, Alix-Panabières C. Liquid biopsy and minimal residual disease—latest advances and implications for cure. *Nat Rev Clin Oncol*. 2019;16(7):409–24.
15. Alix-Panabieres C, Pantel K. Clinical Applications of Circulating Tumor Cells and Circulating Tumor DNA as Liquid Biopsy. *Cancer Discov* [Internet]. 2016;6(5):479–91. Available from: <https://www.ncbi.nlm.nih.gov/pubmed/26969689>

16. Corvigno S, Johnson AM, Wong KK, Cho MS, Afshar-Kharghan V, Menter DG, et al. Novel Markers for Liquid Biopsies in Cancer Management: Circulating Platelets and Extracellular Vesicles. *Mol Cancer Ther.* 2022 Jul 5;21(7):1067–75.
17. Skapek SX, Ferrari A, Gupta AA, Lupo PJ, Butler E, Shipley J, et al. Rhabdomyosarcoma. *Nat Rev Dis Primers* [Internet]. 2019;5(1):1. Available from: <https://www.ncbi.nlm.nih.gov/pubmed/30617281>
18. Trubicka J, Grajkowska W, Dembowska-Bagińska B. Molecular Markers of Pediatric Solid Tumors—Diagnosis, Optimizing Treatments, and Determining Susceptibility: Current State and Future Directions. *Cells.* 2022 Apr 6;11(7):1238.
19. Lawlor ER, Thiele CJ. Epigenetic changes in pediatric solid tumors: promising new targets. *AACR*; 2012.
20. Andersson D, Fagman H, Dalin MG, Stahlberg A. Circulating cell-free tumor DNA analysis in pediatric cancers. *Mol Aspects Med* [Internet]. 2020;72:100819. Available from: <https://www.ncbi.nlm.nih.gov/pubmed/31563277>
21. Lo YMD, Han DSC, Jiang P, Chiu RWK. Epigenetics, fragmentomics, and topology of cell-free DNA in liquid biopsies. *Science (1979).* 2021 Apr 9;372(6538).
22. Rostami A, Lambie M, Yu CW, Stambolic V, Waldron JN, Bratman S v. Senescence, Necrosis, and Apoptosis Govern Circulating Cell-free DNA Release Kinetics. *Cell Rep.* 2020 Jun;31(13):107830.
23. Mouliere F. A hitchhiker's guide to cell-free DNA biology. *Neurooncol Adv.* 2022 Nov 11;4(Supplement_2):ii6–14.
24. Lui YY, Chik KW, Chiu RW, Ho CY, Lam CW, Lo YD. Predominant Hematopoietic Origin of Cell-free DNA in Plasma and Serum after Sex-mismatched Bone Marrow Transplantation. *Clin Chem.* 2002 Mar 1;48(3):421–7.
25. Zheng YWL, Chan KCA, Sun H, Jiang P, Su X, Chen EZ, et al. Nonhematopoietically Derived DNA Is Shorter than Hematopoietically Derived DNA in Plasma: A Transplantation Model. *Clin Chem.* 2012 Mar 1;58(3):549–58.
26. Galimberti S, Balducci S, Guerrini F, del Re M, Cacciola R. Digital Droplet PCR in Hematologic Malignancies: A New Useful Molecular Tool. *Diagnostics.* 2022 May 24;12(6):1305.
27. Basu AS. Digital Assays Part I: Partitioning Statistics and Digital PCR. *SLAS Technol.* 2017 Aug;22(4):369–86.
28. Tan LL, Loganathan N, Agarwalla S, Yang C, Yuan W, Zeng J, et al. Current commercial dPCR platforms: technology and market review. *Crit Rev Biotechnol.* 2023 Apr 3;43(3):433–64.
29. Adalsteinnsson VA, Ha G, Freeman SS, Choudhury AD, Stover DG, Parsons HA, et al. Scalable whole-exome sequencing of cell-free DNA reveals high concordance with metastatic tumors. *Nat Commun.* 2017 Nov 6;8(1):1324.
30. van Wezel EM, Zwijnenburg D, Zappeij-Kannegieter L, Bus E, van Noesel MM, Molenaar JJ, et al. Whole-Genome Sequencing Identifies Patient-Specific DNA Minimal Residual Disease Markers in Neuroblastoma. *The Journal of Molecular Diagnostics.* 2015 Jan;17(1):43–52.
31. Kulis M, Esteller M. DNA Methylation and Cancer. In 2010. p. 27–56.
32. Morgan AE, Davies TJ, Mc Auley MT. The role of DNA methylation in ageing and cancer. *Proceedings of the Nutrition Society.* 2018 Nov 30;77(4):412–22.
33. Jones PA. Functions of DNA methylation: islands, start sites, gene bodies and beyond. *Nat Rev Genet.* 2012 Jul 29;13(7):484–92.
34. Ehrlich M. DNA hypermethylation in disease: mechanisms and clinical relevance. *Epigenetics.* 2019 Dec 2;14(12):1141–63.

35. Capper D, Jones DTW, Sill M, Hovestadt V, Schrimpf D, Sturm D, et al. DNA methylation-based classification of central nervous system tumours. *Nature* [Internet]. 2018/03/15. 2018;555(7697):469–74. Available from: <https://www.ncbi.nlm.nih.gov/pubmed/29539639>
36. Koelsche C, Schrimpf D, Stichel D, Sill M, Sahm F, Reuss DE, et al. Sarcoma classification by DNA methylation profiling. *Nat Commun* [Internet]. 2021;12(1):498. Available from: <https://www.ncbi.nlm.nih.gov/pubmed/33479225>
37. de Koker R.; De Wilde B.; de Preter K.; Callewaert N. A; van P. A versatile method for circulating cell-free DNA methylome profiling by reduced representation bisulfite sequencing. *bioRxiv*. 2019;
38. Paemel R Van, Koker A De, Vandeputte C, Van L, Lammens T, Laureys G, et al. Minimally invasive classification of paediatric solid tumours using reduced representation bisulphite sequencing of cell-free DNA : a proof-of-principle study. *Epigenetics* [Internet]. 2020;00(00):1–13. Available from: <https://doi.org/10.1080/15592294.2020.1790950>
39. Knudson AG. Mutation and Cancer: Statistical Study of Retinoblastoma. *Proceedings of the National Academy of Sciences*. 1971 Apr;68(4):820–3.
40. Wang LH, Wu CF, Rajasekaran N, Shin YK. Loss of Tumor Suppressor Gene Function in Human Cancer: An Overview. *Cellular Physiology and Biochemistry*. 2018;51(6):2647–93.
41. Donninger H, Vos MD, Clark GJ. The RASSF1A tumor suppressor. *J Cell Sci*. 2007/09/20. 2007;120(Pt 18):3163–72.
42. Vos MD, Ellis CA, Bell A, Birrer MJ, Clark GJ. Ras uses the novel tumor suppressor RASSF1 as an effector to mediate apoptosis. *J Biol Chem*. 2000/09/22. 2000;275(46):35669–72.
43. Malpeli G, Innamatori G, Decimo I, Bencivenga M, Nwabo Kamdje AH, Perris R, et al. Methylation Dynamics of RASSF1A and Its Impact on Cancer. *Cancers (Basel)*. 2019/07/22. 2019;11(7).
44. Malpeli G, Amato E, Dandrea M, Fumagalli C, Debattisti V, Boninsegna L, et al. Methylation-associated down-regulation of RASSF1A and up-regulation of RASSF1C in pancreatic endocrine tumors. *BMC Cancer*. 2011/08/16. 2011;11:351.
45. Pan ZG, Kashuba VI, Liu XQ, Shao JY, Zhang RH, Jiang JH, et al. High frequency somatic mutations in RASSF1A in nasopharyngeal carcinoma. *Cancer Biol Ther*. 2005 Oct 27;4(10):1116–22.
46. Donninger H, Schmidt ML, Mezzanotte J, Barnoud T, Clark GJ. Ras signaling through RASSF proteins. *Semin Cell Dev Biol* [Internet]. 2016;58:86–95. Available from: <https://dx.doi.org/10.1016/j.semcdb.2016.06.007>
47. Volodko N, Salla M, Zare A, Abulghasem EA, Vincent K, Benesch MGK, et al. RASSF1A site-specific methylation hotspots in cancer and correlation with RASSF1C and MOAP-1. *Cancers (Basel)*. 2016;8(6).
48. Bin Y, Ding Y, Xiao W, Liao A. RASSF1A: A promising target for the diagnosis and treatment of cancer. *Clinica Chimica Acta* [Internet]. 2020;504(January):98–108. Available from: <https://doi.org/10.1016/j.cca.2020.01.014>
49. Hesson LB, Cooper WN, Latif F. The role of RASSF1A methylation in cancer. *Dis Markers*. 2007;23(1–2):73–87.
50. Grawenda AM, O'Neill E. Clinical utility of RASSF1A methylation in human malignancies. *Br J Cancer* [Internet]. 2015;113(3):372–81. Available from: <https://www.ncbi.nlm.nih.gov/pubmed/26158424>
51. Jahr S, Hentze H, Englisch S, Hardt D, Fackelmayer FO, Hesch RD, et al. DNA Fragments in the Blood Plasma of Cancer Patients: Quantitations and Evidence for Their Origin from Apoptotic and Necrotic Cells. *Cancer Res*. 2001;61(4).
52. Mouliere F, Rosenfeld N. Circulating tumor-derived DNA is shorter than somatic DNA in plasma. *Proceedings of the National Academy of Sciences*. 2015;112(11):3178–9.

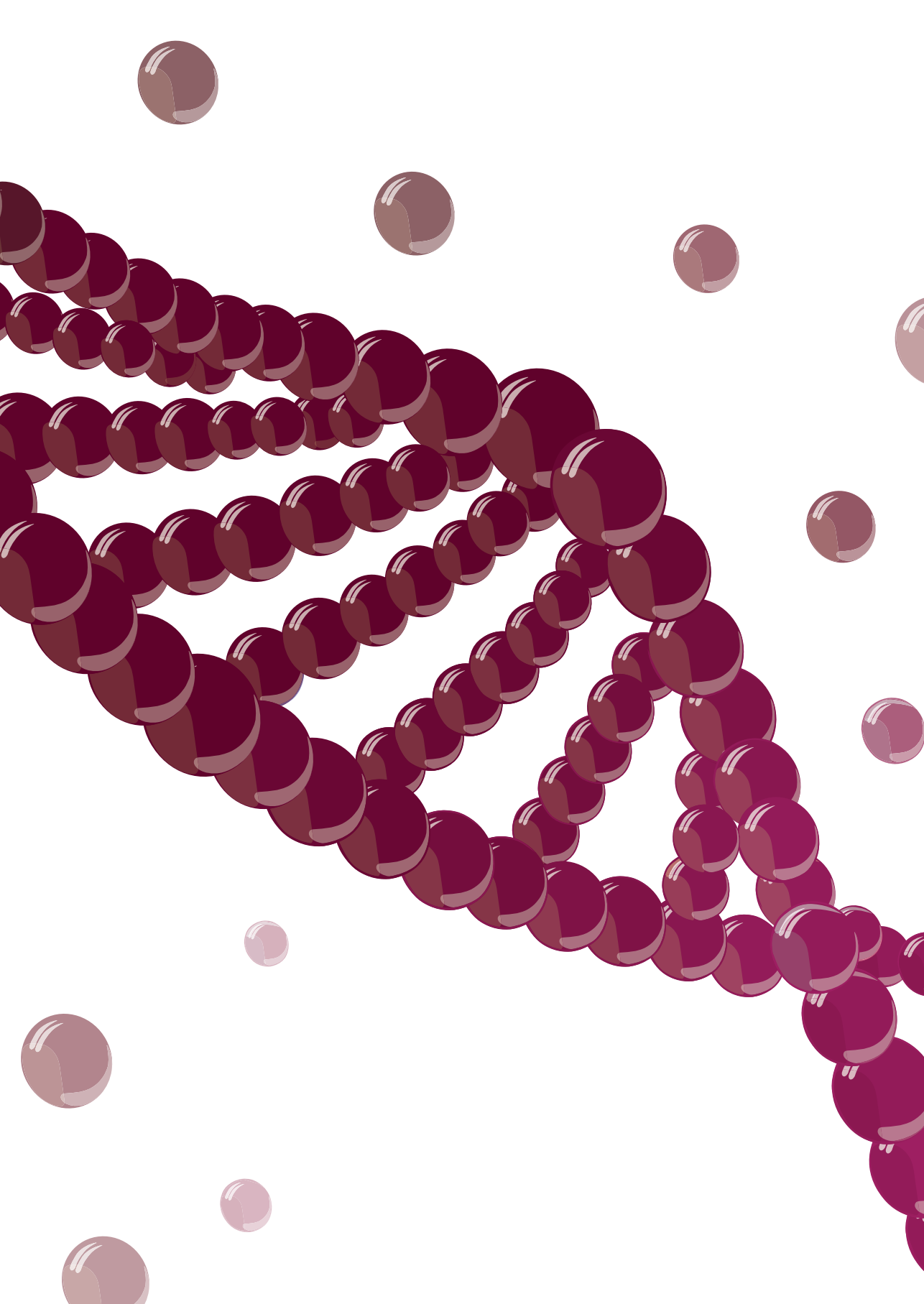
53. Mouliere F, Chandrananda D, Piskorz AM, Moore EK, Morris J, Ahlborn LB, et al. Enhanced detection of circulating tumor DNA by fragment size analysis. *Sci Transl Med* [Internet]. 2018;10(466). Available from: <https://www.ncbi.nlm.nih.gov/pubmed/30404863>
54. Bockhorn M, Jain RK, Munn LL. Active versus passive mechanisms in metastasis: do cancer cells crawl into vessels, or are they pushed? *Lancet Oncol*. 2007 May;8(5):444–8.
55. Krog BL, Henry MD. Biomechanics of the Circulating Tumor Cell Microenvironment. In 2018. p. 209–33.
56. Pereira-Veiga T, Schneegans S, Pantel K, Wikman H. Circulating tumor cell-blood cell crosstalk: Biology and clinical relevance. *Cell Rep*. 2022 Aug;40(9):111298.
57. Noubissi Nzeteu GA, Geismann C, Arlt A, Hoogwater FJH, Nijkamp MW, Meyer NH, et al. Role of Epithelial-to-Mesenchymal Transition for the Generation of Circulating Tumors Cells and Cancer Cell Dissemination. *Cancers (Basel)*. 2022 Nov 8;14(22):5483.
58. Alix-Panabières C, Pantel K. Challenges in circulating tumour cell research. *Nat Rev Cancer*. 2014 Sep 31;14(9):623–31.
59. Cristofanilli M, Pierga JY, Reuben J, Rademaker A, Davis AA, Peeters DJ, et al. The clinical use of circulating tumor cells (CTCs) enumeration for staging of metastatic breast cancer (MBC): International expert consensus paper. *Crit Rev Oncol Hematol*. 2019 Feb;134:39–45.
60. Miller MC, Doyle G v., Terstappen LWMM. Significance of Circulating Tumor Cells Detected by the CellSearch System in Patients with Metastatic Breast Colorectal and Prostate Cancer. *J Oncol*. 2010;2010:1–8.
61. Ghossein RA, Bhattacharaya S, Rosai J. Molecular detection of micrometastases and circulating tumor cells in solid tumors. *Clin Cancer Res*. 1999 Aug;5(8):195060.
62. Stutterheim J, Zappeij-Kannegieter L, Versteeg R, Caron HN, van der Schoot CE, Tytgat GA. The prognostic value of fast molecular response of marrow disease in patients aged over 1 year with stage 4 neuroblastoma. *Eur J Cancer* [Internet]. 2011;47(8):1193–202. Available from: <https://www.ncbi.nlm.nih.gov/pubmed/21429738>
63. Van Wezel EM, Stutterheim J, Vree F, Zappeij-Kannegieter L, Decarolis B, Hero B, et al. Minimal residual disease detection in autologous stem cell grafts from patients with high risk neuroblastoma. *Pediatr Blood Cancer*. 2015;62(8):1368–73.
64. van Zogchel L, de Carolis B, van Wezel E, Stutterheim J, Zappeij-Kannegieter L, van Doornum M, et al. Detection of Minimal Residual Disease (MRD) in High Risk Neuroblastoma Correlates with Outcome: Final Results of International GPOH-DCOG Prospective Validation Study. In: *Pediatric Blood & Cancer*. WILEY 111 RIVER ST, HOBOKEN 07030-5774, NJ USA; 2018. p. S38–S38.
65. van Wezel EM, Decarolis B, Stutterheim J, Zappeij-Kannegieter L, Berthold F, Schumacher-Kuckelkorn R, et al. Neuroblastoma messenger RNA is frequently detected in bone marrow at diagnosis of localised neuroblastoma patients. *Eur J Cancer*. 2016;54:149–58.
66. Stutterheim J, Gerritsen A, Zappeij-Kannegieter L, Yalcin B, Dee R, van Noesel MM, et al. Detecting minimal residual disease in neuroblastoma: the superiority of a panel of real-time quantitative PCR markers. *Clin Chem* [Internet]. 2009;55(7):1316–26. Available from: <https://www.ncbi.nlm.nih.gov/pubmed/19460840>
67. van Zogchel LMJ, Zappeij-Kannegieter L, Javadi A, Lugtigheid M, Gelineau NU, Lak NSM, et al. Specific and Sensitive Detection of Neuroblastoma mRNA Markers by Multiplex RT-qPCR. *Cancers (Basel)*. 2021;13(1):150.
68. Stutterheim J, Gerritsen A, Zappeij-Kannegieter L, Kleijn I, Dee R, Hooft L, et al. PHOX2B is a novel and specific marker for minimal residual disease testing in neuroblastoma. *J Clin Oncol* [Internet]. 2008;26(33):5443–9. Available from: <https://www.ncbi.nlm.nih.gov/pubmed/18838715>

69. HERRIOTT RM, CONNOLLY JH, GUPTA S. Blood Nucleases and Infectious Viral Nucleic Acids. *Nature*. 1961 Mar;189(4767):817–20.
70. Sorber L, Zwaenepoel K, Jacobs J, de Winne K, Goethals S, Reclusa P, et al. Circulating Cell-Free DNA and RNA Analysis as Liquid Biopsy: Optimal Centrifugation Protocol. *Cancers (Basel)*. 2019 Mar 30;11(4):458.
71. Arroyo JD, Chevillet JR, Kroh EM, Ruf IK, Pritchard CC, Gibson DF, et al. Argonaute2 complexes carry a population of circulating microRNAs independent of vesicles in human plasma. *Proceedings of the National Academy of Sciences*. 2011 Mar 22;108(12):5003–8.
72. Raposo G, Stoorvogel W. Extracellular vesicles: exosomes, microvesicles, and friends. *J Cell Biol* [Internet]. 2013;200(4):373–83. Available from: <https://www.ncbi.nlm.nih.gov/pubmed/23420871>
73. Zaborowski MP, Balaj L, Breakefield XO, Lai CP. Extracellular Vesicles: Composition, Biological Relevance, and Methods of Study. *Bioscience*. 2015 Aug 1;65(8):783–97.
74. Akers JC, Gonda D, Kim R, Carter BS, Chen CC. Biogenesis of extracellular vesicles (EV): exosomes, microvesicles, retrovirus-like vesicles, and apoptotic bodies. *J Neurooncol* [Internet]. 2013;113(1):1–11. Available from: <https://www.ncbi.nlm.nih.gov/pubmed/23456661>
75. Simeone P, Bologna G, Lanuti P, Pierdomenico L, Guagnano MT, Pieragostino D, et al. Extracellular Vesicles as Signaling Mediators and Disease Biomarkers across Biological Barriers. *Int J Mol Sci*. 2020 Apr 4;21(7):2514.
76. Cammarata G, de Miguel-Perez D, Russo A, Peleg A, Dolo V, Rolfo C, et al. Emerging noncoding RNAs contained in extracellular vesicles: rising stars as biomarkers in lung cancer liquid biopsy. *Ther Adv Med Oncol*. 2022 Jan 4;14:175883592211312.
77. Suárez B, Solé C, Márquez M, Nanetti F, Lawrie CH. Circulating MicroRNAs as Cancer Biomarkers in Liquid Biopsies. In 2022. p. 23–73.
78. Boing AN, van der Pol E, Grootemaat AE, Coumans FA, Sturk A, Nieuwland R. Single-step isolation of extracellular vesicles by size-exclusion chromatography. *J Extracell Vesicles* [Internet]. 2014;3. Available from: <https://www.ncbi.nlm.nih.gov/pubmed/25279113>
79. Clayton A, Boilard E, Buzas EI, Cheng L, Falcon-Perez JM, Gardiner C, et al. Considerations towards a roadmap for collection, handling and storage of blood extracellular vesicles. *J Extracell Vesicles* [Internet]. 2019;8(1):1647027. Available from: <https://www.ncbi.nlm.nih.gov/pubmed/31489143>
80. Coumans FAW, Brisson AR, Buzas EI, Dignat-George F, Drees EEE, El-Andaloussi S, et al. Methodological Guidelines to Study Extracellular Vesicles. *Circ Res* [Internet]. 2017;120(10):1632–48. Available from: <https://www.ncbi.nlm.nih.gov/pubmed/28495994>
81. Bebelman MP, Smit MJ, Pegtel DM, Baglio SR. Biogenesis and function of extracellular vesicles in cancer. *Pharmacol Ther* [Internet]. 2018;188:1–11. Available from: <https://www.ncbi.nlm.nih.gov/pubmed/29476772>
82. Nanou A, Coumans FAW, van Dalum G, Zeune LL, Dolling D, Onstenk W, et al. Circulating tumor cells, tumor-derived extracellular vesicles and plasma cytokeratins in castration-resistant prostate cancer patients. *Oncotarget* [Internet]. 2018;9(27):19283–93. Available from: <https://www.ncbi.nlm.nih.gov/pubmed/29721202>
83. Nanou A, Miller MC, Zeune LL, de Wit S, Punt CJA, Groen HJM, et al. Tumour-derived extracellular vesicles in blood of metastatic cancer patients associate with overall survival. *Br J Cancer* [Internet]. 2020;122(6):801–11. Available from: <https://www.ncbi.nlm.nih.gov/pubmed/31937922>
84. Hettmer S, Wagers AJ. Muscling in: Uncovering the origins of rhabdomyosarcoma. *Nat Med*. 2010 Feb;16(2):171–3.
85. Yang J, Ren Z, Du X, Hao M, Zhou W. The role of mesenchymal stem/progenitor cells in sarcoma: update and dispute. *Stem Cell Investig*. 2014;1:18.

86. Seki M, Nishimura R, Yoshida K, Shimamura T, Shiraishi Y, Sato Y, et al. Integrated genetic and epigenetic analysis defines novel molecular subgroups in rhabdomyosarcoma. *Nat Commun* [Internet]. 2015;6:7557. Available from: <https://www.ncbi.nlm.nih.gov/pubmed/26138366>
87. Shern JF, Chen L, Chmielecki J, Wei JS, Patidar R, Rosenberg M, et al. Comprehensive Genomic Analysis of Rhabdomyosarcoma Reveals a Landscape of Alterations Affecting a Common Genetic Axis in Fusion-Positive and Fusion-Negative Tumors. *Cancer Discov*. 2014 Feb 1;4(2):216–31.
88. Kohsaka S, Shukla N, Ameer N, Ito T, Ng CKY, Wang L, et al. A recurrent neomorphic mutation in MYOD1 defines a clinically aggressive subset of embryonal rhabdomyosarcoma associated with PI3K-AKT pathway mutations. *Nat Genet*. 2014 Jun 4;46(6):595–600.
89. Arnold MA, Barr FG. Molecular diagnostics in the management of rhabdomyosarcoma. *Expert Rev Mol Diagn*. 2017 Feb 6;17(2):189–94.
90. Skapek SX, Anderson J, Barr FG, Bridge JA, Gastier-Foster JM, Parham DM, et al. PAX-FOXO1 fusion status drives unfavorable outcome for children with rhabdomyosarcoma: a children's oncology group report. *Pediatr Blood Cancer* [Internet]. 2013;60(9):1411–7. Available from: <https://www.ncbi.nlm.nih.gov/pubmed/23526739>
91. Barr FG. Gene fusions involving PAX and FOX family members in alveolar rhabdomyosarcoma. *Oncogene* [Internet]. 2001;20(40):5736–46. Available from: <https://www.ncbi.nlm.nih.gov/pubmed/11607823>
92. Parham DM, Barr FG. Classification of rhabdomyosarcoma and its molecular basis. *Adv Anat Pathol* [Internet]. 2013;20(6):387–97. Available from: <https://www.ncbi.nlm.nih.gov/pubmed/24113309>
93. Linardic CM. PAX3–FOXO1 fusion gene in rhabdomyosarcoma. *Cancer Lett*. 2008 Oct;270(1):10–8.
94. Sorensen PHB, Lynch JC, Qualman SJ, Tirabosco R, Lim JF, Maurer HM, et al. PAX3-FKHR and PAX7-FKHR Gene Fusions Are Prognostic Indicators in Alveolar Rhabdomyosarcoma: A Report From the Children's Oncology Group. *Journal of Clinical Oncology*. 2002 Jun 1;20(11):2672–9.
95. Hettmer S, Linardic CM, Kelsey A, Rudzinski ER, Vokuhl C, Selfe J, et al. Molecular testing of rhabdomyosarcoma in clinical trials to improve risk stratification and outcome: A consensus view from European paediatric Soft tissue sarcoma Study Group, Children's Oncology Group and Cooperative Weichteilsarkom-Studiengruppe. *Eur J Cancer*. 2022 Sep;172:367–86.
96. Oberlin O, Rey A, Sanchez de Toledo J, Martelli H, Jenney ME, Scopinaro M, et al. Randomized comparison of intensified six-drug versus standard three-drug chemotherapy for high-risk nonmetastatic rhabdomyosarcoma and other chemotherapy-sensitive childhood soft tissue sarcomas: long-term results from the International Society of Pediatric Oncology MMT95 study. *J Clin Oncol* [Internet]. 2012;30(20):2457–65. Available from: <https://www.ncbi.nlm.nih.gov/pubmed/22665534>
97. Oberlin O, Rey A, Lyden E, Bisogno G, Stevens MC, Meyer WH, et al. Prognostic factors in metastatic rhabdomyosarcomas: results of a pooled analysis from United States and European cooperative groups. *J Clin Oncol* [Internet]. 2008;26(14):2384–9. Available from: <https://www.ncbi.nlm.nih.gov/pubmed/18467730>
98. Arndt CAS, Bisogno G, Koscielniak E. Fifty years of rhabdomyosarcoma studies on both sides of the pond and lessons learned. *Cancer Treat Rev* [Internet]. 2018;68:94–101. Available from: <https://www.ncbi.nlm.nih.gov/pubmed/29940525>
99. Weiss AR, Lyden ER, Anderson JR, Hawkins DS, Spunt SL, Walterhouse DO, et al. Histologic and clinical characteristics can guide staging evaluations for children and adolescents with rhabdomyosarcoma: a report from the Children's Oncology Group Soft Tissue Sarcoma Committee. *J Clin Oncol* [Internet]. 2013;31(26):3226–32. Available from: <https://www.ncbi.nlm.nih.gov/pubmed/23940218>

100. Schoot RA, Chisholm JC, Casanova M, Minard-Colin V, Georger B, Cameron AL, et al. Metastatic Rhabdomyosarcoma: Results of the European Paediatric Soft Tissue Sarcoma Study Group MTS 2008 Study and Pooled Analysis With the Concurrent BERNIE Study. *Journal of Clinical Oncology*. 2022 Nov 10;40(32):3730–40.
101. Bailey KA, Wexler LH. Pediatric rhabdomyosarcoma with bone marrow metastasis. *Pediatr Blood Cancer* [Internet]. 2020;67(5):e28219. Available from: <https://www.ncbi.nlm.nih.gov/pubmed/32100935>
102. Bisogno G, Jenney M, Bergeron C, Gallego Melcon S, Ferrari A, Oberlin O, et al. Addition of dose-intensified doxorubicin to standard chemotherapy for rhabdomyosarcoma (EpSSG RMS 2005): a multicentre, open-label, randomised controlled, phase 3 trial. *Lancet Oncol* [Internet]. 2018;19(8):1061–71. Available from: <https://www.ncbi.nlm.nih.gov/pubmed/29941280>
103. Chisholm JC, Marandet J, Rey A, Scopinaro M, de Toledo JS, Merks JH, et al. Prognostic factors after relapse in nonmetastatic rhabdomyosarcoma: a nomogram to better define patients who can be salvaged with further therapy. *J Clin Oncol* [Internet]. 2011;29(10):1319–25. Available from: <https://www.ncbi.nlm.nih.gov/pubmed/21357778>
104. Oberlin O, Rey A, Brown KL, Bisogno G, Koscielniak E, Stevens MC, et al. Prognostic Factors for Outcome in Localized Extremity Rhabdomyosarcoma. Pooled Analysis from Four International Cooperative Groups. *Pediatr Blood Cancer* [Internet]. 2015;62(12):2125–31. Available from: <https://www.ncbi.nlm.nih.gov/pubmed/26257045>
105. Bisogno G, De Salvo GL, Bergeron C, Gallego Melcon S, Merks JH, Kelsey A, et al. Vinorelbine and continuous low-dose cyclophosphamide as maintenance chemotherapy in patients with high-risk rhabdomyosarcoma (RMS 2005): a multicentre, open-label, randomised, phase 3 trial. *Lancet Oncol* [Internet]. 2019;20(11):1566–75. Available from: <https://www.ncbi.nlm.nih.gov/pubmed/31562043>
106. NCT04625907: FaR-RMS: An Overarching Study for Children and Adults With Frontline and Relapsed RhabdoMyoSarcoma (FaR-RMS).
107. Chisholm JC, Merks JHM, Casanova M, Bisogno G, Orbach D, Gentet JC, et al. Open-label, multicentre, randomised, phase II study of the EpSSG and the ITCC evaluating the addition of bevacizumab to chemotherapy in childhood and adolescent patients with metastatic soft tissue sarcoma (the BERNIE study). *Eur J Cancer* [Internet]. 2017;83:177–84. Available from: <https://www.ncbi.nlm.nih.gov/pubmed/28738258>
108. Sartori F, Alaggio R, Zanazzo G, Garaventa A, Di Cataldo A, Carli M, et al. Results of a prospective minimal disseminated disease study in human rhabdomyosarcoma using three different molecular markers. *Cancer: Interdisciplinary International Journal of the American Cancer Society*. 2006;106(8):1766–75.
109. Gallego S, Llort A, Roma J, Sabado C, Gros L, de Toledo JS. Detection of bone marrow micrometastasis and microcirculating disease in rhabdomyosarcoma by a real-time RT-PCR assay. *J Cancer Res Clin Oncol* [Internet]. 2006;132(6):356–62. Available from: <https://www.ncbi.nlm.nih.gov/pubmed/16435141>
110. Krsková L, Mrhalová M, Hilská I, Sumerauer D, Drahokoupilová E, Múdry P, et al. Detection and clinical significance of bone marrow involvement in patients with rhabdomyosarcoma. *Virchows Archiv*. 2010;456(5):463–72.
111. Michelagnoli MP, Burchill SA, Cullinane C, Selby PJ, Lewis IJ. Myogenin—a more specific target for RT-PCR detection of rhabdomyosarcoma than MyoD1. *Med Pediatr Oncol* [Internet]. 2003;40(1):1–8. Available from: <https://www.ncbi.nlm.nih.gov/pubmed/12426678>

112. Klega K, Imamovic-Tuco A, Ha G, Clapp AN, Meyer S, Ward A, et al. Detection of Somatic Structural Variants Enables Quantification and Characterization of Circulating Tumor DNA in Children With Solid Tumors. *JCO Precis Oncol* [Internet]. 2018;2018. Available from: <https://www.ncbi.nlm.nih.gov/pubmed/30027144>
113. Eguchi-Ishimae M, Tezuka M, Koikeguchi T, Nagai K, Moritani K, Yonezawa S, et al. Early detection of the PAX3-FOXO1 fusion gene in circulating tumor-derived DNA in a case of alveolar rhabdomyosarcoma. *Genes Chromosomes Cancer* [Internet]. 2019;58(8):521–9. Available from: <https://www.ncbi.nlm.nih.gov/pubmed/30739374>
114. De Vree PJP, De Wit E, Yilmaz M, Van De Heijning M, Klous P, Verstegen MJAM, et al. Targeted sequencing by proximity ligation for comprehensive variant detection and local haplotyping. *Nat Biotechnol*. 2014;32(10):1019–25.
115. Allahyar A, Pieterse M, Swennenhuis J, Los-de Vries GT, Yilmaz M, Leguit R, et al. Robust detection of translocations in lymphoma FFPE samples using targeted locus capture-based sequencing. *Nat Commun* [Internet]. 2021/06/09. 2021;12(1):3361. Available from: <https://www.ncbi.nlm.nih.gov/pubmed/34099699>



Chapter 2

Improving risk stratification for pediatric patients with rhabdomyosarcoma by molecular detection of disseminated disease

Clin Cancer Res. 2021 Oct 15;27(20):5576-5585. doi: 10.1158/1078-0432.CCR-21-1083.

Nathalie S.M. Lak^{1,2}, Timon L. Voormanns², Lily Zappeij-Kannegieter²,
Lieke M.J. van Zogchel^{1,2}, Marta Fiocco^{1,3,4}, Max M. van Noesel¹, Johannes H.M. Merks¹,
C. Ellen van der Schoot², Godelieve A.M. Tytgat^{1,2*}, Janine Stutterheim^{1,2*}.

¹Princess Máxima Center for Pediatric Oncology, Utrecht, the Netherlands

²Sanquin Research, Amsterdam, the Netherlands

³Mathematical Institute, Leiden University, the Netherlands

⁴University of Leiden, Department of Data Science, Medical Statistics section, Leiden University
Medical Centre, the Netherlands

*Contributed equally

Abstract

Background

Survival of children with rhabdomyosarcoma that suffer from recurrent or progressive disease is poor. Identifying these patients upfront remains challenging, indicating a need for improvement of risk stratification. Detection of tumor-derived mRNA in bone marrow (BM) and peripheral blood (PB) using reverse-transcriptase quantitative PCR (RT-qPCR) is a more sensitive method to detect disseminated disease. We identified a panel of genes to optimize risk stratification by RT-qPCR.

Methods

Candidate genes were selected using gene expression data from rhabdomyosarcoma and healthy hematological tissues, and a multiplexed RT-qPCR was developed. Significance of molecular disease was determined in a cohort of 99 Dutch patients with rhabdomyosarcoma (72 localized and 27 metastasized) treated according to the EpSSG RMS2005 protocol.

Findings

We identified the following 11 rhabdomyosarcoma markers: *ZIC1*, *ACTC1*, *MEGF10*, *PDLIM3*, *SNAI2*, *CDH11*, *TMEM47*, *MYOD1*, *MYOG*, *PAX3/7-FOXO1*. RT-qPCR was performed for this 11-marker panel on BM and PB samples from the patient cohort. Five-year EFS was 35.5% (95%CI 17.5-53.5%) for the 33/99 RNA-positive patients, versus 88.0% (95%CI 78.9-97.2%) for the 66/99 RNA-negative patients ($p < 0.0001$). Five-year OS was 54.8% (95%CI 36.2-73.4%) and 93.7% (95%CI 86.6-100.0%), respectively ($p < 0.0001$). RNA panel-positivity was negatively associated with EFS (Hazard Ratio 9.52 95%CI (3.23-28.02)), while the RMS2005 risk group stratification was not, in the multivariate Cox regression model.

Interpretation

This study shows a strong association between PCR-based detection of disseminated disease at diagnosis with clinical outcome in pediatric patients with rhabdomyosarcoma, also compared to conventional risk stratification. This warrants further validation in prospective trials as additional technique for risk stratification.

Translational relevance

This study investigated the clinical relevance of molecular detection of disseminated tumor cells in blood and bone marrow at diagnosis and during treatment in 99 children with rhabdomyosarcoma treated according to the EpSSG RMS2005 protocol.

For molecular detection of disseminated tumor cells in blood and bone marrow we developed an RT-qPCR-based, 11-marker RNA panel to detect tumor-derived RNA. RNA-panel positivity at diagnosis was of significant prognostic value in children with rhabdomyosarcoma, regardless of the risk group. In patients with metastatic as well as localized disease, RNA-positivity was associated with an increased risk of an event.

These data suggest that molecular detection of disseminated disease at diagnosis could be of additional value to risk stratification to improve risk stratification.

Introduction

Each year, more than 200 children in Europe are diagnosed with rhabdomyosarcoma.⁽¹⁾ In the Netherlands, patients were stratified into risk groups and treated according to the European pediatric Soft tissue sarcoma Study Group (EpSSG) RMS2005 protocol with increasing therapy intensities per risk group. Risk stratification depends on several patient- and tumor-dependent factors, such as age, pathology, post-surgical stage (IRS group), nodal stage, tumor size and location.⁽²⁾ Presence of metastases is a crucial prognostic factor. Patients with localized disease have a 5-year overall survival of 75%, and below 40% in patients who present with metastatic disease.⁽³⁻⁵⁾ At diagnosis, 84% of patients have localized disease.⁽⁶⁾ Still, one in three of these patients will suffer relapse.^(2, 7, 8)

Metastases are detected by imaging and bone marrow (BM) immunohistochemistry and cytomorphology.⁽⁹⁾ BM metastases are present in 6% of patients at diagnosis⁽¹⁰⁾, and 3-year event-free survival (EFS) is poorer for these patients than for patients with metastatic disease not involving the BM (3-year EFS 14% vs 34%, respectively).⁽⁵⁾

Two main histological subtypes are described in rhabdomyosarcoma: the most common embryonal, and the alveolar subtype. In 70-80% of alveolar rhabdomyosarcoma a typical fusion gene exists between the PAX3 or PAX7 and FOXO1 locus and its presence is associated with worse prognosis.⁽¹¹⁻¹³⁾ Apart from this translocation, the genetic landscape of rhabdomyosarcoma is heterogeneous. There is a scarcity of recurrent mutations, but various copy number variations and epigenetic modifications are prevalent.⁽¹⁴⁻¹⁶⁾ It is possible to detect tumor-derived cell-free DNA in plasma using targeted or whole genome sequencing techniques.⁽¹⁷⁻¹⁹⁾ However, these approaches often require knowledge on aberrations present in a specific patient and sophisticated equipment and data analysis pipelines. Consequently, we chose to focus on tumor cell-specific mRNA transcripts to detect

circulating tumor cells, aiming to devise a method to cover the entire spectrum of rhabdomyosarcoma. Reverse-transcriptase quantitative PCR (RT-qPCR) represents a cost-efficient and more sensitive approach than immunohistochemistry, with detection of up to 1 positive cell in 1,000,000 non-tumor cells.⁽²⁰⁾ *MYOD1*, *MYOG* and *PAX3/7-FOXO1* fusion genes are known rhabdomyosarcoma markers and the feasibility to detect them with RT qPCR in peripheral blood (PB) and BM has been shown.⁽²¹⁻²³⁾ Several studies from smaller cohorts report that the presence of these markers in liquid biopsies at diagnosis and during follow-up might correlate with a poor prognosis.⁽²²⁻²⁴⁾ As *MYOD1* and *MYOG* are heterogeneously expressed in rhabdomyosarcoma, with *MYOG* predominant in the alveolar subtype⁽²⁵⁾, and the *PAX3/7-FOXO1* fusion gene occurring solely in alveolar rhabdomyosarcomas^(11, 13, 21), we sought additional rhabdomyosarcoma-specific mRNA markers.

We aimed to design an RNA panel with the potential to detect all pediatric rhabdomyosarcoma subtypes, and to evaluate whether minimal disseminated disease detection in liquid biopsies can improve risk stratification at diagnosis and response evaluation during treatment and follow-up in these pediatric rhabdomyosarcoma patients.

Material and methods

Patients and Samples

We included samples from all consecutive Dutch pediatric patients with rhabdomyosarcoma, enrolled in the EpSSG RMS2005 trial (EudraCT number 2005-000217-35) and treated at the Sophia Children's Hospital (Rotterdam, the Netherlands), Emma Children's Hospital (Amsterdam, the Netherlands) and the Princess Máxima Center for Pediatric Oncology (Utrecht, the Netherlands), were collected between 2006 and 2019. Patients included in the trial until 2017 gave informed consent for sample use in the EpSSG RMS2005 add-on study, *Minimal Disseminated Disease monitoring in children with rhabdomyosarcoma (MDD study)*. Samples from patients recruited between 2017 and July 2019 were included if consent was given for biobanking of stored sample residues following routine clinical testing. RNA from 10 primary rhabdomyosarcomas from patients included in this study and from 9 established rhabdomyosarcoma cell lines (RH30, RD, RMS-YM, RUCH2, RUCH3, RH18, RH41, TE617T, HS729T) for assay validation was kindly provided by the Human Genetics department at the Amsterdam UMC location AMC (Amsterdam, the Netherlands) and cDNA was generated. As healthy controls, PB from

47 healthy volunteers and 41 BM samples from children in molecular remission for acute lymphoblastic leukemia were used, as described previously.^(26, 27)

RNA extraction and reverse transcription

Up to 5ml of PB and BM, collected in EDTA tubes (BD, USA), were centrifuged at 1375 G for 10 minutes to separate the cellular fraction from the plasma. For PB, cells were isolated by hemolysis (NH₄Cl). BM was run through a Ficoll gradient (Ficoll Paque, GE Healthcare, USA) according to manufacturer's protocol. Cells were counted, aliquoted per 5 to 10 million cells in TRIzol (Thermo Fisher Scientific, USA) and stored at -80°C. Isolation of total RNA was performed using Direct-Zol DNA/RNA Miniprep (Zymo Research, USA) following the manufacturer's protocol. For cDNA synthesis, High-Capacity RNA-to-cDNA™ Kit (Thermo Fisher Scientific, USA) was used according to manufacturer's protocol.

Candidate gene selection

The Megasearch software in R2⁽²⁸⁾, was used to search for differentially expressed genes. Candidate genes with high expression in rhabdomyosarcomas and low expression in healthy PB and BM were selected, with at least 6 log difference in gene expression (Supplementary figure 1). Affymetrix expression data on RMS tumors from the Human Genome U133A (HG-U133A) microarray chip (n=162) and the Affymetrix Human Genome U133p2 (HG-U133p2) microarray chip (n=9) were compared to expression data on normal PB (n=108) and BM samples (n=5). The U133A contained data of 66 aRMS, 66 eRMS (xtstriche) and 30 other RMS (xtschafwell). It also contained data of 5 BM (xtnormal353) and 108 PB (perbloodbev). The U133p2 chip contained data of 9 RMS (versteeg), 9 PB controls (per blood), 12 PB from the general population (bloodasd56) and 5 BM (xtnormal353). The initial search was performed in May 2007 and resulted in 250 genes. Expression of these genes was compared to the HaemAtlas⁽²⁹⁾, and 62 genes were selected as potential markers, which had low expression in healthy hematopoietic tissues. These 62 candidate markers were then tested in SYBRGreen-based RT-qPCR in the RD and RH30 rhabdomyosarcoma cell lines as previously described⁽²⁷⁾, and healthy PB (n=3) and BM (n=3) (Supplemental table 4). Next, thirteen candidate markers were selected with low/no expression in control PB and BM samples and high expression in the rhabdomyosarcoma cell lines for further analysis with RT-qPCR with Taqman probes. After extensive testing on control BM (n=41) and control PB (n=47), RMS tumors (n=10) and RMS cell lines (n=9), 7 new genes on top of the established genes (*MYOD1*, *Myogenin*, *PAX3-FOXO1* and *PAX7-FOXO1*) were selected for testing of clinical samples using multiplex RT-qPCR with Taqman probes; 7 for PB and 3 for BM (Supplementary figure 1).

RT-qPCR

Samples were analyzed using multiplexed RT-qPCR with Taqman probes. Primers and Taqman probes were ordered from Eurogentec (Belgium). Probes were designed using Oligo 7 (Molecular Biology Insights, USA) and Primer Express 3.0.1 (Thermo Fisher Scientific, USA). For *MYOD1* and *MYOG*, we initially used the sequences as published previously and listed in the EpSSG RMS 2005 MDD study.^(23, 30) RT-qPCR was performed on a Viia7 Real-time PCR system using TaqMan™ Multiplex Master Mix (Thermo Fisher Scientific, USA) for 50 cycles at 60°C. Primer concentration in the reaction was 300 nM and probe concentration 200 nM.

The gene *Glucuronidase-β* (*GUSB*) was used as a reference gene and normalized against *GUSB*-plasmid DNA (ipsogen, Qiagen, Germany) dilutions.⁽³¹⁾ All RT-qPCR experiments were carried out at least in duplicate and median values were used. An RH30 calibration curve was used as an exogenous positive control to ascertain the efficiency of each PCR reaction, except for the *PAX7-FOXO1* assay for which a CW9019 calibration curve was used (CW9019 cell line courtesy of Dr. F. Barr, National Cancer Institute, Bethesda, USA).

Sanger sequencing

Sanger sequencing was performed on products amplified by PCR. Further processing and analysis as described previously, on BioEdit software version 7.2.5.⁽³²⁾

Determining a threshold for positivity in patient samples

For genes with expression in normal hematopoietic tissue, we defined thresholds for positivity using the guidelines for minimal residual disease detection in acute lymphatic leukemia, as defined by the European Study Group⁽³³⁾ and as was described previously by our group in neuroblastoma.⁽²⁷⁾ In short, to correct for differences in RNA input, the Ct value of a marker was normalized to reference gene *GUSB*. Then, the median Δ Ct marker expression in healthy tissue (Δ Ct = Ct of marker – Ct of *GUSB*), was calculated and the threshold for positivity was set 3 Ct above the median Δ Ct (Supplemental figure 2). A patient sample was scored as positive if the Δ Ct of at least one marker in the 11-marker panel was above its threshold.

Statistical analysis

Event-free survival (EFS) and overall survival (OS) from diagnosis were estimated using Kaplan-Meier's methodology; differences in survival outcomes were assessed with the log-rank test. Association between PCR positivity and EFS/OS was estimated using a multivariate Cox regression model with EpSSG risk group stratification as a prognostic factor.⁽³⁴⁾

To estimate the cumulative incidence of relapse or progressive disease from diagnosis for RNA panel positivity/negativity, a competing risks model with death as competing event was employed.⁽³⁵⁾ Gray's test was used to assess statistical significance difference between the cumulative incidence for the RNA panel groups.⁽³⁶⁾ All analyses for the competing risk model were performed by using the mstate library⁽³⁷⁾ in the R environment version 4.4.⁽³⁸⁾ The other statistical analyses were performed in SPSS version 23 and figures were generated in Graphpad Prism version 8.

Results

Assay redesign for MYOD1 detection in liquid biopsies

Initial testing detected high background expression using the *MYOD1* assay as previously developed by Sartori et al⁽²³⁾ in PB and BM samples from healthy donors (Figure 1A). Using Sanger sequencing (Supplemental file 1) of the amplicons and RT-qPCR (Supplemental table 2), we demonstrated that this assay also detected unconverted RNA and genomic DNA. Consequently, we redesigned the forward primer to exclude genomic DNA amplification (Supplemental Table 3, new *MYOD1* sequence Supplemental Table 1). The newly designed *MYOD1* assay was shown to be completely tumor-specific with no background expression in BM and PB from healthy donors (Figure 1A) with similar sensitivity (Supplemental table 3).

Developing the rhabdomyosarcoma-specific RNA marker panel for testing in liquid biopsies

Candidate markers were selected with high expression in rhabdomyosarcoma and low/no expression in normal PB/BM, as described in the methods (Supplemental figure 1 and 3). This selection process identified three new markers for testing in BM and PB (*PDLIM3*, *ACTC1* and *ZIC1*) in addition to the redesigned *MYOD1* and known markers, *MYOG* and fusions of *PAX3* or *PAX7* genes with *FOXO1*.⁽³⁰⁾ Four new markers were selected for use in blood-based monitoring (*SNAI2*, *CDH11*, *TMEM47* *MEGF10*), since background of these markers was high in BM (on SYBR green for *SNAI2*, *CDH11* and *TMEM47* and in the Taqman assay for *MEGF10* (shown in Supplemental table 4 and Figure 1, respectively)).

Thresholds for positivity were set for all markers (Figure 1), except for *MYOD1* and *PAX3/7-FOXO1* fusions since these markers were completely tumor-specific. Mean Ct values of the 11 markers and the reference gene in 10 primary tumors are shown in Supplemental table 5. To detect any occult alveolar subtype, since

immunohistochemistry of the primary tumor can be inconclusive and fusion gene status was not available for every patient, we also tested material from patients diagnosed with an embryonal subtype for the *PAX3/7-FOXO1* fusion genes. Expression of most selected marker genes in tumor samples was variable, justifying the use of the 11-marker panel to increase sensitivity. We performed a sensitivity assay of RH30 cells (an established rhabdomyosarcoma cell line) in healthy blood cells which showed a sensitivity of at least 1 tumor cell in 100 000 healthy blood cells (Supplemental table 6).

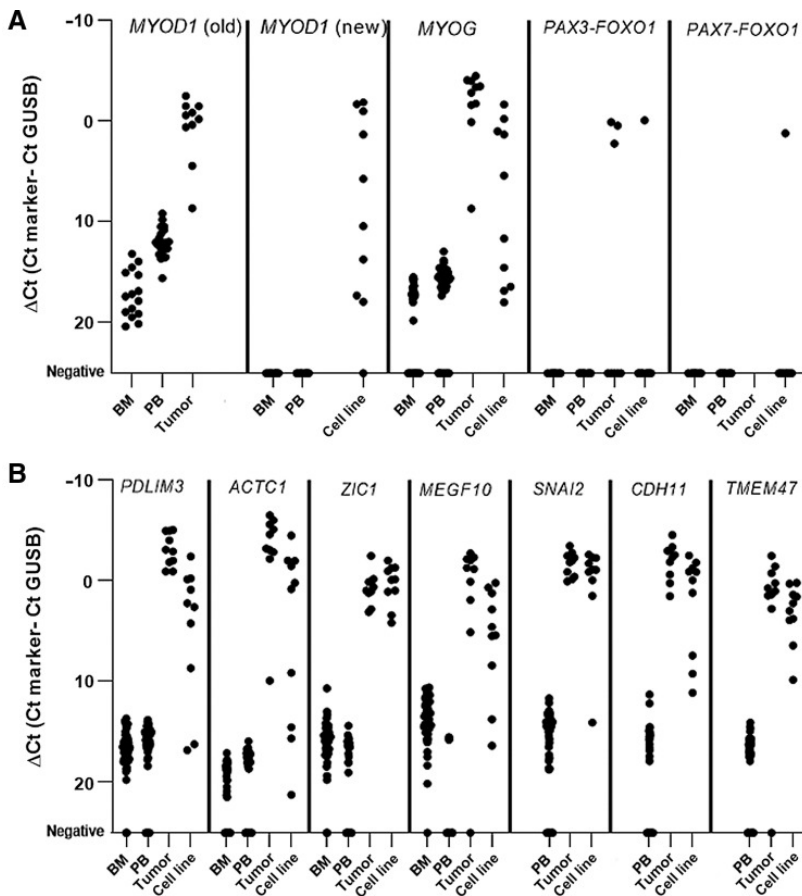


Figure 1. A, Background expression of known markers in control BM and PB, rhabdomyosarcoma (RMS) tumors, and established cell lines. “MYOD1 old design” and MYOG (BM $n = 41$, PB $n = 47$, RMS tumors $n = 10$), “MYOD1 new design” (BM $n = 26$, PB $n = 26$, RMS cell lines $n = 10$), PAX3-FOXO1 fusion gene (BM $n = 17$, PB $n = 10$, RMS tumor $n = 10$, RMS cell lines $n = 10$), and PAX7-FOXO1 (BM $n = 17$, PB $n = 10$, RMS cell lines $n = 10$). **B**, Background expression of PDLIM3, ACTC1, and ZIC1 in healthy control BM ($n = 41$), healthy control PB ($n = 47$), RMS tumors ($n = 10$), and RMS cell lines ($n = 10$). MEGF10, SNAI2, CHD11, and TMEM47 only measured in PB ($n = 47$), RMS tumors ($n = 10$), and RMS cell lines ($n = 10$).

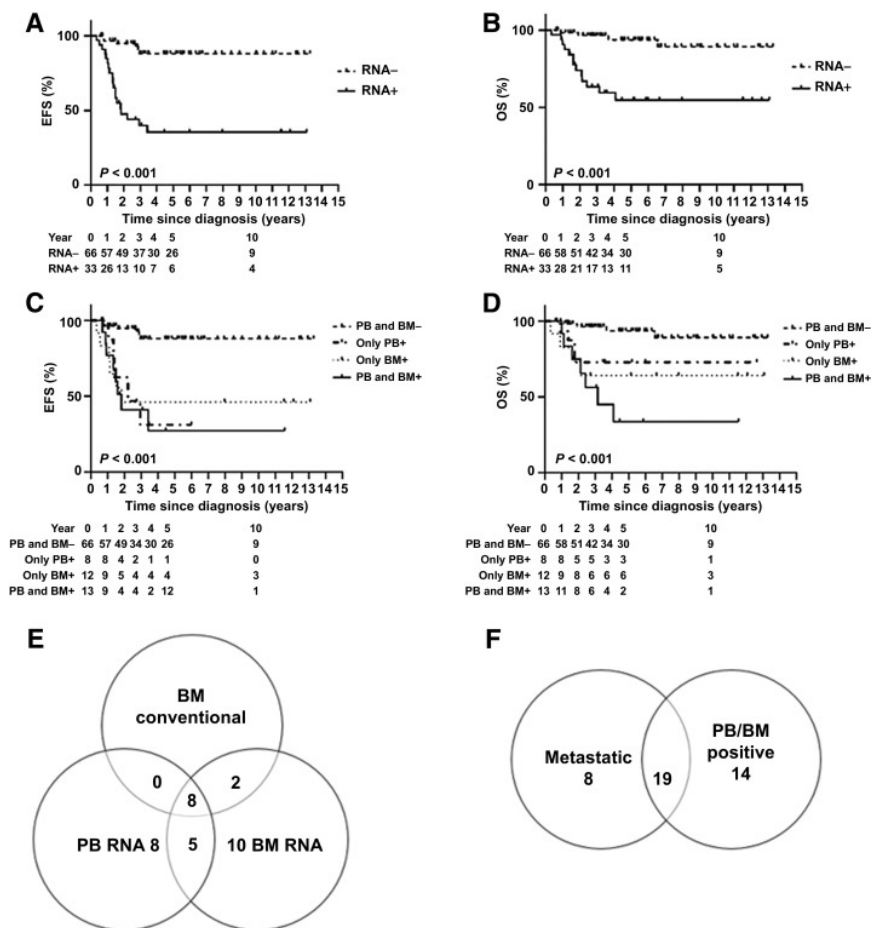


Figure 2. RNA positivity (BM and PB) at diagnosis and clinical outcome **(A)** EFS and **(B)** OS for SR and RNA panel **(C)** EFS and **(D)** OS for patients stratified for PCR testing of BM and PB at diagnosis: negative in PB and BM (PB and BM-), PB positive only (only PB+), BM positive only (only BM+), and positive in PB and BM (PB and BM+). **E**, Venn diagram depicting number of patients that tested positive with the RNA panel in PB, BM, and by conventional IHC in BM at diagnosis. **F**, Venn diagram depicting patients that tested positive for PB and/or BM with the RNA panel and patients with metastatic disease, detected by conventional diagnostics at diagnosis.

Prospective cohort description

After having established the thresholds for positivity for the marker panel, we tested patient samples. We collected diagnostic BM and PB samples of 99 consecutive patients at diagnosis and follow-up samples from 25 patients (14 BM and 78 PB) treated according to the EpSSG RMS2005 protocol. Median follow-up was 3.5 years (minimum 0.34 – maximum 13.29 years). Patient age and the risk group assigned are

shown in table 1 and supplemental table 7. Twenty-seven patients had metastatic disease of which 10 had bone marrow invasion determined by conventional immunohistochemistry. Twenty-eight patients had the alveolar subtype, *PAX3/7-FOXO1* fusion gene status was not recorded in this study. Five-year EFS and OS was 69.7% (95% CI 59.5-79.9) and 79.9% (95% CI 70.9-89.9), respectively.

Liquid biopsy-based 11-marker panel detection at diagnosis correlates with clinical outcome

At diagnosis, in 33 of 99 (33.3%) patients molecular disease was detected in PB and/or BM with our 11-marker panel. Primary tumor material was available for 8 patients (Supplemental table 5). In the samples that tested positive in matched PB and/or BM at diagnosis, most of the markers with a high expression in the primary tumor were also scored as positive in PB and/or BM. Due to low numbers, no statistical analysis was performed. For the 33 RNA-positive patients, paired PB and BM samples were positive in 13 patients, only BM samples were positive in 12 patients and only PB samples were positive in 8 patients (Supplemental table 8).

The 5-year EFS was 35.5% (95% CI 17.5-53.5%) for the RNA-positive patients, while this was 88.0% (95% CI 78.9-97.2%) for 66 RNA-negative patients ($p < 0.001$, figure 2A); the 5-year OS was 54.8% (95% CI 36.2-73.4%), and 93.7% (95% CI 86.6-100.0%), respectively ($p < 0.001$, figure 2B). Patient subgroups defined by molecular detection in BM, PB and paired BM-PB all show poor EFS and OS (Figure 2C and D) compared to RNA panel negative patients. In conclusion, molecular detection of minimal disseminated disease is correlated with outcome.

Liquid biopsy-based molecular detection at diagnosis complements current risk stratification strategies

Our patient cohort included 10 patients with bone marrow disease, determined by immunohistochemistry and cytomorphology. In all 10 BM samples and 8 paired PB samples tumor-derived mRNA was detected (figure 2E). Tumor-derived mRNA in PB/ BM was furthermore detected in 23 additional patients (figure 2E), among 14 with localized disease and 9 with metastases detected in other sites than the BM (figure 2F). Eighteen of the 33 patients testing positive in PB and/or BM had an alveolar subtype.

The numbers of patients with low risk (LR) and very high risk (VHR) disease were too small to allow statistical analyses, so only the larger risk groups (standard risk (SR), high risk (HR) and metastatic disease) according to the risk stratification used in EpSSG RMS2005, were analyzed in relation to RNA panel positivity and survival.

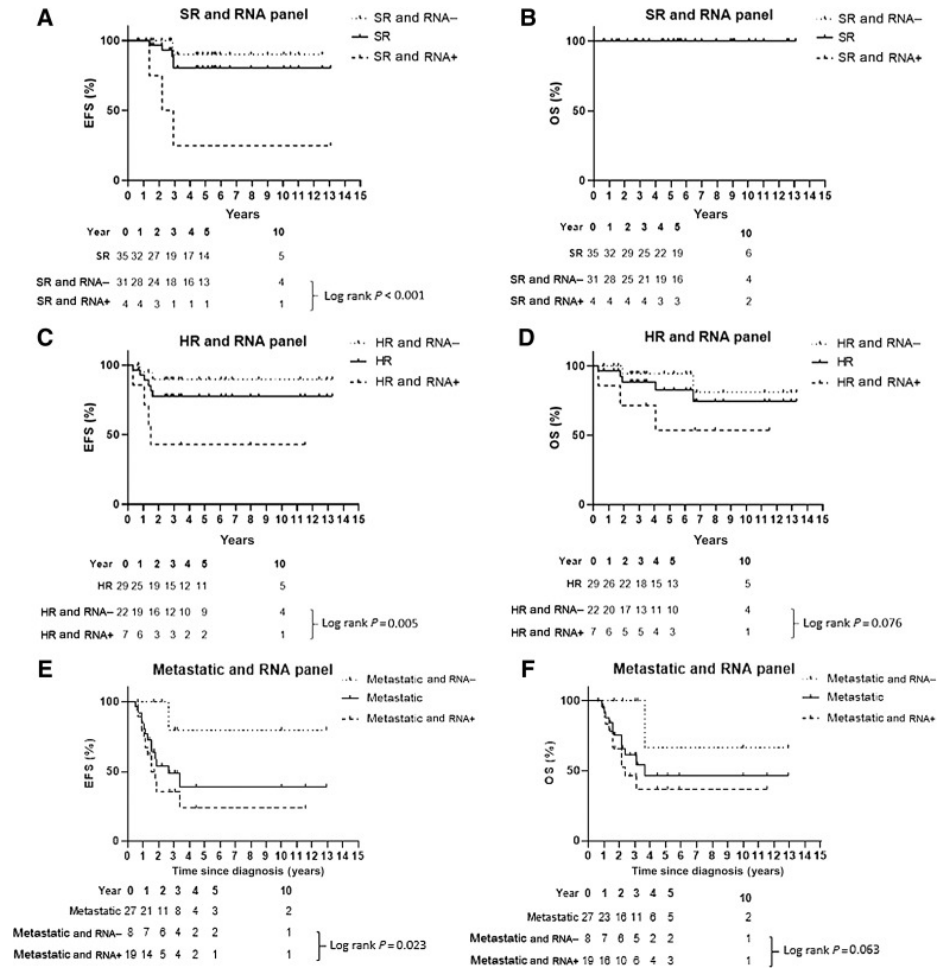


Figure 3. RNA positivity at diagnosis and outcome for different risk groups, stratified according RMS2005. Outcome for different risk groups is given as treated (continuous line) and stratified for RNA positivity (RNA+) and RNA negativity (RNA-) at diagnosis. **A** and **B**, EFS and OS, respectively, for SR group; please note that no P value is reported since there is no mortality in the SR group. **C** and **D**, EFS and OS, respectively, for HR group. **E** and **F**, EFS and OS, respectively, for metastatic disease group.

There was an association between the risk groups and survival outcomes: within each risk group, RNA panel negative patients had better outcome than RNA panel positive patients (Figures 3 A-F).

Considering the entire cohort of 99 patients, 6 of 14 (42.9 %) patients with localized disease and RNA positivity suffered from relapse (3 localized relapses, 3 metastatic relapses) and 3 eventually died (2 after relapse, 1 due to sepsis during primary



treatment), compared to 5 events in the 58 (8.6%) patients with localized disease without RNA-panel positivity (Supplemental Figure 4). Molecular disseminated disease was detected in 19/27 (70.3%) patients diagnosed with metastatic disease in bone, BM, lung and/or distant lymph nodes. Seven of these 19 patients experienced relapse, 5 progressive disease and 10 eventually died of disease. In contrast, 1 of 8 patients with metastatic disease (6/8 pulmonary lesions and 8/8 distant lymph nodes) and negative for our 11-marker panel, suffered from recurrent disease and later died (Supplemental Figure 4). The cumulative incidence of the event of interest (relapse/progressive disease) for RNA panel positivity is significantly different ($p < 0.001$, Figure 4).

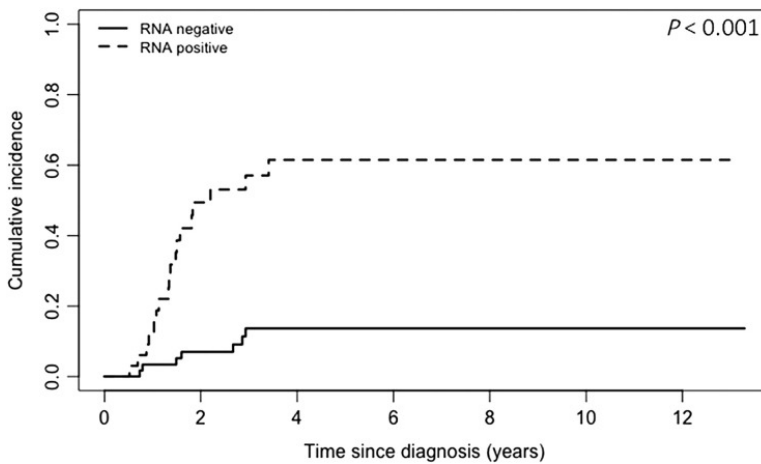


Figure 4. Cumulative incidence for relapse for RNA-negative/positive patients, as defined at diagnosis. Gray's test was used to compute the P value

We evaluated the prognostic impact of liquid biopsy-based molecular minimal disease detection at diagnosis on EFS and OS in univariate and multivariate Cox regression models (respectively, Supplemental table 9 and Table 2) for the largest groups in this cohort (SR, HR and metastatic disease). Risk factors included in the analysis, that all have prognostic value in univariate analysis, were metastatic disease, positive BM immunohistochemistry, age above 10 years, alveolar subtype, tumor size and regional lymph node involvement (Supplemental table 9). Other clinical characteristics like tumor site and IRS group were not included in this analysis due to low number of patients and/or no events in the subgroups. RNA panel-positivity was a prognostic factor for EFS (Hazard Ratio 9.52 95% CI (3.23-28.02)), while RMS2005 risk group stratification was not, in the multivariate model (Table 2). RNA positivity was also associated with EFS for the other risk factors in multivariate analyses. The

low number of events in the SR group in the 5-year follow-up prevented estimation of the effect on overall survival in multivariate analysis. However in multivariate analyses, the RNA panel was significantly associated with OS, where conventional BM immunohistochemistry and alveolar subtype was not (Table 2).

CDH11 is an important novel marker

Molecular testing in liquid biopsies revealed differential impact for certain markers, although the number of markers contributing to the positive score in paired BM and PB samples did not correlate with outcome (Supplemental Table 10). *MYOD1*, *PAX3/7-FOXO1* and *MYOG* were the markers most often contributing to assay positivity in both PB and BM samples (Supplemental Figures 5 and 6). Interestingly, *MYOG* was also positive in 3 out of the 15 patients with non-alveolar subtype testing positive at diagnosis, all 3 suffered from an event. *CDH11* contributed as single marker to positive scoring in diagnostic blood samples from 6/21 patients (Supplemental figure 5), 5 of 6 were histologically diagnosed with an embryonal rhabdomyosarcoma subtype. One of these six *CDH11* positive patients died of disease and two suffered relapses.

The 11-marker panel does not adequately detect minimal residual disease following treatment

We evaluated the potential of the 11-marker panel to detect minimal residual disease in BM and PB samples collected during primary therapy and 5-year follow-up. We tested 42 PB and 4 BM samples from 20 patients during primary treatment (the first 24 weeks after primary diagnosis within the EpSSG RMS2005 trial) and 9 BM and 35 PB samples collected for 20 patients during follow-up after treatment (Supplemental table 11). For the 19 patients who suffered from an event (15 relapse, 4 progressive disease), blood samples were available at first clinical relapse diagnosis from 10, and tested positive in only 3 patients. BM was available for 5 patients and tested positive in one patient (Supplemental table 11). While longitudinal blood sampling was not complete for any of these patients, at least 2 samples were collected for 16 patients during treatment and for 9 patients during follow-up. However, blood samples from only 1 (RMS007) of these 25 patients tested positive for the 11-marker panel during therapy and follow-up. This patient had a complex course with the blood samples at diagnosis, after 3 chemotherapy cycles and shortly before death testing positive (Supplemental table 11). The blood sample following primary treatment was negative, three blood samples during follow-up remained negative even after diagnosis of progressive disease. When tested in a small patient cohort during therapy and follow-up, our 11-marker panel did only detect minimal residual disease in a small proportion of patients who experience an event, even though it clearly identifies patients with risk of an event when tested at diagnosis.

Table 1. Patient and clinical characteristics with risk group stratification according to the EpSSG RMS2005 trial.

	Number of patients
Age at diagnosis (years)	
<1	1
1-10	64
>10	34
Sex	
Female	38
Male	61
Histology	
Alveolar rhabdomyosarcoma	28
Botryoid rhabdomyosarcoma	2
Embryonal Rhabdomyosarcoma	67
Rhabdomyosarcoma not otherwise specified	1
Spindle cell/leiomyomatous rhabdomyosarcoma	1
Pathology	
Favourable	71
Unfavourable	28
Post-surgical tumor staging (IRS grouping)	
I	6
II	13
III	53
IV	27
Tumor size	
≤5 cm	43
>5 cm	56
Regional lymph node involvement	
No evidence of lymph node involvement	69
Evidence of regional lymph node involvement	29
No information about lymph node involvement	1
Risk group	
Low risk	3
Standard risk	35
High risk	29
Very high risk	5
Metastatic	27
Site of origin of primary tumor	
Orbit	17
Head neck	6
Parameningeal	21
Bladder prostate	9
Genitourinary non-bladder prostate	13
Extremities	18
Other sites	15

Table 2. Hazard ratios (HR) with 95% confidence interval (CI) based on the Cox proportional hazard regression model for event-free survival.

	Event-free survival		Overall survival	
	Hazard ratio	95% Confidence Interval	Hazard ratio	95% Confidence Interval
RNA panel: PB and/or BM positive	9.52	3.23-28.02		
Standard Risk	1		Not possible due to low number of events in Standard Risk group	
High Risk	1.15	0.35-3.83		
Metastatic disease	1.52	0.50-4.66		
RNA panel: PB and/or BM positive	8.83	3.38-23.10	7.13	2.19-23.18
Positive BM immunohistochemistry	0.91	0.33-2.54	1.22	0.37-3.98
RNA panel: PB and/or BM positive	6.98	2.58-18.85	4.48	1.32-15.15
Metastatic disease	1.69	0.72-3.98	3.70	1.23-11.16
RNA panel: PB and/or BM positive	7.71	2.85-20.89	5.91	1.71-20.45
Alveolar rhabdomyosarcoma	1.29	0.55-3.02	1.66	0.57-4.85
RNA panel: PB and/or BM positive	8.22	3.25-20.78	6.21	2.00-19.28
Age > 10 years	2.07	0.93-4.61	5.65	1.92-16.59
RNA panel: PB and/or BM positive	7.80	2.89-21.01	4.27	1.23-14.87
Regional lymph node involvement	1.17	0.50-2.78	3.29	1.06-10.18
RNA panel: PB and/or BM positive	6.63	2.53-17.38	4.20	1.33-13.24
Tumor size >5cm	2.33	0.83-6.54	9.57	1.21-75.84

Discussion

We present results of the largest prospective study to date detecting minimal disseminated disease in liquid biopsies from pediatric patients with rhabdomyosarcoma, treated according to uniform guidelines. We identified and optimized new mRNA markers for the sensitive detection of tumor-derived mRNA in PB and BM samples and designed an 11-marker RT-qPCR panel assay. The presence of minimal disseminated disease in liquid biopsies at diagnosis correlates with poor outcome in our patient cohort, supporting inclusion of this assay in future studies to further improve risk stratification for children and adolescents diagnosed with rhabdomyosarcoma.

Our 11-marker panel detected bone marrow disease in all BM samples with positive histology, and in addition in 15 BM immunohistochemistry-negative samples (from 8 patients with localized disease and 7 with metastatic disease without known BM metastasis). Our data concur with findings from Gallego et al,⁽²²⁾ who conducted a study in 16 patients (14 localized, 2 metastatic) with the *PAX-FOXO1* fusion gene, *MYOD1* and acetylcholine receptor as targets for RT-qPCR in PB and BM samples. In their study, all BM samples with positive histology were positive with PCR as well, and 6 additional BM were only positive with PCR. This points out that PCR-based detection of minimal disseminated disease can help improve the diagnosis of BM metastasis since conventional diagnostics of BM metastasis can be inconclusive. In our cohort, two of 8 patients diagnosed with localized disease and molecular disease detected in BM suffered relapse (1 metastatic, 1 localized). An important question for a future validation study of the RNA panel is whether patients diagnosed with occult BM disease detected by PCR alone should be considered for upstaging of their treatment protocol at initial diagnosis. This might spare them additional morbidity due to further treatment for relapse and more importantly increase survival chance, since relapse is associated with lower survival.^(7, 39, 40)

PCR-based detection of minimal disseminated disease in PB and/or BM has been associated with poor outcome in several smaller studies,⁽²²⁻²⁴⁾ consistent with the very poor patient outcome previously correlated with documented BM metastases.^(5, 10) We observed a striking decline in overall survival for patients diagnosed with metastatic disease by both conventional diagnostics and RNA-positivity in liquid biopsies. This suggests the existence of an RNA-positive subgroup within the metastatic risk group with an ultrahigh-risk profile, including patients with histologically documented BM metastases and/or alveolar subtype, who could be considered for further therapy intensification. RT-qPCR-based detection alone was not associated with the type

of relapse (localized versus metastatic) in our study. Since metastatic relapse is associated with worse survival,⁽⁷⁾ this is an interesting question for a follow-up study.

Overall, we observe that patients for whom liquid biopsies test positive for the 11-marker panel at diagnosis have a higher risk of suffering an event. This suggests that the use of the RNA panel in addition to conventional strategies at initial diagnosis could improve risk stratification, however this needs to be further investigated in a larger cohort. We made an effort to avoid selection bias, as we included all consecutive patients treated in the participating centers, regardless of risk groups. However, this also resulted in underrepresented subgroups (LR and VHR). A future study in an independent cohort to evaluate whether the use of the RNA panel improves current risk stratification for these risk groups and for patients that would potentially benefit most from improving risk stratification (patients with metastatic disease testing positive for the 11-marker panel) is crucial.

The 11-marker assay was positive in samples collected after start of treatment for only a small number of patients in our cohort. This is in contrast to data from earlier publications.⁽²²⁻²⁴⁾ Sartori et al. reports *MYOD1* expression in BM samples collected after the first therapy cycle in 5/10 patients.⁽²³⁾ Gallego et al. and Krskova et al. detected *MYOD1* and *PAX3/7-FOXO1* in proportionately more blood and BM samples collected during treatment and follow-up.^(22, 24) The use of the *MYOD1* assay that also detected genomic DNA complicates the comparison. Gallego et al confirmed the potential for false positive results by describing discrete but positive expression of *MYOD1* in healthy PB.⁽²²⁾ Our redesigned *MYOD1* assay eliminates false positive detection from DNA binding. Furthermore, in our study BM samples were important for RNA positivity at diagnosis, but unfortunately only a low number of BM samples after diagnosis was available. Comparison of our cohort, consisting of patients treated completely according to the EpSSG RMS2005 protocol, to these 3 older studies is further complicated by the distinct treatment protocols patients were subjected to more than a decade ago. The absence of circulating tumor cells in patients from our cohort during treatment or even a change in gene expression due to treatment-driven clonal evolution of the disease⁽⁴¹⁻⁴³⁾ can be another explanation. Although we already applied a panel of multiple markers, we cannot exclude that during relapse our panel of markers is less sensitive in relapse samples than at diagnosis. Analysis of RNA Seq data from pre-treated tumors might offer further insight into gene expression during treatment. Also, further investigation into the potential of DNA-based techniques to detect minimal residual disease, which have shown great promise in other solid tumors as well as rhabdomyosarcoma, should be pursued.^(17-19, 44)

Most positively scored samples in our cohort detected the known markers, *MYOD1*, *PAX3/7-FOXO1* fusion and *MYOG*. Due to absence of background expression in healthy PB and BM, our redesigned *MYOD1* is completely tumor-specific which presents a major advantage compared to other markers. *CDH11* was the only marker in our panel that detected additional patients who suffered events later, especially in embryonal rhabdomyosarcoma which is in agreement with a report from 1999 which reports *CDH11* as being specific for fusion gene-negative rhabdomyosarcoma cells.⁽⁴⁵⁾ The majority of the patients with diagnostic liquid biopsies expressing *CDH11*, test negative for all the other markers. This makes *CDH11* an interesting novel marker for detection of minimal disseminated disease in fusion gene-negative tumors and further research should address its potential as a prognostic marker.

Conclusion

Here we demonstrate that RT-qPCR-based detection of minimal disseminated disease in blood and bone marrow samples collected at diagnosis in pediatric patients with rhabdomyosarcoma is associated with survival. We identify *CDH11* as an important novel blood-based marker for detection of minimal disseminated disease. The redesigned *MYOD1* assay supports highly sensitive rhabdomyosarcoma detection in liquid biopsies. The association between molecularly detected minimal disseminated disease at diagnosis and outcome warrants further investigations into the added value of this 11-marker panel at initial diagnosis on conventional diagnostic strategies to improve risk stratification for treatment of pediatric patients with rhabdomyosarcoma.

Acknowledgements

N. Lak, L. Zappeij-Kannegieter and J. Stutterheim were supported by the Children Cancer-Free Foundation (KiKa), project number 312.

The cell line CW9019 was kindly provided by dr. F. Barr, National Cancer Institute, Bethesda, USA.

The authors would like to thank Marcel Kool for his contributions in the early phase of this project and Kathy Astrahantseff for her contribution in the editing of this manuscript.

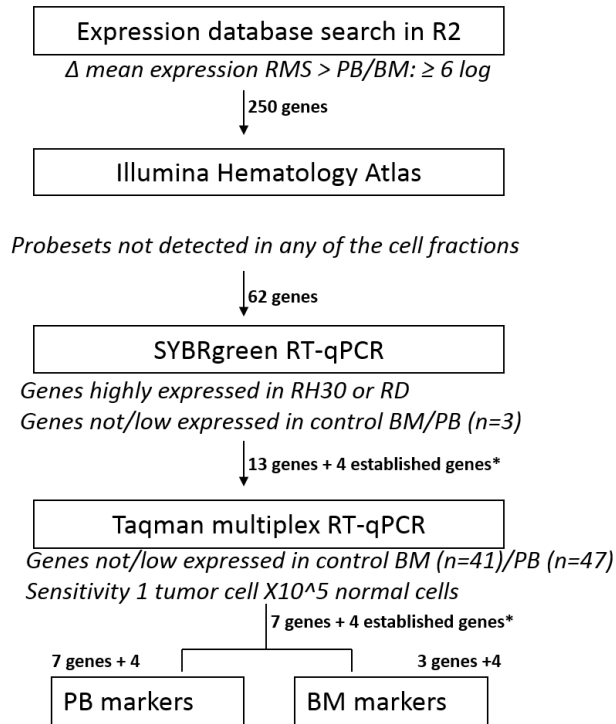
References

1. Gatta G, Botta L, Rossi S, Aareleid T, Bielska-Lasota M, Clavel J, et al.. Childhood cancer survival in Europe 1999–2007: results of EUROCARE-5—a population-based study. *Lancet Oncol* 2014;15:35–47.
2. Bisogno G, Jenney M, Bergeron C, Gallego Melcon S, Ferrari A, Oberlin O, et al.. Addition of dose-intensified doxorubicin to standard chemotherapy for rhabdomyosarcoma (EpSSG RMS 2005): a multicentre, open-label, randomised controlled, phase 3 trial. *Lancet Oncol* 2018;19:1061–71.
3. Oberlin O, Rey A, Sanchez de Toledo J, Martelli H, Jenney ME, Scopinaro M, et al.. Randomized comparison of intensified six-drug versus standard three-drug chemotherapy for high-risk nonmetastatic rhabdomyosarcoma and other chemotherapy-sensitive childhood soft tissue sarcomas: long-term results from the International Society of Pediatric Oncology MMT95 study. *J Clin Oncol* 2012;30:2457–65.
4. Arndt CAS, Bisogno G, Koscielniak E. Fifty years of rhabdomyosarcoma studies on both sides of the pond and lessons learned. *Cancer Treat Rev* 2018;68:94–101.
5. Oberlin O, Rey A, Lyden E, Bisogno G, Stevens MC, Meyer WH, et al.. Prognostic factors in metastatic rhabdomyosarcomas: results of a pooled analysis from United States and European cooperative groups. *J Clin Oncol* 2008;26:2384–9.
6. Weiss AR, Lyden ER, Anderson JR, Hawkins DS, Spunt SL, Walterhouse DO, et al.. Histologic and clinical characteristics can guide staging evaluations for children and adolescents with rhabdomyosarcoma: a report from the Children's Oncology Group Soft Tissue Sarcoma Committee. *J Clin Oncol* 2013;31:3226–32.
7. Chisholm JC, Marandet J, Rey A, Scopinaro M, de Toledo JS, Merks JH, et al.. Prognostic factors after relapse in nonmetastatic rhabdomyosarcoma: a nomogram to better define patients who can be salvaged with further therapy. *J Clin Oncol* 2011;29:1319–25.
8. Oberlin O, Rey A, Brown KL, Bisogno G, Koscielniak E, Stevens MC, et al.. Prognostic factors for outcome in localized extremity rhabdomyosarcoma. Pooled analysis from four international cooperative groups. *Pediatr Blood Cancer* 2015;62:2125–31.
9. Dasgupta R, Fuchs J, Rodeberg D. Rhabdomyosarcoma. *Semin Pediatr Surg* 2016;25:276–83.
10. Bailey KA, Wexler LH. Pediatric rhabdomyosarcoma with bone marrow metastasis. *Pediatr Blood Cancer* 2020;67:e28219.
11. Barr FG. Gene fusions involving PAX and FOX family members in alveolar rhabdomyosarcoma. *Oncogene* 2001;20:5736–46.
12. Selfe J, Olmos D, Al-Saadi R, Thway K, Chisholm J, Kelsey A, et al.. Impact of fusion gene status versus histology on risk-stratification for rhabdomyosarcoma: Retrospective analyses of patients on UK trials. *Pediatr Blood Cancer* 2017;64.
13. Anderson J, Gordon T, McManus A, Mapp T, Gould S, Kelsey A, et al.. Detection of the PAX3-FKHR fusion gene in paediatric rhabdomyosarcoma: a reproducible predictor of outcome? *Br J Cancer* 2001;85:831–5.
14. Seki M, Nishimura R, Yoshida K, Shimamura T, Shiraishi Y, Sato Y, et al.. Integrated genetic and epigenetic analysis defines novel molecular subgroups in rhabdomyosarcoma. *Nat Commun* 2015;6:7557.
15. Parham DM, Barr FG. Classification of rhabdomyosarcoma and its molecular basis. *Adv Anat Pathol* 2013;20:387–97.
16. Anderson J, Gordon A, Pritchard-Jones K, Shipley J. Genes, chromosomes, and rhabdomyosarcoma. *Genes Chromosomes Cancer* 1999;26:275–85.

17. Klega K, Imamovic-Tuco A, Ha G, Clapp AN, Meyer S, Ward A, et al.. Detection of somatic structural variants enables quantification and characterization of circulating tumor DNA in children with solid tumors. *JCO Precis Oncol* 2018;2018:PO.17.00285.
18. Eguchi-Ishimae M, Tezuka M, Kokeyuchi T, Nagai K, Moritani K, Yonezawa S, et al.. Early detection of the PAX3-FOXO1 fusion gene in circulating tumor-derived DNA in a case of alveolar rhabdomyosarcoma. *Genes Chromosomes Cancer* 2019;58:521–9.
19. Tombolan L, Zin A, Bisogno G. Cell-free DNA in pediatric rhabdomyosarcoma: potential and challenges. *Methods Mol Biol* 2019;1909:165–75.
20. Hoon DS, Kuo CT, Wen S, Wang H, Metelitsa L, Reynolds CP, et al.. Ganglioside GM2/GD2 synthetase mRNA is a marker for detection of infrequent neuroblastoma cells in bone marrow. *Am J Pathol* 2001;159:493–500.
21. Michelagnoli MP, Burchill SA, Cullinane C, Selby PJ, Lewis JJ. Myogenin—a more specific target for RT-PCR detection of rhabdomyosarcoma than MyoD1. *Med Pediatr Oncol* 2003;40:1–8.
22. Gallego S, Llord A, Roma J, Sabado C, Gros L, de Toledo JS. Detection of bone marrow micrometastasis and microcirculating disease in rhabdomyosarcoma by a real-time RT-PCR assay. *J Cancer Res Clin Oncol* 2006;132:356–62.
23. Sartori F, Alaggio R, Zanazzo G, Garaventa A, Di Cataldo A, Carli M, et al.. Results of a prospective minimal disseminated disease study in human rhabdomyosarcoma using three different molecular markers. *Cancer* 2006;106:1766–75.
24. Krskova L, Mrhalova M, Hilska I, Sumerauer D, Drahokoupilova E, Mudry P, et al.. Detection and clinical significance of bone marrow involvement in patients with rhabdomyosarcoma. *Virchows Arch* 2010;456:463–72.
25. Dias P, Chen B, Dilday B, Palmer H, Hosoi H, Singh S, et al.. Strong immunostaining for myogenin in rhabdomyosarcoma is significantly associated with tumors of the alveolar subclass. *Am J Pathol* 2000;156:399–408.
26. Stutterheim J, Gerritsen A, Zappeij-Kannegieter L, Kleijn I, Dee R, Hooft L, et al.. PHOX2B is a novel and specific marker for minimal residual disease testing in neuroblastoma. *J Clin Oncol* 2008;26:5443–9.
27. Stutterheim J, Gerritsen A, Zappeij-Kannegieter L, Yalcin B, Dee R, van Noesel MM, et al.. Detecting minimal residual disease in neuroblastoma: the superiority of a panel of real-time quantitative PCR markers. *Clin Chem* 2009;55:1316–26.
28. R2: Genomics Analysis and Visualization Platform. Available from: <http://r2.amc.nl>.
29. Watkins NA, Gusnanto A, de Bono B, De S, Miranda-Saavedra D, Hardie DL, et al.. A HaemAtlas: characterizing gene expression in differentiated human blood cells. *Blood* 2009;113:e1–9.
30. Carli M, Outcome of consortium meeting within EpSSG. Protocol for detection of minimal disease by quantitative real-time PCR in blood and bone marrow of children with RMS. Final version of the protocol with changes as agreed on Sept 1 (2009) conference call.
31. Beillard E, Pallisgaard N, van der Velden VH, Bi W, Dee R, van der Schoot E, et al.. Evaluation of candidate control genes for diagnosis and residual disease detection in leukemic patients using 'real-time' quantitative reverse-transcriptase polymerase chain reaction (RQ-PCR) - a Europe Against Cancer program. *Leukemia* 2003;17:2474–86.
32. van Wezel EM, Zwijnenburg D, Zappeij-Kannegieter L, Bus E, van Noesel MM, Molenaar JJ, et al.. Whole-genome sequencing identifies patient-specific DNA minimal residual disease markers in neuroblastoma. *J Mol Diagn* 2015;17:43–52.

33. van der Velden VH, Cazzaniga G, Schrauder A, Hancock J, Bader P, Panzer-Grumayer ER, et al.. Analysis of minimal residual disease by Ig/TCR gene rearrangements: guidelines for interpretation of real-time quantitative PCR data. *Leukemia* 2007;21:604–11.
34. Group EpStsS. Combination chemotherapy in treating young patients with nonmetastatic rhabdomyosarcoma. 2006. Available from: <https://clinicaltrials.gov/ct2/show/NCT00379457>.
35. Putter H, Fiocco M, Geskus RB. Tutorial in biostatistics: competing risks and multi-state models. *Stat Med* 2007;26:2389–430.
36. Gray RJ. A class of K-sample tests for comparing the cumulative incidence of a competing risk. *The Annals of Statistics* 1988;16:1141–54.
37. de Wreede LC, Fiocco M, Putter H. An R package for the analysis of competing risks and multi-state models. *Journal of Statistical Software* 2011;38.
38. Team RC. R: A language and environment for statistical computing. 2017
39. Winter S, Fasola S, Brisse H, Mosseri V, Orbach D. Relapse after localized rhabdomyosarcoma: evaluation of the efficacy of second-line chemotherapy. *Pediatr Blood Cancer* 2015;62:1935–41.
40. Mascarenhas L, Lyden ER, Breitfeld PP, Walterhouse DO, Donaldson SS, Rodeberg DA, et al.. Risk-based treatment for patients with first relapse or progression of rhabdomyosarcoma: a report from the Children's Oncology Group. *Cancer* 2019;125:2602–9.
41. Meacham CE, Morrison SJ. Tumour heterogeneity and cancer cell plasticity. *Nature* 2013;501:328–37.
42. Roerink SF, Sasaki N, Lee-Six H, Young MD, Alexandrov LB, Behjati S, et al.. Intra-tumour diversification in colorectal cancer at the single-cell level. *Nature* 2018;556:457–62.
43. Schulte M, Koster J, Rahmann S, Schramm A. Cancer evolution, mutations, and clonal selection in relapse neuroblastoma. *Cell Tissue Res* 2018;372:263–8.
44. Chicard M, Colmet-Daage L, Clement N, Danzon A, Bohec M, Bernard V, et al.. Whole-exome sequencing of cell-free DNA reveals temporo-spatial heterogeneity and identifies treatment-resistant clones in neuroblastoma. *Clin Cancer Res* 2018;24:939–49.
45. Markus MA, Reichmuth C, Atkinson MJ, Reich U, Hoffmann I, Balling R, et al.. Cadherin-11 is highly expressed in rhabdomyosarcomas and during differentiation of myoblasts in vitro. *J Pathol* 1999;187:164–72.

Supplemental data



Supplemental figure 1. Flowchart of the selection of the RNA markers. RMS=rhabdomyosarcoma, PB=peripheral blood, BM=bone marrow, RH30 and RD= two established RMS cell lines.

* 4 established genes: MYOD1, MYOG, PAX3-FOXO1 and PAX7-FOXO1.

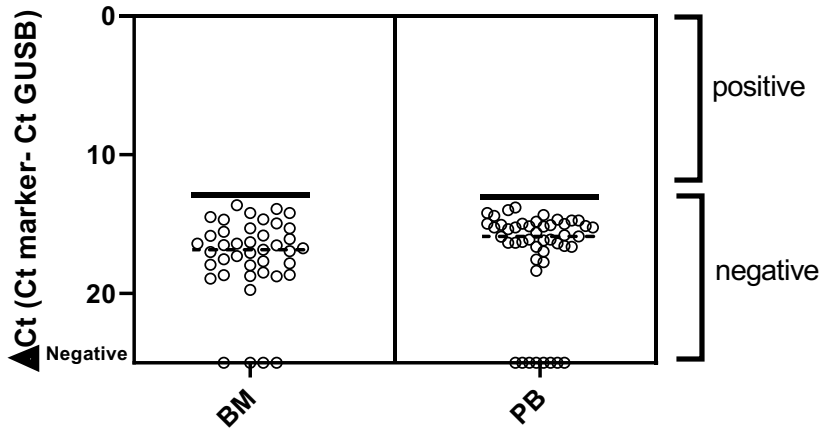
Supplemental table 1. Sequences of primers and probe.

Gene name Function	Sequence	5' modification	3' modification	Multiplex
Myogenic differentiation 1 (MYO1) <i>Transcription factor of muscle-specific target genes and important in muscle differentiation</i>	Forward primer (EpSSG)	AGGCGCTACTACAACGAGG		1 multiplex assay
	Forward primer (new)	CAACTGCTCCGAGGGCAT		
	Reverse primer	CAGGCGAGTCTAGGCTCGACAC		
	Probe	GCCCAGCGAACCCAGGCCCGGGAA	BHQ-2 Dragonfly Orange	
Myogenic factor 4 (MYOG) <i>Transcription factor of muscle-specific target genes and important in muscle differentiation</i>	Forward primer	TGCACCTGGAGTTACGCGC		
	Reverse primer	GGAGTGCAGGTTGTGGGC		
	Probe	AACCCAGGGGATCATCTGCTC	BHQ-1 6-FAM	
PDZ and LIM domain 3 (PDLIM3) <i>Organization of actin filament arrays within muscle cells</i>	Forward primer	ACTTCAACCAGCCTTTGGTCA		
	Reverse primer	ATCCTGTCTGCGCATCAG		
	Probe	CAGCTGCCAACCTGTGTCCTGGAGA	BHQ-1 Yakima Yellow	
Actin Alpha Cardiac muscle 1 (ACTC1) <i>Found in muscle tissues and major constituent of the contractile apparatus</i>	Forward primer	CCAGGCAGTGCTATCCCTGTAT		1 multiplex assay
	Reverse primer	GTGAGTTACACCATCCCCAGAGT		
	Probe	TCTGGCCGTACCACAGGCATTGTTCC	BHQ-1 Yakima Yellow	
Multiple EGF-like domains 10 (MEGF10)* <i>Plays role in muscle cell proliferation, adhesion and motility, essential factor in myogenesis regulation</i>	Forward primer	CGCGTTGATTGGAACAGATT		
	Reverse primer	TGCTTCTCCTCTTTAATGGATTGG		
	Probe	CGCTGCGATTCTCAAGATCTCGACC	BHQ-1 6-FAM	
ZIC family member 1 (ZIC1) <i>Transcription activator of multiple genes, incl PAX3, SNAI2</i>	Forward primer	TCCACAAAAGGACGCACACA		1 single assay
	Reverse primer	TGCACGTGCATGTGCTTCTT		
	Probe	CTGTGACCCGGCGCTTCGCTAACA	BHQ-2 Dragonfly Orange	

Supplemental table 1. Continued

Gene name Function	Sequence	5' modification	3' modification	Multiplex
Snail family zinc finger (SNAI2)* <i>Transcription repressor modulating activator-dependent and basal transcription</i>	Forward primer	GACCTGGTGGTCTCAAGGA		1 multiplex assay
	Reverse primer	GAGCCCTCAGATTTGACCTGTCT		
	Probe	AGAAGCCTTTTTCTTGCCTCACTGCAA	Dragonfly Orange BHQ-2	
Cadherin 11 (CDH11)* Calcium-dependent cell adhesion protein, involved in myogenesis ⁽¹⁾	Forward primer	TGGAACCCAGTTCCTCGTGATAGAG		
	Reverse primer	TCCCATCACCAGAGTCAATATCTG		
	Probe	CCTGACCCCGTCTTGTGGGC	6-FAM BHQ-1	
Transmembrane protein 47 (TMEM47)* <i>Regulates cell junction organization</i>	Forward primer	CAGCTGACCACCAGTACTACTCTGT		
	Reverse primer	AGGAGTAAAGCCAGAGTAGCAATCT		
	Probe	TCTGGCACTGCGAGTCCACGCT	Yakima Yellow BHQ-1	
Paired box 3 (PAX3) <i>Transcription factor regulating cell proliferation, migration, apoptosis and myogenesis</i>	Forward primer	TGAACCCACCATTGGCAAT		1 single assay with FOXO1
	Probe	TCTCACCTCAGAATTC	FAM MGB-Eclipse®	
	Reverse primer	ACATGAACCCCGTTCAGCAA		
Paired box 7 (PAX7) <i>Transcription factor regulating muscle stem cell proliferation, myogenesis and muscle regeneration</i>	Forward primer	ACATGAACCCCGTTCAGCAA		1 single assay with FOXO1
	Probe	CTGTCTCTCAGAATTC	FAM MGB-Eclipse®	
	Reverse primer	CTGTGTAGGGACAGATTATGACGAA		
Forkhead box O1 (FOXO1) Transcription factor involved in glucose metabolism	Reverse primer	CTGTGTAGGGACAGATTATGACGAA		

* Only measured in peripheral blood due to high background in healthy bone marrow. Gene function is summarized from entry per gene from www.uniprot.org, as searched on 3rd of May 2021.



Supplemental figure 2. Example of determining the threshold for positivity using the median background expression (dotted line) of *PDLIM3* in healthy bone marrow (BM) and peripheral blood (PB). Threshold (continuous line) is set 3 Ct above the median.

Supplemental table 2. Mean Ct values of RT-qPCR assay of *MYOD1* assay with the forward primer from the EpSSG protocol.

	Normal	DNase + cDNA	Unconverted RNA	DNA
RH30 10 ⁰	15.7	19.2	27.5	23.2

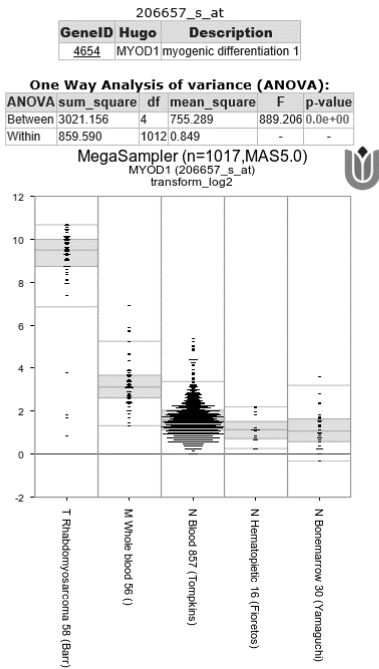
Conditions: normal preparation of cDNA, DNase treated RNA then converted into cDNA, unconverted RNA and DNA from RH30 cells.

Supplemental table 3. Mean Ct values of RT-qPCR assay of *MYOD1* assay with forward primer from EpSSG protocol and new design on a dilution of RH30 cells.

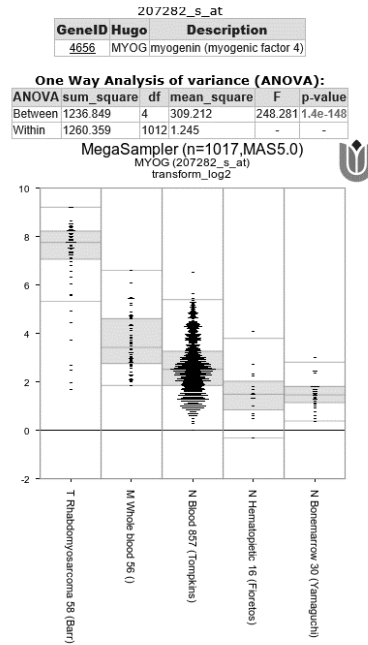
	EpSSG FWD Mean Ct value	New FWD Mean Ct value
RH30 10 ⁻²	22.1	23.2
RH30 10 ⁻³	24.9	25.7
RH30 10 ⁻⁴	28.2	28.9
RH30 10 ⁻⁵	30.6	31.6



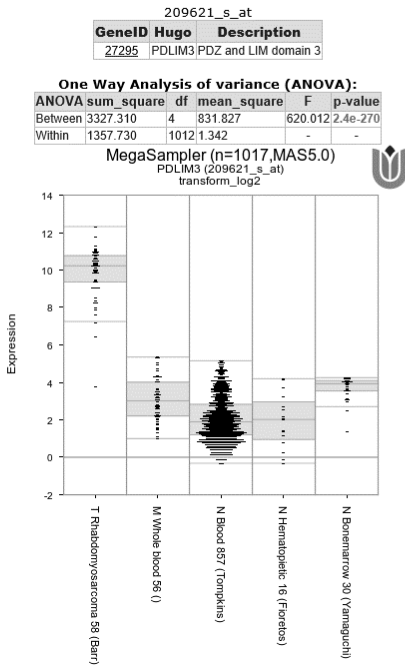
MYOD1:



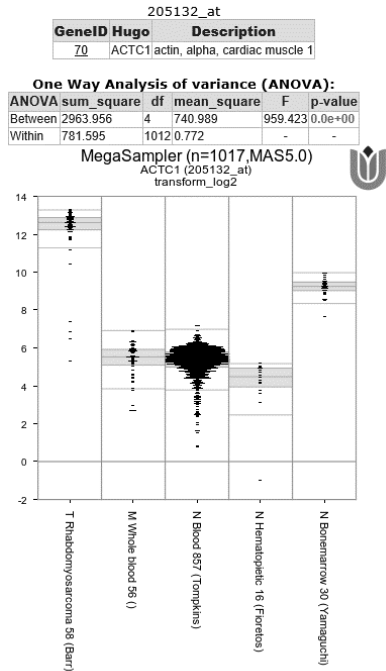
MYOG:



PDLIM3:

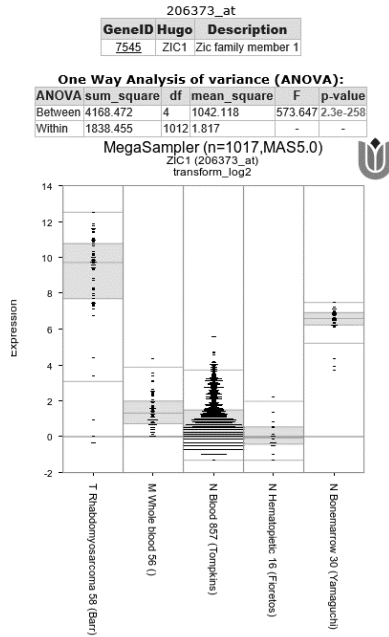


ACTC1:

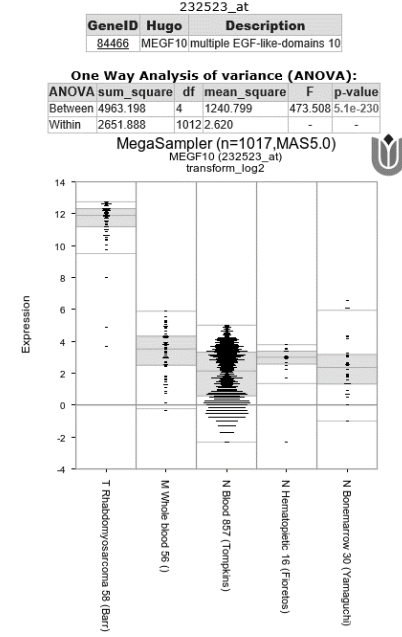


Supplemental figure 3. Expression of selected markers in healthy tissue and rhabdomyosarcoma tumors.

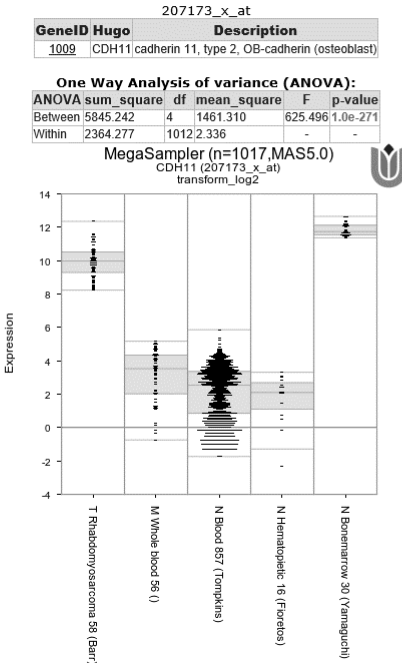
ZIC1:



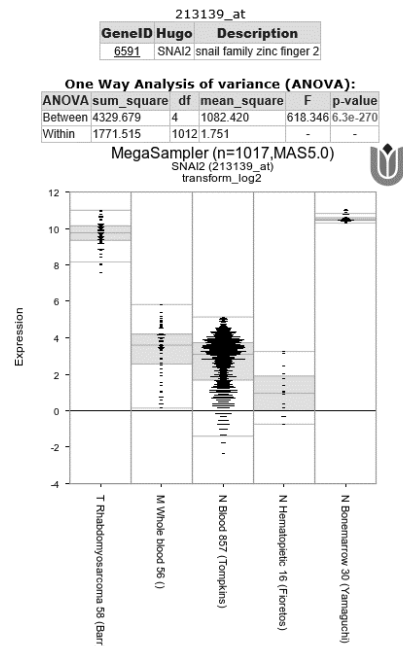
MEGF10:



CDH11:



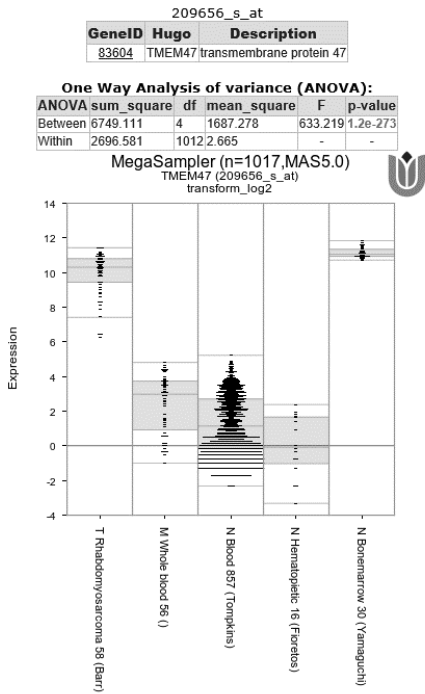
SNAI2:



Supplemental figure 3. Expression of selected markers in healthy tissue and rhabdomyosarcoma tumors.



TMEM47:



Supplemental figure 3. Expression of selected markers in healthy tissue and rhabdomyosarcoma tumors. Data as analyzed on 10th of January 2021 on R2: Genomics Analysis and Visualization Platform (<http://r2.amc.nl>).

Included datasets:

Tumor Rhabdomyosarcoma - Barr - 58 - MAS5.0 - u133p2 gse66533

Mixed Whole blood - 56 - MAS5.0 - u133p2 gse6575

Normal Blood (Trauma Patients) - Tompkins - 857 - MAS5.0 - u133p2 gse36809

Normal Hematopoietic Subgroups - Fioretos - 16 - MAS5.0 - u133p2 gse19599

Normal Bonemarrow Mesenchymal stem cells - Yamaguchi - 30 - MAS5.0 - u133p2 gse7637

Supplemental table 4. SYBR-green results of the 62 genes tested on 2 established rhabdomyosarcoma cell lines (RD and RH30), and healthy PB and BM. Please note that Ct values are not included if all samples were negative for a marker.

Gene	PB					BM				
	RD-1	RH30-1	PB pos	Mean Ct	Min Ct	Max Ct	BM pos	Mean Ct	Min Ct	Max Ct
A2M	33,05	34,97	(4/4)	29,94	28,35	34,47	(3/3)	26,37	25,67	27,15
ACTC1	20,80	19,22	(3/4)	34,54	34,18	35,21	(3/3)	33,50	32,25	34,49
AMOTL1	24,20	22,17	(4/4)	26,97	26,16	28,19	(3/3)	30,94	23,84	31,51
ASP	35,43	23,06	(4/4)	35,08	33,36	34,68	(3/3)	34,03	33,20	34,84
C1S	30,09	31,10	(4/4)	32,76	30,13	35,19	(3/3)	28,33	26,22	30,53
CAPN6	24,37	27,53	(2/5)	35,84	35,26	36,41	(2/3)	34,38	33,19	35,57
CDH11	22,29	23,90	(2/5)	36,26	36,26	37,00	(3/3)	27,30	24,30	30,50
CSRP2	22,40	23,26	(3/3)	26,16	25,32	26,69	(3/3)	26,12	25,62	29,96
CTGF	21,67	24,61	(3/3)	29,73	29,01	31,03	(3/3)	24,29	21,12	26,56
CTHRC1	22,18	26,07	(3/3)	29,86	32,99	34,42	(3/3)	30,98	29,82	32,34
COL3A1	19,70	25,70	(4/5)	34,38	27,46	37,79	(3/3)	26,14	25,90	26,40
COL5A2	18,58	17,82	(3/3)	28,46	28,27	28,81	(3/3)	26,98	26,12	22,06
DCLK1	36,02	31,00	(1/4)	39,40	39,40	39,40	(2/3)	38,55	37,59	39,52
DCN	23,55	32,08	(5/5)	32,81	31,90	33,80	(3/3)	27,17	26,40	35,10
DLK1	30,01	28,68	(3/3)	32,89	31,44	34,62	(3/3)	31,12	29,69	32,78
DNAPT6	18,80	18,37	(3/3)	24,69	24,37	24,90	(3/3)	22,94	22,06	23,95
FBN1	25,22	23,06	(4/4)	27,84	25,85	30,16	(3/3)	29,48	25,07	33,89
FGFR4	21,76	19,20	(4/4)	31,18	28,21	33,64	(3/3)	26,67	24,31	29,72
FND5	21,81	22,70	(3/3)	29,71	29,54	30,33	(3/3)	28,94	25,56	30,75
GJA1	22,32	26,17	(3/3)	24,09	23,50	24,40	(3/3)	25,77	25,30	26,20
GJC1	28,36	25,42	(4/4)	35,98	34,41	37,67	(4/4)	32,92	30,78	35,07



Supplemental table 4. Continued

Gene	PB					BM				
	RD-1	RH30-1	PB pos	Mean Ct	Min Ct	Max Ct	BM pos	Mean Ct	Min Ct	Max Ct
GLT8D4	36,02	24,60	(2/4)	34,26	33,47	35,05	(3/3)	26,10	25,28	26,76
HS6ST2	33,85	34,48	(0/4)	-	-	-	(1/3)	36,01	36,01	36,01
IGF2	17,49	17,46	(4/4)	35,61	33,69	37,64	(3/3)	25,77	24,73	26,29
KBTBD10	21,93	24,18	(3/5)	36,61	35,18	37,99	(3/3)	32,32	31,13	33,99
LAMB1	24,42	26,44	(4/4)	30,66	28,60	31,80	(3/3)	28,23	27,80	28,50
LOXL1	27,42	26,55	(1/1)	26,54	23,93	31,47	(3/3)	27,66	26,82	27,70
LOXL2	29,28	27,93	(3/3)	23,85	22,73	25,04	(3/3)	27,26	26,27	28,99
LPHN2	29,96	28,70	(1/4)	39,47	39,47	39,47	(3/3)	38,15	35,59	38,30
LUM	27,56	33,65	(4/4)	32,81	30,88	33,65	(3/3)	28,54	27,19	29,36
MDK	20,84	20,56	(4/4)	25,23	24,11	26,40	(3/3)	24,72	24,38	25,67
MEGF10	23,25	23,40	(0/3)	-	-	-	(3/3)	31,90	31,06	33,33
MEST	16,63	21,57	(3/3)	24,01	23,65	24,19	(3/3)	22,13	21,82	22,71
MGP	36,82	26,25	(3/3)	25,39	24,50	26,30	(3/3)	27,08	26,10	28,00
MYH3	36,48	38,99	(4/4)	26,72	24,00	26,67	(3/3)	26,81	23,37	29,83
MYL1	21,03	27,20	(0/5)	-	-	-	(0/6)	-	-	-
MXRA5	31,89	27,72	(1/5)	35,42	35,42	35,42	(3/3)	27,77	26,70	29,20
NES	22,12	22,29	(2/3)	39,54	39,24	39,84	(7/7)	38,05	36,35	39,07
PCDH7	33,89	41,20	(0/3)	-	-	-	(0/3)	-	-	-
PDGFRA	33,81	28,09	(4/4)	36,22	33,91	37,58	(3/3)	29,82	28,67	31,93
PDLIM3	20,54	22,70	(3/5)	38,77	38,27	39,15	(3/3)	35,80	35,10	36,70
PEG10	24,27	23,11	(1/1)	23,65	23,65	23,65	-	-	-	-
PLK2	29,21	31,14	(4/4)	24,52	23,27	26,00	(3/3)	23,86	23,09	24,89

Supplemental table 4. Continued

Gene	PB					BM				
	RD-1	RH30-1	PB pos	Mean Ct	Min Ct	Max Ct	BM pos	Mean Ct	Min Ct	Max Ct
PLS3	20,82	18,75	(3/3)	29,44	28,48	30,39	(3/3)	26,72	26,56	26,98
POSTN	24,82	31,50	(2/3)	34,75	34,60	34,90	(3/3)	30,14	29,64	30,84
PTPRD	23,41	24,33	(4/4)	35,73	33,30	39,89	(3/3)	29,56	28,85	30,10
RBM24	22,93	23,13	(3/3)	29,37	28,19	30,45	(3/3)	29,31	27,54	30,40
RBP1	27,78	23,12	(5/5)	34,21	33,70	34,60	(3/3)	32,32	30,00	32,50
RG55	27,44	32,72	(2/3)	36,92	33,60	37,00	(3/3)	30,35	27,40	32,30
RND3	25,92	26,94	(2/2)	33,60	32,32	34,88	-	-	-	-
RUNX1T1	33,99	24,51	(4/4)	34,57	33,91	35,25	(3/3)	31,12	29,59	32,30
SIX1	22,83	21,74	(3/3)	35,10	34,22	36,16	(2/2)	32,48	30,03	36,78
SNAI2	22,76	21,59	(3/3)	35,89	34,00	37,50	(3/3)	28,24	27,30	29,40
SPARCL1	29,54	31,96	(5/5)	35,40	34,50	38,10	(3/3)	32,26	29,90	32,50
TEAD1	23,08	22,30	(3/3)	31,06	23,10	32,30	(3/3)	30,09	28,70	32,20
TMEM47	26,71	23,08	(2/5)	36,18	36,20	36,40	(3/3)	32,38	30,50	34,90
TNNI1	24,01	21,22	(2/6)	36,19	34,63	37,75	(3/3)	35,78	33,71	38,05
TSPAN12	22,45	22,85	(4/4)	35,08	31,56	36,21	(3/3)	30,55	30,14	30,95
TUSC3	22,53	22,40	(3/3)	30,77	29,80	31,60	(3/3)	29,55	29,30	29,70
VASH2	23,37	20,68	(3/4)	35,44	31,08	38,64	(3/3)	30,33	29,57	31,38
YAP1	22,22	23,45	(3/3)	29,17	28,80	29,90	(3/3)	29,18	26,90	30,60
ZIC1	22,54	23,14	(4/6)	34,81	32,12	36,25	(3/7)	35,52	33,86	37,18

PB pos = number of control PB testing positive for a marker, per number of PB tested.

BM pos = number of control BM testing positive for a marker, per number of BM tested.



Supplemental table 5. Expression of the 11 markers in 10 rhabdomyosarcoma tumors and their matching results in PB and BM (when available). Markers in PB and BM are scored as positive according to the defined thresholds.

RMS ID	Subtype	Markers in tumor (mean Ct values)										Markers positive (according to threshold)		
		GUS	MYOD1	MYOG	PAX3- FOXO1	ZIC1	ACTC1	CDH11	MEGF10	PD LIM3	SNAI2	TMEM47	Pb at Dx	BM at Dx
RMS075	ARMS	22.83	21.98	18.82	23.26	22.64	16.33	22.2	20.5	19.91	21.94	22.05	MYOD1, MYOG, PDLIM3, ACTC1, ZIC1, PAX3-FOXO1	MYOD1, MYOG, PDLIM3, ACTC1, ZIC1, PAX3-FOXO1
RMS099	ARMS	28.72	28.52	24.62	Und	29.9	25.86	30.22	30.61	24.68	26.72	29.74	neg	MYOD1
RMS038	ARMS	28.5	27.01	25.03	30.71	31.28	22.9	26.17	27.32	27.55	28.55	29.21	NA	NA
RMS105	ARMS	29.23	26.71	25.85	Und	30.18	24.13	29.46	27.05	24.26	25.75	27.79	neg	NA
RMS045	ARMS	23.15	21.64	18.64	Und	24.19	17.13	21.27	21.86	18.18	20.35	20.67	neg	MYOD1, PAX7- FOXO1
RMS059	ERMS	33.22	33.8	31.62	Und	33.23	29.99	28.65	30.48	28.16	30.91	34.68	NA	NA
RMS069	ERMS	29.22	29.56	27.48	Und	29.82	26.15	25.86	29.3	26.11	28.79	31.97	neg	neg
RMS078	ERMS	24.07	23.49	21.22	Und	21.58	19.44	21.02	22.04	22.06	21.57	24.29	neg	neg
RMS003	ERMS	28.31	36.94	36.97	Und	28.42	38.22	25.32	33.4	27.37	28.15	29.63	neg	neg
RMS095	ERMS	35.34	39.75	35.43	Und	38.43	33.15	32.75	Und	33.49	33.49	Und	neg	neg

Please note: PAX7-FOXO1 RT-qPCR was tested in the clinical diagnostic lab, exact Ct values are not available. Und=undetermined, sample is negative for target. Neg=negative. NA=not available

Supplemental table 6. Sensitivity assay of RH30 cells diluted in PB cells from a healthy controls.

	MYOD1	MYOG	ACTC1	CDH11	MEGF10	PDLIM3	SNAI2	TMEM47
	Mean Ct	Mean Ct	Mean Ct	Mean Ct	Mean Ct	Mean Ct	Mean Ct	Mean Ct
RH30	16,3	16,2	13,4	17,8	19,7	18,7	16,7	20,6
RH30-1	19,6	19,5	17,0	21,4	23,2	22,1	19,9	23,7
RH30-2	23,1	22,8	21,0	24,7	26,5	25,4	23,3	27,1
RH30-3	26,4	26,1	24,6	28,1	29,8	28,9	26,6	29,9
RH30-4	29,7	29,3	28,5	31,4	33,1	32,4	30,2	33,2
RH30-5	33,5	32,4	32,2	33,8	36,1	35,8	33,1	36,0
RH30-6	35,6	35,0	36,1	Und	Und	38,4	35,7	37,4
PbCo	Und	35,2	40,7	Und	Und	44,7	Und	Und

Und= undetermined, sample is negative for target

PbCo= healthy PB cells without mixed in RH30.

Supplemental table 7. Patient and clinical characteristics distributed according to the RMS2005 risk groups.

Risk group	N	Age at diagnosis (years)					Tumor	
		Male	ARMS	<1	1-10	>10	N1	size >5cm
Low risk	3	3	0	0	3	0	0	0
Standard risk	35	22	0	1	27	7	0	6
High risk	29	16	9	0	19	10	5	23
Very high risk	5	3	5	0	3	2	5	5
Metastatic disease	27	17	14	0	12	15	17*	22
Total	99	61	28	1	64	34	27	56

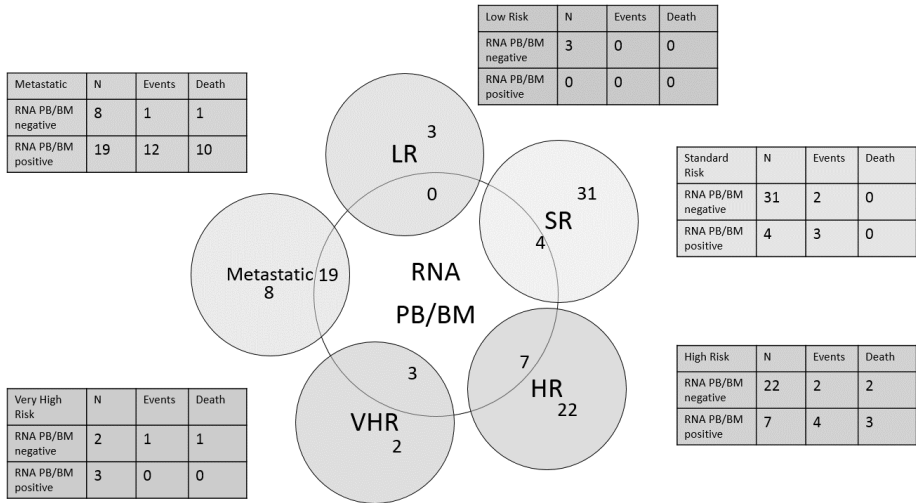
N= total number of patients, ARMS= alveolar rhabdomyosarcoma, N1= regional lymph node involvement

* lymph node status missing for 1 patient

Supplemental table 8. Number of patients distributed according to the RMS 2005 risk group stratification and patients testing positive in peripheral blood only, bone marrow only or positive in both.

Risk group	Number of patients	Only PB+	Only BM+	PB and BM +
Low risk	3	0	0	0
Standard risk	35	3	1	0
High risk	29	2	4	1
Very high risk	5	1	2	0
Metastatic	27	2	5	12

PB = peripheral blood; BM = bone marrow; ARMS = alveolar rhabdomyosarcoma



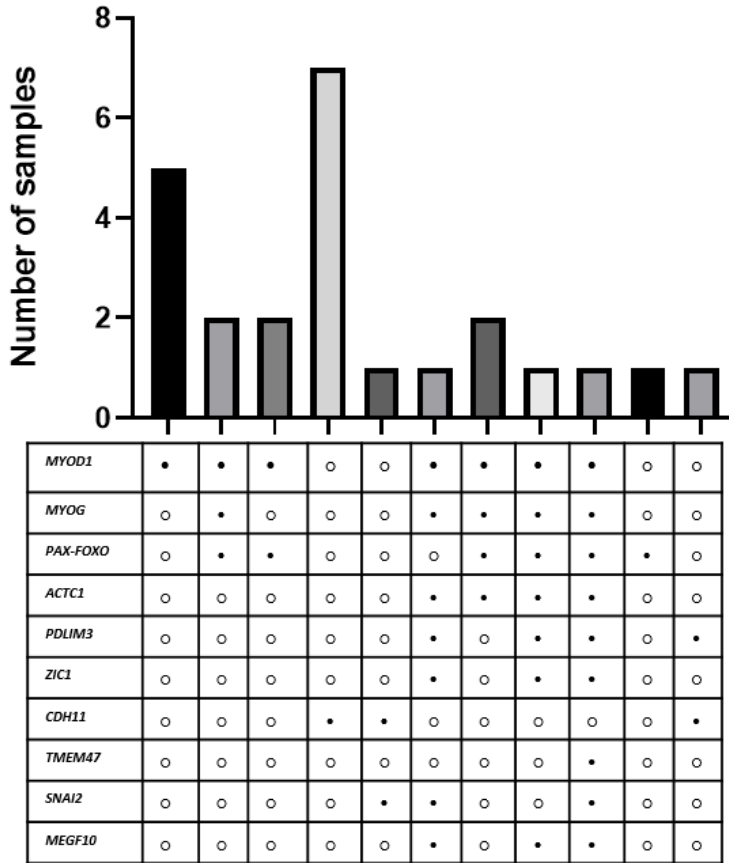
Supplemental figure 4. Distribution of RNA positivity, events (=relapse, progressive disease or death) and death of disease among conventional risk groups according to the RMS 2005 risk stratification. PB=peripheral blood, BM=bone marrow, LR=low risk, SR=standard risk, HR=high risk, VHR=very high risk, N= total number of patients.

Supplemental table 9. Univariate analysis of RNA panel positivity in peripheral blood and/or bone marrow and conventional risk factors.

	Event-free survival		Overall survival	
	Hazard ratio	95% Confidence Interval	Hazard ratio	95% Confidence Interval
RNA panel: PB and/or BM positive	8.62	3.43-21.69	7.54	2.46-23.17
Risk group: Standard Risk	1			
Risk group: High Risk	1.58	0.48-5.17	Not possible due to low events in Standard Risk group	
Risk group: Metastatic	4.73	1.68-13.35		
Metastatic disease	3.81	1.72-8.40	6.83	2.49-18.75
Alveolar rhabdomyosarcoma	3.06	1.39-6.70	3.81	1.44-10.07
Positive BM immunohistochemistry	3.02	1.13-8.06	3.50	1.13-10.80
Age >10 years	2.41	1.09-5.30	6.88	2.38-19.86
Tumor size >5 cm	4.33	1.62-11.58	16.53	2.19-124.84
Regional node involvement	2.72	1.21-6.10	6.29	2.24-17.64

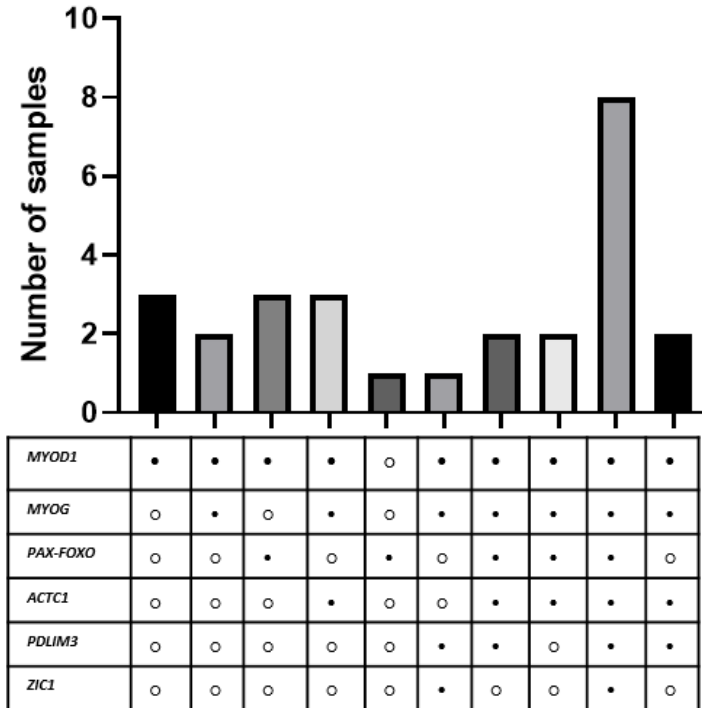
PB = peripheral blood; BM = bone marrow





Supplemental figure 5. Distribution of RNA markers positive in peripheral blood (PB) at diagnosis (21 samples) and during follow up (4 samples).

•=positive sample, o= negative sample



Supplemental figure 6. Distribution of RNA markers positive in bone marrow (BM) at diagnosis (25 samples) and during follow up (1 sample).

•=positive sample, ○= negative sample

Supplemental table 10. Number of positive markers in peripheral blood (PB) and bone marrow (BM) at diagnosis correlating with events (=relapse, progressive disease or death).

		Patients (number of events)		
		Markers positive in PB		
		0 markers	≤2 markers	≥3 markers
Markers positive in BM	0 markers	66 (6)	8 (5)	0 (0)
	≤2 markers	6 (1)	1 (1)	1 (1)
	≥3 markers	6 (5)	4 (3)	7 (3)

Supplemental table 11. Follow-samples of 25 patients. (following page)

RMSnr	Risk group	Dx	PB2	PB3	PB4	PB5	Follow up	1st rel	PD	2 nd rel	Outcome	Follow up time (years)
RMS002	meta	•	-	0	0	-	-	•	-	-	DOD (after 3 rd rel)	3.14
RMS007	meta	•	-	•	-	0	-	-	0-0-0--	-	DOD (ongoing PD)	2.13
RMS010	meta	•	0	0	-	0	-	0-0-0-0	-	-	DOD (after 1 st rel)	1.62
RMS011	meta	0	0	0	-	0	-	0	-	-	DOD (after 1 st rel)	3.67
RMS022	meta	•	0	0	-	0	-	-	0	-	DOD (PD)	.90
RMS024	HR	•	0	-	-	-	-	0	-	0	DOD (after 4 th rel)	4.09
RMS025	SR	0	0	0	-	-	-	-	-	0-0-0	Alive (CR after 2 nd rel)	9.11
RMS026	meta	•	-	0	0	-	0-0	0	-	-	Alive (SD after 2 nd rel)	5.86
RMS037	meta	•	0	0	-	-	0-0	-	-	-	Alive (CR)	3.06
RMS043	VHR	•	0	0	-	-	-	-	-	-	Alive (CR)	5.99
RMS048	SR	0	-	-	-	-	-	0	-	-	Alive (CR after 1 st rel)	6.99
RMS050	HR	0	-	-	-	-	-	0	-	-	DOD (after 1 st rel)	1.91
RMS055	meta	•	-	0	-	0	-	-	-	-	DOD (PD)	1.11
RMS067	meta	•	0	0	0	-	0-0	-	-	-	Alive (CR)	4.45
RMS073	HR	•	-	-	-	-	-	•	-	-	Alive (CR after 2 nd rel)	6.65
RMS074	HR	0	0	0	-	-	0	-	-	-	DOD (PD after 1 st rel)	6.55
RMS075	meta	•	-	-	-	0	0	-	-	-	Alive (CR)	11.55
RMS080	meta	•	-	-	-	-	-	0	-	-	Alive (after 1 st rel)	5.13
RMS084	HR	•	0	-	-	-	-	-	-	-	Alive (CR)	7.97
RMS089	meta	•	0	0	-	0	-	-	-	-	DOD (relapse)	.99
RMS091	meta	•	0	0	-	-	-	-	-	-	DOD (after 1 st rel)	1.61

Supplemental table 11. Continued

RMSnr	Risk group	Dx	PB2	PB3	PB4	PB5	Follow up	1 st rel	PD	2 nd rel	Outcome	Follow up time (years)
RMS092	meta	•	0	0	-	-	0	-	-	-	DOD (PD)	2.40
RMS106	meta	•	-	0	-	-	-	-	-	-	Alive (CR)	2.71
RMS110	SR	•	0	0	0	-	-	-o-o	-	-	Alive (CR after 1 st rel)	3.58
RMS114	SR	0	-	-	-	-	-	-	-	o-o	Alive (CR after 2 nd rel)	8.87

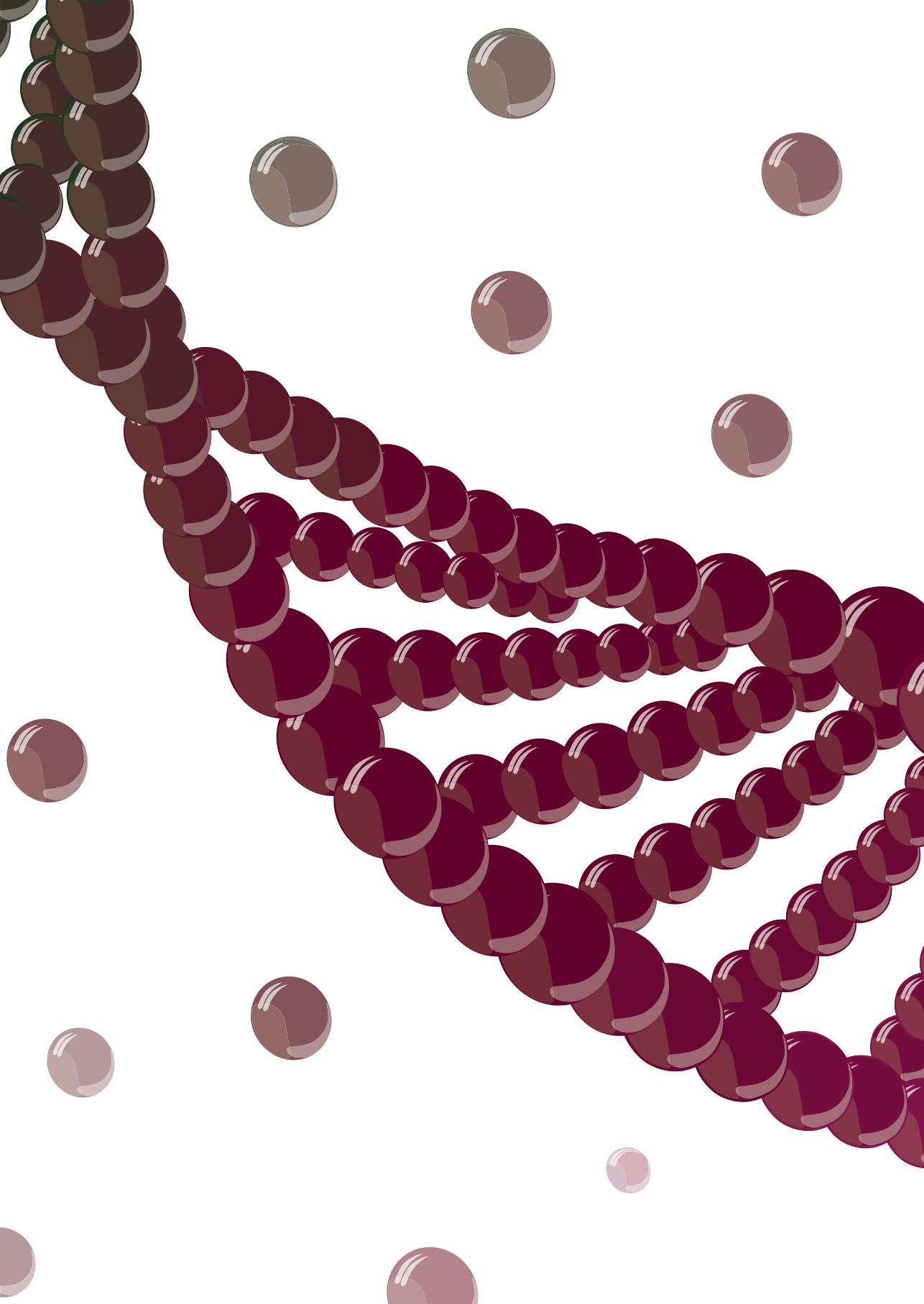
PB=peripheral blood, SR= Standard Risk, HR= High Risk, VHR=Very High Risk, meta=metastatic disease, •=positive sample, - = no sample available, Dx=diagnosis, PB2= after 1st cycle of chemotherapy, PB3= after 3rd cycle of chemotherapy, PB4= after 4th cycle of chemotherapy, PB5= at the end of primary treatment after 9th cycle of chemotherapy, 1st rel= first relapse, DOD=dead of disease, CR=complete remission, PD=progressive disease.



References for supplemental data

1. Markus MA, Reichmuth C, Atkinson MJ, Reich U, Hoffmann I, Balling R, et al. Cadherin-11 is highly expressed in rhabdomyosarcomas and during differentiation of myoblasts in vitro. *J Pathol.* 1999;187(2):164-72.





Chapter 3

Novel circulating hypermethylated RASSF1A ddPCR for liquid biopsies in patients with pediatric solid tumors

JCO Precis Oncol. 2021 Nov 17;5:PO.21.00130. doi: 10.1200/PO.21.00130.

Lieke M.J. van Zogchel^{1,2}, Nathalie S.M. Lak^{1,2}, Onno J.H.M. Verhagen³, Ahmed Tissoudali⁴, Mohammed Gussmalla Nuru², Nina U. Gelineau^{1,2}, Lily Zappeij-Kannengieter^{2,3}, Ahmad Javadi², Eline A.M. Zijtregtop^{1,5}, Johannes H.M. Merks¹, Marry van den Heuvel-Eibrink¹, Antoinette.Y.N. Schouten-van Meeteren¹, Janine Stutterheim¹, C. Ellen van der Schoot², Godelieve A.M. Tytgat¹

1. Princess Máxima Center for Pediatric Oncology, Utrecht, the Netherlands
2. Department of Experimental Immunohematology, Sanquin Research and Landsteiner Laboratory, Amsterdam University Medical Center, Amsterdam, the Netherlands
3. Department of Immunocytology, Sanquin Diagnostic Services, Amsterdam, the Netherlands.
4. Department of Immunohematology Diagnostics, Sanquin Diagnostic Services, Amsterdam, the Netherlands.
5. Department of pediatric oncology, Erasmus Medical Center– Sophia Children's Hospital, the Netherlands

Abstract

Purpose: Liquid biopsies can be used to investigate tumor-derived DNA, circulating in the cell-free DNA (cfDNA) pool in blood. We aimed to develop a droplet digital PCR (ddPCR) assay detecting hypermethylation of tumor suppressor gene RASSF1A as a simple standard test to detect various pediatric tumor types in small volume blood samples, and to evaluate this test for monitoring treatment response of high risk neuroblastoma patients.

Patients and methods: We developed a ddPCR assay to sensitively detect tumor-derived hypermethylated RASSF1A DNA in liquid biopsies. We tested this assay in plasma of 96 patients with neuroblastoma, renal tumors, rhabdomyosarcoma or Hodgkin lymphoma at diagnosis, and in cerebrospinal fluid of 4 patients with brain tumors. We evaluated presence of hypermethylated RASSF1A in plasma samples during treatment and follow-up in 47 patients with neuroblastoma treated according to high-risk protocol and correlated results to blood and bone marrow mRNA-based minimal residual disease detection and clinical outcome.

Results: The total cfDNA level was significantly higher in patients with metastatic neuroblastoma and nephroblastoma compared to healthy adult and pediatric controls. Hypermethylated RASSF1A was present in 41/42 patients with metastatic neuroblastoma and in all nephroblastoma, with a median percentage of 69% and 21% of total RASSF1A respectively. Hypermethylated RASSF1A levels decreased during therapy and recurred at relapse.

Conclusion: Our findings demonstrate the value of ddPCR-based detection of hypermethylated RASSF1A as circulating molecular tumor marker in neuroblastoma. Our preliminary investigation of RASSF1A hypermethylation detection in circulating cfDNA of other pediatric tumor entities demonstrates potential as a pan-tumor marker, but requires investigation in larger cohorts to evaluate its use and limitations.

Context summary

Key objective: Molecular testing of circulating tumor DNA (ctDNA) has the potential to improve pediatric solid tumor diagnosis and discrimination of subtypes as well as monitoring of treatment response. Our aim was to develop a RASSF1A hypermethylation ddPCR as a standard test to detect ctDNA in several pediatric tumor types using small blood volumes, and as a test to monitor treatment response of neuroblastoma patients.

Knowledge generated: We developed a sensitive and quantitative ddPCR-based assay for hypermethylated RASSF1A detection. Our findings demonstrate the value of hypermethylated RASSF1A as molecular circulating tumor marker in neuroblastoma. RASSF1A was frequently hypermethylated in plasma samples from patients with nephroblastoma, rhabdomyosarcoma and Hodgkin lymphoma.

Relevance: Our study supports the use of ctDNA to assist in the monitoring of therapy response in patients with neuroblastoma and show the potential of ctDNA in assisting in the diagnosis of other pediatric solid tumor entities

3

Introduction

Cancer remains one of the most common causes of childhood death in high-income countries.¹ Although the combination of intensive chemotherapy, surgery, radiation therapy, and immunotherapy has improved outcomes in children with solid tumors, disease still recurs in 50% of patients with neuroblastomas;^{2,3} 46% of patients with Ewing sarcomas;⁴ and approximately 30% of patients with localized rhabdomyosarcomas,⁵ osteosarcomas,⁶ and renal tumors.⁷ Response to treatment is primarily based on imaging. In patients with neuroblastoma, bone marrow (BM) histology or (immuno)cytology assesses the extent of disease.⁸ In neuroblastoma and rhabdomyosarcoma, reverse-transcriptase quantitative polymerase chain reaction (RT-qPCR) for the detection of minimal residual disease (MRD) in peripheral blood or BM is shown to be more sensitive⁹⁻¹³ and predictive of outcomes, but even patients with low or negative MRD results can suffer from recurrent disease,^{9,14} or mRNA markers can be downregulated upon epithelial-to-mesenchymal transition.¹⁵

Liquid biopsies, for example, peripheral blood, can also be a source for tumor-derived cell-free DNA (cfDNA). As the genomic view is not limited to the boundaries of a tissue biopsy, liquid biopsies better represent spatial and intratumor heterogeneity. Liquid biopsies have shown promise in assisting diagnosis and monitoring therapy response in adult oncology.¹⁶⁻¹⁸ Pediatric tumors have lower mutational burdens with few recurrent mutations¹⁹ but a variety of copy number alterations²⁰ and epigenetic changes.²¹ The tumor suppressor gene *RASSF1A* is silenced in nearly all adult cancers and associated with poor prognosis and high-risk disease.²²⁻²⁴ Promotor hypermethylation^{23,25,26} or, less frequently, a combination of hypermethylation and 3p21.3 allelic loss^{22,23,27} causes inactivation. *RASSF1A* is hypermethylated in neuroblastoma,^{22,28-35} hepatoblastoma,^{29,36} nephroblastoma,^{29,37,38} medulloblastoma and primitive neuroectodermal tumors,^{29,39} and osteosarcoma and Ewing sarcoma.^{29,40-42} These

accumulating data suggest *RASSF1A* hypermethylation to be as common in pediatric tumor entities as in adult tumor entities. *RASSF1A* hypermethylation is rare in normal tissues,²³ but present in placenta, and therefore is also suited for fetal DNA detection in maternal plasma.^{43,44} We previously investigated hypermethylated *RASSF1A* in cfDNA from patients with neuroblastoma by performing qPCR.³³ We demonstrated the promise of this marker, but observed loss of cfDNA because of bisulfite conversion, and were unable to quantify the low amounts of circulating tumor DNA (ctDNA).³³ In this study, we harnessed the sensitivity and accuracy of droplet digital PCR (ddPCR) and developed a ddPCR method with methylation-sensitive restriction enzymes (MSREs) to overcome these limitations. We furthermore investigated the feasibility of our hypermethylated *RASSF1A* ddPCR assay in detecting different pediatric tumor types in small volume patient plasma samples.

Methods

Methods on patient inclusion, sample collection, cfDNA isolation, and RT-qPCR for mRNA markers⁴⁵ and single nucleotide polymorphism array can be found in the Data Supplement.

Hypermethylated *RASSF1A* ddPCR

To discriminate between methylated and unmethylated *RASSF1A*, every sample was subjected to two different ddPCR reactions (Fig 1): one with MSRE and the other without; all remaining conditions were identical. ACTB-1 primer-probe set was added to control for cfDNA input, and this amplicon is unaffected by the MSRE. ACTB-2 primer-probe set was added to control for MSRE performance since this amplicon is digested by the enzymes. *RASSF1A*, ACTB-1, and ACTB-2 primer and probe sets are listed in the Data Supplement. Primer and probe sequences for *RASSF1A* and ACTB-2 have been described before by O'Brien et al.⁴⁴ A detailed protocol can be found in the Data Supplement. To avoid false positivity, a threshold was based on healthy donors for both the single- and double-digest reactions (see the Results) and a minimum of four positive droplets per duplicate. If a sample was scored positive, the percentage of hypermethylated *RASSF1A* was calculated as $(RASSF1A/ACTB^{with\ MSRE}) / (RASSF1A/ACTB^{without\ MSRE}) \times 100\%$. *RASSF1A* ddPCR performance was compared with that of *RASSF1A* qPCR by testing 16 rhabdomyosarcoma and renal tumor cfDNA samples. *RASSF1A* qPCR was performed as described previously.³³

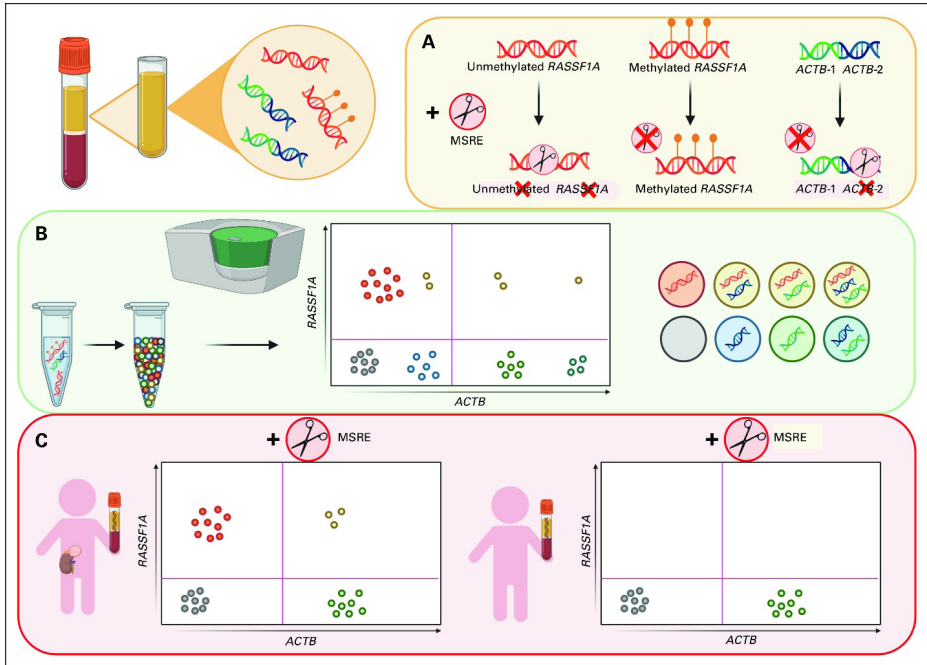


Figure 1. Concept of quantifying methylated *RASSF1A* using MSRE and ddPCR. **(A)** An MSRE incubation of a cfDNA sample results in the digestion of unmethylated *RASSF1A*, whereas methylated *RASSF1A* remains intact. Two amplicons of *ACTB* are added, and *ACTB-1* is unaffected by the MSRE, whereas *ACTB-2* is digested by the MSRE, as a control for MSRE performance. Every sample is subjected to two different ddPCR reactions, **(B)** one without the MSRE and **(C)** the other with the MSRE. *ACTB-2* primers and probe are added in a lower concentration, resulting in a lower amplitude to discriminate between the *ACTB-1* and *ACTB-2* clusters. **(C)** Only in cfDNA from patients with circulating tumor DNA present, *RASSF1A* will be detected after digestion with the MSRE, as the absence of *RASSF1A* methylation will result in *RASSF1A* digestion, preventing the detection of this unmethylated *RASSF1A* allele by ddPCR. cfDNA, cell-free DNA; ddPCR, droplet digital polymerase chain reaction; MSRE, methylation-sensitive restriction enzymes.

Statistical Analysis

As cfDNA and ctDNA levels were not normally distributed, they are presented as median (interquartile range) and statistical significance was determined by the Kruskal–Wallis test. Fisher's exact test was used to analyze the correlation between ctDNA and/or mRNA positivity and outcomes. Correlation analysis between cfDNA, ctDNA, and mRNA levels was performed using Spearman's test. Events were defined as relapse, progressive,⁸ or refractory disease, when the progression was not according to the International Neuroblastoma Response Criteria but resulted in change of treatment protocol. Receiver operating characteristic analysis was used to identify a cutoff for hypermethylated *RASSF1A* copies/mL. This cutoff was used to

identify two subgroups for the comparison of event-free survival using Kaplan-Meier method. All statistical analyses were performed using GraphPad Prism 8 (GraphPad Software, La Jolla, CA) software. Results were considered significant if $P \leq .05$.

Results

Limit of Detection and Limit of Blank: Single and Double MSRE Digest

The dilution series of neuroblastoma cell line IMR32 DNA (100% hypermethylated *RASSF1A*) in DNA from blood from a healthy male and in H₂O showed a good linearity (a detailed description is given in the Data Supplement). The limit of detection, however, is defined by the level of positivity in the control samples, also called the limit of blank. For the limit of blank, we evaluated *RASSF1A* positivity in 22 samples stored at room temperature from adult male controls from which plasma was separated after 24, 48, 72, or 144 hours and 18 pediatric control samples (plasma separation within 24 hours). To test the efficacy of single-digest MSRE (BstUI-only), both hypermethylated *RASSF1A* and *ACTB* were measured in these control samples after digestion. We observed a correlation between the number of hypermethylated *RASSF1A* copies and *ACTB* copies in the adult controls (Spearman $r_s = 0.91$, $P < .0001$) and to a lesser extent in the pediatric controls (Spearman $r_s = 0.69$, $P = .002$), with a maximum of 0.039 *RASSF1A* copies per *ACTB* copies/mL plasma (Data Supplement). Although we cannot formally exclude that hypermethylated *RASSF1A* is derived from necrotic cells during storage of the samples, these data suggest that, although the ACTB-2 cluster was not clearly present, BstUI-only was not able to digest all cfDNA in our samples. A threshold on the basis of this ratio would greatly reduce the sensitivity of the assay and result in many inconclusive samples, and therefore, we investigated the use of two MSREs in a double-digest reaction. Double digestion by MSREs HhaI and Bsh1236I instead of BstUI in 43 adult and 18 pediatric control samples resulted in a more efficient digestion of *RASSF1A*. The number of hypermethylated *RASSF1A* copies was no longer dependent on the cfDNA concentration (Data Supplement). A prolonged time to plasma separation did not result in a significant increase in *RASSF1A* copies/mL, neither for the single-digest nor double-digest method (Data Supplement). On the basis of mean + 3 × standard deviation in hypermethylated *RASSF1A* copies/mL plasma of these controls, we set the threshold on 14 copies/mL plasma. As a large number of patient samples were already tested using the single-digest method, all patient samples with ≥ 4 positive droplets and a ratio ≤ 0.039 *RASSF1A*/*ACTB* copies/ μ L were also tested using the double-digest method and scored according to the new double-digest threshold. To compare *RASSF1A* ddPCR performance with that

of *RASSF1A* qPCR,³³ we tested 16 diagnostic rhabdomyosarcoma and renal tumor plasma samples using both techniques. All 11 samples that were positive by qPCR, of which three were positive-not-quantifiable, tested positive by ddPCR, and 1 in 5 qPCR-negative samples were tested positive by ddPCR.

Total cfDNA Is Increased in Patients With Neuroblastoma and Nephroblastoma

We investigated plasma samples from patients with high-risk neuroblastoma (47) at diagnosis and during therapy and diagnostic plasma samples from pediatric patients with non-high-risk neuroblastoma (17), rhabdomyosarcoma (14), renal tumor (13), Hodgkin lymphoma (five), and cerebrospinal fluid (CSF) from CNS tumors (four). For clinical details, see the Data Supplement. We isolated cfDNA from 200 to 1,000 μ L plasma or CSF and compared diagnostic plasma cfDNA levels (*ACTB*) with 24 healthy adult and 18 healthy pediatric plasma control samples, processed within 24 hours (Fig 2A, Table 1). Total cfDNA levels were significantly higher in patients with metastatic neuroblastoma and nephroblastoma compared with adult and pediatric controls ($P < .0001$, $P < .0001$, $P < .0001$, and $P = .0117$, respectively). Patients with localized neuroblastoma had significantly lower cfDNA levels compared with metastatic neuroblastoma ($P = .0004$) and were not significantly different from the adult and pediatric controls ($P = .4$ and $P > .99$, respectively). There was a trend to higher cfDNA levels in patients with rhabdomyosarcoma and Hodgkin lymphoma, which was only significant compared with adult controls ($P = .015$ and $P = .013$, respectively; Table 1).

Hypermethylated RASSF1A Is Detected in Diagnostic Plasma of Patients With Different Tumor Entities

At diagnosis, *RASSF1A* hypermethylation was detected in 41 of 42 patients with metastatic neuroblastoma (Fig 2B and Table 1). The one negative patient was stage MS and upstaged to stage M because of two new bone lesions. Hypermethylated *RASSF1A* was detected in all diagnostic plasma samples from patients with nephroblastoma and absent in plasma from two patients with Cystic Partially Differentiated Nephroblastoma and bilateral differentiated nephroblastomatosis, providing the possibility that only malignant tumors are detected by this marker. Eight of 14 plasma samples from patients with rhabdomyosarcoma were positive, as were 4 of 5 Hodgkin lymphoma plasma samples. Only one CSF sample from a patient with medulloblastoma was positive, and this was the sample with the highest cfDNA concentration.

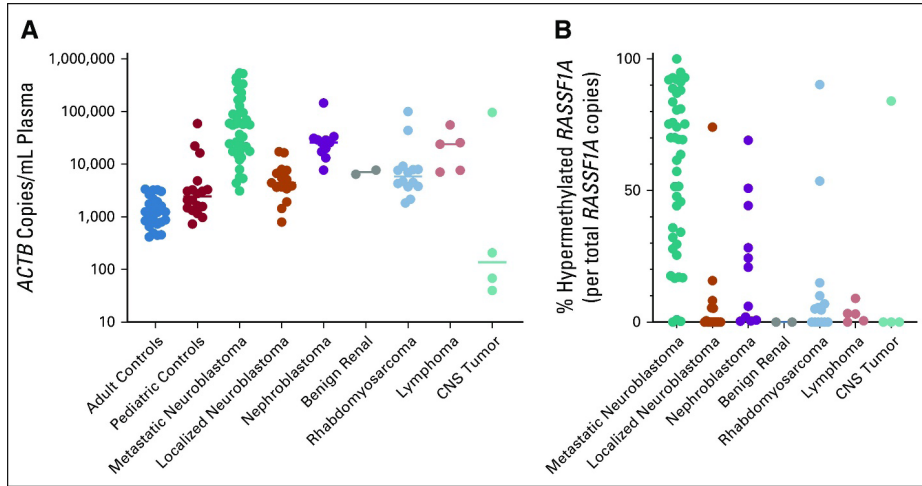


Figure 2. Amount of cfDNA and circulating hypermethylated *RASSF1A*. (A) Level of cfDNA at diagnosis in patients with various pediatric solid tumor entities, compared with healthy adult and pediatric controls. cfDNA was quantified by β -actin (*ACTB*), in copies/mL plasma or CSF (cerebrospinal fluid). Lines indicate the median. (B) The percentage of hypermethylated *RASSF1A* of total *RASSF1A* copies at diagnosis in patients with metastatic neuroblastoma ($n = 42$), localized neuroblastoma ($n = 15$), nephroblastoma ($n = 11$), rhabdomyosarcoma ($n = 14$), lymphoma ($n = 5$), and CNS tumors ($n = 4$). Adult and pediatric controls were used to establish a threshold for positivity. In 41 of 42 patients with metastatic neuroblastoma and 6 of 15 patients with localized neuroblastoma, hypermethylated *RASSF1A* was detected. In all 11 patients with nephroblastoma, 8 of 14 patients with rhabdomyosarcoma, 4 of 5 patients with lymphoma, and 1 of 4 patients with CNS tumor, hypermethylated *RASSF1A* was detected. Two plasma samples of patients with benign renal tumors (a Cystic Partially Differentiated Nephroblastoma and a bilateral differentiated nephroblastomatosis) were negative for hypermethylated *RASSF1A*. cfDNA, cell-free DNA; CFS, cerebrospinal fluid.

Table 1. Levels of cfDNA and Circulating Hypermethylated *RASSF1A* in Various Pediatric Solid Tumor Entities and Adult and Pediatric Controls.

Tumor	Total cfDNA (copies/mL) ^a	Hypermethylated <i>RASSF1A</i> -Positive Samples (No.)	Hypermethylated <i>RASSF1A</i> of Total <i>RASSF1A</i> ^a (%)	Hypermethylated <i>RASSF1A</i> (copies/mL) ^a
Metastatic neuroblastoma	56,996 (17,694-138,639) ^b	41 of 42	69.4 (34.1-83.7)	19,281 (5,170-55,196)
Localized neuroblastoma	4,431 (3,441-7,669)	6 of 15	6.8 (5.4-13.9)	440 (273-546)
Nephroblastoma	26,023 (17,390-31,177) ^b	11 of 11	20.9 (1.4-36.3)	2,250 (421-6,946)
Benign renal	6,462 and 7,731	0 of 2		
Rhabdomyosarcoma	5,893 (3,791-8,319)	8 of 14	8.5 (5.4-24.6)	263 (172-1,905)
Lymphoma	23,949 (7,406-40,873)	4 of 5	3.2 (2.5-4.7)	926 (220-1,638)
Medulloblastoma	138 (47-72,711)	1 of 4	84.1	89,336
Adult controls	1,232 (748-2,143)			
Pediatric controls	2,445 (1,446-3,694)			

Abbreviations: cfDNA, cell-free DNA; IQR, interquartile range.

^aMedian and IQR are given.

^bTotal cfDNA is significantly increased in patients with metastatic neuroblastoma compared with adult and pediatric controls, with $P < .0001$ and $P < .0001$, respectively, and in patients with nephroblastoma.

Cell-Free Detection of Hypermethylated RASSF1A at Diagnosis and During Therapy

Plasma was available from 47 patients with high-risk neuroblastoma during the course of treatment. Clinical details, time of sampling, and ctDNA and mRNA results per sample can be found in the Data Supplement. Single nucleotide polymorphism array data confirmed 3p loss in 9 of 32 tumor samples, and in all nine patients, hypermethylated *RASSF1A* was detected in plasma, indicating that *RASSF1A* hypermethylation can still be identified in neuroblastoma with only one *RASSF1A* allele. At diagnosis, the absolute and relative levels of hypermethylated RASSF1A were significantly higher in the group of patients who will experience an event, although with a substantial overlap (median 37,243 copies/mL [interquartile range: 6,749-174,727] v 8,221 copies/mL [3,951-18,339], $P = .012$, 70.2% [45.0-91.7] v 56.5% [17.1-74.5], $P = .030$, respectively; Figs 3A and 3B). Receiver operating characteristic analysis revealed a cutoff of 27,681 hypermethylated *RASSF1A* copies/mL with a sensitivity of 64% and a specificity of 89% (Data Supplement) that identifies a group that has a significantly poorer event-free survival (Data Supplement, log-rank $P = .0007$). As the majority of the total cfDNA was tumor-derived, this led to a significant increase in cfDNA at diagnosis for patients who will experience an event (59,714 copies/mL [27,547-246,149] v 21,450 copies/mL [16,107-63,446], $P = .023$; Fig 3C). For other time points, there was no significant difference in total cfDNA levels between the patients with and without an event. At relapse, ctDNA levels were comparable with levels at diagnosis. Hypermethylated *RASSF1A* positivity did not correlate with an event for any of the time points (Fig 3D).

Comparison of ctDNA With the Detection of mRNA in BM and Blood

We previously showed that qPCR-based *RASSF1A* hypermethylation correlated with mRNA marker panel positivity or negativity in BM cells in patients when tumor burden was high or no tumor was detected.³³ Marker discrepancies indicated either low-level BM infiltration (ctDNA⁻&mRNA⁺ panel⁺) or primary tumor or soft tissue lesions without BM involvement (ctDNA⁺&mRNA⁻ panel⁻). To confirm these results in the current cohort, we tested cell fractions of corresponding blood (227) and BM (224) samples for mRNA markers⁴⁵ and compared them with hypermethylated *RASSF1A* in plasma by ddPCR. We again observe a strong correlation when the tumor load is to be expected high (at time of diagnosis or event) or absent (Fig 4), but see both ctDNA⁻&mRNA⁺ and vice versa when the tumor load is expected to be lower, for example, during therapy. In 227 matched blood samples, ctDNA was concordant with blood mRNA in 73% (75 ctDNA⁺&mRNA⁺ and 91 ctDNA⁻&mRNA⁻), 47 samples were ctDNA-positive only, and 14 samples mRNA-positive only. Spearman correlation of those 75 ctDNA⁺&mRNA⁺ indicated an association between ctDNA and mRNA results

($r_s = 0.65$, $P > .001$). In 224 matched BM mRNA and ctDNA blood samples, paired positive or negative results were found in 65% (103 and 43 samples, respectively). In contrast to the blood samples, BM mRNA-only identified more positive samples (62) compared with ctDNA-only (16). Twenty-seven of those 62 samples were taken during induction chemotherapy. In 103 ctDNA⁺&mRNA⁺ samples, Spearman correlation indicated a moderate association between ctDNA and mRNA results ($r_s = 0.49$, $P > .001$).

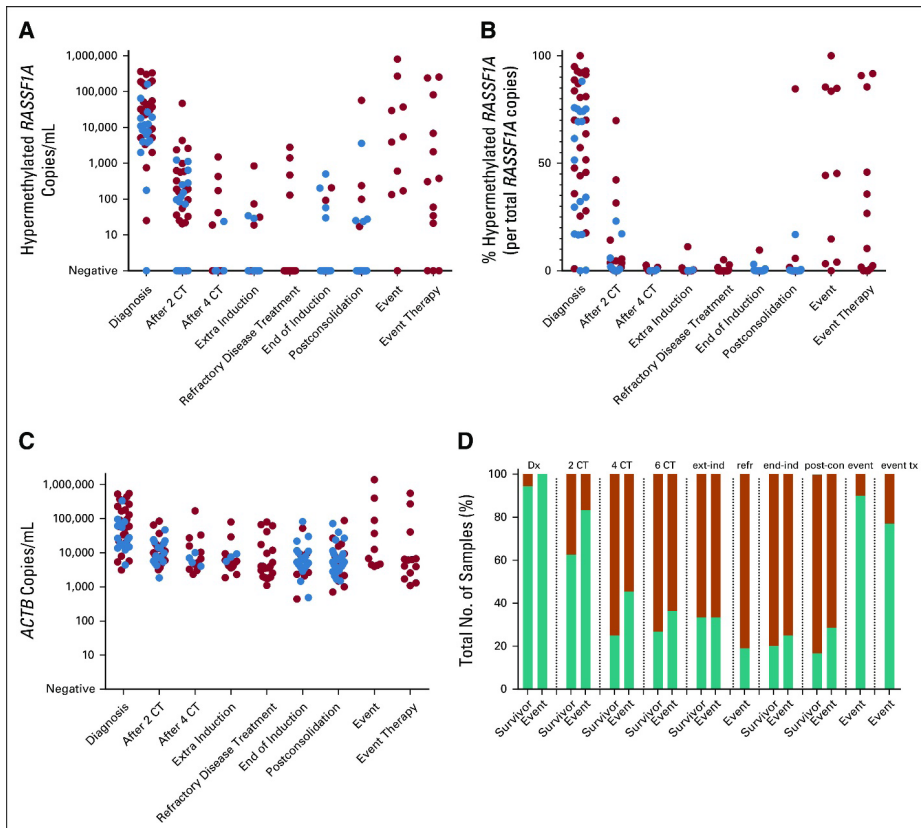


Figure 3. Positivity and levels of circulating hypermethylated *RASSF1A* and total cfDNA during therapy in patients with high-risk neuroblastoma. Red circles indicate samples from a patient who will suffer from an event, and blue circles indicate samples from patients who remain in complete remission (survivor). (A) Amount of hypermethylated *RASSF1A* in copies/mL plasma during therapy. (B) Relative levels of hypermethylated *RASSF1A* per total *RASSF1A* copies during therapy. (C) Levels of cfDNA, measured by β -actin (*ACTB*), in copies/mL plasma during therapy. (D) Fraction of total number of samples tested that were positive for circulating hypermethylated *RASSF1A*. Green bar represents positive samples, and orange bar represents negative samples. cfDNA, cell-free DNA; CT, cycles of chemotherapy; Dx, diagnosis; end-ind, end of induction; event tx, event therapy; ext-ind, extra induction therapy (not for refractory disease); post-con, postconsolidation; refr, refractory disease treatment.

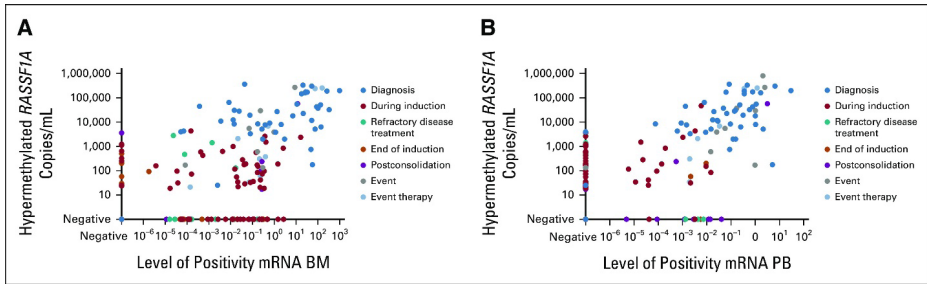


Figure 4. (A) Association between mRNA in BM samples and circulating hypermethylated *RASSF1A* and (B) association between mRNA in blood samples and circulating hypermethylated *RASSF1A*. BM, bone marrow; PB, peripheral blood.

Combined ctDNA and mRNA Detection Correlates With Outcomes

We next studied the kinetics of circulating hypermethylated *RASSF1A* and the mRNA markers from the corresponding BM and blood samples. Representative examples from five patients are depicted in Figures 5A–5E, and the combined outcome of circulating hypermethylated *RASSF1A* and BM mRNA for different time points is shown in Figure 5F. We showed that during therapy, the presence of hypermethylated *RASSF1A* in plasma was not associated with poorer prognosis at any of the time points in this patient cohort (Fig 3D). However, when circulating hypermethylated *RASSF1A* results were combined with BM mRNA, positivity with both techniques after two cycles of chemotherapy was associated with unfavorable clinical outcomes of these patients ($P = .046$; Fig 5F), with the sensitivity and specificity of the ctDNA⁺&mRNA⁺ profile being 74% and 63%, respectively. BM mRNA positivity alone at this time point was not predictive of the outcome in this cohort ($P = .12$). The trend that ctDNA⁺&mRNA⁺ positivity at other time points also correlates with an event was not significant in this small cohort. Remarkably, BM mRNA positivity alone during post consolidation was associated with unfavorable outcomes ($P = .077$). In summary, the level of hypermethylated *RASSF1A* at diagnosis was correlated with unfavorable outcomes. Moreover, the combination of ctDNA with BM mRNA improved the predictive value after two cycles of chemotherapy in this cohort.

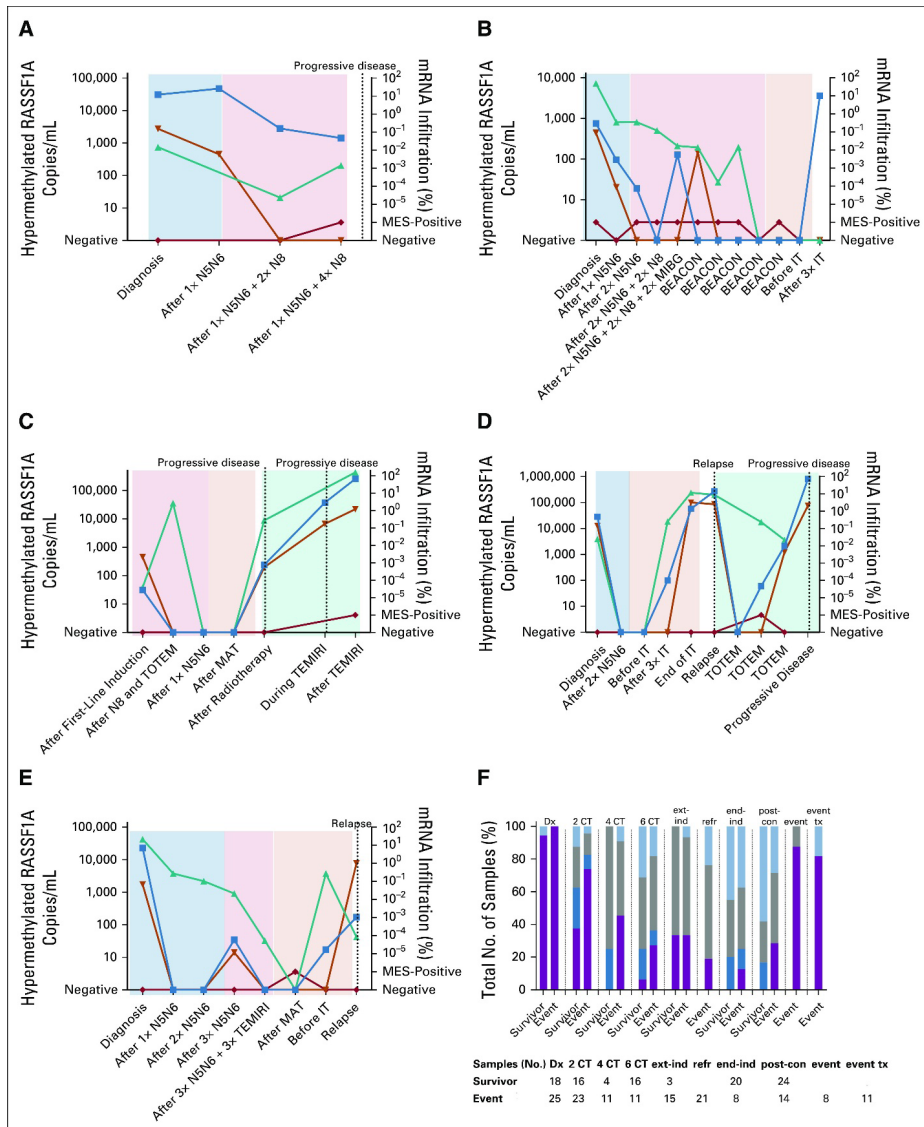


Figure 5. (A-E) For patients with refractory, relapse, or progressive disease, all sequential samples, if available, were analyzed for hypermethylated RASSF1A (blue squares; N2063, N2071, N2099, N2101, and N2123, respectively). Corresponding blood (orange triangles) and BM (green triangles for adrenergic markers and red diamonds for MES markers) samples were tested for mRNA. Colored blocks indicate the treatment: light blue, induction therapy; light red, extra induction therapy; light orange, post consolidation therapy; light green, relapse or progressive disease treatment. **(F)** Fraction of total number of tested samples, which were positive for circulating hypermethylated RASSF1A and/or BM mRNA, of patients who will suffer an event compared with those who remain in complete remission (survivor). Purple bar represents hypermethylated RASSF1A⁺ and mRNA panel⁺ samples, dark blue bar represents hypermethylated RASSF1A ctDNA⁺ and mRNA panel⁻ samples, gray bar represents hypermethylated RASSF1A⁻ and mRNA panel⁺ samples, and light blue bar represents hypermethylated RASSF1A ctDNA⁻ and mRNA panel⁻ samples.

mRNA panel samples. BEACON, TEMIRI, and TOTEM are treatment for refractory or relapsed disease. BEACON, BEACON-Neuroblastoma Trial: bevacizumab, temozolomide \pm irinotecan; BM, bone marrow; CT, cycles of chemotherapy; ctDNA; circulating tumor DNA; Dx, diagnosis; end-ind, end of induction; event tx, event therapy; ext-ind, extra induction therapy (not for refractory disease); IT, immunotherapy; MAT, myeloablative therapy; MES, mesenchymal; MIBG, iodine-131-meta-iodobenzylguanidine; N5, N6, and N8; courses of induction chemotherapy; post-con, postconsolidation; refr, refractory disease treatment; TEMIRI, temozolomide and irinotecan; TOTEM, temozolomide and topotecan.

Discussion

Molecular testing of cfDNA has the potential to improve pediatric solid tumor diagnosis, discrimination of subtypes, and MRD monitoring. Our aim was to complete a first step in this evolution of diagnostic modalities by evaluating our *RASSF1A* hypermethylation ddPCR as a standard test to detect ctDNA in several pediatric tumor types using small blood volumes and as a test to monitor treatment response of patients with neuroblastoma.

We previously described qPCR-based detection of circulating hypermethylated *RASSF1A* in patients with neuroblastoma.³³ In our previous study, the majority of positive samples could not be quantified reliably by qPCR, whereas ddPCR technology is adept for precise quantification of low abundant targets.⁴⁶ Furthermore, like in many other widely used methods to analyze DNA methylation, cfDNA samples in the qPCR study were bisulfite converted, which is known to degrade the majority of DNA.⁴⁷ As cfDNA is often present in low quantities, we investigated the use of an MSRE, previously described by Chan et al and O'Brien et al, as an alternative to bisulfite conversion.^{43,44} We noticed higher hypermethylated *RASSF1A* levels in control samples with high total cfDNA levels, also reported by O'Brien et al.⁴⁴ We successfully introduced a combination of two MSREs, which resulted in better digestion of unmethylated *RASSF1A*. cfDNA may not always be present as double-stranded DNA, but can also appear as (partially) single-stranded DNA fragments.^{48,49} Although the enzyme BstUI performed well in genomic DNA experiments, it is reported to be less active on single-stranded DNA.⁵⁰ The addition of HhaI overcomes this, as this enzyme is capable of digesting single-stranded DNA. The use of two different MSRE, and thus an increase in digestion sites, may result in digestion of DNA that is only partially methylated,⁵¹ potentially underestimating present hypermethylated *RASSF1A*. However, as BstUI-only was clearly unable to digest all unmethylated *RASSF1A*, we proceeded with the use of two MSREs. The frequency of low-level positive results detected in healthy adult and pediatric controls defined the limit of detection. Since lack of remnants precluded the retesting of our qPCR study samples,³³ we showed in 16 rhabdomyosarcoma and renal tumor samples the slight superiority

of the ddPCR method. In summary, the ddPCR is our preferred method to use for hypermethylated *RASSF1A* detection in plasma samples because the MSRE-ddPCR can reliably quantify ctDNA and saves time and sample.

We corroborate the potential of hypermethylated *RASSF1A* as a ctDNA marker for neuroblastoma, for monitoring treatment response and early relapse detection. This study confirms that cell-free hypermethylated *RASSF1A* correlates with mRNA marker panel positivity in BM and blood in patients at the opposite ends of the disease spectrum, when tumor burden was high or no tumor was detected.^{32,33} The difference in kinetics of ctDNA and BM mRNA is illustrated by the prolonged presence of BM mRNA during induction therapy, whereas ctDNA rapidly declines during therapy, but is present again at relapse. The results of this study further support the finding, in an independent cohort, that both ctDNA and mRNA complement each other for the detection of MRD, with the combination showing a correlation with the outcome after two cycles of chemotherapy. Although the detection of ctDNA was shown to be very promising for future MRD studies in neuroblastoma, no definitive conclusions can be made as samples for this study were not prospectively collected, resulting in missing samples. Future research should be undertaken to investigate whether hypermethylated *RASSF1A* can be used as a marker during follow-up for early relapse detection and whether a cutoff can be used to predict event-free survival. As inactivation of *RASSF1A*, for example, by hypermethylation, is advantageous for many tumor entities, in melanoma, demethylation agents lead to apoptosis and cell death⁵²; we think that this marker is not lost in time. We will test this hypothesis in prospective collaborative studies on the use of ctDNA in the new SIOOPEN HR-2 (NCT04221035) patient cohort, which are being initiated within the SIOOPEN liquid biopsy group.

Comparison of the total cfDNA levels in pediatric solid tumors with those of other studies confirms higher levels in patients with neuroblastoma and nephroblastoma tumors.⁵³⁻⁵⁷ Consistent with literature, a high tumor-derived fraction of total cfDNA was found in patients with neuroblastoma and nephroblastoma, demonstrating the potential of liquid biopsies in these tumor entities.^{54,56,58} Plasma samples from patients with other tumor entities in this study were less conclusive, which may indicate differences in the extent that different tumor types shed tumor DNA into circulation, a lower frequency of *RASSF1A* hypermethylation in other tumor entities,²⁹ or may just be artifacts of low sample numbers in the preliminary sample collection evaluated.

In this study, we developed a sensitive and quantitative ddPCR-based assay for hypermethylated *RASSF1A* detection and determined threshold values for positive results. Our findings demonstrate the value of hypermethylated *RASSF1A* as a molecular circulating tumor marker in neuroblastoma. Furthermore, our preliminary investigation of *RASSF1A* hypermethylation detection in circulating cfDNA demonstrates potential as a pan-tumor marker, but requires further investigation to evaluate its use and limitations.

Support

Supported by Liquidhope, a TranScan-2 project by Koningin Wilhelmina Fund, KWF Kankerbestrijding TRANSCAN 8352/TRS-2018-00000715 (L.M.J.v.Z. and N.U.G.), Foundation AMeesing Mees, and Foundation Koppie Au.

References

1. Siegel RL, Miller KD, Jemal A: Cancer statistics, 2019. *CA Cancer J Clin* 69:7-34, 2019
2. Park JR, Kreissman SG, London WB, et al.: Effect of tandem autologous stem cell transplant vs single transplant on event-free survival in patients with high-risk neuroblastoma. *JAMA* 322:746, 2019
3. Van Wezel EM, Zwijnenburg D, Zappeij-Kannegieter L, et al.: Whole-genome sequencing identifies patient-specific DNA minimal residual disease markers in neuroblastoma. *J Mol Diagn* 17:43-52, 2015
4. Stahl M, Ranft A, Paulussen M, et al.: Risk of recurrence and survival after relapse in patients with Ewing sarcoma. *Pediatr Blood Cancer* 57:549-553, 2011
5. Malempati S, Hawkins DS: Rhabdomyosarcoma: review of the Children's Oncology Group (COG) Soft-Tissue Sarcoma Committee experience and rationale for current COG studies. *Pediatr Blood Cancer* 59:5-10, 2012
6. Whelan JS, Davis LE: Osteosarcoma, chondrosarcoma, and chordoma. *J Clin Oncol* 36:188-193, 2018
7. Brok J, Lopez-Yurda M, Tinteren HV, et al.: Relapse of Wilms' tumour and detection methods: A retrospective analysis of the 2001 Renal Tumour Study Group–International Society of Paediatric Oncology Wilms' tumour protocol database. *Lancet Oncol* 19:1072-1081, 2018
8. Park JR, Bagatell R, Cohn SL, et al.: Revisions to the International Neuroblastoma Response Criteria: A consensus statement from the National Cancer Institute clinical trials planning meeting. *J Clin Oncol* 35:2580-2587, 2017
9. Viprey VF, Gregory WM, Corrias MV, et al.: Neuroblastoma mRNAs predict outcome in children with stage 4 neuroblastoma: A European HR-NBL1/SIOPEN study. *J Clin Oncol* 32:1074-1083, 2014
10. Cheung NK, Ostrovnya I, Kuk D, et al.: Bone marrow minimal residual disease was an early response marker and a consistent independent predictor of survival after anti-GD2 immunotherapy. *J Clin Oncol* 33:755-763, 2015
11. Kreissman SG, Seeger RC, Matthay KK, et al.: Purged versus non-purged peripheral blood stem-cell transplantation for high-risk neuroblastoma (COG A3973): A randomised phase 3 trial. *Lancet Oncol* 14:999-1008, 2013
12. Burchill SA, Beiske K, Shimada H, et al.: Recommendations for the standardization of bone marrow disease assessment and reporting in children with neuroblastoma on behalf of the International Neuroblastoma Response Criteria Bone Marrow Working Group. *Cancer* 123:1095-1105, 2017
13. Lak NS, Voormanns TL, Zappeij-Kannegieter L, et al.: Improving risk stratification for pediatric patients with rhabdomyosarcoma by molecular detection of disseminated disease. *Clin Cancer Res* 10.1158/1078-0432.CCR-21-1083 [epub ahead of print on July 20, 2021]
14. Stutterheim J, Zappeij-Kannegieter L, Versteeg R, et al.: The prognostic value of fast molecular response of marrow disease in patients aged over 1 year with stage 4 neuroblastoma. *Eur J Cancer* 47:1193-1202, 2011
15. van Wezel EM, van Zogchel LM, van Wijk J, et al.: Mesenchymal neuroblastoma cells are undetected by current mRNA marker panels: The development of a specific neuroblastoma mesenchymal minimal residual disease panel. *JCO Precis Oncol* 3:1-11, 2019
16. Wan JCM, Massie C, Garcia-Corbacho J, et al.: Liquid biopsies come of age: Towards implementation of circulating tumour DNA. *Nat Rev Cancer* 17:223-238, 2017
17. Siravegna G, Marsoni S, Siena S, et al.: Integrating liquid biopsies into the management of cancer. *Nat Rev Clin Oncol* 14:531-548, 2017

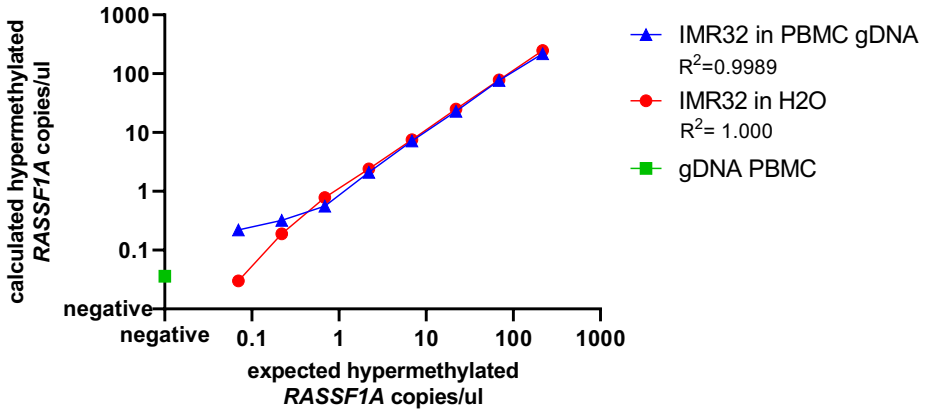
18. Rolfo C, Cardona AF, Cristofanilli M, et al.: Challenges and opportunities of cfDNA analysis implementation in clinical practice: Perspective of the International Society of Liquid Biopsy (ISLB). *Crit Rev Oncol Hematol* 151:102978, 2020
19. Lawrence MS, Stojanov P, Polak P, et al.: Mutational heterogeneity in cancer and the search for new cancer-associated genes. *Nature* 499:214-218, 2013
20. Klega K, Imamovic-Tuco A, Ha G, et al.: Detection of somatic structural variants enables quantification and characterization of circulating tumor DNA in children with solid tumors. *JCO Precis Oncol* 10.1200/PO.17.00285
21. Lawlor ER, Thiele CJ: Epigenetic changes in pediatric solid tumors: Promising new targets. *Clin Cancer Res* 18:2768-2779, 2012
22. Hesson LB, Cooper WN, Latif F: The role of RASSF1A methylation in cancer. *Dis Markers* 23:73-87, 2007
23. Donninger H, Vos MD, Clark GJ: The RASSF1A tumor suppressor. *J Cell Sci* 120:3163-3172, 2007
24. Grawenda AM, O'Neill E: Clinical utility of RASSF1A methylation in human malignancies. *Br J Cancer* 113:372-381, 2015
25. Dubois F, Bergot E, Zalcmán G, et al.: RASSF1A, puppeteer of cellular homeostasis, fights tumorigenesis, and metastasis—An updated review. *Cell Death Dis* 10:928, 2019
26. Malpeli G, Innamorati G, Decimo I, et al.: Methylation dynamics of RASSF1A and its impact on cancer. *Cancers (Basel)* 11:959, 2019
27. Hogg RP, Honorio S, Martínez A, et al.: Frequent 3p allele loss and epigenetic inactivation of the RASSF1A tumour suppressor gene from region 3p21.3 in head and neck squamous cell carcinoma. *Eur J Cancer* 38:1585-1592, 2002
28. Abe M, Ohira M, Kaneda A, et al.: CpG island methylator phenotype is a strong determinant of poor prognosis in neuroblastomas. *Cancer Res* 65:828-834, 2005
29. Harada K, Toyooka S, Maitra A, et al.: Aberrant promoter methylation and silencing of the RASSF1A gene in pediatric tumors and cell lines. *Oncogene* 21:4345-4349, 2002
30. Hoebeeck J, Michels E, Pattyn F, et al.: Aberrant methylation of candidate tumor suppressor genes in neuroblastoma. *Cancer Lett* 273:336-346, 2009
31. Misawa a, Tanaka S, Yagyu S, et al.: RASSF1A hypermethylation in pretreatment serum DNA of neuroblastoma patients: A prognostic marker. *Br J Cancer* 100:399-404, 2009
32. Stutterheim J, Ichou FA, Den Ouden E, et al.: Methylated RASSF1a is the first specific DNA marker for minimal residual disease testing in neuroblastoma. *Clin Cancer Res* 18:808-814, 2012
33. Van Zogchel LMJ, Van Wezel EM, Van Wijk J, et al.: Hypermethylated RASSF1A as circulating tumor DNA marker for disease monitoring in neuroblastoma. *JCO Precis Oncol* 4:291-306, 2020
34. Wong IHN, Chan J, Wong J, et al.: Ubiquitous aberrant RASSF1A promoter methylation in childhood neoplasia. *Clin Cancer Res* 10:994-1002, 2004
35. Kiss NB, Kogner P, Johnsen JI, et al.: Quantitative global and gene-specific promoter methylation in relation to biological properties of neuroblastomas. *BMC Med Genet* 13:1-12, 2012
36. Honda S, Miyagi H, Suzuki H, et al.: RASSF1A methylation indicates a poor prognosis in hepatoblastoma patients. *Pediatr Surg Int* 29:1147-1152, 2013
37. Wagner KJ, Cooper WN, Grundy RG, et al.: Frequent RASSF1A tumour suppressor gene promoter methylation in Wilms' tumour and colorectal cancer. *Oncogene* 21:7277-7282, 2002
38. Ehrlich M, Jiang G, Fiala E, et al.: Hypomethylation and hypermethylation of DNA in Wilms tumors. *Oncogene* 21:6694-6702, 2002

39. Mühlisch J, Schwering A, Grotzer M, et al.: Epigenetic repression of RASSF1A but not CASP8 in supratentorial PNET (sPNET) and atypical teratoid/rhabdoid tumors (AT/RT) of childhood. *Oncogene* 25:1111-1117, 2006
40. Lim S, Yang MH, Park JH, et al.: Inactivation of the RASSF1A in osteosarcoma. *Oncol Rep* 10:897-901, 2003
41. Wang WG, Chen SJ, He JS, et al.: The tumor suppressive role of RASSF1A in osteosarcoma through the Wnt signaling pathway. *Tumour Biol* 37:8869-8877, 2016
42. Avigad S, Shukla S, Naumov I, et al.: Aberrant methylation and reduced expression of RASSF1A in Ewing sarcoma. *Pediatr Blood Cancer* 53:1023-1028, 2009
43. Chan KC, Ding C, Gerovassili A, et al.: Hypermethylated RASSF1A in maternal plasma: A universal fetal DNA marker that improves the reliability of noninvasive prenatal diagnosis. *Clin Chem* 52:2211-2218, 2006
44. O'Brien H, Hyland C, Schoeman E, et al.: Non-invasive prenatal testing (NIPT) for fetal Kell, Duffy and Rh blood group antigen prediction in alloimmunised pregnant women: Power of droplet digital PCR. *Br J Haematol* 189:e90-e94, 2021
45. van Zogchel LM, Zappeij-Kannegieter L, Javadi A, et al.: Specific and sensitive detection of neuroblastoma mRNA markers by multiplex RT-qPCR. *Cancers (Basel)* 13:150, 2021
46. Taylor SC, Laperriere G, Germain H: Droplet digital PCR versus qPCR for gene expression analysis with low abundant targets: From variable nonsense to publication quality data. *Scientific Rep* 7:1-8, 2017
47. Grunau C, Clark S, Rosenthal A: Bisulfite genomic sequencing: Systematic investigation of critical experimental parameters. *Nucleic Acids Res* 29:e65, 2001
48. Sanchez C, Snyder MW, Tanos R, et al.: New insights into structural features and optimal detection of circulating tumor DNA determined by single-strand DNA analysis. *NPJ Genom Med* 3:31, 2018
49. Burnham P, Kim MS, Agbor-Enoh S, et al.: Single-stranded DNA library preparation uncovers the origin and diversity of ultrashort cell-free DNA in plasma. *Scientific Rep* 6:1-9, 2016
50. *The Restriction Enzyme Database (REBASE)*. <http://rebase.neb.com/rebase/rebase.html>
51. Mikeska T, Candiloro IL, Dobrovic A: The implications of heterogeneous DNA methylation for the accurate quantification of methylation. *Epigenomics* 2:561-573, 2010
52. McKenna S, García-Gutiérrez L: Resistance to targeted therapy and RASSF1A loss in melanoma: What are we missing? *Int J Mol Sci* 22:5115, 2021
53. Bettegowda C, Sausen M, Leary RJ, et al.: Detection of circulating tumor DNA in early- and late-stage human malignancies. *Sci Transl Med* 6:224ra24, 2014
54. Chicard M, Boyault S, Daage LC, et al.: Genomic copy number profiling using circulating free tumor DNA highlights heterogeneity in neuroblastoma. *Clin Cancer Res* 22:5564-5573, 2016
55. Chicard M, Colmet-Daage L, Clement N, et al.: Whole-exome sequencing of cell-free DNA reveals temporo-spatial heterogeneity and identifies treatment-resistant clones in neuroblastoma. *Clin Cancer Res* 24:939-949, 2018
56. Jiménez I, Chicard M, Colmet-Daage L, et al.: Circulating tumor DNA analysis enables molecular characterization of pediatric renal tumors at diagnosis. *Int J Cancer* 144:68-79, 2019
57. Su Y, Wang L, Jiang C, et al.: Increased plasma concentration of cell-free DNA precedes disease recurrence in children with high-risk neuroblastoma. *BMC Cancer* 20:102, 2020
58. Paemel RV, Koker AD, Vandeputte C, et al.: Minimally invasive classification of paediatric solid tumours using reduced representation bisulphite sequencing of cell-free DNA: A proof-of-principle study. *Epigenetics* 16:196-208, 2020

Supplemental Data

Supplemental table 1. Primer and probe sequences.

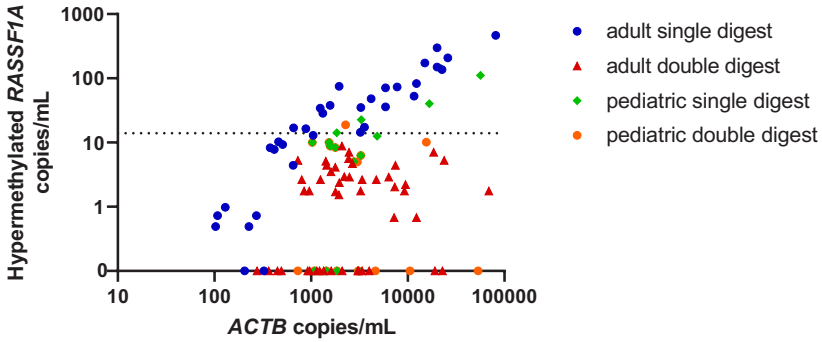
target	forward primer	reverse primer	probe	amplicon size
RASSF1A	AGCCTGAGCTCATTGAGCTG	ACCAAGTGCCTGTGG	/5FAM/CCAACGCGTGCAT/3MGBE/	129
ACTB-1	GTAAGGACAAGTTGGCCCC	TGACTTTGTGGTGTGGCTG	/5HEX/TGCAGGGT/ZEN/CACCTCTGTCGCCCCCA/3IABkFQ/	101
ACTB-2	GCGCCGTCCGAAAGT	CGGCGGATCGGAAA	/5HEX/ACCGCGAGACCGCTC/3MGBE/	137



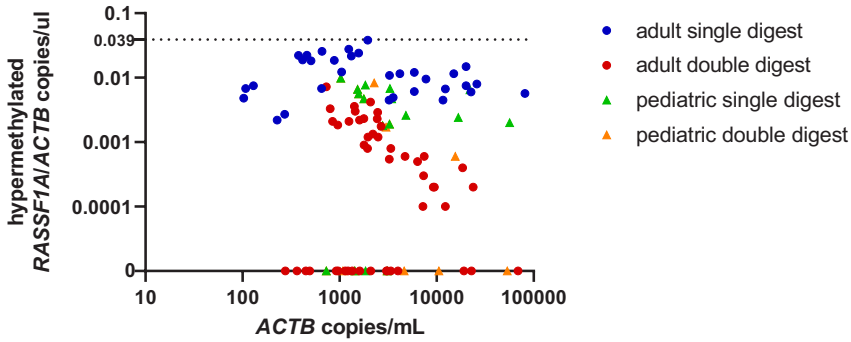
Supplemental figure 1. Dilution series of neuroblastoma cell line IMR32 in DNA of blood mononuclear cells (gDNA PBMC) of a healthy male and in H₂O. While both dilution series showed as expected a good linearity, the PBMC gDNA showed a false positivity of 0.036 copies/ul hypermethylated RASSF1A, explaining why the calculated copies/ul of the lower dilutions of IMR32 in PBMC gDNA is slightly higher than IMR32 in H₂O.



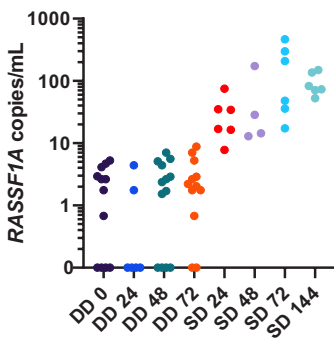
A



B



C

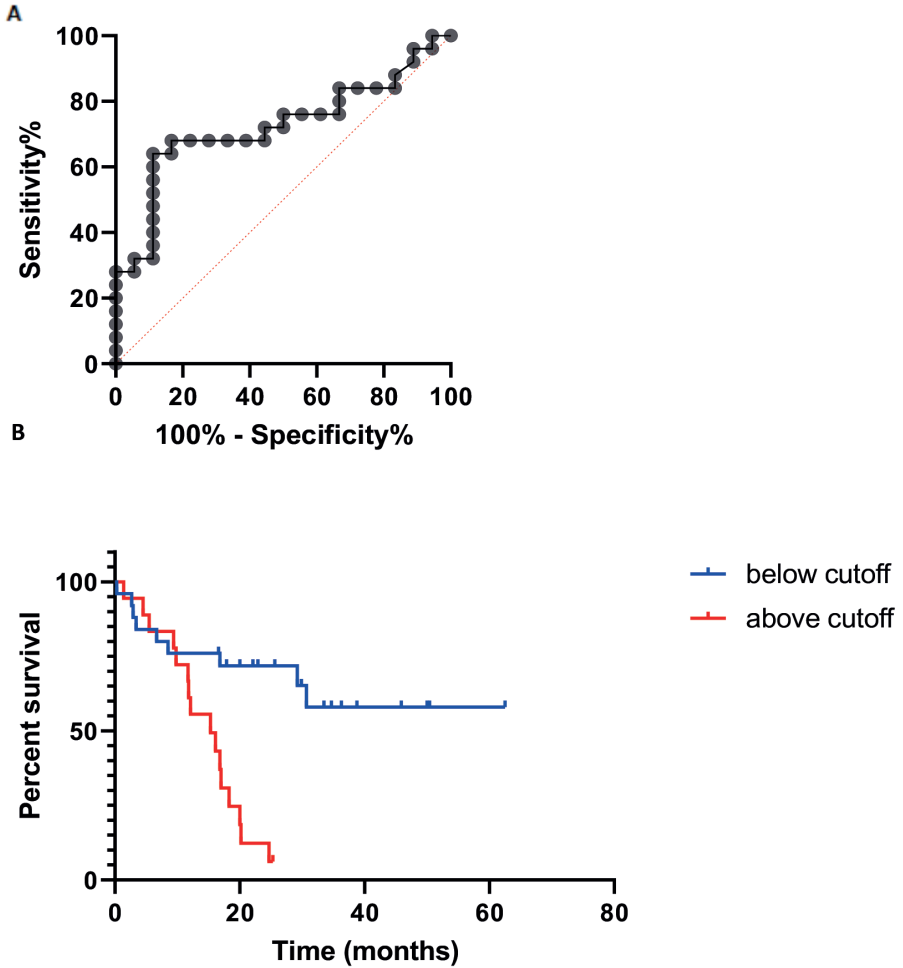


Supplemental figure 2. (A) Association between the number of hypermethylated *RASSF1A* copies/mL plasma and the number of total *ACTB* copies/mL plasma. **(B)** Association between the ratio of hypermethylated *RASSF1A* copies/*ACTB* copies per μL in the ddPCR reaction and the number of total *ACTB* copies/mL plasma. **(C)** *RASSF1A* copies/mL analyzed in EDTA samples, analyzed separately per time to plasma separation, for both double digestion (DD) and single digestion (SD). Numbers indicate the hours from collection to plasma separation.

Supplemental table 3. Clinical data of patients with non-high risk neuroblastoma and other tumor entities (following page)

Sample ID	Tumor	stage	Risk group	age at diagnosis (months)	Hypermethylated RASSF1A copies/mL
2059	neuroblastoma	L2	MR	33	346
2060	neuroblastoma	L2	MR	41	0
2061	neuroblastoma	MS	LR	5	1659
2064	neuroblastoma	L1	LR	36	27
2065	neuroblastoma	L2	LR	16	0
2073	neuroblastoma	L2	MR	129	0
2076	neuroblastoma	L2	LR	3	0
2077	neuroblastoma	L1	LR	69	0
2079	neuroblastoma	L1	LR	29	0
2080	neuroblastoma	L2	LR	2	534
2091	neuroblastoma	L2	LR	162	550
2094	neuroblastoma	MS	LR	3	157
2097	neuroblastoma	L1	LR	6	0
2098	neuroblastoma	MS	LR	3	35
2115	neuroblastoma	L1	LR	4	0
2126	neuroblastoma	L1	LR	13	0
2129	neuroblastoma	L2	MR	13	248
K002	nephroblastoma	IV	IR	29	49
K003	nephroblastoma	II	HR	68	7857
K004	nephroblastoma	II	IR	20	15890
K008	nephroblastoma	II	IR	21	7757
K009	nephroblastoma	I	IR	16	117
K010	nephroblastoma	III	IR	39	515
K014	nephroblastoma	III	IR	30	6135
K015	nephroblastoma	II	IR	43	5720
K018	nephroblastoma	III	IR	7	327
K019	nephroblastoma	III	IR	11	2250
K006	nephroblastoma	III	IR	40	1544
K005	CPDN	III	LR	6	0
K017	Diffuse bilateral nephroblastomatosis			13	0
NL-03-105	Lymphoma	IVB	TL-3	186	1603
NL-03-106	Lymphoma	IVB	TL-3	142	0
NL-03-107	Lymphoma	IV	TL-3	197	250
NL-03-111	Lymphoma	IVB	TL-3	144	1744
NL-03-112	Lymphoma	IIA	TL-2	193	132
14-1662	ATRT	II		9	89336
14-1881	intracranial germ cell tumor	IV		109	0
15-0485	Medulloblastoma	M1		21	0
15-3756	Medulloblastoma	M0		19	0
RMS030	aRMS		VHR	193	267
RMS026	aRMS		M	105	163821
RMS080	aRMS		M	63	1179
RMS037	aRMS		M	126	0
RMS007	aRMS		M	206	0
RMS061	aRMS		M	21	4086
RMS039	eRMS		SR	33	0
RMS010	eRMS		M	195	0
RMS017	eRMS		M	121	259
RMS051	eRMS		SR	121	0
RMS032	eRMS		SR	86	63
RMS004	eRMS		M	170	193
RMS022	eRMS		M	37	110
RMS096	eRMS		HR	34	0

Abbreviations: CPDN, Cystic Partially Differentiated Nephroblastoma; ATRT, Atypical Teratoid Rhabdoid Tumor; aRMS, alveolar rhabdomyosarcoma; eRMS, embryonal rhabdomyosarcoma, L1, L2 and MS, stage according to the International Neuroblastoma Risk Group (INRG) Staging System; LR, low risk; MR, medium risk; IR, intermediate risk; TL, treatment level; VHR, very high risk; HR, high risk; M, medium risk; SR, standard risk

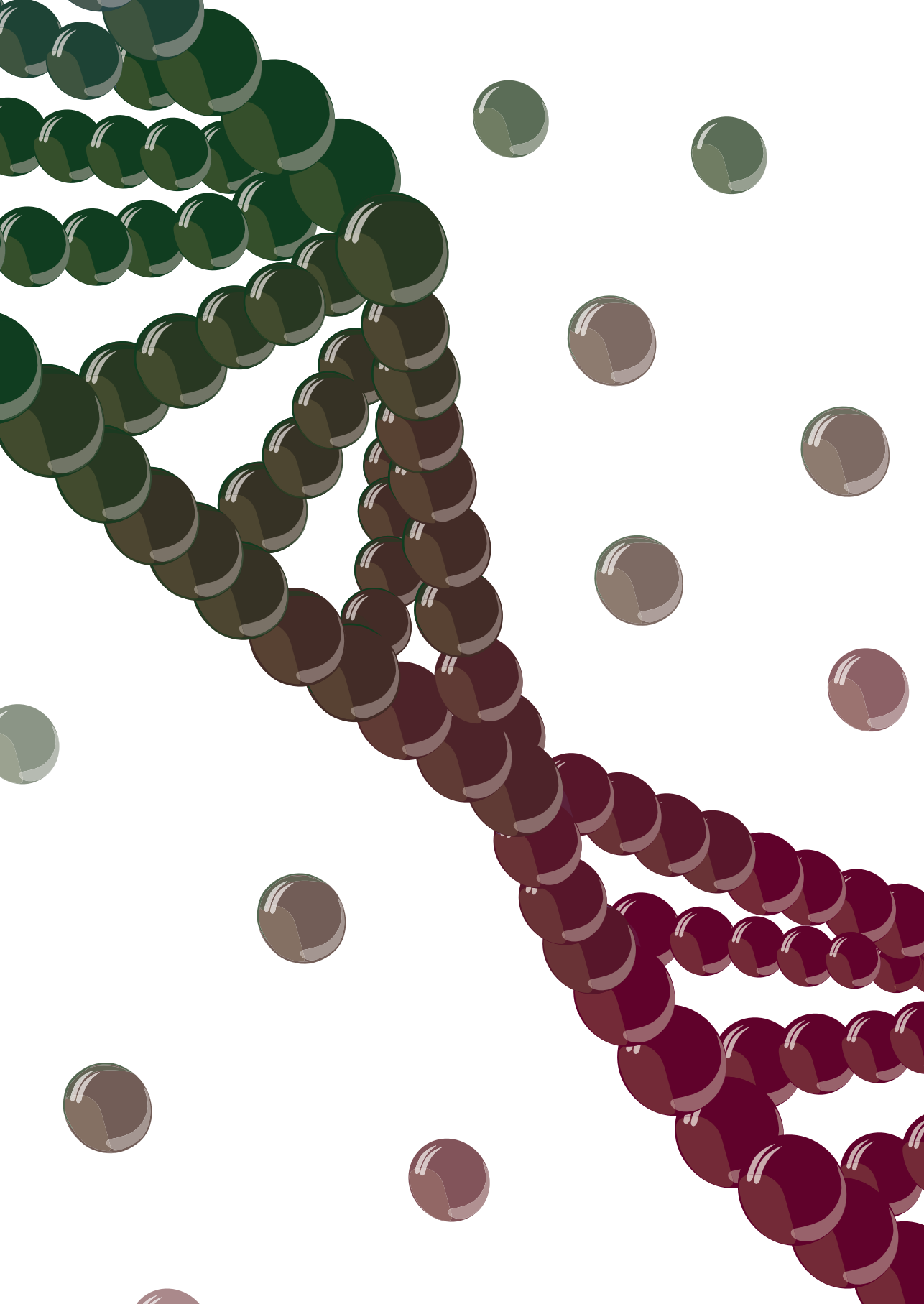


Subjects at risk

months	0	12	24	36	48	60
Below cutoff	25	19	12	6	3	1
Above cutoff	18	11	2	0	0	0

Supplemental figure 3. (A) Receiver operating characteristic analysis with the hypermethylated RASSF1A copies/mL at diagnosis versus events at a later stage. The datapoint with the optimal sensitivity and specificity was chosen as a cutoff. This cutoff was used in the Kaplan Meier-analysis (B).





Cell-free DNA as a diagnostic and prognostic biomarker in pediatric rhabdomyosarcoma

JCO Precis Oncol. 2023 Jan;7:e2200113. doi: 10.1200/PO.22.00113.

Nathalie S.M. Lak^{1,2}, Lieke M.J. van Zogchel^{1,2}, Lily Zappeij-Kannegieter², Ahmad Javadi², Ruben van Paemel³, Charlotte Vandeputte³, Katleen De Preter³, Bram De Wilde³, M. Chicard⁴, Y. Iddir⁴, G. Schleiermacher⁵, O. Ruhen⁶, J. Shipley⁶, Marta Fiocco^{7,8}, Johannes H.M. Merks¹, Max M. van Noesel^{1,9}, C. Ellen van der Schoot², Godelieve A.M. Tytgat^{1,2*}, Janine Stutterheim^{1,2*}

¹ Princess Máxima Center for Pediatric Oncology, Utrecht, the Netherlands

² Sanquin Research Department, Amsterdam, the Netherlands

³ Translational Oncogenomics and Bioinformatics Lab, Department of Biomolecular Medicine & Cancer Research Institute Ghent, Ghent University Hospital, Ghent, Belgium

⁴ Equipe SiRIC RTOP Recherche Translationelle en Oncologie Pédiatrique, andINSERM U830, Laboratoire de Génétique et Biologie des Cancers, Institut Curie, Paris, France

⁵ SIREDO: Care, Innovation and Research for Children, Adolescents and Young Adults with Cancer, Institut Curie, Paris, France

⁶ Divisions of Molecular Pathology and Cancer Therapeutics, The Institute of Cancer Research, London, UK.

⁷ Mathematical Institute, Leiden University, the Netherlands

⁸ Department of Data Science, Medical Statistics section, Leiden University Medical Center, the Netherlands

⁹ UMC Utrecht, Division Oncology & Cancer, Utrecht, the Netherlands

* Authors contributed equally

Abstract

Background and aims: Total cell-free DNA (cfDNA) and tumor-derived cfDNA (ctDNA) can be used to study tumor-derived genetic aberrations. We analyzed the diagnostic and prognostic potential of cfDNA and ctDNA, obtained from pediatric patients with rhabdomyosarcoma.

Methods: cfDNA was isolated from diagnostic plasma samples from 57 patients enrolled in the EpSSG RMS2005 study. To study the diagnostic potential, shallow whole-genome sequencing (shWGS) and cell-free reduced representation bisulphite sequencing (cfRRBS) were performed in a subset of samples and all samples were tested using droplet digital PCR (ddPCR) to detect methylated *RASSF1A* (*RASSF1A-M*). Correlation with outcome was studied by combining cfDNA *RASSF1A-M* detection with analysis of our rhabdomyosarcoma-specific RNA panel in paired cellular blood and bone marrow fractions, and survival analysis in 56 patients.

Findings: At diagnosis, ctDNA was detected in 16/30 and 24/26 patients using shWGS and cfRRBS, respectively. Furthermore, 21/25 samples were correctly classified as embryonal by cfRRBS. *RASSF1A-M* was detected in 21/57 patients. The presence of *RASSF1A-M* was significantly correlated with poor outcome (the 5-year event-free survival rate was 46.2% for 21 *RASSF1A-M*-positive patients, compared to 84.9% for 36 *RASSF1A-M*-negative patients ($p < 0.001$)). *RASSF1A-M* positivity had the highest prognostic effect among patients with metastatic disease. Patients both negative for *RASSF1A-M* and the rhabdomyosarcoma-specific RNA panel (28/56 patients) had excellent outcome (5-year event-free survival 92.9%), while double-positive patients (11/56) had poor outcome (5-year event-free survival 13.6%, $p < 0.001$).

Interpretation: Analyzing ctDNA at diagnosis using various techniques is feasible in pediatric rhabdomyosarcoma and has potential for clinical use. Measuring *RASSF1A-M* in plasma at initial diagnosis correlated significantly with outcome, particularly when combined with paired analysis of blood and bone marrow using a rhabdomyosarcoma-specific RNA panel.

Context Summary

Key objective: In pediatric rhabdomyosarcoma, the use of liquid biopsies can assist in generating a more comprehensive view of the molecular landscape of the tumor. We explore different methods for analysis of cell-free DNA (cfDNA) from plasma by cell-free reduced representation bisulphite sequencing (cfRRBS), shallow whole genome sequencing (shWGS) and ddPCR for *RASSF1A* methylation (*RASSF1A-M*).

Furthermore, we study whether combining cfDNA analyses with detection of rhabdomyosarcoma-specific RNA in the cellular fraction of blood and bone marrow has a complementary value.

Knowledge generated: Both cfRRBS and shWGS have diagnostic potential, whereas the presence of RASSF1A-M at diagnosis correlates to poor survival, especially in patients testing positive for rhabdomyosarcoma-specific RNA in cells from blood and bone marrow.

Relevance: Analysis of cfDNA through different molecular approaches can be of additional value to current clinical risk stratification, especially the detection of RASSF1A-M in cfDNA and rhabdomyosarcoma-specific RNA in paired blood and bone marrow.

Introduction

Rhabdomyosarcoma, the most common sarcoma among children and adolescents, accounts for approximately 3% of pediatric tumors¹. Despite considerable research regarding treatment and risk stratification, 1/3 patients will experience relapse²⁻⁶. The use of liquid biopsies in pediatric patients is drawing growing interest^{7,8}. Our group reported that the presence of rhabdomyosarcoma-derived mRNA in the cellular fraction of peripheral blood (PB) and bone marrow (BM) at initial diagnosis is correlated with poor outcome, and could potentially improve current risk stratification⁹. Studies on other pediatric solid tumors demonstrated cell-free DNA (cfDNA) analysis from plasma to provide added value for diagnostics, prognostics, and response monitoring¹⁰⁻¹⁶. In rhabdomyosarcoma, the presence of tumor-derived cfDNA (ctDNA) has been shown to correlate to tumor burden throughout treatment in a few small case series^{17,18}. ctDNA can be studied using various techniques, using genetic aberrations present in rhabdomyosarcoma. The alveolar subtype has a tumor-driving fusion between the PAX3 or PAX7 gene and the FOXO1 gene. Epigenetic analyses revealed distinct methylation profiles in alveolar and embryonal rhabdomyosarcoma, allowing for the classification of cases into fusion-positive vs. fusion-negative tumors^{19,20}. Van Paemel *et al.* showed that these distinct methylation patterns can be detected in ctDNA from diagnostic plasma, using cell-free reduced representation bisulphite sequencing (cfRRBS) to correctly classify rhabdomyosarcoma as either the embryonal or alveolar subtype²¹. Copy number aberrations (CNAs) have been found to occur in several chromosomes^{3,22}. These can be analyzed in cfDNA by shallow whole-genome sequencing (shWGS)²³. Recently, Van Paemel *et al.*¹⁶ showed that shWGS data from cfDNA can be complementary to CNA analysis on the primary tumor.

However, cfDNA typically contains a relatively small amount of ctDNA; the remaining cfDNA is derived from healthy cells, which can cause high background noise and limit the ability to detect a tumor-derived signal²⁴. To overcome this, a tumor-specific assay can be used, such as droplet digital PCR (ddPCR) which is highly sensitive and less expensive²⁵. A target suited for analysis by ddPCR is methylation of the tumor-suppressor gene *RASSF1A*; this gene has been shown to be silenced by methylation in several adult²⁶ and pediatric²⁷⁻³⁰ tumors. Moreover, methylated *RASSF1A* (*RASSF1A-M*) has been detected in cfDNA in patients with neuroblastoma^{31,32}. Recently, we developed a methylation-specific enzyme-based approach involving ddPCR to detect *RASSF1A-M* in several pediatric solid tumors, including rhabdomyosarcoma¹⁴.

Here, we report the detection of ctDNA in plasma of patients with rhabdomyosarcoma for diagnostic purposes, such as cfRRBS and shWGS. Furthermore, we study the prognostic potential of *RASSF1A-M* detection in cfDNA and measure the added value of combining *RASSF1A-M* ctDNA detection with our rhabdomyosarcoma-specific mRNA panel in paired BM and PB samples.

Methods

Patients and sample collection

Plasma samples were collected prospectively from the same cohort described in our previous paper⁹, consisting of all patients included in the Dutch Minimal Residual Disease add-on study within the EpSSG RMS2005 trial (EudraCT number: 2005-000217-35) from 2013 through July 2019. Informed consent was given via the EpSSG RMS2005 trial until 2017. From 2017, consent was provided if the patients/caretakers consented to the collection of samples for biobanking. PB was collected in EDTA tubes (Becton-Dickinson) and processed within 24 hours. Plasma was obtained by centrifuging the blood samples at 1,375xg for 10 minutes and stored at -20°C until further processing. Matched tumor material was not available.

CfRRBS and shWGS

We performed cfRRBS³³ and shWGS^{16,34} on cfDNA as described and validated previously. In brief, cfDNA was isolated from 200 µl of plasma as described previously^{16,33,34}. For shWGS, the modified copy number profile abnormality (CPAm) score was calculated in order to quantify the copy number tumor burden present in the cfDNA¹⁶. Based on 80 healthy volunteers, the level corresponding to a 1% false discovery rate (FDR) was set at 0.355 for shWGS.

ddPCR assay for measuring RASSF1A-M

For ddPCR, cfDNA was isolated from plasma samples using the Quick-cfDNA Serum & Plasma kit (Zymo Research). The *RASSF1A*-M ddPCR assay was performed using double digestion with the methylation-sensitive restriction enzymes *HhaI* and *Bsh1236I* (*Bst*UI) (Thermo-Fisher Scientific) using a thermocycler T100 and QX200 reader (Bio-Rad) as described previously¹⁴. The sequences and concentrations of the primers and probes, cycling conditions, and analyses were performed as described previously, with the threshold for *RASSF1A*-M positivity per sample set at ≥ 14 copies/ml and ≥ 4 *RASSF1A*-M positive droplets, as determined in 18 healthy pediatric and 22 adult control plasmas¹⁴. The percentage of *RASSF1A*-M was calculated relative to total *RASSF1A*. Based on the plasma volume available (ranging from 150 μ l to 1 ml), different amounts of plasma were used to isolate cfDNA. To correct for variations in the amount of input plasma, cfDNA is reported in ng/ml plasma. In all ddPCR assays, total cfDNA was determined using the reference gene *ACTB*.

Since there was no matched tumor material available, we used data on *RASSF1A*-M in rhabdomyosarcoma tumors from published datasets from Clay *et al*³⁵, Koelsche *et al*³⁶ and specifically requested data from Seki *et al*²⁰. Data from Clay and Koelsche were analyzed in R2³⁷. We focused on hypermethylation of the promotor region of *RASSF1A* as this is typically hypermethylated in cancer³⁸. We calculated the mean beta-value and report the range of the beta values^{39,40}.

Detection of rhabdomyosarcoma-specific mRNA using an RNA panel

Rhabdomyosarcoma-specific mRNA was detected in the cellular fractions of matched diagnostic patient PB and BM samples using our previously reported 11-marker RNA panel^{9,10}. The RNA panel was considered positive if either PB or BM was positive.

Statistical analysis

Statistical analyses were performed using SPSS version 23. Figures were generated using GraphPad Prism version 8. The correlation between continuous variables was determined using Pearson's test. Continuous variables were analyzed using the non-parametric Mann-Whitney *U* test, and 2 or more groups were analyzed using the Kruskal-Wallis test. Independence between 2 categorical variables was determined using the non-parametric Pearson chi-square test. Event-free survival and overall survival were estimated using the Kaplan-Meier approach, and differences in survival were analyzed using the log-rank test. Differences were considered significant at $p < 0.05$.

Results

Patient and sample characteristics

We collected a total of 152 plasma samples from 65 patients, treated according to the EpSSG RMS2005 protocol; diagnostic plasma samples were available for 57 patients. The patient characteristics, assigned risk group and tumor histology, are summarized in Table 1. The median follow-up was 4.21 years (range: 0.34–10.60 years).

Diagnostic potential of various molecular techniques for detecting ctDNA

First, total cfDNA levels at diagnosis were determined by measuring *ACTB* using ddPCR for all samples. No significant differences in total cfDNA levels were observed between patients with respect to tumor histology, risk group, localized versus metastatic disease, tumor size or event-free survival (Supplemental Figure S1A-E). Next, we examined the feasibility to detect ctDNA using cfRRBS, shWGS and ddPCR (Table 2, Supplemental Tables S1, S2, S3 and Supplemental Figure S2). Overall, in 39 out of 57 patients (68.4%), at least one of these techniques detected ctDNA in diagnostic plasma samples. Please note that cfRRBS and shWGS were tested on a subset of samples.

Methylation profiling for diagnostic classification

As negative control, cfRRBS was performed on 31 samples from healthy controls, all classified correctly as normal (Supplemental figure S3). We applied cfRRBS to diagnostic samples from 24 patients with the embryonal subtype, 1 with botryoid subtype, and 1 with alveolar subtype, successfully detecting rhabdomyosarcoma DNA in 24 of these 26 samples (92.3% of cases). Twenty of these samples were correctly identified as embryonal tumors. Three cases with embryonal histology were classified as alveolar, one case of botryoid rhabdomyosarcoma was classified as embryonal, and no tumor DNA was detected in 2 samples (one alveolar and one embryonal).

Copy number aberrations

We performed shWGS on 30 plasma samples and obtained a median CPAm score of 0.35 (range: 0.27-3.94), (Supplemental Figure S4). In three cases (2 embryonal and 1 alveolar), the analysis failed (Table 2, Supplemental Table S2). Twelve embryonal cases (7/12 metastatic) and 4 alveolar (all metastatic) cases had CNAs, while 10 embryonal cases and 1 botryoid case had no CNA. Most CNAs were detected in patients with metastatic disease and 7/16 (43.8%) patients with detectable CNAs suffered from an event.

Table 1. Patient characteristics of the patients with rhabdomyosarcoma (n=65)

	N (%)
Age at diagnosis	
<1 year	1 (1.5)
1-10 years	38 (58.5)
>10 years	26 (40.0)
Sex	
Female	23 (35.4)
Male	42 (64.6)
Histology	
Alveolar rhabdomyosarcoma	22 (33.8)
Embryonal rhabdomyosarcoma	40 (61.5)
Botryoid rhabdomyosarcoma	1 (1.5)
Spindle cell/leiomyomatous rhabdomyosarcoma	1 (1.5)
Rhabdomyosarcoma not otherwise specified	1 (1.5)
Post-surgical tumor staging (IRS grouping)	
I	4 (6.3)
II	11 (16.9)
III	27 (41.5)
IV	23 (35.4)
Tumor size	
≤5 cm	29 (44.6)
>5 cm	36 (55.4)
Regional lymph node involvement	
No evidence of lymph node involvement	42 (64.6)
Evidence of regional lymph node involvement	22 (33.8)
No information about lymph node involvement	1 (1.5)
Risk group	
Low risk	1 (1.5)
Standard risk	24 (36.9)
High risk	14 (21.5)
Very high risk	3 (4.6)
Metastatic	23 (35.4)
Site of origin of primary tumor	
Orbit	10 (15.4)
Head neck non-parameningeal	5 (7.7)
Parameningeal	10 (15.4)
Bladder prostate	8 (12.3)
Genitourinary non-bladder prostate	10 (15.4)
Extremities	14 (21.5)
Other sites	8 (12.3)

Methylated RASSF1A

Using data from Clay *et al*³⁵, Koelsche *et al*³⁶ and Seki *et al*²⁰, the mean beta-value of *RASSF1A-M* was 0.550 (range 0.032-0.933) (Supplemental Figures S5 A-D). We next examined the presence of *RASSF1A-M* in plasma using ddPCR. Methylated *RASSF1A* was detectable in 21/57 diagnostic plasma samples; 9/37 embryonal cases, 10/17 alveolar cases, 1/1 spindle case, 0 botryoid case, and 1 not-otherwise-specified case, with a median *RASSF1A-M* concentration of 2.46 ng/ml (range: 0.22-273.11 ng/ml). In patients with alveolar tumors and metastatic disease, methylated *RASSF1A* was more frequently detected, compared to embryonal histology ($p=0.014$) and localized disease (*RASSF1A-M* positive in 9/37 patients with localized, 12/20 patients with metastatic disease $p=0.008$). The total level of *RASSF1A-M* varied widely within the *RASSF1A-M*-positive samples and was correlated with tumor histology (Supplemental Figure S6A). To correct for variations in total cfDNA, we calculated the percentage of *RASSF1A-M* relative to total *RASSF1A* for each patient, yielding a median percentage of 15.1% (range: 2.0-92.7%) for the *RASSF1A-M*-positive samples. Although metastatic and alveolar tumors more often show the presence of *RASSF1A-M* in cfDNA, the *RASSF1A-M* percentage in positive samples was similar in alveolar and embryonal tumors ($p=0.55$) and in localized and metastatic cases ($p=0.35$). We found no correlation between tumor size at diagnosis and either total *RASSF1A-M* ($r=0.132$ and $p=0.64$; Supplemental Figure S6B) or the percentage of *RASSF1A-M* ($r=-0.229$ and $p=0.41$; Figure 2C). Finally, we found no difference in total cfDNA levels (*ACTB*) between *RASSF1A-M*-positive and *RASSF1A-M*-negative cases ($p=0.96$; Figure 1D).

Cell-free RASSF1A-M correlates with poor outcome

We examined whether the detection of ctDNA in 57 diagnostic plasma samples was associated with patient outcome. Eleven out of 21 (52,3%) *RASSF1A-M* positive patients suffered from an event.

The 5-year EFS rate was 46.2% for the *RASSF1A-M*-positive patients, compared to 84.9% for the *RASSF1A-M*-negative patients ($p=0.001$; Figure 2A); and, the 5-year overall survival (OS) rate was 55.7% for the *RASSF1A-M*-positive patients compared to 100% for the *RASSF1A-M*-negative patients ($p<0.001$; Figure 2B). The prognostic value of detecting *RASSF1A-M* at diagnosis was attributed almost exclusively to patients with metastasized disease (Figure 2B-C, Supplemental Figure S7).

In 27 samples both shWGS and *RASSF1A-M* was performed (Supplemental table S4). In 6 patients shWGS was positive while *RASSF1A-M* was negative, and only one patient suffered from an event, while 6/10 double positive patients suffered from an

event, suggesting that the presence of both RASSF1A-M and ctDNA by shWGS may be more prognostic than detection of ctDNA by shWGS alone.

We next examined whether combining *RASSF1A*-M detection with detection of rhabdomyosarcoma-specific mRNA (based on our previously published mRNA panel⁹) tested in 56 matched diagnostic PB and BM samples, could improve the predictive value. Rhabdomyosarcoma-specific mRNA was detected in 18/56 PB and/or BM samples (8/18 tested positive on conventional BM histology, Supplemental Table S5). Five-year EFS ranged from 92.9% to 13.6% for *RASSF1A*-M^{neg}/mRNA panel^{neg} and *RASSF1A*-M^{pos}/mRNA panel^{pos}, ($p=0.006$) and 5 years OS from 100% to 36.4% for *RASSF1A*-M^{neg}/mRNA panel^{neg} and *RASSF1A*-M^{pos}/mRNA panel^{pos}, respectively ($p<0.001$) (Figure 3A and 3B).

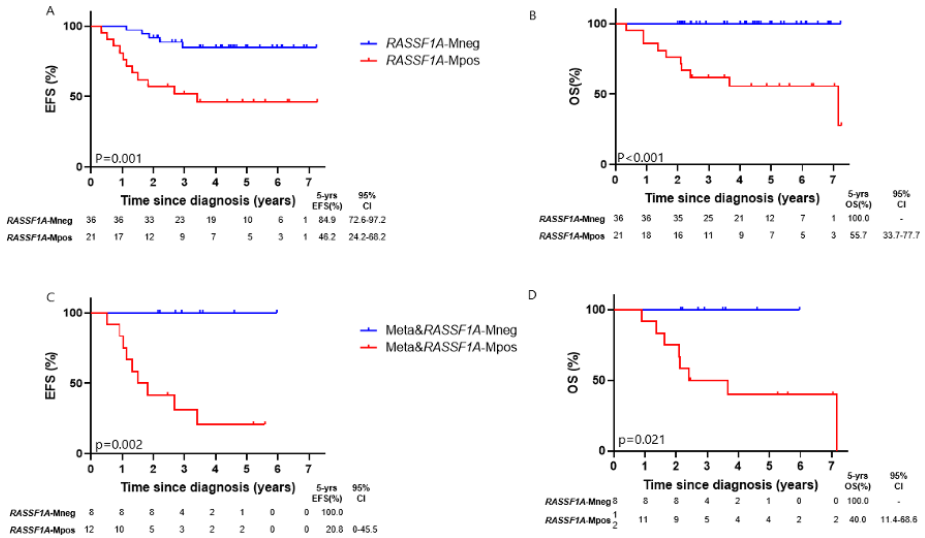


Figure 2. Survival outcome defined by detection of cell-free methylated RASSF1A (RASSF1A-M) at diagnosis. **A** and **B**. Event-free survival (EFS) and overall survival (OS), respectively, of patients with no detectable methylated *RASSF1A* in the diagnostic plasma (*RASSF1A*-Mneg) ($n=36$) and patients with detectable methylated *RASSF1A* in the diagnostic plasma (*RASSF1A*-Mpos) ($n=21$). **C** and **D**. EFS and OS of *RASSF1A*-M-negative patients ($n=8$) and *RASSF1A*-M-positive patients ($n=12$) with metastatic disease. Shown below each plot are the number of patients at each time point, and 5-years survival with the 95% confidence interval.

To validate the association of *RASSF1A*-M to clinical outcome, we performed univariate and multivariable Cox regression analyses for EFS (Supplemental Tables S6 and Table 3, respectively). In the multivariable model, only *RASSF1A*-M, RNA panel, and tumor size larger than 5 cm had a significant effect on outcome. The known EpSSG RMS2005 risk group classification, metastatic disease, alveolar subtype, over

10 years of age, and lymph node involvement were not significantly associated with outcome in our multivariable model. Lastly, OS could not be analyzed due to the low number of events in this cohort.

Table 2. Overview of the results of different approaches on cfDNA of n= 57 diagnostic plasma samples.

Technique	Result	N (%)
<i>RASSF1A</i> -M ddPCR (n=57)	Positive	21 (36.8)
	Negative	36 (63.2)
cfRRBS (n=26)	Embryonal subtype	21 (80.8) ^a
	Alveolar subtype	3 (11.5) ^b
	No tumor DNA	2 (7.7)
shWGS (n=30)	CNA present	16 (53.3)
	Flat	11 (36.7)
	Fail	3 (10.0)

RASSF1A-M, methylated *RASSF1A*; cfRRBS, cell-free reduced representation bisulphite sequencing; shWGS, shallow whole genome sequencing;

^a 1 case was originally classified as botryoid based on the clinical diagnosis.

^b All 3 of these cases were originally classified as embryonal based on the clinical diagnosis.

RASSF1A-M during treatment and clinical follow-up

For 33 patients, a total of 95 samples drawn during primary treatment and/or subsequent clinical follow-up were available. *RASSF1A*-M was measured in the follow-up samples only if the patient was *RASSF1A*-M-positive at diagnosis or—if a diagnostic sample was not available—at relapse. Among the 23 patients for whom samples were collected during primary treatment, only 2 patients (Supplemental Table S7/S8) were *RASSF1A*-M-positive after two cycles of chemotherapy, but *RASSF1A*-M-negative in all subsequent samples. In 8 patients, *RASSF1A*-M was measured in a sample taken during a clinical event (5 at first relapse, 2 at second relapse, and 1 at progressive disease during primary treatment). Five of these 8 samples were *RASSF1A*-M-positive (3 at first relapse and 2 at second relapse); no samples at initial diagnosis were available for these 5 patients. After initiating relapse therapy, all subsequent samples from these patients were *RASSF1A*-M-negative. The sample taken from the patient at progressive disease (patient RMS133) was *RASSF1A*-M-negative, and no previous plasma samples were available for this patient.

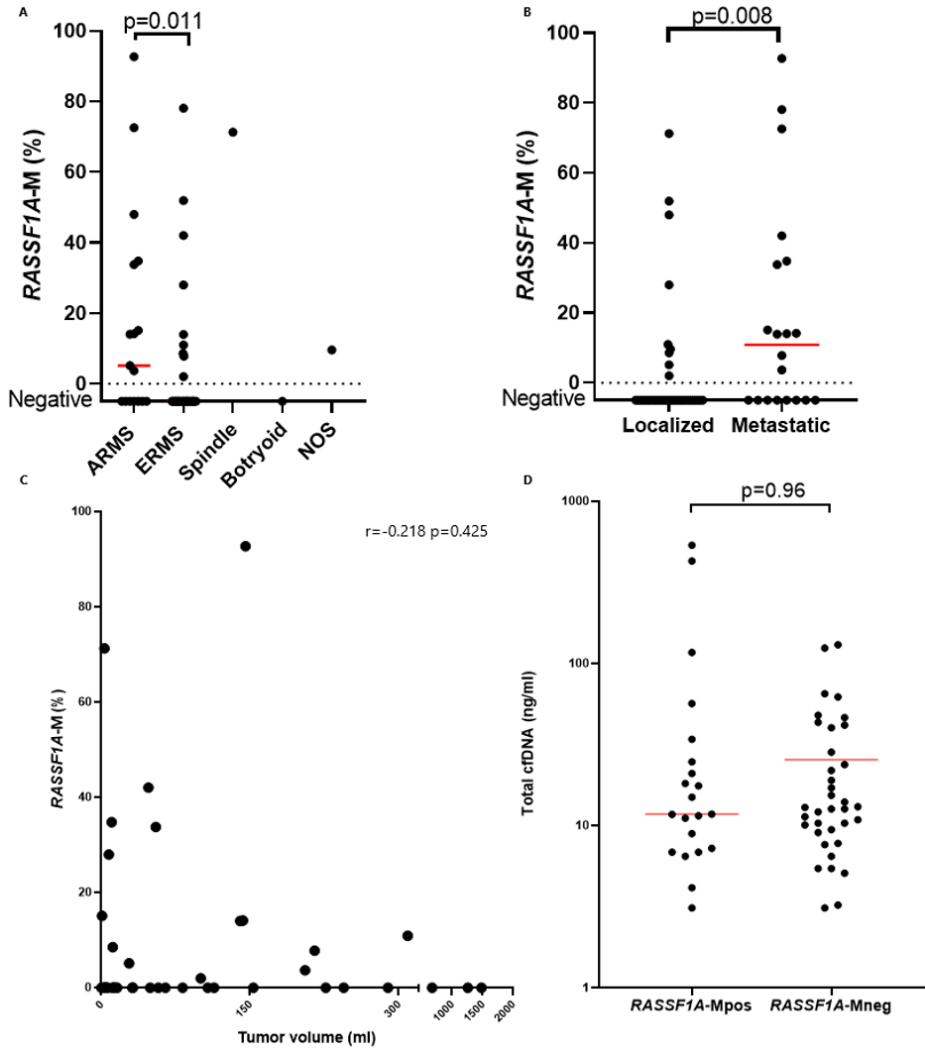


Figure 1. Methyated *RASSF1A* (*RASSF1A-M*) in diagnostic plasma samples of patients with rhabdomyosarcoma. The percentage of cell-free methylated-*RASSF1A* (*RASSF1A-M*) is calculated according to total *RASSF1A* copies at diagnosis in patients: **A.** with different subtypes; **B.** with localized and metastatic disease and **C.** plotted against tumor volume at diagnosis. **D.** Level of cfDNA (quantified by *beta-Actin* (*ACTB*)) at diagnosis in plasma samples with detectable *RASSF1A-M* and with no detectable *RASSF1A-M*; note that the y-axis is plotted on a log scale.

In this figure, each symbol represents an individual patient, and the red horizontal lines represent the median values. Tumor size was determined by MRI, CT-scan or ultrasonography.

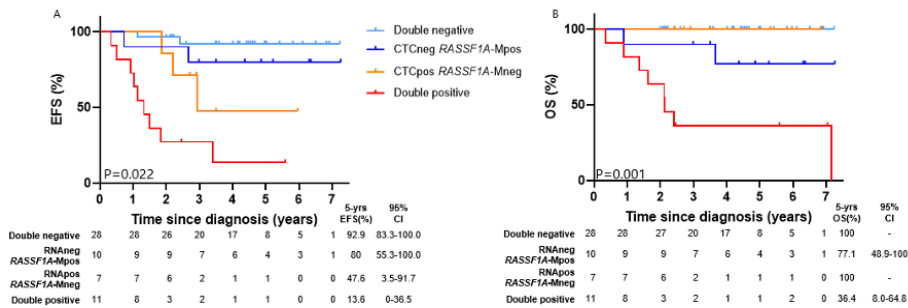


Figure 3. Survival outcome defined by detection of cell-free methylated *RASSF1A* (*RASSF1A-M*) from plasma and rhabdomyosarcoma-specific RNA in blood and bone marrow at diagnosis. **A** and **B**. Event-free survival (EFS) and overall survival (OS) of 56 patients based on the absence or presence of rhabdomyosarcoma-specific RNA (RNA-negative and RNA-positive, respectively) combined with *RASSF1A-M* status. Shown below each plot are the number of patients at each time point, and 5-years survival with the 95% confidence interval.

Table 3. Hazard ratios with 95% CI estimated with a multivariable Cox proportional hazard regression model for event-free survival.

	Hazard ratio (95% CI)
<i>RASSF1A-M-positive</i>	4.52 (1.34-15.27)*
Standard Risk	1
High Risk	1.29 (0.22-7.74)
Metastatic disease	2.69 (0.69-10.47)
<i>RASSF1A-M-positive</i>	4.15 (1.38-12.49)*
Localized vs metastatic disease	1.99 (0.70-5.61)
<i>RASSF1A-M-positive</i>	3.38 (1.14-9.97)*
RNA panel	7.60 (2.37-24.36)*
<i>RASSF1A-M-positive</i>	4.82 (1.60-14.51)*
Alveolar rhabdomyosarcoma	1.16 (0.42-3.25)
<i>RASSF1A-M-positive</i>	5.72 (1.96-16.69)*
Age at diagnosis >10 years	2.14 (0.99-7.44)
<i>RASSF1A-M-positive</i>	5.87 (2.02-17.07)*
Tumor size >5cm	8.05 (1.81-35.81)*
<i>RASSF1A-M-positive</i>	4.27 (1.39-13.13)*
Lymph node involvement	1.34 (0.46-3.88)

* indicates significance at $p < 0.05$

Discussion

Based on our findings, we propose that each cfDNA-based technique can address a specific clinical need, ranging from assisting at initial tumor diagnosis to fine-tuning of risk stratification. In our cohort, cfRRBS proved its potential as a highly sensitive method for identifying rhabdomyosarcoma-derived cfDNA at initial diagnosis, and the majority was classified correctly as embryonal. Van Paemel *et al.*²¹ found that cfRRBS was also able to correctly identify alveolar ctDNA. Thus, cfRRBS can provide added value at initial diagnosis, particularly if the ability to perform a tumor biopsy is restricted by clinical features such as tumor location or the patient's condition, and when the ability to distinguish between other types of pediatric solid tumors is important²¹.

We detected CNAs in 53.3% of samples analyzed by shWGS, mostly metastatic cases. Based on literature, CNAs are present in nearly all fusion-negative rhabdomyosarcomas^{20,41} and in approximately one-third of all fusion-positive rhabdomyosarcomas^{41,42}. We detected CNAs in the cfDNA of only half of the patients with fusion-negative tumors. This relatively low rate may have been due in part to contamination of the cfDNA with genomic DNA, as the protocol for drawing and storing blood was not standardized, which can lower the sensitivity to detect CNA¹⁶. Van Paemel *et al.* noted that performing shWGS on cfDNA can provide additional value with respect to analyzing CNAs in the primary tumor, resulting in a more complete overview of the patient's genetic landscape and bypassing any potential heterogeneity within the tumor and/or metastatic lesions. This is important to consider when designing further studies.

Based on the previous reports, demonstrating feasibility to use *RASSF1A-M* ddPCR as a tumor-specific marker with a high specificity due to extremely low background in plasma from healthy controls^{14,15}, we studied *RASSF1A-M* ddPCR in cfDNA of rhabdomyosarcoma patients. One of the limitations of this study, was the absence of paired primary tumor samples. However, the presence of *RASSF1A-M*, as extracted from data published by several groups^{20,35,36}, indicated the potential to detect *RASSF1A-M* in primary tumors, with admittedly a large variation in the level of *RASSF1A-M*. Still, for the patients in our cohort who were *RASSF1A-M*-negative, based on cfDNA obtained at diagnosis, we were unable to determine whether this was due to absence of *RASSF1A* methylation or no detectable ctDNA. This is underlined by the 18 samples testing negative for *RASSF1A-M*, in which ctDNA was detected by cfRRBS and/or shWGS. Future studies should include matching tumor material to establish the contribution of different approaches for cfDNA analysis. Nonetheless, we were

able to detect *RASSF1A-M* in cfDNA in 36% of diagnostic samples, and found a strong correlation between *RASSF1A-M* positivity and event-free and overall survival. Importantly, this predictive value was obtained almost exclusively in the group of patients with metastatic disease. This finding might suggest that more aggressive tumors contain methylated *RASSF1A* and deserves further investigations in a follow-up study, including matching primary tumor material. Interestingly, in the samples that were tested by both shWGS and *RASSF1A-M*, results suggest that detection of ctDNA by both methods may be more prognostic than detection of ctDNA by shWGS alone. This should be studied further in a larger cohort.

As we previously showed rhabdomyosarcoma-specific RNA detection in PB and/or BM at diagnosis to detect additional disseminated disease and to correlate with outcome⁹, we now showed that combining mRNA and ctDNA (*RASSF1A-M*) in paired diagnostic samples identifies patients with very good and very poor outcome. Our multivariable analysis revealed that combining the cfDNA *RASSF1A-M* assay with rhabdomyosarcoma-specific RNA detection in PB and BM samples provides an even better tool for discriminating between low-risk patients and patients with a poor prognosis. Given the relatively small number of patients in our cohort, however, we were unable to investigate the effect of adding both *RASSF1A-M* and the RNA panel to established prognostic factors, particularly in the EpSSG RMS2005 risk group; nevertheless, our results can form a starting point for future studies involving a prospective cohort.

An interesting finding from our study is the dynamics of ctDNA. Prior to our study, we hypothesized that ctDNA would still be present during primary treatment and decrease slowly, tracking the decrease in tumor burden. However, in our rhabdomyosarcoma cohort, we found that most of the samples were negative for ctDNA after the first course of chemotherapy. This rapid transition to a ctDNA-negative state is consistent with results reported by Klega *et al.*¹⁸, who found that most samples were negative for ctDNA prior to the second course of chemotherapy. Thus, an interesting question is whether performing earlier sampling and obtaining multiple samples during the first 2 weeks after the start of treatment would reveal the presence of ctDNA, and—if so—would lead to the development of a prognostic marker, similar to the marker for minimal residual disease developed for use in leukemia^{43,44}.

Conclusions

Here, we demonstrate the feasibility to study ctDNA in pediatric rhabdomyosarcoma by different approaches. The choice of a given technique will depend on whether the underlying question is diagnostic or prognostic. We show that the presence of methylated *RASSF1A* in cfDNA is associated with poor outcome and can be used to improve risk stratification at diagnosis. Furthermore, we show that combining detection of methylated *RASSF1A* in plasma with analysis of tumor-specific RNA in blood and bone marrow identified patients with good vs. poor outcome.

Acknowledgements

We thank Masafumi Seki for sharing detailed data regarding *RASSF1A* methylation from their published cohort. We thank Maisa Renata Ferro dos Santos from Ghent University for the analysis of cfRRBS data from healthy controls.

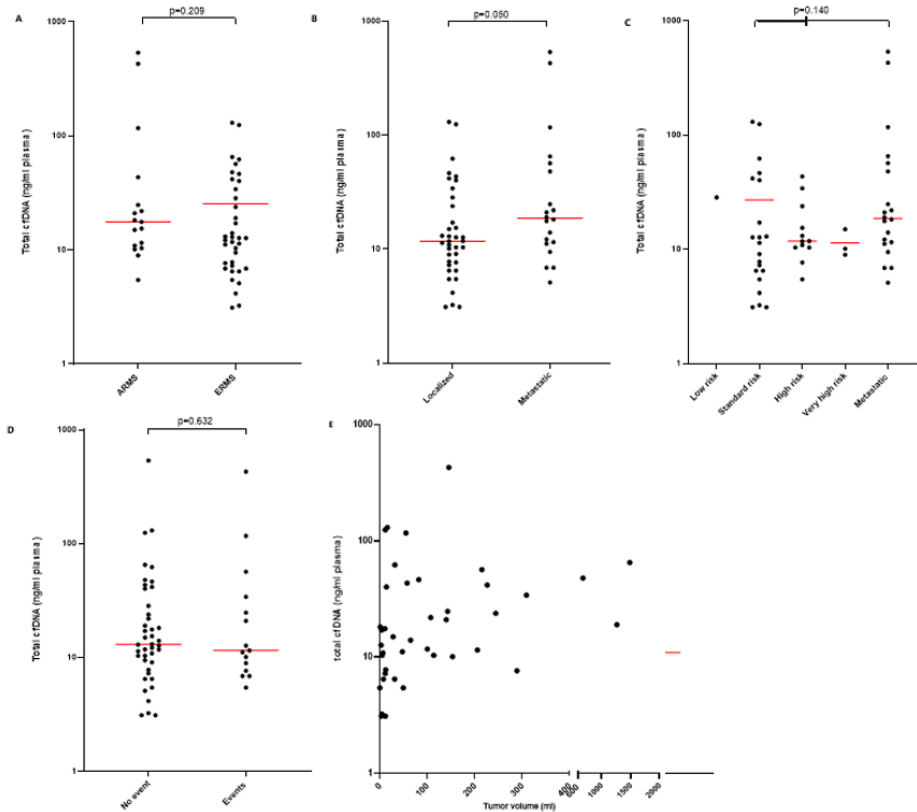
References

1. https://www.prinsesmaximacentrum.nl/storage/configurations/prinsesmaximacentrumnl/files/hetprinsesmaximacentrum-jaarverslag_cenr2020_06-21_s_interactive.pdf.
2. Gartrell J, Pappo A: Recent advances in understanding and managing pediatric rhabdomyosarcoma. *F1000Res* 9, 2020
3. Skapek SX, Ferrari A, Gupta AA, et al: Rhabdomyosarcoma. *Nat Rev Dis Primers* 5:1, 2019
4. Oberlin O, Rey A, Lyden E, et al: Prognostic factors in metastatic rhabdomyosarcomas: results of a pooled analysis from United States and European cooperative groups. *J Clin Oncol* 26:2384-9, 2008
5. Oberlin O, Rey A, Sanchez de Toledo J, et al: Randomized comparison of intensified six-drug versus standard three-drug chemotherapy for high-risk nonmetastatic rhabdomyosarcoma and other chemotherapy-sensitive childhood soft tissue sarcomas: long-term results from the International Society of Pediatric Oncology MMT95 study. *J Clin Oncol* 30:2457-65, 2012
6. Chisholm JC, Marandet J, Rey A, et al: Prognostic factors after relapse in nonmetastatic rhabdomyosarcoma: a nomogram to better define patients who can be salvaged with further therapy. *J Clin Oncol* 29:1319-25, 2011
7. Van Paemel R, Vlug R, De Preter K, et al: The pitfalls and promise of liquid biopsies for diagnosing and treating solid tumors in children: a review. *Eur J Pediatr* 179:191-202, 2020
8. Andersson D, Fagman H, Dalin MG, et al: Circulating cell-free tumor DNA analysis in pediatric cancers. *Mol Aspects Med* 72:100819, 2020
9. Lak NSM, Voormanns TL, Zappeij-Kannegieter L, et al: Improving Risk Stratification for Pediatric Patients with Rhabdomyosarcoma by Molecular Detection of Disseminated Disease. *Clin Cancer Res*, 2021
10. van Zogchel LMJ, van Wezel EM, van Wijk J, et al: Hypermethylated RASSF1A as Circulating Tumor DNA Marker for Disease Monitoring in Neuroblastoma. *JCO Precis Oncol* 4, 2020
11. Jimenez I, Chicard M, Colmet-Daage L, et al: Circulating tumor DNA analysis enables molecular characterization of pediatric renal tumors at diagnosis. *Int J Cancer* 144:68-79, 2019
12. Chicard M, Boyault S, Colmet Daage L, et al: Genomic Copy Number Profiling Using Circulating Free Tumor DNA Highlights Heterogeneity in Neuroblastoma. *Clin Cancer Res* 22:5564-5573, 2016
13. Chicard M, Colmet-Daage L, Clement N, et al: Whole-Exome Sequencing of Cell-Free DNA Reveals Temporo-spatial Heterogeneity and Identifies Treatment-Resistant Clones in Neuroblastoma. *Clin Cancer Res* 24:939-949, 2018
14. van Zogchel LMJ, Lak NSM, Verhagen OJHM, et al: Novel Circulating Hypermethylated RASSF1A ddPCR for liquid biopsies in patients with pediatric solid tumors. *JCO Precis Oncol* 5:1738-1748, 2021
15. Lobo J, van Zogchel LMJ, Nuru MG, et al: Combining Hypermethylated RASSF1A Detection Using ddPCR with miR-371a-3p Testing: An Improved Panel of Liquid Biopsy Biomarkers for Testicular Germ Cell Tumor Patients. *Cancers (Basel)* 13, 2021
16. Van Paemel R, Vandeputte C, Raman L, et al: The feasibility of using liquid biopsies as a complementary assay for copy number aberration profiling in routinely collected paediatric cancer patient samples. *Eur J Cancer*, 2021
17. Eguchi-Ishimae M, Tezuka M, Kokeyuchi T, et al: Early detection of the PAX3-FOXO1 fusion gene in circulating tumor-derived DNA in a case of alveolar rhabdomyosarcoma. *Genes Chromosomes Cancer* 58:521-529, 2019

18. Klega K, Imamovic-Tuco A, Ha G, et al: Detection of Somatic Structural Variants Enables Quantification and Characterization of Circulating Tumor DNA in Children With Solid Tumors. *JCO Precis Oncol* 2018, 2018
19. Sun W, Chatterjee B, Wang Y, et al: Distinct methylation profiles characterize fusion-positive and fusion-negative rhabdomyosarcoma. *Mod Pathol* 28:1214-24, 2015
20. Seki M, Nishimura R, Yoshida K, et al: Integrated genetic and epigenetic analysis defines novel molecular subgroups in rhabdomyosarcoma. *Nat Commun* 6:7557, 2015
21. Van Paemel R, De Koker A, Vandeputte C, et al: Minimally invasive classification of paediatric solid tumours using reduced representation bisulphite sequencing of cell-free DNA: a proof-of-principle study. *Epigenetics* 16:196-208, 2021
22. Parham DM, Barr FG: Classification of rhabdomyosarcoma and its molecular basis. *Adv Anat Pathol* 20:387-97, 2013
23. De Koker AvP, R.; De Wilde, B.; de Preter, K.; Callewaert, N. : A versatile method for circulating cell-free DNA methylome profiling by reduced representation bisulfite sequencing. *bioRxiv* 2019
24. Wan JCM, Massie C, Garcia-Corbacho J, et al: Liquid biopsies come of age: towards implementation of circulating tumour DNA. *Nat Rev Cancer* 17:223-238, 2017
25. Vessies DCL, Greuter MJE, van Rooijen KL, et al: Performance of four platforms for KRAS mutation detection in plasma cell-free DNA: ddPCR, Idylla, COBAS z480 and BEAMing. *Sci Rep* 10:8122, 2020
26. Grawenda AM, O'Neill E: Clinical utility of RASSF1A methylation in human malignancies. *Br J Cancer* 113:372-81, 2015
27. Lim S, Yang MH, Park JH, et al: Inactivation of the RASSF1A in osteosarcoma. *Oncol Rep* 10:897-901, 2003
28. Wagner KJ, Cooper WN, Grundy RG, et al: Frequent RASSF1A tumour suppressor gene promoter methylation in Wilms' tumour and colorectal cancer. *Oncogene* 21:7277-82, 2002
29. Honda S, Miyagi H, Suzuki H, et al: RASSF1A methylation indicates a poor prognosis in hepatoblastoma patients. *Pediatr Surg Int* 29:1147-52, 2013
30. Astuti D, Agathangelou A, Honorio S, et al: RASSF1A promoter region CpG island hypermethylation in pheochromocytomas and neuroblastoma tumours. *Oncogene* 20:7573-7, 2001
31. van Zogchel LMJ, van Wezel EM, van Wijk J, et al: Hypermethylated RASSF1A as circulating tumor DNA marker for disease monitoring in neuroblastoma. *J Clin Oncol Precision Oncology*, 2020
32. Stutterheim J, Ichou FA, den Ouden E, et al: Methylated RASSF1a is the first specific DNA marker for minimal residual disease testing in neuroblastoma. *Clin Cancer Res* 18:808-14, 2012
33. Van Paemel R, De Koker A, Vandeputte C, et al: Minimally invasive classification of paediatric solid tumours using reduced representation bisulphite sequencing of cell-free DNA: a proof-of-principle study. *Epigenetics*:1-13, 2020
34. Van Roy N, Van Der Linden M, Menten B, et al: Shallow Whole Genome Sequencing on Circulating Cell-Free DNA Allows Reliable Noninvasive Copy-Number Profiling in Neuroblastoma Patients. *Clin Cancer Res* 23:6305-6314, 2017
35. Clay MR, Patel A, Tran Q, et al: Methylation profiling reveals novel molecular classes of rhabdomyosarcoma. *Sci Rep* 11:22213, 2021
36. Koelsche C, Schrimpf D, Stichel D, et al: Sarcoma classification by DNA methylation profiling. *Nat Commun* 12:498, 2021
37. R2: Genomics Analysis and Visualization Platform
38. Raos D, Ulamec M, Katusic Bojanac A, et al: Epigenetically inactivated RASSF1A as a tumor biomarker. *Bosn J Basic Med Sci* 21:386-397, 2021

39. Niu H, Yang J, Yang K, et al: The relationship between RASSF1A promoter methylation and thyroid carcinoma: A meta-analysis of 14 articles and a bioinformatics of 2 databases (PRISMA). *Medicine (Baltimore)* 96:e8630, 2017
40. Xu G, Zhou X, Xing J, et al: Identification of RASSF1A promoter hypermethylation as a biomarker for hepatocellular carcinoma. *Cancer Cell Int* 20:547, 2020
41. Chen L, Shern JF, Wei JS, et al: Clonality and evolutionary history of rhabdomyosarcoma. *PLoS Genet* 11:e1005075, 2015
42. Lynn M, Shah N, Conroy J, et al: A study of alveolar rhabdomyosarcoma copy number alterations by single nucleotide polymorphism analysis. *Appl Immunohistochem Mol Morphol* 22:213-21, 2014
43. Laughton SJ, Ashton LJ, Kwan E, et al: Early responses to chemotherapy of normal and malignant hematologic cells are prognostic in children with acute lymphoblastic leukemia. *J Clin Oncol* 23:2264-71, 2005
44. van Dongen JJ, Seriu T, Panzer-Grumayer ER, et al: Prognostic value of minimal residual disease in acute lymphoblastic leukaemia in childhood. *Lancet* 352:1731-8, 1998

Supplemental figures and tables



Supplemental Figure S1. Total cell-free DNA (cfDNA), as measured by gene *ACTB* (actin beta) in ddPCR, in plasma from patients with rhabdomyosarcoma at diagnosis **A**. Total level of cfDNA in patients with alveolar rhabdomyosarcoma (ARMS; n=17) and embryonal rhabdomyosarcoma (ERMS; n=37). Not shown are 1 case of spindle rhabdomyosarcoma (3.11 ng/ml), 1 case of botryoid rhabdomyosarcoma (9.08 ng/ml), and 1 case of rhabdomyosarcoma not-otherwise-specified (11.80 ng/ml). **B**. Total level of cfDNA in cases with localized disease and cases with metastatic disease. **C**. Total level of cfDNA in the indicated risk groups stratified according to the EpSSG RMS2005 study. **D**. Total level of cfDNA in ddPCR in the patients who experienced an event (relapse, progressive disease, or disease-related death). **E**. Total cfDNA concentration plotted against tumor volume at diagnosis. Note that the y-axes are on a log scale, and note the break in the x-axis in panel E. In this figure, each symbol represents an individual patient, and the red horizontal lines represent the median values. Tumor size was determined by MRI, CT-scan or ultrasonography.

Supplemental Table S1. Patient characteristics, cell-free (cfDNA) techniques applied at diagnosis, and outcome.

RMSnr	Patient characteristics					cfDNA technique			RNA	Survival outcome	
	Age ^a	Gender ^b	Histology ^c	Size ^d	Risk ^e	RASSF1A ^f	cfRRBS ^g	shWGS ^h	PB/BM ⁱ	Event ^j	DOD ^k
RMS004	2	2	0	2	5	1	-	-	1	1	1
RMS005	1	2	0	1	2	0	1	2	0	0	0
RMS007	2	1	1	2	5	1	-	1	1	1	1
RMS010	1	1	0	2	5	1	1	1	2	1	1
RMS011	1	1	1	2	5	1	0	2	0	1	1
RMS012	2	2	1	2	3	0	-	-	0	0	0
RMS013	1	2	0	1	2	0	-	-	0	0	0
RMS014	1	1	0	1	5	0	2	0	0	0	0
RMS017	2	1	0	2	5	1	1	1	2	1	1
RMS018	1	2	0	2	3	0	-	-	-	0	0
RMS022	1	1	0	2	5	1	1	1	2	1	1
RMS026	1	2	1	2	5	1	-	-	1	1	1
RMS027	2	1	0	1	2	0	1	1	0	0	0
RMS030	2	1	1	2	4	1	-	-	0	1	1
RMS032	1	1	2	1	2	1	-	-	0	0	0
RMS033	1	1	0	2	2	0	1	0	0	0	0
RMS037	2	1	1	2	5	0	-	-	1	0	0
RMS039	1	1	0	1	2	1	-	-	0	0	0
RMS044	1	1	0	1	2	0	1	0	0	0	0
RMS046	2	1	0	2	5	0	1	1	0	0	0
RMS047	0	1	0	1	2	1	1	1	0	0	0
RMS051	2	1	0	1	2	1	-	-	0	0	0
RMS052	2	1	0	2	3	0	2	0	0	0	0
RMS053	1	2	3	1	2	0	1	0	0	0	0
RMS060	1	1	0	2	3	0	1	2	0	0	0
RMS061	1	2	1	1	5	1	-	1	0	0	0
RMS063	2	1	0	1	2	0	1	0	0	0	0
RMS067	1	1	1	1	5	1	-	1	1	0	0
RMS071	2	2	1	1	3	0	-	-	0	0	0
RMS080	1	1	1	2	5	1	-	-	2	1	0
RMS083	1	2	1	2	4	1	-	-	0	0	0
RMS086	2	2	1	2	3	0	-	-	0	0	0
RMS087	1	2	0	1	2	0	2	1	1	1	0
RMS090	2	2	0	2	3	1	1	1	2	1	1
RMS092	2	1	1	2	5	1	-	1	1	1	1

Supplemental Table S1. Continued

RMSnr	Patient characteristics					cfDNA technique			RNA	Survival outcome	
	Age ^a	Gender ^b	Histology ^c	Size ^d	Risk ^e	RASSF1A ^f	cfRRBS ^g	shWGS ^h	PB/BM ⁱ	Event ^j	DOD ^k
RMS096	1	2	4	2	3	1	-	-	0	0	0
RMS102	2	1	0	1	2	0	1	0	0	0	0
RMS106	2	2	0	2	5	0	1	1	2	0	0
RMS109	1	2	1	2	3	0	-	-	0	0	0
RMS110	1	2	0	1	2	0	0	0	1	1	0
RMS116	1	1	0	1	2	0	1	0	0	0	0
RMS118	1	1	1	1	3	0	-	-	0	0	0
RMS120	1	1	0	2	2	0	1	0	0	0	0
RMS121	1	1	0	2	5	0	1	1	1	0	0
RMS122	2	1	0	2	5	0	1	1	0	0	0
RMS123	2	1	0	1	3	1	1	1	0	0	0
RMS125	1	2	0	1	2	0	1	0	0	0	0
RMS126	2	1	0	2	2	0	-	-	0	0	0
RMS127	2	1	1	1	5	1	-	-	1	0	0
RMS128	2	2	1	2	4	0	-	-	2	1	0
RMS129	1	2	0	2	5	0	-	-	1	0	0
RMS132	2	1	0	2	2	0	-	-	0	0	0
RMS136	1	1	0	2	2	0	-	-	0	0	0
RMS138	2	1	0	2	3	0	-	-	0	1	0
RMS139	1	1	0	1	1	0	-	-	0	0	0
RMS140	1	1	0	1	2	0	-	-	0	0	0
RMS141	1	1	0	2	5	0	-	-	0	0	0

-, test not performed; BM, bone marrow; cfRRBS, cell-free reduced representation bisulphite sequencing; DOD, died of disease; PB, peripheral blood; *RASSF1A*-M, methylated *RASSF1A*; RMSnr, patient research ID number (unique identifier); RNA, outcome of tumor-specific RNA panel as measured in blood and bone marrow; shWGS, shallow whole-genome sequencing;

^a 0, <1 year; 1, 1-10 years; 2, >10 years

^b 1, male; 2, female

^c 0, embryonal; 1, alveolar; 2, spindle; 3, botryoid; 4, not otherwise specified

^d 0, unknown; 1, <5 cm; 2, ≥5 cm

^e EpSSG RMS2005 risk group: 1, low risk; 2, standard risk; 3, high risk; 4, very high risk; 5, metastatic

^f 0, negative; 1, positive

^g 0, negative; 1, embryonal; 2, alveolar

^h 0, flat; 1, positive; 2, fail

ⁱ 0, negative in both PB and BM; 1, positive in PB; 2, positive in BM

^j 0, no event; 1, event (relapse, progressive disease, or disease-related death)

^k 0, alive; 1; died of disease

Supplemental Table S2. Detailed results of the various cell-free DNA (cfDNA) techniques performed on diagnostic plasma samples.

RMSnr	Result ^a	RASSF1A		cfRRBS		shWGS
		% RASSF1A-M ^b	Total cfDNA(ng/ml) ^c	Result ^d	Result ^e	CPAmscore
RMS004	1	13.94	6.87	-	-	
RMS005	0	0	40.19	1	2	
RMS007	1	14.04	21	-	1	
RMS010	1	7.8	56.65	1*	1†	3.6268
RMS011	1	3.67	11.51	0*	2†	
RMS012	0	0	15.4	-	-	
RMS013	0	0	12.71	-	-	
RMS014	0	0	9.46	2	0	0.3362
RMS017	1	42.04	11.15	1*	1†	
RMS018	0	0	13.09	-	-	
RMS022	1	78.14	6.87	1*	1†	
RMS026	1	92.75	428.69	-	-	
RMS027	0	0	12.96	1	1	0.3626
RMS030	1	48.03	8.95	-	-	
RMS032	1	71.28	3.11	-	-	
RMS033	0	0	6.48	1	0	0.3028
RMS037	0	0	21.91	-	-	
RMS039	1	8.54	7.26	-	-	
RMS044	0	0	62.23	1	0	0.3187
RMS046	0	0	12.16	1	1	0.4198
RMS047	1	27.98	6.48	1	1	3.831
RMS051	1	51.96	4.15	-	-	
RMS052	0	0	10.37	2	0	0.3437
RMS053	0	0	9.08	1	0	0.2884
RMS060	0	0	23.85	1	2	
RMS061	1	34.8	17.63	-	1†	
RMS063	0	0	7.78	1	0	0.2705
RMS067	1	15.12	18.21	-	1†	
RMS071	0	0	10.89	-	-	
RMS080	1	14.13	24.76	-	-	
RMS083	1	5.15	14.99	-	-	
RMS086	0	0	43.39	-	-	
RMS087	0	0	12.71	2	1	0.3573
RMS090	1	10.95	34.1	1	1	1.5756

Supplemental Table S2. Continued

RMSnr	RASSF1A			cfRRBS	shWGS	
	Result ^a	% RASSF1A-M ^b	Total cfDNA(ng/ml) ^c	Result ^d	Result ^e	CPAmscore
RMS092	1	33.77	117.07	-	1†	
RMS096	1	9.63	11.8	-	-	
RMS102	0	0	124.46	1	0	0.3532
RMS106	0	0	190.675	1	1	0.3568
RMS109	0	0	5.445	-	-	
RMS110	0	0	5.445	0	0	0.3095
RMS116	0	0	17.11	1	0	0.3409
RMS118	0	0	10.37	-	-	
RMS120	0	0	11.36	1	0	0.2782
RMS121	0	0	5.1	1	1	0.7034
RMS122	0	0	65.13	1	1	3.9445
RMS123	1	2	11.75	1	1	1.4441
RMS125	0	0	3.11	1	0	0.3143
RMS126	0	0	46.41	-	-	
RMS127	1	72.58	536.72	-	-	
RMS128	0	0	10.11	-	-	
RMS129	0	0	47.97	-	-	
RMS132	0	0	41.75	-	-	
RMS136	0	0	130.55	-	-	
RMS138	0	0	7.65	-	-	
RMS139	0	0	28.39	-	-	
RMS140	0	0	3.24	-	-	
RMS141	0	0	14	-	-	

-, test not performed; BM, bone marrow; cfRRBS, cell-free reduced representation bisulphite sequencing; CPAmscore, copy number tumor burden score; RASSF1A-M, methylated RASSF1A; RMSnr, patient research ID number (unique identifier); shWGS, shallow whole-genome sequencing.

^a 0, negative; 1, positive

^b Percentage of RASSF1A-M, calculated relative to total RASSF1A

^c Total level of cell-free DNA as determined using the reference gene ACTB

^d 0, negative; 1, embryonal; 2, alveolar

^e 0, flat; 1, positive; 2, fail

†= samples already included in paper by van Paemel et al (1)

Supplemental Table S3. Detailed results of diagnostic plasmas analyzed by RASSF1A-M ddPCR.

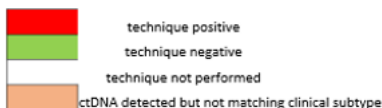
	RASSF1A	Droplets	ACTB	RASSF1A-M
RMSnr	Result ^a	RASSF1A-M+ ^b	copies/ml plasma	copies/ml plasma
RMS004	1	14	2082	251
RMS005	0	2	12179	19.6
RMS007	1	44	6364	707
RMS010	1	46	17168	825
RMS011	1	7	3488.571	97.43
RMS012	0	0	4667	0
RMS013	0	0	3850	0
RMS014	0	0	2868	0
RMS017	1	96	3379	1689
RMS018	0	2	3968	10
RMS022	1	80	2082	1257
RMS026	1	9223	129905	82762
RMS027	0	1	3929	24
RMS030	1	77	2711	1139
RMS032	1	24	943	358
RMS033	0	0	1964	0
RMS037	0	0	6639	0
RMS039	1	10	2200	165
RMS044	0	0	18857	0
RMS046	0	2	0	3685
RMS047	1	45	1964	483
RMS051	1	25	1257	511
RMS052	0	0	3143	0
RMS053	0	0	2750	0
RMS060	0	1	7229	31
RMS061	1	150	5343	2671
RMS063	0	0	2357	0
RMS067	1	142	5520	746
RMS071	0	0	3300	0
RMS080	1	47	7504	982
RMS083	1	43	4541	184
RMS086	0	0	13148	0
RMS087	0	0	3850	0
RMS090	1	160	10332	1159
RMS092	1	537	35475	11039

Supplemental Table S3. Continued

RMSnr	RASSF1A Result ^a	Droplets RASSF1A-M+ ^b	ACTB copies/ml plasma	RASSF1A-M copies/ml plasma
RMS096	1	11	3575	216
RMS102	0	0	37714	0
RMS106	0	0	5775	0
RMS109	0	0	1650	0
RMS110	0	0	1650	0
RMS116	0	0	5186	0
RMS118	0	0	3143	0
RMS120	0	0	3441	0
RMS121	0	3	1545	21.0
RMS122	0	2	19737	7.86
RMS123	1	9	3562	65.48
RMS125	0	1	943	7.9
RMS126	0	0	14064	0
RMS127	1	6162	162643	120607
RMS128	0	3	3064	59
RMS129	0	0	14536	0
RMS132	0	0	12650	0
RMS136	0	0	39561	0
RMS138	0	0	2318	0
RMS139	0	0	8604	0
RMS140	0	0	982	0
RMS141	0	0	4243	0

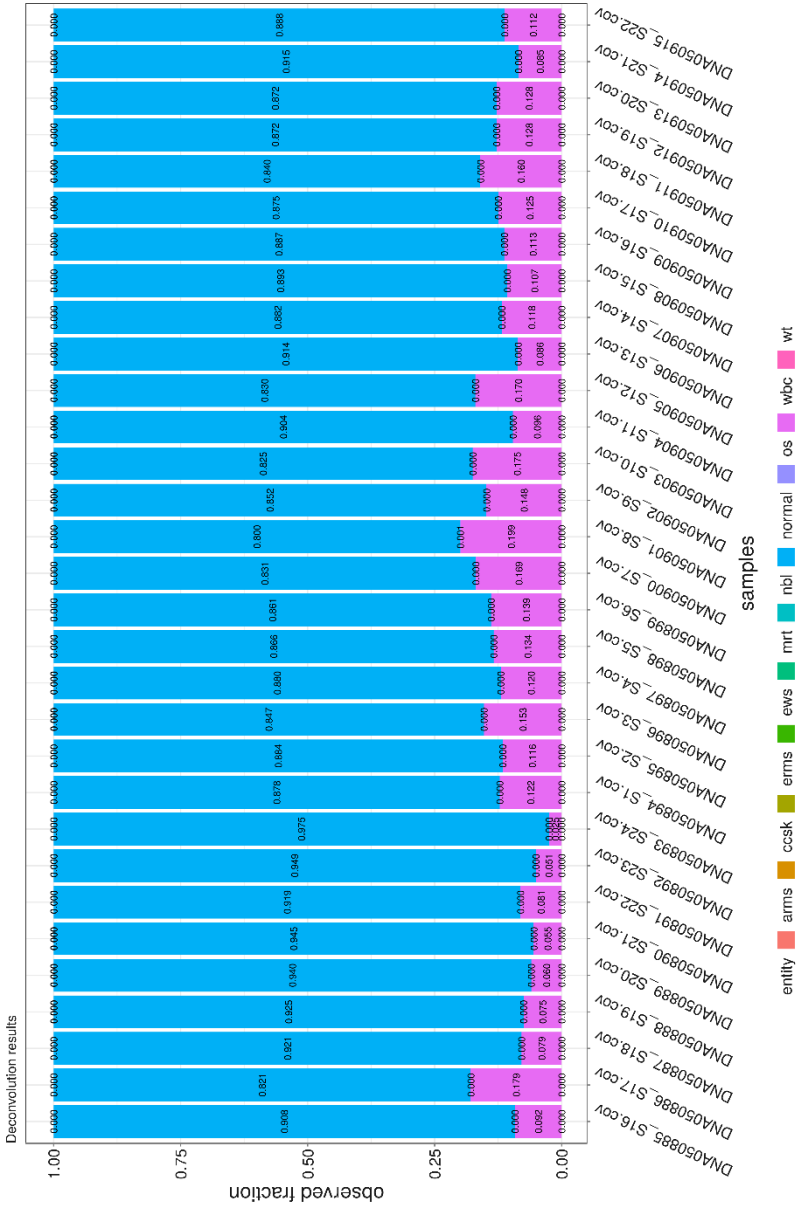
^a 0, negative; 1, positive^b number of RASSF1A-M positive droplets per sample

RMSnr	cfDNA			RNA panel	Outcome	
	cRRBS	shWGS	RASSF1A		Event	DOD
RMS092					1	1
RMS010					1	1
RMS017					1	1
RMS022					1	1
RMS047					0	0
RMS090					1	1
RMS123					0	0
RMS027					0	0
RMS046					0	0
RMS087					1	0
RMS106					0	0
RMS121					0	0
RMS122					0	0
RMS033					0	0
RMS044					0	0
RMS053					0	0
RMS063					0	0
RMS102					0	0
RMS116					0	0
RMS120					0	0
RMS125					0	0
RMS014					0	0
RMS052					0	0
RMS026					1	1
RMS080					1	0
RMS037					0	0
RMS128					1	0
RMS007					1	1
RMS061					0	0
RMS067					0	0
RMS011					1	1
RMS005					0	0
RMS060					0	0
RMS110					1	0
RMS004					1	1
RMS030					1	1
RMS032					0	0
RMS039					0	0
RMS051					0	0
RMS083					0	0
RMS096					0	0
RMS127					0	0
RMS012					0	0
RMS013					0	0
RMS018					0	0
RMS071					0	0
RMS086					0	0
RMS109					0	0
RMS118					0	0
RMS126					1	0
RMS129					0	0
RMS132					0	0
RMS136					0	0
RMS138					1	0
RMS139					0	0
RMS140					0	0
RMS141					0	0



Supplemental Figure S2. Results of the cell-free (cfDNA) techniques performed on diagnostic plasma samples, as well as testing rhabdomyosarcoma-specific RNA and survival outcome.

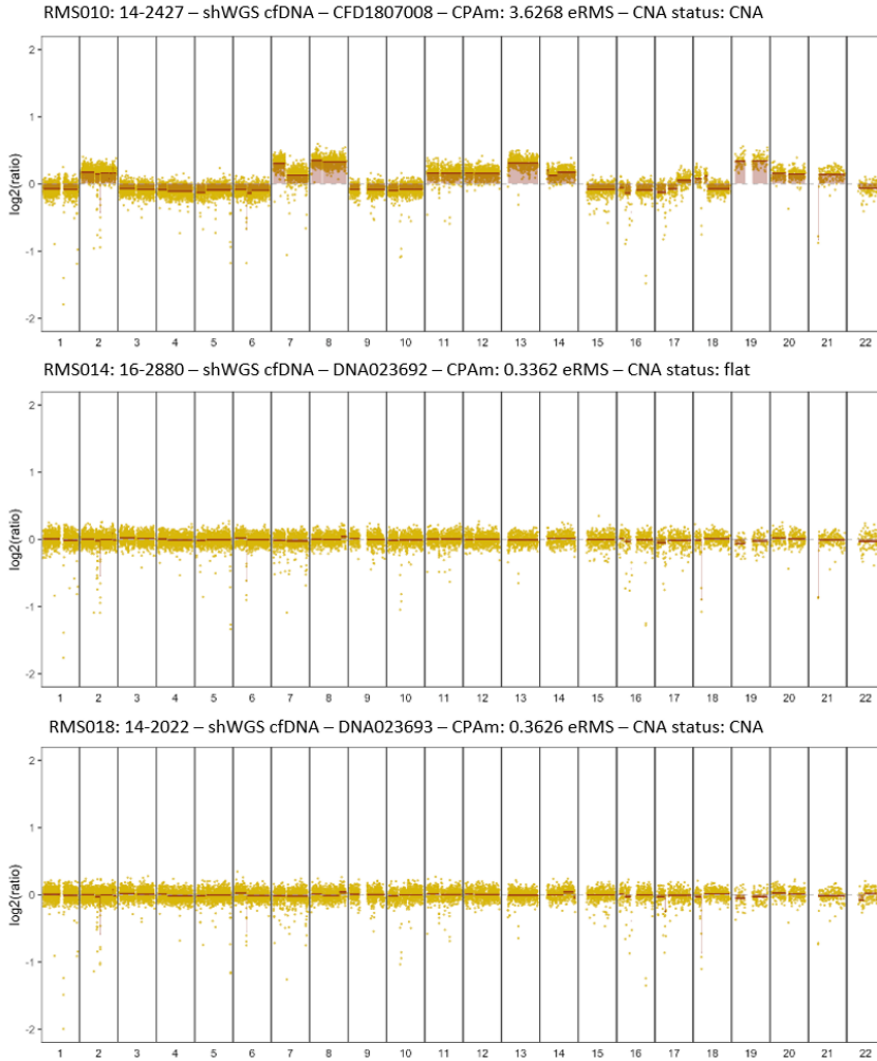
cfRRBS, cell-free reduced representation bisulphite sequencing; RNA panel, presence of rhabdomyosarcoma-specific RNA in the cellular fraction of blood and/or bone marrow; *RASSF1A*-M, methylated *RASSF1A*; RMSnr, patient research ID number (unique identifier); shWGS, shallow whole-genome sequencing. For events: 0, no event; 1, event (relapse, progressive disease, or disease-related death). For DOD: 0, alive; 1; died of disease.



Supplemental Figure S3. Results of cfRRBS on 31 cfDNA samples from plasma drawn from healthy controls.

Entities:

- arms: alveolar rhabdomyosarcoma
- ccsk: clear cell sarcoma of the kidney
- ems: embryonal rhabdomyosarcoma
- ewe: Ewing sarcoma
- mrt: malignant rhabdoid tumor
- nbl: neuroblastoma
- os: osteosarcoma
- wbc: white blood cell
- wt: Wilms tumor



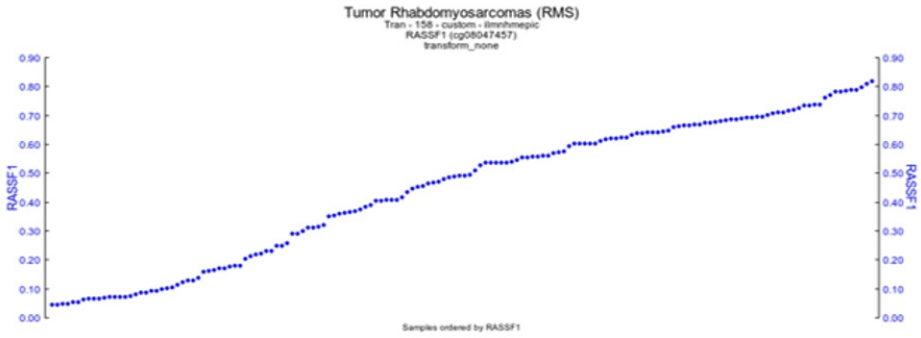
Supplemental Figure S4. Three representative examples of shWGS data obtained for three separate patients. Above each plot is the RMS patient ID, sample ID number, technique performed (shWGS on cfDNA), ID number for the technique, CPAm score, histologic subtype (in all case, embryonal), and CNA (copy number aberration) status. For this analysis, a 1% false discovery rate was set at 0.3549618.

A **Tumor Rhabdomyosarcomas (RMS) - Tran - 158 - custom - ilmnhmepic** public 4
 158 samples, transform_none

GeneID	Hugo	Description
11188	RASSF1	Ras association (Raf/GDS/AF-6) domain family member 1

R2 gene categories
RASSF1: low cycle, signal transduction

Significance of correlation:
r-value=1.000 p-value= 0.00e+00 T-value=279284800.875 degrees of freedom=156

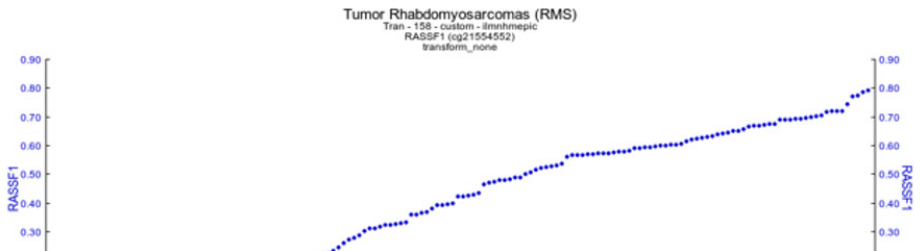


Tumor Rhabdomyosarcomas (RMS) - Tran - 158 - custom - ilmnhmepic public 4
 158 samples, transform_none

GeneID	Hugo	Description
11188	RASSF1	Ras association (Raf/GDS/AF-6) domain family member 1

R2 gene categories
RASSF1: low cycle, signal transduction

Significance of correlation:
r-value=1.000 p-value= 0.00e+00 T-value=279284800.875 degrees of freedom=156



Supplemental Figure S5. Overview of RASSF1A methylation in rhabdomyosarcoma tumors from 3 different datasets.



B Tumor Sarcoma classification - Deimling - 1020 - custom - ilmnhmepic ^{publ} ma(pleomorphic),rhabdomyosarcoma(spindlecell),rhabdomyosarcoma_(alveolar),rhabdomyo (n=82), transform_none

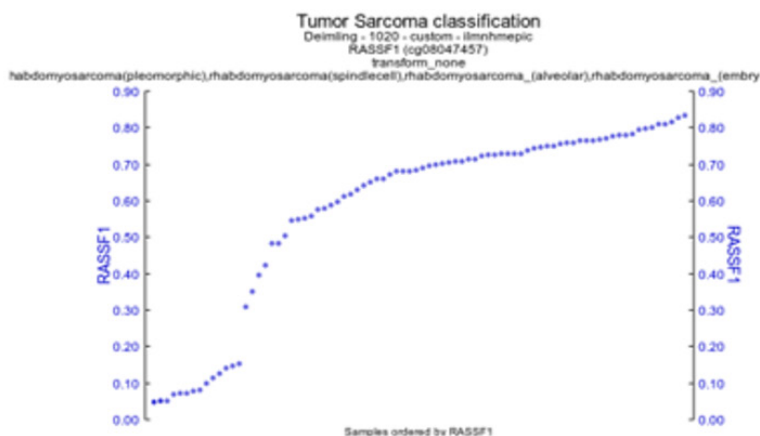
GeneID	Hugo	Description
11186	RASSF1	Ras association (Raf/GDS/AF-6) domain family member 1

R2 gene categories

RASSF1 *cell cycle, signal transduction*

Significance of correlation:

r-value=1.000 p-value= 0.00e+00 T-value=200000000.000 degrees of freedom=80



Tumor Sarcoma classification - Deimling - 1020 - custom - ilmnhmepic ^{publ} ma(pleomorphic),rhabdomyosarcoma(spindlecell),rhabdomyosarcoma_(alveolar),rhabdomyo (n=82), transform_none

GeneID	Hugo	Description
11186	RASSF1	Ras association (Raf/GDS/AF-6) domain family member 1

R2 gene categories

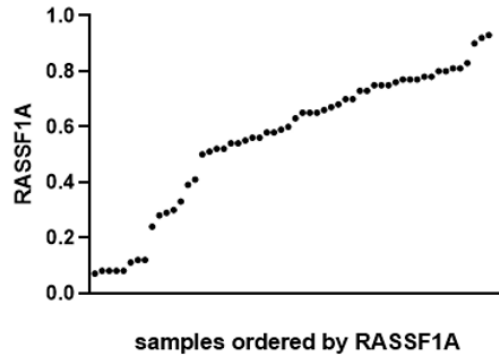
RASSF1 *cell cycle, signal transduction*

Significance of correlation:

r-value=1.000 p-value= 0.00e+00 T-value=200000000.000 degrees of freedom=80



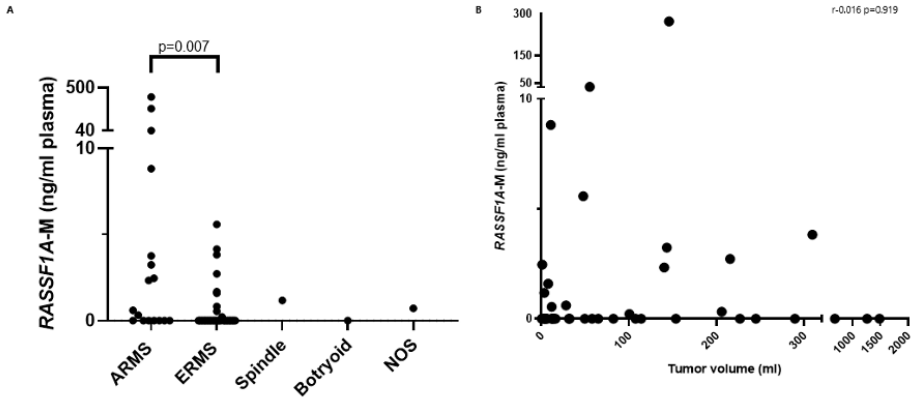
C Methylation of *RASSF1A* (cg00777121) in rhabdomyosarcoma (n=56) data from Seki et al



D

Dataset	Number of rhabdomyosarcoma tumors	Probe	Mean	Range
Tran	82	cg08047457	0.444	0.044-0.818
		cg21554552	0.394	0.032-0.791
Deimling	158	cg08047457	0.580	0.049-0.833
		cg21554552	0.540	0.04-0.850
Seki	56	cg00777121	0.790	0.073-0.933

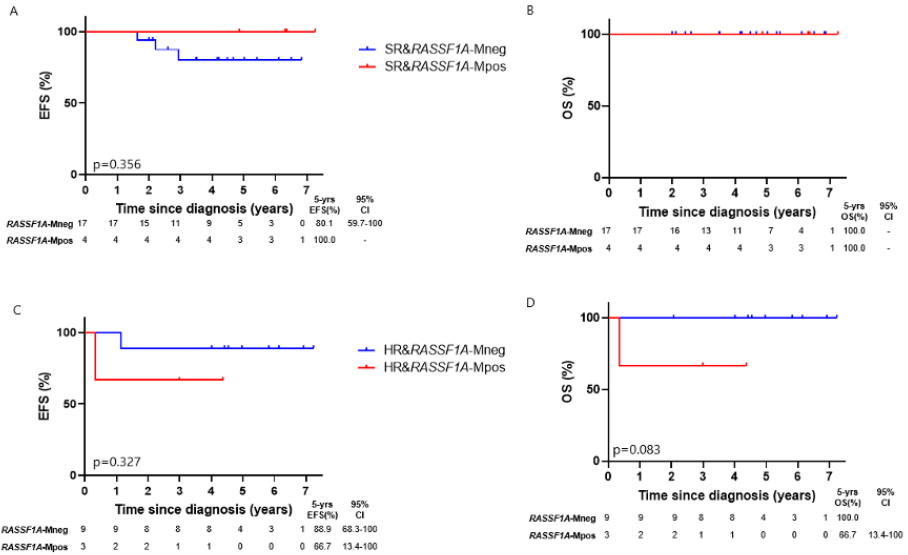
Supplemental Figure S5. Overview of *RASSF1A* methylation in rhabdomyosarcoma tumors from 3 different datasets. **A.** Data from Tran (as published in the paper by Clay *et al*(2)) analyzed in R2(3), on methylation of *RASSF1A* in 158 rhabdomyosarcoma tumors on cg08047457 and cg21554552, respectively (cg00777121 not available in this dataset). **B.** Data from Deimling (as published in the paper by Koelsche *et al*(4)) analyzed in R2(3), on methylation of *RASSF1A* in 82 rhabdomyosarcoma tumors on cg08047457 and cg21554552, respectively (cg00777121 not available in this dataset) **C.** Data on methylation of *RASSF1A* from the dataset from Seki et al (5) on cg00777121 (data on cg08047457 and cg21554552 not available), received on specific request. **D.** Overview of mean methylation (beta values) of the different datasets according to their respective Illumina probes and the range.



Supplemental Figure S6. Tumor-derived methylated *RASSF1A* (*RASSF1A*-M) in diagnostic plasma samples taken from patients with rhabdomyosarcoma. **A.** Total plasma levels of *RASSF1A*-M at diagnosis for patients with the indicated rhabdomyosarcoma subtypes. **B.** Total *RASSF1A*-M plotted against tumor volume. Note the break in the y-axis in panels A and B, and the break in the x-axis in panel B.

In this figure, each symbol represents an individual patient. Tumor size was determined by MRI, CT-scan or ultrasonography.

NOS, not otherwise specified.



Supplemental Figure S7. Survival outcome defined by detection of cell-free methylated *RASSF1A* (*RASSF1A-M*) at diagnosis. **A** and **B.** Event-free survival (EFS) overall survival (OS) of *RASSF1A-M*-negative patients (n=17) and *RASSF1A-M*-positive patients (n=4) with standard risk. **C** and **D.** EFS and OS of *RASSF1A-M*-negative patients (n=9) and *RASSF1A-M*-positive patients (n=3) with high risk.

Supplemental table S4. Number of patients tested by both *RASSF1A-M* ddPCR and shWGS for copy number aberration and number of events (in brackets).

RASSF1A-M	shWGS		
	Negative (events)	Positive (events)	Total (events)
Negative	11 (1)	6 (1)	17 (2)
positive	0	10 (6)	10 (6)
Total	11 (1)	16 (7)	27 (8)

Supplemental Table S5. Details on the samples that tested positive in the cellular fraction of blood and or bone marrow for the rhabdomyosarcoma-specific RNA panel.

RMSnr	RASSF1A-M ^a	RNA panel ^b	BM histology ^c	Event ^d	DOD ^e
RMS004	1	0	0	1	1
RMS007	1	2	1	1	1
RMS010	1	1	0	1	1
RMS017	1	1	0	1	1
RMS022	1	1	1	1	1
RMS026	1	2	1	1	1
RMS037	0	2	0	0	0
RMS067	1	2	1	0	0
RMS080	1	1	0	1	0
RMS087	0	0	0	1	0
RMS090	1	1	0	1	1
RMS092	1	2	1	1	1
RMS106	0	1	1	0	0
RMS110	0	0	0	1	0
RMS121	0	2	1	0	0
RMS127	1	2	1	0	0
RMS128	0	1	0	1	0
RMS129	0	0	0	0	0

BM, bone marrow; DOD, died of disease; *RASSF1A-M*, methylated *RASSF1A* as measured by ddPCR on cfDNA; RMSnr, patient research ID number (unique identifier);

^a 0, negative; 1, positive

^b 0, only peripheral blood positive; 1, only bone marrow positive; 2, blood and bone marrow positive

^c 0, bone marrow negative by conventional immunohistochemistry; 1, bone marrow positive by conventional immunohistochemistry

^d 0, no event; 1, event (relapse, progressive disease, death)

^e 0, alive; 1, died of disease

Supplemental Table S6. Hazard ratios with 95% CI estimated with an univariate Cox proportional hazard regression model for event-free survival.

	Hazard ratio (95% CI)
<i>RASSF1A</i>-M-positive	5.03 (1.75-14.52)
RNA-positive	10.01 (3.22-31.09)
Standard risk	1
High risk	1.79 (0.36-8.87)
Metastatic disease	4.19 (1.13-15.53)
Localized vs metastatic disease	2.97 (1.10-8.01)
Alveolar rhabdomyosarcoma subtype	2.07 (0.80-5.35)
Age >10 years	2.38 (0.90-6.27)
Tumor size >5cm	7.21 (1.64-31.62)
Lymph node involvement	1.89 (0.70-5.08)

RASSF1A-M, methylated *RASSF1A*; RNA-positive, positive for rhabdomyosarcoma-specific RNA panel in blood and/or bone marrow.

Supplemental Table S7. Overview of all plasma samples available for 10 patients tested positive for *RASSF1A-M* during primary treatment or during an event.

RMSnr	Time point	<i>RASSF1A-M</i>	
		% <i>RASSF1A-M</i>	Total cfDNA (ng/ml)
RMS025	2nd relapse	0.63	10.94
RMS025	3 month 2nd relapse	0	9.13
RMS025	Eot 2nd relapse	0	17.89
RMS026	Diagnosis	92.75	428.69
RMS026	Before 5 CT	0	9.85
RMS026	6 month maint	0	5.70
RMS026	FUP	0	13.14
RMS061	Diagnosis	34.8	17.63
RMS061	After 2 CT	64.25	15.82
RMS061	After 4 CT	0	23.72
RMS061	1 month maint	0	27.38
RMS061	3 month maint	0	10.8
RMS061	9 month maint	0	9.33
RMS061	4 months after end of maint	0	12.71
RMS073	1st relapse	3.83	7.67
RMS080	Diagnosis	14.13	24.76
RMS080	1st relapse	0.59	11.1
RMS083	Diagnosis	5.15	14.99
RMS083	After 2 CT	0.33	62.02
RMS083	After 3 CT	0	9.44
RMS083	After 4 CT	0	12.86
RMS083	Eot	0	9.01
RMS083	3 month maint	0	16.49
RMS083	End of maint	0	10.16
RMS092	Diagnosis	33.77	117.07
RMS092	Before 2 CT	0	27.61
RMS092	After 3 CT	0	20.48
RMS092	Eot	0	44.60
RMS092	4 month PD	0	22.30
RMS092	10 month PD	0	9.33
RMS092	14 month PD	0	14.57
RMS131	2nd relapse	0	8.30
RMS133	PD in prim	0	8.29
RMS137	1st relapse	13.49	34.54

-, test not performed; 3 month 2nd relapse, 3 months of relapse therapy for the second relapse; 3 month PD, 3 months of progressive disease therapy; 6 month maint, 6 months of maintenance therapy; Bkpt, patient-specific fusion gene breakpoint; CT, chemotherapy course; Eot, end of treatment; FUP, during clinical follow-up without therapy; PD in prim, progressive disease during primary treatment; *RASSF1A-M*, methylated *RASSF1A*; RMSnr, patient research ID number (unique identifier).

Supplemental Table S3. Detailed results of follow-up plasmas analyzed by RASSF1A-M ddPCR.

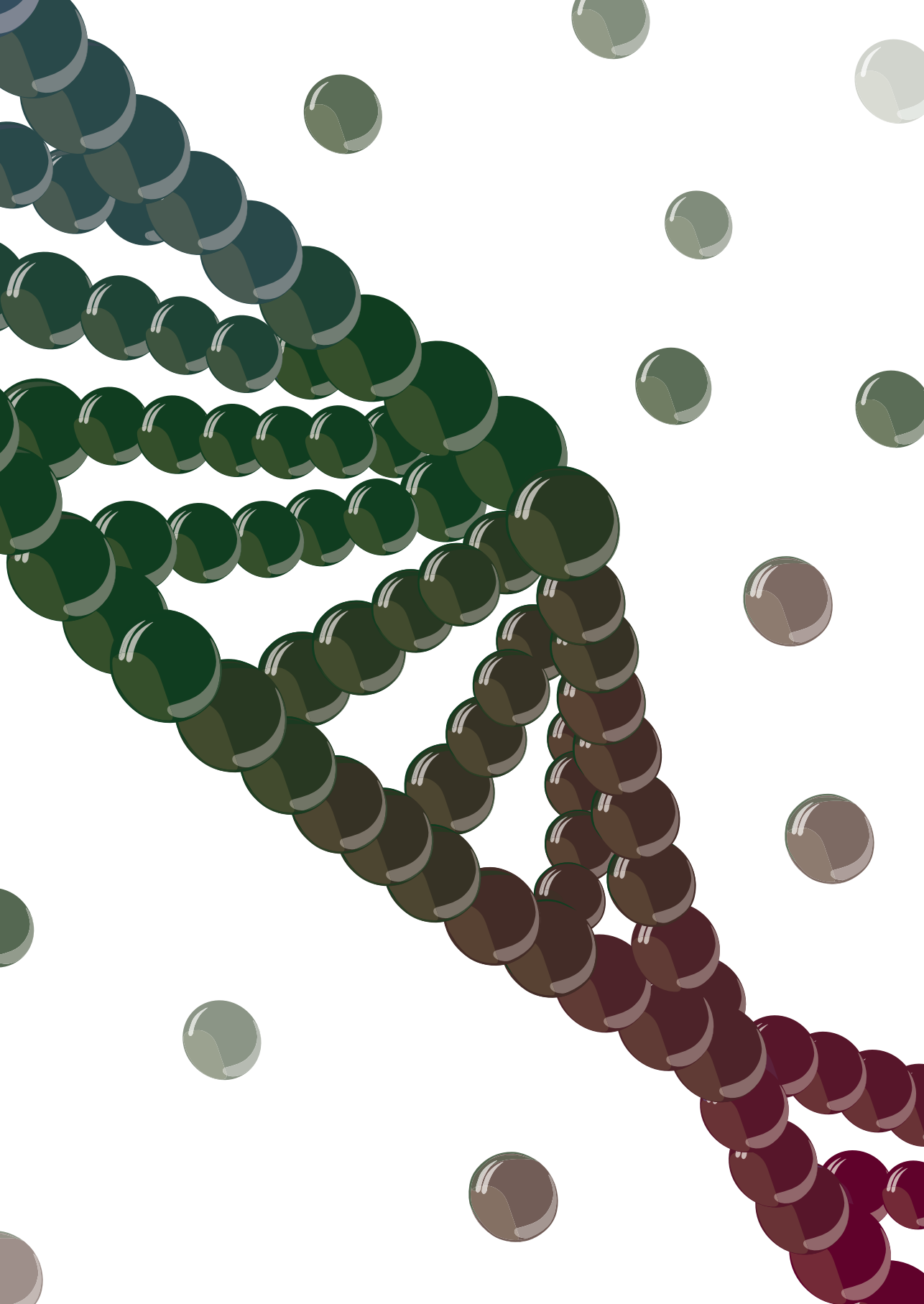
RMSnr	Time point	RASSF1A-M result ^a	RASSF1A-M+ droplets ^b	ACTB copies/ml plasma	RASSf1A-M copies/ml plasma
RMS025	3 month 2nd relapse	0	0	2766	0
RMS025	Eot 2nd relapse	0	0	5421	0
RMS026	Diagnosis	1	9223	129905	82762
RMS026	Before 5 CT	0	1	2986	8
RMS026	6 month maint	0	0	1729	0
RMS026	FUP	0	0	3981	0
RMS061	Diagnosis	1	150	5343	2671
RMS061	After 2 CT	1	0	27284	0
RMS061	After 4 CT	0	0	7189	0
RMS061	1 month maint	0	0	8297.142857	0
RMS061	3 month maint	0	0	3274	0
RMS061	9 month maint	0	1	2828.571429	31
RMS061	4 months after end of maint	0	1	3850	8
RMS073	1st relapse	1	19	2325.714286	77
RMS080	Diagnosis	1	47	7503.571429	982
RMS080	1st relapse	1	4	3362.857143	20
RMS083	Diagnosis	1	43	4541	184
RMS083	After 2 CT	1	16	18794	72
RMS083	After 3 CT	0	1	2860	5
RMS083	After 4 CT	0	0	3897	0
RMS083	Eot	0	0	2730	0
RMS083	3 month maint	0	0	4997	0
RMS083	End of maint	0	0	3080	0
RMS092	Diagnosis	1	537	35475	11039
RMS092	Before 2 CT	0	1	8368	6
RMS092	After 3 CT	0	0	6207	0
RMS092	Eot	0	1	13514	12
RMS092	4 month PD	0	0	6757	0
RMS092	10 month PD	0	0	2829	0
RMS092	14 month PD	0	0	4416	0
RMS131	2nd relapse	0	7854	54057	37871
RMS133	PD in prim	0	0	2514	0
RMS137	1st relapse	1	268	10466	1226

^a 0, negative; 1, positive^b number of RASSF1A-M positive droplets per sample

References for Supplemental Figures and Tables

1. Van Paemel R, Vandeputte C, Raman L, Van Thorre J, Willems L, Van Dorpe J, et al. The feasibility of using liquid biopsies as a complementary assay for copy number aberration profiling in routinely collected paediatric cancer patient samples. *Eur J Cancer*. 2021.
2. Clay MR, Patel A, Tran Q, Hedges DJ, Chang TC, Stewart E, et al. Methylation profiling reveals novel molecular classes of rhabdomyosarcoma. *Sci Rep*. 2021;11(1):22213.
3. R2: Genomics Analysis and Visualization Platform
4. Koelsche C, Schrimpf D, Stichel D, Sill M, Sahm F, Reuss DE, et al. Sarcoma classification by DNA methylation profiling. *Nat Commun*. 2021;12(1):498.
5. Seki M, Nishimura R, Yoshida K, Shimamura T, Shiraishi Y, Sato Y, et al. Integrated genetic and epigenetic analysis defines novel molecular subgroups in rhabdomyosarcoma. *Nat Commun*. 2015;6:7557.





Molecular characterisation of circulating tumor DNA in pediatric rhabdomyosarcoma: a feasibility study

JCO Precis Oncol. 2022 Oct;6:e2100534. doi: 10.1200/PO.21.00534.

Olivia Ruhen,¹ Nathalie S.M. Lak^{2,3} Janine Stutterheim^{2,3} Sara G. Danielli,⁴ Mathieu Chicard,⁵ Yasmine Iddir,⁵ Alexandra Saint-Charles,⁵ Virginia Di Paolo,⁶ Lucia Tombolan,⁷ Susanne A. Gatz,^{1,8} Ewa Aladowicz,¹ Paula Proszek,^{1,9} Sabri Jamal,^{1,9} Reda Stankunaite,^{1,9,10} Deborah Hughes,^{1,9} Paul Carter,^{1,9} Elisa Izquierdo,^{1,9} Ajla Wasti,¹¹ Julia C. Chisholm,^{11,12} Sally L. George,^{1,11} Erika Pace,^{11,13} Louis Chesler,^{1,11} Isabelle Aerts,⁵ Gaëlle Pierron,⁵ Sakina Zaidi,¹⁴ Olivier Delattre,¹⁴ Didier Surdez,^{14,15} Anna Kelsey,¹⁶ Michael Hubank,^{1,9} Paolo Bonvini,⁷ Gianni Bisogno,¹⁷ Angela Di Giannatale,⁶ Gudrun Schleiermacher,^{5,18} Beat W. Schäfer,⁴ Godelieve A.M. Tytgat,^{2,3} and Janet Shipley,¹

¹Division of Molecular Pathology, The Institute of Cancer Research, London, United Kingdom ²Princess Máxima Center for Pediatric Oncology, Utrecht, the Netherlands ³Experimental Immunohematology, Sanquin, Amsterdam, the Netherlands ⁴Department of Oncology and Children's Research Centre, University Children's Hospital, Zurich, Switzerland ⁵SiRIC RTOP (Recherche Translationnelle en Oncologie Pédiatrique), Institut Curie, Paris, France ⁶Department of Pediatric Haematology/Oncology, Bambino Gesù Children's Hospital, IRCCS, Rome, Italy ⁷Institute of Pediatric Research, Fondazione Città della Speranza, Padova, Italy ⁸Institute of Cancer and Genomic Sciences, University of Birmingham, Birmingham, United Kingdom ⁹Molecular Diagnostics, Royal Marsden NHS Foundation Trust, London, United Kingdom ¹⁰Centre for Evolution and Cancer, The Institute of Cancer Research, London, United Kingdom ¹¹Children & Young People's Unit, Royal Marsden NHS Foundation Trust, London, United Kingdom ¹²Division of Clinical Studies, The Institute of Cancer Research, London, United Kingdom ¹³Department of Diagnostic Radiology, Royal Marsden NHS Foundation Trust, London, United Kingdom ¹⁴INSERM U830, Équipe Labellisée LNCC, PSL Research University, SIREDO Oncology Centre, Institut Curie, Paris, France ¹⁵Bone Sarcoma Research Laboratory, Balgrist University Hospital, University of Zurich, Zurich, Switzerland ¹⁶Department of Pediatric Histopathology, Manchester University Foundation Trust, Manchester, United Kingdom ¹⁷Department of Woman's and Children's Health, Hematology and Oncology Unit, University of Padova, Padova, Italy ¹⁸Department of Pediatric Oncology, Hospital Group, Institut Curie, Paris, France

Abstract

Purpose: Rhabdomyosarcomas (RMS) are rare neoplasms affecting children and young adults. Efforts to improve patient survival have been undermined by a lack of suitable disease markers. Plasma circulating tumor DNA (ctDNA) has shown promise as a potential minimally-invasive biomarker and monitoring tool in other cancers; however, it remains under-explored in RMS. We aimed to determine the feasibility of identifying and quantifying ctDNA in plasma as a marker of disease burden and/or treatment response using blood samples from RMS mouse models and patients.

Patients and methods: We established mouse models of RMS and applied qPCR and droplet digital PCR (ddPCR) to detect ctDNA within the mouse plasma. Potential driver mutations, copy number alterations, and DNA breakpoints associated with PAX3/7- FOXO1 gene fusions were identified in the RMS samples collected at diagnosis. Patient-matched plasma samples collected from 28 RMS patients prior to, during, and after treatment were analyzed for the presence of ctDNA via ddPCR, panel sequencing and/or whole-exome sequencing.

Results: Human tumor-derived DNA was detectable in plasma samples from mouse models of RMS and correlated with tumor burden. In patients, ctDNA was detected in 14/18 pre-treatment plasma samples with ddPCR and 7/7 cases assessed by sequencing. Levels of ctDNA at diagnosis were significantly higher in patients with unfavorable tumor sites, positive nodal status, and metastasis. In patients with serial plasma samples (n=18), fluctuations in ctDNA levels corresponded to treatment response.

Conclusions: Comprehensive ctDNA analysis combining high sensitivity and throughput can identify key molecular drivers in RMS models and patients, suggesting potential as a minimally-invasive biomarker. Preclinical assessment of treatments using mouse models and further patient testing through prospective clinical trials are now warranted

Context summary

Key objective: Whilst overall survival for children with rhabdomyosarcoma has improved, patients with high-risk and refractory disease continue to experience poor outcomes. This international collaborative pilot study aimed to assess the feasibility of detecting and quantifying circulating tumor DNA (ctDNA) in mouse models of and patients with rhabdomyosarcoma and investigate its relationship with clinical variables and outcome.

Knowledge generated: We provide evidence to suggest that ctDNA is a surrogate marker of tumor burden in animal models of rhabdomyosarcoma and demonstrate feasibility for detecting and quantifying ctDNA in serial plasma samples from rhabdomyosarcoma patients via several approaches including whole-exome and targeted sequencing and droplet digital PCR.

Relevance: Our data indicates that ctDNA holds potential as a minimally-invasive biomarker in rhabdomyosarcoma, providing evidence for its assessment in future preclinical animal model trials and prospective clinical trials

Introduction

Rhabdomyosarcoma (RMS), the most common soft tissue sarcoma in children, is a major cause of pediatric cancer-related death.¹ Outcomes for patients with high-risk or relapsed RMS remain particularly poor.² There is an urgent need to develop accurate prognostic and predictive markers and monitoring tools that can better identify patients at risk of treatment failure. This knowledge can aid in treatment decision making and the identification of patients who may benefit from participation in trials of novel therapeutics.

Molecular profiling of RMS tumors has identified several oncogenic drivers that hold potential as disease biomarkers. Alveolar subtype neoplasms (aRMS) commonly harbor the chromosomal translocations t(2;13) (q35;q14) or t(1;13) (p36;q14), which result in a fusion between the genes FOXO1 and PAX3 or PAX7, respectively.^{3,4} Crucially, PAX3-FOXO1 fusions are associated with an unfavorable patient prognosis.^{2,5} By contrast, embryonal RMS (eRMS) is characterized by mutations to key members of the AKT-PI3K and RAS pathways, some of which are predictive for response to certain molecular therapies.⁶ RMS can also carry copy-number variants such as amplifications of the CDK4 and MYCN genes.⁶ Hence, there is increasing evidence to support the screening of RMS for clinically relevant molecular alterations.

Recent research has focused on the assessment of blood-based biomarkers, such as cell-free DNA (cfDNA) and its malignant counterpart circulating tumor DNA (ctDNA), as a minimally invasive modality for tumor molecular profiling. This liquid biopsy approach is advantageous over tissue biopsies as it can provide a dynamic measurement of tumor activity in real time, allowing patient response to treatment to be monitored throughout their disease. Many studies have demonstrated the feasibility of using ctDNA for the diagnosis, prognosis, and monitoring of

adult cancers.⁷ However, the assessment of ctDNA in pediatric patients with RMS has thus far been limited. Quantitative polymerase chain reaction (qPCR), targeted sequencing panels, and whole-genome sequencing have previously been used to detect the PAX3-FOXO1 gene fusion in ctDNA from a limited number of patients with aRMS.⁸⁻¹⁰ However, more evidence is needed (particularly for eRMS or fusion-negative patients) to support the clinical utility of ctDNA in this tumor type.

In this large international collaborative study, we applied several techniques including panel sequencing, whole-exome sequencing (WES), qPCR, and droplet digital PCR (ddPCR) to identify molecular drivers in pediatric RMS and quantify ctDNA in RMS patients and models.

Methods

Animal Experiments

Three patient-derived xenografts (PDX) were established by implanting RMS patient tumor biopsy samples in immunodeficient non scid gamma (NSG) mice, as previously described (Data Supplement for PDX characteristics).¹¹ For the aRMS PDX experiments, dissociated tumor cells from established xenografts were expanded in culture and labeled with enhanced green fluorescent protein (EGFP) (Data Supplement). One million IC-pPDX-104 EGFP or IC-pPDX-29 EGFP cells were injected orthotopically into the hind limb muscle of seven and five NSG mice, respectively. Tumor size was measured 3 times per week using calipers. Blood (100 μ L) was collected via the lateral tail vein every week in IC-pPDX-29–injected mice and from the day tumors started to be visible in IC-pPDX-104–injected mice (day 32) until the end point of the experiment, upon which the mice were anesthetized with a lethal dose of ketamine-xylazine and 250–1,000 μ L blood was collected through cardiac puncture. Plasma ctDNA and cfDNA were measured by SYBR Green-based qPCR using hLINE-1 and mPtger2 primer sets, respectively (Data Supplement). For the eRMS PDX experiments in ICR-PDX-RMS008, blood was collected from NSG mice during routine passaging of PDX tumor pieces. These pieces were implanted bilaterally in five NSG mice, with four mice developing tumors and one mouse no tumors. Blood (230–550 μ L) was collected through cardiac puncture after lethal anesthetic. Tumor-specific variants in cfDNA were quantified with ddPCR.

Patients and Samples

Blood and tissue samples were obtained from pediatric cancer patients ($n = 48$) with RMS according to institutional review board–approved protocols. To be included in the study, subjects had to be between age 0 and 18 years with a pathologic diagnosis of RMS. There

were no exclusion criteria. Samples were collected after obtaining written informed consent from patients, parents, or legal guardians. Participating institutions included Bambino Gesù Children's Hospital, Rome (protocol number 578); University-Hospital, Padova (4115/AO/17); Institut Curie, Paris (ClinicalTrials.gov identifier: NCT02546453); University Children's Hospital, Zurich (2020-01609); Princess Máxima Centre for Pediatric Oncology, Utrecht (METC2006-148 and PMCLAB2019-053); and The Institute of Cancer Research/Royal Marsden Hospital, London (13/LO/0254, 15/LO/0719 and 18/LO/1860).

Plasma was separated from blood collected in EDTA and DNA extracted from patient's plasma, and fresh, cultured, or formalin-fixed paraffin-embedded tumor tissue according to local standard operating procedures (Data Supplement). Targeted locus amplification, WES, and targeted sequencing with two custom sequencing panels were performed on patient tumor DNA and germline DNA (where available) to identify patient-specific genetic variants of interest (Data Supplement).¹²

ddPCR

Patient and ICR-PDX-RMS008 cfDNA were assessed for the presence of tumor-specific genetic variants by ddPCR, which was performed on the Bio-Rad QX200 ddPCR system as per manufacturer's instructions (Data Supplement). Plasma ctDNA and cfDNA were measured by assays targeting tumor-specific variants and reference genes, respectively (Data Supplement).

Targeted Sequencing

Baseline cfDNA samples from seven cases with sufficient DNA (10 ng) were analyzed by WES alongside patient-matched germline DNA and tumor DNA from fresh-frozen material, as previously described (Data Supplement).¹³ Serial cfDNA samples were also sequenced with a targeted sequencing panel that was designed to encompass 196 single-nucleotide variants (SNVs), corresponding to all SNVs observed in WES sequencing and 44 single-nucleotide polymorphisms to identify each sample. Libraries of cfDNA were constructed using a double-capture procedure. Samples were multiplexed for the capture and sequenced with HiSeq reagents (Illumina, Cambridgeshire, UK; expected coverage: 5,000×). Variants were filtered according to an established bioinformatic pipeline.¹³ For serial plasma samples, variants with < 10 supporting reads were excluded from the final data set.

Statistical Analysis

Statistical analysis was performed using GraphPad Prism v9.0 (GraphPad Software). Pearson's correlation was performed to assess the relationship between mouse plasma ctDNA levels and tumor size or weight. To test whether detection of ctDNA

at baseline was associated with clinical features such as tumor size, a two-sided Fisher's exact test was used. A two-tailed Mann-Whitney U test was used to verify the hypothesis that patients with tumors in an unfavorable site (favorable tumor sites include the biliary tract, orbit, head and neck [excluding parameningeal sites] and the genitourinary tract [excluding bladder and prostate]; unfavorable tumor sites are those arising in all other anatomical locations, including [but not limited to] parameningeal sites, the bladder or prostate, and extremities), nodal spread, or metastases had higher pretreatment ctDNA levels than those who did not. The results were considered statistically significant when $P < .05$.

Results

CtDNA Can Be Detected in Animal Models of RMS and Correlates With Tumor Burden

In PDX models, human tumor DNA can be easily discriminated from host mouse DNA by targeting human-specific or tumor-specific sequences such as the chromosomal translocation PAX3-FOXO1 breakpoint or SNVs. Using serial dilutions of human tumor DNA and mouse plasma cfDNA, we established that hLINE-1 primers were optimal for detecting human DNA and mPtger2 for identifying mouse DNA in aRMS models (Data Supplement). We then tested whether ctDNA could be found in the blood of mice transplanted with aRMS PDXs. Blood samples were collected weekly until mice reached maximal tumor size (Fig 1A). Plasma ctDNA and cfDNA levels were quantified with hLINE-1 and mPtger2 primer sets, respectively. At the earliest time points after tumor injection, ctDNA was detected in only a fraction of the animals, but detection rates increased to 100% at later time points (Figs 1B and 1C). Similar to tumor volumes, ctDNA levels increased during the course of the experiment and ranged from nondetectable up to 25.3 ± 2.0 ng/mL blood in IC-pPDX-29 (Fig 1D), and 17.7 ± 2.3 ng/mL blood in IC-pPDX-104 (Fig 1E). A significantly positive Pearson correlation was observed between ctDNA and tumor volume in both aRMS PDXs (Figs 1F and 1G). Importantly, no significant correlation was observed between tumor volume and cfDNA (Figs 1H and 1I), whose levels remained relatively stable during the entire course of the experiment (IC-pPDX-29: 33.9 ± 3.8 ng/mL blood; IC-pPDX-104: 14.4 ± 3.1 ng/mL blood). In the eRMS PDX, tumor-specific variants (Data Supplement) were identified in all four cfDNA samples from tumor-bearing mice, whereas the plasma sample from the mouse that did not grow a tumor had no detectable ctDNA (Data Supplement). These results demonstrate feasibility to detecting human ctDNA in mouse models of RMS and using ctDNA as a marker to monitor tumor growth, providing the rationale for moving forward with patients' samples.

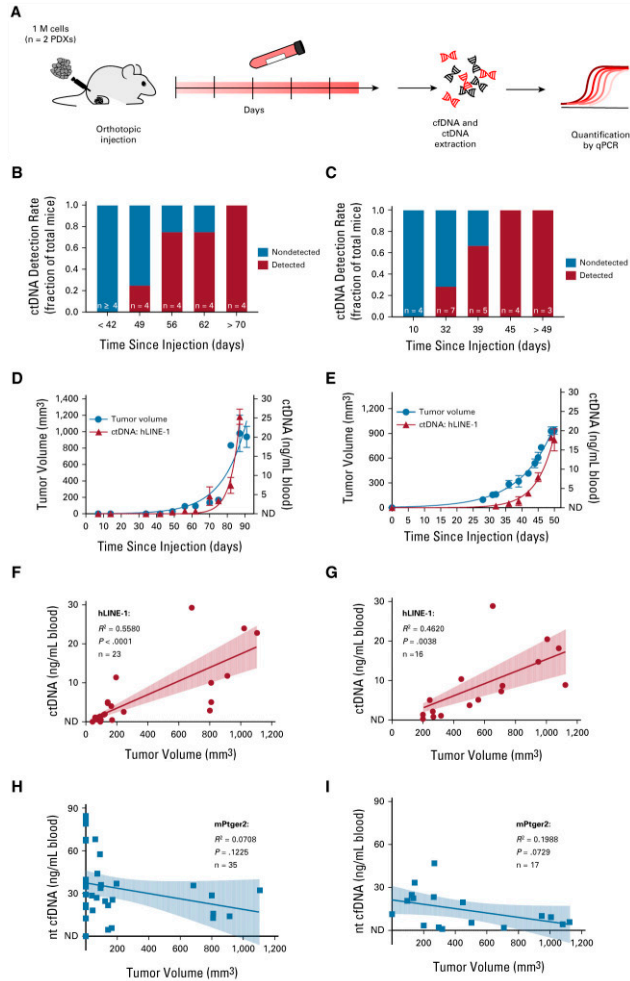


Figure 1. ctDNA correlates with tumor burden in RMS PDX models. **(A)** Experimental design. After orthotopic PDX injection, blood was collected weekly until the end point of the experiment. Plasma ctDNA was measured by qPCR using hLINE-1 primer sets; nontumor cfDNA was quantified with mPter2 primer set. Detection rate of plasma ctDNA at different time points after tumor injection of IC-pPDX-29 **(B)** or ICpPDX-104 cells **(C)**. The number of mice at the selected time points is indicated. Monitoring of ctDNA concentration and tumor volume over time in mice injected with **(D)** IC-pPDX-29 or **(E)** ICpPDX-104 cells. Tumor volume was measured 3 times a week, whereas plasma ctDNA was measured at the selected time points. Data are represented as mean \pm SEM of $n \geq 2$ animals and connected with an exponential growth curve fit. Correlation between tumor volume and plasma **(F and G)** ctDNA or **(H and I)** cfDNA in mice injected with **(F and H)** IC-pPDX-29 or **(G and I)** ICpPDX-104 cells. Data points are interpolated with a linear regression. Correlation coefficient (R^2), statistical significance (P), and number of data points (n) are indicated. cfDNA, cell-free DNA; ctDNA, circulating tumor DNA; ND, nondetectable; PCR, polymerase chain reaction; PDX, patient-derived xenograft; qPCR, quantitative PCR; RMS, rhabdomyosarcoma.

Patient Cohort

A summary of the samples collected and successfully analyzed is illustrated in Figure 2A. Of the 48 patients, 28 had targetable tumor variants and sufficient cfDNA to analyze (see Tables 1 and 2 for clinical characteristics). Baseline plasma samples (collected at diagnosis) were available for 25/28 (89%) patients (20 frontline and five relapse), whereas serial plasma samples collected during treatment (mean 4, range 2-7) were available for 18/28 (64%) patients (17 frontline and one relapse).

CtDNA Can Be Detected in Baseline Plasma Samples by ddPCR and Is Associated With Clinical Features in Patients With RMS

Across all baseline plasma samples assessed by ddPCR ($n = 18$), the median total cfDNA yield was 38.2 ng/mL plasma (range 3.9-1,857.5 ng/mL). Patients with nodal spread (N1) had significantly higher baseline cfDNA compared with those without it (N0; $P = .035$; Fig 2B), but there was no significant association between plasma cfDNA levels and characteristics such as tumor size, histology, site, or patient clinical risk group.

A tumor-specific variant was detected in 14/18 baseline samples, demonstrating 78% concordance with tumor tissue (Table 3). A patient-specific PAX3/7-FOXO1 fusion was exhibited in 10/11 (91%) baseline cfDNA samples from fusion-positive patients, whereas mutations and copy-number variants were seen in 3 of 5 (60%) and 1 of 2 (50%) patients, respectively.

Baseline ctDNA levels were significantly higher in frontline patients with an unfavorable tumor site and positive nodal status (mean = 0, median = 0 v mean = 124.9, median = 13.9 ng/mL plasma for favorable v unfavorable, $P = .021$, Fig 2C; and mean = 2.2, median = 1.1 v mean = 176.5, median = 41.6 ng/mL plasma for N0 versus N1, $P = .043$, Fig 2D). Both frontline and relapsed patients with metastasis at diagnosis had significantly higher ctDNA levels at baseline (mean = 97.3, median = 6.6 ng/mL plasma) compared with those without it (mean = 0.5, median = 0 ng/mL plasma, $P = .0201$, Fig 2E). These results support the utility of ddPCR for the detection of ctDNA in patients with RMS and suggest that diagnostic ctDNA levels are related to disease aggressiveness.

The Molecular Profile of Baseline ctDNA Demonstrates Concordance With That of the Primary Tumor in Frontline RMS Patients

To more comprehensively assess the extent to which the genomic landscape of patient ctDNA reflects that of the primary tumor, we performed WES on seven

patients with matched tumor, germline, and baseline cfDNA. ctDNA was detected in all (100%) baseline plasma samples. A mean of nine SNVs per case were common to both the baseline cfDNA and primary tumor (range 3-26 SNVs), with a mean of 1 (range 0-2) SNV detected only in the cfDNA, and a mean of 10 SNVs (range 0-48) seen only in the tumor (Fig 2F). The latter were mainly observed in eRMS. These data demonstrate that patient ctDNA collected at the time of diagnosis largely reflects the molecular profile of the tumor in RMS, and that WES of cfDNA is a useful tool for highlighting variants that may not have been sampled in the tissue biopsy.

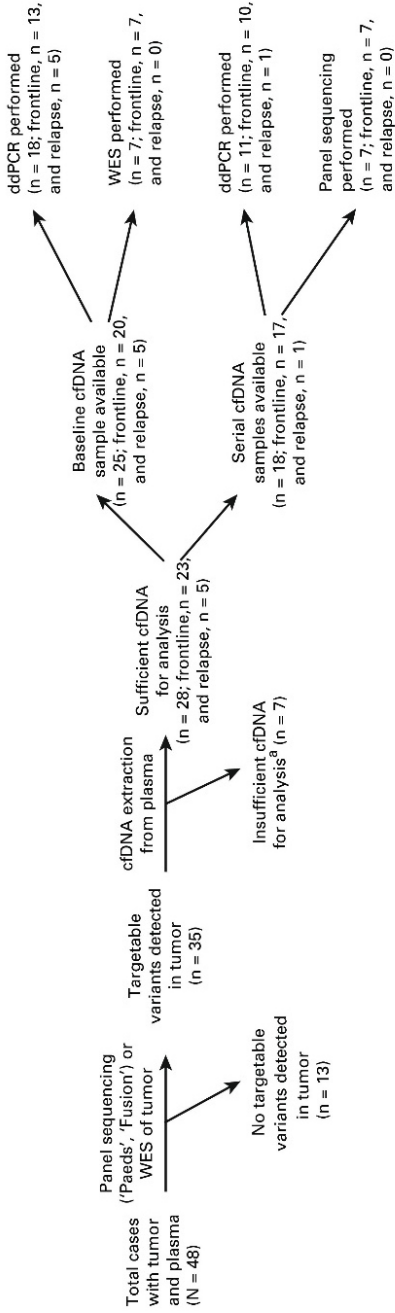
CtDNA Levels Reflect the Disease Burden in Patients With RMS Over Time

In cases where serial plasma samples were available (n = 18), we used ddPCR or panel sequencing to track tumor variants over the course of patient treatment. In most of these patients, ctDNA levels decreased after the onset of chemotherapy and remained stable, corresponding with favorable response to therapy (Fig 3A and Data Supplement). However, there were three patients in whom ctDNA was detectable at various time points after treatment commenced, which coincided with disease progression or relapse (Figs 3B-3D). These results provide evidence to support the notion that ctDNA can act as a surrogate marker for disease aggressiveness in patients with RMS and suggest that ctDNA levels reflect patient response to treatment.

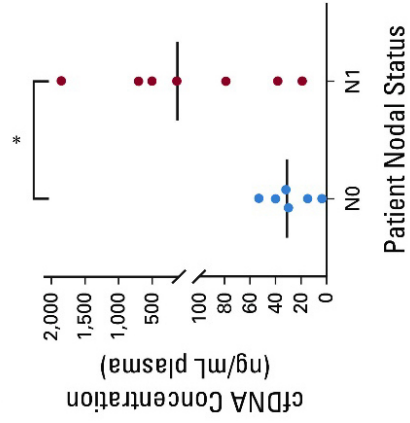
Discussion

Analysis of ctDNA is rapidly being introduced into the clinic for the diagnosis, prognosis, and monitoring of adult patients with cancer.⁷ However, its utility for pediatric cancers is yet to be fully realized. In this study, we aimed to assess the feasibility of detecting and quantifying plasma ctDNA in pediatric RMS. Using techniques offering high sensitivity (such as qPCR and ddPCR) and multiplexing of targets (whole-exome and panel sequencing), we have demonstrated that we can detect molecular markers in cfDNA from RMS animal models and patients, including variants of clinical significance, such as PAX3-FOXO1 fusions and MYOD1 mutations.^{5,6} The detection of mutations is of particular importance, as ctDNA studies of RMS have focused on identifying gene fusions with little evidence for detection of ctDNA in fusion-negative patients.^{8-10,14} In this study, we have also developed a custom sequencing panel, suitable for formalin-fixed paraffin-embedded tissue, to define the unique PAX3/7-FOXO1 DNA breakpoints. This is more practical for clinical implementation than a requirement for fresh-frozen material.

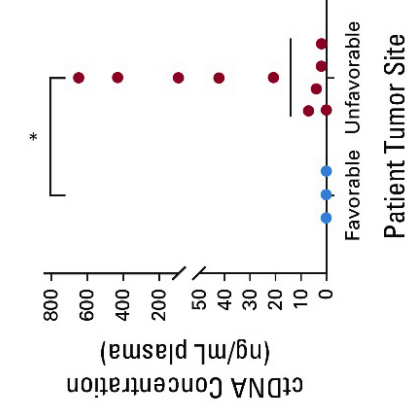
A



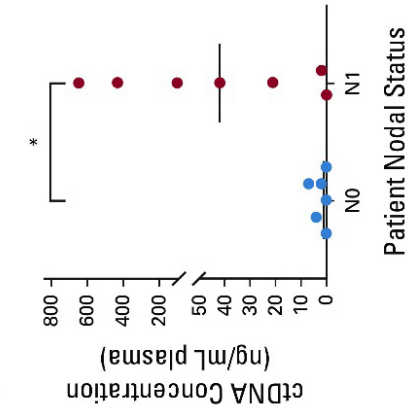
B



C



D



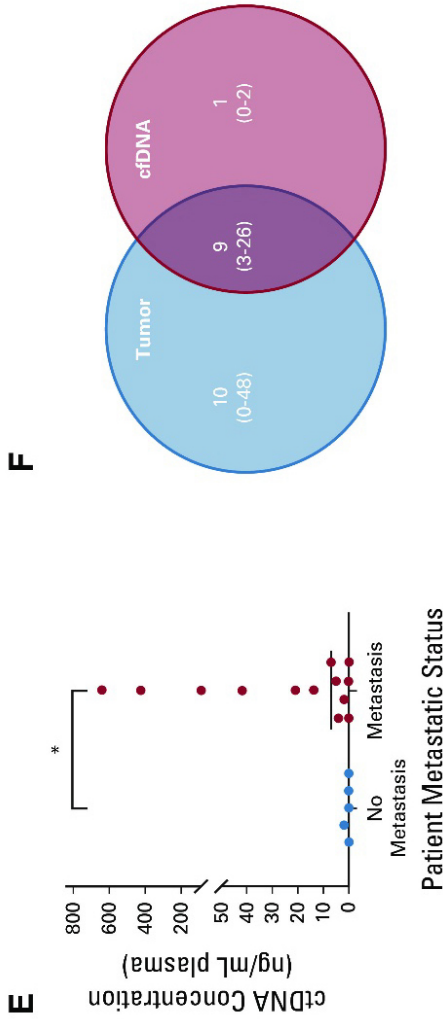
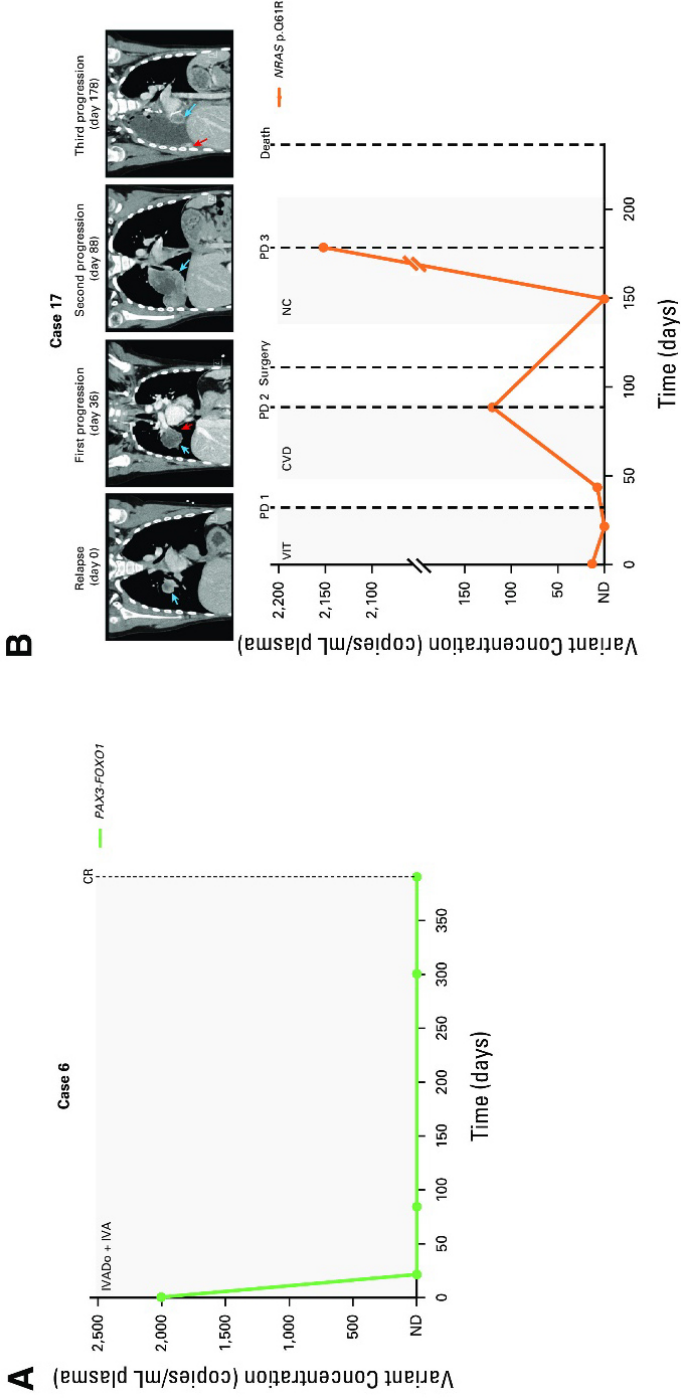


Figure 2. Baseline cfDNA analysis. (A) Overview of samples collected (n = 48 tumor and plasma) and successfully analyzed (n = 28 cfDNA), insufficient cfDNA yield is defined as < 1 ng for ddPCR and < 10 ng for WES/panel sequencing. (B) Frontline patients with nodal spread (N1, n = 7) had significantly higher baseline cfDNA yields (ng/mL plasma) compared with those without it (N0, n = 6; P = .035). Baseline ctDNA yields (ng/mL plasma) were significantly higher in frontline patients with (C) tumors in an unfavorable site (n = 10) compared with those with tumors in a favorable site (n = 3; P = .0210) and (D) nodal involvement (N1, n = 7) compared with those without it (N0, n = 6; P = .043). (E) Baseline ctDNA yields (ng/mL plasma) were significantly higher in both frontline and relapsed patients with metastases at diagnosis (n = 13) compared with those without it (n = 5; P = .0201). Median cfDNA or ctDNA yields indicated by horizontal lines on graphs. (F) There was considerable overlap in the molecular profile of matched patient tumor DNA and baseline cfDNA, as illustrated by mean number (and ranges) of variants detected in each via WES, cfDNA, cell-free DNA; ctDNA, circulating tumor DNA; ddPCR, droplet digital polymerase chain reaction.



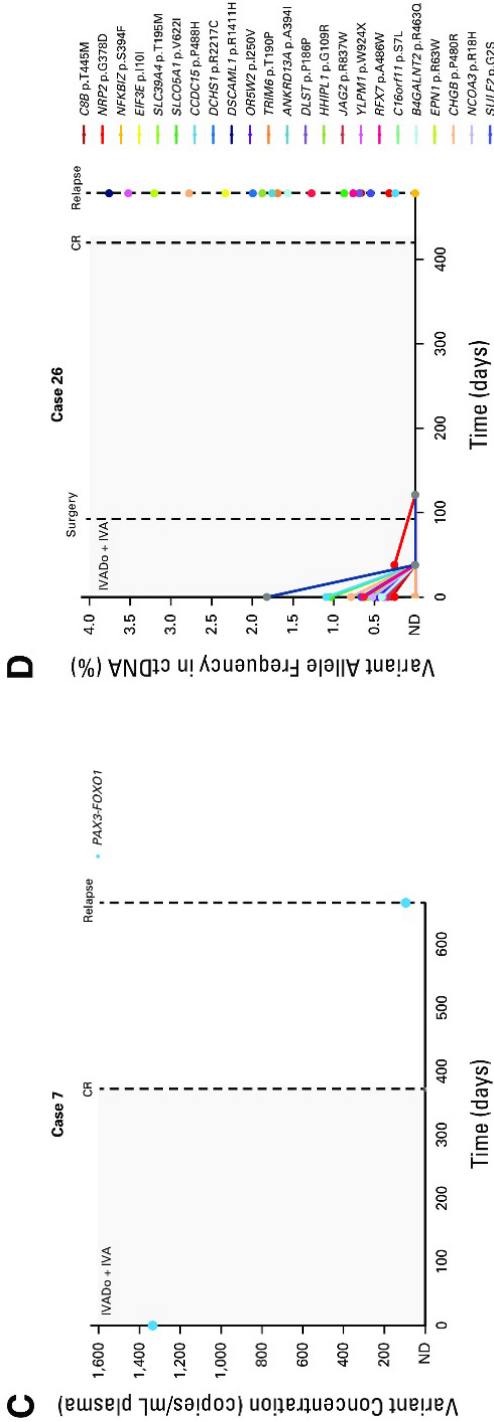


Figure 3. Patient ctDNA levels reflect disease burden over time. **(A)** A PAX3-FOXO1 rearrangement in the pretreatment ctDNA of a frontline patient with aRMS became undetectable via ddPCR in plasma samples collected during chemotherapy. The patient ended therapy with a complete response. **(B)** Plasma levels of an NRAS variant in a relapsed eRMS patient with pulmonary metastasis (day 0 CT image, blue arrow) initially decreased after initiation of chemotherapy but increased as the patient's neoplasm enlarged (see enlarged nodule indicated by blue arrow and narrowing of right lower bronchus indicated by red arrow, CT images at days 36 and 88, respectively). The patient was deemed to have disease progression according to the RECIST 1.1.24 Following surgery and adjuvant chemotherapy, ctDNA became undetectable via ddPCR, but a subsequent plasma sample illustrated a re-emergence of the variant, coinciding with further progression in the patient (new pulmonary metastasis in the surgical bed denoted by blue arrow and scattered vascularized ipsilateral pleural deposits indicated by red arrow in CT image day 178; note the broken y-axis of the graph). The patient died 2 months later. **(C)** A PAX3-FOXO1 fusion initially identified in the pretreatment ctDNA of a patient with frontline aRMS was also detected in a ctDNA sample collected at time of relapse via ddPCR, albeit at a lower concentration. **(D)** Targeted sequencing of ctDNA from an aRMS patient illustrates an initial response to frontline treatment, as evidenced by decreasing variant allele frequencies (%) in serial plasma samples. However, ctDNA was detected in a blood sample collected 2 months after the completion of treatment, coinciding with clinical relapse. Day 0 for all patients is the day that the pretreatment blood sample was collected. Dots on the line graph correspond to the days in which plasma samples were obtained. Gray boxes indicate the chemotherapy duration. Dashed lines indicate clinical time point (surgery, response as assessed on imaging). cfDNA, cell-free DNA; CR, complete response; CT, computed tomography; ctDNA, circulating tumor DNA; CVD, cyclophosphamide, vincristine, and doxorubicin; ddPCR, droplet digital polymerase chain reaction; eRMS, embryonal RMS; IVA, ifosfamide, vincristine, and actinomycin D; IVADo, ifosfamide, vincristine, actinomycin D, and doxorubicin; NC, navelbine (vinorelbine) and cyclophosphamide; ND, not detected; PD, progressive disease; RMS, rhabdomyosarcoma; VIT, vincristine, irinotecan, and temozolomide.

The sensitivity for detection of ctDNA in diagnostic patient plasma samples (78% and 100% for ddPCR and WES, respectively) was on par with that of previous studies in pediatric sarcomas.^{9,10,14-17} Interestingly, all three frontline patients in whom baseline ctDNA could not be detected by ddPCR had tumors in a favorable anatomic site (genitourinary tract, excluding the bladder and prostate) and were fusion-negative, which are both positive survival indicators in RMS.² Two of the three patients had their tumors resected before collecting baseline blood samples, which explains why no ctDNA could be found in them. However, the fourth subject who was ctDNA-negative at baseline had a locoregional recurrence, which is generally associated with longer survival compared with distant relapse.¹⁸ This suggests that ctDNA detection at diagnosis may be linked to disease aggressiveness in RMS, although survival data were not available for all patients to test this hypothesis. A recent study by members of our group found that the presence of circulating tumor cells in blood and bone marrow, as detected by an RMS-specific RNA panel at diagnosis, was negatively associated with survival in patients with RMS.¹⁹ The identification of novel prognostic markers, such as ctDNA and circulating tumor cells at diagnosis, has the potential to further improve risk stratification for children with RMS, and thus, it will be of great value to assess the prognostic significance of these in future clinical studies.

Plasma ctDNA concentration correlated with tumor size in animal models, suggesting that analysis of ctDNA from models may prove useful for real-time assessment of tumor response to treatment. We believe this approach will better enable the RMS research community to conduct preclinical and coclinical testing of personalized therapies that have the potential to improve patient outcomes. In patients, baseline ctDNA levels were higher in those with advanced disease, supporting the notion that ctDNA acts as a surrogate measure of disease status and, thus, as a minimally invasive biomarker for RMS. This contrasts with nontumor cfDNA levels, which did not correlate with tumor burden in animal models, and was only associated with nodal status in frontline patients (possibly because of increased inflammation, a known trigger of cfDNA release, in cancer-infiltrated lymph nodes).²⁰ Although every effort was made to process blood and extract cfDNA in such a way as to minimize cell lysis and enrich for fragmented DNA, we cannot exclude the possibility of contamination with high-molecular-weight DNA.²¹ Furthermore, blood collection for this study was only performed ad hoc, resulting in a small sample size, which limits the power of our statistical analysis. As such, these results should be validated in a larger cohort with standardized collection procedures.

We have also provided evidence to support serial monitoring of ctDNA in patients with RMS using both ddPCR and targeted sequencing, alongside current tools such as imaging. Changes in ctDNA levels corresponded to changes in disease burden and are consistent with the frequent initial responsiveness of RMS to current treatments.¹ We were also able to detect ctDNA at the time of disease relapse in three patients, indicating that ctDNA analysis has utility in the follow-up of patients after completion of frontline treatment. In this study, ctDNA was collected when relapse was clinically apparent. Future prospective studies will be required to determine whether ctDNA is detectable before imaging modalities and/or onset of disease symptoms in relapse patients, and whether earlier detection and treatment of relapse provides a survival benefit.

We initially used ddPCR for detection of ctDNA as it affords high sensitivity (down to 0.03% frequency in some assays) and absolute quantification of target molecules, enabling direct comparison among serial cfDNA samples. We found it ideal for cases with only one variant (eg, PAX3/7-FOXO1 fusions); however, its capacity for multiplexing targets is limited. In cases with matched fresh-frozen tumor tissue and serial plasma, we instead performed targeted sequencing to assess ctDNA. This allowed for longitudinal monitoring of tumor evolution across multiple genomic targets and the identification of potential treatment-resistant variants that may have been unsampled or below the level of detection in the tumor biopsy, or which arose during therapy. As such, sequencing approaches to monitor ctDNA may be more appropriate for patients who have more than one driver mutation, although for some cases, there were several variants that could not be detected in the ctDNA via WES. Future studies will explore the use of approaches such as ultra-deep panel sequencing for detection of rare variants and/or minimal residual disease.²²

Limited starting material can also impact upon the test sensitivity, particularly in pediatric cancers, where blood volumes (and resulting cfDNA yields) may be very small.²³ We excluded cases with < 1 ng cfDNA for ddPCR, and < 10 ng for sequencing. However, it is possible that some low-input samples may have generated false-negative results because of limited amplification of target molecules. As such, caution in the interpretation of these results and consideration of other patient variables will be required for clinical application.

In summary, we have demonstrated that we can detect tumor-specific variants in the plasma of children with both aRMS and eRMS, and have provided preliminary evidence for the use of ctDNA to monitor disease burden in these patients. We believe that this approach warrants further investigation in the context of large-

scale prospective clinical trials, such as the international Frontline and Relapsed Rhabdomyosarcoma study (ClinicalTrials.gov identifier: NCT04625907).

Acknowledgement

The authors would like to thank all patients and their families for their participation in this study. The authors are also grateful to Harma Feitsma, Ellen Stelloo, Irina Sergeeva, and Max van Min from Cergentis BV (Utrecht, The Netherlands) for performing the TLA procedure, and to Vladimir Kirkin and Gary Box for helping to create the ICR-PDX-RMS008 mouse model and collect blood samples.

Support

This project was carried out with the support of the KickCancer Fund, managed by the King Baudouin Foundation and Innovative Therapies for Children with Cancer. O.R. was supported by the children's cancer charity Alice's Arc. N.L. and J.St. were supported by KiKa (Children Cancer Free), grant number 312. S.G.D. received support from the Swiss National Science Foundation grant 31003A_175558 (to B.W.S.). V.D.P. was supported by Fondazione Umberto Veronesi. L.T. was supported by Peter Pan Onlus (Bolzen, Italy). E.I. was supported by Christopher's Smile, the National Institute of Health Research (NIHR) Royal Marsden Biomedical Research Centre (BRC). E.P. is supported by The Royal Marsden Cancer Charity.

This work represents independent research supported by the National Institute for Health Research (NIHR) Biomedical Research Centre at The Royal Marsden NHS Foundation Trust and the Institute of Cancer Research, London (J.C.C., A.W., S.L.G., E.P).

Table 1. Clinical characteristics of patients with frontline rhabdomyosarcoma included in the study

Clinical Variable	Patients, No. (%)
Sex	
Male	10 (43)
Female	5 (22)
Unknown	8 (35)
Age at primary diagnosis, years	
< 1	2 (9)
1-10	10 (43)
> 10	11 (48)
Histologic subtype	
Alveolar	13 (57)
Embryonal	9 (39)
Other	1 (4)
Fusion status	
Positive	11 (48)
Negative	6 (26)
Not assessed	6 (26)
IRS clinical group	
I	0 (0)
II	3 (13)
III	7 (30)
IV	13 (57)
Primary tumor site	
Favorable ^a	6 (26)
Unfavorable ^b	17 (74)
Tumor size, cm	
< 5	2 (9)
≥ 5	21 (91)
Nodal involvement	
N _x	1 (4)
N ₀	9 (39)
N ₁	13 (57)
Metastasis present	
Yes	14 (61)
No	9 (39)

Abbreviation: IRS, Intergroup Rhabdomyosarcoma Studies.

^aFavorable tumor sites include the biliary tract, orbit, head and neck (excluding parameningeal sites), and the genitourinary tract (excluding bladder and prostate).

^bUnfavorable tumor sites are those arising in all other anatomic locations, including (but not limited to) parameningeal sites, the bladder or prostate, and extremities.

Table 2. Clinical characteristics of patients with relapsed rhabdomyosarcoma included in the study.

Clinical Variable	Patients, No. (%)
Sex	
Male	4 (80)
Female	1 (20)
Age at diagnosis, years	
< 1	0 (0)
1-10	4 (80)
> 10	1 (20)
Histologic subtype	
Alveolar	4 (80)
Embryonal	1 (20)
Other	0 (0)
Fusion status	
Positive	4 (80)
Negative	1 (20)
Not assessed	0 (0)
Site of relapse	
Locoregional	1 (20)
Distant	4 (80)

Table 3. Tumor-specific variants detected in patient baseline cfDNA by droplet digital polymerase chain reaction

Patient	Variant Type	Variant	Variant Fractional Abundance (%)	Copy Number ^a	Variant Concentration (copies/mL plasma)	ctDNA Concentration (ng/mL plasma)	Reference Concentration (copies/mL plasma)	cfDNA _{WT} Concentration (ng/mL plasma)	Total cfDNA (ng/mL plasma)
1	Gene fusion	<i>PAX3-FOXO1</i> variant 1	28.20		5,758.00	19.00	17,554.02	57.93	76.93
	Gene fusion	<i>PAX3-FOXO1</i> variant 2	32.20		7,036.00	23.22	17,722.18	58.48	81.70
2	SNV	<i>KRAS</i> G13D	2.00		22.88	0.08	1,144.00	3.78	3.85
3	Gene fusion	<i>PAX3-FOXO1</i>	21.60		28,214.26	93.11	123,591.25	407.85	500.96
4	No baseline cfDNA available								
5	Gene fusion	<i>PAX3-FOXO1</i>	23.09		129,957.14	428.86	432,928.57	1,428.66	1,857.52
6	Gene fusion	<i>PAX3-FOXO1</i>	21.89		2,003.57	6.61	7,150.00	23.60	30.21
7	Gene fusion	<i>PAX3-FOXO1</i>	13.93		1,335.71	4.41	8,250.00	27.23	31.63
8	SNV	<i>NRAS</i> ^{G61K}	/	/	/	/	5,814.29	19.19	19.19
9	CNV	<i>MDM2</i> amp		2.04	/	/	16,185.71	53.41	53.41
10	CNV	<i>FGFR2</i> amp		24.94	196,428.57	648.21	15,753.57	51.99	700.20
11	SNV	<i>NRAS</i> ^{G61K}	/	/	/	/	12,060.71	39.80	39.80
12	No baseline cfDNA available								
13	Gene fusion	<i>PAX3-FOXO1</i>	34.20		12,615.85	41.63	26,132.38	86.24	127.87
14	Gene fusion	<i>PAX3-FOXO1</i> variant 1	2.60		280.00	0.92	10,862.85	35.85	36.77
	Gene fusion	<i>PAX3-FOXO1</i> variant 2	9.30		1,083.00	3.57	10,931.99	36.08	39.65
15	SNV	<i>BRAF</i> ^{V600E}	17.50		927.60	3.06	4,333.44	14.30	17.36
	SNV	<i>MYO1L</i> ^{L122R}	10.50		410.80	1.36	3,493.47	11.53	12.88
16	No baseline cfDNA available								
17	SNV	<i>NRAS</i> ^{G61R}	0.70		13.11	0.04	1,847.57	6.10	6.14
18	Gene fusion	<i>PAX3-FOXO1</i>	/	/	/	/	2,642.35	8.72	8.72
19	Gene fusion	<i>PAX3-FOXO1</i>	3.00		120.97	0.40	3,998.00	13.19	13.59
20	Gene fusion	<i>PAX7-FOXO1</i>	58.10		4,286.25	14.14	3,148.67	10.39	24.54
21	Gene fusion	<i>PAX3-FOXO1</i> variant 1	10.70		2,256.00	7.44	19,626.00	64.77	72.21
	Gene fusion	<i>PAX3-FOXO1</i> variant 2	2.70		515.00	1.70	19,433.00	64.13	65.83

NOTE. Patients 8, 11, and 18 had no detectable variants (/). Patient 9's tumor had a *MDM2* copy number > 21, but the cfDNA copy number was 2 (normal) and thus, ctDNA was not detected.

Abbreviations: amp, amplification; cfDNA, cell-free DNA; CNV, copy-number variant; ctDNA, circulating tumor DNA; SNV, single nucleotide variant; WT, wild-type.

^aCopy number 1.5-3 defined as normal diploid cells, 3-8 defined as a gain, and > 8 defined as an amplification.

References

1. Skapek SX, Ferrari A, Gupta AA, et al.: Rhabdomyosarcoma. *Nat Rev Dis Primers* 5:1, 2019
2. Hibbitts E, Chi YY, Hawkins DS, et al.: Refinement of risk stratification for childhood rhabdomyosarcoma using FOXO1 fusion status in addition to established clinical outcome predictors: A report from the Children's Oncology Group. *Cancer Med* 8:6437-6448, 2019
3. Barr FG, Galili N, Holick J, et al.: Rearrangement of the PAX3 paired box gene in the pediatric solid tumor alveolar rhabdomyosarcoma. *Nat Genet* 3:113-117, 1993
4. Davis RJ, D'Cruz CM, Lovell MA, et al.: Fusion of PAX7 to FKHR by the variant t(1;13)(p36;q14) translocation in alveolar rhabdomyosarcoma. *Cancer Res* 54:2869-2872, 1994
5. Missiaglia E, Williamson D, Chisholm J, et al.: PAX3/FOXO1 fusion gene status is the key prognostic molecular marker in rhabdomyosarcoma and significantly improves current risk stratification. *J Clin Oncol* 30:1670-1677, 2012
6. Shern JF, Selfe J, Izquierdo E, et al.: Genomic classification and clinical outcome in rhabdomyosarcoma: A report from an International Consortium. *J Clin Oncol* 39:2859-2871, 2021
7. Cescon DW, Bratman SV, Chan SM, Siu LL: Circulating tumor DNA and liquid biopsy in oncology. *Nat Cancer* 1:276-290, 2020
8. Eguchi-Ishimae M, Tezuka M, Kokeguchi T, et al.: Early detection of the PAX3-FOXO1 fusion gene in circulating tumor-derived DNA in a case of alveolar rhabdomyosarcoma. *Genes Chromosomes Cancer* 58:521-529, 2019
9. Klega K, Imamovic-Tuco A, Ha G, et al.: Detection of somatic structural variants enables quantification and characterization of circulating tumor DNA in children with solid tumors. *JCO Precis Oncol* 2:1-9, 2018
10. Shah AT, Azad TD, Breese MR, et al.: A comprehensive circulating tumor DNA assay for detection of translocation and copy-number changes in pediatric sarcomas. *Mol Cancer Ther* 20:2016-2025, 2021
11. Manzella G, Schreck LD, Breunis WB, et al.: High throughput drug profiling with a living biobank of primary rhabdomyosarcoma cells unravels disease heterogeneity and detects an AKT inhibitor sensitive subgroup. *Nat Commun* 11:4629, 2020
12. Izquierdo E, Yuan L, George S, et al.: Development of a targeted sequencing approach to identify prognostic, predictive and diagnostic markers in paediatric solid tumours. *Oncotarget* 8:112036-112050, 2017
13. Chicard M, Colmet-Daage L, Clement N, et al.: Whole-exome sequencing of cell-free DNA reveals temporo-spatial heterogeneity and identifies treatment-resistant clones in neuroblastoma. *Clin Cancer Res* 24:939-949, 2018
14. Tombolan L, Rossi E, Binatti A, et al.: Clinical significance of circulating tumor cells and cell-free DNA in pediatric rhabdomyosarcoma. *Mol Oncol* 16:2071-2085, 2022
15. Kurihara S, Ueda Y, Onitake Y, et al.: Circulating free DNA as non-invasive diagnostic biomarker for childhood solid tumors. *J Pediatr Surg* 50:2094-2097, 2015
16. Krumbholz M, Hellberg J, Steif B, et al.: Genomic EWSR1 fusion sequence as highly sensitive and dynamic plasma tumor marker in Ewing sarcoma. *Clin Cancer Res* 22:4356-4365, 2016
17. Barris DM, Weiner SB, Dubin RA, et al.: Detection of circulating tumor DNA in patients with osteosarcoma. *Oncotarget* 9:12695-12704, 2018
18. Heske CM, Mascarenhas L: Relapsed rhabdomyosarcoma. *J Clin Med* 10:804, 2021

19. Lak NSM, Voormanns TL, Zappeij-Kannegieter L, et al.: Improving risk stratification for pediatric patients with rhabdomyosarcoma by molecular detection of disseminated disease. *Clin Cancer Res* 27:5576-5585, 2021
20. Lin LH, Chang KW, Kao SY, et al.: Increased plasma circulating cell-free DNA could be a potential marker for oral cancer. *Int J Mol Sci* 19:3303, 2018
21. Risberg B, Tsui DWY, Biggs H, et al.: Effects of collection and processing procedures on plasma circulating cell-free DNA from cancer patients. *J Mol Diagn* 20:883-892, 2018
22. Stankunaite R, George SL, Gallagher L, et al.: Circulating tumour DNA sequencing to determine therapeutic response and identify tumour heterogeneity in patients with paediatric solid tumours. *Eur J Cancer* 162:209-220, 2022
23. Quan PL, Sauzade M, Brouzes E: dPCR: A technology review. *Sensors (Basel)* 18:1271, 2018
24. Eisenhauer EA, Therasse P, Bogaerts J, et al.: New response evaluation criteria in solid tumors: Revised RECIST guideline (version 1.1). *Eur J Cancer* 45:228-247, 2009

Supplementary methods

Establishment of RMS PDX

Patient-derived xenografts (PDX) of alveolar and embryonal RMS were established by implanting tumor samples collected from patients at the Institut Curie and Royal Marsden Hospital (see Table S1 for PDX characteristics) as previously described.¹ To produce *in vitro* cultures of alveolar RMS PDXs, dissociated tumor cells were grown on plates coated with Matrigel (Corning, 354234) diluted 1:10 in Advanced DMEM/F-12 medium (Thermofisher Scientific, 12634010) and left at room temperature for 30-60 min to solidify. IC-pPDX-104 cells were cultured in Advanced DMEM/F-12 (Thermofisher Scientific, 12634010) medium supplemented with 100 U/ml penicillin/streptomycin (Thermofisher Scientific, 15140122), 2 mM Glutamax (Thermofisher Scientific, 35050061), 0.75x B-27 (Thermofisher Scientific, 17504044), 20 ng/ml bFGF (PeproTech, AF-100-18B) and 20 ng/ml EGF (PeproTech, AF-100-15), whereas IC-pPDX-29 cells were grown in Neurobasal medium (Thermo Fisher Scientific) supplemented with 100 U/ml penicillin/streptomycin (Thermofisher, 15140122), 2 mM Glutamax (Thermofisher Scientific, 35050061), 2x B-27 (Thermofisher Scientific, 17504044), 20 ng/ml bFGF (PeproTech, AF-100-18B) and 20 ng/ml EGF (PeproTech, AF-100-15). For further passaging, cells were washed with PBS and detached with Accutase (Sigma-Aldrich, A6964) diluted 1:2 to 1:3 in PBS.

EGFP transduction

Lentiviral particles containing EGFP were produced in HEK293T cells with 2nd generation packaging plasmids (psPAX2 #12260 and pVSV #36399, both from Addgene) and the respective transfer plasmid (Plasmid #19070, Addgene) using calcium phosphate. Supernatants containing EGFP-lentivirus were collected 72 hours after transduction and concentrated with Amicon Ultra centrifugal filter units (Sigma-Aldrich UFC910024). IC-pPDX-104 and IC-pPDX-29 cells (below passage 20) were transduced with EGFP lentivirus and sorted on a BD FACSAria™ Fusion.

Animal experiments

Alveolar: Mouse experiments were approved by the cantonal guidelines (License no 213/17). Six-to-ten-week-old NOD scid gamma (NSG) mice were used throughout the study. For orthotopic injection, mice were anesthetized using isoflurane. IC-pPDX-104 EGFP and IC-pPDX-29 EGFP cells were resuspended in Matrigel (10 M/mL) and kept on ice for the remaining of the procedure. 0.1 mL cell suspension were injected into the right hind limb muscle of each mouse.

Embryonal: For the eRMS PDX experiments in ICR-PDX-RMS008 (conducted under license number PD498FF8D), tumor pieces were implanted bilaterally in 5 NSG mice, with 3 mice developing bilateral tumors, 1 mouse a unilateral tumor and 1 mouse no tumors (negative control). Blood (230-550 μ L) was collected through cardiac puncture at the end of the experiment after human killing of the mouse in K3EDTA 2.5 ml tubes or into an Eppendorf tube through a 0.5M EDTA prewetted syringe.

Mouse plasma DNA extraction

Blood samples were kept on ice and were processed within 1 hour from collection. Plasma was separated from blood via a double centrifugation step (1,200 g for 10 min then 16,000 g for 10 min, 4°C) and stored at -80°C. Circulating DNA was extracted with the QIAmp Circulating Nucleic Acid Kit (Qiagen, 55114) according to manufacturer's instructions and eluted in 50 μ L nuclease-free water. To test the sensitivity and specificity of the aRMS assays, genomic DNA was extracted from PDX-cultured cells or from the mouse cell line C2C12 with the DNeasy Blood & Tissue Kit (Qiagen, 69504). For the eRMS assays, tumor DNA was extracted from FFPE, fresh frozen and cultured PDX tumor tissue with the QIAamp DNA FFPE Tissue kit (Qiagen) and the DNeasy Blood & Tissue Kit (Qiagen).

PDX tumor variant determination

To detect *PAX3-FOXO1* translocation sequences, genomic DNA was isolated from IC-pPDX-104 and IC-pPDX-29 cultured cells and processed according to an established Targeted Locus Amplification protocol (Cergentis, Utrecht, Netherlands).² Droplet digital PCR (ddPCR) was performed on DNA from ICR-PDX-RMS008 PDX tumors to confirm the PDX tumors contained the same genetic variants (*MYOD1* L122R, *NRAS* G12A, *PIK3CA* H1044K) detected in the patient primary tumor (see 'ddPCR').

qPCR

We first tested the sensitivity and species-specificity of different primer sets that have been previously described to be selective for either human or mouse DNA. Primer sets, listed in Table S2, were purchased from Microsynth in liquid form (100 μ M). Probes were coupled to FAM at the 5'-end and to TAMRA at the 3'-end.

SYBR Green-based qPCR was used for primer sets hPtger2, hGAPDH, hAluJ, hLINE-1 and mPtger2, whereas Taqman-based qPCR was used for *PAX3-FOXO1*-breakpoint-specific primer sets and for mGAPDH. For SYBR Green qPCR, each reaction well of a 384 well plate consisted of 2 μ L DNA (100-0.001 ng), 5 μ L PowerUpTM SYBRTM Green Master Mix (Thermo Fischer Scientific, A25778), 4.8 μ L nuclease-free water (not DEPC-treated) (ThermoFisher Scientific, AM9937) and the gene mix (0.1 μ L forward and 0.1 μ L

reverse primer). All samples were prepared on ice and run in triplicate on a 7900HT Fast Real-Time PCR System (Applied Biosystems) with the following cycling conditions: 50 °C for 2 min, 95 °C for 10 min, 40 cycles of 95 °C for 15 sec and 60 °C for 1 min, followed by a dissociation stage of 95 °C for 15 sec, 60 °C for 15 sec and 95 °C for 15 sec.

For real-time qPCR, each reaction well consisted of 4.5 µL DNA (100-0.001 ng), 5 µL TaqMan™ Gene Expression Master Mix (Thermo Fischer Scientific, 4369016), 0.43 µL nuclease-free water (not DEPC- treated) (ThermoFisher Scientific, AM9937) and the primer mix (0.03 µL forward, 0.03 µL reverse primer and 0.01 µL probe). All samples were prepared on ice and run in triplicate on a 7900HT Fast Real-Time PCR System (Applied Biosystems) with the following cycling conditions: 50 °C for 2 min, 95 °C for 10 min, followed by 40 cycles of 95 °C for 15 sec and 60 °C for 1 min.

For ctDNA and nt-cfDNA quantification, SYBR Green qPCR with primer sets hLINE-1 and mPtger2 was performed as described above, except that DNA samples were diluted 1:5 in nuclease-free water (not DEPC-treated) (ThermoFisher Scientific, AM9937). Standard curves and negative controls (water and cfDNA extracted from plasma of healthy mice) were included in every run. The LoD was set 2-Ct-values below background of negative controls.

Patient blood sample processing

Whole blood was collected in EDTA tubes (BD, Reading, UK) and processed at participating sites according to local standard operating procedures:

Bambino Gesù Children's Hospital, Rome: Blood was centrifuged at 500 g for 10 min. Plasma was then collected and centrifuged at 3,000 g and then at 12,000 g for 20 min. Clarified plasma was then aliquoted and stored at -80°C prior to use.

University-Hospital, Padova: Blood was centrifuged for 10 minutes at 890 g. The plasma fraction was transferred to new tubes and centrifuged for 10 minutes at 16,000 g. Clarified plasma was aliquoted into new tubes and stored at -80°C.

Princess Máxima Centre, Utrecht: Blood was centrifuged for 10 minutes at 1,375 g. The plasma fraction was aliquoted into new tubes and stored at -20°C prior to use.

Institute of Cancer Research, London: Blood was centrifuged for 10 minutes at 1,600 g. The plasma fraction was transferred to new tubes and centrifuged for 10 minutes at 1,600 g. Clarified plasma was aliquoted into new tubes and stored at -80°C.

Institut Curie, Paris: Blood was centrifuged for 10 minutes at 2,000 rpm. The plasma fraction was aliquoted into new tubes and stored at -80°C.

Plasma cell-free DNA extraction

Cell-free DNA was extracted from patient plasma at local sites according to established procedures.

University-Hospital, Padova: Cell-free DNA was extracted from 0.5-1 mL of plasma using the QIAamp MinElute ccfDNA kit (Qiagen, Hilden, Germany) according to the manufacturers' instructions.

Princess Máxima Centre, Utrecht: Cell-free DNA was extracted from 0.2-1 mL of plasma using the Quick-cfDNA Serum & Plasma kit (Zymo Research, Irvine, USA) according to the manufacturer's protocol.

Institute of Cancer Research, London: Cell-free DNA was extracted from 0.5-8 mL of plasma using the QIAamp Circulating Nucleic Acid kit (Qiagen) according to the manufacturers' instructions.

Institut Curie, Paris: Cell-free DNA was extracted from 0.5-1 mL of plasma using the QIAamp Circulating Nucleic Acid kit (Qiagen) according to the manufacturers' instructions.

Tumor DNA extraction

Patient tumor samples were shipped to either Utrecht, London or Paris for DNA extraction as follows:

FFPE tissue: Tumor cases were assessed by an expert pediatric rhabdomyosarcoma pathologist prior to extraction to estimate tumor cellularity. Only cases with tumor cellularity greater than 50% were considered for extraction. DNA from FFPE tissue was isolated with the Maxwell RSC FFPE Plus DNA kit (Promega; Princess Maxima Centre, Utrecht) or the QIAamp DNA FFPE Tissue kit (Qiagen; Institute of Cancer Research, London) according to manufacturer's protocol. DNA quantity and quality were assessed with the Qubit HS dsDNA Kit (Thermo Fisher Scientific; both sites) and the Agilent HS D1000 Screen Tape (Agilent Technologies; Institute of Cancer Research, London).

Fresh-frozen tissue: Fresh-frozen tumor samples were processed if they had at least 30% of tumor cellularity determined by an experienced pathologist. Extraction was

performed with the AllPrep DNA Mini kit (Qiagen) according to the manufacturer's instructions (Institut Curie, Paris).

Germline DNA extraction

In some cases where peripheral blood mononuclear cells were available, germline DNA was extracted with the DNeasy Blood and Tissue kit (Qiagen) according to the manufacturer's instructions (Institut Curie, Paris).

Targeted Locus Amplification

In *PAX3-FOXO1*-rearranged cases where fresh tumor tissue was available, targeted locus amplification (TLA) was performed to determine the translocation breakpoints. TLA was performed according to established methods (Cergentis).² The input was 3-5 million cells from cultured patient-derived organoids.

Targeted sequencing

For FFPE tumors, targeted sequencing was performed with two custom sequencing panels to identify tumor-specific variants of interest. The first panel ('Paeds') was for the detection of single nucleotide variants (SNVs), insertions and deletions (indels), or copy number variants (CNVs) recurrently altered in pediatric solid tumors, including RMS (see Table S3 for list of gene targets).^{3,4} This panel has been validated to Good Laboratory and Clinical Practice standards and is now offered as part of routine diagnostic testing across the UK.

For FFPE tumor samples positive for the *PAX3/7-FOXO1* gene fusions, DNA was sequenced with a second panel ('RMS fusion 01') to detect the genomic position of translocation breakpoints. This panel was designed to detect any translocations involving the *PAX3*, *PAX7* and *FOXO1* genes, which account for >95% of all gene fusions in fusion-positive pediatric RMS. The genomic locations of the panel baits are listed in Table S4.

For both panels, tumor DNA samples (and, where available, germline DNA) were concentrated to >1.6 ng/μL with the DNA Clean and Concentrator kit (Zymo Research) according to the manufacturer's instructions. Between 29 and 226 ng of DNA per sample was input into the library preparation, which was performed with the KAPA Hyper Plus kits (Kapa Biosystems) with barcoded adapters (Roche) according to the manufacturer's instructions. Libraries were pooled and hybridised to the panel baits overnight at 47°C for 'RMS fusion 01' and 55°C for 'Paeds'. Sequencing was performed on the NovaSeq 6000 (Illumina). Sequencing data was analysed as previously described.^{3,4}

Whole-exome sequencing

WES was performed on fresh-frozen tumor material, as previously described.⁵ Briefly, libraries were prepared using the KAPA Library Preparation kit (Kapa Biosystems) as per manufacturer's instructions, except for a modified overnight ligation at 20°C with a 10:1 adapter:insert ratio. The SeqCap EZ Exome Enrichment kit (Roche) was used for exome capture, with sequencing performed on the HiSeq 2500 (Illumina) to a mean coverage depth of 100x. Sequences were aligned to the human genome (hg19) with Bowtie2 and variant calling was performed with GenomeAnalysisTK-3.5 UnifiedGenotyper, HaplotypeCaller, and Samtools-0.1.18. Variants were filtered according to an established bioinformatic pipeline.⁵

Droplet digital PCR

ddPCR primers and probes for tumor-specific variants and reference genes were purchased from Bio-Rad or Thermo Fisher Scientific, or were custom-designed using Primer3Plus and ordered through Integrated DNA Technologies. All assays were run against a temperature gradient to determine the optimal annealing temperature. Details of the custom and commercial assays used to assess cell-free DNA for *PAX3/7-FOXO1* gene fusions, mutations and copy number changes are listed in Table S5 and S6, respectively. ddPCR was performed on the Bio-Rad QX200 ddPCR system as per manufacturer's instructions using 2X ddPCR Supermix for Probes (Bio-Rad), assay mixes (with a final concentration of 900 nM of primers and 250 nM of probe) and 1.0-30 ng of cfDNA. Each assay included a positive control (patient tumor DNA harbouring the variant of interest), a negative control (patient germline DNA or Human Genomic DNA, Promega) and a no-template control (Nuclease-free water, Ambion). All samples were run in duplicate where possible. Reaction mixes were partitioned into droplets on the QX200 Auto Droplet Generator. After droplet generation, PCR was performed with the following condition: 95 °C for 10 min (1 cycle); 94 °C for 30 s and 55–60 °C for 1 min (40 cycles); 98 °C for 10 min (1 cycle), 4 °C hold. Droplets were analysed in the QX200 ddPCR Droplet Reader and analysis performed with the QuantaSoft Analysis Pro software.

Fractional abundance of variants (*PAX3/7-FOXO1* gene fusions or SNVs such as *NRAS* G35C) in patient cfDNA was determined by the following formula:

$$\text{Variant Fractional Abundance (\%)} = [C_{\text{var}} / (C_{\text{var}} + C_{\text{ref}})] * 100$$

Where: C_{var} = Variant concentration in copies/μL
 C_{ref} = Reference concentration in copies/μL

The reference genes for *PAX3/7-FOXO1* gene fusions and copy number alterations was human *RPP30* and *RPPH1* (Bio-Rad) and *ACTB* (custom, see Table S5) and the reference for SNVs was the wild-type sequence at the target allele.

Plasma concentration of variant-positive cell-free DNA ('ctDNA') was calculated as follows:

$$\text{ctDNA (copies/mL plasma)} = C_{\text{var}} \times V_{\text{rx}} \times V_{\text{elu}} / V_{\text{dna}} \times V_{\text{plasma}}$$

Where:

- C_{var} = Variant concentration (copies/ μL)
- V_{rx} = Total volume of ddPCR reaction mix (μL)
- V_{elu} = Total volume of eluate from DNA extraction (μL)
- V_{dna} = Volume of DNA input into ddPCR reaction (μL)
- V_{plasma} = Volume of plasma DNA was extracted from (mL)

Plasma concentration of wild-type cell-free DNA ('cfDNA_{WT}') was calculated as follows:

$$\text{cfDNA}_{\text{WT}} \text{ (copies/mL plasma)} = C_{\text{ref}} \times V_{\text{rx}} \times V_{\text{elu}} / V_{\text{dna}} \times V_{\text{plasma}}$$

Where:

- C_{ref} = Reference concentration (copies/ μL)
- V_{rx} = Total volume of ddPCR reaction mix (μL)
- V_{elu} = Total volume of eluate from DNA extraction (μL)
- V_{dna} = Volume of DNA input into ddPCR reaction (μL)
- V_{plasma} = Volume of plasma DNA was extracted from (mL)

Amount of ctDNA, cfDNA_{WT} and total cfDNA ('cfDNA') in ng/mL plasma was calculated as per the following equations:

$$\text{ctDNA (ng/mL plasma)} = \text{ctDNA (copies/mL plasma)} \times 0.0033$$

$$\text{cfDNA}_{\text{WT}} \text{ (ng/mL plasma)} = \text{cfDNA}_{\text{WT}} \text{ (copies/mL plasma)} \times 0.0033$$

$$\text{cfDNA (ng/mL plasma)} = [\text{cfDNA}_{\text{WT}} \text{ (copies/mL plasma)} \times 0.0033] + [\text{ctDNA (copies/mL plasma)} \times 0.0033]$$

Where 0.0033 = approximate mass of the haploid genome in ng

Supplementary data

Animal experiments

For the alveolar mouse models, we first verified the presence of individual *PAX3-FOXO1* breakpoints in two aRMS PDXs using a targeted locus amplification (TLA) approach. In both samples, the translocation was successfully identified, and the breakpoint sequences determined (Table S7). We then determined the sensitivity and specificity of *PAX3-FOXO1*-specific primers (Figure S1A and B) and of previously published human-specific sequences (hLINE, hAluJ, hPtgerhGAPDH) (Figure S1C) by using serial dilutions of human tumor gDNA in water as template for quantitative PCR. Water and plasma cfDNA extracted from healthy mice were used as negative controls for background determination. All tested primers exhibited linearity of responses over four or more orders of magnitude of input DNA (Figure S1A-F). Among the human-specific primers, only tumor-specific *PAX3-FOXO1* breakpoint sequences resulted in high specificity, with no detectable murine unspecific signal. Among mouse-specific assays, only mPtger (Figure S1G) was considered for further studies, as Ct values of mGAPDH (Figure S1H) were not reproducible below 0.1 ng input DNA (coefficient of variation >15%). We next assessed the limit of detection (LoD) of the tested primers based on a threshold cycle of 40 or of the corresponding species-unspecific background (Figure S1 I). Highest sensitivity for human DNA was achieved with primers targeting multi-copy DNA (hLINE-1: LoD = 0.1 ± 0.1 pg; hAluJ: LoD = 7.1 ± 1.9 pg), and with tumor-specific *PAX3-FOXO1* breakpoint sequences (IC-pPDX-29: LoD = 4.5 ± 1.2 pg; IC-pPDX-104: LoD = 16.3 ± 3.7 pg). For mouse DNA, mPtger2 could detect down to 5.0 ± 1.6 pg. Given our experimental set-up and the necessity to detect and quantify ctDNA from very small amounts of blood, hLINE-1 and mPtger2 were chosen for further animal experiments. Data for the detection of SNVs in cfDNA from ICR-PDX-RMS008 is presented in Figure S2.

Detection of key oncogenic drivers in patient tumors

DNA from patient FFPE tumor tissue was sequenced with the 'Paeds' targeted sequencing panel (n=35) and the 'RMS fusion 01' sequencing panel (n=14) to detect key tumor-specific variants (and, in the case of the 'RMS fusion 01' panel, determine the translocation breakpoints resulting in the fusions between the *PAX3* or *PAX7* and *FOXO1* genes). Cases had a tumor cellularity between 50 and 95% (as estimated by an expert pediatric rhabdomyosarcoma pathologist). The mean depth of coverage for samples sequenced with the 'Paeds' panel was 264x (range 14-1145x, median 164x), while that of the 'RMS fusion 01' panel was 974x (range 49-6432x, median 118x). Variants were identified in 31 (89%) cases sequenced with the 'Paeds' panel, with an average of 3 variants detected per case (range 0-6; Figure S3). *PAX3/7-FOXO1*

breakpoints were identified in 12 (86%) cases sequenced with the 'RMS fusion 01' panel (see Table S7 for breakpoint locations). Three cases had two unique *PAX3-FOXO1* gene fusions detected, whilst 1 case had two unique *PAX7-FOXO1* gene fusions. These do not appear to be reciprocal translocations as the breakpoints occur at different genomic locations, and ddPCR testing determined that they were present at different concentrations in patient cfDNA from the same timepoint (see Table 3). Variant-positive patients who had sufficient cfDNA for testing and for whom a ddPCR assay could be purchased/developed to target variants in cfDNA (e.g., those who had a 'targetable variant') were carried forward into the final cohort (n=28; See Figure 2A for sample overview).

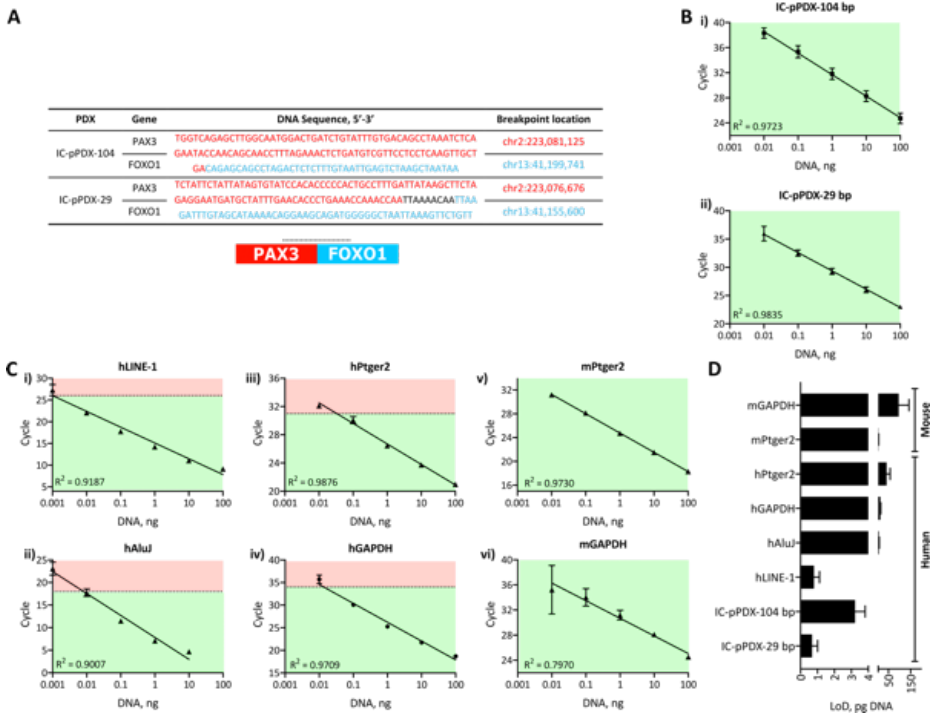


Figure S1. Design of a human-specific qRT-PCR assay to quantify ctDNA in alveolar RMS PDXs. (A-F) Genomic DNA from human RMS PDXs was serially diluted in water and detected by qRT-PCR using primer sets specific for *PAX3-FOXO1* breakpoint sequences (A and B), or for previously published human hPtger2 (C), hGAPDH (D), hLINE-1 (E), hAluJ (F) sequences. Plasma cfDNA from murine controls was used to set the limit of detection (LoD) (dotted lines) for each assay. (G-H) Mouse DNA was serially diluted in water and detected with previously published primer sets specific for mouse DNA (mPtger2, G; mGAPDH, H). Data are represented as mean \pm SEM from at least two independent experiments. Correlation coefficient values (R^2) are shown for each graph. (I) Limit of detection (LoD) of the different primer sets. LoD was set based on a threshold cycle of 40 or the corresponding species-unspecific background (LoD set 2-Ct-values below background signal). Data are represented as mean \pm SEM from at least two independent experiments.

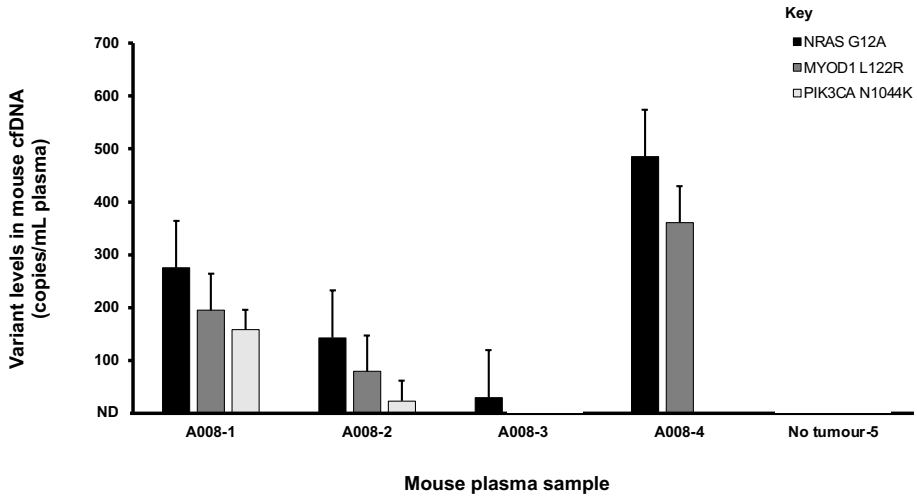


Figure S2. Levels of key genetic variants *NRAS*^{G12A}, *MYOD1*^{L122R} and *PIK3CA*^{H1044K} detected in mouse plasma samples by ddPCR (copies/mL plasma). Plasma samples 1 to 4 were collected from mice who had grown the ICR-PDX-RMS008 embryonal RMS PDX, whilst plasma sample 5 was collected from an NSG mouse which did not develop tumors.

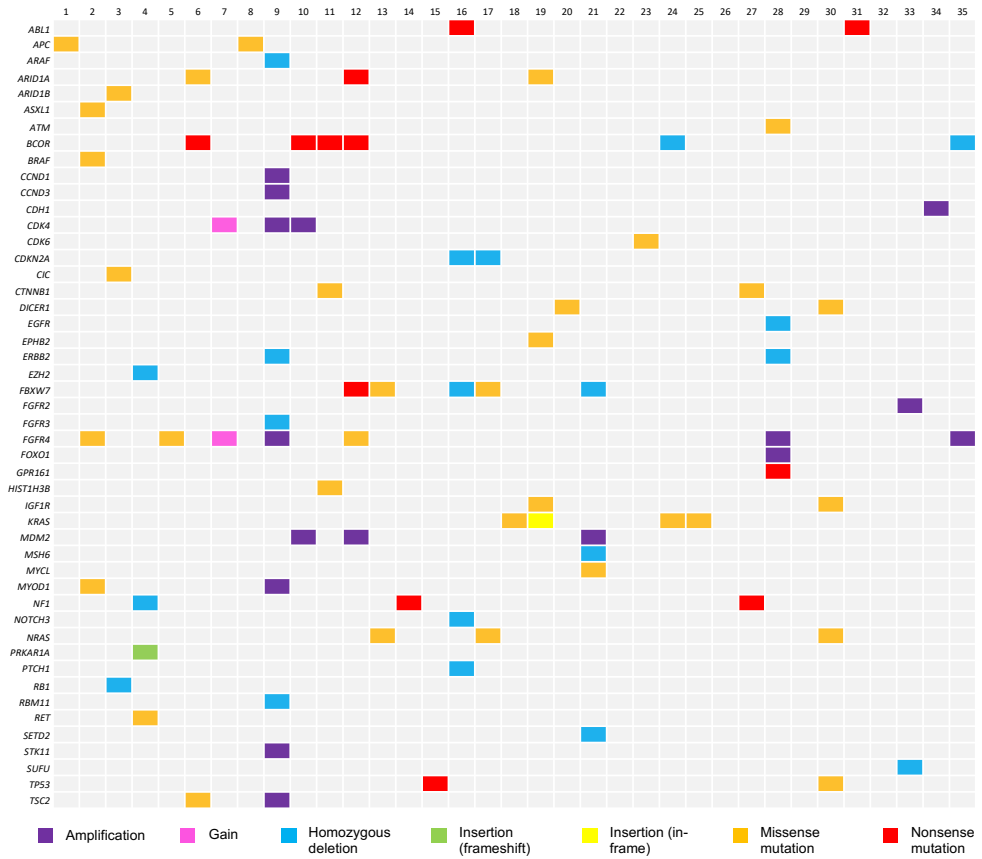


Figure S3: OncoPrint map of SNVs and CNVs detected in patient tumor DNA via targeted sequencing with the Paeds panel.³ Each column represents a case (1-35), with the type of variant in each gene detected in each case represented by a coloured square. Grey shading indicates that no variant was detected in that gene in that patient. *Note:* Not all cases presented here were subject to cfDNA analysis. Patients were excluded from the final liquid biopsy cohort if no variants were detected in their tumor, a ddPCR assay to target variants detected was not available, or there was insufficient cfDNA to test (see Figure 2A for sample overview).

Figure S4. Variant levels in patient cfDNA over time as assessed by ddPCR or panel sequencing (n=14; remaining 4 cases illustrated in Figure 3). Although some variants exhibited marginal increases in concentration over time (<10% increase from baseline), Case 4 (B) and Case 22 (I) were deemed to have stable ctDNA levels during treatment. (previous page)

Table S1. Characteristics of PDXs and patient clinical data.

PDX	Histology	Disease status at biopsy	Tumor sampled	Tumor site	Metastatic infiltration	Tumor-specific variants (AF%)
IC-pPDX-104	Alveolar	Relapse	Primary tumor	Anterior compartment of leg	No evidence in bone marrow	PAX3-FOXO1
IC-pPDX-29	Alveolar	Relapse	Primary tumor	Paravertebral	Pleural infiltration	PAX3-FOXO1
ICR-PDX-RMS008	Embryonal	Primary progressive	Primary tumor	Jaw (non-parameningeal)	None	NRAS ^{G12A} (54.7%) MYOD1 ^{L1226} (48.0%) PIK3CA ^{H1044K} (39.8%)

Table S2. Characteristics of qPCR primer-probe sets used for cfDNA analysis in PDX.

Species	Target sequence	Oligo	Oligo sequence (5'-3')	T _m (°C)	Amplicon size (bp)
Human	IC-pPDX-104 <i>PAX3-FOXO1</i>	F	TGA GGG GCT GGT GTG AAG CAG TGT	68.5	-
		R	AGG CTG CTC TGT CAG CAA CTT GAG G	69.1	
		P	TCA GGG AGG TCA CAC CTG TCC A	65.8	
	IC-pPDX-29 <i>PAX3-FOXO1</i>	F	CCA CTG CCT TTG ATT ATA AGC TTC TAG	65.3	-
		R	CTG CTT CCT GTT TTA TGC TAC AAA TC	62.9	
		P	TGA TGC TAT TTG AAC ACC CTG AAA CCA AAC C	69.7	
	hPtger2 ^{6,7}	F	GCT GCT TCT CAT TGT CTC GG	60.5	189
		R	GCC AGG AGA ATG AGG TGG TC	62.5	
	hGAPDH ⁸	F	ATC ATC CCT GCC TCT ACT GG	60.5	121
		R	GTC AGG TCC ACC ACT GAC AC	62.5	
	hAluJ ⁹	F	CAC CTG TAA TCC CAG CAC TTT	59.5	240
		R	CCC AGG CTG GAG TGC AGT	60.8	
hLINE-1 ¹⁰	F	TCA CTC AAA GCC GCT CAA CTA C	62.1	81	
	R	TCT GCC TTC ATT TCG TTA TGT ACC	62.0		
Mouse	mGAPDH ¹¹	F	CCT CAC AAT CTG TCT CAC CTT ATT	62.0	-
		R	GAC CTC TGT AAG TCC GCT TTG	61.2	
		P	AGC CTT ATT GTC CTC GGG CAT	61.2	
	mPtger2 ^{6,7}	F	CCT GCT GCT TAT CGT GGC TG	62.5	189
		R	GCC AGG AGA ATG AGG TGG TC	62.5	

Abbreviations: F = forward primer; R = reverse primer; P = probe

Table S3. List of genes targeted in the Pediatric Solid Tumor ('Paeds') panel.³

<i>ABL1</i>	<i>CDK4</i>	<i>FGFR2</i>	<i>MRE11A</i>	<i>PTEN</i>
<i>ACVR1</i>	<i>CDK6</i>	<i>FGFR3</i>	<i>MSH2</i>	<i>PTPN11</i>
<i>AKT1</i>	<i>CDKN1A</i>	<i>FGFR4</i>	<i>MSH6</i>	<i>RAD51B</i>
<i>ALK</i>	<i>CDKN2A</i>	<i>GPR161</i>	<i>MYC</i>	<i>RAD51C</i>
<i>AMER1</i>	<i>CDKN2B</i>	<i>H3F3A</i>	<i>MYCL</i>	<i>RAD51D</i>
<i>APC</i>	<i>CHEK1</i>	<i>HIST1H3B</i>	<i>MYCN</i>	<i>RAD54L</i>
<i>ARID1A</i>	<i>CHEK2</i>	<i>HIST1H3C</i>	<i>MYOD1</i>	<i>RAF1</i>
<i>ARID1B</i>	<i>CIC</i>	<i>HIST2H3C</i>	<i>NF1</i>	<i>RB1</i>
<i>ASXL1</i>	<i>CREBBP</i>	<i>HRAS</i>	<i>NF2</i>	<i>RET</i>
<i>ATM</i>	<i>CTNNB1</i>	<i>IDH1</i>	<i>NRAS</i>	<i>SETD2</i>
<i>ATR</i>	<i>DAXX</i>	<i>IDH2</i>	<i>PALB2</i>	<i>SMARCA4</i>
<i>ATRX</i>	<i>DDX3X</i>	<i>IGF1R</i>	<i>PDGFRA</i>	<i>SMARCB1</i>
<i>BARD1</i>	<i>DICER1</i>	<i>KIT</i>	<i>PHOX2B</i>	<i>SMARCE1</i>
<i>BBC3</i>	<i>DROSHA</i>	<i>KMT2A</i>	<i>PIK3CA</i>	<i>SMO</i>
<i>BCOR</i>	<i>EGFR</i>	<i>KRAS</i>	<i>PIK3R1</i>	<i>SUFU</i>
<i>BRAF</i>	<i>EMSY</i>	<i>LIN28B</i>	<i>PIN1</i>	<i>TERT</i>
<i>BRCA1</i>	<i>EPHB2</i>	<i>MAP2K1</i>	<i>PMS1</i>	<i>TFE3</i>
<i>BRCA2</i>	<i>ERBB2</i>	<i>MAP2K2</i>	<i>PMS2</i>	<i>TP53</i>
<i>BRIP1</i>	<i>EZH2</i>	<i>MAPK1</i>	<i>PPM1D</i>	<i>TSC1</i>
<i>CCND1</i>	<i>FANCI</i>	<i>MDM2</i>	<i>PPP2R2A</i>	<i>TSC2</i>
<i>CCND2</i>	<i>FANCL</i>	<i>MDM4</i>	<i>PRKAR1A</i>	<i>VHL</i>
<i>CCNE1</i>	<i>FBXW7</i>	<i>MET</i>	<i>PTCH1</i>	<i>WT1</i>
<i>CDK12</i>	<i>FGFR1</i>	<i>MLH1</i>	<i>PTCH2</i>	<i>YAP1</i>

Table S4. Genomic locations of the 'RMS fusion 01' panel baits.

Chromosome	Gene	Start	End
chr1	<i>PAX7_upstream</i>	18945508	18946114
chr1	<i>PAX7_upstream</i>	18946133	18946669
chr1	<i>PAX7_upstream</i>	18947028	18947239
chr1	<i>PAX7_upstream</i>	18947533	18947826
chr1	<i>PAX7_upstream</i>	18948158	18948437
chr1	<i>PAX7_upstream</i>	18948468	18948713
chr1	<i>PAX7_upstream</i>	18948723	18948943
chr1	<i>PAX7_upstream</i>	18949543	18949645
chr1	<i>PAX7_upstream</i>	18949673	18950588
chr1	<i>PAX7_upstream</i>	18950783	18952680
chr1	<i>PAX7_upstream</i>	18952688	18952829
chr1	<i>PAX7_upstream</i>	18953293	18954552
chr1	<i>PAX7_upstream</i>	18954558	18954632
chr1	<i>PAX7_upstream</i>	18954658	18955643
chr1	<i>PAX7_upstream</i>	18955708	18957311
chr1	<i>PAX7</i>	18957323	18958182
chr1	<i>PAX7</i>	18958183	18959142
chr1	<i>PAX7</i>	18959143	18960796
chr1	<i>PAX7</i>	18960797	18961032
chr1	<i>PAX7</i>	18961033	18961604
chr1	<i>PAX7</i>	18961605	18961734
chr1	<i>PAX7</i>	18961735	18961944
chr1	<i>PAX7</i>	18962033	18962278
chr1	<i>PAX7</i>	18962323	18962730
chr1	<i>PAX7</i>	18962731	18962865
chr1	<i>PAX7</i>	18962866	18963261
chr1	<i>PAX7</i>	18963278	18963377
chr1	<i>PAX7</i>	18963393	18966617
chr1	<i>PAX7</i>	18966623	18968571
chr1	<i>PAX7</i>	18968638	18969226
chr1	<i>PAX7</i>	18969243	18970856
chr1	<i>PAX7</i>	18970863	18974834
chr1	<i>PAX7</i>	18975103	18979683
chr1	<i>PAX7</i>	18979703	18979843
chr1	<i>PAX7</i>	18979853	18981285
chr1	<i>PAX7</i>	18981308	18982249

Table S4. Continued

Chromosome	Gene	Start	End
chr1	<i>PAX7</i>	18982293	18982719
chr1	<i>PAX7</i>	18983008	18983217
chr1	<i>PAX7</i>	18983498	18984243
chr1	<i>PAX7</i>	18984258	18984741
chr1	<i>PAX7</i>	18984753	18985415
chr1	<i>PAX7</i>	18985608	18986957
chr1	<i>PAX7</i>	18986983	18988068
chr1	<i>PAX7</i>	18988153	18988919
chr1	<i>PAX7</i>	18988933	18989031
chr1	<i>PAX7</i>	18989418	18989874
chr1	<i>PAX7</i>	18990158	18990717
chr1	<i>PAX7</i>	18990728	18991859
chr1	<i>PAX7</i>	18992453	18992526
chr1	<i>PAX7</i>	18992658	18993716
chr1	<i>PAX7</i>	18993718	18993848
chr1	<i>PAX7</i>	18993938	18994860
chr1	<i>PAX7</i>	18995188	18996346
chr1	<i>PAX7</i>	18996593	18998193
chr1	<i>PAX7</i>	18998483	18999092
chr1	<i>PAX7</i>	18999383	18999623
chr1	<i>PAX7</i>	18999643	19002996
chr1	<i>PAX7</i>	19003008	19004303
chr1	<i>PAX7</i>	19004898	19006310
chr1	<i>PAX7</i>	19006323	19006565
chr1	<i>PAX7</i>	19006578	19007380
chr1	<i>PAX7</i>	19007678	19008196
chr1	<i>PAX7</i>	19008508	19008647
chr1	<i>PAX7</i>	19008648	19010057
chr1	<i>PAX7</i>	19010343	19012407
chr1	<i>PAX7</i>	19012433	19013374
chr1	<i>PAX7</i>	19013673	19015107
chr1	<i>PAX7</i>	19015428	19017482
chr1	<i>PAX7</i>	19017753	19017964
chr1	<i>PAX7</i>	19017988	19018247
chr1	<i>PAX7</i>	19018248	19018447
chr1	<i>PAX7</i>	19018448	19018751

Table S4. Continued

Chromosome	Gene	Start	End
chr1	<i>PAX7</i>	19019068	19020696
chr1	<i>PAX7</i>	19021008	19021709
chr1	<i>PAX7</i>	19021718	19022556
chr1	<i>PAX7</i>	19022883	19022963
chr1	<i>PAX7</i>	19022978	19023057
chr1	<i>PAX7</i>	19023238	19023341
chr1	<i>PAX7</i>	19023458	19024494
chr1	<i>PAX7</i>	19024518	19024760
chr1	<i>PAX7</i>	19024788	19025591
chr1	<i>PAX7</i>	19025618	19026065
chr1	<i>PAX7</i>	19026338	19026440
chr1	<i>PAX7</i>	19026448	19026553
chr1	<i>PAX7</i>	19026603	19026891
chr1	<i>PAX7</i>	19026918	19027127
chr1	<i>PAX7</i>	19027138	19027146
chr1	<i>PAX7</i>	19027147	19027312
chr1	<i>PAX7</i>	19027313	19027886
chr1	<i>PAX7</i>	19028048	19028454
chr1	<i>PAX7</i>	19028473	19028552
chr1	<i>PAX7</i>	19028843	19029154
chr1	<i>PAX7</i>	19029168	19029309
chr1	<i>PAX7</i>	19029318	19029587
chr1	<i>PAX7</i>	19029588	19029790
chr1	<i>PAX7</i>	19029791	19030717
chr1	<i>PAX7</i>	19030743	19030843
chr1	<i>PAX7</i>	19031203	19032920
chr1	<i>PAX7</i>	19033258	19033581
chr1	<i>PAX7</i>	19033613	19033887
chr1	<i>PAX7</i>	19034218	19034396
chr1	<i>PAX7</i>	19034403	19034778
chr1	<i>PAX7</i>	19035068	19036142
chr1	<i>PAX7</i>	19036143	19039285
chr1	<i>PAX7</i>	19039573	19040420
chr1	<i>PAX7</i>	19040723	19041107
chr1	<i>PAX7</i>	19041118	19042507
chr1	<i>PAX7</i>	19042528	19042988

Table S4. Continued

Chromosome	Gene	Start	End
chr1	<i>PAX7</i>	19043003	19045146
chr1	<i>PAX7</i>	19045423	19047007
chr1	<i>PAX7</i>	19047023	19047189
chr1	<i>PAX7</i>	19047223	19051579
chr1	<i>PAX7</i>	19051583	19052463
chr1	<i>PAX7</i>	19052528	19052626
chr1	<i>PAX7</i>	19052668	19053517
chr1	<i>PAX7</i>	19053523	19053612
chr1	<i>PAX7</i>	19053613	19053745
chr1	<i>PAX7</i>	19053898	19054069
chr1	<i>PAX7</i>	19054083	19055091
chr1	<i>PAX7</i>	19055373	19056701
chr1	<i>PAX7</i>	19056703	19056919
chr1	<i>PAX7</i>	19056923	19057922
chr1	<i>PAX7</i>	19057923	19058511
chr1	<i>PAX7</i>	19058538	19058824
chr1	<i>PAX7</i>	19058828	19062125
chr1	<i>PAX7</i>	19062126	19062632
chr1	<i>PAX7_downstream</i>	19062633	19062685
chr1	<i>PAX7_downstream</i>	19062973	19063358
chr1	<i>PAX7_downstream</i>	19063368	19063894
chr1	<i>PAX7_downstream</i>	19063918	19064635
chr1	<i>PAX7_downstream</i>	19064648	19066973
chr1	<i>PAX7_downstream</i>	19066978	19067189
chr1	<i>PAX7_downstream</i>	19067983	19068380
chr1	<i>PAX7_downstream</i>	19068393	19068630
chr1	<i>PAX7_downstream</i>	19068933	19069708
chr1	<i>PAX7_downstream</i>	19069713	19070384
chr1	<i>PAX7_downstream</i>	19070388	19070918
chr1	<i>PAX7_downstream</i>	19071043	19071154
chr1	<i>PAX7_downstream</i>	19071228	19074279
chr1	<i>PAX7_downstream</i>	19074318	19074483
chr1	<i>PAX7_downstream</i>	19074488	19075784
chr1	<i>PAX7_downstream</i>	19075883	19079140
chr1	<i>PAX7_downstream</i>	19079148	19079750
chr1	<i>PAX7_downstream</i>	19079753	19081503

Table S4. Continued

Chromosome	Gene	Start	End
chr1	<i>PAX7_downstream</i>	19081508	19081718
chr1	<i>PAX7_downstream</i>	19081728	19082146
chr1	<i>PAX7_downstream</i>	19082233	19082704
chr1	<i>PAX7_downstream</i>	19082768	19082887
chr1	<i>PAX7_downstream</i>	19082938	19083015
chr1	<i>PAX7_downstream</i>	19083083	19083283
chr1	<i>PAX7_downstream</i>	19083568	19083788
chr1	<i>PAX7_downstream</i>	19083848	19084136
chr1	<i>PAX7_downstream</i>	19084143	19084323
chr1	<i>PAX7_downstream</i>	19084388	19085417
chr1	<i>PAX7_downstream</i>	19085798	19086011
chr1	<i>PAX7_downstream</i>	19086588	19087002
chr2	<i>PAX3</i>	223064571	223066161
chr2	<i>PAX3</i>	223066162	223066539
chr2	<i>PAX3</i>	223066551	223066662
chr2	<i>PAX3</i>	223066663	223066909
chr2	<i>PAX3</i>	223066910	223067142
chr2	<i>PAX3</i>	223067156	223067416
chr2	<i>PAX3</i>	223067426	223067736
chr2	<i>PAX3</i>	223067766	223068044
chr2	<i>PAX3</i>	223068066	223068790
chr2	<i>PAX3</i>	223068826	223069668
chr2	<i>PAX3</i>	223069676	223070856
chr2	<i>PAX3</i>	223070861	223071113
chr2	<i>PAX3</i>	223071116	223071398
chr2	<i>PAX3</i>	223071421	223071724
chr2	<i>PAX3</i>	223071731	223072668
chr2	<i>PAX3</i>	223072741	223074310
chr2	<i>PAX3</i>	223074608	223075573
chr2	<i>PAX3</i>	223075868	223076304
chr2	<i>PAX3</i>	223076308	223077344
chr2	<i>PAX3</i>	223077363	223079278
chr2	<i>PAX3</i>	223079288	223081401
chr2	<i>PAX3</i>	223081448	223082491
chr2	<i>PAX3</i>	223082508	223083525
chr2	<i>PAX3</i>	223083533	223084504

Table S4. Continued

Chromosome	Gene	Start	End
chr2	<i>PAX3</i>	223084523	223084858
chr2	<i>PAX3</i>	223084859	223085073
chr2	<i>PAX3</i>	223085074	223085940
chr2	<i>PAX3</i>	223085941	223086106
chr2	<i>PAX3</i>	223086107	223087135
chr2	<i>PAX3</i>	223087393	223089277
chr2	<i>PAX3</i>	223089293	223091643
chr2	<i>PAX3</i>	223091648	223091783
chr2	<i>PAX3</i>	223091798	223092042
chr2	<i>PAX3</i>	223092338	223092442
chr2	<i>PAX3</i>	223092453	223093359
chr2	<i>PAX3</i>	223093683	223094631
chr2	<i>PAX3</i>	223095588	223095663
chr2	<i>PAX3</i>	223095668	223096796
chr2	<i>PAX3</i>	223096797	223097002
chr2	<i>PAX3</i>	223097003	223097484
chr2	<i>PAX3</i>	223097498	223097788
chr2	<i>PAX3</i>	223097818	223098998
chr2	<i>PAX3</i>	223099003	223100501
chr2	<i>PAX3</i>	223100503	223100985
chr2	<i>PAX3</i>	223101078	223102030
chr2	<i>PAX3</i>	223102068	223102525
chr2	<i>PAX3</i>	223102528	223104187
chr2	<i>PAX3</i>	223104198	223104542
chr2	<i>PAX3</i>	223104553	223105490
chr2	<i>PAX3</i>	223105493	223105668
chr2	<i>PAX3</i>	223105678	223109457
chr2	<i>PAX3</i>	223109468	223109603
chr2	<i>PAX3</i>	223109888	223110402
chr2	<i>PAX3</i>	223110718	223111202
chr2	<i>PAX3</i>	223111223	223111294
chr2	<i>PAX3</i>	223111318	223112512
chr2	<i>PAX3</i>	223112518	223113943
chr2	<i>PAX3</i>	223113948	223115312
chr2	<i>PAX3</i>	223115323	223115809
chr2	<i>PAX3</i>	223116558	223118358

Table S4. Continued

Chromosome	Gene	Start	End
chr2	<i>PAX3</i>	223118673	223118874
chr2	<i>PAX3</i>	223118878	223119506
chr2	<i>PAX3</i>	223119788	223120492
chr2	<i>PAX3</i>	223120778	223121929
chr2	<i>PAX3</i>	223121933	223123219
chr2	<i>PAX3</i>	223123233	223123550
chr2	<i>PAX3</i>	223123578	223123779
chr2	<i>PAX3</i>	223123783	223124623
chr2	<i>PAX3</i>	223124883	223124989
chr2	<i>PAX3</i>	223125068	223125274
chr2	<i>PAX3</i>	223125588	223126286
chr2	<i>PAX3</i>	223126348	223127035
chr2	<i>PAX3</i>	223127068	223127399
chr2	<i>PAX3</i>	223127408	223127689
chr2	<i>PAX3</i>	223127693	223127826
chr2	<i>PAX3</i>	223127833	223127908
chr2	<i>PAX3</i>	223127918	223127995
chr2	<i>PAX3</i>	223128018	223128118
chr2	<i>PAX3</i>	223128133	223128274
chr2	<i>PAX3</i>	223128283	223128904
chr2	<i>PAX3</i>	223129003	223129316
chr2	<i>PAX3</i>	223129358	223130093
chr2	<i>PAX3</i>	223130403	223132529
chr2	<i>PAX3</i>	223132543	223134383
chr2	<i>PAX3</i>	223134388	223135193
chr2	<i>PAX3</i>	223135218	223138044
chr2	<i>PAX3</i>	223138048	223138474
chr2	<i>PAX3</i>	223138483	223139247
chr2	<i>PAX3</i>	223139258	223140147
chr2	<i>PAX3</i>	223140158	223140585
chr2	<i>PAX3</i>	223140603	223142353
chr2	<i>PAX3</i>	223142738	223143643
chr2	<i>PAX3</i>	223144043	223144646
chr2	<i>PAX3</i>	223145163	223146766
chr2	<i>PAX3</i>	223146768	223148051
chr2	<i>PAX3</i>	223148053	223148220

Table S4. Continued

Chromosome	Gene	Start	End
chr2	<i>PAX3</i>	223148223	223149313
chr2	<i>PAX3</i>	223149358	223150651
chr2	<i>PAX3</i>	223150948	223151965
chr2	<i>PAX3</i>	223151983	223152848
chr2	<i>PAX3</i>	223152853	223155647
chr2	<i>PAX3</i>	223155653	223156679
chr2	<i>PAX3</i>	223156728	223158058
chr2	<i>PAX3</i>	223158113	223158431
chr2	<i>PAX3</i>	223158438	223158574
chr2	<i>PAX3</i>	223158588	223158885
chr2	<i>PAX3</i>	223158886	223159020
chr2	<i>PAX3</i>	223159021	223159513
chr2	<i>PAX3</i>	223159538	223160246
chr2	<i>PAX3</i>	223160247	223160376
chr2	<i>PAX3</i>	223160377	223160907
chr2	<i>PAX3</i>	223160928	223161166
chr2	<i>PAX3</i>	223161173	223161696
chr2	<i>PAX3</i>	223161697	223161932
chr2	<i>PAX3</i>	223161933	223162813
chr2	<i>PAX3</i>	223162838	223163249
chr2	<i>PAX3</i>	223163250	223163735
chr13	<i>FOXO1_downstream</i>	41118832	41119089
chr13	<i>FOXO1_downstream</i>	41119357	41119544
chr13	<i>FOXO1_downstream</i>	41119797	41119895
chr13	<i>FOXO1_downstream</i>	41119957	41121089
chr13	<i>FOXO1_downstream</i>	41121102	41121625
chr13	<i>FOXO1_downstream</i>	41121637	41122575
chr13	<i>FOXO1_downstream</i>	41122877	41123072
chr13	<i>FOXO1_downstream</i>	41123122	41124372
chr13	<i>FOXO1_downstream</i>	41124422	41125918
chr13	<i>FOXO1_downstream</i>	41125967	41126523
chr13	<i>FOXO1_downstream</i>	41126537	41126882
chr13	<i>FOXO1</i>	41127197	41133171
chr13	<i>FOXO1</i>	41133172	41133337
chr13	<i>FOXO1</i>	41133347	41133645
chr13	<i>FOXO1</i>	41133646	41134997

Table S4. Continued

Chromosome	Gene	Start	End
chr13	<i>FOXO1</i>	41134998	41135210
chr13	<i>FOXO1</i>	41135502	41135812
chr13	<i>FOXO1</i>	41136097	41136263
chr13	<i>FOXO1</i>	41136267	41138425
chr13	<i>FOXO1</i>	41138432	41140526
chr13	<i>FOXO1</i>	41140807	41141829
chr13	<i>FOXO1</i>	41142107	41143921
chr13	<i>FOXO1</i>	41144022	41144164
chr13	<i>FOXO1</i>	41144462	41145332
chr13	<i>FOXO1</i>	41145512	41147844
chr13	<i>FOXO1</i>	41147867	41148243
chr13	<i>FOXO1</i>	41148307	41149210
chr13	<i>FOXO1</i>	41149462	41150372
chr13	<i>FOXO1</i>	41150377	41152924
chr13	<i>FOXO1</i>	41152967	41156356
chr13	<i>FOXO1</i>	41156357	41156590
chr13	<i>FOXO1</i>	41156657	41156732
chr13	<i>FOXO1</i>	41156872	41157073
chr13	<i>FOXO1</i>	41157182	41157327
chr13	<i>FOXO1</i>	41157377	41157546
chr13	<i>FOXO1</i>	41157777	41157850
chr13	<i>FOXO1</i>	41158057	41158484
chr13	<i>FOXO1</i>	41158787	41159475
chr13	<i>FOXO1</i>	41159497	41161412
chr13	<i>FOXO1</i>	41161417	41162958
chr13	<i>FOXO1</i>	41163252	41164896
chr13	<i>FOXO1</i>	41164907	41165838
chr13	<i>FOXO1</i>	41166127	41167168
chr13	<i>FOXO1</i>	41167447	41168539
chr13	<i>FOXO1</i>	41168542	41168830
chr13	<i>FOXO1</i>	41169107	41169677
chr13	<i>FOXO1</i>	41169687	41170067
chr13	<i>FOXO1</i>	41170092	41172640
chr13	<i>FOXO1</i>	41172647	41173269
chr13	<i>FOXO1</i>	41173272	41175989
chr13	<i>FOXO1</i>	41176007	41176660

Table S4. Continued

Chromosome	Gene	Start	End
chr13	<i>FOXO1</i>	41176667	41176978
chr13	<i>FOXO1</i>	41176992	41177486
chr13	<i>FOXO1</i>	41177612	41178317
chr13	<i>FOXO1</i>	41178332	41179150
chr13	<i>FOXO1</i>	41179267	41179361
chr13	<i>FOXO1</i>	41179382	41180117
chr13	<i>FOXO1</i>	41180127	41180435
chr13	<i>FOXO1</i>	41180737	41181675
chr13	<i>FOXO1</i>	41181677	41184792
chr13	<i>FOXO1</i>	41184847	41185466
chr13	<i>FOXO1</i>	41185472	41185919
chr13	<i>FOXO1</i>	41186237	41186825
chr13	<i>FOXO1</i>	41186837	41186910
chr13	<i>FOXO1</i>	41186922	41187542
chr13	<i>FOXO1</i>	41187562	41187876
chr13	<i>FOXO1</i>	41187887	41188086
chr13	<i>FOXO1</i>	41188092	41189383
chr13	<i>FOXO1</i>	41189702	41190410
chr13	<i>FOXO1</i>	41190422	41191293
chr13	<i>FOXO1</i>	41191577	41192216
chr13	<i>FOXO1</i>	41192487	41193150
chr13	<i>FOXO1</i>	41193447	41194942
chr13	<i>FOXO1</i>	41195217	41196511
chr13	<i>FOXO1</i>	41196532	41197265
chr13	<i>FOXO1</i>	41197277	41197653
chr13	<i>FOXO1</i>	41197657	41197968
chr13	<i>FOXO1</i>	41198252	41198456
chr13	<i>FOXO1</i>	41198472	41199480
chr13	<i>FOXO1</i>	41199482	41199757
chr13	<i>FOXO1</i>	41199802	41200111
chr13	<i>FOXO1</i>	41200242	41201674
chr13	<i>FOXO1</i>	41201987	41202172
chr13	<i>FOXO1</i>	41202192	41202313
chr13	<i>FOXO1</i>	41202327	41202500
chr13	<i>FOXO1</i>	41202527	41202775
chr13	<i>FOXO1</i>	41202842	41203288

Table S4. Continued

Chromosome	Gene	Start	End
chr13	<i>FOXO1</i>	41203572	41203777
chr13	<i>FOXO1</i>	41203827	41204525
chr13	<i>FOXO1</i>	41204807	41205434
chr13	<i>FOXO1</i>	41205612	41205713
chr13	<i>FOXO1</i>	41205872	41205943
chr13	<i>FOXO1</i>	41205957	41206048
chr13	<i>FOXO1</i>	41206417	41206547
chr13	<i>FOXO1</i>	41207197	41207298
chr13	<i>FOXO1</i>	41207312	41207385
chr13	<i>FOXO1</i>	41207392	41208634
chr13	<i>FOXO1</i>	41209132	41210091
chr13	<i>FOXO1</i>	41210372	41210513
chr13	<i>FOXO1</i>	41210947	41211153
chr13	<i>FOXO1</i>	41211157	41211317
chr13	<i>FOXO1</i>	41211602	41212197
chr13	<i>FOXO1</i>	41212207	41212514
chr13	<i>FOXO1</i>	41212532	41212816
chr13	<i>FOXO1</i>	41212822	41213060
chr13	<i>FOXO1</i>	41213347	41214884
chr13	<i>FOXO1</i>	41215207	41215521
chr13	<i>FOXO1</i>	41215567	41215701
chr13	<i>FOXO1</i>	41215702	41215846
chr13	<i>FOXO1</i>	41216137	41216758
chr13	<i>FOXO1</i>	41217062	41217190
chr13	<i>FOXO1</i>	41217497	41217872
chr13	<i>FOXO1</i>	41217877	41218027
chr13	<i>FOXO1</i>	41218042	41219940
chr13	<i>FOXO1</i>	41220212	41220430
chr13	<i>FOXO1</i>	41220592	41220727
chr13	<i>FOXO1</i>	41221017	41221116
chr13	<i>FOXO1</i>	41221132	41221545
chr13	<i>FOXO1</i>	41221832	41224140
chr13	<i>FOXO1</i>	41224277	41224380
chr13	<i>FOXO1</i>	41224572	41224880
chr13	<i>FOXO1</i>	41225347	41226429
chr13	<i>FOXO1</i>	41226662	41227108

Table S4. Continued

Chromosome	Gene	Start	End
chr13	<i>FOXO1</i>	41227397	41227581
chr13	<i>FOXO1</i>	41227597	41228342
chr13	<i>FOXO1</i>	41228657	41229218
chr13	<i>FOXO1</i>	41229497	41229768
chr13	<i>FOXO1</i>	41230057	41230972
chr13	<i>FOXO1</i>	41231197	41231448
chr13	<i>FOXO1</i>	41231757	41232872
chr13	<i>FOXO1</i>	41233482	41233608
chr13	<i>FOXO1</i>	41233612	41233780
chr13	<i>FOXO1</i>	41233817	41234975
chr13	<i>FOXO1</i>	41235117	41235422
chr13	<i>FOXO1</i>	41235722	41236029
chr13	<i>FOXO1</i>	41236332	41237351
chr13	<i>FOXO1</i>	41237377	41238151
chr13	<i>FOXO1</i>	41238397	41239719
chr13	<i>FOXO1</i>	41239720	41240734
chr13	<i>FOXO1_upstream</i>	41240735	41240982
chr13	<i>FOXO1_upstream</i>	41240992	41243152
chr13	<i>FOXO1_upstream</i>	41243402	41243921
chr13	<i>FOXO1_upstream</i>	41244222	41244314
chr13	<i>FOXO1_upstream</i>	41244322	41244951
chr13	<i>FOXO1_upstream</i>	41244977	41245782
chr13	<i>FOXO1_upstream</i>	41246032	41248301
chr13	<i>FOXO1_upstream</i>	41248632	41249463
chr13	<i>FOXO1_upstream</i>	41249467	41249883
chr13	<i>FOXO1_upstream</i>	41250167	41250609
chr13	<i>FOXO1_upstream</i>	41250797	41250934
chr13	<i>FOXO1_upstream</i>	41251212	41251561
chr13	<i>FOXO1_upstream</i>	41251577	41251666
chr13	<i>FOXO1_upstream</i>	41251672	41251746

Table S5. Characteristics of custom ddPCR primer-probe sets used for analysis of genetic variants in patient cfDNA.

Assay ID	Target gene	Oligo	Oligo sequence (5'-3')	Annealing temp (°C)	Amplicon size (bp)	Probe dye
1 Variant 1	PAX3-FOXO1	F	TCC AGG AGA TGC AAT GAC C	58	97	FAM
		R	GAG ACC TCC ATA GTT GCT CA			
		P	CCC C+AG CCT +AAT G+AA CAA CC			
1 Variant 2	PAX3-FOXO1	F	GCT CTG AAC ATG GCT TTG G	58	98	FAM
		R	GAA CAC CTG ACT ACT TAA GAA CA			
		P	AGG A+AT TCT +TGG TTC +ACG TCT T			
3	PAX3-FOXO1	F	ATA GAG ACA CAC AGC CAC AG	56	102	FAM
		R	GTT CAT GTC TAA CAC CCT GG			
		P	ACG CCT G+AT TAT AGG TCA CAA GCC			
5	PAX3-FOXO1	F	GTAGACATGGGGTTTCACC	58	141	FAM
		R	TCCTGGTCTAGGATCTTGC			
		P	TGACTAAAACCTCTCGCATCTGTTT			
6	PAX3-FOXO1	F	TGCCTCAAGAGCAAATGACA	57	120	FAM
		R	TCCTTCC TAATGAATTTCTAACG			
		P	AGCAGCAACTTTGGCAGTCGC			
7	PAX7-FOXO1	F	TTGTCCCCCACTCTAGGTT	56	121	FAM
		R	CCTCCCTCACTTCTGAAG			
		P	AAAGGGCCAGGAGAGAGAAG			
12 Variant 1	PAX7-FOXO1	F	CACTCCAGCTTGGTGACAGA	57	85	FAM
		R	TTAGCCTTCCAGAGCTGCAT			
		P	AATTGCATTCTTCCCACCAAGC			

Table S5. Continued

Assay ID	Target gene	Oligo	Oligo sequence (5'-3')	Annealing temp (°C)	Amplicon size (bp)	Probe dye
12 Variant 2	PAX7-FOXO1	F	CATCACTGACGGAGCAGAAA	57	125	FAM
		R	GCACCAGGATCTCACACTTG			
		P	ACCCATATTGTTCCTAGTTGGTTTTGAC			
13	PAX3-FOXO1	F	AAT AGA GAC ACA GAG CCA CA	56	86	FAM
		R	CAC TTC TCT GTA ATG ACA CTG T			
		P	ACA CAC GCC TT+A GC+A AAA GT			
14 Variant 1	PAX3-FOXO1	F	ACA AGA AGG TAC AGA AGC T	58	116	FAM
		R	GAC CAA CAT CAT GAG ACC CT			
		P	TAC AGC TGT GTG CC+A CCA CG			
14 Variant 2	PAX3-FOXO1	F	GAG TGA GGT GGC TCG ATC	58	94	FAM
		R	GAC AGC ACC AAT AGA GTT CAA			
		P	CCT CCC +AGG TCC +AAG CAA			
18	PAX3-FOXO1	F	AGA GAG ATT ACA CCA CGT CC	56	119	FAM
		R	ATC TGA ACA ACA TCC TGG AC			
		P	TCT GTC GGT TTT TG+A GGT GAC CT			
19	PAX3-FOXO1	F	TCT GAA TGG TCC ATG AGC	56	94	FAM
		R	CAA CCA TTT TCT TCC TTT AGC A			
		P	AGC TGC ATT +ACC CCG GGA AG			
20	PAX7-FOXO1	F	AGA CAG GAA CAC CAC ACC	56	79	FAM
		R	TGC CTC TTC CCT TCT AAT CC			
		P	TTC +ACC TCC CCG ACA CCT CT			

Table S5. Continued

Assay ID	Target gene	Oligo	Oligo sequence (5'-3')	Annealing temp (°C)	Amplicon size (bp)	Probe dye
21 Variant 1	PAX3-FOXO1	F	ATC TCC ATC CTT GAA CGG TT	58	97	FAM
		R	CTT GCC TTT CTC TTG TGC TG			
		P	TGA CCC +ACC CTG +ATC ACT TCT			
21 Variant 2	PAX3-FOXO1	F	ATA GGT TGG TTG CAG GCT AC	58	119	FAM
		R	GCA GGG ATT TGA GTC AGG AT			
		P	AGC TTT +AGG +AAG AG+A TGT +AGC TTT G			
β-actin (reference gene)	ACTB	F	GTAAGGACAAGTTGGCCCCC	55-60	101	HEX
		R	TGACTTTGTGGTGTGGCTGG			
		P	TGCAGGGTTCACCCCTCTGCTGCCCCCA			

Abbreviations: F = forward primer; R = reverse primer; P = probe

Table S6. Characteristics of commercial ddPCR primer-probe sets used for analysis of tumor variants in patient cfDNA.

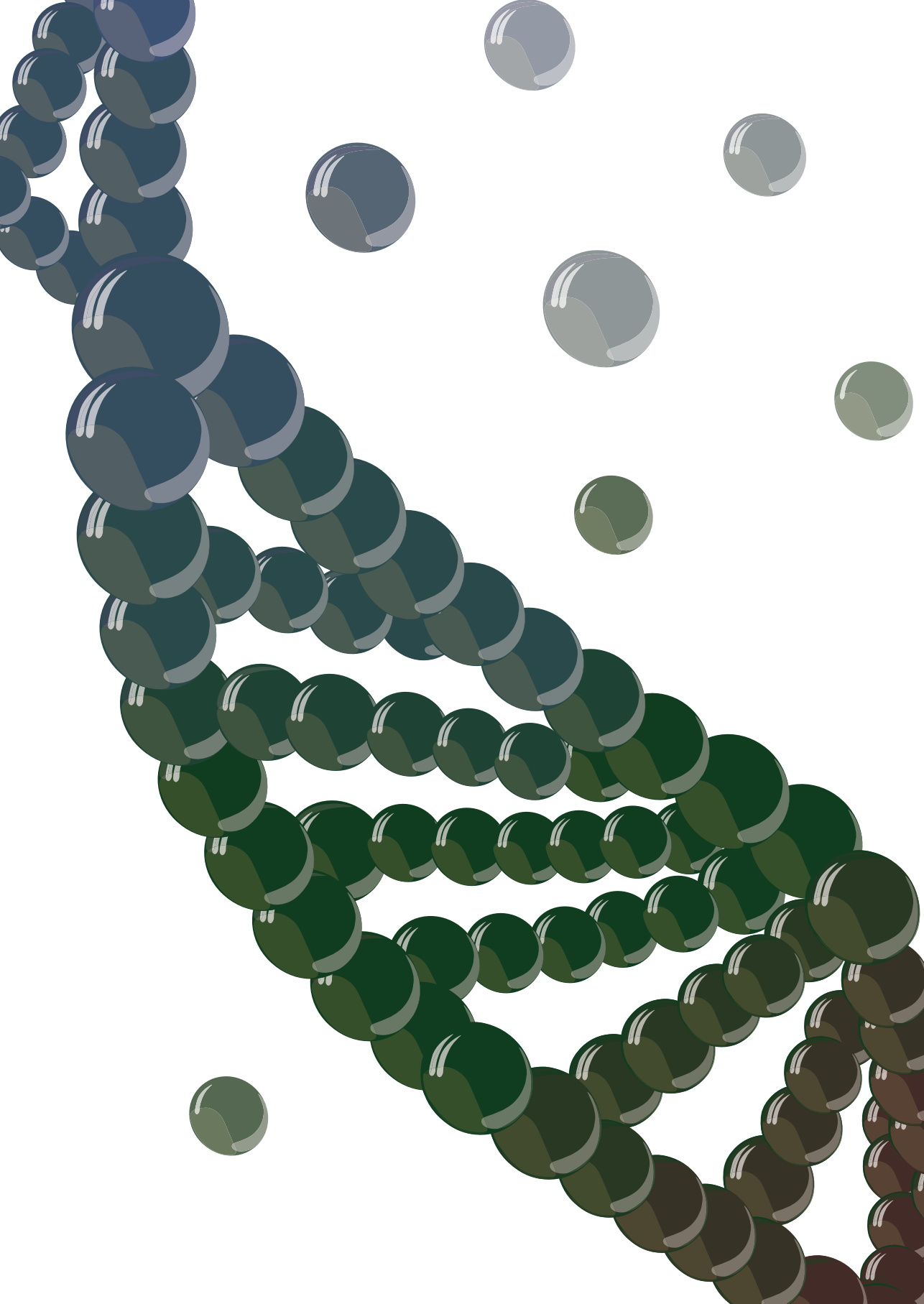
Assay ID	Target	Source	Annealing temp (°C)	Dye
dHsaCP2500374 (Copy number assay)	<i>CDK4</i>	Bio-Rad	60	FAM
dHsaCP2500320 (Copy Number assay)	<i>FGFR2</i>	Bio-Rad	60	FAM
228443642 (SNP Genotyping Assay)	<i>KRAS</i> ^{G13D}	IDT	60	FAM
dHsaCP2500317 (Copy number assay)	<i>MDM2</i>	Bio-Rad	60	FAM
dHsaMDS579992170	<i>NRAS</i> ^{Q61K}	Bio-Rad	55	FAM
4331349 (Custom Taqman SNP Genotyping Assay)	<i>BRAF</i> ^{V600E}	Thermo Fisher	60	FAM
4331349 (Custom Taqman SNP Genotyping Assay)	<i>NRAS</i> ^{G12A}	Thermo Fisher	60	FAM
4331349 (Custom Taqman SNP Genotyping Assay)	<i>NRAS</i> ^{Q61R}	Thermo Fisher	60	FAM
4331349 (Custom Taqman SNP Genotyping Assay)	<i>MYO1</i> ^{L122R}	Thermo Fisher	55	FAM
4331349 (Custom Taqman SNP Genotyping Assay)	<i>PIK3CA</i> ^{H1044K}	Thermo Fisher	55	FAM
dHsaCP2500350 (Copy number assay)	<i>RPP30</i>	Bio-Rad	58	HEX
dHsaCNS674780718 (Copy number assay)	<i>RPPH1</i>	Bio-Rad	58	HEX

Table S7. *PAX3-FOXO1* and *PAX7-FOXO1* breakpoint locations identified in fusion-positive patient tumor DNA via targeted sequencing

Case	Gene fusion	Fusion partner 1		Fusion partner 2	
		Chromosome	Location	Chromosome	Location
1	<i>PAX3-FOXO1</i>	2	223,071,019	13	41,162,803
	<i>PAX3-FOXO1</i>	2	223,071,615	13	41,157,856
3	<i>PAX3-FOXO1</i>	2	223,082,412	13	41,191,753
5	<i>PAX3-FOXO1</i>	2	223,082,041	13	41,195,136
6	<i>PAX3-FOXO1</i>	2	223,069,832	13	41,161,236
7	<i>PAX7-FOXO1</i>	1	19,042,580	13	41,176,358
12	<i>PAX7-FOXO1</i>	1	19,041,354	13	41,229,493
	<i>PAX7-FOXO1</i>	1	19,048,182	13	41,229,523
13	<i>PAX3-FOXO1</i>	2	223,082,528	13	41,191,754
14	<i>PAX3-FOXO1</i>	2	223,076,047	13	41,165,979
	<i>PAX3-FOXO1</i>	2	223,076,078	13	41,165,949
18	<i>PAX3-FOXO1</i>	2	223,067,214	13	41,143,785
19	<i>PAX3-FOXO1</i>	2	223,073,869	13	41,157,501
20	<i>PAX7-FOXO1</i>	1	19,056,569	13	41,151,743
21	<i>PAX3-FOXO1</i>	2	223,078,665	13	41,169,915
	<i>PAX3-FOXO1</i>	2	223,078,489	13	41,170,565

References for Supplementary data

- Manzella G, Schreck LD, Breunis WB, Molenaar J, Merks H, Barr FG, Sun W, Römmele M, Zhang L, Tchinda J, Ngo Q, Bode PK, Delattre O, Surdez D, Rekhi B, Niggli FK, Schäfer BW, Wachtel M. High throughput drug profiling with a living biobank of primary rhabdomyosarcoma cells unravels disease heterogeneity and detects an AKT inhibitor sensitive subgroup. *Nat Commun.* 2020 Sep 15;11(1):4629. doi.org/10.1038/s41467-020-18388-7
- de Vree PJP, de Wit E, Yilmaz M, et al. Targeted sequencing by proximity ligation for comprehensive variant detection and local haplotyping. *Nat Biotechnol.* 2014 32(10):1019-25
- Izquierdo E, Yuan L, George S, et al. Development of a targeted sequencing approach to identify prognostic, predictive and diagnostic markers in pediatric solid tumors. *Oncotarget*, 2017 8(67):112036-112050.
- George SL, Izquierdo E, Campbell J, et al. A tailored molecular profiling programme for children with cancer to identify clinically actionable genetic alterations. *Eur J Cancer.* 2019 21:224-235.
- Chicard M, Colmet-Daage L, Clement N, Danzon A, Bohec M, Bernard V, Baulande S, Bellini A, Deveau P, Pierron G, Lapouble E, Janoueix-Lerosey I, Peuchmaur M, Corradini N, Defachelles AS, Valteau-Couanet D, Michon J, Combaret V, Delattre O, Schleiermacher G. Whole-Exome Sequencing of Cell-Free DNA Reveals Temporo-spatial Heterogeneity and Identifies Treatment-Resistant Clones in Neuroblastoma. *Clin Cancer Res.* 2018 Feb 15;24(4):939-949. doi: 10.1158/1078-0432.CCR-17-1586.
- Alcoser SY et al. Real-time PCR-based assay to quantify the relative amount of human and mouse tissue present in tumor xenografts. *BMC Biotechnol.* 2011. doi:10.1186/1472-6750-11-124
- Deng W, McLaughlin SL & Klinke DJ. Quantifying spontaneous metastasis in a syngeneic mouse melanoma model using real time PCR. *Analyst.* 2017. doi:10.1039/c7an00623c
- Gorges TM et al. Cancer therapy monitoring in xenografts by quantitative analysis of circulating tumor DNA. *Biomarkers.* 2012. doi:10.3109/1354750X.2012.689133
- Schneider T, Osl F, Friess T et al. Quantification of human Alu sequences by real-time PCR - An improved method to measure therapeutic efficacy of anti- metastatic drugs in human xenotransplants. *Clin. Exp. Metastasis.* 2002. doi:10.1023/A:1020992411420
- Rago C et al. Serial assessment of human tumor burdens in mice by the analysis of circulating DNA. *Cancer Res* 2007. doi:10.1158/0008-5472.CAN-07-0605
- Rakhit CP et al. Early detection of pre-malignant lesions in a KRAS G12D-driven mouse lung cancer model by monitoring circulating free DNA. *DMM Dis. Model. Mech.* 2019. doi:10.1242/dmm.036863



Chapter 6

Targeted Locus Amplification to develop robust patient-specific assays for liquid biopsies in pediatric solid tumors

Front Oncol. 2023 Apr 20;13:1124737. doi: 10.3389/fonc.2023.1124737.

Lieke M. Van Zogchel^{1,2*}, Nathalie S. Lak^{2,1*}, Nina U. Gelineau^{2,1}, Irina Sergeeva³, Ellen Stelloo³, Joost Swennenhuis³, Harma Feitsma³, Max van Min³, Erik Splinter³, Margit Bleijs¹, Marian Groot Koerkamp¹, Willemijn Breunis^{1,4}, Michael T. Meister^{1,5}, Waleed H. Kholosy¹, Frank C. Holstege^{1,6}, Jan J. Molenaar¹, Wendy W. de Leng⁷, Janine Stutterheim¹, Ellen Van Der Schoot², Lieve Tytgat¹

¹ Princess Maxima Center for Pediatric Oncology, Netherlands,

² Sanquin Research, Netherlands,

³ Cergentis B.V., Netherlands,

⁴ University Children's Hospital Zurich, Switzerland,

⁵ Oncode Institute, Netherlands,

⁶ Center for Molecular Medicine, University Medical Center Utrecht, Netherlands,

⁷ Department of Pathology, UMC Utrecht, Netherlands

Abstract

Background: Liquid biopsies combine minimally invasive sample collection with sensitive detection of residual disease. Pediatric malignancies harbor tumor-driving copy number alterations or fusion genes, rather than recurrent point mutations. These regions contain tumor-specific DNA breakpoint sequences. We investigated the feasibility to use these breakpoints to design patient-specific markers to detect tumor-derived cell-free DNA (cfDNA) in plasma from patients with pediatric solid tumors.

Materials and methods: Regions of interest (ROI) were identified through standard clinical diagnostic pipelines, using SNP array for CNAs, and FISH or RT-qPCR for fusion genes. Using targeted locus amplification (TLA) on tumor organoids grown from tumor material or targeted locus capture (TLC) on FFPE material, ROI-specific primers and probes were designed, which were used to design droplet digital PCR (ddPCR) assays. cfDNA from patient plasma at diagnosis and during therapy was analyzed.

Results: TLA was performed on material from 2 rhabdomyosarcoma, 1 Ewing sarcoma and 3 neuroblastoma. FFPE-TLC was performed on 8 neuroblastoma tumors. For all patients, at least one patient-specific ddPCR was successfully designed and in all diagnostic plasma samples the patient-specific markers were detected. In the rhabdomyosarcoma and Ewing sarcoma patients, all samples after start of therapy were negative. In neuroblastoma patients, presence of patient-specific markers in cfDNA tracked tumor burden, decreasing during induction therapy, disappearing at complete remission and re-appearing at relapse.

Conclusion: We demonstrate the feasibility to determine tumor-specific breakpoints using TLA/TLC in different pediatric solid tumors and use these for analysis of cfDNA from plasma. Considering the high prevalence of CNAs and fusion genes in pediatric solid tumors, this approach holds great promise and deserves further study in a larger cohort with standardized plasma sampling protocols.

Contribution to the field

An important challenge in the treatment of children with solid tumors is monitoring therapy response. In current clinical practice, treatment response is evaluated by different imaging modalities, which have several limitations. In young children, most evaluation scans require general anesthesia. Moreover, subtle changes in the primary tumor or appearance of relapse are not detected by imaging until the tumor burden reaches a certain threshold. Precise monitoring of treatment response and relapse

detection are essential to improve survival. Liquid biopsies offer another approach to monitor tumor activity on a molecular level. Studying tumor-derived cell-free DNA in blood plasma combines minimal invasiveness with a high sensitivity, which makes this extremely suitable for use in pediatric patients. Pediatric solid tumors have a low mutational burden, often harboring tumordriving copy number alterations or fusion genes. In this study, we demonstrate the feasibility of designing patient-specific markers within these regions using targeted locus amplification (TLA) and evaluate the use of these assays on diagnostic and serial plasma samples from patients with pediatric solid tumors (neuroblastoma, rhabdomyosarcoma and Ewing sarcoma). This workflow for the analysis of liquid biopsies in pediatric solid tumors can be considered ready for the transition from bench to bedside.

Introduction

Despite advances in treatment and survival, mortality for pediatric patients with solid tumors that suffer of metastatic or relapsed disease remains high (1–7). During the course of the disease, children face many invasive procedures to acquire tumor material as well as imaging under general anesthesia to determine disease dissemination and response evaluation. Sampling of blood or other liquids produced by the human body, e.g. ‘liquid biopsies’ form a potential source of biomarkers that can be collected in a less invasive manner which could reduce the number of stressful procedures. Moreover, liquid biopsies contain material from both the primary tumor and metastatic lesions, thereby offering a more comprehensive view of the disease and could assist in clinical decision making (8–10). An important challenge is the correct choice of the marker. Studies focusing on the detection of tumor-derived mRNA from blood and bone marrow using a tumor-specific RNA panel have shown promising results for improving risk stratification at diagnosis, as seen in neuroblastoma and rhabdomyosarcoma (10–12). However, these methods still require the use of bone marrow, and the potential for response monitoring with this approach has not been shown yet for rhabdomyosarcoma (10). Cell-free DNA (cfDNA) from plasma holds great potential for diagnostic and prognostic purposes in pediatric solid tumors (13–16). We have previously described hypermethylated RASSF1A as a marker for cell free tumor DNA in several pediatric tumors. However, the level of methylation of RASSF1A differs in different types of pediatric tumors, which limits its use (16). In contrast to adult malignancies, mutations in pediatric tumors are scarce. Often, they have copy number alterations (CNAs) or translocations resulting in fusion genes which are considered early tumor-driving events and remain present during the entire course of the disease (17–19). In rhabdomyosarcoma,

the fusion gene between PAX3 or PAX7 and FOXO1 is an important characteristic within the alveolar subtype (3, 20–22). In Ewing sarcoma, EWSR1 pairs with several fusion partners from the ETS family of transcription factors (5, 17). Neuroblastoma tumors often have amplification of MYCN, loss of heterozygosity of chromosome 1p and 11p and gain of 17q (4). Most of these CNAs result in a unique chromosomal fusion, however it is mostly unknown to which chromosome. These genetic events are formed by DNA sequences which are exclusive to a patient, thereby forming a perfect target to detect tumor-derived DNA since these sequences are not present in the background of healthy cell-free DNA, which is always present in blood. For pediatric patients with a solid tumor, fluorescent in situ hybridization (FISH), shallow whole genome sequencing (sWGS) or single nucleotide polymorphism (SNP) array has become available for routine diagnostics to identify clinically relevant fusion genes, as well as genomic deletions or amplifications. As these genomic aberrations are independent of gene activity, their presence could potentially be used to detect and quantify tumor burden. Historically, the identification of the exact breakpoint sequence has been time- and resource consuming, as WGS followed by Sanger sequencing validation was necessary (23). However, this procedure can be sped up by using a targeted approach for genomic breakpoint sequencing, like targeted locus amplification/capture (TLA/TLC). TLA/TLC is a technique that uses crosslinking of physically proximal sequences to selectively amplify and sequence regions of >100 kb surrounding specific primer or probe binding sites without prior detailed locus information. TLA can be applied to cells, while TLC is optimized for formalin fixed paraffin embedded (FFPE) material (24–27). The breakpoint sequence revealed by the TLA/TLC technique can be used to design an assay that targets the patient-specific breakpoint. We use droplet digital PCR (ddPCR) to detect these targets in small volumes of plasma from patients with pediatric solid tumors, since ddPCR allows for absolute quantification combined with high sensitivity. In this report, we investigate the possibility of designing patient-specific assays for cell free tumor DNA detection in patients with neuroblastoma, rhabdomyosarcoma and Ewing sarcoma, using TLA/TLC – based breakpoint sequences. Furthermore, we study whether the presence of these specific breakpoints correlates to residual and recurrent disease and, thus, its potential as marker for treatment response.

Methods

For a graphical overview of the methods, see Figure 1.

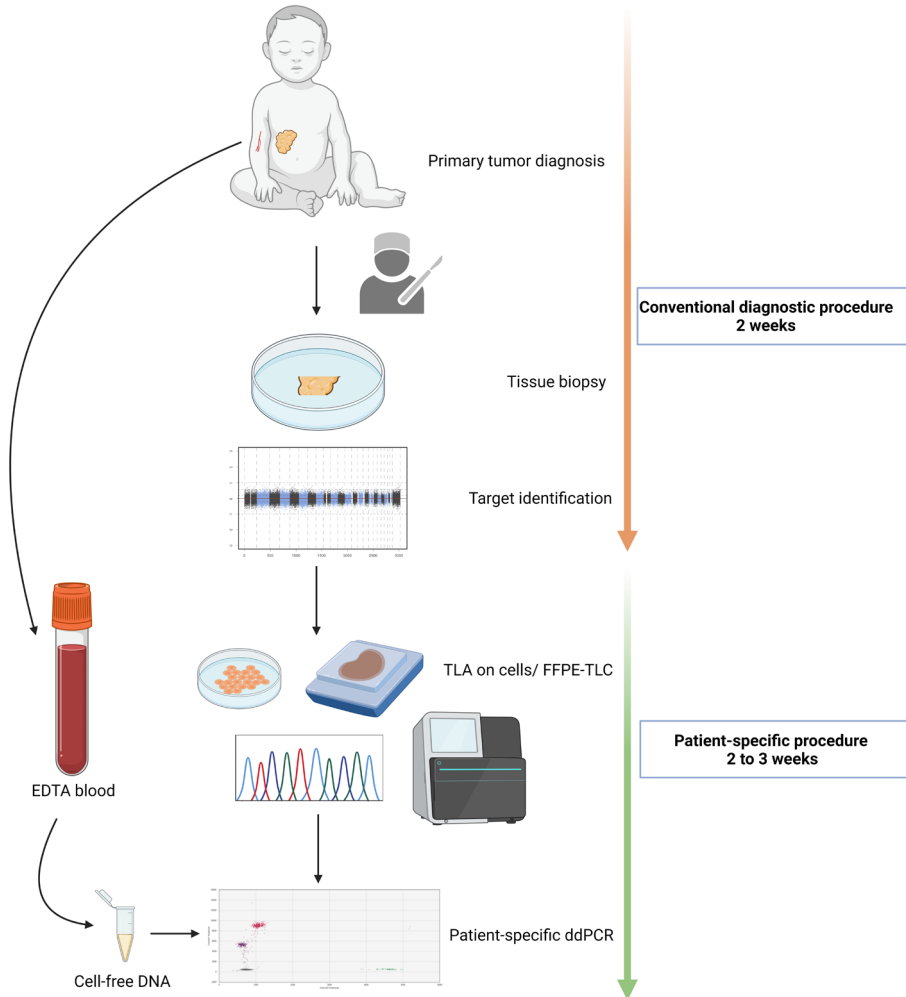


Figure 1. Workflow for the development of a patient-specific assay. At primary diagnosis, tumor material is collected through biopsy or resection. The tissue is then analyzed in the regular diagnostic pipeline. This means copy number analysis through SNP array for neuroblastoma tumors, and fusion gene detection through immunohistochemistry or RT-qPCR for rhabdomyosarcoma and Ewing sarcoma. Based on the identified altered regions/copy number aberrations and fusion partner, for targeted locus amplification (TLA) or targeted locus capture (TLC) is performed on cells or FFPE material, respectively. The breakpoint sequence(s) are then used for a patient-specific ddPCR design which is then measured on cell-free DNA from EDTA blood.

Tumor and plasma samples

Patients with neuroblastoma, rhabdomyosarcoma and Ewing sarcoma, diagnosed in 2016 and 2017 and treated at the Princess Máxima Center (Utrecht, the Netherlands), of whom tumor material (viable or FFPE) and genetic information of the tumor and plasma samples were available, were included in this study. Tumor samples were collected if patients/caretakers gave informed consent for biobanking. Plasma samples from neuroblastoma patients were collected within the Minimal Residual Disease study of the DCOG high-risk protocol (MEC07/219#08.17.0836) and from patients with rhabdomyosarcoma within the Minimal Residual Disease study (add-on within the EpSSG RMS2005, EudraCT number: 2005-000217-35). Plasma samples from the patient with Ewing sarcoma was collected after informed consent for the biobank. Peripheral blood was collected in EDTA tubes (Becton-Dickinson, NJ, USA) and processed within 24 hours. Plasma was obtained by centrifuging the blood samples at 1,375g for 10 minutes and stored at -20°C until further processing.

Identification of regions of interest

For neuroblastoma tumors, chromosomal regions with aberrations in copy numbers were identified through SNP array. SNP array copy number profiling and analysis of regions of homozygosity were performed according to standard procedures using the CytoSNP-850 K BeadChip (Illumina, San Diego, CA). Visualizations of SNP array results and data analysis were performed using NxClinical software (BioDiscovery, Los Angeles, CA), using Human genome build February 2009 GRCh37/hg1. Chromosomal aberrations that are known to be tumor driving or associated with high-risk disease were preferentially selected for TLA/TLC breakpoint identification (e.g. chromosome 1p, 1q, 2p (including *MYCN* locus), 3p, 11q, 17q) (4). The fusion partners of *FOXO1* in the fusion-positive alveolar rhabdomyosarcomas were validated through RT-qPCR on tumor organoid models (tumoroids) grown from primary tumor material, as described previously (28). In the Ewing sarcoma sample, the fusion between *EWSR1* and *FLI1* was validated through RT-qPCR on the tumoroid with primers located on *EWSR1* exon 8 (AGGAGAGAACCGGAGCATGA) and *FLI1* exon 5 (CCCTGAGGTAAGTGGTGTG).

Identification of the patient-specific breakpoint(s) using TLA and FFPE-TLC

After the regions of interest (ROI) were identified through standard clinical diagnostic pipelines, ROI-specific primers or probe panels were designed for TLA and FFPE-TLC sequencing by Cergentis (Utrecht, the Netherlands), to sequence tumor-specific breakpoints (24, 25). As starting material for TLA, 2 to 5 million tumoroid cells were used. For tumors for which only FFPE material was available, targeted locus capture (FFPE-TLC) was performed as described previously (27). For FFPE-TLC, 2-3 slides of 10µm

with >30% tumor were used. The region-specific primers used for TLA and location of capture probes used for TLC are provided in Supplemental Table S1. For TLA, PCR products were library prepped using the Illumina Nextera DNA Flex protocol (Illumina, San Diego, CA, USA) after ROI amplification, whereas for TLC, libraries were created with the KAPA library preparation kit (Roche Kapa Hyperprep, Kapa Unique Dual indexed adapter kit) and subsequently subjected to targeted capture. Sequencing for both TLA and TLC was performed on an Illumina sequencer. 151 bp reads were mapped using BWA-SW, version 0.7.15-r1140, settings `bwasw -b 7`. The NGS reads were aligned to the human genome (hg19). Breakpoint sites were identified based on coverage peak(s) in the genome and the detection of fusion-reads between different parts of the genome.

cfDNA isolation and ddPCR

cfDNA was isolated from plasma samples using the Quick-cfDNA Serum & Plasma kit (Zymo Research, CA, USA). Based on the plasma volume available, different amounts of plasma were used to isolate cfDNA based on availability, ranging from 200µl to 1000µl. To correct for variations in the amount of input plasma, cfDNA is reported in copies/mL plasma. In every analysis, *Actin beta* (*ACTB*) was included as a reference gene to determine total cfDNA input.

Using the patient-specific DNA sequence, a ddPCR assay was designed using Primer 3 Plus (<https://primer3plus.com/>). The design was tested for specificity using Primer Blast (<https://www.ncbi.nlm.nih.gov/tools/primer-blast/index.cgi>). Designs yielding amplicons in the human reference genome below 1000 bp were excluded to avoid aspecific amplification. The ddPCR assay conditions were optimized using DNA from the primary tumor. In every run, DNA from a healthy leukocyte pool and H₂O were included as negative controls. The patient-specific primers, probes, and assay conditions are provided in Supplemental Table S2.

Reaction mixes for ddPCR were prepared to a final volume of 22 µl using 11 µl ddPCR Supermix for probes (no dUTP) (Bio-Rad Laboratories, Hercules, CA, USA), 1 µl of target assay and 1 µl of *ACTB* assay (final concentration of 900 nM of each primer and 250 nM of each probe, unless otherwise specified), 5 µl of DNA eluate and 3 µl H₂O. Droplets were generated using the QX200™ Droplet Generator (Bio-Rad) or QX200™ Automated Droplet Generator (Bio-Rad). Incubation and thermal cycling were performed using the C1000 Touch Thermal Cycler (Bio-Rad), with the following program: 95°C for 10 min; 40 cycles of 94°C for 30s, annealing temperature variable per assay, for 1 min; 98°C for 10 min; 4°C hold. Following PCR, droplets were read and quantified using the QX200 Droplet reader and analyzed by QuantaSoft 1.7.4.0917 (Bio Rad) software for single targets on FAM and HEX. Analysis on assays with multiple targets on FAM

were done in QX Manager 1.2 Standard Edition software (Bio-Rad). The assay for methylated *RASSF1A* (*RASSF1A-M*) was performed as described previously (16).

Results

Patient-specific breakpoints were successfully identified in different pediatric solid tumors

An overview of the clinical characteristics of the patient cohort can be found in Table 1. Tumor material grown from primary tumor cells was available for TLA for 2 patients with rhabdomyosarcoma, 1 patient with Ewing sarcoma and 4 with neuroblastoma. For 8 patients with neuroblastoma, FFPE material was available for analysis by FFPE-TLC. An overview of the tested tumor material and identified breakpoints is shown in Table 2. In 4 patients with neuroblastoma, multiple breakpoints were detected by TLA and/or FFPE-TLC. In NB2056 2 breakpoints were identified in different locations: between chromosome 2 and 4, and between chromosome 11 and 17. In NB2050 4 breakpoints were identified in chromosome 2. Based on in-silico design results we proceeded with only 2 of these 4 breakpoints for ddPCR design. In 3 samples, NB2066, NB2086 and NB2100, some of the candidate breakpoint sequences were also found in the normal human reference genome (hg38) and therefore were not suited as tumor-specific target. For NB2100, no tumor-specific ddPCR could be designed, in NB2086 and NB2100, other suitable breakpoints were identified in these tumors. In all 14 tumors at least one breakpoint was identified by TLA/FFPE-TLC, and for 13/14 a tumor-specific ddPCR could be designed. These findings illustrate that TLA can be applied successfully both in freshly grown cells and FFPE material, for different tumor entities and different types of genetic aberrations: copy number aberrations and fusion genes.

Results of ddPCR assay in single and multiple breakpoints

Patient-specific ddPCR assays were designed for 15 breakpoints identified in 13 cases. An illustrative example of a ddPCR assay with one breakpoint is shown in Figure 2 for the cfDNA from diagnostic plasma and genomic DNA from the primary tumor from patient NB2049. In case more than one tumor-specific ddPCR could be designed, we aimed to combine these in a multiplex assay (Figure 3). For NB2050, two breakpoints, both chromosome 2-2 breakpoints in the amplified *MYCN* locus, were massively amplified relative to the reference gene, resulting in overloading of the droplets and failure to quantify the cfDNA targets accurately in undiluted cfDNA from diagnostic plasma. cfDNA diluted 500 times enabled correct quantification of the different targets. Both Figures 2, 3 illustrate the range that can be covered by ddPCR and the possibilities of absolute quantification.

Table 1. Clinical characteristics of patients analyzed by targeted locus amplification (TLA)/capture (TLC).

PtID	Age (years)	Gender	Tumor type	Tumor location	Risk group	Metastatic	Primary tumor volume (ml)	Molecular characteristics	Survival
RMS108	8.8	Female	Fusion-positive rhabdomyosarcoma	Bladder	M	Lung, bone	145.8	PAX3-FOXO1(Chr13-Chr2)	2x relapse, died of disease
RMS006	11.6	Male	Fusion-positive rhabdomyosarcoma	Leg	M	Lung, bone	55.3	PAX3-FOXO1(Chr13-Chr2)	Progressive disease, died of disease
EWS010			Ewing sarcoma					EWSR1-FLI1(Chr22-Chr11)	
NB2049	10.8	Male	Neuroblastoma	Abdominal	HR	Bone marrow	3198.8	MYCN gain, Chr17 gain	Refractory disease, died of disease
NB2050	4.1	Male	Neuroblastoma	Abdominal	HR	Bone marrow	1276.6	Chr17 gain	Progressive disease, died of disease
NB2053	1.8	Male	Neuroblastoma	Adrenal	HR	Bone marrow, lung, liver	1517	MYCN amp, LOH1p, Chr17 gain, ALK F1174L mutation	Relapse, died of disease
NB2054	0.7	Male	Neuroblastoma	Adrenal, paravertebral	HR	Bone marrow	2.1	MYCN amp, Chr17 gain LOH1p	Complete remission
NB2056	3.2	Female	Neuroblastoma	Adrenal	HR	Bone marrow	210.0	MYCN gain, Chr17 gain	Refractory disease, Complete remission
NB2061	0.4	Male	Neuroblastoma	Adrenal	LR	Bone marrow, liver	204	LOH1p	Progressive disease, died of disease

Table 1. Continued

PtID	Age (years)	Gender	Tumor type	Tumor location	Risk group	Metastatic	Primary tumor volume (ml)	Molecular characteristics	Survival
NB2066	1.8	Female	Neuroblastoma	Adrenal	HR	Bone marrow	4.7	<i>MYCN</i> gain, Chr17 gain	Complete remission
NB2074	1.9	Male	Neuroblastoma	Adrenal	HR	Bone marrow	491	Chr1p gain, Chr17q gain, <i>MYCN</i> amp	Progressive disease, died of disease
NB2086	2.0	Male	Neuroblastoma	Adrenal	HR	Bone marrow	unknown	LOH1p, LOH11q, <i>MYCN</i> amp	Progressive disease, died of disease
NB2100	2.4	Male	Neuroblastoma	Adrenal	HR	Bone marrow	1281	LOH1p, gain 17q, <i>MYCN</i> amp	Relapse, died of disease
NB2101	4.7	Male	Neuroblastoma	Adrenal	HR	Bone marrow	1767	Chr1p gain, Chr17q gain, <i>MYCN</i> amp	Relapse, died of disease

PtID, unique patient identifier; Risk group; M; metastatic, HR; high risk disease; amp, amplification; LOH, loss of heterozygosity.

Table 2. Overview of tumor material and breakpoints. (following page)

PtID	Tumor material	Timing of tumor sample	Region	Type of genetic aberration	Breakpoint partner 1	Breakpoint partner 2	Details on breakpoint	ddPCR assay successful
RMS108	Tumoroid	Relapse surgery	Chr 13- Chr 2 (PAX3- FOXO1)	Fusion gene	Chr13:4119 5136 (fwd)	Chr2:22308 2041	no overlapping base	yes
RMS006	Tumoroid	Relapse surgery	Chr 13- Chr 2 (PAX3- FOXO1)	Fusion gene	Chr13:4113 6846	Chr2:22308 2995	1 overlapping base	yes
ES010	Tumoroid	Relapse surgery	Chr 22- Chr 11 (EWSR- FLI)	Fusion gene	Chr22:2929 2022	Chr11:1287 72451	2 homologous bases	yes
NB2049	FFPE	Primary biopsy	Chr 1-Chr1	Amplification	Chr1:53649 791	Chr1:32092 640	7 inserted bases	yes
NB2050	FFPE	Resection	Chr2-Chr2	Amplification	Chr2:16022 293	Chr2:15960 456	5 inserted bases	NA
			Chr2-Chr2	Amplification	Chr2:21514 327	Chr2:15957 643	4 homologous bases	yes
			Chr2-Chr2	Amplification	Chr2:21511 794	Chr2:15957 693	2 homologous bases	NA
			Chr2-Chr2	Amplification	Chr2:16108 256	Chr2:20989 391	3 homologous bases	yes
NB2053	Tumoroid	Relapse biopsy	Chr 1- Chr 17	Translocation & gain	Chr1:47886 678	Chr17:3304 8245	2 homologous bases	yes
NB2054	FFPE	Resection	Chr2-Chr2	Amplification	Chr2:14863 510	Chr2:15987 902	1 homologous base	yes
NB2056	FFPE	Resection	Chr4-Chr2	Translocation	Chr4:19104 4254	Chr2:57488 356	1 homologous base	yes
			Chr 17- Chr 11	Amplification	Chr17:3094 7919	Chr11:7122 1924	17 inserted bases	yes
NB2061	Tumoroid	Relapse biopsy	Chr 1- Chr 16	Translocation	Chr16:6852 9301	Chr1:29295 626	2 homologous bases	yes
NB2066	FFPE	Primary biopsy	Chr 3- Chr 3	Amplification	Chr3:56630 532	Chr3:56630 543	20 homologous bases	no, sequence was found in normal hg38 genome
NB2074	FFPE	Resection	Chr 2	Amplification	Chr2:18597 249	Chr2:27751 059		yes
NB2086	Tumoroid	Relapse biopsy	Chr 11-9	Translocation	Chr11:8830 1222	Chr9:92443 417		no, sequence was found in normal hg38 genome
			Chr 2	Amplification	Chr2:16893 201	Chr2:15757 504	2 homologous bases	yes
NB2100	Tumoroid and FFPE	Organoid: relapse biopsy	Chr 1	Deletion	Chr 1: 92107327	Chr 1: 95347109	1 homologous base	yes
		FFPE: resection	Chr 2	Amplification	Chr2:16670 567	Chr2:15943 507	2 homologous bases	no, sequence was found in normal hg38 genome
			Chr 17	NA			In telomeric sequence	NA
NB2101	FFPE	Primary biopsy	Chr 2	Amplification (multiple breakpoints)	Chr2:15179 926	Chr2:16075 495		yes

Presence of patient-specific targets correlates with disease stage

Sequential cfDNA samples obtained during the clinical disease course were measured by ddPCR for the patient-specific breakpoint and by the *RASSF1A-M* assay (Figure 4 for patients with neuroblastoma, Figure 5 for patients with rhabdomyosarcoma and Ewing sarcoma). In all plasma samples taken at initial diagnosis in patients with neuroblastoma and rhabdomyosarcoma, the patient-specific targets were present. In neuroblastoma, presence of tumor-derived targets followed the clinical course, decreasing after start of treatment and reappearing before or at relapse. In patients NBL2061 and NBL2101 the tumor-specific target is clearly detectable in the cfDNA before a relapse is detected by imaging or standard bone marrow evaluation. In the two patients with rhabdomyosarcoma, the targets in the tumor-derived cfDNA disappeared quickly after start of therapy and did not reappear during therapy for relapse (RMS108) or progressive disease (RMS006). In both cases, no samples were drawn at diagnosis of relapse or progressive disease. For the patient with Ewing sarcoma, the specific breakpoint target was not detected in two cfDNA samples taken during therapy for relapse, even though design of a patient-specific breakpoint was successful, as determined in the positive control. Unfortunately, no sample taken at initial diagnosis was available for this patient.

For NBL2053, NBL2061, NBL2086, NBL2100, RMS006 and RMS108, the tumoroid that was used to identify the patient-specific breakpoint for TLA was grown from a tumor sample taken at relapse. However, we could detect the exact same breakpoints in plasma taken at initial diagnosis. This illustrates clearly that the targeted chromosomal breakpoints in neuroblastoma and the *PAX3-FOXO1* fusion gene in the rhabdomyosarcoma patient remain stable during the course of the disease.

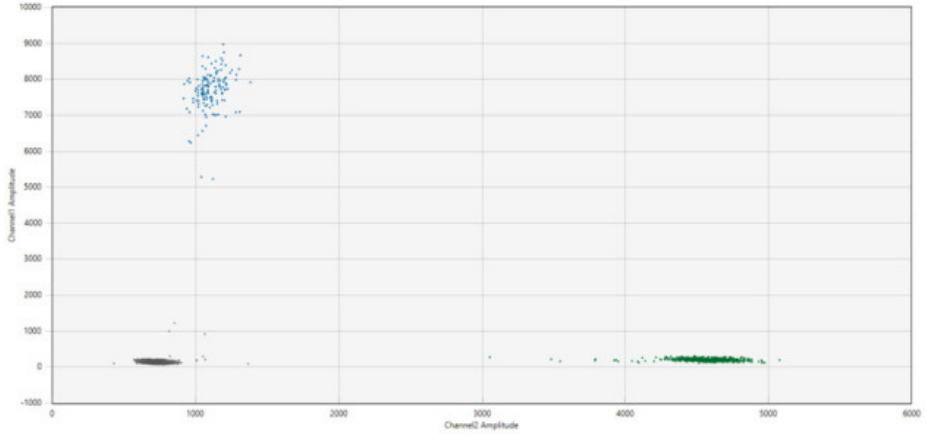
We show that patient-specific targets identified in tumor material by TLA can be detected in cfDNA from diagnostic plasma, furthermore, the presence of these targets track clinical course in neuroblastoma.

Levels of patient-specific target in cfDNA comparable to *RASSF1A-M*

Levels of the patient-specific marker and *RASSF1A-M* were comparable at initial diagnosis in patients with neuroblastoma and rhabdomyosarcoma. During the course of treatment minor discrepancies were found between *RASSF1A-M* and the patient-specific marker (NBL2054, NBL2056, NBL2061, NBL2100, NBL2101) (Figure 4), reflecting the presence of minimal residual disease. Note that in patient NBL2050 the patient-specific marker targets the highly amplified *MYCN* sequence and therefore has an increased sensitivity compared to the *RASSF1A-M* assay. Similar to the breakpoint levels, all sequential samples in the patients with rhabdomyosarcoma

were negative for *RASSF1A-M* (Figure 5). For the patient with Ewing sarcoma, all samples were negative for both *RASSF1A-M* and the breakpoint.

A



B

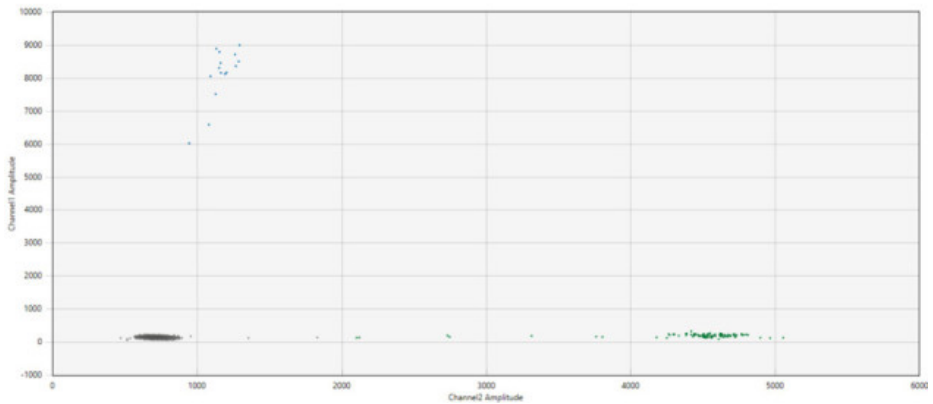


Figure 2. 2D plot from the ddPCR assay for NB2049 with **(A)**. cfDNA from the diagnostic plasma sample (total cfDNA input 25.6 ng/well) and **(B)**. positive control with DNA from FFPE material from the primary tumor (total cfDNA input 3.3 ng/well). Blue dots; droplets positive for patient-specific breakpoint (FAM channel) Green dots; droplets positive for ACTB(HEX channel) Grey dots; droplets negative for both targets.

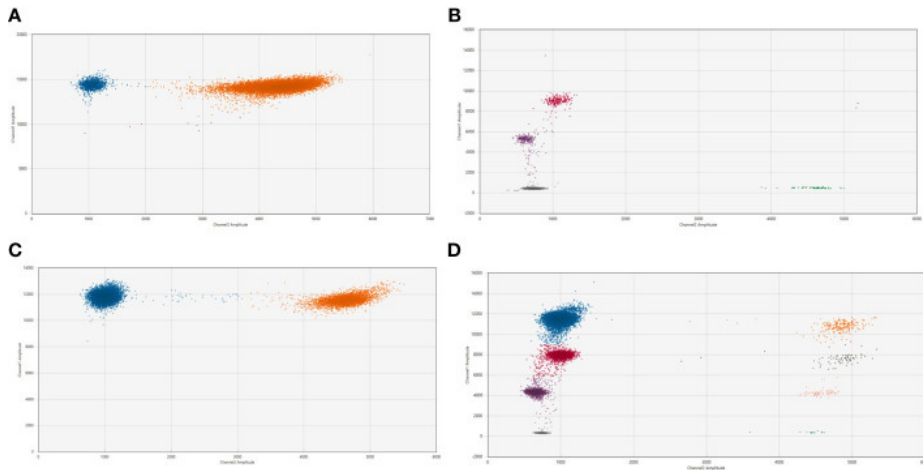
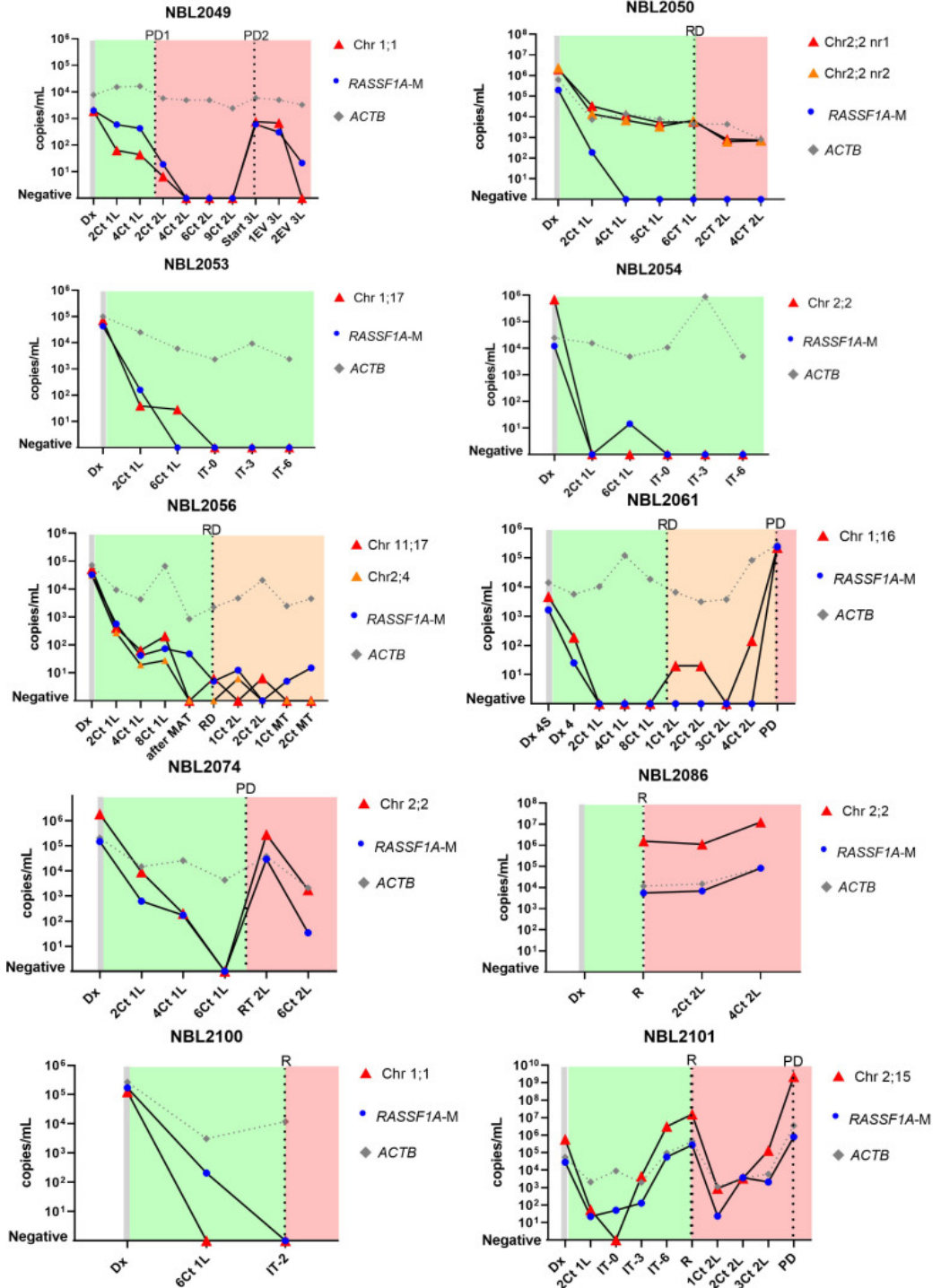


Figure 3. 2D plot from the ddPCR assay for NB2050 with 2 patient-specific breakpoints **(A)**. cfDNA from the diagnostic plasma sample (total cfDNA input can not be determined due to overload of the droplets) **(B)**. positive control with DNA from FFPE material from the primary tumor (total cfDNA input 1.7 ng/well). **(C)** Dilution of diagnostic plasma 50 times and **(D)**. 500 times Blue dots; droplets positive for both patient-specific breakpoint (FAM channel) Green dots; droplets positive for Actin Beta (HEX channel) Pink dots; droplets positive for breakpoint Chr 2;2 nr 1 Purple dots; droplets positive for breakpoint Chr 2;2 nr 2 (with 450 nM and 125 nM primer and probe concentrations, respectively) Orange dots; droplets positive for both breakpoints and Actin Beta Black dots; droplets positive for breakpoint nr 1 and Actin Beta Salmon-colored dots; droplets positive for breakpoint nr 2 and Actin Beta Grey dot; droplets negative for both targets.

Figure 4 (next page). Levels of patient-specific targets, reference gene ACTIN beta (ACTB) and methylated RASSF1A (RASSF1A-M) in cell-free DNA (cfDNA) from 10 neuroblastoma patients at diagnosis and during the course of the disease. Dx, diagnosis; Dx 4S, diagnosis INSS stage 4S; Dx 4, diagnosis INSS stage 4; nCt 1L, after n courses in first line therapy; nCt 2L, after courses in second line therapy; 3L, third line therapy; 1EV 3L, first evaluation third line therapy; 2EV 3L, second evaluation third line therapy; IT-0, before GD-2 immunotherapy IT-3 after 3 cycles of GD-2 immunotherapy; IT-6, after 6 cycles of GD-2 immunotherapy; MAT, myeloablative therapy and autologous stem cell transplantation; RT 2L, after radiotherapy during second line therapy; MT, maintenance treatment. PD, progressive disease; R, relapse; RD, refractory disease. Green blocks indicate first line treatment, orange blocks indicate added treatment for refractory disease, red blocks indicate treatment for progressive or relapsed disease.



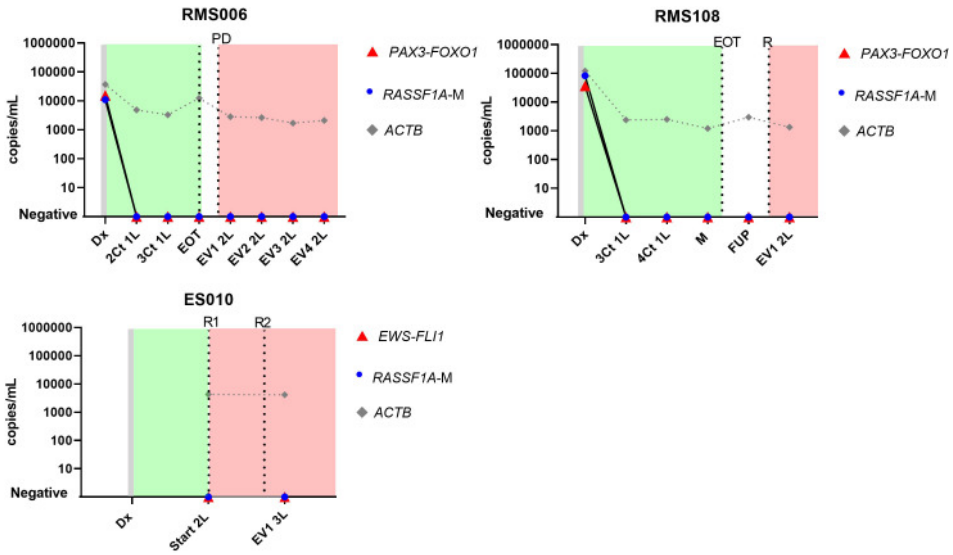


Figure 5. Levels of patient-specific targets, reference gene ACTIN beta (ACTB) and methylated RASSF1A (RASSF1A-M) in cell-free DNA (cfDNA) in 2 patients with rhabdomyosarcoma (RMS026 and RMS092) and 1 patient with Ewing sarcoma (ES010) at diagnosis and during the course of the disease. Dx, diagnosis; nCt 1L, after n courses in first line therapy; M, maintenance; FUP-follow up; EVn 2L, evaluation number n during second line therapy; EOT, end of treatment; R, relapse; Start 2L, start second line therapy; R, relapse; PD, progressive disease. Green blocks indicate first line treatment, red blocks indicate treatment for progressive or relapsed disease.

Discussion

In this study we demonstrate the feasibility to identify a patient-specific target, based on chromosomal structural variants, and design a patient-specific assay for use in liquid biopsies in different pediatric solid tumors. Moreover, we show that the presence of these targets in plasma at initial diagnosis for neuroblastoma and rhabdomyosarcoma, and that its presence during the course of the disease, corresponds to detectable or minimal residual disease status in neuroblastoma.

In patients with neuroblastoma, we observed that the level of tumor-derived cfDNA, as measured by the patient-specific targets, already increased before the clinical diagnosis of relapse or progressive disease was made. This finding suggests a potential for monitoring treatment response in neuroblastoma by detecting tumor-derived cfDNA. This is in line with data from our previous study on hypermethylated *RASSF1A* (16), but is also shown by others. Su et al. reported that the total amount of cfDNA increases before the recurrence of high risk neuroblastoma (29), which can be explained as the majority of the present cfDNA at relapse is tumor derived (16). More recently, Lodrini et al., showed the applicability of detecting tumor-derived cfDNA MYCN and ALK copy number alterations and ALK hotspot mutations in longitudinal plasma samples from patients with neuroblastoma (30). The study of Bosse et al., that predominantly included neuroblastoma patients with an event (91%), showed at least one pathogenic genomic alteration detected in 56% of the samples (31). However, only 20% and 10% of neuroblastoma tumors harbor MYCN amplification or ALK mutation, respectively (4). With the development of TLA/TLC, patient-specific targets for use in liquid biopsies can be detected for any CNAs, as illustrated in our study, which significantly increases the number of patients eligible for monitoring of disease with tumor-derived cfDNA.

In our study, we did not observe re-appearance of the patient-specific breakpoint in samples from patients with rhabdomyosarcoma and Ewing sarcoma. This might be due to a lack of well-timed samples, especially for the patient with Ewing sarcoma. Re-appearance of the patient-specific breakpoint has been described by Eguchi-Ishimae in a patient with fusion-positive rhabdomyosarcoma that suffered from relapse (32). Recently, Ruhen et al. published analysis of cfDNA from plasma in a cohort of 18 patients with rhabdomyosarcoma, which showed a rapid decrease of cfDNA targets after initiation of therapy and an increase at relapse (33). This rapid decrease of tumor-derived cfDNA was also observed by Klega et al. in patients with Ewing sarcoma and fusion-positive rhabdomyosarcoma, often becoming undetectable at the start of the second cycle of chemotherapy (34). Moreover, they

observed that in patients with Ewing sarcoma the detection of tumor-derived cfDNA after start of treatment was related to the level of tumor necrosis (34). The relation to tumor burden and monitoring of relapse in Ewing sarcoma was also demonstrated in the recent study by Shulman et al. (35) They also designed a patient-specific assay for the fusion genes in 6 patients with Ewing sarcoma, using data from WGS of the tumor material. In 2 patients that remained in complete remission, the fusion breakpoint disappeared after initiation of treatment. In 4 patients that suffered from relapse, cfDNA levels of the breakpoint reflected presence of relapse and response to therapy (35). These findings from other reports underline the potential of a patient-specific target as a treatment response marker and early relapse detection. But the timing of blood sampling is crucial. In the 2 patients with rhabdomyosarcoma in our study, we did not have samples taken right before or at diagnosis of relapse, only samples taken after start of relapse therapy. Standardized and uniform sampling in a larger cohort of patients with rhabdomyosarcoma and Ewing sarcoma is essential to validate these markers for clinical use. Clinical trials are now being conducted, with liquid biopsy sampling being implemented in the current EpSSG FaR RMS trial for pediatric and adult rhabdomyosarcoma in Europe and in the US a focused trial in adults into liquid biopsies for solid tumors (36, 37).

The use of a patient-specific molecular target as marker for minimal residual disease has been implemented firmly in leukemia (38, 39). In solid tumors, our group has previously described the feasibility to design patient-specific DNA markers from aberrations detected by WGS, and successful marker detection in BM of patients with neuroblastoma (23), but this has not reached clinical practice yet. Some important factors contributing to this lack of translation should be considered. One challenge is defining a target. At initial diagnosis, the search for potential targets can be guided by clinical information and tumor histology, focusing on early oncogenic events that remain present throughout the course of the disease, for example the PAX3-FOXO1 fusion in rhabdomyosarcoma. This fusion gene is considered the tumor-driving event in this tumor entity (3, 20, 40). Also for neuroblastoma, amplification of the MYCN gene, gain of 17q and loss of heterozygosity of chromosome 1 have been found to be recurring events, occurring extremely early in tumor development and remaining present during the course of the disease (41–43). Clonal evolution can affect the suitability of targets. Studies of paired primary and relapse neuroblastoma tumor have shown that mutations detected at relapse represent outgrowth of clones already present at diagnosis or *de novo* events, but most structural events remain present in the relapse sample (41, 44). Combining a panel of targets from diagnosis and then updating this panel again at relapse, using fresh genetic data from the relapsed tumors, might maintain sensitivity of the patient-specific ddPCR assays.

In other types of pediatric solid tumors, it might be more challenging to identify patient-specific targets that remain stable throughout the course of the disease. For example, in osteosarcoma, many structural variations have been reported throughout the genome in primary tumors (45, 46), but extensive studies on the stability of these regions in recurrent and progressive disease is lacking. Nonetheless, as many pediatric tumors harbor any structural variant (insertions, deletions, translocations) (18), this approach could benefit cfDNA research in other pediatric tumors as well (42, 45). In our center, regions involved in translocations and copy numbers were previously evaluated by FISH, RT-qPCR and SNP arrays as part of regular clinical investigations and this information can direct the investigations into patient-specific targets. Considering these recurrent regions with copy number aberrations, it would be interesting to explore a multiplex approach of TLA/TLC for neuroblastoma, targeting several regions often carrying amplifications. This approach has shown its potential for detection of translocations in acute leukemia (26).

Another important challenge is the time and effort necessary to identify a patient-specific target. The procedure for FFPE-TLC takes 2 to 3 weeks, shorter than the process based on WGS as described by Subhash et al. (47) Furthermore, FFPE-TLC opens up the possibility to analyze archived samples of patients presenting with late relapse. If no FFPE material is available and not enough cells are available directly after biopsy or surgery, then the time depends on growth of the tumoroids. This can differ significantly. TLA-based approaches to determine the patient-specific breakpoint also preclude the known objections to WGS, with the risk of unsolicited findings and their impact on patients' lives (48, 49).

In this study, we used a ddPCR-based approach for the detection of the patient-specific targets in cfDNA. Other reports have used hybrid capture sequencing (e.g., TranSS-Seq by Klega et al.) (34). All approaches correlate well with each other (34, 50, 51). The choice of a platform for cfDNA detection depends on the availability at a specific center, the costs and whether multiplexing is necessary, in tumors with multiple targets. A next generation sequencing platform can offer a wider range of targets to be tested, but on the other hand it can be time-consuming to validate, is less flexible and more costly. The possibility of multiplexing targets in cfDNA on the ddPCR is more limited but not impossible, as reported here and in previous publications (52, 53). ddPCR thereby offers a rapid testing modality, also very suited for monitoring of residual disease during treatment and follow-up in a clinical setting.

In some cases, it might be impossible to design a patient-specific assay, which might be due to absence of an appropriate chromosomal region or presence of the

sequence in the normal genome (as illustrated by case NB2100). Alternative liquid biopsy-based platforms could be explored, as we have demonstrated previously. We have developed and validated RNA panels for the detection of circulating tumor cells in the cellular compartment of blood and bone marrow for patients with neuroblastoma and rhabdomyosarcoma (10–12). Furthermore, as we also applied in the current study, an enzyme-based ddPCR for methylated RASSF1A in cfDNA is also suited for the detection of tumor-derived cfDNA. Since hypermethylation of RASSF1A has been found in many types of tumors (54–60), this assay offers another approach for liquid biopsy-based disease monitoring. The combination of both RNA and DNA-based platforms for the analysis of liquid biopsies could be complementary, as we have showed previously in a cohort of patients with rhabdomyosarcoma (61).

Conclusion

In this study, we demonstrate that patient-specific targets can be identified using targeted locus amplification in different pediatric solid tumors. Furthermore, we show that these patient-specific targets can be detected in cfDNA from plasma and their presence may correlate to (minimal) residual or recurrent disease. This approach holds promise for use in daily clinical practice.

References

1. Chisholm JC, Marandet J, Rey A, Scopinaro M, de Toledo JS, Merks JH, et al.. Prognostic factors after relapse in nonmetastatic rhabdomyosarcoma: a nomogram to better define patients who can be salvaged with further therapy. *J Clin Oncol* (2011) 29(10):1319–25. doi: 10.1200/JCO.2010.32.1984
2. Selfe J, Olmos D, Al-Saadi R, Thway K, Chisholm J, Kelsey A, et al.. Impact of fusion gene status versus histology on risk-stratification for rhabdomyosarcoma: Retrospective analyses of patients on UK trials. *Pediatr Blood Cancer* (2017) 64(7). doi: 10.1002/pbc.26386
3. Skapek SX, Ferrari A, Gupta AA, Lupo PJ, Butler E, Shipley J, et al.. Rhabdomyosarcoma. *Nat Rev Dis Primers* (2019) 5(1):1. doi: 10.1038/s41572-018-0051-2
4. Matthay KK, Maris JM, Schleiermacher G, Nakagawara A, Mackall CL, Diller L, et al.. Neuroblastoma. *Nat Rev Dis Primers* (2016) 2:16078. doi: 10.1038/nrdp.2016.78
5. Grunewald TGP, Cidre-Aranaz F, Surdez D, Tomazou EM, de Alava E, Kovar H, et al.. Ewing Sarcoma. *Nat Rev Dis Primers* (2018) 4(1):5. doi: 10.1038/s41572-018-0003-x
6. Park JR, Kreissman SG, London WB, Naranjo A, Cohn SL, Hogarty MD, et al.. Effect of tandem autologous stem cell transplant vs single transplant on event-free survival in patients with high-risk neuroblastoma. *JAMA* (2019) 322(8):746. doi: 10.1001/jama.2019.11642
7. Stahl M, Ranft A, Paulussen M, Bolling T, Vieth V, Bielack S, et al.. Risk of recurrence and survival after relapse in patients with Ewing sarcoma. *Pediatr Blood Cancer* (2011) 57(4):549–53. doi: 10.1002/pbc.23040
8. van Paemel R, Vlugg R, de Preter K, van Roy N, Speleman F, Willems L, et al.. The pitfalls and promise of liquid biopsies for diagnosing and treating solid tumors in children: a review. *Eur J Pediatr* (2020) 179(2):191–202. doi: 10.1007/s00431-019-03545-y
9. Alix-Panabieres C, Pantel K. Clinical applications of circulating tumor cells and circulating tumor DNA as liquid biopsy. *Cancer Discov* (2016) 6(5):479–91. doi: 10.1158/2159-8290.CD-15-1483
10. Lak NSM, Voormans TL, Zappeij-Kannegieter L, van Zogchel LMJ, Fiocco M, van Noesel MM, et al.. Improving risk stratification for pediatric patients with rhabdomyosarcoma by molecular detection of disseminated disease. *Clin Cancer Res* (2021) 27(20):5576–85. doi: 10.1158/1078-0432.CCR-21-1083
11. Stutterheim J, Gerritsen A, Zappeij-Kannegieter L, Yalcin B, Dee R, van Noesel MM, et al.. Detecting minimal residual disease in neuroblastoma: the superiority of a panel of real-time quantitative PCR markers. *Clin Chem* (2009) 55(7):1316–26. doi: 10.1373/clinchem.2008.117945
12. van Zogchel LMJ, Zappeij-Kannegieter L, Javadi A, Lugtigheid M, Gelineau NU, Lak NSM, et al.. Specific and sensitive detection of neuroblastoma mRNA markers by multiplex RT-qPCR. *Cancers (Basel)* (2021) 13(1). doi: 10.3390/cancers13010150
13. van Paemel R, de Koker A, Vandeputte C, Van L, Lammens T, Laureys G, et al.. Minimally invasive classification of paediatric solid tumours using reduced representation bisulphite sequencing of cell-free DNA : a proof-of-principle study. *Epigenetics* (2020) 00(00):1–13. doi: 10.1080/15592294.2020.1790950
14. van Paemel R, Vandeputte C, Raman L, van Thorre J, Willems L, van Dorpe J, et al.. The feasibility of using liquid biopsies as a complementary assay for copy number aberration profiling in routinely collected paediatric cancer patient samples. *Eur J Cancer* (2021) 160:12–23. doi: 10.1016/j.ejca.2021.09.022
15. van Paemel R, de Koker A, Vandeputte C, van Zogchel L, Lammens T, Laureys G, et al.. Minimally invasive classification of paediatric solid tumours using reduced representation bisulphite sequencing of cell-free DNA: a proof-of-principle study. *Epigenetics* (2021) 16(2):196–208. doi: 10.1080/15592294.2020.1790950

16. van Zogchel LMJ, Lak NSM, Verhagen OJHM, Tissoudali A, Gusmalla Nuru M, Gelineau NU, et al.. Novel circulating hypermethylated RASSF1A ddPCR for liquid biopsies in patients with pediatric solid tumors. *JCO Precis Oncol* (2021) 5:1738–48. doi: 10.1200/PO.21.00130
17. Jones DTW, Banito A, Grünewald TGP, Haber M, Jäger N, Kool M, et al.. Molecular characteristics and therapeutic vulnerabilities across paediatric solid tumours. *Nat Rev Cancer* (2019) 19(8):420–38. doi: 10.1038/s41568-019-0169-x
18. Gröbner SN, Worst BC, Weischenfeldt J, Buchhalter I, Kleinheinz K, Rudneva VA, et al.. The landscape of genomic alterations across childhood cancers. *Nature* (2018) 555(7696):321–7. doi: 10.1038/nature25480
19. Bosse KR, Maris JM. Advances in the translational genomics of neuroblastoma: from improving risk stratification and revealing novel biology to identifying actionable genomic alterations. *Cancer* (2016) 122(1):20–33. doi: 10.1002/cncr.29706
20. Barr FG. Gene fusions involving PAX and FOX family members in alveolar rhabdomyosarcoma. *Oncogene* (2001) 20(40):5736–46. doi: 10.1038/sj.onc.1204599
21. Barr FG, Biegel JA, Sellinger B, Womer RB, Emanuel BS. Molecular and cytogenetic analysis of chromosomal arms 2q and 13q in alveolar rhabdomyosarcoma. *Genes Chromosomes Cancer* (1991) 3(2):153–61. doi: 10.1002/gcc.2870030212
22. Parham DM, Barr FG. Classification of rhabdomyosarcoma and its molecular basis. *Adv Anat Pathol* (2013) 20(6):387–97. doi: 10.1097/PAP.0b013e3182a92d0d
23. van Wezel EM, Zwijnenburg D, Zappeij-Kannegieter L, Bus E, van Noesel MM, Molenaar JJ, et al.. Whole-genome sequencing identifies patient-specific DNA minimal residual disease markers in neuroblastoma. *J Mol Diagn* (2015) 17(1):43–52. doi: 10.1016/j.jmoldx.2014.09.005
24. de Vree PJP, de Wit E, Yilmaz M, van de Heijning M, Klous P, Versteegen MJAM, et al.. Targeted sequencing by proximity ligation for comprehensive variant detection and local haplotyping. *Nat Biotechnol* (2014) 32(10):1019–25. doi: 10.1038/nbt.2959
25. Hottentot QP, van Min M, Splinter E, White SJ. Targeted locus amplification and next-generation sequencing. *Methods Mol Biol* (2017) 1492:185–96. doi: 10.1007/978-1-4939-6442-0_13
26. Alimohamed MZ, Johansson LF, de Boer EN, Splinter E, Klous P, Yilmaz M, et al.. Genetic screening test to detect translocations in acute leukemias by use of targeted locus amplification. *Clin Chem* (2018) 64(7):1096–103. doi: 10.1373/clinchem.2017.286047
27. Allahyar A, Pieterse M, Swennenhuis J, Los-de Vries GT, Yilmaz M, Leguit R, et al.. Robust detection of translocations in lymphoma FFPE samples using targeted locus capture-based sequencing. *Nat Commun* (2021) 12(1):3361. doi: 10.1038/s41467-021-23695-8
28. Meister MT, Groot Koerkamp MJA, de Souza T, Breunis WB, Frazer-Mendelewska E, Brok M, et al.. Mesenchymal tumor organoid models recapitulate rhabdomyosarcoma subtypes. *EMBO Mol Med* (2022) 14(10). doi: 10.15252/emmm.202216001
29. Su Y, Wang L, Jiang C, Yue Z, Fan H, Hong H, et al.. Increased plasma concentration of cell-free DNA precedes disease recurrence in children with high-risk neuroblastoma. *BMC Cancer* (2020) 20(1):102. doi: 10.1186/s12885-020-6562-8
30. Lodrini M, Graef J, Thole-Kliesch TM, Astrahantseff K, Sprussel A, Grimaldi M, et al.. Targeted analysis of cell-free circulating tumor DNA is suitable for early relapse and actionable target detection in patients with neuroblastoma. *Clin Cancer Res* (2022) 28(9):1809–20. doi: 10.1158/1078-0432.CCR-21-3716
31. Bosse KR, Giudice AM, Lane MV, McIntyre B, Schürch PM, Pascual-Pasto G, et al.. Serial profiling of circulating tumor DNA identifies dynamic evolution of clinically actionable genomic alterations in high-risk neuroblastoma. *Cancer Discov* (2022) 12(12):2800–19. doi: 10.1158/2159-8290.CD-22-0287

32. Eguchi-Ishimae M, Tezuka M, Kokeyuchi T, Nagai K, Moritani K, Yonezawa S, et al.. Early detection of the PAX3-FOXO1 fusion gene in circulating tumor-derived DNA in a case of alveolar rhabdomyosarcoma. *Genes Chromosomes Cancer* (2019) 58(8):521–9. doi: 10.1002/gcc.22734
33. Ruhen O, Lak NSM, Stutterheim J, Danielli S, Chicard M, Iddir Y, et al.. Molecular characterisation of circulating tumor DNA in pediatric rhabdomyosarcoma: a feasibility study. *JCO Precis Oncol* (2022) 6. doi: 10.1200/PO.21.00534
34. Klega K, Imamovic-Tuco A, Ha G, Clapp AN, Meyer S, Ward A, et al.. Detection of somatic structural variants enables quantification and characterization of circulating tumor DNA in children with solid tumors. *JCO Precis Oncol* (2018) 2018. doi: 10.1200/PO.17.00285
35. Seidel MG, Kashofer K, Moser T, Thueringer A, Liegl-Atzwanger B, Leithner A, et al.. Clinical implementation of plasma cell-free circulating tumor DNA quantification by digital droplet PCR for the monitoring of Ewing sarcoma in children and adolescents. *Front Pediatr* (2022) 10. doi: 10.3389/fped.2022.926405
36. NCT04625907: *FaR-RMS: an overarching study for children and adults with frontline and relapsed RhabdoMyoSarcoma (FaR-RMS)*.
37. NCT04354064 *circulating tumor DNA (ctDNA) for early treatment response assessment of solid tumors*.
38. Borowitz MJ, Wood BL, Devidas M, Loh ML, Raetz EA, Salzer WL, et al.. Prognostic significance of minimal residual disease in high risk b-ALL: a report from children's oncology group study AALL0232. *Blood* (2015) 126(8):964–71. doi: 10.1182/blood-2015-03-633685
39. della Starza I, Chiaretti S, de Propriis MS, Elia L, Cavalli M, de Novi LA, et al.. Minimal residual disease in acute lymphoblastic leukemia: technical and clinical advances. *Front* (2019) 9:726. doi: 10.3389/fonc.2019.00726
40. Chen L, Shern JF, Wei JS, Yohe ME, Song YK, Hurd L, et al.. Clonality and evolutionary history of rhabdomyosarcoma. *PLoS Genet* (2015) 11(3):e1005075. doi: 10.1371/journal.pgen.1005075
41. Eleveld TF, Oldridge DA, Bernard V, Koster J, Colmet Daage L, Diskin SJ, et al.. Relapsed neuroblastomas show frequent RAS-MAPK pathway mutations. *Nat Genet* (2015) 47(8):864–71. doi: 10.1038/ng.3333
42. Mlakar V, Jurkovic Mlakar S, Lopez G, Maris JM, Ansari M, Gumy-Pause F. 11q deletion in neuroblastoma: a review of biological and clinical implications. *Mol Cancer*. (2017) 16(1):1–12. doi: 10.1186/s12943-017-0686-8
43. Guan J, Hallberg B, Palmer RH. Chromosome imbalances in Neuroblastoma—Recent molecular insight into chromosome 1p-deletion, 2p-gain, and 11q-deletion identifies new friends and foes for the future. *Cancers (Basel)* (2021) 13(23):5897. doi: 10.3390/cancers13235897
44. Schulte M, Köster J, Rahmann S, Schramm A. Cancer evolution, mutations, and clonal selection in relapse neuroblastoma. *Cell Tissue Res* (2018) 372(2):263–8. doi: 10.1007/s00441-018-2810-5
45. Rickel K, Fang F, Tao J. Molecular genetics of osteosarcoma. *Bone* (2017) 102:69–79. doi: 10.1016/j.bone.2016.10.017
46. Chen X, Bahrami A, Pappo A, Easton J, Dalton J, Hedlund E, et al.. Recurrent somatic structural variations contribute to tumorigenesis in pediatric osteosarcoma. *Cell Rep* (2014) 7(1):104–12. doi: 10.1016/j.celrep.2014.03.003
47. Subhash VV, Huang L, Kamili A, Wong M, Chen D, Venn NC, et al.. Whole-genome sequencing facilitates patient-specific quantitative PCR-based minimal residual disease monitoring in acute lymphoblastic leukaemia, neuroblastoma and Ewing sarcoma. *Br J Cancer* (2021) 126:482–91. doi: 10.1038/s41416-021-01538-z
48. Pinxten W, Howard HC. Ethical issues raised by whole genome sequencing. *Best Pract Res Clin Gastroenterol* (2014) 28(2):269–79. doi: 10.1016/j.bpg.2014.02.004

49. Schoot VV, Viellevoyje SJ, Tammer F, Brunner HG, Arens Y, Yntema HG, et al.. The impact of unsolicited findings in clinical exome sequencing, a qualitative interview study. *Eur J Hum Genet* (2021) 29(6):930–9. doi: 10.1038/s41431-021-00834-9
50. Deveson IW, Gong B, Lai K, LoCoco JS, Richmond TA, Schageman J, et al.. Evaluating the analytical validity of circulating tumor DNA sequencing assays for precision oncology. *Nat Biotechnol* (2021) 39(9):1115–28. doi: 10.1038/s41587-021-00857-z
51. Garcia J, Forestier J, Dusserre E, Wozny AS, Geiguer F, Merle P, et al.. Cross-platform comparison for the detection of RAS mutations in cfDNA (ddPCR biorad detection assay, BEAMing assay, and NGS strategy). *Oncotarget* (2018) 9(30):21122–31. doi: 10.18632/oncotarget.24950
52. de Kock R, van den Borne B, Youssef-El Soud M, Belderbos H, Brunsveld L, Scharnhorst V, et al. Therapy monitoring of EGFR-positive non-Small-Cell lung cancer patients using ddPCR multiplex assays. *J Mol Diagn* (2021) 23(4):495–505. doi: 10.1016/j.jmoldx.2021.01.003
53. Ostorbin I, Kechin A, Boyarskikh U, Filipenko M. Multiplex ddPCR assay for screening copy number variations in BRCA1 gene. *Breast Cancer Res Treat* (2019) 178(3):545–55. doi: 10.1007/s10549-019-05425-3
54. Bin Y, Ding Y, Xiao W, Liao A. RASSF1A: a promising target for the diagnosis and treatment of cancer. *Clinica Chimica Acta* (2020) 504:98–108. doi: 10.1016/j.cca.2020.01.014
55. Dubois F, Bergot E, Zalcmán G, Levallet G. RASSF1A, puppeteer of cellular homeostasis, fights tumorigenesis, and metastasis-an updated review. *Cell Death Dis* (2019) 10(12):928. doi: 10.1038/s41419-019-2169-x
56. Donniger H, Vos MD, Clark GJ. The RASSF1A tumor suppressor. *J Cell Sci* (2007) 120(Pt 18):3163–72. doi: 10.1242/jcs.010389
57. Lim S, Yang MH, Park JH, Nojima T, Hashimoto H, Unni KK, et al.. Inactivation of the RASSF1A in osteosarcoma. *Oncol Rep* (2003) 10(4):897–901. doi: 10.3892/or.10.4.897
58. Hesson LB, Cooper WN, Latif F. The role of RASSF1A methylation in cancer. *Dis Markers* (2007) 23(1–2):73–87. doi: 10.1155/2007/291538
59. Wong IHN, Chan J, Wong J, Tam PKH. Ubiquitous aberrant RASSF1A promoter methylation in childhood neoplasia. *Clin Cancer Res* (2004) 10(3):994–1002. doi: 10.1158/1078-0432.CCR-0378-3
60. Grawenda AM, O'Neill E. Clinical utility of RASSF1A methylation in human malignancies. *Br J Cancer* (2015) 113(3):372–81. doi: 10.1038/bjc.2015.221
61. Lak NSM, van Zogchel LMJ, Zappeij-Kannegieter L, Javadi A, van Paemel R, Vandeputte C, et al.. Cell-free DNA as a diagnostic and prognostic biomarker in pediatric rhabdomyosarcoma. *JCO Precis Oncol* (2023) 7. doi: 10.1200/PO.22.00113

Supplementary data

Supplemental Table S1. Primer location and sequences for TLA, and capture probe locations for TLC

PtID	TLA/TLC	Primer name	Direction	Binding position	Sequence
NB2053	TLA	Chr 17	RV	chr17:33078551	TCTTTGGGTAACAAGGCTTT
			FW	chr17:33078702	AAAGTAAGCATCACTGAGCA
		Chr 1	RV	chr1:47894882	TCCACATTGCTTGTAAAGACA
			FW	chr1:47894975	CAGACAAATCCAATGACTGC
		Chr 11	RV	chr11:69560644	AGTGATTCAAAGGACACA
			FW	chr11:69560726	AGGGACTGGAGCTGATTT
NB2061	TLA	Chr 1	RV	chr1:29310092	CAGGCTCAGTAAACAAGGTA
			FW	chr1:29310232	AGTATCTGCATCCCTCCAAG
		Chr 16-gain	RV	chr16:68569701	GAATACCGAGAAGCCCAA
			FW	chr16:68569926	CTTACTATTGTGAAGTGC
		Chr 16-gain	RV	chr16:69899652	TAAGTGCCATCTCAAAGGG
			FW	chr16:69899886	CGACACTGAGGAAAGAAAGA
		Chr 16-gain	RV	chr16:71251358	AGTGTATTCTACTGGGCA
			FW	chr16:71251584	ATAACTGCTTACTTGTGGGC
NB2086	TLA	Chr 11	RV	chr11:88295587	TGCACGGTGAGAATACTTG
			FW	chr11:88295918	ACACCTGACACGCCATTT
		NMYC	RV	chr2:15785316	GATCCCTGGTTTCTTTGACT
			FW	chr2:15785594	CAATCACGCACCAAATCC
		NMYC	RV	chr2:16886121	GCTAGAAATGTTCCACCTGT
			FW	chr2:16886227	GATATTTAAACCTCAGCTCCTG
NB2100	TLA	Chr 2	RV	Chr2:15948909	CTAATTAATTCTCGGTACACC
			FW	Chr2:15949614	TGCTAATTAATTCTCGCCCTTT
		Chr 2	RV	Chr2:16669425	TGAATGAATGTGAACAGACAAA
			FW	Chr2:16669521	CTTCAGCACATTGGTTGGT
		Chr 17	RV	Chr17:45935137	CCCCTCCAAGCTACAGG
			FW	Chr17:45935709	TAAGCTTGCTTACCTCACTG
		Chr 17	RV	Chr17:45960196	CTTCACAGTCAGGATTCCAG
			FW	Chr17:45960293	AAATGGGCTTGAATGAGTCA
		Chr 17	RV	Chr17:45979674	GTGTGACCTAACCTCTTTCA
			FW	Chr17:45979710	TACTTTGAGTGGGAGATGG
		Chr 17	RV	Chr17:46000144	TGGCGAATGTTGACTATTGA
			FW	Chr17:46000752	CATAGCTTAAGGGTACGTCC
		Chr 1	RV	Chr17:92088225	AATGGTCCACTTTGCTCTTT
			FW	Chr17:92088352	CCTCTGGCACCTTGATG
		Chr 1	RV	Chr17:95353980	CTCAAAGCACATCTGTAGGA
			FW	Chr17:95354220	CATCTGACGTCTCACTGAAA



Supplemental Table S1. Continued

PtID	TLA/TLC	Primer name	Direction	Binding position	Sequence
RMS026	TLA	PAX3 exon 9	RV	chr2:223066247	ATGACATTGTCAGCCTGTAG
			FW	chr2:223066337	CATATGATCCTGGAGCTGAC
		PAX3 exon 7	RV	chr2:223086048	TGGCTTTCAACCATCTCATT
			FW	chr2:223086281	GTGTCAAAGGTCAGTAGAGG
RMS092	TLA	PAX3 exon 9	RV	chr2:223066247	ATGACATTGTCAGCCTGTAG
			FW	chr2:223066337	CATATGATCCTGGAGCTGAC
		PAX3 exon 7	RV	chr2:223086048	TGGCTTTCAACCATCTCATT
			FW	chr2:223086281	GTGTCAAAGGTCAGTAGAGG
ES010	TLA	EWSR1	RV	chr22:29,287,610	CATCCAAGATGTTAGCTGGA
			FW	chr22:29,287,807	CTATTGCAGGCCACTATGAT
		FLI1	RV	chr11:128,786,438	ATGTACGAACGTACAGTTGT
			FW	chr11:128,786,734	CAATCAGCACATCTCTTCT

PtID	TLA/TLC	Probe targeted region (hg19)
NB2049	TLC	chr1:53625000-53665000
NB2050	TLC	chr2:15952000-15962000
		chr2:16104000-16114000
NB2054	TLC	
NB2056	TLC	chr2:57465000-57515000
	TLC	chr11:71200000-71250000
NB2066	TLC	chr3:56610000-56650000
NB2074	TLC	chr2:18585000-18615000
		chr2:27740000-27780000
		chr2:31100000-31130000
NB2100	TLC	chr2:15928000-15958000
		chr2:16655000-16685000
NB2101	TLC	NA, SV identified with sWGS FFPE-TLC preps

PtID= unique patient identifier

Supplemental Table S2. Primer and probe sequences for patient-specific ddPCR

PTID	Region	Start	End	Oligo	Oligo sequence (5'-3')	Amplicon size (bp)	Reporter	Quencher	Annealing temperature (°C)
NB2049	Chr1-1	53625000	53665000	Fwd	ATAACCTGGTTCATGCCATC	111	FAM	ZEN/lowa Black™ FQ	57
				Rev	CAGAGTCACACAGGCAGAAA				
				Probe	AGCTGGATGTGGTGAAGGCT				
NB2050	Chr2-chr2	15952000	15962000	Fwd	CTCCTGTCTACCAGGAAGTG	100	FAM	ZEN/lowa Black™ FQ	57
				Rev	TGCTTGGTTCATGACGAGA				
				Probe	ACTCTACTCCAGGAGATCTTTTGTAGA				
	Chr2-Chr2	15952000	15962000	Fwd ²	CCTTATACCTGGCCTTCC ²	117	FAM	ZEN/lowa Black™ FQ	57
				Rev ²	ACAGACAGGGGTTGGGAAC ²				
				Probe ¹⁸	TGCCTGCACATAGGCCAT ⁸				
NB2053	Chr1-Chr17	47886678	33048245	Fwd	CCATCAGTCCAGATGAGCAG	94	FAM	ZEN/lowa Black™ FQ	59
				Rev	TGTAACCTATGCAGCCCTGTG				
				Probe ¹	TGGGGCATCTCTCCGAACCTCCA				
NB2054	Chr2-Chr2	14863510	15987902	Fwd	ACCATGGAACCATGAGACA	123	FAM	ZEN/lowa Black™ FQ	59
				Rev	ATTACAGGTGCTACACAC				
				Probe ¹	ACTGTCAGTTTCACTCATTCCGCAGCACACA				
NB2056	Chr4-chr2	57465000	57515000	Fwd	GGGTTAGGGTTCGGTTT	116	FAM	ZEN/lowa Black™ FQ	57
				Rev	CAAAATGCAGGATTACAGG				
				Probe	AAAACGGAGACCAGGAGCG				
	Chr 17/11	71200000	71250000	Fwd ²	GCACTTTGGATAAGGTACTCAA	119	FAM	ZEN/lowa Black™ FQ	57
				Rev ²	GTCCTGTTCCCTCCCTA				
				Probe ³	TGTATATATGTTTCATGGATACGACC				
NB2061	Chr16-Chr1	68529301	29295626	Fwd	CAGAGTTTCACTCTTGCTGC	81	FAM	ZEN/lowa Black™ FQ	59
				Rev	CTTGGGTGACAGGCAAG				
				Probe	AGATCATGCCATTGCACTCCAGCCTGG				
NB2074	Chr2-Chr2 amplification	31120077	98796284	Fwd	GCCTGCCCTTCTTGTTTC	106	FAM	ZEN/lowa Black™ FQ	57
				Rev	GAGGGAGGAAGSAGAGAGAA				
				Probe ¹	ACAAGCAGGCTGAAGACAAGCACACA				
NB2086	Chr2-Chr2 amplification	16893201	15757504	Fwd	AACAAAGGATATTACCATCT	120	FAM	MGB Eclipse™	55
				Rev	AGGTAGTAGGATCATGACTGAA				
				Probe ¹	TGCCATTGTAGTATGGA				
NB2100	Chr 1-Chr1 deletion	92107327	95347109	Fwd	CTCTTTTTCAGCCAGGCGT	75	FAM	ZEN/lowa Black™ FQ	55
				Rev	GCTGGGACTACAGGCACC				
				Probe	AATTTAGCCAGGCATGTGGCG				

Supplemental Table S2. Continued

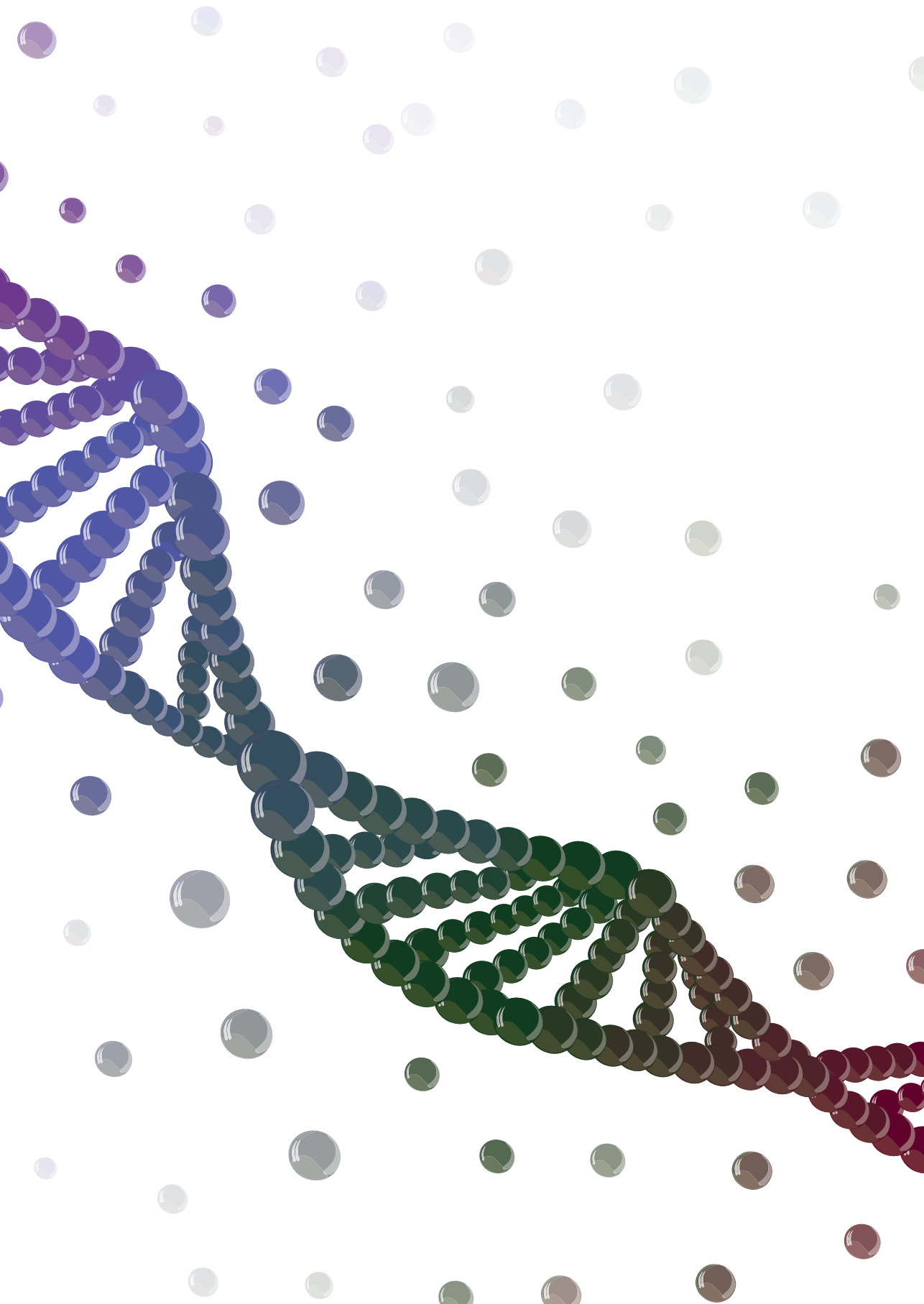
NB2101	Chr2-Chr2 amplification	15179926	16075495	Fwd	CACCTTTFAGCAGAGCTTGGA	118	FAM	ZEN/lowa Black™ FQ	57
				Rev	GACAATCAGTCAGGTGGAGG				
				Probe ¹	AGGACAGCCTGGGAGGCTGATCATCTCC				
RMS026	Chr13-Chr2 (PAX3-FOXO1)	41136846	223082995	Fwd	GTAGACATGGGGTTTCACC	141	FAM	ZEN/lowa Black™ FQ	58
				Rev	TCCTGGTCTAGGATCTTGTC				
				Probe	TGACTAAAACCTCCTGCACTGTTT				
RMS092	Chr13-Chr2 (PAX3-FOXO1)	41136846	223082995	Fwd	AAGTAGAATTGCTAGAATGTG	116	FAM	ZEN/lowa Black™ FQ	55
				Rev	AGTCCTGCTCTCTATTCCT				
				Probe	TGCAGTTGTGGTTTGTATCTGT				
ES010	Chr 22-Chr11 (EWS-FU)	29292022	128772451	Fwd	GCTCCATTTTAGCAGTGGC	111	FAM	ZEN/lowa Black™ FQ	58
				Rev	GGAGAGCAGTTGGAACCTTT				
				Probe ¹	CACAGACCCCGGACCAACTCAAAATGACC				

¹ Probe on reverse sequence

² Primer concentration 450 nM

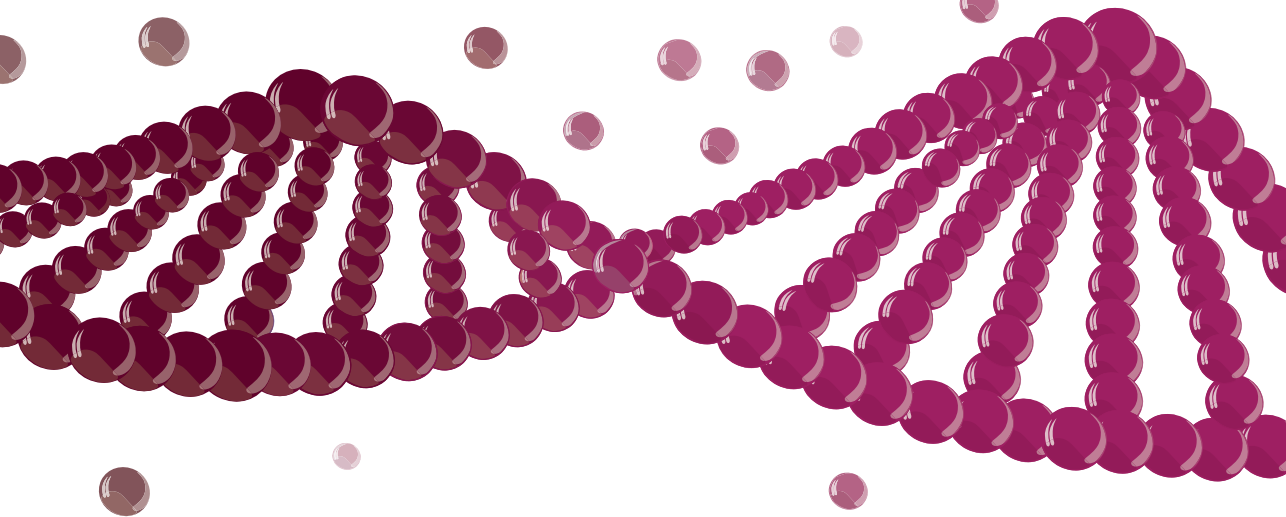
³ Probe concentration 125 nM

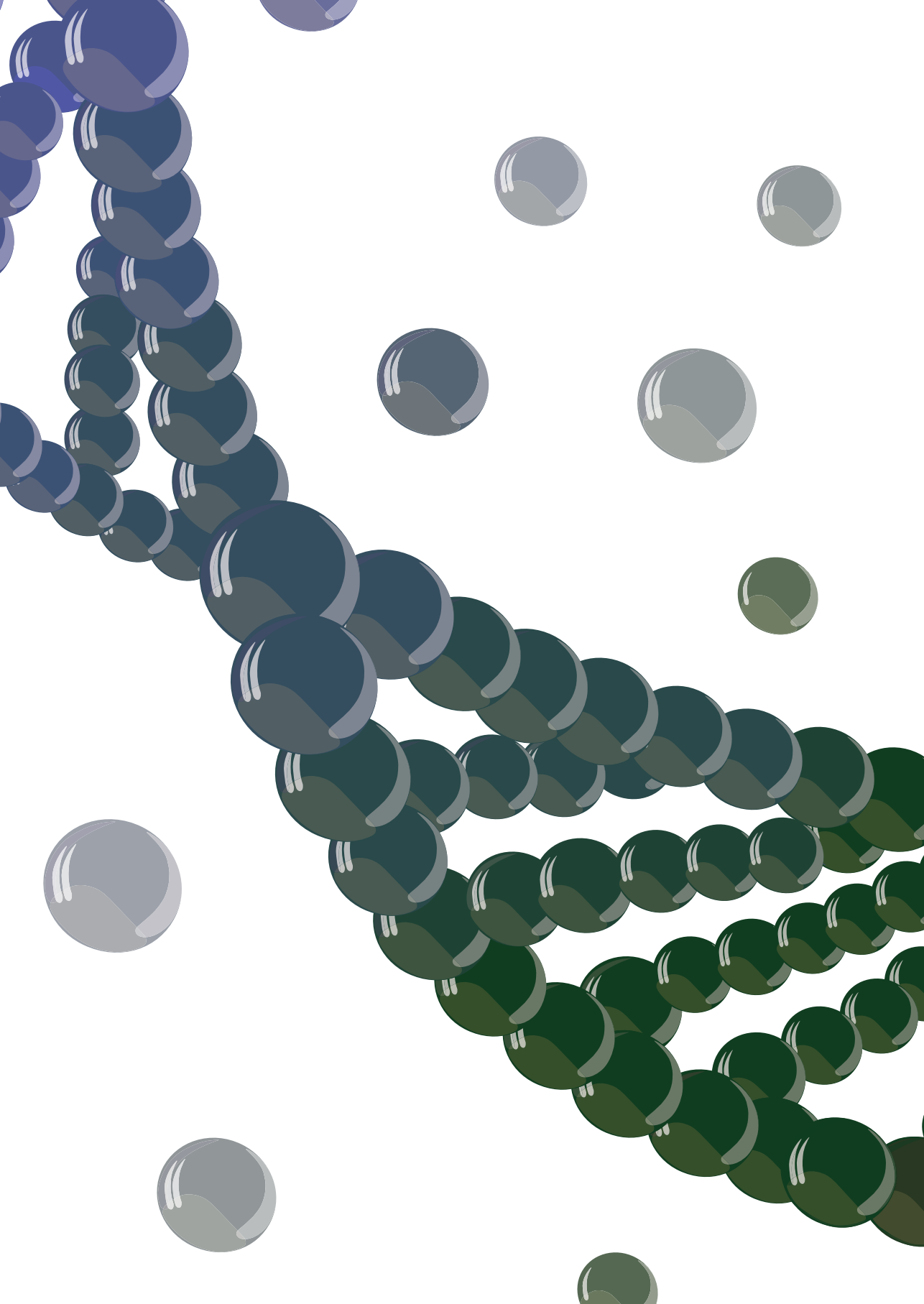




PART II

Extracellular vesicles and cell-free RNA





Chapter 7

Extracellular vesicles: a new source of biomarkers in pediatric solid tumors? A systematic review

Front Oncol. 2022 May 24;12:887210. doi: 10.3389/fonc.2022.887210.

Nathalie S.M. Lak^{1,2}, Elvera J. van der Kooi², Agustin Enciso-Martinez³,
Estefanía Lozano-Andrés⁴, Cees Otto³, Marca H.M. Wauben⁴, Godelieve A.M. Tytgat^{1,2}

¹ Princess Máxima Center for Pediatric Oncology, Utrecht, the Netherlands

² Department of Experimental Immunohematology, Sanquin Research, Amsterdam, the Netherlands

³ Medical Cell Biophysics Group, University of Twente, Enschede, the Netherlands

⁴ Department of Biomolecular Health Sciences, Faculty of Veterinary Medicine, Utrecht University, Utrecht, the Netherlands.

Abstract

Virtually every cell in the body releases extracellular vesicles (EVs), the contents of which can provide a “fingerprint” of their cellular origin. EVs are present in all bodily fluids and can be obtained using minimally invasive techniques. Thus, EVs can provide a promising source of diagnostic, prognostic, and predictive biomarkers, particularly in the context of cancer. Despite advances using EVs as biomarkers in adult cancers, little is known regarding their use in pediatric cancers. In this review, we provide an overview of published clinical and *in vitro* studies in order to assess the potential of using EV-derived biomarkers in pediatric solid tumors. We performed a systematic literature search, which yielded studies regarding desmoplastic small round cell tumor, hepatoblastoma, neuroblastoma, osteosarcoma, and rhabdomyosarcoma. We then determined the extent to which the *in vivo* findings are supported by *in vitro* data, and vice versa. We also critically evaluated the clinical studies using the GRADE (Grading of Recommendations Assessment, Development, and Evaluation) system, and we evaluated the purification and characterization of EVs in both the *in vivo* and *in vitro* studies in accordance with MISEV guidelines, yielding EV-TRACK and PedEV scores. We found that several studies identified similar miRNAs in overlapping and distinct tumor entities, indicating the potential for EV-derived biomarkers. However, most studies regarding EV-based biomarkers in pediatric solid tumors lack a standardized system of reporting their EV purification and characterization methods, as well as validation in an independent cohort, which are needed in order to bring EV-based biomarkers to the clinic.

Introduction

Extracellular vesicles (EVs) are released by virtually every cell in the body (1). EVs therefore play a key role in intercellular communication and are involved in several aspects of cancer (2, 3), making cancer-associated EVs a promising source of biomarkers (4, 5). EVs are highly heterogeneous, and many subtypes of EVs have been defined based on their size, cell type of origin, biogenesis route, and the cellular processes in which they are involved (1). Intraluminal vesicles (ILVs) are formed within the endosomal network and are released by the fusion of multivesicular bodies (MVBs) with the plasma membrane; the resulting EVs are thereafter called exosomes (1). In contrast, microvesicles (MVs) are formed and released via direct budding of the plasma membrane (1). Other EV subtypes include apoptotic bodies, ectosomes, oncosomes, and microparticles (1, 6). Because the various EV subtypes overlap with respect to their size and composition, their classification and nomenclature remain open for debate (1, 2, 7). For the purposes of this review, however, we will use the rather general term “EVs”. EVs play an essential role in both physiological and pathological processes by mediating cell-cell communication (8). The precise effect exerted by a given EV is determined primarily by its surface molecules and its cargo, which can include proteins, lipids, nucleic acids such as DNA and RNA, and metabolites derived from the cell of origin (9). Lipid encapsulation protects the cargo from degradation and allows the EV to be transported throughout the body and across physiological barriers (10). Thus, EVs can be recovered from various bodily fluids, including blood (Figure 1) (4, 11, 12), cerebrospinal fluid (13), urine (14), and breast milk (15). Moreover, EVs can also be isolated from liquid biopsies, providing a minimally invasive, clinically relevant method for monitoring patients with cancer (16).

In cancer, EVs play a role in both disease progression and metastasis by mediating the crosstalk between tumor cells and their environment (3, 17, 18). EVs can also induce a tumor-promoting phenotype in recipient cells (19), and EVs have been associated with the induction of multi-drug resistance in several cancer types (20). Compared to non-malignant cells, cancer cells release relatively high amounts of EVs (2, 21, 22), thus translating to higher numbers of EVs present in the blood of cancer patients compared to healthy controls. Moreover, the cargo contained in tumor-derived EVs differs from the cargo in EVs released by healthy cells, and the contents of tumor-derived EVs can change during tumor progression, reflecting the stage of the tumor (23).

Compared to other biomarkers from liquid biopsies for the use in pediatric solid tumors, EVs have some potential advantages (24). The use of cell-free DNA from plasma has been extensively studied for different tumor entities using various molecular techniques. The presence of the methylated tumor suppressor gene

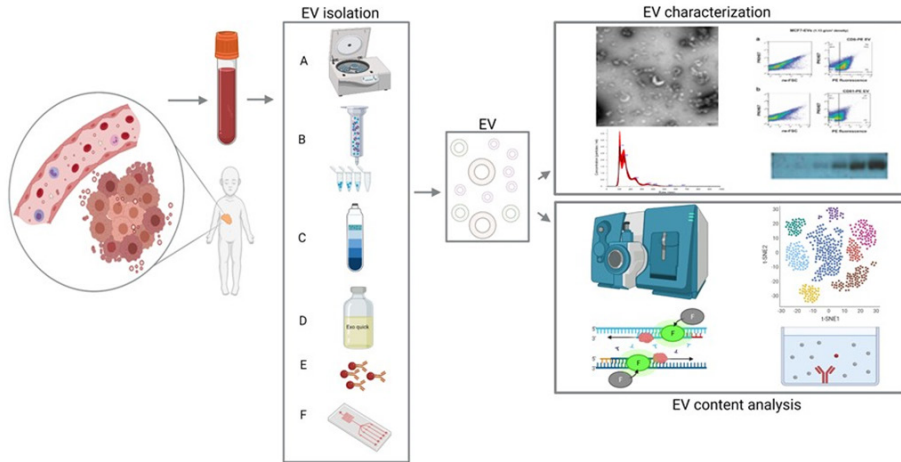


Figure 1. Extracellular vesicles (EVs) from blood as a liquid biopsy: isolation methods and downstream analyses. Left: EVs (including tumor-derived EVs) are isolated from peripheral blood and purified using differential centrifugation/ultrafiltration (A), size exclusion chromatography (SEC; B), density gradient (C), commercially available precipitating agents (e.g., Exoquick; D), immunoprecipitation/capture (E) or microfluidic/nanostructure approaches (F). Right, top panel: the isolated EVs are then characterized using (from the top-left, moving clockwise) electron microscopy, flow cytometry, western blot analysis, and/or nanoparticle tracking analysis (NTA). Right, bottom panel: the EV contents are analyzed using (from the top left, moving clockwise) mass spectrometry, RNA sequencing, enzyme-linked immunosorbent assay (ELISA), and/or RT-qPCR.

RASSF1A can be detected in plasma for several types of pediatric solid tumors, and can be used to monitor therapy response (25, 26). For neuroblastoma, tumor-specific aberrations in the MYCN and ALK genes (mutations and copy number alterations) can be monitored during the course of the disease (27, 28). Copy number profiling can be performed on cell-free DNA to detect a tumor-derived signal, and this can be combined with the copy number profile from the primary tumor, offering a more comprehensive overview of the genetic landscape of the tumor and its metastatic lesions (29). However, since plasma mostly contains non-tumor cell-free DNA, the signal-to-noise reduction can be challenging, especially considering that not all tumors shed large amounts of cell-free DNA (25, 30). Another option that has been explored, is detection of circulating tumor cells in blood, or bone marrow, using tumor-specific targets. This has been shown to be of clinical value in neuroblastoma and rhabdomyosarcoma (31-33). Still, it is hard to identify targets for specific tumors, especially for the detection of relapse since tumor cells can change their molecular characteristics under influence of therapy, and not all tumors shed large numbers of tumor cells into circulation (34-37). Biomarkers that are isolated from purified EVs

benefit from a decrease of background noise and, since all cells in the body shed EVs, are not depending on the presence of circulating tumor cells. Furthermore, the lipid bilayer of EVs offers protection from RNase naturally present in plasma (38, 39).

Importantly, the outcome of an EV study can be affected by the methods used to enrich (including isolation and purification) and analyze the EVs. Over the past decade alone, a wide range of methods have been used to isolate EVs, including ultracentrifugation, size-exclusion chromatography, density gradient centrifugation, precipitation, and immunocapture (Figure 1) (40). Apart from these conventional approaches to EV purification, microfluidic and nanostructure-based techniques have emerged in recent years. Potentially, these approaches pair high-throughput testing to low sample input, which makes them very interesting for clinical, point-of-care use. Most of these techniques depend on differences in size and/or (immuno-) labelling of the EVs (41-43). The reproducibility and reliability of EV-derived data depend heavily on the enrichment method used, as demonstrated back in 2014 by Van Deun *et al.* (44), who used several methods to isolate EVs from conditioned medium from a breast cancer cell line and found clear differences with respect to the number of co-isolates, EV morphology, EV quantity, and EV content. The authors found that the OptiPrep density gradient method outperformed both ultracentrifugation and commercially available precipitating agents with respect to the purity of the resulting EVs; they also found that their downstream analysis of protein and RNA content was greatly affected by the enrichment method used, thus potentially compromising the reproducibility and validation of EV studies (44). Apart from the purity of EVs, an important aspect to consider is the workflow and costs from every technique. Size exclusion chromatography and precipitation approaches are relatively rapid considering the workflow, whereas differential centrifugation requires specific material and is time-consuming, as is density gradient centrifugation. Immunocapture demands knowledge on markers present on the surface of EVs, which restricts unbiased studying of a heterogeneous EV population. (40, 42). The combination of different techniques, like size exclusion chromatography followed by density gradient centrifugation is considered as an approach for pure EV recovery. However, this is very time consuming and also results in a loss of total EV (40, 45). Various techniques for EV characterization and validation are used. Western blot is available in most laboratories and several established EV-related markers are often used, e.g. CD9, CD63, CD81 or TSG101 (40). However, this approach depends on the assumption that all EV of interest contain these markers, which can turn into a self-fulfilling prophecy. Nanoparticle tracking analysis can determine size and concentration of particles in a solution, however it does not only measure EVs but also other particles like lipoproteins or protein aggregates (40) Flowcytometry is

often performed to confirm the presence of EV. This approach is prone to erroneous measurements, since detection of EVs depends on specific instrument requirements and correct interpretation of data, which can be ambiguous (46, 47).

In an attempt to improve both precision and standardization in the EV field, the International Society for Extracellular Vesicles (ISEV) published a position paper in 2014 with guidelines regarding the minimal experimental requirements for studies involving EVs (48); this was followed in 2018 by a research community-based update entitled Minimal Information for Studies of Extracellular Vesicles (MISEV) (49). Together, these guidelines provide researchers with criteria for isolating, enriching, and analyzing EVs, as well as guidelines for the standardized reporting of their findings, thus improving both reproducibility and validity, and paving the way towards the clinical application of EVs as a biomarker (48, 49). Moreover, the online crowdsourced knowledge base EV-TRACK (transparent reporting and centralizing knowledge in extracellular vesicle research; <https://evtrack.org/>)—to which essential information regarding methods for enriching and characterizing EVs can be published and submitted manuscripts can be uploaded—also contributes to increasing the accuracy, rigor, and reproducibility of EV research (50, 51). When a new study is submitted to EV-TRACK, a so-called EV-METRIC score is calculated and controlled by the EV-TRACK administrators for inclusion in the database, allowing other researchers to objectively evaluate the technical reproducibility and detailed reporting of the study (50, 51).

In several adult cancers, EV-based biomarkers have been shown to be correlated with both disease stage and outcome (21, 22, 52-56). Due to significant differences in pathophysiology between adult and pediatric cancers, however, this knowledge cannot simply be extrapolated from adults to pediatric patients. For example, in adults cancer progression is often driven by multiple genetic aberrations, whereas pediatric tumors have a distinct genomic landscape typically characterized by a paucity of recurrent mutations and structural variants (57-59). Furthermore, the genes that are mutated in childhood tumors often differ from those in adult tumors and tend to be specific to certain cancer types and individual patients (60, 61).

To date, relatively few studies examined the clinical relevance of EVs in pediatric solid tumors, despite the high potential of using liquid biopsies in pediatric patients. To illustrate this research gap, we counted the number of articles published since 1990 involving EVs, pediatric solid tumors, tumor-derived EVs, and EVs in pediatric solid tumors; the results are shown in Figure 2. Over the past decade, the number of publications regarding EVs and tumor-derived EVs (in adult cancer) has increased

exponentially, and publications regarding pediatric solid tumors also increased, albeit gradually; strikingly, however, the number of publications regarding EVs in pediatric solid tumors has remained extremely low.

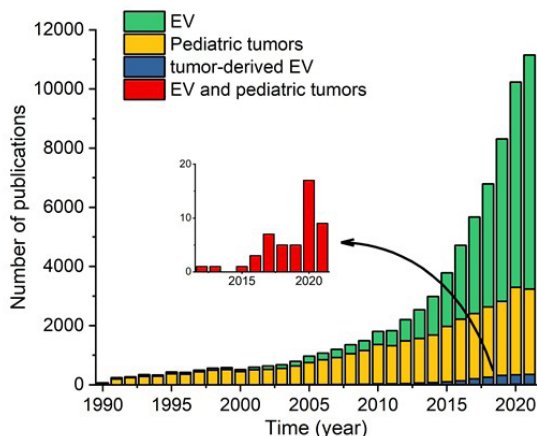


Figure 2. Number of papers published in the indicated years regarding extracellular vesicles (EVs), pediatric solid tumors, tumor-derived EVs, and both EVs and pediatric solid tumors. The inset shows only the publications regarding both EVs and pediatric solid tumors.

In this review, we critically assessed the published *in vivo* and *in vitro* studies involving EVs in pediatric solid tumors, and we discuss the barriers that must be overcome in order to bring EVs from the bench to the pediatric bedside. We focused primarily on studies that report patient-derived EVs, and we examined whether the conclusions drawn from these studies were supported by *in vitro* data. Given the importance of studying EVs using standardized methods with respect to reproducibility, we also evaluated the methods used to isolate and characterize EVs, and we assessed whether validation studies using either patient cohorts or *in vitro* methods were reported.

Methodology

Search strategy

The literature search and review strategy is depicted in Figure 3. In brief, we performed an electronic search of the PubMed, Cochrane Library, Web of Science, and Embase databases, as well as the *Journal of Extracellular Vesicles (JEV)* website, using the following search terms:

“(“extracellular vesicle” OR “extracellular vesicles” OR EV OR EVs OR exosom* OR ectosom* OR oncosom* OR microvesicle* OR microparticle* OR nanosom* OR nanoparticle* OR “shedding vesicles” OR “exosome-like vesicles”) AND (pediatric OR child OR children OR infant) AND (neuroblastoma OR rhabdomyosarcoma OR sarcoma OR “rhabdoid tumor*” OR “rhabdoid tumor*” OR Wilms OR nephroblastoma OR “renal medullary carcinoma” OR “renal cell carcinoma” OR “renal tumor*” OR leiomyosarcoma OR osteosarcoma OR hepatoblastoma OR “hepatocellular carcinoma” OR “Ewing”)”

Additional eligible studies were identified by screening the references listed in relevant reviews. The final search was performed on April 28, 2020, and EndNote X9 was used to identify and remove duplicate records. We updated the search on March 16th 2022. After pre-screening by two independent investigators (authors EK and NL) based on the title and abstract, followed by subsequent full text screening, a total of 27 studies (15 *in vivo* studies and 12 *in vitro* studies) were included in the final analysis.

Study selection

The literature was searched for studies that investigated the use of EVs as a biomarker of pediatric solid tumors. Because we were interested primarily in the clinical relevance of EVs in children with solid tumors, the starting point of our search was *in vivo* studies involving pediatric patients. We then identified *in vitro* studies that investigated the same tumors and included the same authors and/or used the same downstream analysis platform to identify potential biomarkers. Using this approach, we were able to compare studies and investigate whether the *in vitro* data supported the *in vivo* findings. For the *in vivo* part of this review, we included clinical studies that used EVs derived from patients ≤ 25 years old with pediatric solid tumors. For the *in vitro* part of this review, we included studies that: *i*) assessed EVs from cell lines derived from the same tumor entities as the *in vivo* studies, and *ii*) either used the same platform as the *in vivo* studies or were performed by the same research group as the *in vivo* studies. Only primary reports of original studies were included, and we excluded studies that were published in non-peer-reviewed form such as conference abstracts.

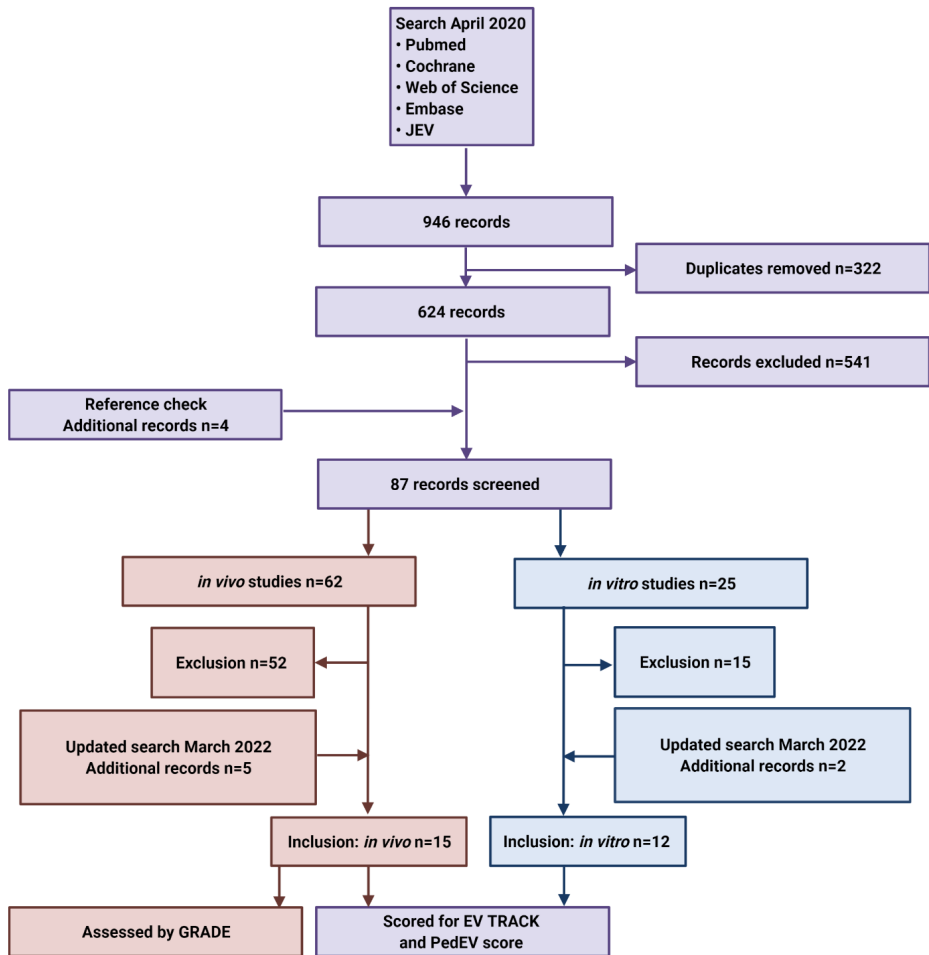


Figure 3. Flow diagram depicting the search strategy and inclusion and exclusion of studies. JEV: Journal of Extracellular Vesicles



Grading of studies

We graded the studies using three approaches. First, we assessed the quality of the clinical studies using the GRADE (Grading of Recommendations, Assessment, Development, and Evaluations) system (Supplemental Table S1) (62, 63). Second, we assessed all selected publications (both *in vivo* and *in vitro* studies) by importing all methodological details from these studies into EV-TRACK (<https://evtrack.org>) in order to obtain their corresponding EV-METRIC scores (50). Although scoring via EV-TRACK is highly rigorous and detailed, studies involving pediatric patients are challenging due to the relatively limited volumes of peripheral blood available, which limits the number of techniques that can be applied. Therefore, we also developed a PedEV score. Based on the MISEV guidelines and EV-TRACK score, we defined 11 criteria that are essential to improve reproducibility in pediatric EV studies and included these criteria in our PedEV score (Supplemental Table S2). The difference between PedEV and EV-TRACK lies primarily in the score allocated for the EV characterization technique, with PedEV providing a more lenient scoring system of EV characterization compared to EV-TRACK. Data for the evaluation were retrieved from the Materials and Methods sections of the included articles and from the supplementary materials. The 22 publications included in our review are listed in Table 4, including each publication's unique EV-TRACK ID number.

Results and Discussion

Literature search

The initial literature search yielded 241 papers in PubMed, 2 papers in the Cochrane Library, 160 papers in Web of Science, 515 papers in Embase, and 28 papers published in the *Journal of Extracellular Vesicles* (Figure 3). After duplicates were removed, pre-screening of the remaining 652 articles led to the exclusion of an additional 541 articles due to a lack of relevance. An additional 4 papers were then identified by checking the reference lists. The full text articles describing 62 *in vivo* studies and 30 *in vitro* studies were then assessed for the inclusion and exclusion criteria, and on 16th of March 2022 the search was updated. Finally, this resulted in the inclusion of 15 *in vivo* studies (7 only *in vivo* experiments and 8 both *in vivo* and *in vitro* experiments) and 12 fully *in vitro* studies. We found publications describing six tumor entities (desmoplastic small round cell tumor, hepatoblastoma, neuroblastoma, osteosarcoma, rhabdomyosarcoma and Ewing sarcoma); no other pediatric solid tumors were described.

Table 1. Overview of *in vivo* studies involving EVs derived from pediatric solid tumors.


Tumor type	EV source	Method	Cohort	Result	Biological function
<i>Author Year</i>	<i>Starting amount</i>	<i>Isolation Platform</i>	<i>Patients: Test cohort Validation cohort</i>		
			Healthy controls		
Desmoplastic small round cell tumor					
Colletti 2018 (70)	Plasma 0.6 mL	Precipitation (miRCURY Exosome Serum/Plasma Kit) Exiqon miRNA PCR panel (175 targets)	Test cohort: DSRCT n=3 (3 metastatic) Time: diagnosis (n=1), disease progression (n=2) Validation cohort: NR	miRNA ↑ miR-34a-5p ↑ miR-22-3p ↑ miR-324-5p ↓ miR-150-5p ↓ miR-342-3p	Cell growth, proliferation, migration, invasion 
Hepatoblastoma					
Liu 2016 (75)	Serum NR	Precipitation (ExoQuick) TaqMan miRNA assay (target: miR-21)	Test cohort: HB n=32 (8 metastatic, 24 localised) Stage: I (n=3), II (n=5), III (n=10), IV (n=14) Validation cohort: NR	miRNA ↑ miR-21	NR



Table 1. Continued



Tumor type	EV source	Method	Cohort	Result	Biological function
Jiao 2017 (77)	Serum NR	Precipitation (ExoQuick) TaqMan miRNA assay (targets: miR-34a, miR-34b, miR-34c)	Test cohort: HB n=63 (14 metastatic, 49 localised) Stage: I (n=7), II (n=10), III (n=20), IV (n=26) Validation cohort: HB n=26 (7 metastatic, 19 localised) Stage: I (n=2), II (n=2), III (n=9), IV (n=13)	HC n=63 miRNA ↓ miR-34a ↓ miR-34b ↓ miR-34c	Tumor initiation, metastasis, progression 
Neuroblastoma					
Ma 2019 (85)	Plasma 2 mL	Membrane-based affinity binding (exoRNeasy Serum /Plasma Midi Kit) BGISEQ-500 miRNA platform (500 targets)	Test cohort: NBL n=9, GNBi n=6 (12 FH, 3 UFH) INSS stage: I (n=2), II (n=4), III (n=5), IV (n=4) Validation cohort: NBL n=8 (6 FH, 2 UFH) INSS stage: I (n=1), II (n=3), III (n=2), IV (n=2)	HC n=7 miRNA ↑ miR-199a-3p	Cell proliferation, migration 

Table 1. Continued






Tumor type	EV source	Method	Cohort	Result	Biological function
Morini 2019 (86)	Plasma 0.5 mL	Membrane-based affinity binding (exoRNeasy Serum /Plasma Midi Kit) TaqMan miRNA array (381 targets)	Test cohort: NB n=52 Time: before + after induction chemotherapy INSS stage: IV (n=47), III (n=4), IVS (n=1) Validation cohort: NR	miRNA ↓ miR-29c ↓ miR-342-3p ↓ let-7b	Response to induction  Tumor progression, chemoresistance, survival 
Osteosarcoma					
Xu 2017 (96)	Serum NR	Differential centrifugation (10 min 1,000 g, 10 min 2,000 g, 30 min 10,000 g, 2 x 70 min 100,000 g) TaqMan miRNA array (746 targets)	Test cohort: OS n=28 (poor response), OS n=25 (good response) Validation cohort: OS n=20 (poor response), OS n=20 (good response)	miRNA ↑ miR-135b ↑ miR-148a ↑ miR-27a ↑ miR-9 ↓ miR-124 ↓ miR-133a ↓ miR-199a-3p ↓ miR-385	Response to chemotherapy  Proliferation, invasion, migration, tumor progression 
		Differential centrifugation (10 min 1,000 g, 10 min 2,000 g, 30 min 10,000 g, 2 x 70 min 100,000 g) TaqMan mRNA assay (8 targets)	Test cohort: OS n=20 (poor response) OS n=20 (good response) Validation cohort: NR	mRNA ↑ Annexin2 ↑ Smad2 ↑ Cdc5L ↑ P27 ↓ MTAP ↓ CIP4 ↓ PEDF ↓ WWOX	Response to chemotherapy 



Table 1. Continued







Tumor type	EV source	Method	Cohort	Result	Biological function
Baglio 2017 (97)	Serum 1.5 mL	Size exclusion chromatography ELISA (target: TGFβ)	Test cohort: OS n=10 Stage: IB (n=4), IIA (n=2), IIB (n=2), III (n=2) Validation cohort: NR	HC n=10 Protein ↑ TGFβ	Tumor growth, metastasis 
Shen 2016 (98)	Serum NR	Precipitation (ExoQuick) Western blotting (target: G6PD)	Test cohort: OS n=15 Time: diagnosis Validation cohort: NR	HC n=15 Protein ↑ G6PD	Cell adhesion, migration, viability 
Gong 2018 (99)	Plasma NR	Differential centrifugation (10 min 300 g, 10 min 2,000 g, 30 min 10,000 g, 2x 70 min 100,000 g) Small RNA library sequencing (Illumina)	Test cohort: OS n=2 (localised) Time: diagnosis + postoperative metastasis Validation cohort: NR	miRNA ↑ miR-675	Migration, invasion Metastasis  
Ye 2020 (106)	Plasma NR	Differential centrifugation (20 min 1,500G, 30 min 10,000G, 120 min 100,000G) Small RNA sequencing (BGISEQ-500) RT-qPCR	Test cohort: OS n=25 Validation cohort: NR	HC n=10 miRNA ↑ miR92a-3p ↑ miR130a-3p ↑ miR195-3p ↑ miR335-5 ↑ let7f-3p	Proliferation, apoptosis inhibition, G2/M cell cycle arrest, invasion  

Table 1. Continued



Tumor type	EV source	Method	Cohort	Result	Biological function
Cambier 2021(107)	Serum 0.3ml	Precipitation (Exoquick)	Test cohort: OS n=12	HC n=12 DNA ↑HSATII	NR
		Precipitation (PEG)	Validation cohort: OS n=8	HC n=12 ↑LINE1-P1 ↑Charlie3 RNA =HSATII =LINE1-P1 =Charlie3	
Rhabdomyosarcoma					
Ghamloush 2019 (116)	Serum 0.4 mL	Differential centrifugation (10 min 300 g, 10 min 2,000 g, 30 min 10,000 g, 2x 70 min 100,000 g) + precipitation (ExoQuick)	Test cohort: RMS n=7 (ERMS n=6, ARMS n=1), control n=6 (benign tumor) Time: diagnosis Follow-up n=2 (ERMS n=1, ARMS n=1) Time: follow-up after treatment	miRNA ↑ miR-486-5p	Response to chemotherapy in ARMS  Invasion, migration, proliferation 
Ewing sarcoma					
Dong 2020 (123)	Plasma 0.3 mL	ES-EV Click Chip RT-ddPCR	Test cohort: ES n=4 Time: NR	HC=4 mRNA EWSR1 rearrangement	NR
Samuel 2020 (124)	Plasma 0.25 mL	Immunoprecipitation qRT-PCR	Test cohort: ES n=10	HC=6 mRNA EWSR1-ETS fusion	NR

Table 1. Continued

Tumor type	EV source	Method	Cohort	Result	Biological function
Sun 2022 (125)	Plasma 1.0 mL	Click Beads RT-dPCR	Test cohort: ES n=28 (35 patients)	HC=10 mRNA EWSR1-FLI1	NR

DSRCT: desmoplastic small round cell tumor; HC: healthy control; HB: hepatoblastoma; NR: not reported; PRETEXT: pre-treatment extent of disease; NBL: neuroblastoma; GNB1: ganglioneuroblastoma intermixed; FH: favourable histology; UFH: unfavourable histology; INSS: International Neuroblastoma Staging System; OS: osteosarcoma; ERMS: embryonal rhabdomyosarcoma; ARMS: alveolar rhabdomyosarcoma; RMS: rhabdomyosarcoma. Function derived from: 📖 : literature; 🧪 : in vitro; 🐭 : mice.

Table 2. Overview of the in vitro studies involving pediatric solid tumors and EVs. (following page)

Tumor type	Cell lines	Method	Result	Biological function
Neuroblastoma				
Ma 2019 (85)	SK-N-SH SH-SY5Y SK-N-BE(2)	Isolation Platform Differential centrifugation (10 min 300 g, 10 min 2,000 g, 30 min 10,000 g, 70 min 100,000 g, 60 min 100,000 g) BGISEQ-500 miRNA platform (500 targets)	miRNA ↑ miR-199a-3p	Cell proliferation, migration 
Challagundla 2015 (87)	SK-N-BE(2) CHLA-255 IMR-32	Precipitation (ExoQuick) Affymetrix human exon arrays (> 10 ⁶ targets)	miRNA ↑ miR-21-5p	Drug resistance 
Haug 2015 (88)	MYCN-amplified Kelly MYCN-amplified SK-N-BE(2)-C SK-N-AS	Differential centrifugation (10 min 200 g, 20 min 2,000 g, 30 min 10,000 g, 70 min 110,000 g) miRCURY qPCR panels 1+2 V2.M (752 targets)	miRNA ↑ miR-92a-3p ↑ miR-23a-3p ↑ miR-218-5p ↑ miR-320a ↑ miR-24-3p ↑ miR-27b-3p ↑ miR-16-5p ↑ miR-25-3p ↑ miR-21-5p ↑ miR-125b-5p ↑ miR-320b	Survival, proliferation, apoptosis, angiogenesis, differentiation, invasion, metastasis 
Osteosarcoma				
Baglio 2017 (97)	MG63 HOS 143B	Differential centrifugation (2x 10 min 500 g, 2x 15 min 2,000 g, 2x 30 min 10,000 g, 2x 60 min 70,000 g) ELISA (target: TGFβ)	Protein ↑ TGFβ	Tumor growth, metastasis 

Table 2. Continued











Tumor type	Cell lines	Method	Result	Biological function
Gong 2018 (99)	MG63 HOS 143B Well5	Differential centrifugation (10 min 300 g, 10 min 2,000 g, 30 min 10,000 g, 2x 70 min 100,000 g) Small RNA library sequencing (Illumina)	miRNA ↑ miR-675	Migration, invasion  Metastasis 
Jerez 2017 (100)	SAOS2 MG63 U2OS HOS 143B	Ultracentrifugation (90 min 100,000 g) Proteomics (MS)	Protein 565 unique proteins	Angiogenesis, adhesion, migration, metastasis 
Yoshida 2018 (103)	143B U2OS	Ultracentrifugation (2x 70 min 110,000 g) RT-qPCR (target miR-25-3p)	miRNA ↑ miR-25-3p	Proliferation, invasion, migration, angiogenesis, drug resistance 
Fujiwara 2017 (102)	U2OS HOS 143B SaOS2	Ultracentrifugation (70 min 110,000 g) RT-qPCR (target miR-25-3p)	miRNA ↑ miR-25-3p ↑ miR-17-5p	Cell proliferation, tumor growth  Survival 
Macklin 2016 (104)	KHOS (HiMet-C1, HiMet-C6, LoMet-C4, LoMet-C5)	Precipitation (ExoQuick) Proteomics (MS)	Protein 31 unique proteins	Migration, invasion  Lung metastasis 
Jerez 2019 (101)	SAOS2 MG63 HOS 143B U2OS hFOB1.19	Ultracentrifugation (90 min 100,000 g) NEBNext Small RNA library (Illumina)	miRNA ↑ miR-21-5p ↑ miR-143-3p ↑ miR-181a-5p ↑ miR-148a-3p	Tumor progression, metastasis 

Table 2. Continued

Tumor type	Cell lines	Method	Result	Biological function
Raimondi 2020 (105)	SAOS2 MG63 U2	Differential centrifugation (5 min 300 g, 15 min 3,000 g, 30 min, 10,000 g, 90 min 100,000 g) MiSeq Reagent Kit v3 (Illumina)	miRNA ↑ miR-21-5p ↑ miR-148a-3p	Carcinogenesis
Ye 2020 (106)	NHOst U2OS 143B	EV isolation not reported RT-qPCR	miRNA miR130a-30 miR195-3p	Proliferation, apoptosis inhibition, G2/M cell cycle arrest, invasion
Rhabdomyosarcoma				
Gayad 2016 (114)	Rh30 Rh41 RD JR1 Rh36	Differential centrifugation (10 min 300 g, 10 min 2,000 g, 30 min 10,000 g, 2x 70 min 100,000 g) Affymetrix GeneChip miRNA 3.0 Arrays kit (19724 targets)	miRNA ↑ miR-1246 ↑ miR-1268	Proliferation, migration, invasion, metastasis
Rammal 2019 (115)	Rh30 Rh41 RD JR1 Rh36	Differential centrifugation (10 min 300 g, 20 min 2,000 g, 30 min 10,000 g, 2x 70 min 100,000 g) Proteomics (MS)	Protein 36 unique proteins	Invasion, proliferation, metastasis
Ghamloush 2019 (116)	Rh30 Rh41 RD JR1 Rh36	Differential centrifugation (10 min 300 g, 10 min 2,000 g, 30 min 10,000 g, 2x 70 min 100,000 g) TaqMan miRNA assay (target: miR-486)	miRNA ↑ miR-486-5p	Invasion, migration, proliferation
Ewing sarcoma				
Miller 2013 (121)	A673 SK-N-MC SB-KMS-KS1	Differential centrifugation (10 min 300 g, 10 min 2,000g, 30 min 10,000, 70 min 100,000, 60 min 100,000) Affymetrix HumanGene 1.0 ST arrays	mRNA NR0B1, NKX2.2, STEAP1, LIPI, EWSR1-FLI fusion	Signal transduction, stemness



Table 2. Continued

Tumor type	Cell lines	Method	Result	Biological function
Zhang 2018 (122)	Hs919.T CHLA-258 CHLA-9	Differential centrifugation 5 min 2500 rpm, 45 min 10,000 g, 120 min 100,000 g	mRNA EWSR1-FLI1 fusion	NR
Dong 2020 (123)	A673 SKES 1 ES5838	Differential centrifugation (10 min 300 g, 30 min 4600 g, 120 min 100,000 g) Exoquick Immunomagnetic beads ES-EV Click Chips	mRNA EWSR1 rearrangement	NR
Samuel 2020 (124)	TC-71 RD-ES SK-ES-1 CHLA-258 COG-E-352 Hs919.T	RT-ddPCR Differential centrifugation 5 min 2500 rpm, 45 min 10,000 g, 75 min 110,000 g, 60 min 35,800 rpm Proteomics Immunoprecipitation	Protein Bulk analysis CD99, NGFR mRNA EWSR1-ETS fusion	Bulk: Exosomal proteins (membrane transport and fusion), metabolic enzymes, antigen presenting, cytoskeletal, protein binding 
Sun 2022 (125)	A673	RT-qPCR Differential centrifugation 10 min 300 g, 10 min 2800 g, 90 min 100,000 g Click beads ExoQuick Magnetic biotin-PEG-DSPE beads RT-dPCR	mRNA EWSR1-FLI1 fusion	NR

MS: mass spectrometry. Function derived from:  : literature;  : in vitro;  : clinical;  : mice.

Table 3. Critical appraisal of the clinical studies using the GRADE system.

Reference	Study design	Patient inclusion	Patient characteristics	Selection bias	Reproducibility	In vitro validation	End point	Outcome	Funding	Score
Colletti 2018 (70)	2	0	1	0	0	0	1	2	1	7
Liu 2016 (75)	2	1	1	0	0	0	1	2	1	8
Jiao 2017 (77)	1	1	1	0	1	0	1	2	1	8
Ma 2019 (85)	2	1	1	0	2	1	1	2	1	11
Morini 2019 (86)	2	1	1	0	0	0	1	2	1	8
Xu 2017 (96)	2	1	1	0	2	0	1	2	1	10
Baglio 2017 (97)	2	0	1	0	0	1*	1	2	0	7
Shen 2016 (98)	2	1	1	0	0	0	1	2	1	8
Gong 2018 (99)	2	1	0	0	2	1*	1	2	1	10
Ye 2020 (106)	2	0	1	1	0	1	1	1	0	7
Cambier 2021 (107)	2	0	1	0	1	0	1	2	0	7
Ghamloush 2019 (116)	1	0	0	0	0	1*	1	2	0	5
Dong 2020 ((123)	1	0	0	0	0	2	1	0	1	5
Samuel 2020 ((124)	1	1	0	1	0	1	1	1	1	7
Sun 2020 (125)	1	1	1	1	0	1	1	2	0	8

See Supplementary Table S1 for a detailed description of the criteria. *: in vivo validation of in vitro findings.



Table 4. Critical appraisal of the EV isolation and characterization in the *in vivo* and *in vitro* studies using the criteria for PedEV score and EV-TRACK.

Reference	Nomenclature	Prenalytical variables	Isolation method	Source volume & EV abundance	EV-enriched proteins	Non-EV-enriched proteins	Antibody & lysis buffer	Single vesicle characterisation	Electron microscopy	Characterisation platform	Inclusion of controls	PedEV Score (%)	EV Track ID	EV-METRIC <i>in vivo</i> (%)	EV-METRIC <i>in vitro</i> (%)
Colletti 2019 (70)	0	5.5	11	11	0	0	NA	11	5.5	11	0	55	EV200162	17	-
Liu 2016 (75)	0	5.5	11	0	0	0	NA	0	0	11	0	27.5	EV200163	0	-
Jiao 2017 (77)	0	5.5	11	0	0	0	NA	0	0	11	0	27.5	EV200164	0	-
Ma 2019 (85)	5.5	5.5	11	5.5*	5.5*	5.5*	5.5*	11*	5.5*	11*	0	71.5	EV200165	38	0
Morini 2019 (86)	5.5	5.5	11	5.5	5.5	0	5.5	5.5	0	11	0	55	EV200166	0	-
Challagundla 2015 (87)	0	5.5	11	5.5	5.5	0	11	5.5	0	11	5.5	60.5	EV210115	-	0
Haug 2015 (88)	5.5	11	11	0	11	5.5	11	11	5.5	11	5.5	88	EV210117	-	44
Xu 2017 (96)	0	0	5.5**	0	0	0	NA	0	0	5.5	0	11	EV210073	0	-
Baglio 2017 (97)	5.5	5.5	11	5.5	5.5*	0	11*	5.5*	5.5*	11	0	66	EV210074	0	22
Shen 2016 (98)	0	5.5	11	0	5.5	0	11	5.5	5.5	5.5	0	49.5	EV210080	25	-
Gong 2018 (99)	0	5.5*	11	0	11*	5.5*	11*	11*	5.5*	5.5	0	66	EV210072	0	44
Jerez 2017 (100)	5.5	5.5	11	0	11	0	11	5.5	5.5	11	5.5	71.5	EV210071	-	22
Jerez 2019 (101)	5.5	5.5	11	5.5	11	0	11	5.5	0	11	5.5	71.5	EV210070	-	14
Fujiwara 2017 (102)	0	5.5	11	0	0	0	NA	0	0	11	0	27.5	EV210116	-	0
Yoshida 2018 (103)	0	5.5	11	0	5.5	0	11	11	5.5	11	5.5	66	EV210079	-	22
Macklin 2016 (104)	5.5	11	11	5.5	11	0	11	11	5.5	11	0	82.5	EV210078	-	38

Table 4. Continued

Reference	Nomenclature	Prenalytical variables	Isolation method	Source volume & EV abundance	EV-enriched proteins	Non-EV-enriched proteins	Antibody & lysis buffer	Single vesicle characterisation	Electron microscopy	Characterisation platform	Inclusion of controls	PedEV Score (%)	EV Track ID	EV-METRIC in vivo (%)	EV-METRIC in vitro (%)
Raimondi 2019 (105)	5.5	11	5.5	0	5.5	5.5	11	5.5	0	11	0	60.5	EV210081	-	44
Ye 2020 (106)	0	5.5	11	5.5	11*	0	5.5	5.5*	5.5*	11	5.5	66	EV220086	11	0
Cambier 2021 (107)	5.5	11	5.5	5.5	0	0	0	5.5	0	11	11	55	EV220085	29	-
Ghayad 2016 (114)	0	5.5	11	5.5	11	5.5	11	5.5	5.5	11	0	71.5	EV210077	-	33
Rammal 2019 (115)	0	5.5	11	0	11	5.5	11	5.5	5.5	11	0	66	EV210082	-	33
Ghamloush 2019 (116)	0	5.5	5.5	5.5	11*	5.5*	11*	5.5*	5.5*	11	0	66	EV200167	0	38
Miller, 2013 (121)	5.5	5.5	11	11	5.5	5.5	0	11	5.5	11	5.5	77	EV130146	-	25
Zhang 2018 (122)	5.5	5.5	11	5.5	0	0	0	11	5.5	11	5.5	60.5	EV220168	-	29
Dong 2020 (123)	0	5.5	11	5.5	5.5	0	0	5.5	5.5	11	5.5	55	EV220170	0	0
Samuel 2020 (124)	5.5	5.5	11	5.5	5.5	0	0	5.5	0	11	11	60.5	EV220169	0	11
Sun 2022 (125)	5.5	11	11	5.5	0	0	0	5.5	5.5	11	5.5	60.5	EV220167	0	0

See Supplementary Table S2 for a detailed description of the used criteria. *: performed either in vitro or in vivo, but not both. **: in the Materials and Methods section, EV isolation from conditioned media is mentioned, but from the rest of the article it is clear that this should be serum.
 Note: if different EV-METRIC scores were given to different experiments, only the highest score is reported.



Extracellular vesicles in pediatric solid tumors

The *in vivo* and *in vitro* studies are summarized in Table 1 and Table 2, respectively. Regarding the *in vivo* studies, we reviewed the following information: tumor type, the sample used to detect EVs, and the sample volume, the latter of which is particularly important in pediatric patients, as sample volumes are typically relatively low. To assess the possible effects of specific EV enrichment techniques on the results, we also examined the enrichment protocols used in each study. We also noted any details regarding the patient cohorts and—if included in the study—healthy controls. As an outcome, we examined the biomarkers, including their function and how this was determined in the study.

Next, we critically assessed the clinical studies using the GRADE system (62, 63) and the EV methodology using our own PedEV score and EV-TRACK score(51). The mean GRADE score was 7.7 points (range: 5-11 points), and the mean PedEV score was 59.1% (range: 11-88%). Finally, the mean EV-TRACK score was 8% (range: 0-38%) for the *in vivo* studies and 21% (range: 0-44%) for the *in vitro* studies. Below, we discuss the output for each of the six tumor entities.

Desmoplastic small round cell tumor

Desmoplastic small round cell tumor (DSRCT) is an aggressive and rare sarcoma that occurs primarily in adolescents and young adults, with an increased prevalence among males (64). The majority of DSRCT cases present intra-abdominally, often with widespread metastasis throughout the abdomen (65). At the molecular level, DSRCT is characterized by a t(11:22)(p13;q12) translocation, causing fusion of the *EWSR1* and *WT1* genes (66). The resulting fusion gene generates the oncogenic EWSR1-WT1 fusion protein, which regulates transcriptional activity and is essential for tumor cell proliferation (67). Patients with DSRCT have extremely poor outcome, and sparse research has been performed with respect to diagnostic and prognostic biomarkers (68, 69). Our literature search identified only one clinical study involving EV in DSRCT and no *in vitro* studies.

Colletti *et al.* examined the miRNA profiles of EVs isolated from plasma samples obtained from three patients with DSRCT and compared the results with EVs obtained from four healthy controls (Table 1) (70). They found that five miRNAs were highly dysregulated in all three patients, and the dysregulated miRNAs were correlated with both tumor aggressiveness and clinical outcome, suggesting that this EV-derived miRNA profile could be used as a possible prognostic marker. Moreover, bioinformatics analysis showed that the genes targeted by the dysregulated miRNAs are involved in oncogenic signaling pathways. A potential limitation of this study

is that the authors reported, using western blot analysis, to detect EV-related and non-EV-related proteins, but did not show the results of these experiments. Other methodological limitations include the relatively small cohort size (with 3 patients and 4 controls), no clear list of inclusion and exclusion criteria, and no validation in an independent cohort, which complicates the translation to clinical practice. These limitations are reflected in the relatively low GRADE and EV-TRACK scores of 7 and 17%, respectively, although the PedEV score (55%) was average, indicating a more permissive assessment of their EV characterization.

Given that DSRCT is extremely rare, validation in an independent cohort may be difficult. However, *in vitro* validation of the results would likely increase their applicability and provide important insights into the pathology underlying DSRCT.

Hepatoblastoma

Hepatoblastoma is the most common primary pediatric liver tumor, typically presenting in children between 6 months and 4 years of age (71). Hepatoblastoma is an embryonal tumor, presumably arising from hepatocyte precursor cells and displaying histological patterns that recapitulate the liver's developmental stages (72). Although most hepatoblastoma cases are sporadic in origin, some are associated with genetic syndromes such as Beckwith-Wiedemann syndrome or familial adenomatous polyposis (73). In recent decades, the overall survival rate among patients with hepatoblastoma has improved considerably; however, the outcome for patients with advanced disease remains unfavorable, and effective biomarkers for early diagnosis and for predicting outcome are still lacking (74). Our literature search revealed two clinical studies regarding EV in hepatoblastoma, and no *in vitro* studies.

Liu *et al.* examined the diagnostic and prognostic potential of measuring miR-21 in serum EVs in patients with hepatoblastoma (Table 2) (75). The authors found significantly higher expression of miR-21 in both the serum and serum-derived EVs in patients compared to healthy controls. They also showed that miR-21 expression in EVs is a better diagnostic marker for hepatoblastoma than serum AFP (alpha-fetoprotein) levels, the currently used biomarker (76). miR-21 expression was also found to be an independent predictor of low event-free survival, suggesting that it could be used as both a diagnostic and prognostic biomarker for hepatoblastoma. Although they did not assess the function of miR-21 in hepatoblastoma, the authors noted that this will be examined in a follow-up study. In addition, future studies are needed in order to determine the precise prognostic value of miR-21, as well as the relationship between this marker and other risk factors, which may confer a possible



bias. Finally, the size of their study cohort (n=32 patients) was relatively large given the rarity of this tumor, and the authors included a control group consisting of healthy age- and gender-matched children; nevertheless, a validation cohort and/or *in vitro* validation is needed in order to support their conclusions.

Jiao *et al.* studied the diagnostic and prognostic value of measuring miR-34 expression in serum-derived EVs in patients with hepatoblastoma (Table 2) and found lower levels of miR-34a, miR-34b, and miR-34c in EV-enriched samples obtained from patients compared to healthy age- and gender-matched controls (77). With respect to diagnosing hepatoblastoma, they found that a panel comprised of all three miRNAs performed better than serum AFP levels, indicating its potential as a diagnostic biomarker. Moreover, this miRNA panel appeared to be superior at predicting poor prognosis compared to other risk factors. The authors also reported that miR-34 miRNAs have been shown previously to play a role in the initiation, progression, and metastasis of several types of tumors. Although the authors did not investigate the function of miR-34 miRNAs specifically in hepatoblastoma, their study included a relatively large patient cohort (n=63) and an age- and gender-matched control group; moreover, they also included a validation cohort (n=26 patients). On the other hand, a potential limitation of their study is that it was retrospective.

Remarkably, although the studies by Liu *et al.* (75) and Jiao *et al.* (77) were performed by two different groups at two different research centers, their publications contained large sections of identical text (particularly their description of the methods), and the studies were performed during the same time period with comparable cohorts. In addition, although the two groups used a similar approach, they studied different miRNAs, without discussing their choice of miRNAs.

An important limitation common to both studies is a general lack of EV characterization. Furthermore, they provided no evidence that the miRNAs were EV-associated, nor did they report the initial volume of serum. These limitations are reflected in the low EV-METRIC and PedEV scores (0% and 27.5%, respectively, for both studies), although their GRADE score of 8 was average.

Neuroblastoma

Neuroblastoma is the most common pediatric extracranial solid tumor, predominantly occurring in children in the first 2 years of life (78). Neuroblastoma arises from the developing sympathetic nervous system, resulting in tumors in the adrenal glands and/or sympathetic ganglia. Neuroblastoma is characterized by biological heterogeneity and unique clinical properties such as a tendency for spontaneous

regression in infants, even in cases with metastatic disease (79). These features translate to a highly variable outcome, with a survival rate higher than 90% in low-risk and intermediate-risk cases, but only 40-50% survival in high-risk cases (80). Several genetic aberrations have been associated with neuroblastoma, including mutations in the *ALK* (81) and *PHOX2B* (82) genes, amplification of the *MYCN* gene (83), and segmental chromosome alterations (84). Importantly, new biomarkers for the early detection of neuroblastoma and for predicting the patient's response to therapy are urgently needed. With respect to EVs in neuroblastoma, our literature search revealed two clinical studies regarding EVs in neuroblastoma (one of which also assessed EVs *in vitro*) and two *in vitro* studies.

Ma *et al.* identified EV-derived miRNA biomarkers *in vivo* and then examined the underlying molecular mechanism in an *in vitro* study (Tables 1 and 2)(85). In their *in vivo* study, they used next-generation sequencing of EV-derived miRNA and found that the expression of miR-199a-3p was significantly higher in EVs isolated from plasma obtained at the initial diagnosis of patients with neuroblastoma (in all risk groups) compared to healthy age- and gender-matched controls. Moreover, this upregulation of miR-199a-3p in patients appeared to be correlated with a high risk profile. In their *in vitro* study, the authors found that miR-199a-3p was expressed at significantly higher levels in neuroblastoma cell lines and their corresponding EVs compared to control human cell lines, including HUVEC (human umbilical vein endothelial cells), HEK293, and MRC-5 (fibroblast) cells. This miRNA was also shown to promote the proliferation and migration of neuroblastoma cells. Based on their results, the authors suggest that miR-199a-3p may be used as a rapid, easy, non-invasive biomarker for the detection of neuroblastoma, even though their study included only 7 healthy controls. With respect to the authors' *in vitro* validation of their *in vivo* findings, it is important to note that they used different methods to isolate EVs, and only the patient-derived EVs were characterized. Moreover, their *in vivo* study had a relatively small cohort (n=15 patients) and was cross-sectional; thus, longitudinal studies involving several time points and larger cohorts may provide more insights into the progression of neuroblastoma and facilitate the discovery of new biomarkers. Nevertheless, their validation using both a clinical validation cohort (n=8) and *in vitro* data increase their study's reproducibility. The resulting GRADE score of 11 indicates that this was a well-balanced study; in addition, the study used a sound methodological approach for the *in vivo* experiments, reflected by the relatively high EV-TRACK and PedEV scores of 38% and 71.5%, respectively.

Morini *et al.* investigated whether EV-derived miRNA can be used to predict the patient's response to induction chemotherapy (Table 1)(86). The authors found that



plasma samples from patients with high-risk neuroblastoma contained significant levels of neuroblastoma-derived EVs, and these levels decreased and developed a differential miRNA expression profile in response to chemotherapy. Specifically, they found that a signature consisting of three miRNAs (miR-29c, miR-342-3p, and let-7b) could discriminate between patients with a poor clinical response and patients with a good clinical response. These three miRNAs have tumor-suppressor functions, and pathway analysis indicated that they play a role in tumor progression, survival, and chemoresistance. Notably, for each patient the authors also calculated a chemoresistance index for the specific drugs used in neuroblastoma treatment, based on changes in EV-derived miRNAs; they found that this index reliably defined each patient's response to specific drugs, creating new opportunities for applications involving personalized medicine. Despite these strengths, their study was retrospective and lacked *in vivo* and *in vitro* validation. Thus, a prospective study involving a validation cohort would likely support the prognostic value of these miRNAs. Moreover, their characterization of EVs did not use conventional techniques such as western blot analysis or electron microscopy, which resulted in an EV-METRIC score of 0%. In contrast, the PedEV score was 55%; this higher PedEV score was due to their use of flow cytometry to analyze EVs. However, all of the essential information regarding the use of flow cytometry needs to be properly reported to avoid an erroneous interpretation of the data, particularly when analyzing single EV-based flow cytometry data (47).

Challagundla *et al.* examined the role of EV-derived miRNAs in the development of drug resistance in neuroblastoma (Table 2) (87). They measured the expression of several pro-inflammatory miRNAs in three neuroblastoma cell lines and found that only miR-21-5p was expressed in all three cell lines. The authors also claimed that they used a noncoding RNA array to screen for miRNA expression in EVs released by five neuroblastoma cell lines; however, these data were not shown. Co-culture experiments showed that secreted miR-21-5p could be transferred to human monocytes via EVs. Thus, although the potential of using miR-21-5p as a biomarker for neuroblastoma was not examined, it would be interesting to analyze whether this miRNA is upregulated *in vivo*. Another interesting question is if miR-21-5p is upregulated only in *MYCN*-amplified neuroblastoma, as the *MYCN* amplification status of the cell lines was not clearly stated. Similar to the study by Morini *et al.* (86), we found a relatively large discrepancy between the EV-METRIC score (0%) and PedEV score (60.5%). Moreover, the study by Challagundla *et al.* did not meet the strict criteria established by EV-TRACK, including failing to report an analysis of EV-enriched and non-EV-enriched proteins, and not using a density gradient to purify the EV-enriched fraction. However, the authors did provide details regarding their

EV enrichment method, their characterization of EVs using nanoparticle tracking analysis (NTA), and their analysis of the EV cargo, which is reflected in the relatively higher PedEV score (60.5%).

Haug *et al.* examined the miRNA profile of EVs derived from two *MYCN*-amplified neuroblastoma cell lines (Table 2) (88) and found a total of 11 EV-derived miRNAs that were expressed at high levels in both cell lines. Functional enrichment analysis showed that these miRNAs are involved in several processes in cancer, including tumor survival, proliferation, and metastasis. A strength of this study is that they validated the origin of the isolated miRNAs by measuring the expression of EV-derived miRNAs in a single neuroblastoma cell line using two different isolation protocols, yielding nearly identical expression levels. Among all of the publications that we analyzed, this study had the highest EV-METRIC (44%) and PedEV (88%) scores, reflecting its sound methodology and study design.

Among these four studies, miR-199a-3p was the only miRNA reported to be upregulated in neuroblastoma both *in vivo* and *in vitro* (85). In addition, miR-21-5p was upregulated in two *in vitro* studies (87, 88). Based on the various groups' reporting of their EV methodologies, we found disparity between the EV-METRIC and PedEV scores. This disparity reflects the efforts that the researchers put into characterizing EVs, but it also reflects possible limitations with respect to EV-specific equipment and/or the knowledge available at the various research centers.

Osteosarcoma

Osteosarcoma is a highly aggressive primary bone tumor that typically presents in children and adolescents, although a second peak in incidence can occur among individuals >60 years of age (89). The primary tumors typically arise in the appendicular skeleton, with metastatic disease commonly occurring in the lungs and other bones (90). The tumor is mesenchymal in origin and is characterized by the production of osteoid (91), and includes a wide range of distinct histological subtypes (92). Although the genetic landscape of osteosarcoma varies widely between tumors, osteosarcoma has been associated with recurrent somatic mutations in several genes, including *TP53*, *RB1*, *ARTX*, and *DLG2* (93, 94). The survival rate among patients with metastatic disease remains low, emphasizing the urgent need to identify reliable biomarkers for diagnosis and tracking the disease progression (95). Our search revealed six *in vivo* studies involving EVs in osteosarcoma (of which three studies also included *in vitro* experiments) and six distinct *in vitro* studies.

Xu *et al.* examined the potential of using serum EV-derived miRNA expression profiles to predict the response to chemotherapy in patients with osteosarcoma (Table 1) (96). The authors identified the differential expression of 30 miRNAs, 8 of which were confirmed in a validation cohort, and they found that the expression levels were correlated with poor response. Comparative pathway analysis revealed that the differentially regulated miRNAs affect several pathways involved in cancer. Based on these results, the authors suggest that both miRNAs and mRNAs derived from EVs could be used as markers to monitor and predict disease progression in patients with osteosarcoma undergoing chemotherapy. This study had several strengths, including the use of a uniform method for EV enrichment in all samples, the relatively large size of the patient cohort (n=53) and validation cohort (n=40), and their assessment of both miRNA and mRNA. On the other hand, a limitation of their study is that pre-analysis factors such as the collection and processing of the serum samples were not described, and no results were reported with respect to EV characterization or validation. These limitations are reflected in both a low EV-METRIC score (0%) and a low PedEV score (11%). In contrast, the GRADE score was 10, which is relatively good.

Baglio *et al.* studied the effect of tumor EV-educated mesenchymal stem cells on osteosarcoma progression (Tables 1 and 2) (97). They found that EVs derived from three osteosarcoma cell lines contained higher levels of transforming growth factor β (TGF β) compared to EVs derived from fibroblast cells (as a control group). They also studied the effect of osteosarcoma-derived EVs on tumor growth and metastasis in a preclinical mouse model. Finally, they measured serum TGF β levels in osteosarcoma patients and healthy controls and found increased levels in the patient group; however, they did not indicate whether the healthy controls were age-matched. Importantly, this study was not designed to identify biomarkers for osteosarcoma, but rather to perform an *in vitro* analysis of osteosarcoma-derived EVs. Furthermore, they used different EV isolation protocols for the *in vitro* and *in vivo* samples. This difference is reflected in the EV-METRIC scores of 0% and 22% for the *in vivo* and *in vitro* experiments, respectively. This difference between the *in vivo* and *in vitro* protocols cannot be captured by the PedEV score (66%), which scores overall methodological quality. Finally, the GRADE score for this study was 7, as the authors failed to report their patient inclusion criteria and no validation cohort was included.

Shen *et al.* found that serum-derived EVs obtained from patients with osteosarcoma can affect the adhesion, migration, and viability of MG-63 cells, a human pre-osteoblastic cell line (Table 1) (98). They then used mass spectrometry (MS) to identify the proteins in these EVs, finding that 233 proteins were expressed in the osteosarcoma patients but not in healthy (albeit not age- or gender-matched)

controls. KEGG (Kyoto Encyclopedia of Genes and Genomes) pathway analysis revealed that these proteins play a role in four pathways that are important for osteosarcoma progression. Interestingly, the protein G6PD (glucose-6-phosphate dehydrogenase) was expressed at particularly high levels in the EVs obtained from patients with osteosarcoma and was suggested as a diagnostic and/or therapeutic target in osteosarcoma; however, this finding should be substantiated in a validation cohort. More extensive characterization of the EVs and the inclusion of age- and gender-matched healthy controls would have increased the study's validity; these limitations resulted in a GRADE score of 8. The PedEV score of 49.5% indicates that the EV characterization was reported in sufficient detail; however, the EV-METRIC score was only 25% based on the authors failing to report EV quantitation and not mentioning whether they purified the EV-enriched fraction using a density gradient.

Gong *et al.* examined the miRNA profiles of EVs isolated from metastatic osteosarcoma cell lines and non-metastatic osteosarcoma cell lines (Tables 1 and 2) (99). Small RNA sequencing identified a total of 61 miRNAs that were differentially expressed in EVs between the metastatic and non-metastatic cell lines, as well as patient serum. miR-675 was the most significantly upregulated miRNA in EVs isolated from the metastatic cell lines, and this result was confirmed both *in vitro* and *in vivo* using RT-qPCR. *In vitro* functional studies indicated that miR-675 can increase tumor cell migration and invasion by targeting expression of the calcium-binding protein CALN1 (Calneuron-1); thus, miR-675 might serve as a valuable mechanism-based prognostic biomarker for osteosarcoma metastasis. A strength of this study is that it included both *in vivo* and *in vitro* data. However, it is limited by the small patient cohort (n=2) and the fact that the patient characteristics are not reported. The GRADE score was therefore 10. A follow-up study with a larger clinical cohort is needed in order to validate these findings. The PedEV and EV-METRIC scores were relatively high for the *in vitro* experiments (66% and 44%, respectively); however, the *in vivo* experiments lacked sufficient EV characterization.

Jerez *et al.* performed a proteomic analysis of EVs derived from three osteosarcoma cell lines (Table 2) (100). The authors identified a total of 1,741 proteins that were unique to the osteosarcoma-derived EVs, 565 of which were found in all three cell lines. Gene Ontology analysis revealed that these proteins are involved in angiogenesis, adhesion, and cell migration.

In a separate, more recent study the same group used next-generation sequencing to characterize the miRNAs in EVs derived from five osteosarcoma cell lines, some of which were included in their previous report (Table 2) (101). They found 237 miRNAs

that were present exclusively in the osteosarcoma cell lines, and they found that the metastatic cell lines clustered differently than the non-metastatic cell lines. In particular, they found four miRNAs (miR-21-5p, miR-143-3p, miR-181a-5p, and miR-148a-3p) that were enriched in the metastatic SaOS2 cell line. Gene Ontology analysis revealed that the genes targeted by these highly abundant miRNAs in osteosarcoma cell lines are related to tumor progression and metastasis. The EV methodology used in both the 2017 and 2019 studies had rather high standards with respect to EV isolation and characterization, resulting in a PedEV score of 71.5% for both studies. However, in their 2019 paper (101) they did not report the results regarding EV characterization by EV-enriched proteins, resulting in a slightly lower EV-METRIC score for this paper (14%) compared to their previous publication (22%).

Fujiwara *et al.* screened circulating miRNAs in patient serum samples and in EVs secreted by osteosarcoma cell lines (Table 2) (102). They found that miR-25-3p and miR-17-5p were upregulated in the osteosarcoma cell lines and culture media, and the expression of these two miRNAs was even higher in EVs derived from the osteosarcoma cell lines than in the cells themselves. They also found that the serum levels of these miRNAs were higher in patients with osteosarcoma than in healthy controls. Due to the limited volume of serum, miRNAs were isolated only from total serum and not from EV-enriched samples. Moreover, the low EV-METRIC and PedEV scores of 0% and 5, respectively, reflect the limited effort that the authors put into providing a detailed description of their isolation and characterization of EVs.

In a follow-up study by the same group, Yoshida *et al.* assessed the role of miR-25-3p in osteosarcoma (Table 2) (103) and found that high expression levels of miR-25-3p were correlated with poor prognosis. They also performed functional analyses and found that this miRNA is involved in proliferation, invasion, migration, and multi-drug resistance in osteosarcoma cells. The encapsulation of the miRNAs in the lipid vesicles was believed to increase the stability of miR-25-3p and facilitate delivery to the tumor microenvironment, promoting tumor progression. In this follow-up study, the authors included more details regarding their EV methodology and characterization, as reflected by the PedEV and EV-METRIC scores of 66% and 22%, respectively.

Macklin *et al.* analyzed EVs secreted by both high and low metastatic clonal variants of the KHOS human osteosarcoma cell line (Table 2) (104). The authors found that the high metastatic cells secreted three times more EVs than the low metastatic cells, and transfer of these EVs to low metastatic cells induced a migratory and invasive phenotype in those cells. Using MS, they identified 64 proteins in the

high metastatic cell-derived EVs, 31 of which were unique to these vesicles. In *in vivo* mouse experiments, they also found that high metastatic EVs preferentially colonized the lung tissue, which is the principal site of metastatic development in osteosarcoma(90). The quality of reporting their EV methodology was high, with EV-METRIC and PedEV scores of 38% and 15%, respectively.

Raimondi *et al.* performed small RNA sequencing on osteosarcoma-derived EVs and on their parental cells (Table 2) (105). The authors found a total of 21 differentially expressed miRNAs, and bioinformatic analysis revealed that these miRNAs are associated with carcinogenesis. In addition, they found that expression of miR-21-5p and miR-148a was increased in cultured osteoclast-like and endothelial cells that were treated with osteosarcoma-derived EVs, promoting osteoclast formation and angiogenesis; this finding confirmed the notion that these miRNAs are transferred from EVs to their target cells, in which they exert functional effects. The PedEV score of 82.5% and EV-METRIC score of 44% reflect the fact that the authors reported more details regarding their EV methodology than the other publications assessed in our review.

Ye *et al.* also performed small RNA sequencing on EV derived from osteosarcoma patients and healthy controls (106). They identified 10 miRNA that were upregulated in patients. They went on to perform RT-qPCR on a selection of these miRNA and compared that to EV from 3 osteosarcoma cell lines. This comparison found only miR195-3p and miR130a-3p to be upregulated in both patient and cell line-derived EV. They further analyzed the function of miR195-3p in several experiments with an osteosarcoma cell line and mice, from which they concluded that miR195-3p promotes cell proliferation and migration, and inhibits apoptosis. The investigators do not state the exact starting volume for EV isolation from plasma. They also do not report the EV isolation method from the cell lines for the functional experiments, nor if these EVs were analyzed by transmission electron microscopy and/or western blot, as was done for the EVs from plasma. Considering the clinical part of the study, a validation cohort is missing, as is a clear description of patient inclusion criteria. This results in a PedEV score of 66% and an EV-METRIC score of 11%, and a GRADE score of 7.

Cambier *et al.* analyzed repetitive DNA and RNA elements present in EVs isolated from serum from patients and healthy controls (107). In this report, different EV isolation and purification approaches were used: ExoQuick in the discovery cohort and PEG precipitation, SEC and immunoaffinity capture in different subgroups within the validation cohort. In both the discovery and validation cohort, size and concentration



of EV were analyzed by nanoparticle analysis after each EV purification method. However, the samples isolated by PEG precipitation and immunoaffinity were also analyzed by ExoView. This visualization technique depends on immunocapture of EVs to a microarray chip by different EV-enriched surface proteins (107). In the discovery cohort sequencing of RNA and DNA resulted in identification of 4 repetitive elements upregulated in serum from patients with osteosarcoma, in comparison to healthy controls. This finding was then confirmed in the validation cohort. The complex subgrouping and different techniques within the validation weakens the possibility to draw any conclusions. It demands further validation in a patient cohort analyzed with a uniform approach to EV isolation, visualization and characterization. These limitations result in a PedEV score of 55% and EV-METRIC score of 14%. Patient inclusion and exclusion is not clearly described, which precludes assessment of selection bias. The presence of a validation cohort is good, however it is not fully independent to the discovery cohort since 2 samples from the discovery cohort were also analyzed in the validation cohort. Furthermore, the validation cohort is divided in several subgroups with different techniques. This results in a GRADE score of 7.

In summary, several miRNAs were identified in several osteosarcoma studies, including miR-25-3p (102, 103) and miR-21-5p (101, 105). Interestingly, miR-675 (99), miR-148a (96, 101, 105) were found in both *in vivo* and *in vitro* studies. With respect to EV methodology, we found differences in the extent of details reported for EV characterization between the *in vitro* and *in vivo* experiments.

Rhabdomyosarcoma

Rhabdomyosarcoma is a highly malignant cancer that develops from skeletal myoblast-like cells (108). Rhabdomyosarcoma is the most common soft tissue sarcoma in children and has a slight male predominance (109). The primary tumor can arise in a variety of anatomical sites, including the head, neck, and extremities, and metastases in the lungs, bone, and/or bone marrow are quite common (110, 111). Two major histological subtypes of rhabdomyosarcoma—embryonal and alveolar—have been identified. Alveolar tumors are often associated with the recurrent chromosomal translocations t(2;13) and t(1;13), which generate fusion oncoproteins between *PAX3* and *FOXO1* and between *PAX7* and *FOXO1*, respectively (112). Although the 5-year overall survival rate is now as high as 70% due to therapeutic advances, the cure rate among patients with metastatic and/or recurrent rhabdomyosarcoma is still low (113). Our literature study identified one study that examined EVs in rhabdomyosarcoma using both *in vivo* and *in vitro* experiments and two additional *in vitro* studies; all three studies were performed by the same group.

In their first study, Ghayad *et al.* characterized the miRNA expression profiles of EVs secreted by five rhabdomyosarcoma cell lines (Table 2) (114). They found miRNAs that were differentially expressed between rhabdomyosarcoma-derived EVs and the corresponding cell lysates, and they also found differential expression between cell lines. Two miRNAs—miR-1246 and miR-1268—were enriched in the EVs of all five rhabdomyosarcoma cell lines. Rhabdomyosarcoma-derived EVs were also shown to increase the proliferation of recipient fibroblasts and rhabdomyosarcoma cells. Moreover, these EVs also induced the migration and invasion of normal fibroblasts, and they promoted angiogenesis in endothelial cells. Subsequently, Rammal *et al.* examined the protein composition of EVs derived from five rhabdomyosarcoma cell lines using liquid chromatography-MS/MS (LC-MS/MS) (Table 2) (115). They found a total of 80 proteins that were common to all five cell lines, as well as 81 that were specific to embryonal rhabdomyosarcoma cells and 42 that were specific to alveolar rhabdomyosarcoma cells. Pathway analysis revealed that these EV proteins are involved in pathways related to tumor cell invasion, proliferation, and metastasis. Thus, these proteins may serve as potential biomarkers, although this should be tested in a clinical study.

Finally, in their recent study, Ghamloush *et al.* found that expressing the PAX3-FOXO1 fusion protein in murine myoblasts modulated the miRNA content and paracrine function of their EVs, promoting the proliferation, migration, and invasion of recipient fibroblasts (Tables 1 and 2) (116). Hierarchical clustering of miRNA microarray profiling data showed that expressing the PAX3-FOXO1 fusion protein altered the EVs' miRNA content. Interestingly, miR-486-5p was identified as a downstream effector of PAX3-FOXO1 expressed in the EVs of all five rhabdomyosarcoma cell lines, albeit at higher levels in the alveolar rhabdomyosarcoma cell lines compared to the embryonal cell lines. The authors also found this miRNA in serum-derived EVs obtained from patients with rhabdomyosarcoma; in one patient with an alveolar tumor, the levels of miR-486-5p decreased after chemotherapy when the patient was in remission. Despite the relatively small patient cohort, these findings suggest that this miRNA may play a clinically relevant role in patients with rhabdomyosarcoma. A follow-up study with a larger cohort may provide additional insights into the potential use of miR-486-5p as a diagnostic biomarker and for assessing the patient's response to chemotherapy. However, this study received a GRADE score of only 5, as the patient cohort and inclusion criteria were not described in sufficient detail, and their findings were not validated in an independent cohort.

With respect to the EV methodology for the *in vitro* experiments, these three reports had good EV-METRIC scores (33%, 33%, and 38% for the first, second, and

third studies, respectively) and PedEV scores (71.5%, 66%, and 66%, respectively). However, for the *in vivo* experiments EV characterization was not performed, and—importantly—no healthy controls were included.

Overall, miR-486-5p was the only miRNA that was found to be upregulated in the rhabdomyosarcoma-derived EVs isolated from both patient serum samples and cell lines (116). However, given the low number of patients with rhabdomyosarcoma included in this study, additional fundamental work regarding characterization of the EVs is warranted before EV-derived diagnostics can be applied in clinical practice.

Ewing sarcoma

Ewing sarcoma is the second most common bone tumor, mostly presenting in adolescents (117, 118). It is characterized by the presence of a tumor-driving fusion gene, the most common one is EWSR1-FLI1, but several other combinations by members from the FET and ETS gene families have been described, e.g. EWSR1-ERG or FUS-FEV (117). Currently, risk stratification at initial diagnosis relies on imaging and molecular pathology. The first step is often FISH and/or RT-qPCR for the detection of the most common EWSR1 rearrangements (119). Prognosis depends heavily on the presence of metastatic lesions at diagnosis, which mostly presents in the lungs, bone and bone marrow (117). Treatment consists of a combination of chemotherapy, local control by surgery and radiotherapy (117, 118). Evaluation of treatment response is an important challenge, since relapse is associated with <10% 5-years survival (117). Currently, response evaluation depends on imaging. However, liquid biopsies are also gaining attention. The use of cell-free DNA has been explored in several reports (29, 30, 120) but often the level of tumor-derived cell-free DNA is low which limits sensitivity. Detection of circulating tumor cells from blood is also an option, but sensitivity is challenging, due to a high signal-to-noise ratio in peripheral blood cells and not all tumors shedding cells into circulation (34, 119). Considering the limitations of other liquid biopsy-based targets, EVs are also an interesting source of biomarkers in Ewing sarcoma. We identified 3 reports that studied EVs from Ewing sarcoma both *in vivo* and *in vitro*, and 2 that contained only *in vitro* data.

Miller et al. (121) were one of the first in 2013 to demonstrate the presence of the EWSR1 fusion gene in RNA isolated from Ewing sarcoma cell line-derived EV. They identified several other potential Ewing sarcoma-specific genes through analysis of publicly available array data and then confirmed the presence of this panel in their own EV preparations. They went one step further, using RNase experiments to show that these mRNA markers are truly present within EV. Lastly, they mixed EVs derived from Ewing sarcoma cell lines with plasma from healthy controls, and were also able

to detect these markers. On the contrary, in the plasma from 20 healthy controls without EV, these markers were not present. This study reports the EV methodology in detail, which is reflected by a good PedEV score of 77% and also EV METRIC score is quite good with 25%. No clinical samples were included.

Zhang et al. (122) present a microfluidic, chip-based approach for the quantification of tumor-specific mRNA from EV. All their experiments were performed on EVs purified from conditioned culture medium originating from Ewing sarcoma cell lines, without any *in vivo* validation. PedEV score was 60.5%, resulting from a detailed reporting on EV-enrichment and characterization, but lacking any report on the analysis of EV-derived protein. EV-METRIC score is 29%, which is quite high and is mostly caused by very detailed reporting on the qualitative and quantitative analysis, and the ultracentrifugation specifics.

Dong et al. (123) present a new technique for purifying EVs from plasma from patients with Ewing sarcoma. In their report, they describe in detail the development, optimization and validation of the 'ES-EV Click Chip', first in conditioned culture medium from Ewing sarcoma cell lines. The ES-EV Click Chip combines click chemistry-mediated EV capture within a nanostructure-embedded microchip, which depends on the presence of the protein LINGO1 on Ewing sarcoma-derived EVs. LINGO1 is presented as a Ewing sarcoma-specific marker by the authors. The presence of tumor-specific EVs is then confirmed by RT-ddPCR targeted to the EWSR1 rearrangement. Dong *et al.* compared this novel ES-EV Click Chip technique to more conventional EV purification approaches, e.g. differential centrifugation, immunocapture and Exoquick. The focus is clearly on the development and optimization of this new technique and the small number of plasma samples included at the end just serves as a small validation. There are no details reported on pre-analytical variables for the plasma samples, such as type of blood tube. Patient characteristics and timing of sampling are also not reported. This results in a low GRADE score of 5. PedEV is more average (55%) since the *in vitro* details are well described, however conventional EV characterization techniques are not reported (or not detailed enough) which leads to an EV-METRIC score of 0%.

Samuel *et al.* (124) also report on a new approach to isolating Ewing sarcoma-specific EVs. They started by performing proteomics on EVs isolated from different Ewing sarcoma cell lines. By comparing these data to proteomics data from healthy human plasma, they identified Ewing sarcoma-specific markers CD99 and NGFR. The next step was to develop an immunocapture approach combining CD99 and NGFR and thereby purifying tumor-specific EVs. They confirmed the presence of Ewing sarcoma-

specific mRNA by performing RT-qPCR for the EWSR1 fusions. Finally, they performed this Ewing-EV-specific immunocapture on plasma of a small cohort of patients and compared this to healthy controls. It is an impressive effort, however especially the details on the clinical samples (type of blood tube, preparation of plasma) are not reported, as are some details of the Western Blot procedures, resulting in an EV METRIC score of 0% for the *in vivo* and 11% for the *in vitro* part. Within PedEV, *in vivo* and *in vitro* are taken together, which results in a score of 60.5%. Considering the clinical part of the study, patient details are not reported in detail and there is no independent validation cohort, resulting in a GRADE score of 7.

Sun *et al.* (125) also developed a click chemistry-based approach for the purification of EV. They first optimized this approach in conditioned medium from an Ewing sarcoma cell line, and then validated its *in vivo* potential in plasma from Ewing sarcoma patients and even patients with pancreatic cancer, coupled to a cohort of healthy controls. To confirm that the EVs from patient plasma are originating from the tumor, RT-dPCR is performed for the EWSR1-FLI1 fusion gene. For 2 patients, sequential samples were also tested and the number of EWSR1-FLI1 copies tracks the course of the disease, as is determined by clinical imaging. This is an interesting finding, suggesting a true potential as a minimal residual disease marker for these EVs isolated with click chemistry. Concerning the GRADE score, this report has an average score (8), with one of the most important limitations being a lack of a validation cohort. The reporting of the methodology behind the report is also sound, only characterization of the EV-related proteins is lacking. This is reflected in a PedEV score of 60.5%. However, EV METRIC score for both *in vivo* and *in vitro* experiments is 0%, since the level of details of the EV enrichment and characterization techniques is not sufficient for EV-TRACK.

Overview of the miRNAs identified in EVs derived from pediatric solid tumors, and the role of the miRNAs in the hallmarks of cancer

The majority of studies included in our systematic review involved an analysis of miRNA, and nearly all studies reported their putative biological function. This allowed us to provide an overview of the reported miRNAs (both from *in vivo* and *in vitro* studies) in relation to the hallmarks of cancer. In Figure 4A, we summarize the miRNAs involved in the “classic” hallmarks of cancer described by Hanahan and Weinberg first in 2000 (126) and again in 2011 (127), and we included an emerging cancer trait: drug resistance (19). In addition, changes in several miRNAs were found in different tumor entities, as illustrated in Figure 4B. For example, miR-21—which is known to play a role in metastasis and tumor progression(128)—was upregulated in neuroblastoma (87, 88), hepatoblastoma (75) and osteosarcoma (101, 105). Consistent

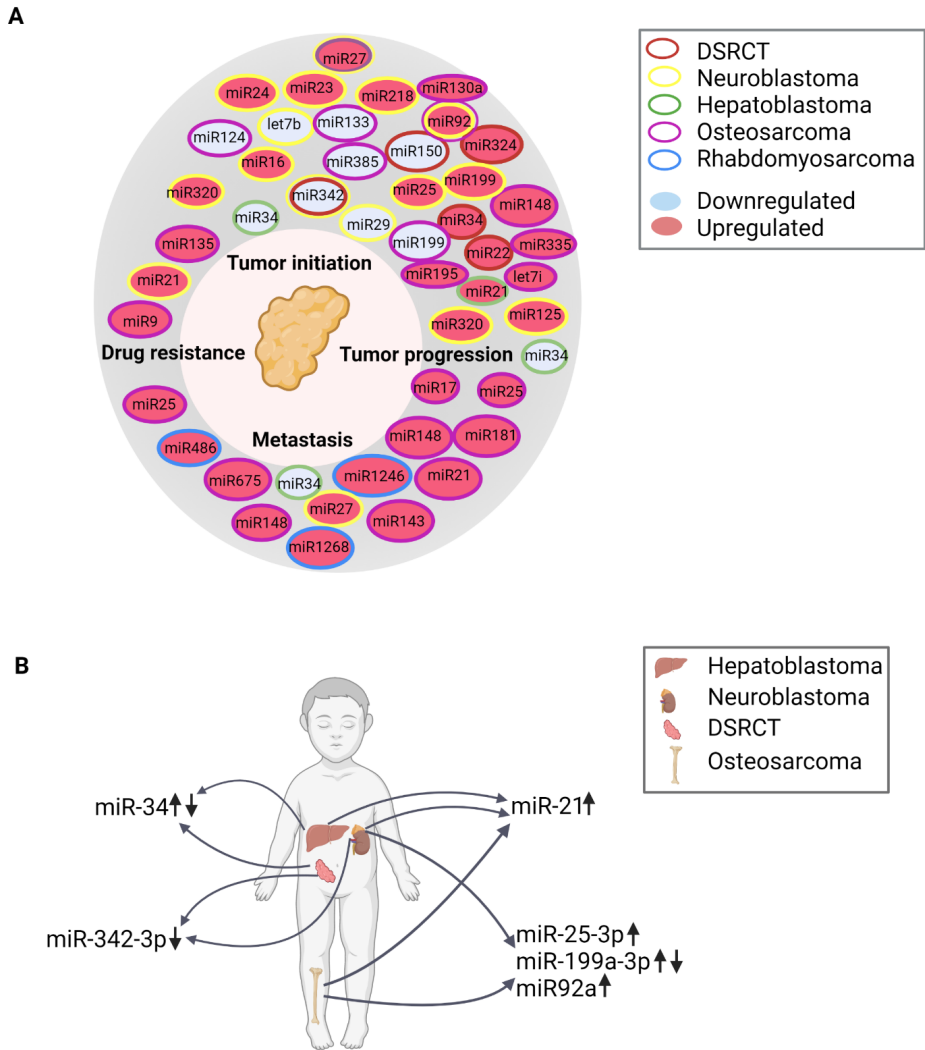


Figure 4. A. Overview of the hallmarks of cancer and the differentially regulated miRNAs described in the various in vitro and in vivo reports, classified according to their function. DSRCT, desmoplastic small round cell tumor **B.** Differentially regulated miRNAs in the indicated solid tumors (hepatoblastoma, neuroblastoma, DSRCT, and osteosarcoma) based on the in vivo and in vitro publications (↑, upregulated; ↓, downregulated). References for miR-21: (75, 87, 88, 101, 105); for miR-25-3p: (88, 102, 103); for miR199a-3p: (85, 96); for miR-34: (70, 77); for miR92a: (88, 106) and for miR-342-3p: (70, 86).

with this finding, miR-21 has been shown to be overexpressed in many types of solid tumors (129). In addition, miR-25-3p was upregulated in both neuroblastoma (88) and osteosarcoma (102, 103). This miRNA was shown previously to play a role in these two tumor types (130, 131), as well as in other types of cancer, particularly with respect to tumor initiation and progression (132); miR-25-3p has also been reported as a potential biomarker for breast cancer and hepatocarcinoma (133, 134). miR-34a-5p was upregulated in DSRCT (70), while miR-34 miRNAs were downregulated in hepatoblastoma (77). The miR-34 family members play an important role in tumor suppression and are dysregulated in several cancers (135-137). miR-199a-3p was upregulated in neuroblastoma (85) but downregulated in osteosarcoma (96); this miRNA is known to exert opposite effects in different tumors (138), acting as a promoter of leukemic transformation (139) and as a tumor-suppressor gene in both renal cancer (140) and esophageal cancer (141). Finally, miR-342-3p was downregulated in both neuroblastoma (86) and DSRCT (70); this miRNA has been shown to suppress cell proliferation and migration in several types of cancer (142-144).

Summary and future directions

EVs have high potential as diagnostic and prognostic biomarkers for both adult and pediatric cancers (145, 146). However, major discrepancies exist between the number of novel EV-based biomarkers that are reported and the biomarkers that have been successfully incorporated into daily clinical practice, and many obstacles must still be overcome along the road to developing and implementing these biomarkers (147).

Peripheral blood is a suitable source of EVs, as it can be obtained by minimally invasive sampling methods and contains high levels of tumor-derived EVs (148, 149). However, challenges have arisen with respect to the isolation, purification, and analysis of blood-derived EVs. For example, pre-analytical factors such as the type of collection tubes and the conditions used to store the samples can affect several EV characteristics, ranging from the final EV concentration to the origin of the EVs (e.g., platelet-derived versus tumor-derived) (150-154). The method used to enrich EVs from the blood can also affect the subsequent RNA (44, 155, 156) and protein (157, 158) analyses, thereby affecting the final result. Moreover, the complex composition of blood—including non-EV-bound proteins and lipoprotein particles—can complicate the identification of bona fide EV-derived molecules and can potentially hinder the discovery and validation of these biomarkers (159-162). This issue is illustrated by two recent reports by Palviainen *et al.* (154) and Chiam *et al.* (163). In their study, Palviainen *et al.* found that serum contains more platelet-derived EVs compared to plasma; moreover, they found that the protein composition differs

between plasma and serum, as well as between samples obtained using different anticoagulants(154). Chiam *et al.* examined miRNAs in EVs purified from serum and plasma samples obtained from patients with esophageal carcinoma and found that although the plasma contained more miRNA than serum, the plasma also contained more non-EV-derived miRNA (163). With respect to pediatric solid tumors, the clinical studies that we identified from our literature search evaluated EVs that were derived from either serum or plasma; however, detailed descriptions of the pre-analytical factors and the starting sample volumes were often absent, for example in studies involving hepatoblastoma (75, 77) and osteosarcoma (99, 164, 165). Moreover, a wide range of methods were used for enriching and characterizing the EVs, in some cases even within the same publication (85, 97). These missing details limit the studies' reproducibility and our ability to correctly interpret the resulting data, thereby preventing subsequent validation in a clinical setting.

Our search of the literature for *in vitro* studies assessing EV-derived biomarkers in pediatric solid tumors yielded >3000 hits. However, when focusing on clinical studies that described EVs derived from liquid biopsies from children with solid tumors, and when we evaluated whether these *in vivo* findings were supported using *in vitro* data, we found only the 27 reports that we discussed in this review. It is interesting that we did not find many reports studying the use of microfluidics or nanostructure-based approaches, apart from the two reports in Ewing sarcoma (122, 123), even though in theory these approaches would be suited for low input samples and point-of-care use. Also, more novel particle characterization platforms like Raman scattering (166, 167) were not used in the reports that we found. However, these techniques are often still in early development phases, and pre-clinical testing, which is challenging considering the limited sample number and volumes available in pediatric oncology.

The majority of studies included in this review, were *in vitro* and focused on EVs secreted from cultured cancer cell lines, whereas validation of these biomarkers in physiologically relevant biofluids was often not performed. With respect to the *in vivo* studies, important details regarding the enrichment and characterization platforms of EVs were often not reported, as reflected by the relatively low PedEV scores for these studies. Moreover, many studies did not report using—and therefore may not have used—a density gradient for EV enrichment and/or purification, and they did not report in details on EV characterization, thus resulting in low EV-METRIC scores. Overall, many studies yielded relatively higher scores from PedEV than from EV-TRACK. This is probably caused by the rigorous EV-TRACK scoring system, with points allocated for reporting on specific techniques, e.g. density gradient and details on both qualitative and quantitative analysis. As mentioned before, pediatric studies on



patient samples are limited by sample volumes which results in a limitation in the number of techniques that can be performed. The PedEV score requires no specific techniques to be performed and allocates scores for more generally defined criteria (e.g. at least one method for particle characterization not further specified). This also increases the PedEV scores for studies using less conventional EV enrichment approaches, e.g. click chemistry-based approaches. Furthermore, PedEV allocates a general score for the entire report, creating the possibility for a report with less detailed reporting on *in vivo* experiments but with a very detailed report of *in vitro* experiments to still receive a good score. In this respect, it is important to emphasize that EV-TRACK was developed as a general tool for scoring the reproducibility and reporting of EV research and is based on studies using conditioned culture medium or biofluids collected from adults. Given that pediatric studies are far more limited with respect to patient numbers and the volume of biofluids, the extent of EV characterization is limited, as is the inclusion of healthy controls, particularly age-matched controls. Another consideration is that because the field of EV research in pediatric oncology is relatively new and often limited to pediatric oncology centers, EV-specific knowledge and equipment are not yet widely available. Thus, our PedEV score may provide a more lenient and flexible scoring system for EV characterization, at least until the pediatric research community reaches the level of standards that are only now emerging in adult studies involving EVs. Indeed, the EV field is not the first to experience a gap in the quality of study designs between pediatric and adult research (168). Closing this gap will require collaboration beyond the borders of the respective centers and countries, as well as collaboration between scientists in the fields of pediatrics and adult medicine.

Altered regulation of miRNAs has been associated with the initiation and progression of cancer (169). Moreover, the potential of miRNAs was previously demonstrated in adults, with several ongoing clinical trials investigating the potential of using EV-derived miRNAs as diagnostic, predictive, and/or prognostic biomarkers (170). In the studies we evaluated in this review, the same miRNAs were upregulated both *in vivo* and *in vitro* in neuroblastoma(85), osteosarcoma (99), and rhabdomyosarcoma (96, 99, 101, 105). This finding suggests that *in vitro* screening of candidate biomarkers can be highly valuable before moving to *in vivo* validation. However, it is important to note that most of these biomarkers were identified within the same study and/or by the same group. In addition, a study using alveolar rhabdomyosarcoma cell lines suggests that gene expression can differ between *in vitro* conditions and the primary tumor (171). This finding calls into question the value of *in vitro* validation studies, as they may not fully recapitulate the clinical situation. Nevertheless, if *in vitro* studies are performed, we recommend using the same techniques that were used in the

corresponding clinical studies, thus reducing technical variations and improving the resulting conclusions. An even better strategy would be to validate the *in vivo* findings in an independent cohort, thus strengthening the claim of identifying a promising new biomarker.

The finding that the same miRNAs are differentially regulated in different tumor types suggests that a panel of miRNAs may be more suitable than any given miRNA as a general pediatric oncology marker, as it may span the entire spectrum of pediatric solid tumors. Studying the changes in this miRNA panel throughout the course of the disease may even lead to the use of miRNAs as a marker of minimal residual disease, as shown previously in adults with Hodgkin lymphoma (4).

To conclude, EVs remain a promising diagnostic biomarker for use in pediatric solid tumors. However, for many tumor types the methodical research—and in particular, *in vivo* validation—is currently lacking. Thus, studies using standardized methods and clear reporting of each step in the enrichment and analysis of EVs derived from liquid biopsies are urgently needed in the field of pediatric oncology. Such studies will likely accelerate both the validation of EV-based techniques and the translation of these biomarkers from the bench to the bedside.

References

1. van Niel G, D'Angelo G, Raposo G. Shedding light on the cell biology of extracellular vesicles. *Nat Rev Mol Cell Biol.* 2018;19(4):213-28.
2. Bebelman MP, Smit MJ, Pegtel DM, Baglio SR. Biogenesis and function of extracellular vesicles in cancer. *Pharmacol Ther.* 2018;188:1-11.
3. Becker A, Thakur BK, Weiss JM, Kim HS, Peinado H, Lyden D. Extracellular Vesicles in Cancer: Cell-to-Cell Mediators of Metastasis. *Cancer Cell.* 2016;30(6):836-48.
4. van Eijndhoven MA, Zijlstra JM, Groenewegen NJ, Drees EE, van Niele S, Baglio SR, et al. Plasma vesicle miRNAs for therapy response monitoring in Hodgkin lymphoma patients. *JCI Insight.* 2016;1(19):e89631.
5. Merchant ML, Rood IM, Deegens JKJ, Klein JB. Isolation and characterization of urinary extracellular vesicles: implications for biomarker discovery. *Nat Rev Nephrol.* 2017;13(12):731-49.
6. Raposo G, Stoorvogel W. Extracellular vesicles: exosomes, microvesicles, and friends. *Journal of Cell Biology.* 2013;200(4):373-83.
7. Willms E, Cabañas C, Mäger I, Wood MJA, Vader P. Extracellular Vesicle Heterogeneity: Subpopulations, Isolation Techniques, and Diverse Functions in Cancer Progression. *Frontiers in immunology.* 2018;9:738-.
8. Yuana Y, Sturk A, Nieuwland R. Extracellular vesicles in physiological and pathological conditions. *Blood Reviews.* 2013;27(1):31-9.
9. Zaborowski MP, Balaj L, Breakefield XO, Lai CP. Extracellular Vesicles: Composition, Biological Relevance, and Methods of Study. *BioScience.* 2015;65(8):783-97.
10. Simeone P, Bologna G, Lanuti P, Pierdomenico L, Guagnano MT, Pieragostino D, et al. Extracellular Vesicles as Signaling Mediators and Disease Biomarkers across Biological Barriers. *International journal of molecular sciences.* 2020;21(7):2514.
11. Caby MP, Lankar D, Vincendeau-Scherrer C, Raposo G, Bonnerot C. Exosomal-like vesicles are present in human blood plasma. *Int Immunol.* 2005;17(7):879-87.
12. Berckmans RJ, Lacroix R, Hau CM, Sturk A, Nieuwland R. Extracellular vesicles and coagulation in blood from healthy humans revisited. *J Extracell Vesicles.* 2019;8(1):1688936.
13. Akers J, Ramakrishnan V, Kim R, Phillips S, Kaimal V, Mao Y, et al. miRNA contents of cerebrospinal fluid extracellular vesicles in glioblastoma patients. *Journal of neuro-oncology.* 2015;123.
14. Gonzales PA, Zhou H, Pisitkun T, Wang NS, Star RA, Knepper MA, et al. Isolation and purification of exosomes in urine. *Methods Mol Biol.* 2010;641:89-99.
15. Zonneveld MI, Brisson AR, van Herwijnen MJC, Tan S, van de Lest CHA, Redegeld FA, et al. Recovery of extracellular vesicles from human breast milk is influenced by sample collection and vesicle isolation procedures. *Journal of extracellular vesicles.* 2014;3:10.3402/jev.v3.24215.
16. Weiser DA, West-Szymanski DC, Frait E, Weiner S, Rivas MA, Zhao CWT, et al. Progress toward liquid biopsies in pediatric solid tumors. *Cancer and Metastasis Reviews.* 2019;38(4):553-71.
17. Nakata R, Shimada H, Fernandez GE, Fanter R, Fabbri M, Malvar J, et al. Contribution of neuroblastoma-derived exosomes to the production of pro-tumorigenic signals by bone marrow mesenchymal stromal cells. *J Extracell Vesicles.* 2017;6(1):1332941.
18. Tamura T, Yoshioka Y, Sakamoto S, Ichikawa T, Ochiya T. Extracellular Vesicles in Bone Metastasis: Key Players in the Tumor Microenvironment and Promising Therapeutic Targets. *Int J Mol Sci.* 2020;21(18).

19. Xavier CP, Caires HR, Barbosa MA, Bergantim R, Guimarães JE, Vasconcelos MH. The Role of Extracellular Vesicles in the Hallmarks of Cancer and Drug Resistance. *Cells*. 2020;9(5):1141.
20. Namee NM, O'Driscoll L. Extracellular vesicles and anti-cancer drug resistance. *Biochim Biophys Acta Rev Cancer*. 2018;1870(2):123-36.
21. Nanou A, Coumans FAW, van Dalum G, Zeune LL, Dolling D, Onstenk W, et al. Circulating tumor cells, tumor-derived extracellular vesicles and plasma cytokeratins in castration-resistant prostate cancer patients. *Oncotarget*. 2018;9(27):19283-93.
22. Nanou A, Miller MC, Zeune LL, de Wit S, Punt CJA, Groen HJM, et al. Tumour-derived extracellular vesicles in blood of metastatic cancer patients associate with overall survival. *Br J Cancer*. 2020;122(6):801-11.
23. Kosaka N, Kogure A, Yamamoto T, Urabe F, Usuba W, Prieto-Vila M, et al. Exploiting the message from cancer: the diagnostic value of extracellular vesicles for clinical applications. *Experimental & molecular medicine*. 2019;51(3):1-9.
24. Van Paemel R, Vlug R, De Preter K, Van Roy N, Speleman F, Willems L, et al. The pitfalls and promise of liquid biopsies for diagnosing and treating solid tumors in children: a review. *Eur J Pediatr*. 2020;179(2):191-202.
25. van Zogchel LMJ, Lak NSM, Verhagen OJHM, Tissoudali A, Gusmalla Nuru M, Gelineau NU, et al. Novel Circulating Hypermethylated RASSF1A ddPCR for liquid biopsies in patients with pediatric solid tumors. *JCO Precis Oncol*. 2021;5:1738-48.
26. van Zogchel LMJ, van Wezel EM, van Wijk J, Stutterheim J, Bruins WSC, Zappeij-Kannegieter L, et al. Hypermethylated RASSF1A as circulating tumor DNA marker for disease monitoring in neuroblastoma. *J clin Oncol Precision Oncology*. 2020.
27. Lodrini M, Graef J, Thole-Kliesch TM, Astrahantseff K, Sprussel A, Grimaldi M, et al. Targeted analysis of cell-free circulating tumor DNA is suitable for early relapse and actionable target detection in patients with neuroblastoma. *Clin Cancer Res*. 2022.
28. Lodrini M, Sprussel A, Astrahantseff K, Tiburtius D, Konschak R, Lode HN, et al. Using droplet digital PCR to analyze MYCN and ALK copy number in plasma from patients with neuroblastoma. *Oncotarget*. 2017;8(49):85234-51.
29. Van Paemel R, Vandeputte C, Raman L, Van Thorre J, Willems L, Van Dorpe J, et al. The feasibility of using liquid biopsies as a complementary assay for copy number aberration profiling in routinely collected paediatric cancer patient samples. *Eur J Cancer*. 2021.
30. Klega K, Imamovic-Tuco A, Ha G, Clapp AN, Meyer S, Ward A, et al. Detection of Somatic Structural Variants Enables Quantification and Characterization of Circulating Tumor DNA in Children With Solid Tumors. *JCO Precis Oncol*. 2018;2018.
31. Lak NSM, Voormans TL, Zappeij-Kannegieter L, van Zogchel LMJ, Fiocco M, van Noesel MM, et al. Improving Risk Stratification for Pediatric Patients with Rhabdomyosarcoma by Molecular Detection of Disseminated Disease. *Clin Cancer Res*. 2021.
32. Stutterheim J, Gerritsen A, Zappeij-Kannegieter L, Kleijn I, Dee R, Hooft L, et al. PHOX2B is a novel and specific marker for minimal residual disease testing in neuroblastoma. *J Clin Oncol*. 2008;26(33):5443-9.
33. Stutterheim J, Gerritsen A, Zappeij-Kannegieter L, Yalcin B, Dee R, van Noesel MM, et al. Detecting minimal residual disease in neuroblastoma: the superiority of a panel of real-time quantitative PCR markers. *Clin Chem*. 2009;55(7):1316-26.
34. Tellez-Gabriel M, Brown HK, Young R, Heymann MF, Heymann D. The Challenges of Detecting Circulating Tumor Cells in Sarcoma. *Front Oncol*. 2016;6:202.

35. Chicard M, Colmet-Daage L, Clement N, Danzon A, Bohec M, Bernard V, et al. Whole-Exome Sequencing of Cell-Free DNA Reveals Temporo-spatial Heterogeneity and Identifies Treatment-Resistant Clones in Neuroblastoma. *Clin Cancer Res*. 2018;24(4):939-49.
36. Eleveld TF, Oldridge DA, Bernard V, Koster J, Colmet Daage L, Diskin SJ, et al. Relapsed neuroblastomas show frequent RAS-MAPK pathway mutations. *Nat Genet*. 2015;47(8):864-71.
37. Van Wezel EM, Van Zogchel LMJ, Van Wijk J, Timmerman I, Vo N, Zappeij-Kannegieter L, et al. Mesenchymal neuroblastoma cells are undetected by current mRNA marker panels: the development of a specific neuroblastoma mesenchymal minimal residual disease panel. *J Clin Oncol Precision Oncology*. 2019.
38. Cui M, Wang H, Yao X, Zhang D, Xie Y, Cui R, et al. Circulating MicroRNAs in Cancer: Potential and Challenge. *Front Genet*. 2019;10:626.
39. Mussbacher M, Pirabe A, Brunnthaler L, Schrottmaier WC, Assinger A. Horizontal MicroRNA Transfer by Platelets - Evidence and Implications. *Front Physiol*. 2021;12:678362.
40. Coumans FAW, Brisson AR, Buzas EI, Dignat-George F, Drees EEE, El-Andaloussi S, et al. Methodological Guidelines to Study Extracellular Vesicles. *Circ Res*. 2017;120(10):1632-48.
41. Shirejini SZ, Inci F. The Yin and Yang of exosome isolation methods: conventional practice, microfluidics, and commercial kits. *Biotechnol Adv*. 2022;54:107814.
42. Abreu CM, Costa-Silva B, Reis RL, Kundu SC, Caballero D. Microfluidic platforms for extracellular vesicle isolation, analysis and therapy in cancer. *Lab Chip*. 2022;22(6):1093-125.
43. Singh PK, Patel A, Kaffenes A, Hord C, Kesterson D, Prakash S. Microfluidic Approaches and Methods Enabling Extracellular Vesicle Isolation for Cancer Diagnostics. *Micromachines (Basel)*. 2022;13(1).
44. Van Deun J, Mestdagh P, Sormunen R, Cocquyt V, Vermaelen K, Vandesompele J, et al. The impact of disparate isolation methods for extracellular vesicles on downstream RNA profiling. *J Extracell Vesicles*. 2014;3.
45. Vergauwen G, Dhondt B, Van Deun J, De Smedt E, Berx G, Timmerman E, et al. Confounding factors of ultrafiltration and protein analysis in extracellular vesicle research. *Sci Rep*. 2017;7(1):2704.
46. Arkesteijn GJ, Lozano-Andrés E, Libregts SF, Wauben MHM. Improved flow cytometric light scatter detection of submicron-sized particles by reduction of optical backgrounds signals. *Cytometry A*. 2020.
47. Welsh JA, Van Der Pol E, Arkesteijn GJA, Bremer M, Brisson A, Coumans F, et al. MIFlowCyt-EV: a framework for standardized reporting of extracellular vesicle flow cytometry experiments. *J Extracell Vesicles*. 2020;9(1):1713526.
48. Lotvall J, Hill AF, Hochberg F, Buzas EI, Di Vizio D, Gardiner C, et al. Minimal experimental requirements for definition of extracellular vesicles and their functions: a position statement from the International Society for Extracellular Vesicles. *J Extracell Vesicles*. 2014;3:26913.
49. Théry C, Witwer KW, Aikawa E, Alcaraz MJ, Anderson JD, Andriantsitohaina R, et al. Minimal information for studies of extracellular vesicles 2018 (MISEV2018): a position statement of the International Society for Extracellular Vesicles and update of the MISEV2014 guidelines. *Journal of extracellular vesicles*. 2018;7(1):1535750.
50. Consortium E-T, Van Deun J, Mestdagh P, Agostinis P, Akay O, Anand S, et al. EV-TRACK: transparent reporting and centralizing knowledge in extracellular vesicle research. *Nat Methods*. 2017;14(3):228-32.
51. Van Deun J, Hendrix A, consortium E-T. Is your article EV-TRACKed? *J Extracell Vesicles*. 2017;6(1):1379835.
52. Peng J, Wang W, Hua S, Liu L. Roles of Extracellular Vesicles in Metastatic Breast Cancer. *Breast Cancer (Auckl)*. 2018;12:1178223418767666.

53. Linxweiler J, Junker K. Extracellular vesicles in urological malignancies: an update. *Nature Reviews Urology*. 2019;1-17.
54. Tang MK, Wong AS. Exosomes: Emerging biomarkers and targets for ovarian cancer. *Cancer letters*. 2015;367(1):26-33.
55. Skog J, Wurdinger T, van Rijn S, Meijer DH, Gainche L, Sena-Esteves M, et al. Glioblastoma microvesicles transport RNA and proteins that promote tumour growth and provide diagnostic biomarkers. *Nat Cell Biol*. 2008;10(12):1470-6.
56. Kadota T, Yoshioka Y, Fujita Y, Kuwano K, Ochiya T, editors. *Extracellular vesicles in lung cancer—From bench to bedside. Seminars in cell & developmental biology*; 2017: Elsevier.
57. Lee RS, Stewart C, Carter SL, Ambrogio L, Cibulskis K, Sougnez C, et al. A remarkably simple genome underlies highly malignant pediatric rhabdoid cancers. *J Clin Invest*. 2012;122(8):2983-8.
58. Crompton BD, Stewart C, Taylor-Weiner A, Alexe G, Kurek KC, Calicchio ML, et al. The genomic landscape of pediatric Ewing sarcoma. *Cancer Discov*. 2014;4(11):1326-41.
59. Pugh TJ, Morozova O, Attiyeh EF, Asgharzadeh S, Wei JS, Auclair D, et al. The genetic landscape of high-risk neuroblastoma. *Nat Genet*. 2013;45(3):279-84.
60. Ma X, Liu Y, Liu Y, Alexandrov LB, Edmonson MN, Gawad C, et al. Pan-cancer genome and transcriptome analyses of 1,699 paediatric leukaemias and solid tumours. *Nature*. 2018;555(7696):371-6.
61. Gröbner SN, Worst BC, Weischenfeldt J, Buchhalter I, Kleinheinz K, Rudneva VA, et al. The landscape of genomic alterations across childhood cancers. *Nature*. 2018;555(7696):321-7.
62. Guyatt GH, Oxman AD, Vist GE, Kunz R, Falck-Ytter Y, Alonso-Coello P, et al. GRADE: an emerging consensus on rating quality of evidence and strength of recommendations. *BMJ*. 2008;336(7650):924-6.
63. <https://www.gradeworkinggroup.org/>. GRADE working group.
64. Thomas R, Rajeswaran G, Thway K, Benson C, Shahabuddin K, Moskvic E. Desmoplastic small round cell tumour: the radiological, pathological and clinical features. *Insights Imaging*. 2013;4(1):111-8.
65. Gerald WL, Ladanyi M, de Alava E, Cuatrecasas M, Kushner BH, LaQuaglia MP, et al. Clinical, pathologic, and molecular spectrum of tumors associated with t(11; 22)(p13; q12): desmoplastic small round-cell tumor and its variants. *Journal of Clinical Oncology*. 1998;16(9):3028-36.
66. Gerald WL, Haber DA. The EWS-WT1 gene fusion in desmoplastic small round cell tumor. *Semin Cancer Biol*. 2005;15(3):197-205.
67. Gedminas JM, Chasse MH, McBairty M, Beddows I, Kitchen-Goosen SM, Grohar PJ. Desmoplastic small round cell tumor is dependent on the EWS-WT1 transcription factor. *Oncogenesis*. 2020;9(4):41.
68. Lal DR, Su WT, Wolden SL, Loh KC, Modak S, La Quaglia MP. Results of multimodal treatment for desmoplastic small round cell tumors. *J Pediatr Surg*. 2005;40(1):251-5.
69. Bent MA, Padilla BE, Goldsby RE, DuBois SG. Clinical Characteristics and Outcomes of Pediatric Patients with Desmoplastic Small Round Cell Tumor. *Rare Tumors*. 2016;8(1):6145.
70. Colletti M, Paolini A, Galardi A, Di Paolo V, Pascucci L, Russo I, et al. Expression profiles of exosomal miRNAs isolated from plasma of patients with desmoplastic small round cell tumor. *Epigenomics*. 2019;11(5):489-500.
71. Aronson DC, Meyers RL. Malignant tumors of the liver in children. *Semin Pediatr Surg*. 2016;25(5):265-75.
72. Sumazin P, Chen Y, Treviño LR, Sarabia SF, Hampton OA, Patel K, et al. Genomic analysis of hepatoblastoma identifies distinct molecular and prognostic subgroups. *Hepatology*. 2017;65(1):104-21.

73. Czauderna P, Lopez-Terrada D, Hiyama E, Häberle B, Malogolowkin MH, Meyers RL. Hepatoblastoma state of the art: pathology, genetics, risk stratification, and chemotherapy. *Current Opinion in Pediatrics*. 2014;26(1):19-28.
74. Horton JD, Lee S, Brown SR, Bader J, Meier DE. Survival trends in children with hepatoblastoma. *Pediatric surgery international*. 2009;25(5):407.
75. Liu W, Chen S, Liu B. Diagnostic and prognostic values of serum exosomal microRNA-21 in children with hepatoblastoma: a Chinese population-based study. *Pediatr Surg Int*. 2016;32(11):1059-65.
76. Meyers RL, Maibach R, Hiyama E, Haberle B, Krailo M, Rangaswami A, et al. Risk-stratified staging in paediatric hepatoblastoma: a unified analysis from the Children's Hepatic tumors International Collaboration. *Lancet Oncol*. 2017;18(1):122-31.
77. Jiao C, Jiao X, Zhu A, Ge J, Xu X. Exosomal miR-34s panel as potential novel diagnostic and prognostic biomarker in patients with hepatoblastoma. *J Pediatr Surg*. 2017;52(4):618-24.
78. Matthay KK, Maris JM, Schleiermacher G, Nakagawara A, Mackall CL, Diller L, et al. Neuroblastoma. *Nat Rev Dis Primers*. 2016;2:16078.
79. Louis CU, Shohet JM. Neuroblastoma: molecular pathogenesis and therapy. *Annual review of medicine*. 2015;66:49-63.
80. Ahmed AA, Zhang L, Reddivalla N, Hetherington M. Neuroblastoma in children: Update on clinicopathologic and genetic prognostic factors. *Pediatr Hematol Oncol*. 2017;34(3):165-85.
81. Mossé YP, Laudenslager M, Longo L, Cole KA, Wood A, Attiyeh EF, et al. Identification of ALK as a major familial neuroblastoma predisposition gene. *Nature*. 2008;455(7215):930-5.
82. Trochet D, Bourdeaut F, Janoueix-Lerosey I, Deville A, de Pontual L, Schleiermacher G, et al. Germline mutations of the paired-like homeobox 2B (PHOX2B) gene in neuroblastoma. *Am J Hum Genet*. 2004;74(4):761-4.
83. Deyell RJ, Attiyeh EF. Advances in the understanding of constitutional and somatic genomic alterations in neuroblastoma. *Cancer Genet*. 2011;204(3):113-21.
84. Schleiermacher G, Janoueix-Lerosey I, Ribeiro A, Klijanienko J, Couturier J, Pierron G, et al. Accumulation of segmental alterations determines progression in neuroblastoma. *J Clin Oncol*. 2010;28(19):3122-30.
85. Ma J, Xu M, Yin M, Hong J, Chen H, Gao Y, et al. Exosomal hsa-miR199a-3p Promotes Proliferation and Migration in Neuroblastoma. *Front Oncol*. 2019;9:459.
86. Morini M, Cangelosi D, Segalera D, Marimpietri D, Raggi F, Castellano A, et al. Exosomal microRNAs from Longitudinal Liquid Biopsies for the Prediction of Response to Induction Chemotherapy in High-Risk Neuroblastoma Patients: A Proof of Concept SIOPEX Study. *Cancers (Basel)*. 2019;11(10).
87. Challagundla KB, Wise PM, Neviani P, Chava H, Murtadha M, Xu T, et al. Exosome-mediated transfer of microRNAs within the tumor microenvironment and neuroblastoma resistance to chemotherapy. *J Natl Cancer Inst*. 2015;107(7).
88. Haug BH, Hald OH, Utnes P, Roth SA, Lokke C, Flaegstad T, et al. Exosome-like Extracellular Vesicles from MYCN-amplified Neuroblastoma Cells Contain Oncogenic miRNAs. *Anticancer Res*. 2015;35(5):2521-30.
89. Mirabello L, Troisi RJ, Savage SA. Osteosarcoma incidence and survival rates from 1973 to 2004: data from the Surveillance, Epidemiology, and End Results Program. *Cancer: Interdisciplinary International Journal of the American Cancer Society*. 2009;115(7):1531-43.
90. Geller DS, Gorlick R. Osteosarcoma: a review of diagnosis, management, and treatment strategies. *Clin Adv Hematol Oncol*. 2010;8(10):705-18.
91. Luetke A, Meyers PA, Lewis I, Juergens H. Osteosarcoma treatment—where do we stand? A state of the art review. *Cancer treatment reviews*. 2014;40(4):523-32.

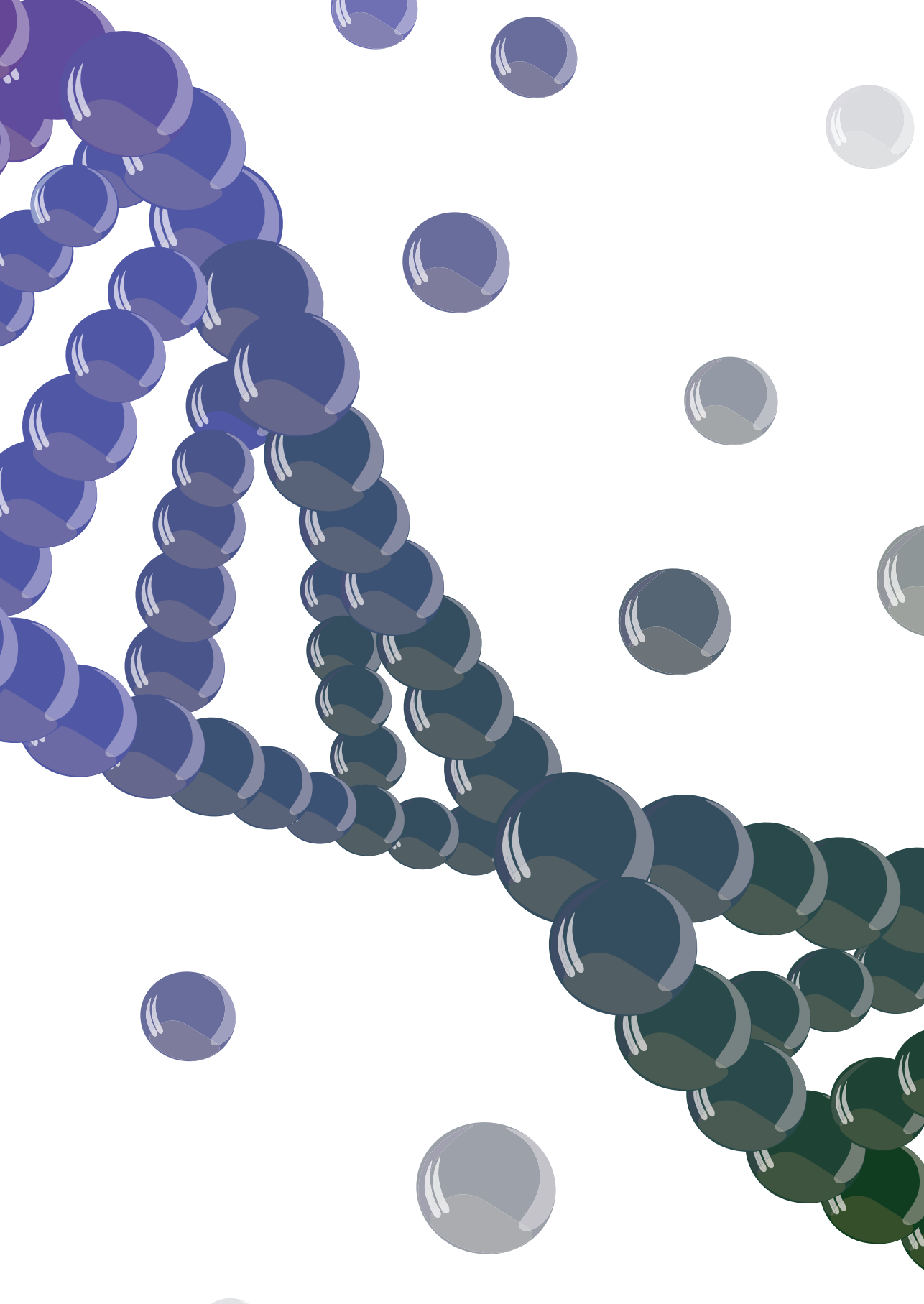
92. Klein MJ, Siegal GP. Osteosarcoma: anatomic and histologic variants. *American journal of clinical pathology*. 2006;125(4):555-81.
93. Martin JW, Squire JA, Zielenska M. The genetics of osteosarcoma. *Sarcoma*. 2012;2012:627254-.
94. Chen X, Bahrami A, Pappo A, Easton J, Dalton J, Hedlund E, et al. Recurrent somatic structural variations contribute to tumorigenesis in pediatric osteosarcoma. *Cell Rep*. 2014;7(1):104-12.
95. Simpson E, Brown HL. Understanding osteosarcomas. *Journal of the American Academy of PAs*. 2018;31(8):15-9.
96. Xu J-F, Wang Y-P, Zhang S-J, Chen Y, Gu H-F, Dou X-F, et al. Exosomes containing differential expression of microRNA and mRNA in osteosarcoma that can predict response to chemotherapy. *Oncotarget*. 2017;8(44):75968-78.
97. Baglio SR, Lagerweij T, Perez-Lanzon M, Ho XD, Leveille N, Melo SA, et al. Blocking Tumor-Educated MSC Paracrine Activity Halts Osteosarcoma Progression. *Clin Cancer Res*. 2017;23(14):3721-33.
98. Shen RK, Zhu X, Yi H, Wu CY, Chen F, Dai LQ, et al. Proteomic identification of osteosarcoma-derived exosomes and their activation of pentose phosphate pathway. *Int J Clin Exp Pathol*. 2016;9(3):4140-8.
99. Gong L, Bao Q, Hu C, Wang J, Zhou Q, Wei L, et al. Exosomal miR-675 from metastatic osteosarcoma promotes cell migration and invasion by targeting CALN1. *Biochem Biophys Res Commun*. 2018;500(2):170-6.
100. Jerez S, Araya H, Thaler R, Charlesworth MC, López-Solís R, Kalergis AM, et al. Proteomic Analysis of Exosomes and Exosome-Free Conditioned Media From Human Osteosarcoma Cell Lines Reveals Secretion of Proteins Related to Tumor Progression. *J Cell Biochem*. 2017;118(2):351-60.
101. Jerez S, Araya H, Hevia D, Irarrazaval CE, Thaler R, van Wijnen AJ, et al. Extracellular vesicles from osteosarcoma cell lines contain miRNAs associated with cell adhesion and apoptosis. *Gene*. 2019;710:246-57.
102. Fujiwara T, Uotani K, Yoshida A, Morita T, Nezu Y, Kobayashi E, et al. Clinical significance of circulating miR-25-3p as a novel diagnostic and prognostic biomarker in osteosarcoma. *Oncotarget*. 2017;8(20):33375-92.
103. Yoshida A, Fujiwara T, Uotani K, Morita T, Kiyono M, Yokoo S, et al. Clinical and Functional Significance of Intracellular and Extracellular microRNA-25-3p in Osteosarcoma. *Acta Med Okayama*. 2018;72(2):165-74.
104. Macklin R, Wang H, Loo D, Martin S, Cumming A, Cai N, et al. Extracellular vesicles secreted by highly metastatic clonal variants of osteosarcoma preferentially localize to the lungs and induce metastatic behaviour in poorly metastatic clones. *Oncotarget*. 2016;7(28):43570-87.
105. Raimondi L, De Luca A, Gallo A, Costa V, Russelli G, Cuscino N, et al. Osteosarcoma cell-derived exosomes affect tumor microenvironment by specific packaging of microRNAs. *Carcinogenesis*. 2019.
106. Ye Z, Zheng Z, Peng L. MicroRNA profiling of serum exosomes in patients with osteosarcoma by high-throughput sequencing. *J Investig Med*. 2020;68(4):893-901.
107. Cambier L, Stachelek K, Triska M, Jubran R, Huang M, Li W, et al. Extracellular vesicle-associated repetitive element DNAs as candidate osteosarcoma biomarkers. *Sci Rep*. 2021;11(1):94.
108. Skapek SX, Ferrari A, Gupta AA, Lupo PJ, Butler E, Shipley J, et al. Rhabdomyosarcoma. *Nat Rev Dis Primers*. 2019;5(1):1.
109. Ognjanovic S, Linabery AM, Charbonneau B, Ross JA. Trends in childhood rhabdomyosarcoma incidence and survival in the United States, 1975-2005. *Cancer: Interdisciplinary International Journal of the American Cancer Society*. 2009;115(18):4218-26.

110. Oberlin O, Rey A, Lyden E, Bisogno G, Stevens MC, Meyer WH, et al. Prognostic factors in metastatic rhabdomyosarcomas: results of a pooled analysis from United States and European cooperative groups. *J Clin Oncol*. 2008;26(14):2384-9.
111. Dasgupta R, Fuchs J, Rodeberg D. Rhabdomyosarcoma. *Semin Pediatr Surg*. 2016;25(5):276-83.
112. Parham DM, Barr FG. Classification of rhabdomyosarcoma and its molecular basis. *Adv Anat Pathol*. 2013;20(6):387-97.
113. Rodeberg D, Paidas C. Childhood rhabdomyosarcoma. *Semin Pediatr Surg*. 2006;15(1):57-62.
114. Ghayad SE, Rammal G, Ghamloush F, Basma H, Nasr R, Diab-Assaf M, et al. Exosomes derived from embryonal and alveolar rhabdomyosarcoma carry differential miRNA cargo and promote invasion of recipient fibroblasts. *Sci Rep*. 2016;6:37088.
115. Rammal G, Fahs A, Kobeissy F, Mechref Y, Zhao J, Zhu R, et al. Proteomic Profiling of Rhabdomyosarcoma-Derived Exosomes Yield Insights into Their Functional Role in Paracrine Signaling. *Journal of Proteome Research*. 2019;18(10):3567-79.
116. Ghamloush F, Ghayad SE, Rammal G, Fahs A, Ayoub AJ, Merabi Z, et al. The PAX3-FOXO1 oncogene alters exosome miRNA content and leads to paracrine effects mediated by exosomal miR-486. *Sci Rep*. 2019;9(1):14242.
117. Grunewald TGP, Cidre-Aranaz F, Surdez D, Tomazou EM, de Alava E, Kovar H, et al. Ewing sarcoma. *Nat Rev Dis Primers*. 2018;4(1):5.
118. Zollner SK, Amatruda JF, Bauer S, Collaud S, de Alava E, DuBois SG, et al. Ewing Sarcoma-Diagnosis, Treatment, Clinical Challenges and Future Perspectives. *J Clin Med*. 2021;10(8).
119. Salguero-Aranda C, Amaral AT, Olmedo-Pelayo J, Diaz-Martin J, Alava E. Breakthrough Technologies Reshape the Ewing Sarcoma Molecular Landscape. *Cells*. 2020;9(4).
120. Van Paemel R, De Koker A, Vandeputte C, van Zogchel L, Lammens T, Laureys G, et al. Minimally invasive classification of paediatric solid tumours using reduced representation bisulphite sequencing of cell-free DNA: a proof-of-principle study. *Epigenetics*. 2021;16(2):196-208.
121. Miller IV, Raposo G, Welsch U, Prazeres da Costa O, Thiel U, Lebar M, et al. First identification of Ewing's sarcoma-derived extracellular vesicles and exploration of their biological and potential diagnostic implications. *Biol Cell*. 2013;105(7):289-303.
122. Zhang P, Crow J, Lella D, Zhou X, Samuel G, Godwin AK, et al. Ultrasensitive quantification of tumor mRNAs in extracellular vesicles with an integrated microfluidic digital analysis chip. *Lab Chip*. 2018;18(24):3790-801.
123. Dong J, Zhang RY, Sun N, Hu J, Smalley MD, Zhou A, et al. Coupling Nanostructured Microchips with Covalent Chemistry Enables Purification of Sarcoma-Derived Extracellular Vesicles for Downstream Functional Studies. *Adv Funct Mater*. 2020;30(49).
124. Samuel G, Crow J, Klein JB, Merchant ML, Nissen E, Koestler DC, et al. Ewing sarcoma family of tumors-derived small extracellular vesicle proteomics identify potential clinical biomarkers. *Oncotarget*. 2020;11(31):2995-3012.
125. Sun N, Tran BV, Peng Z, Wang J, Zhang C, Yang P, et al. Coupling Lipid Labeling and Click Chemistry Enables Isolation of Extracellular Vesicles for Noninvasive Detection of Oncogenic Gene Alterations. *Advanced Science*. n/a(n/a):2105853.
126. Hanahan D, Weinberg RA. The hallmarks of cancer. *Cell*. 2000;100(1):57-70.
127. Hanahan D, Weinberg RA. Hallmarks of cancer: the next generation. *Cell*. 2011;144(5):646-74.
128. Bautista-Sanchez D, Arriaga-Canon C, Pedroza-Torres A, De La Rosa-Velazquez IA, Gonzalez-Barrios R, Contreras-Espinosa L, et al. The Promising Role of miR-21 as a Cancer Biomarker and Its Importance in RNA-Based Therapeutics. *Mol Ther Nucleic Acids*. 2020;20:409-20.

129. Volinia S, Calin GA, Liu CG, Ambs S, Cimmino A, Petrocca F, et al. A microRNA expression signature of human solid tumors defines cancer gene targets. *Proc Natl Acad Sci U S A*. 2006;103(7):2257-61.
130. Wang XH, Cai P, Wang MH, Wang Z. microRNA-25 promotes osteosarcoma cell proliferation by targeting the cell-cycle inhibitor p27. *Molecular medicine reports*. 2014;10(2):855-9.
131. Ren CL, L.; Zhang, H.; Gao, L., Li, A. The role of miR-25 in pediatric neuroblastoma. *Biomed Res* 2017;28(16):7261-7.
132. Ding X, Zhong T, Jiang L, Huang J, Xia Y, Hu R. miR-25 enhances cell migration and invasion in non-small-cell lung cancer cells via ERK signaling pathway by inhibiting KLF4. *Molecular medicine reports*. 2018;17(5):7005-16.
133. Hu Z, Dong J, Wang L-E, Ma H, Liu J, Zhao Y, et al. Serum microRNA profiling and breast cancer risk: the use of miR-484/191 as endogenous controls. *Carcinogenesis*. 2012;33(4):828-34.
134. Li LM, Hu ZB, Zhou ZX, Chen X, Liu FY, Zhang JF, et al. Serum microRNA profiles serve as novel biomarkers for HBV infection and diagnosis of HBV-positive hepatocarcinoma. *Cancer Res*. 2010;70(23):9798-807.
135. Guessous F, Zhang Y, Kofman A, Catania A, Li Y, Schiff D, et al. microRNA-34a is tumor suppressive in brain tumors and glioma stem cells. *Cell cycle*. 2010;9(6):1031-6.
136. Jafari N, Abediankenari S. MicroRNA-34 dysregulation in gastric cancer and gastric cancer stem cell. *Tumour Biol*. 2017;39(5):1010428317701652.
137. Imani S, Wu RC, Fu J. MicroRNA-34 family in breast cancer: from research to therapeutic potential. *J Cancer*. 2018;9(20):3765-75.
138. Gu S, Chan WY. Flexible and versatile as a chameleon-sophisticated functions of microRNA-199a. *Int J Mol Sci*. 2012;13(7):8449-66.
139. Alemdehy MF, Haanstra JR, de Looper HW, van Strien PM, Verhagen-Oldenampsen J, Caljouw Y, et al. ICL-induced miR139-3p and miR199a-3p have opposite roles in hematopoietic cell expansion and leukemic transformation. *Blood*. 2015;125(25):3937-48.
140. Tsukigi M, Bilim Y, Yuuki K, Ugolkov A, Naito S, Nagaoka A, et al. Re-expression of miR-199a suppresses renal cancer cell proliferation and survival by targeting GSK-3 β . *Cancer letters*. 2012;315(2):189-97.
141. Phatak P, Burrows WM, Chesnick IE, Tulapurkar ME, Rao JN, Turner DJ, et al. MiR-199a-3p decreases esophageal cancer cell proliferation by targeting p21 activated kinase 4. *Oncotarget*. 2018;9(47):28391-407.
142. Xue X, Fei X, Hou W, Zhang Y, Liu L, Hu R. miR-342-3p suppresses cell proliferation and migration by targeting AGR2 in non-small cell lung cancer. *Cancer Lett*. 2018;412:170-8.
143. Li XR, Chu HJ, Lv T, Wang L, Kong SF, Dai SZ. miR-342-3p suppresses proliferation, migration and invasion by targeting FOXM1 in human cervical cancer. *FEBS Lett*. 2014;588(17):3298-307.
144. Zhao L, Zhang Y. miR-342-3p affects hepatocellular carcinoma cell proliferation via regulating NF- κ B pathway. *Biochem Biophys Res Commun*. 2015;457(3):370-7.
145. Galardi A, Colletti M, Di Paolo V, Vitullo P, Antonetti L, Russo I, et al. Exosomal MiRNAs in Pediatric Cancers. *Int J Mol Sci*. 2019;20(18).
146. Xu R, Rai A, Chen M, Suwakulsiri W, Greening DW, Simpson RJ. Extracellular vesicles in cancer—implications for future improvements in cancer care. *Nature reviews Clinical oncology*. 2018;15(10):617.
147. Yekula A, Muralidharan K, Kang KM, Wang L, Balaj L, Carter BS. From laboratory to clinic: Translation of extracellular vesicle based cancer biomarkers. *Methods*. 2020;177:58-66.
148. Logozzi M, De Milito A, Lugini L, Borghi M, Calabrò L, Spada M, et al. High levels of exosomes expressing CD63 and caveolin-1 in plasma of melanoma patients. *PLoS One*. 2009;4(4):e5219.

149. Eldh M, Olofsson Bagge R, Lässer C, Svanvik J, Sjöstrand M, Mattsson J, et al. MicroRNA in exosomes isolated directly from the liver circulation in patients with metastatic uveal melanoma. *BMC Cancer*. 2014;14:962.
150. Momen-Heravi F, Balaj L, Alian S, Trachtenberg AJ, Hochberg FH, Skog J, et al. Impact of biofluid viscosity on size and sedimentation efficiency of the isolated microvesicles. *Front Physiol*. 2012;3:162.
151. Menck K, Bleckmann A, Wachter A, Hennies B, Ries L, Schulz M, et al. Characterisation of tumour-derived microvesicles in cancer patients' blood and correlation with clinical outcome. *J Extracell Vesicles*. 2017;6(1):1340745.
152. Ramirez MI, Amorim MG, Gadelha C, Milic I, Welsh JA, Freitas VM, et al. Technical challenges of working with extracellular vesicles. *Nanoscale*. 2018;10(3):881-906.
153. Clayton A, Boilard E, Buzas EI, Cheng L, Falcon-Perez JM, Gardiner C, et al. Considerations towards a roadmap for collection, handling and storage of blood extracellular vesicles. *J Extracell Vesicles*. 2019;8(1):1647027.
154. Palviainen M, Saraswat M, Varga Z, Kitka D, Neuvonen M, Puhka M, et al. Extracellular vesicles from human plasma and serum are carriers of extravesicular cargo-Implications for biomarker discovery. *PLoS One*. 2020;15(8):e0236439.
155. Helwa I, Cai J, Drewry MD, Zimmerman A, Dinkins MB, Khaled ML, et al. A comparative study of serum exosome isolation using differential ultracentrifugation and three commercial reagents. *PLoS one*. 2017;12(1):e0170628.
156. Andreu Z, Rivas E, Sanguino-Pascual A, Lamana A, Marazuela M, González-Alvaro I, et al. Comparative analysis of EV isolation procedures for miRNAs detection in serum samples. *Journal of extracellular vesicles*. 2016;5(1):31655.
157. Kalra H, Adda CG, Liem M, Ang CS, Mechler A, Simpson RJ, et al. Comparative proteomics evaluation of plasma exosome isolation techniques and assessment of the stability of exosomes in normal human blood plasma. *Proteomics*. 2013;13(22):3354-64.
158. Macías M, Rebmann V, Mateos B, Varo N, Perez-Gracia JL, Alegre E, et al. Comparison of six commercial serum exosome isolation methods suitable for clinical laboratories. Effect in cytokine analysis. *Clinical Chemistry and Laboratory Medicine (CCLM)*. 2019;57(10):1539-45.
159. Million R, Tolin S, Puricelli L, Sbrignadello S, Fadini GP, Tessari P, et al. High abundance proteins depletion vs low abundance proteins enrichment: comparison of methods to reduce the plasma proteome complexity. *PLoS One*. 2011;6(5):e19603.
160. Simonsen JB. What are we looking at? Extracellular vesicles, lipoproteins, or both? *Circulation research*. 2017;121(8):920-2.
161. Yuana Y, Koning RI, Kuil ME, Rensen PC, Koster AJ, Bertina RM, et al. Cryo-electron microscopy of extracellular vesicles in fresh plasma. *J Extracell Vesicles*. 2013;2.
162. Yuana Y, Levels J, Grootemaat A, Sturk A, Nieuwland R. Co-isolation of extracellular vesicles and high-density lipoproteins using density gradient ultracentrifugation. *Journal of extracellular vesicles*. 2014;3:10.3402/jev.v3.23262.
163. Chiam K, Mayne GC, Wang T, Watson DI, Irvine TS, Bright T, et al. Serum outperforms plasma in small extracellular vesicle microRNA biomarker studies of adenocarcinoma of the esophagus. *World J Gastroenterol*. 2020;26(20):2570-83.
164. Xu JF, Wang YP, Zhang SJ, Chen Y, Gu HF, Dou XF, et al. Exosomes containing differential expression of microRNA and mRNA in osteosarcoma that can predict response to chemotherapy. *Oncotarget*. 2017;8(44):75968-78.

165. Shen RK, Zhu X, Yi H, Wu CY, Chen F, Dai LQ, et al. Proteomic identification of osteosarcoma-derived exosomes and their activation of pentose phosphate pathway. *Int J Clin Exp Pathol.* 2016;9(3):4140-8.
166. Enciso-Martinez A, Van Der Pol E, Hau CM, Nieuwland R, Van Leeuwen TG, Terstappen L, et al. Label-free identification and chemical characterisation of single extracellular vesicles and lipoproteins by synchronous Rayleigh and Raman scattering. *J Extracell Vesicles.* 2020;9(1):1730134.
167. Enciso-Martinez A, van der Pol E, Lenferink ATM, Terstappen L, van Leeuwen TG, Otto C. Synchronized Rayleigh and Raman scattering for the characterization of single optically trapped extracellular vesicles. *Nanomedicine.* 2020;24:102109.
168. Martinez-Castaldi C, Silverstein M, Bauchner H. Child versus adult research: the gap in high-quality study design. *Pediatrics.* 2008;122(1):52-7.
169. Calin GA, Croce CM. MicroRNA signatures in human cancers. *Nat Rev Cancer.* 2006;6(11):857-66.
170. Mills J, Capece M, Cocucci E, Tessari A, Palmieri D. Cancer-Derived Extracellular Vesicle-Associated MicroRNAs in Intercellular Communication: One Cell's Trash Is Another Cell's Treasure. *International journal of molecular sciences.* 2019;20(24):6109.
171. Batchu S, Kellish AS, Hakim AA. Assessing alveolar rhabdomyosarcoma cell lines as tumor models by comparison of mRNA expression profiles. *Gene.* 2020:145025.



Chapter 8

Cell-free RNA from plasma in patients with neuroblastoma: exploring the technical and clinical potential

Cancers (Basel). 2023 Mar 31;15(7):2108. doi: 10.3390/cancers15072108.

Nathalie S.M. Lak^{1,2}, Anne Seijger³, Lieke M.J. van Zogchel^{1,2}, Nina U. Gelineau^{1,2}, Ahmad Javadi², Lily Zappeij-Kannegieter², Laura Bongiovanni^{3,4}, Anneloes Andriessen³, Janine Stutterheim¹, C. Ellen van der Schoot¹, Alain de Bruin³, Godelieve A.M. Tytgat^{1,2}

¹Princess Máxima Center for Pediatric Oncology, Utrecht, the Netherlands

²Department of Experimental Immunohematology, Sanquin Research, Amsterdam, the Netherlands

³Department of Biomolecular Health Sciences, Faculty of Veterinary Medicine, Utrecht University, Utrecht, the Netherlands

⁴Department of Veterinary Medicine, University of Teramo, Teramo, Italy.

Abstract

Neuroblastoma affects mostly young children, bearing a high morbidity and mortality. Liquid biopsies, e.g., molecular analysis of circulating tumor-derived nucleic acids in blood, offer a minimally invasive diagnostic modality. Cell-free RNA (cfRNA) is released by all cells, especially cancer. It circulates in blood packed in extracellular vesicles (EV) or attached to proteins. We studied the feasibility of analyzing cfRNA and EV, isolated by size exclusion chromatography (SEC), from platelet-poor plasma from healthy controls (n = 40) and neuroblastoma patients with localized (n = 10) and metastatic disease (n = 30). The mRNA content was determined using several multiplex droplet digital PCR (ddPCR) assays for a neuroblastoma-specific gene panel (PHOX2B, TH, CHRNA3) and a cell cycle regulation panel (E2F1, CDC6, ATAD2, H2AFZ, MCM2, DHFR). We applied corrections for the presence of platelets. We demonstrated that neuroblastoma-specific markers were present in plasma from 14/30 patients with metastatic disease and not in healthy controls and patients with localized disease. Most cell cycle markers had a higher expression in patients. The mRNA markers were mostly present in the EV-enriched SEC fractions. In conclusion, cfRNA can be isolated from plasma and EV and analyzed using multiplex ddPCR. cfRNA is an interesting novel liquid biopsy-based target to explore further.

Simple summary

Neuroblastoma mostly affects young children and despite intensive treatment, many children die of progressive disease. It remains challenging to identify those patients at risk. Analyzing blood, as liquid biopsies, is not invasive and can help to identify these patients. We studied whether RNA molecules can be detected in these liquid biopsies. In blood plasma, RNA can be free-floating or packed in small particles, 'extracellular vesicles'. We present a workflow to analyze this cell-free RNA from small volumes of blood plasma of children with neuroblastoma. We have used neuroblastoma-specific markers and markers involved in cell proliferation. These latter genes can be upregulated in many different tumor types. We demonstrate that both types of markers have a higher expression in patients with metastatic disease, compared to healthy controls and patients with localized disease. These findings are essential for future studies on cell-free RNA, hopefully leading to improved survival for these patients.

Introduction

Neuroblastoma is the most common extracranial solid tumor in children [1]. Most patients present with disseminated disease which requires intensive treatment, consisting of chemotherapy, surgery and immunotherapy [1]. Still, more than half of patients suffer from refractory disease or relapse, which is associated with low survival [2,3]. At initial diagnosis and during the first courses of chemotherapy, it is hard to identify patients with treatment-resistant disease or at risk for relapse. Currently, response evaluation depends on imaging which often demands general anesthesia in these young patients. Liquid biopsy-based monitoring might decrease the number of diagnostic procedures and potentially even improve sensitivity of response monitoring [4,5].

The presence of neuroblastoma-specific mRNA in the cellular compartment of blood and bone marrow, such as PHOX2B, TH and CHRNA3, has been shown to correlate with outcome, enabling response monitoring in patients with high-risk disease [6,7,8,9]. Additionally, several targets in cell-free DNA (cfDNA) from plasma have been described to track therapy response, disappearing as tumor burden decreases and re-appearing as the disease relapses [10,11,12,13]. However, the presence of tumor-specific mRNA is often attributed to circulating tumor cells, which are not always present in every stage of the disease. cfDNA targets such as mutations in the ALK gene, amplification of MYCN or hypermethylation of the tumor suppressor gene RASSF1A (RASSF1A-M) are only applicable in patients with high-risk disease [10,12]. Therefore, apart from cfDNA, other liquid biopsy-based biomarkers in the plasma compartment deserve to be investigated. cfDNA is often shed through apoptosis or necrosis [14], whereas RNA is also actively secreted by living cells [15], presumably presenting a more comprehensive perspective on the ongoing disease [16]. Due to the presence of RNases in plasma [17], RNA has historically been considered unstable in plasma and therefore cfRNA not suitable for biomarker studies. However, in recent years, it has been discovered that plasma contains several types of RNA, which are mostly protected from degradation through their association with extracellular vesicles (EVs) or protein aggregates [16,18,19,20,21]. Furthermore, platelets contain RNA which also bears biomarker potential [22,23,24].

In the field of neuroblastoma, Morini et al. identified a panel of miRNA and showed that upregulation of these miRNA in plasma after induction therapy was associated with better chemotherapy response [25]. Ma et al. identified a single miRNA (miR199a-3p) which was upregulated in plasma from patients with neuroblastoma in all risk groups [26]. Recently, Matthew et al. have performed an impressive sequencing effort and characterized cell-free mRNA from plasma from both healthy

controls and adults with lung and breast cancer [27]. They demonstrated that cfRNA expression profiles in patients differed from healthy controls, and they were able to identify tumor tissue-specific signatures. So far, similar sequencing studies in neuroblastoma have not been performed.

Another example of the possibilities of cell-free mRNA from plasma in cancer comes from studies in canines. Duplication of genomic DNA and distribution amongst the new daughter cells is a normal process in healthy cells. This process, named 'cell cycle', consists of well-defined phases, all guarded by checkpoints and their respective regulatory genes [28]. Tumor cells are highly proliferative due to dysregulation of the cell cycle [29]. A pivotal gene for the progression of the G2 phase to the S phase is E2F1 [29,30]. In canines, Bongiovanni et al. identified several genes within the E2F1 pathway to be overexpressed in tissue from canine melanomas, amongst them E2F1, DHFR, CDC6, ATAD2, MCM2 and H2AFZ [31]. Subsequently, Andriessen et al. reported that CDC6, DHFR, H2AFZ and ATAD2 transcripts were present in plasma of canines with malignancies and that these genes were mainly associated with EV [32]. Cell cycle dysregulation is an important feature of the pathogenesis of neuroblastoma [1,33], and we therefore postulated that transcripts of cell cycle proteins might potentially serve as novel biomarkers for this disease.

In this study, we explore the feasibility of detecting and studying cfRNA in plasma from patients with neuroblastoma by studying both a neuroblastoma-specific and a cell cycle panel for use on cell-free mRNA from plasma in patients with neuroblastoma. We report on the development of several multiplex panels for droplet digital PCR (ddPCR) and investigate whether these mRNA targets from plasma are associated with EVs. Finally, we describe technical challenges arising from the study of cfRNA from plasma.

Methods

Patients and Samples

Peripheral blood samples from neuroblastoma patients were collected within the Minimal Residual Disease study of the DCOG high-risk protocol, approved by the ethical committee of the Academic Medical Center, Amsterdam, The Netherlands (MEC07/219#08.17.0836). Samples from patients with International Neuroblastoma Staging System (INSS) stage 1 (localized disease that can be fully resected) and INSS stage 4 (metastatic disease) were included. Peripheral blood was collected in EDTA tubes (Becton-Dickinson, Franklin Lakes, NJ, USA) and processed within 24 h. Plasma

was obtained by centrifugating blood samples at $1375\times g$ for 10 min and stored at $-20\text{ }^{\circ}\text{C}$ until further processing. For controls, blood was collected from healthy adult volunteers and prepared similar to patients' samples, including storage at $-20\text{ }^{\circ}\text{C}$.

Preparation of Platelets from Peripheral Blood

Peripheral blood was collected in EDTA tubes (Becton-Dickinson) and processed within 2 h. First, platelet-rich plasma was obtained by centrifugation at $235\times g$ for 15 min. The supernatant was collected and 10% anticoagulant citrate dextrose, solution A (ACD-A, Terumo, Japan) was added and centrifuged at $16,873\times g$ for 4 min to pellet the platelets. Leukocyte and platelet counts were measured with the Sysmex XN1000 Hematology analyzer (Sysmex, Kobe, Japan) according to manufacturer's protocol.

Isolation of Cell-Free RNA and cDNA Synthesis

RNA was isolated from 200 μL of plasma, unless otherwise specified, with the miRNeasy micro serum/plasma kit (Qiagen, Germantown, TN, USA) following manufacturer's protocol. RNA was eluted in 12 μL of H_2O and subsequently used for cDNA synthesis with the High Capacity RNA-to-cDNA kit (Thermo Fisher, Waltham, MA, USA).

Design and Optimization of the Multiplex ddPCR Assays

For the detection of PHOX2B, TH and CHRNA3, the same primers and probes as previously described for RT-qPCR were used [6,9,34]. As potential cfRNA reference genes, GUSB and B2M were included, as previously described for RT-qPCR [35]. Genes involved in the E2F1 pathway were CDC6, ATAD2, DHFR, H2AFZ and MCM2. To quantify the presence of platelets in the plasma, we applied an assay for platelet-specific ITG3B, designed to amplify and detect both polymorphic alleles (HPA-1A and HPA-1B) of this gene [29]. ddPCR assays were designed using Primer3Plus (www.primer3plus.com (accessed on 1 February 2021)). All sequences are shown in Supplemental Table S1. The QX200™ Droplet Generator (Bio Rad, Hercules, CA, USA) or QX200™ Automated Droplet Generator (Bio Rad) were used for droplet generation. Thermal cycling was performed using the C1000 Touch Thermal Cycler (Bio Rad) with the following program: $95\text{ }^{\circ}\text{C}$ for 10 min; 40 cycles of $94\text{ }^{\circ}\text{C}$ for 30 s, annealing temperature variable per assay for 1 min; $98\text{ }^{\circ}\text{C}$ for 10 min; $4\text{ }^{\circ}\text{C}$ hold. Following PCR, droplets were read and quantified using the QX200 Droplet reader (Bio Rad). Assays were optimized using RNA isolated from the neuroblastoma cell line IMR32 or RNA isolated from healthy platelets. All patient samples were tested in duplicate and 'no template controls' were included with every assay. ddPCR assay analyses were done in QX Manager 1.2 Standard Edition software (Bio Rad), except if indicated, then analyzed in Quantasoft 1.7.4 software (Bio Rad). Results are represented in copies/mL plasma, unless otherwise specified.

Isolation of Cell-Free DNA and ddPCR Assays

cfDNA was isolated using the Quick cfDNA Serum & Plasma kit (Zymo Research, Irvine, CA, USA). The methylation-sensitive restriction enzyme-based ddPCR for methylated tumor suppressor gene RASSF1A (RASSF1A-M) and ACTB was performed as described previously [10].

Isolation of EVs from Plasma and Electron Microscopy on EVs

EVs from plasma were isolated from 500 μ L plasma by size exclusion chromatography (SEC) columns (qEV Original 70 nm from Izon Science, Christchurch, New Zealand) according to manufacturer's protocol. SEC fractions 6 to 20 were collected. Electron microscopy was performed as reported previously [30].

Western Blot

Protein content of each SEC fraction was measured by micro BCA protein assay (Thermo Fisher Scientific), and input from the separate SEC fractions was adjusted accordingly to obtain equal loading of every SEC fraction onto the 4–12% SDS PAGE gel (Bio Rad). Protein concentration was eventually determined by a precipitation assay with trichloroacetic acid (Sigma, Kanagawa, Japan). After transfer to a nitrocellulose membrane (Bio Rad), the membrane was cut into two parts to allow for staining for different targets simultaneously. The membrane was blocked with PBS containing 5% (w/v) bovine serum albumin and then incubated with CD9 (Santa Cruz Biotechnology, Dallas, TX, USA, sc52519, 1:1000) and CD63 (BD Biosciences, San Jose, CA, USA, 556019, 1:1000). Antibody binding was visualized with anti-mouse IgG coupled to horse radish peroxidase at a 1:5000 dilution. Subsequently, the membranes were stripped by incubating with 1% Na₂S₂O₃ for an hour, and after blocking, incubated with CD81 (Santa Cruz Biotechnology, Santa Cruz, Dallas, TX, USA, SC9158, 1:1000) and TSG101 (Sigma, St. Louis, MI, USA, T5701, 1:1000).

Statistical Analysis

Statistical analyses were performed using SPSS version 23. Venn diagrams were generated using Lucid chart (www.lucidchart.com (accessed on 18 February 2022)). All other figures were generated using GraphPad Prism version 8. Continuous variables were analyzed using the non-parametric Mann–Whitney U test; differences were considered significant at $p < 0.05$.

Results

Neuroblastoma-Specific mRNA Is Present in Plasma

To study cfRNA in limited volume samples of pediatric patients with neuroblastoma, we first designed and optimized a multiplex ddPCR which included the neuroblastoma-specific targets PHOX2B, CHRNA3 and TH, and GUSB as a reference gene (Supplemental Figure S1). In 40 healthy controls, there were no transcripts of PHOX2B, TH or CHRNA3 detected, whereas in all donors, GUSB transcripts could be demonstrated (mean 96 copies/mL plasma, range 36–238 copies/mL) (Supplemental Table S2).

We tested the neuroblastoma-specific multiplex ddPCR panel in a first cohort, consisting of 38 samples from 22 patients with neuroblastoma, which were collected at different timepoints during treatment (patient characteristics and outcome in Supplemental Table S3). In these 38 samples, only 24 samples were positive for GUSB and at lower concentrations (mean of positive samples 14.9 copies/mL plasma (range 2.0–127 copies/mL)). In the 24 samples positive for GUSB, 2 samples were positive for PHOX2B and GUSB (1 at initial diagnosis (2.1 and 2.1 copies/mL, respectively) and 1 at relapse (11 and 127 copies/mL), Supplemental Table S4). No samples were positive for TH or CHRNA3. As it is known that freeze–thaw cycles can affect cfRNA quality [27], we hypothesized that the cfRNA in the samples from these archived samples might be degenerated. Unfortunately, no RNA or plasma was left for analysis of RNA quality through another modality, e.g., Bioanalyzer.

To overcome this problem, we subsequently used only pre-treatment plasma samples that had not been thawed before, 10 samples from patients with INSS stage 1 (localized disease) and 30 INSS stage 4 neuroblastoma patients (metastatic disease), to form a second cohort. Patient characteristics and outcomes are shown in Supplemental Table S3. Results for the neuroblastoma-specific markers are shown in Figure 1 and Supplemental Table S5. In all 40 neuroblastoma samples, GUSB was detectable; for patients with localized disease, the mean was 38.2 copies/mL plasma (range 2.3–95 copies/mL plasma) and metastatic disease, 53 copies/mL plasma (range 10–220 copies/mL plasma). In none of the samples of patients with localized disease were PHOX2B, TH and CHRNA3 detected. In contrast, in 14/30 samples of patients with metastatic disease, PHOX2B (n = 13, 9.2 copies/mL, range 0.4–47 copies/mL) and/or CHRNA3 (n = 4, mean 5.4 copies/mL, range 2.1–11 copies/mL) was detected. No samples were positive for TH. In the samples with at least one marker positive, 10/14 (71%) suffered from an event vs. 11/16 (69%) in the negative samples.

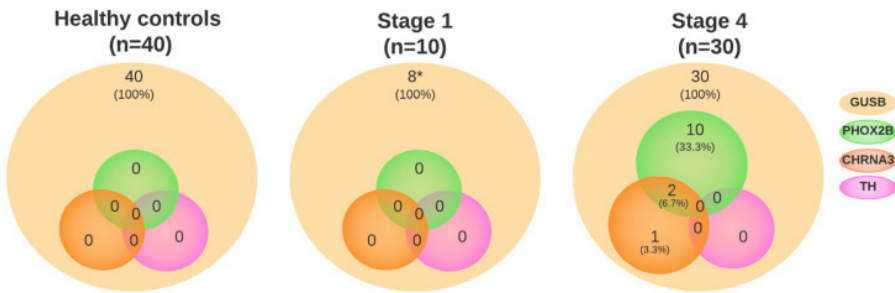


Figure 1. Expression of neuroblastoma-specific genes in cell-free RNA from healthy controls (n = 40), and diagnostic plasmas from patients with neuroblastoma with localized (n = 10) and metastatic (n = 30) disease. * Not enough material was left for 2 patients to perform the ddPCR for these neuroblastoma-specific markers.

Cell Cycle Genes in Plasma and Correction for the Presence of Platelets

Next, we investigated the presence of transcripts of cell cycle genes in cfRNA (Supplemental Figure S2 for the cell cycle panel ddPCR assays). We found that platelets also contain these transcripts (Supplemental Figure S3 for expression in platelets). Since plasma was isolated by centrifugation at 1375× g for 10 min, contaminating platelets might have been present in the plasma thereby affecting the analysis. Indeed, in EDTA blood from four healthy controls that were treated similarly as our plasma samples, using the Sysmex system, we measured that after the centrifugation step, 25–50% of the platelets were still present in plasma (Supplemental Table S6). As platelet counts can vary between patients and healthy controls, the cfRNA was corrected for the presence of platelet-specific RNA using the platelet-specific ITGB3 ddPCR. The ratio between ITGB3 expression and the different cell cycle gene transcripts was stable between donors, which enabled a correction co-efficient for each marker, as indicated in Supplemental Table S7.

Cell Cycle Genes in Plasma from Patients at Diagnosis

We measured the expression of the six cell cycle genes (CDC6, ATAD2, E2F1, H2AFZ, MCM2 and DHFR), the two potential references genes (GUSB and B2M) and the platelet-specific marker ITGB3 in 200 μL of plasma from 20 healthy controls (Supplemental Table S8). We then proceeded to measure these genes in our cohort of 40 patients. After correcting for platelets, CDC6, ATAD2, DHFR, E2F1, H2AFZ, GUSB and B2M were significantly higher in patients with localized disease than in healthy controls. CDC6, DHFR, E2F1, H2AFZ, MCM2, GUSB and B2M were significantly higher in patients with metastatic disease than in healthy controls, and CDC6, DHFR and E2F1 were significantly higher in metastatic patients than in localized patients (Figure 2 and Supplemental Table S9).

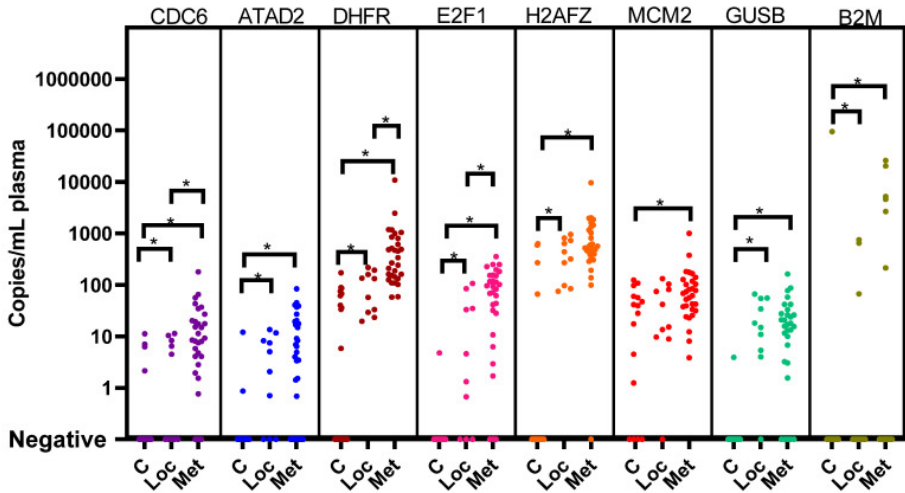


Figure 2. Expression of cell cycle genes (CDC6, ATAD2, DHFR, E2F1, H2AFZ and MCM2) and reference genes (GUSB and B2M) in cell-free RNA from healthy controls ($n = 40$) and diagnostic plasmas from patients with neuroblastoma with localized ($n = 10$) and metastatic ($n = 30$) disease, as measured by ddPCR from 200 μ L plasma and corrected for platelet contamination. C; healthy controls. Loc; patients with localized disease. Met; patients with metastatic disease. * Significance at $p < 0.05$.

We hypothesized that these cell cycle panels could assist in differentiating patients from healthy controls and could possibly differentiate between low- and high-risk disease. For this purpose, we determined the background expression of the cell cycle markers in 20 healthy plasma samples and set a threshold for positivity (Supplemental Table S8). When applying the thresholds for positivity per marker (after correcting for platelets), none of the 10 patients with localized disease were positive, whereas 14 out of 30 patients with metastatic disease had markers that were above the threshold (Supplemental Table S9). All of these 14 patients were positive for DHFR, and only 3 patients were also positive for MCM2 in combination with CDC6 ($n = 2$) and H2AFZ ($n = 1$). All three patients suffered from relapse. Eleven other patients were only positive for DHFR. A total of 7/11 suffered from relapse or refractory disease, and 4 eventually died from the disease. In this small cohort, we observed that, when correcting for platelets and background expression, DHFR was elevated in 14/30 patients with metastatic disease at diagnosis. When compared with the neuroblastoma genes, 7/14 DHFR-positive patients were also positive for PHOX2B and/or CHRNA3.

cfRNA during Treatment

To explore the potential of cfRNA measurements to monitor residual disease during treatment, we measured 66 samples drawn during treatment from 11 patients with

metastatic disease (Supplemental Table S10). Patients were chosen according to their clinical outcome and availability of follow-up samples. All neuroblastoma-specific markers were negative in all follow-up samples, except for one sample at the first course of first-line chemotherapy in patient NBL 2187. This sample was positive for CHRNA3 (2.0 copies/mL plasma). We also measured the cell cycle markers in the sequential samples. Many neuroblastoma patients suffer from bone marrow depression due to toxicity of chemotherapy during treatment, which results in low platelet counts. Since we do not know how this affects the RNA content of platelets and if the cell cycle/ITGB3 ratios are affected, we decided not to use the ITGB3-corrected ratios for these samples but to only use the absolute number of copies present in the samples. Supplemental Figure S4 displays the course of the markers for all 11 patients, sorted per clinical outcome. From seven patients, at least three samples during the first line of therapy were available, and from three patients, two samples during the first line of therapy. In all patients, B2M always had the highest expression throughout the entire treatment. The other transcripts varied greatly per patient. No marker showed an evident increase or decrease in expression in patients with good vs. poor clinical outcome. Therefore, it is impossible to draw a conclusion on the level of specific markers in relation to clinical outcome in this small cohort, considering the variation in sampled time points, the unknown platelet counts and variation in expression levels between the different patients.

The mRNA in Plasma Is Concentrated in EV-Enriched SEC Fractions

Subsequently, we investigated in which compartment the neuroblastoma-derived transcripts were present in a patient with metastatic disease by size exclusion chromatography (SEC) on 500 μ L of plasma, yielding SEC fractions of 500 μ L each. The mRNA markers were tested in parallel to cfDNA using the reference gene ACTB and tumor-specific RASSF1A-M. The presence of EV was confirmed on western blot by the presence of EV-enriched proteins CD9, CD63, CD81 and TSG101 in SEC fractions 7 to 10 isolated from a healthy control and a patient with metastatic disease (Supplemental Figures S5–S7). Electron microscopy on SEC fractions from the same patient also confirmed the presence of EV in fractions 7 to 10 (Supplemental Figure S8), whereas the higher fractions contained aggregated proteins. ddPCR of the RNA markers (both neuroblastoma-specific and cell cycle) and DNA markers from 200 μ L of each SEC fraction from two other patients with metastatic disease (one (NBL2196) being PHOX2B-positive in unfractionated plasma and one PHOX2B-negative (NBL2187)) showed that the mRNA markers were mostly present in the EV-enriched fractions, whereas the DNA targets were mostly present in the higher, protein-enriched fractions (Figure 3A,B,D,E, Supplemental Table S11).

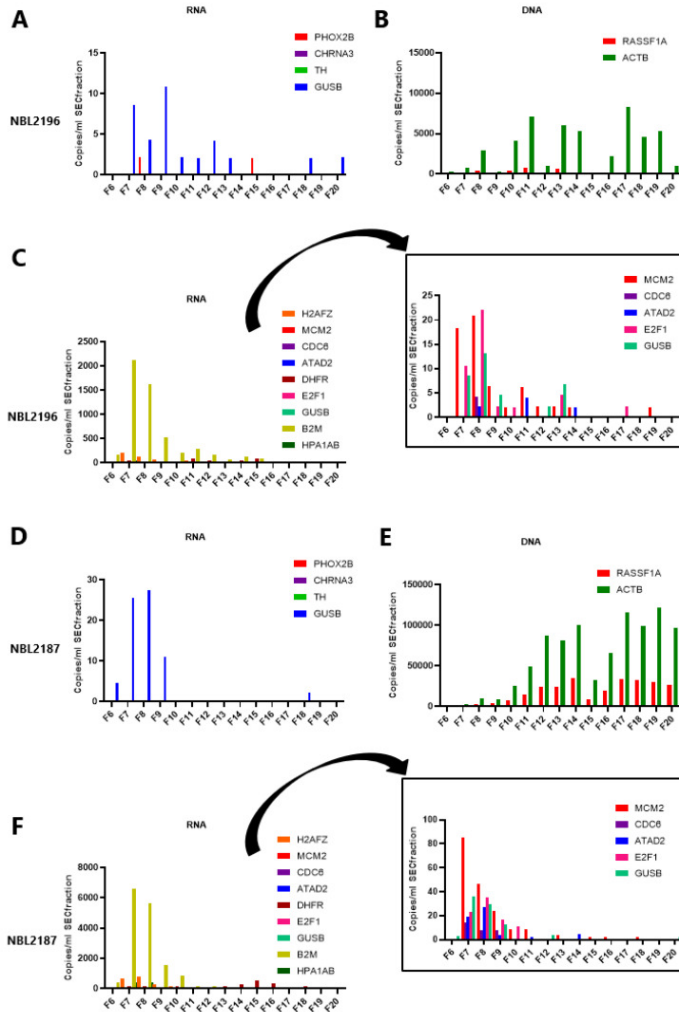


Figure 3. Expression of the mRNA markers and cell-free DNA markers in fractions isolated by size exclusion chromatography (SEC) and analyzed by ddPCR. Fractions F7 to F10 are considered as enriched in extracellular vesicles (EV). For patient NBL2196, **(A)** shows the expression of the neuroblastoma-specific mRNA markers, PHOX2B, CHRNA3 and TH, and reference gene GUSB in cell-free RNA from 200 μ L per SEC fraction: only GUSB and PHOX2B are expressed. **(B)** shows the cfDNA tumor-specific target methylated RASSF1A (RASSF1A-M) and reference gene ACTB in cfDNA from 200 μ L per SEC fraction. **(C)** illustrates the expression of the cell cycle markers (H2AFZ, MCM2, CDC6, ATAD2, DHFR, E2F1, GUSB, B2M and HPA1A/B) in 200 μ L per SEC fraction from the same patient. For patient NBL2187, **(D)** shows the expression of the neuroblastoma-specific mRNA markers, PHOX2B, CHRNA3 and TH, and reference gene GUSB in cell-free RNA from 200 μ L per SEC fraction: only GUSB is expressed. **(E)** shows the cfDNA tumor-specific target methylated RASSF1A (RASSF1A-M) and reference gene ACTB in cfDNA from 200 μ L per SEC fraction. **(F)** illustrates the expression of the cell cycle markers (H2AFZ, MCM2, CDC6, ATAD2, DHFR, E2F1, GUSB, B2M and HPA1A/B) in 200 μ L per SEC fraction from the same patient. Please note that due to a high concentration of B2M, H2AFZ and HPA1A/B, the insert in Figure 3C,F displays an adjusted y-axis without these markers to show the concentration of the other markers.

The presence of mRNA (neuroblastoma-specific and cell cycle markers) in the EV fractions was confirmed in a subsequent experiment with another patient (NBL2177) and a healthy control in which the input in the cDNA reaction was increased 2.5-fold by using the complete 500 μL of SEC fractions. The results are shown in Figure 4 and Supplemental Table S12. Overall, the sum of the positive droplets from all SEC fractions corresponds well to what is found in 500 μL of whole plasma. Unexpectedly, DHFR is increased in the higher, protein-enriched fraction in the patient sample and is even higher than B2M.

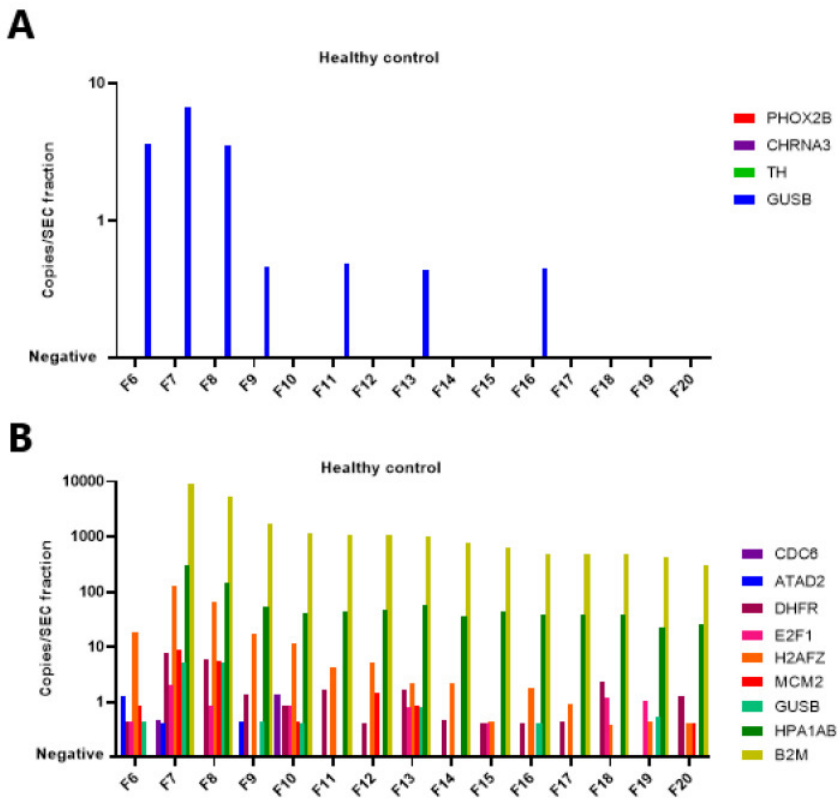


Figure 4. Expression of neuroblastoma-specific and cell cycle genes in 500 μL of SEC (size exclusion chromatography) fractions, as isolated from 500 μL plasma, from one healthy control and one patient with metastatic neuroblastoma. Fractions F7 to F10 are considered as enriched in extracellular vesicles (EV). In the healthy control, **(A)** shows the expression of the neuroblastoma-specific genes (PHOX2B, CHRNA3 and TH with reference gene GUSB) and **(B)** shows the expression of the cell cycle markers (CDC6, ATAD2, DHFR, E2F1, H2AFZ and MCM2 with GUSB, HPA1A/B and B2M). In the patient NBL 2177, **(C)** shows the expression of the neuroblastoma-specific genes (PHOX2B, CHRNA3 and TH with reference gene GUSB) and **(D)** shows the expression of the cell cycle markers (CDC6, ATAD2, DHFR, E2F1, H2AFZ and MCM2 with GUSB, HPA1A/B and B2M). Please note that the y-axis is represented on a log scale.

Discussion

This study addressed the potential for cfRNA analysis from small volumes of plasma using multiplex ddPCR assays and EV enrichment. Within this first exploratory study, we did not aim to draw conclusions on added value to current clinical practice. However, we demonstrated that in patients with neuroblastoma, neuroblastoma-specific cfRNA is only present in patients with metastatic disease and that this RNA is associated with EV. Even with low volumes of plasma, neuroblastoma-specific and quantifiable signals can be obtained when using multiplex ddPCR assays. In this small patient cohort, no correlation with outcome of the disease was observed.

However, we did identify several challenges that are essential to further studies on cfRNA in neuroblastoma. Firstly, pre-analytical variables concerning the preparation and storage of the plasma are critical [20]. The plasma samples we used were prepared within 24 h after collection and then stored at -20°C . In our first cohort, we used plasma samples that had gone through several cycles of thawing and freezing, and from many of these plasmas, no intact mRNA could be isolated, in contrast to plasma from healthy controls that was only thawed once for the cfRNA isolation. This observation that one freeze–thaw cycle does not affect RNA content is also described by Matthew et al. [27].

The plasma preparation protocol is an equally important consideration if one aims to study cfRNA and the transcripts of interest are also expressed in platelets. In this cohort, a one-step centrifugation protocol was applied to obtain platelet-poor plasma (as we confirmed). Since cell cycle genes are expressed in healthy platelets, the quantitative data had to be corrected for the presence of the variable number of platelets. As we showed that the ratio between our transcripts of interest and the platelet-specific transcript ITGB3 was similar between platelets of different healthy donors, it was possible to correct our data. For future studies, the use of platelet-free plasma might be preferable. Platelet-free plasma was not collected for our cohort but is worth considering in future prospective studies on cfRNA.

Considering the lack of literature on reference genes for cfRNA, we pragmatically included GUSB, which is regularly used as a reference gene for the cellular compartment of peripheral blood for patients with neuroblastoma [9]. In addition, we included B2M as a reference gene [35] as it has been described that B2M is one of the genes highly expressed in plasma, although this finding might partly be caused by its high expression in platelets, as is shown in our data and known from the literature [23,27]. B2M is also an interesting gene specifically for neuroblastoma.

It is part of the major histocompatibility complex (MHC), and neuroblastoma cells downregulate MHC proteins, probably in order to evade the immune system [36,37]. Our data suggest that this downregulation is not mediated by specific expulsion of B2M mRNA from the neuroblastoma cells.

The literature on cfRNA analysis in neuroblastoma patients is scarce. Only a single report by Corrias et al. reports on the analysis of cfRNA by RT-qPCR in neuroblastoma patients, stages 1 to 4, using TH as the only neuroblastoma-specific marker and several reference genes, including B2M [38]. This study aimed to investigate whether the analysis of cfRNA was useful in monitoring disease status, as compared to analysis with the same markers in whole blood. In this study, 6 out of 47 samples were positive for TH (1/4 patients with stage 3 disease at diagnosis, 0/15 patients with stage 4 at diagnosis, 1/13 patients with stage 4 during treatment, and 4/15 patients at relapse). In our study, we increased the number of neuroblastoma-specific genes, and by using the ddPCR instead of RT-qPCR, we could increase sensitivity and were able to precisely quantitate the number of transcripts. Interestingly, in our study, no samples were positive for TH, but almost half of the stage 4 samples were positive for PHOX2B and/or CHRNA3 at diagnosis. In contrast, none of the 10 diagnostic samples from patients with localized disease tested positive, strongly suggesting that the presence of cfRNA is related to the stage of the disease. Corrias et al. conclude that the analysis of cfRNA with TH was not superior for monitoring of treatment response compared to RNA analysis from blood cells. Although our discovery study was not aimed or powered to study this question, our study also found that in only one of the 66 samples obtained during treatment could tumor-specific cfRNA be demonstrated. In addition, we did not find a prognostic difference for patients testing positive for the neuroblastoma-specific cfRNA at diagnosis compared to the negative patients (71% vs. 69%, respectively).

It is known that cell cycle genes belonging to the E2F1 pathway can be highly expressed in malignancies. For neuroblastoma, it is known that MYCN amplification is a feature of aggressive disease [1] and that this in turn can upregulate E2F1 and MCM2 [39,40,41]. CDC6, one of the genes of the E2F1 pathway, is also described as an important player in cell proliferation and cell death in neuroblastoma cells, as illustrated by knockdown experiments by Feng et al. [42]. Recently, Andriessen et al. demonstrated that CDC6 was significantly elevated in plasma from canine patients with malignancies compared to healthy controls [32]. This prompted us to study cell cycle genes in our cohort as well, aiming to overcome the low expression of the neuroblastoma-specific markers in cfRNA. Although CDC6 as well as E2F1 and DHFR were, after correcting for platelet presence, significantly higher in patients

with metastatic disease compared to patients with localized disease and healthy controls, these markers cannot be easily used to discriminate between healthy individuals and neuroblastoma patients at the individual level. Only two patients had increased levels of CDC6 and MCM2 after correcting for background expression; one patient had increased levels of MCM2 and other genes were not increased, except for DHFR. This latter gene was elevated in 14/30 patients with metastatic disease. DHFR plays a role in the cell cycle as an enzyme in the folate biosynthesis pathway and is thereby essential for cell proliferation. Inhibition of DHFR has been used historically in antimicrobial agents (e.g., trimethoprim), rheumatoid disease and cancer (e.g., methotrexate) [43,44]. Our findings on elevated DHFR at diagnosis in neuroblastoma patients with metastatic disease support its crucial role, corresponding to a high proliferation rate in metastatic disease. However, if the level of DHFR would have a linear association with tumor burden, we would expect this to be reflected in the longitudinal samples. But this was not observed in our cohort.

Indeed, in the longitudinal samples, all cell cycle markers had a high variation in expression between patients and within individual patients, whereas B2M was consistently high. Sample collection was not consistent in our cohort beyond the induction treatment phase, which further complicated speculations on their potential as markers for early treatment failure or relapse detection. This underlines that further studies with standardized sampling are essential for future cfRNA research. In addition, studies broadening the perspective on mRNA markers specifically for cfRNA research are necessary since current RNA markers are mostly based on the cellular compartment of blood and might not be suited for cfRNA. Specifically for patients with neuroblastoma, a study including RNA sequencing of the transcriptome of the cell-free compartment at different timepoints could improve understanding of this field immensely and help identify cfRNA markers with diagnostic and prognostic value.

We confirmed that most of the mRNA markers are concentrated in the EV-enriched fractions [18,21,32]. However, unexpectedly, DHFR was found to be mostly present in the higher SEC fractions. This could be due to elution of smaller EV in later fractions or also to packaging of mRNA into protein aggregates; both hypotheses are supported by the literature [21,45,46,47,48] and the presence of B2M and GUSB in these SEC fractions. Further studies using RNase and proteinase on the different SEC fractions could elucidate further if mRNA is truly packaged within EV or only associated with EV. The same approach is possible for cfDNA using DNase, since we mostly demonstrate the presence of cfDNA in the protein-enriched fractions. The literature is still conflicting on this subject [49,50], and it is not inconceivable

that EV cargo could even differ per disease. Furthermore, the method chosen for EV enrichment heavily affects the result of the downstream analysis, and after SEC, the presence of similar-sized lipoprotein particles in the EV-enriched fractions might also result in less pure EV preparations [51,52].

Considering a possible implementation in clinical practice, our study does not immediately show a benefit for EV enrichment prior to cfRNA isolation, especially in respect to time and cost effectiveness. In children, the amount of plasma is the major limiting step, and it seems simpler to just isolate RNA from full plasma than first performing density gradient centrifugation for EV isolation. However, that the concentration of EV can result in enrichment of tumor RNA was indeed recently shown by Stegmaier et al. [53]. They show that their target of interest, the transcripts of the PAX-FOXO or SYT-SSX fusion genes from alveolar rhabdomyosarcoma and synovial sarcoma, respectively, had a higher concentration in EV-derived cfRNA from patient plasma than cfRNA directly from plasma [53]. In future studies, it is important to determine which question needs to be answered. The purity of EV through elaborate isolation procedures can be essential to increase the knowledge of EV cargo and function, whereas a translational goal to improve diagnostic procedures might benefit more from a quick EV enrichment procedure through commercially available precipitating agents which increase the target concentration and thereby the sensitivity of the test.

Conclusions

In this study, we explore the possibilities of different cfRNA markers from plasma as novel biomarkers in patients with neuroblastoma. We discuss the possible variables affecting the detection of cfRNA-based markers and present approaches for correcting for the presence of platelets and background marker expression in plasma. Considering the neuroblastoma-specific markers, we conclude that these are only present in patients with metastatic disease. For the cell cycle markers, we find that many markers are higher in patients than in healthy controls, but only elevated above background expression levels in some metastatic patients. Our experiments on EV using SEC isolation illustrate that the mRNA markers are mostly expressed in EV-enriched SEC fractions, whereas cfDNA is mostly present in EV-poor SEC fractions. This study can form a starting point for further research into the potential of cfRNA-based analysis of liquid biopsies since this can be an additional approach to the more common analysis of cfDNA for liquid biopsies.

Acknowledgements

We are grateful to Jalenka van Wijk for performing the pilot experiments for this study. We thank Floris van Alphen for his help with the TCA assays and Herbert Koster for his help with the experiments on the platelets. We are grateful to Nicole van der Wel and Anita Grootemaat for their help with the electron microscopy on the SEC fractions.



References

1. Matthay K.K., Maris J.M., Schleiermacher G., Nakagawara A., Mackall C.L., Diller L., Weiss W.A. Neuroblastoma. *Nat. Rev. Dis. Prim.* 2016;2:16078. doi: 10.1038/nrdp.2016.78.
2. Pearson A.D., Pinkerton C.R., Lewis I.J., Imeson J., Ellershaw C., Machin D. High-dose rapid and standard induction chemotherapy for patients aged over 1 year with stage 4 neuroblastoma: A randomised trial. *Lancet Oncol.* 2008;9:247–256. doi: 10.1016/S1470-2045(08)70069-X.
3. Kreissman S.G., Seeger R.C., Matthay K.K., London W.B., Sposto R., A Grupp S., A Haas-Kogan D., LaQuaglia M.P., Yu A.L., Diller L., et al. Purged versus non-purged peripheral blood stem-cell transplantation for high-risk neuroblastoma (COG A3973): A randomised phase 3 trial. *Lancet Oncol.* 2013;14:999–1008. doi: 10.1016/S1470-2045(13)70309-7.
4. Van Paemel R., Vlug R., De Preter K., Van Roy N., Speleman F., Willems L., Lammens T., Laureys G., Schleiermacher G., Tytgat G.A.M., et al. The pitfalls and promise of liquid biopsies for diagnosing and treating solid tumors in children: A review. *Eur. J. Pediatr.* 2020;179:191–202. doi: 10.1007/s00431-019-03545-y.
5. Alix-Panabières C., Pantel K. Clinical Applications of Circulating Tumor Cells and Circulating Tumor DNA as Liquid Biopsy. *Cancer Discov.* 2016;6:479–491. doi: 10.1158/2159-8290.CD-15-1483.
6. Stutterheim J., Gerritsen A., Zappeij-Kannegieter L., Kleijn I., Dee R., Hooft L., van Noesel M.M., Bierings M., Berthold F., Versteeg R., et al. *PHOX2B* Is a Novel and Specific Marker for Minimal Residual Disease Testing in Neuroblastoma. *J. Clin. Oncol.* 2008;26:5443–5449. doi: 10.1200/JCO.2007.13.6531.
7. Yáñez Y., Hervás D., Grau E., Oltra S., Pérez G., Palanca S., Bermúdez M., Márquez C., Cañete A., Castel V. TH and DCX mRNAs in peripheral blood and bone marrow predict outcome in metastatic neuroblastoma patients. *J. Cancer Res. Clin. Oncol.* 2016;142:573–580. doi: 10.1007/s00432-015-2054-7.
8. Van Wezel E.M., van Zogchel L.M.J., van Wijk J., Timmerman I., Vo N.K., Zappeij-Kannegieter L., deCarolis B., Simon T., van Noesel M.M., Molenaar J.J., et al. Mesenchymal Neuroblastoma Cells Are Undetected by Current mRNA Marker Panels: The Development of a Specific Neuroblastoma Mesenchymal Minimal Residual Disease Panel. *JCO Precis. Oncol.* 2019;3:1–11. doi: 10.1200/PO.18.00413.
9. Stutterheim J., Gerritsen A., Zappeij-Kannegieter L., Yalcin B., Dee R., van Noesel M.M., Berthold F., Versteeg R., Caron H.N., van der Schoot C.E., et al. Detecting Minimal Residual Disease in Neuroblastoma: The Superiority of a Panel of Real-Time Quantitative PCR Markers. *Clin. Chem.* 2009;55:1316–1326. doi: 10.1373/clinchem.2008.117945.
10. Van Zogchel L.M.J., Lak N.S.M., Verhagen O.J.H.M., Tissoudali A., Nuru M.G., Gelineau N.U., Zappeij-Kannegieter L., Javadi A., Zijtregtop E.A.M., Merks J.H.M., et al. Novel Circulating Hypermethylated RASSF1A ddPCR for Liquid Biopsies in Patients With Pediatric Solid Tumors. *JCO Precis. Oncol.* 2021;5:1738–1748. doi: 10.1200/PO.21.00130.
11. Lodrini M., Sprüssel A., Astrahantseff K., Tiburtius D., Konschak R., Lode H.N., Fischer M., Keilholz U., Eggert A., Deubzer H.E. Using droplet digital PCR to analyze *MYCN* and *ALK* copy number in plasma from patients with neuroblastoma. *Oncotarget.* 2017;8:85234–85251. doi: 10.18632/oncotarget.19076.
12. Lodrini M., Graef J., Thole-Kliesch T.M., Astrahantseff K., Sprüssel A., Grimaldi M., Peitz C., Linke R.B., Hollander J.F., Lankes E., et al. Targeted Analysis of Cell-free Circulating Tumor DNA is Suitable for Early Relapse and Actionable Target Detection in Patients with Neuroblastoma. *Clin. Cancer Res.* 2022;28:1809–1820. doi: 10.1158/1078-0432.CCR-21-3716.

13. Van Zogchel L.M.J., van Wezel E.M., van Wijk J., Stutterheim J., Bruins W.S.C., Zappeij-Kannegieter L., Tirza J.E., Iedan R.N., Verly C., Godelieve A.M., et al. Hypermethylated RASSF1A as Circulating Tumor DNA Marker for Disease Monitoring in Neuroblastoma. *JCO Precis. Oncol.* 2020;4:291–306. doi: 10.1200/PO.19.00261.
14. Wan J.C.M., Massie C., Garcia-Corbacho J., Mouliere F., Brenton J.D., Caldas C., Pacey S., Baird R., Rosenfeld N. Liquid biopsies come of age: Towards implementation of circulating tumour DNA. *Nat. Rev. Cancer.* 2017;17:223–238. doi: 10.1038/nrc.2017.7.
15. Skog J., Wurdinger T., van Rijn S., Meijer D.H., Gainche L., Curry W.T., Jr., Sena-Esteves M., Carter B.S., Krichevsky A.M., Breakefield X.O. Glioblastoma microvesicles transport RNA and proteins that promote tumour growth and provide diagnostic biomarkers. *Nat. Cell Biol.* 2008;10:1470–1476. doi: 10.1038/ncb1800.
16. Hulstaert E., Morlion A., Avila Cobos F., Verniers K., Nuytens J., Vanden Eynde E., Yigit N., Anckaert J., Geerts A., Hindryckx P., et al. Charting Extracellular Transcriptomes in The Human Biofluid RNA Atlas. *Cell Rep.* 2020;33:108552. doi: 10.1016/j.celrep.2020.108552.
17. Herriott R.M., Connolly J.H., Gupta S. Blood Nucleases and Infectious Viral Nucleic Acids. *Nature.* 1961;189:817–820. doi: 10.1038/189817a0.
18. Bebelman M.P., Smit M.J., Pegtel D.M., Baglio S.R. Biogenesis and function of extracellular vesicles in cancer. *Pharmacol. Ther.* 2018;188:1–11. doi: 10.1016/j.pharmthera.2018.02.013.
19. Xavier C.P.R., Caires H.R., Barbosa M.A.G., Bergantim R., Guimarães J.E., Vasconcelos M.H. The Role of Extracellular Vesicles in the Hallmarks of Cancer and Drug Resistance. *Cells.* 2020;9:1141. doi: 10.3390/cells9051141.
20. Grözl D., Hauch S., Schlumpberger M., Guenther K., Voss T., Sprenger-Haussels M., Oelmüller U. Liquid Biopsy Preservation Solutions for Standardized Pre-Analytical Workflows—Venous Whole Blood and Plasma. *Curr. Pathobiol. Rep.* 2018;6:275–286. doi: 10.1007/s40139-018-0180-z.
21. Arroyo J.D., Chevillet J.R., Kroh E.M., Ruf I.K., Pritchard C.C., Gibson D.F., Mitchell P.S., Bennett C.F., Pogosova-Agadjanyan E.L., Stirewalt D.L., et al. Argonaute2 complexes carry a population of circulating microRNAs independent of vesicles in human plasma. *Proc. Natl. Acad. Sci. USA.* 2011;108:5003–5008. doi: 10.1073/pnas.1019055108.
22. Wurdinger T., In 't Veld S.G.J.G., Best M.G. Platelet RNA as Pan-Tumor Biomarker for Cancer Detection. *Cancer Res.* 2020;80:1371–1373. doi: 10.1158/0008-5472.CAN-19-3684.
23. Rowley J.W., Oler A.J., Tolley N.D., Hunter B.N., Low E.N., Nix D.A., Yost C.C., Zimmerman G.A., Weyrich A. Genome-wide RNA-seq analysis of human and mouse platelet transcriptomes. *Blood.* 2011;118:e101–e111. doi: 10.1182/blood-2011-03-339705.
24. Rowley J.W., Schwertz H., Weyrich A.S. Platelet mRNA. *Curr. Opin. Hematol.* 2012;19:385–391. doi: 10.1097/MOH.0b013e328357010e.
25. Morini M., Cangelosi D., Segalerba D., Marimpietri D., Raggi F., Castellano A., Fruci D., de Mora J.F., Cañete A., Yáñez Y., et al. Exosomal microRNAs from Longitudinal Liquid Biopsies for the Prediction of Response to Induction Chemotherapy in High-Risk Neuroblastoma Patients: A Proof of Concept SIOPEN Study II. *Cancers.* 2019;11:1476. doi: 10.3390/cancers11101476.
26. Ma J., Xu M., Yin M., Hong J., Chen H., Gao Y., Xie C., Shen N., Gu S., Mo X. Exosomal hsa-miR199a-3p Promotes Proliferation and Migration in Neuroblastoma. *Front. Oncol.* 2019;9:459. doi: 10.3389/fonc.2019.00459.
27. Larson M.H., Pan W., Kim H.J., Mauntz R.E., Stuart S.M., Pimentel M., Zhou Y., Knudsgaard P., Demas V., Aravanis A.M., et al. A comprehensive characterization of the cell-free transcriptome reveals tissue- and subtype-specific biomarkers for cancer detection. *Nat. Commun.* 2021;12:2357. doi: 10.1038/s41467-021-22444-1.

28. Harashima H., Dissmeyer N., Schnittger A. Cell cycle control across the eukaryotic kingdom. *Trends Cell Biol.* 2013;23:345–356. doi: 10.1016/j.tcb.2013.03.002.
29. Matthews H.K., Bertoli C., de Bruin R.A.M. Cell cycle control in cancer. *Nat. Rev. Mol. Cell Biol.* 2021;23:74–88. doi: 10.1038/s41580-021-00404-3.
30. Thurlings I., de Bruin A. E2F Transcription Factors Control the Roller Coaster Ride of Cell Cycle Gene Expression. *Methods Mol. Biol.* 2016;1342:71–88.
31. Bongiovanni L., Andriessen A., Silvestri S., Porcellato I., Brachelente C., de Bruin A. H2AFZ: A Novel Prognostic Marker in Canine Melanoma and a Predictive Marker for Resistance to CDK4/6 Inhibitor Treatment. *Front. Vet. Sci.* 2021;8:705359. doi: 10.3389/fvets.2021.705359.
32. Andriessen A., Bongiovanni L., Driedonks T.A.P., van Liere E., Seijger A., Hegeman C.V., van Nimwegen S.A., Galac S., Westendorp B., Hoen E.N.M.N., et al. CDC6: A novel canine tumour biomarker detected in circulating extracellular vesicles. *Veter Comp. Oncol.* 2021;20:381–392. doi: 10.1111/vco.12781.
33. Ando K., Nakagawara A. Acceleration or Brakes: Which Is Rational for Cell Cycle-Targeting Neuroblastoma Therapy? *Biomolecules.* 2021;11:750. doi: 10.3390/biom11050750.
34. Van Zogchel L., de Carolis B., van Wezel E., Stutterheim J., Zappeij-Kannegieter L., van Doornum M., Schumacher-Kuckelkorn R., Gecht J., Simon T., Caron H., et al. *Pediatric Blood & Cancer.* Wiley; Hoboken, NJ, USA: 2018. Detection of Minimal Residual Disease (MRD) in High Risk Neuroblastoma Correlates with Outcome: Final Results of International GPOH-DCOG Prospective Validation Study; p. 538.
35. Beillard E., Pallisgaard N., van der Velden V.H.J., Bi W., Dee R., van der Schoot E., Delabesse E., Macintyre E., Gottardi E., Saglio G., et al. Evaluation of candidate control genes for diagnosis and residual disease detection in leukemic patients using ‘real-time’ quantitative reverse-transcriptase polymerase chain reaction (RQ-PCR)—A Europe against cancer program. *Leukemia.* 2003;17:2474–2486. doi: 10.1038/sj.leu.2403136.
36. Corrias M.V., Occhino M., Croce M., De Ambrosio A., Pistillo M.P., Bocca P., Pistoia V., Ferrini S. Lack of HLA-class I antigens in human neuroblastoma cells: Analysis of its relationship to TAP and tapasin expression. *Tissue Antigens.* 2001;57:110–117. doi: 10.1034/j.1399-0039.2001.057002110.x.
37. Spel L., Schiepers A., Boes M. NFκB and MHC-1 Interplay in Neuroblastoma and Immunotherapy. *Trends Cancer.* 2018;4:715–717. doi: 10.1016/j.trecan.2018.09.006.
38. Corrias M.V., Pistorio A., Cangemi G., Tripodi G., Bs B.C., Scaruffi P., Fardin P., Garaventa A., Pistoia V., Haupt R. Detection of cell-free RNA in children with neuroblastoma and comparison with that of whole blood cell RNA. *Pediatr. Blood Cancer.* 2010;54:897–903. doi: 10.1002/pbc.22498.
39. Koppen A., Ait-Aissa R., Koster J., Van Sluis P.G., Øra I., Caron H.N., Volckmann R., Versteeg R., Valentijn L.J. Direct regulation of the minichromosome maintenance complex by MYCN in neuroblastoma. *Eur. J. Cancer.* 2007;43:2413–2422. doi: 10.1016/j.ejca.2007.07.024.
40. Liu X., Cai Y., Cheng C., Gu Y., Hu X., Chen K., Wu Y., Wu Z. PCLAF promotes neuroblastoma G1/S cell cycle progression via the E2F1/PTTG1 axis. *Cell Death Dis.* 2022;13:178. doi: 10.1038/s41419-022-04635-w.
41. Wang H., Wang X., Xu L., Zhang J., Cao H. Prognostic significance of MYCN related genes in pediatric neuroblastoma: A study based on TARGET and GEO datasets. *BMC Pediatr.* 2020;20:314. doi: 10.1186/s12887-020-02219-1.
42. Feng L., Barnhart J.R., Seeger R.C., Wu L., Keshelava N., Huang S.-H., Jong A. Cdc6 knockdown inhibits human neuroblastoma cell proliferation. *Mol. Cell. Biochem.* 2008;311:189–197. doi: 10.1007/s11010-008-9709-5.

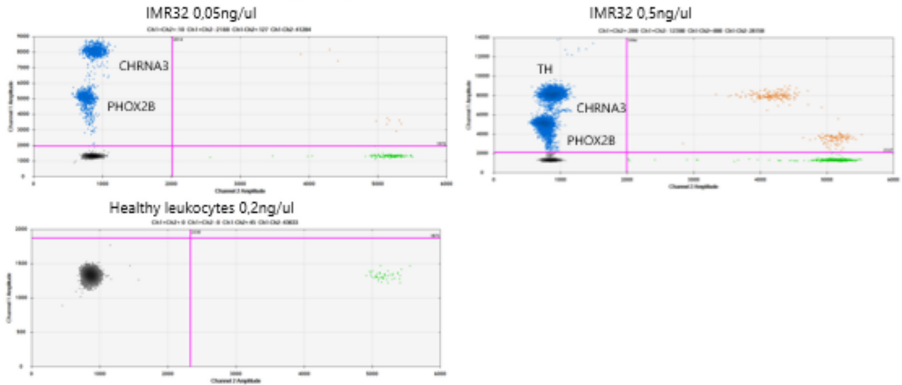
43. Bhagat K., Kumar N., Gulati H.K., Sharma A., Kaur A., Singh J.V., Singh H., Bedi P.M.S. Dihydrofolate reductase inhibitors: Patent landscape and phases of clinical development (2001–2021) *Expert Opin. Ther. Patents*. 2022;32:1079–1095. doi: 10.1080/13543776.2022.2130752.
44. Raimondi M.V., Randazzo O., La Franca M., Barone G., Vignoni E., Rossi D., Collina S. DHFR Inhibitors: Reading the Past for Discovering Novel Anticancer Agents. *Molecules*. 2019;24:1140. doi: 10.3390/molecules24061140.
45. Böing A.N., van der Pol E., Grootemaat A.E., Coumans F.A.W., Sturk A., Nieuwland R. Single-step isolation of extracellular vesicles by size-exclusion chromatography. *J. Extracell. Vesicles*. 2014;3:23430. doi: 10.3402/jev.v3.23430.
46. Clayton A., Boilard E., Buzas E.I., Cheng L., Falcón-Perez J.M., Gardiner C., Gustafson D., Gualerzi A., Hendrix A., Hoffman A., et al. Considerations towards a roadmap for collection, handling and storage of blood extracellular vesicles. *J. Extracell. Vesicles*. 2019;8:1647027. doi: 10.1080/20013078.2019.1647027.
47. Théry C., Witwer K.W., Aikawa E., Alcaraz M.J., Anderson J.D., Andriantsitohaina R., Antoniou A., Arab T., Archer F., Atkin-Smith G.K., et al. Minimal information for studies of extracellular vesicles 2018 (MISEV2018): A position statement of the International Society for Extracellular Vesicles and update of the MISEV2014 guidelines. *J. Extracell. Vesicles*. 2018;7:1535750. doi: 10.1080/20013078.2018.1535750.
48. Coumans F.A.W., Brisson A.R., Buzas E.I., Dignat-George F., Drees E.E.E., El-Andaloussi S., Emanuelli C., Gasecka A., Hendrix A., Hill A.F., et al. Methodological Guidelines to Study Extracellular Vesicles. *Circ. Res*. 2017;120:1632–1648. doi: 10.1161/CIRCRESAHA.117.309417.
49. Liu H., Tian Y., Xue C., Niu Q., Chen C., Yan X. Analysis of extracellular vesicle DNA at the single-vesicle level by nano-flow cytometry. *J. Extracell. Vesicles*. 2022;11:12206. doi: 10.1002/jev2.12206.
50. Thakur B.K., Zhang H., Becker A., Matei I., Huang Y., Costa-Silva B., Zheng Y., Hoshino A., Brazier H., Xiang J., et al. Double-stranded DNA in exosomes: A novel biomarker in cancer detection. *Cell Res*. 2014;24:766–769. doi: 10.1038/cr.2014.44.
51. Van Deun J., Mestdagh P., Sormunen R., Cocquyt V., Vermaelen K., Vandesompele J., Bracke M., De Wever O., Hendrix A. The impact of disparate isolation methods for extracellular vesicles on downstream RNA profiling. *J. Extracell. Vesicles*. 2014;3:24858. doi: 10.3402/jev.v3.24858.
52. Vergauwen G., Tulkens J., Pinheiro C., Cobos F.A., Dedeyne S., De Scheerder M., Vandekerckhove L., Impens F., Miinalainen I., Braems G., et al. Robust sequential biophysical fractionation of blood plasma to study variations in the biomolecular landscape of systemically circulating extracellular vesicles across clinical conditions. *J. Extracell. Vesicles*. 2021;10:e12122. doi: 10.1002/jev2.12122.
53. Stegmaier S., Sparber-Sauer M., Aakcha-Rudel E., Münch P., Reeh T., Feuchtgruber S., Hallmen E., Blattmann C., Bielack S., Klingebiel T., et al. Fusion transcripts as liquid biopsy markers in alveolar rhabdomyosarcoma and synovial sarcoma: A report of the Cooperative Weichteilsarkom Studiengruppe (CWS) *Pediatr. Blood Cancer*. 2022;69:29652. doi: 10.1002/pbc.29652.

Supplemental data

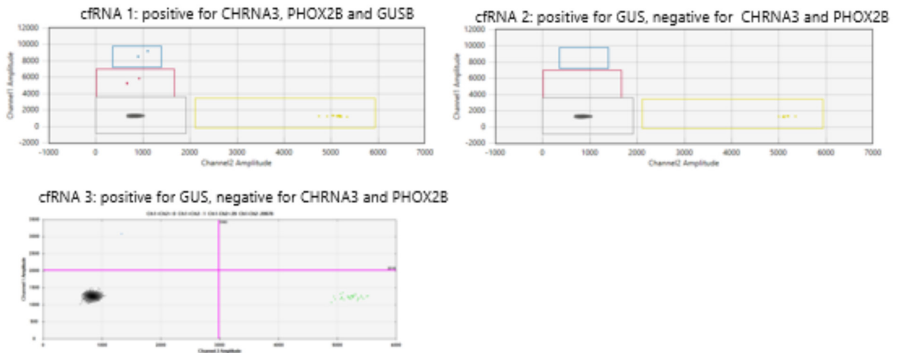
Supplemental table 1. Sequences of ddPCR assays.

MCM2	Forward	CACATCCATGTCCGCATCTC
	Reverse	GTTGCAGTTGACTTGACCATGC
	Probe	/5HEX/ACTGGCGTC/ZEN/CTGCCCCAGCTC/3IABkFQ/
CDC6	Forward	CAAATTCTGAGCAGAGATGTCCACT
	Reverse	TGACATCCATCTCCCTTTCCC
	Probe	/56-FAM/CCCAGATCG/ZEN/GCTGCCTGCCA/3IABkFQ/
H2AFZ	Forward	GTTTCCCGCTCGCAGAGA
	Reverse	GTGAGGTACTCCAGGATGGCTG
	Probe	/56-FAM/CATGGACGT/ZEN/GTGGGCGCGACT/3IABkFQ/
ATAD2	Forward	CAACTTGCTAATGGCAGGCA
	Reverse	TTCTAGCCCTCAATGACCGAGTA
	Probe	/5HEX/AGCCTGCTG/ZEN/TCTGGCCAACTGCCT/3IABkFQ/
E2F1	Forward	CAGCTGGACCACCTGATGAATA
	Reverse	GGTCTGCAATGCTACGAAGGTC
	Probe	/56-FAM/CCTCGGAGA/ZEN/GCAGGCGCAGC/3IABkFQ/
DHFR	Forward	GGTTCGCTAAACTGCATCGTC
	Reverse	AGAGGTTGTGGTCATTCTCTGGA
	Probe	/56-FAM/CGGTGGCCA/ZEN/GGGCAGGTCC/3IABkFQ/
PHOX2B	Forward	GGCACCCCTCAGGGACCA
	Reverse	CTGCGCGCTCCTGCTT
	Probe	/56-FAM/CCAGAACCG/ZEN/CCGCGCCAA/3IABkFQ/
B2M	Forward	GAGTATGCCTGCCGTGTG
	Reverse	AATCCAAATGCGGCATCT
	Probe	/5HEX/CCTCCATGA/ZEN/TGCTGCTTACATGTCTC/3IABkFQ/
GUSB	Forward	GAAAATATGTGGTTGGAGAGCTCATT
	Reverse	CCGAGTGAAGATCCCCTTTTTA
	Probe	/5HEX/CCAGCACTC/ZEN/TCGTGGTGACTGTTCA/3IABkFQ/
TH	Forward	ATT GCT GAG ATC GCC TTC CA
	Reverse	AAT CTC CTC GGC GGT GTA CTC
	Probe	/56-FAM/ACA GGC ACG GCG/ZEN/ ACC CGA TTC /3IABkFQ/
CHRNA3	Forward	GTCCATGTCTCAGCTGGTGAAG
	Reverse	TTCCATTTTCAGCTTGTAGTCATTCC
	Probe	/56-FAM/CAGATCATG/ZEN/GAGACCAACCTGTGGCTC/3IABkFQ/
HPA1A/B	Forward	CCAACATCTGTACCACGCGA
	Reverse	GGCACAGTTATCCTTCAG
	HPA1A probe	/56-FAM/CCTGCCTCT/ZEN/GGGCTCACCTC/3IABkFQ/
	HPA1B probe	/56-FAM/CCTGCCTCC/ZEN/GGGCTCACCTC/3IABkFQ/

A Positive controls for neuroblastoma-specific panel



B 3 patient plasma examples for neuroblastoma-specific panel



Supplemental Figure 1. 2D plots from the ddPCR assays illustrating gating strategies for the neuroblastoma-specific genes. **A.** Neuroblastoma-specific assay in controls (positive control: neuroblastoma cell line IMR32 0,05 ng/ul, 0,5 ng/ul and negative control: healthy leukocytes 0,2 ng/ul). **B.** cfrNA detection by ddPCR from plasma of 3 patients, cfrNA1 was positive for *CHRNA3*, *PHOX2B* and *GUSB*, cfrNA2 and cfrNA3 only for *GUSB*.

Please note that cfrNA 1 and 2 were analyzed with QX Manager 1.2 Standard Edition software (Bio Rad): pink droplets represent *PHOX2B*, blue droplets *CHRNA3* and yellow droplets *GUSB*. cfrNA 3 was analyzed in QuantaSoft 1.7.4 software (Bio Rad), green droplets represent *GUSB*.

Droplets are only counted as positive for *PHOX2B* if they are located exactly above the negative cluster around an amplitude of 5000.

Supplemental Table 2. Results of the neuroblastoma-specific panel and *GUSB* in plasma of 40 healthy controls.

Control	GUS	PHOX2B	TH	CHRNA3
ID	copies/ml	copies/ml	copies/ml	copies/ml
1	56.49	0.00	0.00	0.00
2	196.11	0.00	0.00	0.00
3	153.71	0.00	0.00	0.00
4	42.40	0.00	0.00	0.00
5	97.68	0.00	0.00	0.00
6	237.75	0.00	0.00	0.00
7	40.66	0.00	0.00	0.00
8	111.30	0.00	0.00	0.00
9	102.98	0.00	0.00	0.00
10	52.47	0.00	0.00	0.00
11	104.49	0.00	0.00	0.00
12	96.92	0.00	0.00	0.00
13	91.62	0.00	0.00	0.00
14	58.38	0.00	0.00	0.00
15	51.56	0.00	0.00	0.00
16	81.77	0.00	0.00	0.00
17	36.42	0.00	0.00	0.00
18	180.21	0.00	0.00	0.00
19	67.39	0.00	0.00	0.00
20	60.65	0.00	0.00	0.00
21	50.73	0.00	0.00	0.00
22	10.60	0.00	0.00	0.00
23	35.59	0.00	0.00	0.00
24	6.81	0.00	0.00	0.00
25	62.09	0.00	0.00	0.00
26	12.87	0.00	0.00	0.00
27	15.14	0.00	0.00	0.00
28	49.97	0.00	0.00	0.00
29	24.99	0.00	0.00	0.00
30	31.80	0.00	0.00	0.00
31	15.14	0.00	0.00	0.00
32	15.14	0.00	0.00	0.00
33	6.81	0.00	0.00	0.00
34	6.81	0.00	0.00	0.00
35	29.53	0.00	0.00	0.00
36	15.14	0.00	0.00	0.00
37	19.69	0.00	0.00	0.00
38	10.60	0.00	0.00	0.00
39	67.39	0.00	0.00	0.00
40	6.06	0.00	0.00	0.00

Supplemental Table 3. Patient characteristics of the first and second cohort.

	NBLnr	Gender	Age at Dx (months)	Stage	Risk	MYCN	LOH1p	Gain17q	ALK	Tumor location	BM	Event	DOD	
First cohort	834	0	21	3	2	1	1	1	1	0	1	2	0	
	865	0	19	3	2	1	NA	NA	NA	NA	NA	0	0	
	2011	1	43	3	2	0	0	NA	1	0	1	0	0	
	2012	1	56	3	2	1	1	1	1	0	1	2	1	
	2016	1	86	3	2	0	0	1	0	0	1	1	1	
	2022	0	26	3	2	1	1	2	1	0	1	2	1	
	2024	0	224	3	2	2	0	1	2	0	1	2	1	
	2026	1	28	2	2	1	1	2	0	2	0	0	0	
	2029	1	78	3	2	2	1	2	2	0	1	2	1	
	2032	1	133	3	2	2	0	2	2	0	NA	0	0	
	2033	1	5	3	1	0	3	2	1	0	1	0	0	
	2034	1	59	3	2	2	0	1	0	0	0	0	0	
	2043	0	76	3	2	0	0	1	2	3	1	2	1	
	2046	1	79	3	2	0	0	2	0	NA	1	2	1	
	2047	0	14	3	2	1	1	1	0	0	1	2	0	
	2048	1	50	3	2	0	0	1	0	2	1	4	1	
	2049	0	128	3	2	2	0	1	2	1	1	1	1	
	2050	0	49	3	2	0	1	1	0	0	1	1	1	
	2051	0	57	3	2	0	0	2	0	0	1	2	1	
	2052	0	17	3	2	0	0	1	0	1	0	0	0	
	2054	0	8	3	2	1	1	1	0	5	0	0	0	
	2055	0	35	2	1	2	0	0	2	0	0	1	0	
	Second cohort	2079	0	28.3	0	0	0	1	1	0	0	0	0	0
		2097	0	5.9	0	0	0	0	1	0	0	0	0	0
		2102	1	20.6	3	2	0	0	0	0	0	0	1	1
2115		1	3.7	0	0	0	2	1	0	0	0	0	0	
2117		0	13.6	3	2	0	1	1	0	0	1	0	0	
2124		1	32.8	0	0	0	0	0	0	0	0	0	0	
2126		0	13.6	0	0	0	0	0	0	1	0	0	0	
2141		1	45.1	3	2	0	0	1	0	1	1	1	0	
2143		1	56.8	3	2	2	1	1	1	1	1	1	0	
2144		0	52.6	3	2	2	1	1	0	1	1	0	0	
2146		1	32.9	3	2	0	0	1	0	1	1	2	1	
2147		1	62.9	2	0	0	1	1	0	1	0	2	0	
2148		0	17.5	0	0	2	0	1	0	2	0	0	0	
2149		1	10.4	0	0	0	0	1	0	2	0	0	0	
2150		1	95.5	3	2	0	1	1	0	1	1	0	0	
2151		1	36.7	3	2	1	1	1	0	1	1	2	0	
2152		0	12.3	3	2	1	1	1	0	2	0	1	1	
2153		0	33.4	3	2	1	1	1	0	1	0	1	1	
2155		1	1.2	0	0	0	0	1	0	1	0	3	0	
2157		1	9.7	3	2	1	1	1	1	1	1	1	0	
2160		1	8.2	3	2	1	1	1	0	1	0	1	1	
2161		1	11.1	3	1	0	0	1	0	1	1	1	0	
2163		1	52.5	3	2	0	1	1	0	2	0	0	0	
2164		0	29.2	3	2	0	0	1	0	2	0	0	0	
2165		1	141.4	0	0	0	0	0	1	1	0	0	0	
2166		1	13.2	3	2	1	1	1	0	2	1	2	1	
2169		0	0.1	0	0	0	0	0	0	2	0	0	0	
2171		1	9.8	3	1	0	0	1	0	3	1	0	0	
2172		1	153.7	3	2	0	0	0	0	1	1	1	0	
2174		1	1.5	3	1	0	NA	NA	NA	1	1	0	0	
2175		0	138.4	3	2	1	1	0	0	0	1	0	0	
2177		0	30.3	3	2	0	0	1	0	1	1	2	0	
2179		1	11	3	1	0	0	1	0	1	1	1	1	
2181		1	49.3	3	2	0	0	1	0	0	0	0	0	
2183		0	56.8	3	2	0	0	1	0	1	1	0	0	
2184		1	25.1	3	2	0	0	1	0	0	1	1	1	
2187		0	76.3	3	2	0	0	1	0	0	1	1	0	
2193		0	35.8	3	2	1	1	1	1	0	1	1	0	
2194		0	13.33	3	2	1	1	1	0	0	0	1	1	
2196		0	4.4	3	1	0	1	1	0	0	1	1	1	
2211	1	41.73	3	2	0	0	0	1	0	1	1	0		

ALK; 0=ALK gene wild type, 1=ALK mutation, 2=gain of ALK

BM; 0=no bone marrow invasion, 1=bone marrow invasion

DOD; 0=did not die of disease, 1=died of disease

Dx; diagnosis

Event; 0=no event, 1=progressive disease, 2=relapse, 3=second malignancy, 4=death to other cause

Gain 17q; 0=no gain of chromosome 17q, 1= gain of 17q, 2=partial gain of 17q

Gender; 0=male, 1=female

LOH1p; 0=no loss of heterozygosity of chromosome 1p, 1=LOH1p, 2=partial LOH1p

MYCN; 0=no aberration in MYCN gene, 1=MYCN amplification, 2=gain in MYCN

NBLnr; unique patient identifier

Stage; number corresponds to International Neuroblastoma Staging System Committee (INSS) stage for neuroblastoma

Tumor location; 0=adrenal, 1=abdominal, 2=thoracic, 3=thoracic-abdominal, 4=paravertebral, 5=adrenal paravertebral thoracic



Supplemental Table 4. Results of ddPCR (copies/ml) of the genes in the first cohort.

NBL ID	Moment	ddPCR (copies/ml plasma)			
		PHOX2B	CHRNA3	TH	GUSBnbl
834	Relapse	0.00	0.00	0.00	2.04
834	After 2nd N8 Relapse therapy	0.00	0.00	0.00	4.18
865	Before ASCT	0.00	0.00	0.00	2.18
2011	3 month after eot	0.00	0.00	0.00	0.00
2012	After IT during relapse	0.00	0.00	0.00	0.00
2016	Relapse therapy	0.00	0.00	0.00	0.00
2016	after Gemcitabine-MIBG	0.00	0.00	0.00	2.17
2022	Relapse	0.00	0.00	0.00	2.21
2022	2 months relapse therapy	0.00	0.00	0.00	2.22
2024	Before start high-dose chemotherapy	0.00	0.00	0.00	0.00
2024	After ASCT	0.00	0.00	0.00	4.53
2026	EOT	0.00	0.00	0.00	13.33
2029	During anti GD2	0.00	0.00	0.00	0.00
2032	After salvage N8	0.00	0.00	0.00	2.22
2033	Before N7	0.00	0.00	0.00	0.00
2034	After ASCT	0.00	0.00	0.00	0.00
2043	Relapse	10.98	0.00	0.00	127.21
2043	After N5/N6 and 2xN8	0.00	0.00	0.00	16.73
2043	After 3rd N5/N6 relapse therapy	0.00	0.00	0.00	95.40
2043	After 2nd relapse Ct	0.00	0.00	0.00	2.23
2046	Diagnosis	0.00	0.00	0.00	8.63
2046	After 2nd N5/N6	0.00	0.00	0.00	37.40
2046	After 2nd N5/N6	0.00	0.00	0.00	2.16
2047	After 3rd N5/N6	0.00	0.00	0.00	8.40
2047	Before ASCT	0.00	0.00	0.00	15.75
2047	After 1st N5/N6	0.00	0.00	0.00	8.48
2048	Diagnosis	0.00	0.00	0.00	4.12
2048	After 1st N5/N6	0.00	0.00	0.00	0.00
2048	After 2nd N5/N6	0.00	0.00	0.00	2.20
2049	Diagnosis	0.00	0.00	0.00	2.23
2049	After 2nd N5/N6	0.00	0.00	0.00	4.22
2050	Diagnosis	2.07	0.00	0.00	2.07
2050	After 1st N5/N6	0.00	0.00	0.00	0.00
2051	Relapse	0.00	0.00	0.00	2.33
2052	Diagnosis	0.00	0.00	0.00	0.00
2052	After 2nd N5/N6	0.00	0.00	0.00	0.00
2054	Diagnosis	0.00	0.00	0.00	0.00
2055	Tumor growth during wait-and-see	0.00	0.00	0.00	13.63

ASCT; autologous stem cell transplantation

EOT; end of treatment

GUSBnbl; GUSB as included in the neuroblastoma-specific assay

GUSBc; GUSB as included in the 'cell cycle' assay

NBL ID; unique patient identifier

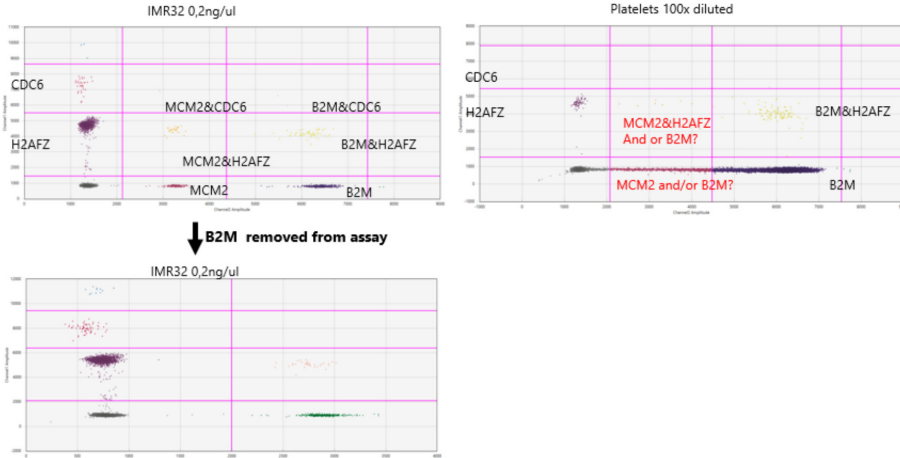
Supplemental Table 5. Results of the ddPCR for DNA-based targets (methylated RASSF1A and ACTB), mRNA based targets (neuroblastoma-specific panel with PHOX2B, CHRNA3, TH and GUSB and cell cycle markers CDC6, ATAD2, DHFR, E2F1, H2AFZ, MCM2, GUSB, HPA1A/B and B2M) in the second cohort. Please note that the cell cycle markers are not corrected for platelets in this table.

NBL ID	Stage	DNA targets				Neuroblastoma specific mRNA markers				Cell cycle mRNA markers						
		RASSF1A-M copies/ml	ACTB (M) plus copies/ml	PHOX2B copies/ml	CHRNA3 TH copies/ml	GUSnb1 copies/ml	CDC6 copies/ml	ATAD2 copies/ml	DHFR copies/ml	E2F1 copies/ml	H2AFZ copies/ml	MCM2 copies/ml	GUSB copies/ml	HPA1A/B copies/ml	B2M copies/ml	
2079	1	3142.9	3661.4	0.0	0.0	0.0	4.6	2.3	29.5	6.8	277.9	13.6	15.8	78.0	3831.3	
2097	1	17600.0	17285.7	0.0	0.0	22.1	11.8	17.8	147.6	188.5	1052.5	106.8	78.7	3642.0	73218.7	
2115	1	785.7	801.4	0.0	0.0	0.5	0.0	0.0	23.5	2.4	90.9	9.8	4.7	58.8	1438.6	
2124	1	0.0	3465.0	0.0	0.0	6.3	0.0	2.3	59.8	11.5	389.2	15.7	18.4	607.3	12720.5	
2126	1	2734.3	3441.4	0.0	0.0	NA	0.0	0.0	20.1	4.5	109.8	0.0	6.7	109.8	2877.3	
2148	1	286.0	9328.0	0.0	0.0	20.9	2.3	22.3	173.4	89.3	1113.0	44.5	95.4	3331.6	49594.9	
2149	1	0.0	19305.0	0.0	0.0	3.5	6.8	12.6	136.3	45.4	483.8	75.1	22.7	376.3	15522.1	
2155	1	79.8	17847.5	0.0	0.0	1.4	11.1	6.7	220.3	51.6	885.9	81.8	74.1	645.9	25592.1	
2165	1	8.3	2282.5	0.0	0.0	2.6	0.0	0.0	34.1	2.3	102.2	9.1	2.3	236.2	4217.5	
2169	1	535.3	10413.3	0.0	0.0	10.4	11.9	9.0	195.4	123.4	1022.2	133.3	62.8	592.9	20216.5	
2102	4	64606.7	119533.3	0.0	0.0	14.0	4.9	7.1	1007.0	142.3	908.6	141.6	52.2	832.9	28848.3	
2117	4	48714.3	55471.4	0.0	0.0	3.7	0.0	4.6	268.8	34.4	424.8	31.7	16.1	224.1	8783.2	
2141	4	23430.0	86460.0	0.0	0.0	27.0	19.4	6.6	855.6	62.1	848.0	79.5	17.7	1953.5	39297.3	
2143	4	9845.0	22825.0	0.0	0.0	60.1	9.2	2.2	170.4	305.9	454.3	9.2	77.2	6617.7	124100.8	
2144	4	8690.0	34782.0	4.4	0.0	35.1	15.6	8.1	189.3	44.7	493.7	24.5	26.4	446.7	17869.3	
2146	4	22110.0	69410.0	10.8	2.2	0.0	73.7	58.8	1181.2	335.4	2210.9	184.0	55.4	3051.4	57393.8	
2150	4	6160.0	28985.0	0.0	0.0	19.3	0.0	4.4	63.8	35.2	353.6	26.7	24.2	1415.9	52245.0	
2151	4	72160.0	108020.0	2.1	0.0	25.1	6.5	11.0	489.9	171.9	477.8	8.7	35.2	742.0	11039.6	
2152	4	3476.0	5984.0	0.0	0.0	22.6	2.1	0.0	61.3	19.0	355.9	12.7	23.2	605.7	28545.5	
2153	4	52085.0	78705.0	0.0	0.0	4.8	9.9	2.3	495.2	138.6	380.9	24.8	31.7	2460.8	34678.6	
2157	4	8052.0	15642.0	0.0	0.0	21.5	16.3	0.0	107.5	134.8	636.0	34.7	21.0	1468.9	46263.3	
2160	4	4818.0	22462.0	0.0	0.0	25.4	8.9	8.7	135.5	87.1	622.4	62.5	24.0	885.9	40205.9	
2161	4	17343.3	47813.3	4.5	0.0	56.2	27.7	19.6	246.1	117.4	1113.0	104.5	26.1	742.0	13757.9	
2163	4	250.8	5456.0	0.0	0.0	44.4	2.1	3.9	109.8	7.8	583.8	42.3	35.2	170.4	32709.9	
2164	4	46676.7	103400.0	0.0	0.0	44.5	2.1	8.5	480.0	230.2	647.4	70.3	36.2	2688.0	126599.5	
2166	4	591360.0	632720.0	15.5	6.6	53.2	45.1	44.0	2468.4	160.5	1574.9	118.9	46.0	2067.1	20746.6	
2171	4	23100.0	102080.0	0.0	2.1	0.0	55.7	19.5	461.1	238.5	1673.4	103.7	66.0	1953.5	30968.4	
2172	4	37693.3	84993.3	2.1	0.0	21.0	8.4	4.4	162.0	53.3	535.3	52.5	31.1	416.4	8359.4	
2174	4	4253.3	149820.0	46.7	10.6	0.0	81.0	38.4	45.0	1188.8	1832.4	177.2	98.4	1703.6	10812.4	
2175	4	17160.0	88366.7	0.0	0.0	77.2	4.5	6.1	628.5	360.4	583.8	77.2	105.2	3891.9	45809.0	
2177	4	485100.0	1129700.0	3.3	0.0	4.7	21.4	20.2	10827.6	192.3	1309.9	128.0	10.1	1294.8	15749.2	
2179	4	5060.0	30250.0	1.0	0.0	19.5	13.0	7.2	243.8	198.4	1279.6	62.9	88.6	8480.3	87756.5	
2181	4	11220.0	30800.0	0.0	0.0	6.3	13.7	0.0	346.8	295.3	870.8	41.0	39.8	2423.0	53607.9	
2183	4	22073.3	37033.3	0.4	0.0	6.1	5.2	11.3	165.1	103.7	581.5	82.5	29.3	1120.6	39297.3	
2184	4	47.7	4546.7	0.0	0.0	3.9	8.6	19.6	152.2	12.3	490.6	42.7	12.3	53.8	1718.8	
2187	4	96525.0	355025.0	0.0	0.0	184.0	79.5	66.9	863.2	477.0	3740.4	386.9	141.6	15166.2	295297.9	
2193	4	80885.0	93885.0	2.3	0.0	46.9	20.2	17.2	112.1	107.5	654.2	38.5	34.5	870.8	12357.1	
2194	4	6966.7	64460.0	0.0	0.0	50.1	183.2	96.2	1067.6	487.6	10221.8	1007.0	220.3	4709.6	28545.5	
2196	4	346.5	49060.0	26.3	0.0	115.1	35.3	39.4	514.1	137.0	2059.5	165.8	96.9	817.7	34981.4	
2211	4	7315.0	9680.0	0.4	0.0	8.0	11.4	0.0	133.3	30.9	817.7	86.3	54.6	2195.8	56333.7	

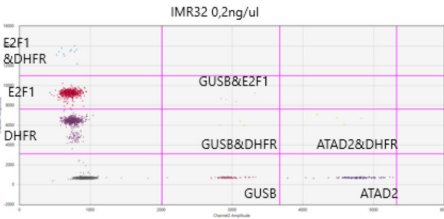
NBL ID; unique patient identifier
 Stage; number corresponds to
 International Neuroblastoma
 Staging System Committee
 (INSS) stage for neuroblastoma



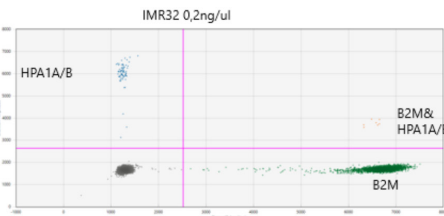
A Positive controls for cell cycle panel 1



B Positive control for cell cycle panel 2

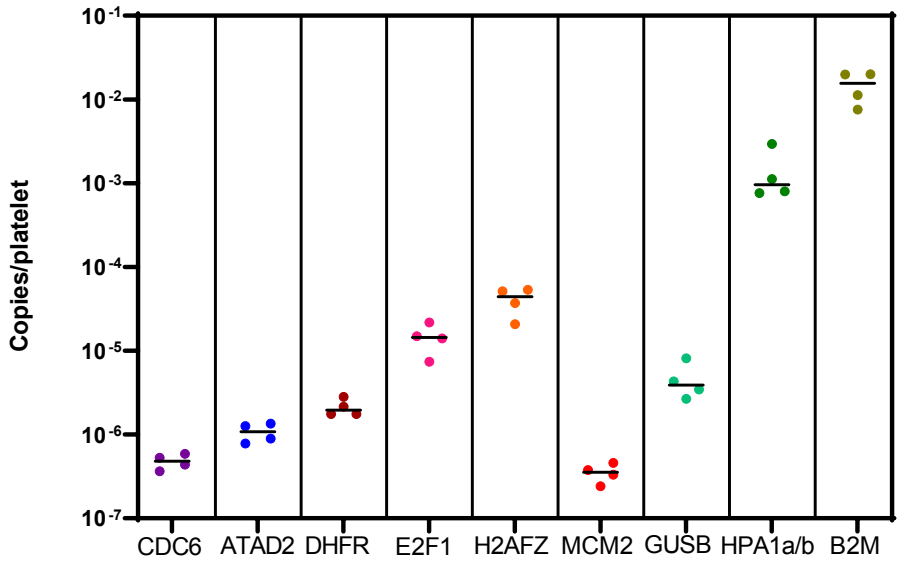


C Positive control for cell cycle panel 3



Supplemental Figure 2. 2D plots from the ddPCR assays illustrating gating strategies for the cell cycle genes. **A.** 2D plots for cell cycle panel 1 (top left and right: CDC6 (bright red droplets, H2AFZ dark purple, turquoise double positive for CDC6 and H2AFZ, MCM2 burgundy droplets, B2M dark violet, green double positive for B2M and MCM2, orange positive for MCM2 and H2AFZ, yellow positive for B2M and H2AFZ, pink positive for CDC6 and MCM2, blue positive for B2M and CDC6) (below left (after removal from B2M from this panel): CDC6 bright red droplets, H2AFZ dark purple, turquoise double positive for CDC6 and H2AFZ, MCM2 green droplets, orange positive for MCM2 and H2AFZ). **B.** 2D plot for cell cycle panel 2 (bright red droplets E2F1, DHFR dark purple, turquoise E2F1 and DHFR double positive, GUSB burgundy, ATAD2 dark violet, orange GUSB and DHFR, light pink GUSB and E2F1, yellow ATAD2 and DHFR). **C.** 2D plot for cell cycle panel 3 (turquoise droplets positive for HPA1A/B, dark green B2M, orange B2M and HPA1A/B).

Please note that these 2D plots were all generated in QX Manager 1.2 Standard Edition (BioRad).



Supplemental Figure 3. Expression of cell cycle genes (CDC6, ATAD2, DHFR, E2F1, H2AFZ and MCM2), reference genes (GUSB and B2M) and platelet-specific gene HPA1a/b in platelets from 4 healthy donors as measured by ddPCR.

Supplemental table 6. Overview of number of leukocytes and platelets recovered at the different centrifugation steps during the preparation of platelet poor plasma, and their percentages to whole blood.

Healthy control ID	Whole blood				After 1x centrifugation in plasma				After 1x centrifugation in cellular fraction				
	number/ul	Total in 9 ml	number/ul	Total in PPP (ml)	number/ul	Total in PPP	% of whole blood	number/ul	Total in cell fraction	% of whole blood	number/ul	Total in cell fraction	% of whole blood
Control 1	8 330	74 970 000	0.70	4	2800	0.00	13 050.00	6 000.00	78 300 000.00	104.44			
	298 000	2 682 000 000	236 000.00	4	944 000 000.00		35.20	351 000.00	6 000.00	2 106 000 000.00			78.52
Control 2	5 590	50 310 000	0.80	3.5	2 800.00	0.01	8 120.00	6 000.00	48 720 000.00	96.84			
	189 000	1 701 000 000	234 000.00	3.5	819 000 000.00		48.15	210 000.00	6 000.00	1 260 000 000.00			74.07
Control 3	6 840	61 560 000	1.50	3	4 500.00	0.01	8 650.00	7 000.00	60 550 000.00	98.36			
	240 000	2 160 000 000	159 000.00	3	477 000 000.00		22.08	276 000.00	7 000.00	1 932 000 000.00			89.44
Control 4	3 730	33 570 000	0.90	4	3 600.00	0.01	6 010.00	7 000.00	42 070 000.00	125.32			
	257 000	2 313 000 000	175 000.00	4	700 000 000.00		30.26	275 000.00	7 000.00	1 925 000 000.00			83.23

Supplemental Table 7. Expression of cell cycle genes in 4 samples of platelets isolated from healthy controls and the corresponding correction co-efficients, as calculated by the following formula:

Control ID	CDC6 (copies)	Ratio marker/HPA3.ub	ATAD2 (copies)	Ratio marker/HPA3.ub	DHFR (copies)	Ratio marker/HPA3.ub	E2F1 (copies)	Ratio marker/HPA3.ub	H2AFZ (copies)	Ratio marker/HPA3.ub	MCM2 (copies)	Ratio marker/HPA3.ub	GUSB (copies)	Ratio marker/HPA3.ub	B2M (copies)	Ratio marker/HPA3.ub	HPA1a/b (copies)
Tr1	352.84	0.000472	522.45	0.000698	1441.66	0.001927	9964.41	0.013320	24956.46	0.033360	222.61	0.000298	2301.81	0.003077	7526309.56	10.060729	748087.91
Tr3	215.04	0.000174	526.99	0.000426	1038.84	0.000841	8268.34	0.006691	12266.22	0.009926	142.20	0.000115	1574.92	0.001275	8328914.00	6.740196	1235707.97
Tr2	246.84	0.000524	564.85	0.001199	1176.65	0.002498	9101.23	0.019325	21443.17	0.045531	192.32	0.000408	3407.28	0.007235	4452183.12	9.453376	470962.23
Tr4	305.90	0.000571	885.89	0.001653	1228.14	0.002291	5179.07	0.009661	37525.54	0.070000	263.50	0.000492	3028.70	0.005650	14007719.00	26.129944	536079.19
Mean copies	280.15	0.000435	625.05	0.000994	1221.32	0.001889	8128.26	0.012249	24047.85	0.039704	205.16	0.000328	2578.18	0.004309	8578781.42	13.096061	747709.33
Standard deviation	215.04	0.000174	522.45	0.000426	1038.84	0.000841	5179.07	0.006691	12266.22	0.009926	142.20	0.000115	1574.92	0.001275	4452183.12	6.740196	470962.23
Minimum	352.84	0.000571	885.89	0.001653	1441.66	0.002498	9964.41	0.019325	37525.54	0.070000	263.50	0.000492	3407.28	0.007235	14007719.00	26.129944	1235707.97
Maximum	61.36	0.000179	174.93	0.000543	167.22	0.000738	2084.50	0.005441	10457.29	0.025025	51.11	0.000163	811.02	0.002651	3986322.76	8.808358	346178.71
Correction co-efficient		0.000971		0.002624		0.004103		0.028571		0.114779		0.000816		0.012262		39.521135	

Supplemental Table 8. Expression of cell cycles genes in plasma from the 20 healthy controls (as shown previously in Supplemental Table 6) with adjacent the levels after correction for platelets using the correction co-efficient per marker and below the calculated thresholds for positivity. The following 2 formulas were used:

	CDCC6	After (copies/m platelets)	ATAD2	After (copies/m subtraction platelets)	DHR8	After (copies/m subtraction platelets)	E2F1	After (copies/m subtraction platelets)	H2AZ	After (copies/m subtraction platelets)	MCM2	After (copies/m subtraction platelets)	GUS	After (copies/ml subtraction platelets)	B2M	After (copies/ml subtraction platelets)	HPA1A/B
1	15.45	11.29	12.11	75.55	127.21	4.76	1082.76	590.86	NA	56.49	3.94	NA	56.49	3.94	NA	4285.60	
2	28.92	-50.41	55.05	-229.21	434.62	1658.21	1658.21	-1895.61	1658.21	196.11	-805.69	NA	196.11	-805.69	NA	81699.07	
3	23.02	-75.35	36.42	-229.42	224.88	-2608.31	-2608.31	-2608.31	-2608.31	153.71	-1088.56	NA	153.71	-1088.56	NA	101309.88	
4	6.75	2.14	24.53	12.08	87.08	67.60	129.48	-6.16	1173.62	42.40	-15.81	NA	42.40	-15.81	NA	4747.48	
5	10.37	-18.52	18.02	-60.06	127.96	5.87	199.89	-650.29	3377.00	81.02	81.02	81.02	56.74	97.68	-267.20	843643.27	
6	23.32	-2.78	22.72	-47.82	150.68	40.39	301.33	-416.65	2218.52	866.70	866.70	866.70	237.75	-91.85	664874.49	-397440.85	
7	4.94	-3.67	2.91	-20.34	69.74	33.39	203.68	-49.43	686.76	330.06	330.06	330.06	47.14	-67.97	132429.73	8858.94	
8	5.91	-61.95	9.24	-174.15	145.38	-141.37	259.71	-1737.04	1892.94	-18.64	-18.64	-18.64	111.30	-745.65	605436.33	-215685.56	
9	3.32	-26.90	2.28	-79.38	89.35	-38.34	166.58	-722.55	999.47	29.91	29.91	29.91	4.51	102.98	-278.62	201029.70	
10	11.51	6.24	4.37	-9.86	83.29	61.05	48.08	-106.81	688.27	66.01	66.01	66.01	41.94	52.47	-14.00	137124.21	
11	5.05	-10.32	5.21	-36.32	151.43	86.51	117.36	-334.77	1590.07	-226.30	-226.30	-226.30	108.23	104.49	-89.56	79500.40	
12	24.38	-60.68	3.35	-226.53	100.70	-258.74	274.85	-2228.11	938.90	-52.56	-52.56	-52.56	96.92	96.92	-977.29	586734.13	
13	13.25	-38.14	18.32	-120.56	89.35	-127.81	215.04	-1297.12	1370.48	-4704.36	-4704.36	-4704.36	91.62	-557.37	499431.97	-1592281.90	
14	6.35	-26.00	23.85	-63.57	109.03	-27.66	353.60	-598.26	726.89	-3097.05	-3097.05	-3097.05	-1.74	58.38	-350.14	311879.97	
15	4.59	-26.66	3.03	-81.41	102.98	-29.06	279.40	-640.01	908.61	-2784.97	-2784.97	-2784.97	17.35	51.56	-343.03	188309.17	
16	11.51	-44.07	13.10	-137.10	134.78	-100.09	91.62	-1543.85	878.32	-5691.90	-5691.90	-5691.90	39.61	81.77	-620.13	217990.39	
17	6.04	0.00	6.83	-9.50	61.48	35.95	25.06	-152.76	984.33	269.95	33.24	33.24	28.16	36.42	-39.90	341561.19	
18	24.23	-77.01	37.56	-236.03	198.38	-229.41	404.33	-2574.56	2135.23	-9831.96	-9831.96	-9831.96	1.24	180.21	-1098.26	789202.46	
19	4.55	-5.01	12.27	-13.56	128.72	88.33	137.81	-143.43	730.67	-399.13	-399.13	-399.13	60.26	67.39	-53.31	200348.24	
20	16.51	7.02	6.06	-19.57	212.01	171.93	69.74	-208.33	1060.04	-61.07	-61.07	-61.07	96.52	60.65	-59.12	269251.07	
Mean	12.50	-25.04	15.86	-85.58	123.32	-35.30	208.78	-895.72	1358.79	-3078.33	-3078.33	-3078.33	33.08	96.05	-377.98	379277.92	
Standard deviation	8.23	28.43	14.14	81.99	46.04	124.80	119.07	892.71	693.21	3692.53	3692.53	3692.53	49.05	55.97	384.44	248706.29	
Minimum	3.32	-77.01	2.28	-236.03	61.48	-258.74	25.06	-2608.31	686.76	-9831.96	-9831.96	-9831.96	-52.56	36.42	-1098.26	79200.40	
Maximum	28.92	11.29	55.05	12.08	224.88	171.93	434.62	4.76	3377.00	628.71	146.13	146.13	124.20	237.75	-3.94	843643.27	
Control threshold	37.19	60.24	58.29	160.40	261.45	339.11	565.99	1782.41	3438.40	7995.25	377.58	377.58	180.22	263.95	775.33	112596.80	



Supplemental Table 9. Overview of the cell cycle marker results and the levels corrected for presence of platelets using the above-mentioned correction co-efficients. Cells in red are positive according to the thresholds (as shown in Supplemental Table 8).

NBL ID	Stage	CDCC6	Corrected for HPA	ATAD2	Corrected for HPA	DHFR	Corrected for HPA	E2F1	Corrected for HPA	H2AFX	Corrected for HPA	MCM2	Corrected for HPA	GUS	Corrected for HPA	ELM	Corrected for HPA	HPA1A1B	
2079	1	4.550616	4.474885	2.8595	2.0593073	29.45407	29.1340801	6.791851	4.526562	277.8829	268.93137	13.62913	13.56493	15.82494	14.8683644	3831.3	749.000115	77.98892	
2097	1	11.81191	8.275527	17.79359	8.2369628	147.6489	132.70576	1.883567	84.480546	1052.472	634.44959	106.7615	103.789656	78.7461	34.0878069	73218.73	70717.504	3642.007	
2104	1	0	-0.0571263	0	-0.154376	23.54811	23.30672	2.354811	0.6739101	90.86088	84.108154	9.767545	9.71953735	4.709622	3.988219148	1438.631	-886.49311	58.83242	
2115	1	0	-0.889432	2.301809	0.7083757	59.81675	57.3251847	11.59004	-5.8407963	389.8174	31.48748	15.6735	15.177838	18.39933	10.95318519	12720.52	-11278.823	607.2535	
2126	1	0	-0.1066063	0	-0.28809	20.06511	19.6146417	4.459755	1.329382	109.7920	97.188617	0	-0.08958883	6.53959862	5.33959862	2877.261	-1461.7728	109.7920	
2148	1	2.347239	-0.887108	22.6692	13.518887	173.3928	159.723432	89.34455	-5.8393288	1113.046	70.65201	44.52183	41.8032737	95.40392	54.55222661	49594.9	-82072.34	3331.566	
2149	1	6.829709	6.4643072	12.64481	11.657354	136.2913	134.747298	45.43054	34.96783	483.8342	404.64107	11.51166	74.8045874	22.71522	18.10083961	15522.07	649.654073	376.3155	
2155	1	11.05474	10.427601	6.731217	5.0365155	220.3376	217.687632	51.63929	33.162397	885.8936	811.76133	81.77479	8.23747626	74.127132	66.20768375	2559.48	66.9918101	645.8694	
2165	1	0	-0.2293874	0	-0.619889	34.07283	33.1035443	2.271522	-4.4784211	102.1185	75.103296	9.086088	8.89331756	2.271522	-0.62523189	4217.459	-51118.9449	236.2383	
2169	1	1.88763	11.311398	9.010371	7.454687	195.3509	192.918358	123.4194	106.48505	1022.185	954.13619	131.2626	23.778844	62.84544	55.57507388	20216.55	-3214.2375	802.8672	
2162	4	4.866629	4.0598913	0.198864	4.9243568	1007.041	1003.62307	142.3487	118.55517	908.6088	813.010396	141.9525	140.91899	52.16929	41.95637025	2884.833	-4068.4799	832.8914	
2117	4	0	-0.2176239	4.588474	4.003744	268.7968	267.877191	34.3757	27.972267	424.7746	399.04994	31.72559	31.5427058	16.62029	13.30388639	8783.218	-74.395738	224.1235	
2141	4	19.38365	17.486797	6.647988	1.521980	855.6066	846.591373	605.8983	6.274566	848.0349	623.138102	79.50327	77.9092067	77.17187	-6.23605478	39297.33	-37907.549	1953.509	
2143	4	9.237523	2.8117354	2.150374	-15.21447	170.3642	143.211724	32.08823	116.82397	454.3004	-305.26868	24.83531	3.83747898	77.23173	-3.91449872	124100.8	-137438.19	6611.701	
2144	4	15.59778	15.164007	8.101762	6.9295353	189.2935	187.460556	44.67327	31.909667	493.6774	442.40192	24.45672	24.0921863	26.42537	20.94753672	17869.31	-13.926869	446.7327	
2146	4	58.83242	55.8695	53.0779	45.070994	1181.191	1168.6715	335.4281	248.24621	2210.948	1860.7102	183.9933	181.50333	55.42514	18.00873242	57393.79	-63201.43	3051.411	
2150	4	0	-1.3748538	4.399181	0.688319	63.75405	57.94455	35.20859	-5.2455273	353.6003	191.08291	26.65322	25.48971378	24.15385	6.79189621	52245.01	-3713.5698	1415.915	
2151	4	6.534412	5.8139	10.97902	9.0319349	489.8916	486.847027	171.8785	150.67794	477.7768	392.60727	8.707501	8.102004	35.20859	26.10981276	11039.6	-18286.288	742.0305	
2152	4	2.127659	1.5394862	0	-1.58946	61.25538	58.7700287	19.00507	1.6984927	355.8718	286.34564	12.72052	12.22624	23.24524	15.81766773	28545.46	4605.96213	605.7392	
2153	4	9.918979	7.5295275	2.6395	-4.19323	495.1918	485.09507	138.5628	68.254882	380.8585	98.40858	24.83531	22.8272818	31.72559	1.551070939	34678.57	-62575.64	2460.816	
2157	4	16.27924	14.852922	0	-3.85444	107.5187	101.491739	134.777	92.808528	636.0262	467.42527	34.67857	33.4799325	21.04944	3.037570079	46263.33	-11789.95	1468.918	
2160	4	8.934653	8.0784505	8.074505	8.130232	87.07501	61.764145	62.2397	570.71505	62.46686	61.7439658	24.00242	13.13958872	40205.94	5194.42406	885.8936			
2161	4	27.1257	26.99207	19.61081	17.663719	246.0639	243.036999	117.362	96.16416	1113.046	1027.863	104.49	103.884515	26.1225	17.03372476	13757.85	-15568.033	742.0305	
2163	4	1.112515	1.947019	3.907018	3.4599823	109.7902	109.091226	17.98892	2.9314181	583.7812	564.22693	42.32603	42.1870095	35.20859	33.11998579	32709.92	25976.9331	170.3642	
2166	4	2.067085	-0.5429316	8.480349	1.4271216	480.0483	469.019585	230.1809	153.38297	647.3838	338.86153	70.34146	68.148083	36.19292	3.233057263	126599.5	20367.9719	2687.968	
2164	4	45.12757	43.120431	43.99181	38.567778	2468.387	2459.90599	160.5209	101.4622	1574.922	1337.664	118.8761	117.18957	46.03618	20.68958268	20746.57	-60946.968	2067.085	
2171	4	19.53509	17.638232	25.51676	20.390756	461.119	453.103719	238.5098	182.89611	1673.355	1449.1327	103.7328	102.138775	66.02557	42.07164642	30968.42	-46236.463	1953.509	
2172	4	8.404631	8.0002626	4.43704	3.3442861	162.0352	160.326559	53.30505	41.40678	535.322	487.5228	52.54788	52.2080559	31.11985	26.01339403	8359.201	-8069.2037	416.4457	
2174	4	38.38872	36.734486	44.97614	40.50578	1188.763	1181.77314	246.8387	198.16398	1832.361	1636.8188	177.1787	175.788545	98.43262	77.5426793	10812.44	-56517.392	1708.642	
2175	4	4.543044	6.74034	6.064964	-1.47315	628.4544	612.448606	360.4148	249.22008	583.7812	1370.07571	172.7315	12.0559785	105.2472	57.5250226	45809.03	-108020.25	3891.874	
2177	4	21.35231	20.095088	20.21875	16.819076	10827.59	10822.2758	193.3222	155.32939	1309.911	1161.2999	197.9624	126.905786	10.14613	-5.73030798	15749.22	-35421.457	1294.768	
2179	4	13.02339	4.7889741	7.170438	-15.082	243.81	209.01557	198.3796	-43.912458	1279.624	306.25811	62.92116	56.001948	88.58936	-14.339679	87756.47	-247396.5	8480.349	
2181	4	13.70485	11.352158	0	-6.357839	36.7857	336.8443	295.2979	226.07156	870.7501	592.64554	41.03883	39.916981	39.75164	10.04133872	53607.92	-42150.071	2422.957	
2183	4	1.565655	4.682353	11.28189	8.3413922	165.0639	160.466038	103.7328	71.715675	581.5096	452.88627	82.53197	81.6158542	29.30263	15.56162177	39297.33	-4990.7401	1120.618	
2184	4	8.556666	6.5038659	19.61081	19.469742	152.192	151.971399	123.2622	10.73026	490.6488	484.47831	42.70461	42.660746	12.26622	11.67020216	1718.785	-405.84544	53.75935	
2187	4	79.5027	64.776894	66.93478	27.1380855	863.1784	800.951461	477.0196	43.706256	3740.44	1999.6788	386.9159	374.540289	141.5915	-44.3763478	295297.9	-304087.31	15166.2	
2193	4	20.21655	19.18785	14.903002	12.06618	108.489064	107.5187	82.605407	654.1983	554.25451	38.46444	38.46444	1003.19837	220.3376	162.5882456	28545.46	-157584.8	4709.621	
2194	4	183.2361	178.60306	96.1611	83.803049	1067.615	1048.29176	487.201	353.06144	1021.815	968.12833	1007.041	1003.19837	165.153824	96.91827	86.891047	34981.44	2663.11695	817.7479
2196	4	35.28431	34.490275	39.37905	37.227277	514.1211	510.765926	137.0485	113.6862	2059.513	1965.653	165.8211	165.153824	96.91827	86.891047	34981.44	2663.11695	817.7479	
2211	4	11.35761	9.2324837	0	-5.761791	133.2626	124.252828	30.8927	-31.849634	817.7479	565.715066	86.31794	84.5260594	54.59225	27.66728939	56333.75	-30446.933	2195.805	

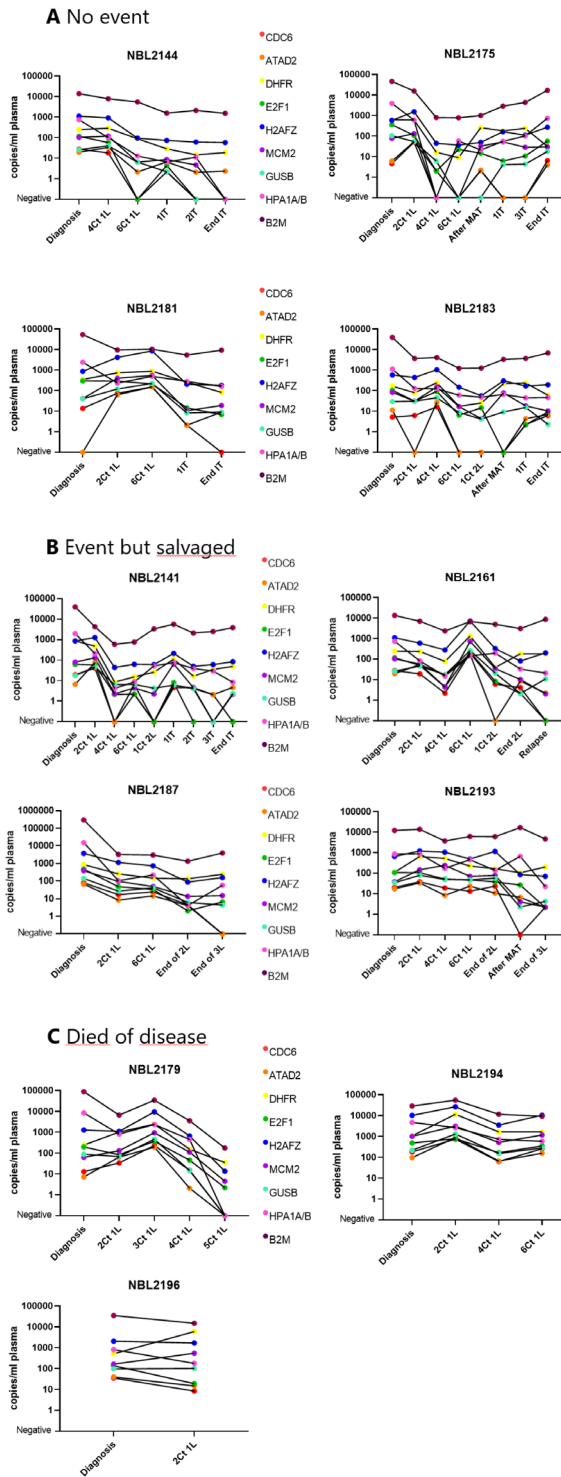
NBL ID; unique patient identifier
 Stage; number corresponds to International Neuroblastoma Staging System Committee (INSS) stage for neuroblastoma

Supplemental Table 10. Levels of the neuroblastoma-specific markers and cell cycle genes in sequential plasma samples from 11 patients with metastatic neuroblastoma. (following page).

NBL ID	Time point	CDC6 (copies/ml)	ATAD2 (copies/ml)	DHFR (copies/ml)	EF1 (copies/ml)	H2AF2 (copies/ml)	MCM2 (copies/ml)	GUS (copies/ml)	HPA1AB (copies/ml)	B2M (copies/ml)	
2141	Diagnosis	19.38365	6.647988	855.6066	62.08827	848.0349	79.50327	17.71787	1953.509	39297.33	
	After 2Ct 1L	40.81168	74.80879	475.5053	57.69666	1249.337	129.4768	47.02051	209.7372	4255.318	
	After 4Ct 1L	0	0	8.556066	2.142802	43.91609	2.309381	6.428407	4.149314	585.2953	
	After 6Ct 1L	2.233663	6.57222	15.29491	2.188233	62.46686	4.459755	6.57222	8.783218	750.3594	
	1Ct 2L	0	0	25.81363	0	60.87679	2.248807	4.300748	51.94214	3323.394	
	1IT	4.626333	6.04982	111.3046	8.101762	212.7659	64.81409	0.04982	75.7174	5572.801	
	2IT	4.543044	4.149314	16.58211	0	49.97348	4.543044	4.149314	39.1450	2067.085	
2144	Diagnosis	27.71257	19.61081	246.0816	117.362	1113.046	104.49	26.1225	742.0305	13757.85	
	After 4Ct 1L	18.09646	33.39137	287.7261	57.84809	916.1805	119.6335	40.0545	100.7041	7798.892	
	After 6Ct 1L	0	2.157946	88.58936	0	94.64675	6.458694	6.473838	12.79624	5451.653	
	1IT	2.180661	6.640416	28.77261	4.429468	74.05162	8.707501	2.210948	6.564699	1559.778	
	2IT	0	2.074657	14.53774	0	61.17966	4.702051	0	11.13046	2112.515	
	End IT	0	2.347239	18.77792	0	57.54522	0	0	0	1514.348	
	2161	Diagnosis	27.71257	19.61081	246.0816	117.362	1113.046	104.49	26.1225	742.0305	13757.85
After 2Ct 1L		19.23222	55.12227	239.267	50.57922	602.7105	57.77238	45.96046	82.53197	7155.294	
After 4Ct 1L		2.210948	17.33928	77.98892	4.331035	281.6687	4.421896	17.33928	14.84061	2377.526	
After 6Ct 1L		197.6224	174.15	1340.198	221.0948	7276.442	741.2733	264.2537	145.3774	6880.283	
1Ct 2L		6.087679	0	39.6002	8.328914	324.8276	34.45142	20.82229	195.9188	5035.207	
End 2L		4.081168	8.556066	183.9933	2.135231	81.77479	10.22185	2.135231	32.93707	3157.416	
Relapse		0	2.188233	183.9933	0	202.9226	2.029226	10.90331	20.898	8858.936	
2175	Diagnosis	4.543044	6.064964	628.4544	360.4148	583.7812	77.23175	105.2472	3891.874	45809.03	
	After 2Ct 1L	50.88209	54.06222	610.2822	108.2759	1537.063	133.2626	54.06222	598.1675	15597.78	
	After 4Ct 1L	0	2.036798	16.27924	2.036798	45.12757	0	0	6.102822	802.6044	
	After 6Ct 1L	0	0	9.010371	22.48807	36.42007	0	0	58.22668	779.8892	
	After MAT	2.173089	2.097372	255.9248	14.68918	50.0492	32.6342	0	21.12515	1007.041	
	3IT	0	0	181.7216	6.117966	163.5496	52.54788	4.081168	55.95156	2869.689	
	End IT	6.405692	3.96002	31.72559	57.46951	271.8255	29.90837	17.79359	739.0018	16809.26	
2179	Diagnosis	13.02329	7.170438	243.81	198.3796	1279.624	62.92116	88.58926	9480.249	97756.47	
	After 2Ct 1L	33.76996	64.35979	1014.613	84.04631	1097.902	130.9511	68.82712	817.7479	6647.988	
	After 3Ct 1L	232.4524	193.8365	2430.529	370.2581	9540.392	954.0292	466.4192	2347.239	34375.7	
	After 4Ct 1L	14.99205	2.082229	154.4635	45.88474	662.5273	111.3046	14.61346	454.3044	3581.433	
	After 5Ct 1L	0	0	35.13287	2.195805	13.55341	4.512757	0	0	177.1787	
	Diagnosis	13.70485	0	346.7857	295.2979	870.7501	41.03883	39.75164	2422.957	53607.92	
	After 2Ct 1L	74.88451	62.76972	736.7303	290.7548	4141.742	402.0594	121.1478	233.2096	9464.675	
2181	After 6Ct 1L	152.192	151.4348	885.8936	212.7659	8556.066	555.7657	225.6739	498.9777	10373.28	
	1IT	2.104944	2.074657	258.9535	14.53774	204.437	10.52472	8.253197	281.6687	5421.366	
	End IT	0	9.086088	81.77479	6.829709	180.9646	18.92935	9.086088	159.0065	9313.24	
	2183	Diagnosis	5.156355	11.28189	165.0639	103.7328	581.5096	82.53197	29.30263	1120.618	39297.33
		After 2Ct 1L	6.170968	0	78.7461	30.58983	436.8894	30.8927	30.58983	128.7196	3649.579
		After 4Ct 1L	16.27924	26.80396	241.5385	91.61805	1044.9	152.9491	44.74898	121.905	4096.311
		After 6Ct 1L	0	0	17.18785	6.451122	147.6489	16.65783	8.631784	60.0439	1219.05
1Ct 2L		0	0	24.91102	14.53774	56.71233	4.361322	4.149314	47.32338	1256.909	
After MAT		0	0	216.5518	0	299.0837	77.98892	9.161805	65.57127	3339.137	
End IT		2.256379	4.353751	235.4811	2.180661	168.8498	18.02074	15.2192	44.52183	3702.581	
2187	Diagnosis	79.50327	66.93418	863.1784	477.0196	3740.44	386.9159	141.5915	15166.2	295299.7	
	2Ct 1L	17.11213	8.328914	257.4392	47.70196	1143.333	96.1611	26.95539	105.2472	3263.42	
	6Ct 1L	24.53244	14.53774	146.8918	33.16422	728.4014	49.14059	41.41742	220.3376	3005.981	
	End of 2L	4.512757	4.103883	135.5341	2.051942	87.83218	13.55341	6.163396	4.111455	1332.626	
	End of 3L	0	0	243.81	6.587414	158.2494	15.14348	4.391609	57.77238	3929.733	
	Diagnosis	20.21655	17.18785	112.0618	107.5187	654.1983	38.46444	34.45142	870.7501	12357.08	
	After 2Ct 1L	38.61587	33.9214	660.2557	106.0044	1219.05	148.4061	80.26044	890.6259	14102.37	
2193	After 4Ct 1L	19.08078	8.328914	529.2646	52.01785	1067.615	243.81	49.89777	171.8783	3763.155	
	After 6Ct 1L	13.32626	23.69955	224.8807	47.47481	497.4633	71.17436	47.47481	458.8474	6246.686	
	End of 2L	23.69955	10.67615	166.5783	38.28872	1166.048	77.98892	57.54522	137.0485	6155.825	
	After MAT	0	6.708562	105.2472	26.80396	87.07501	4.058453	2.236663	673.1277	1712.13	
	End of 3L	2.226092	2.142802	203.6798	2.142802	71.25007	2.226092	4.285605	22.6395	4785.34	
	Diagnosis	183.2361	96.1611	1067.615	487.6201	10221.85	1007.041	220.3376	4709.622	28545.46	
	2194	After 2Ct 1L	749.6023	893.4653	11584.76	779.8982	26425.37	3119.557	137.4883	2657.681	54819.4
After 4Ct 1L		62.76972	65.57127	1650.639	167.3355	3498.144	514.1211	152.192	727.6442	11509.04	
After 6Ct 1L		258.9535	157.4922	1650.639	351.3287	10373.28	1173.62	284.6974	586.8099	9237.523	
Diagnosis		35.28431	39.37305	514.1211	137.0485	2059.513	165.8211	96.91827	817.7479	34981.44	
After 2Ct 1L	8.328914	14.76489	5898.385	19.00507	1696.07	545.9225	101.4613	178.6931	14916.33		

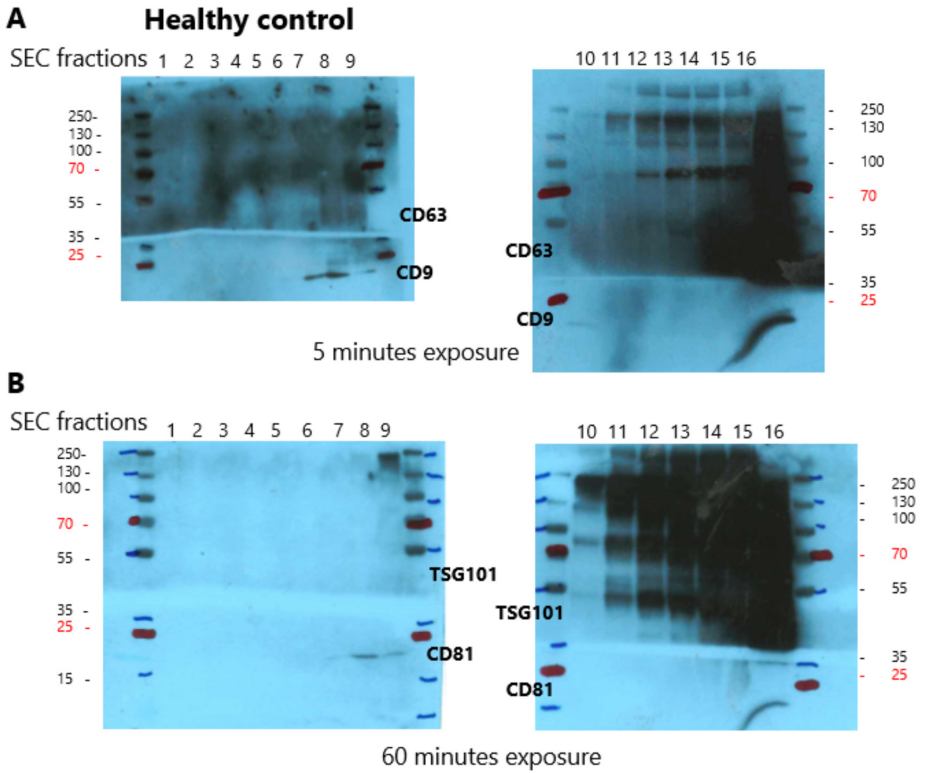
1 IT= at first course of anti-GD2 immunotherapy
 After 2Ct 1L= after 2 courses of chemotherapy in first line therapy
 After MAT= after myeloablative therapy and autologous stem cell treatment
 End of 2L= end of second line therapy
 End of 3L= end of third line therapy
 End of IT=at the end of anti-GD2 immunotherapy courses





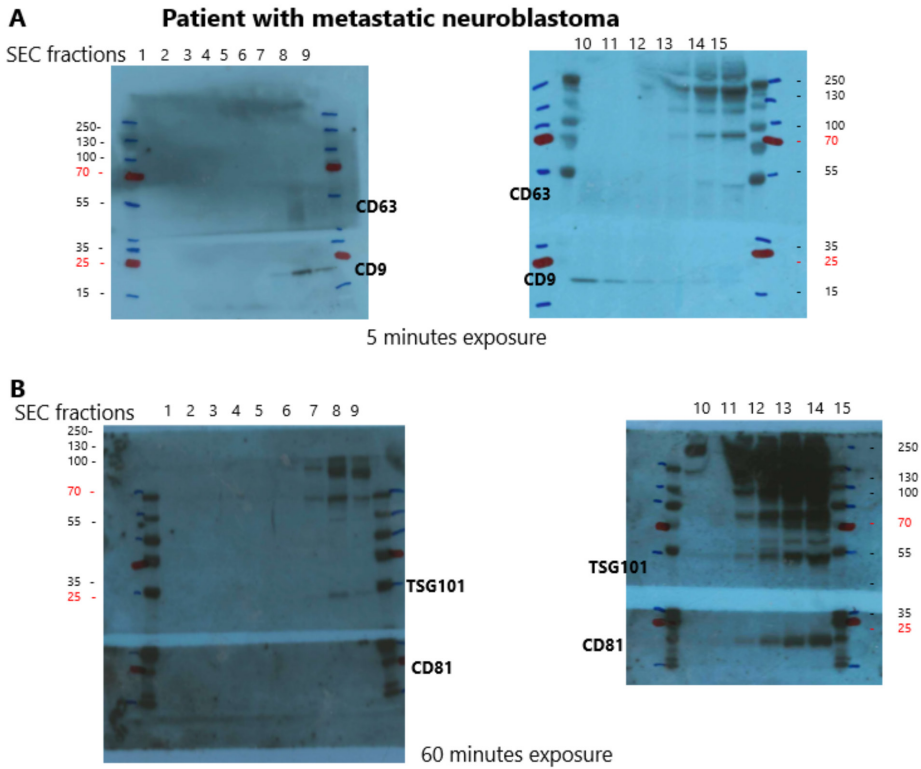
Supplemental figure 4. Level of the cell cycle markers in sequential plasma samples from 11 patients with metastatic neuroblastoma. Patients are classified according to clinical outcome. **A.** No event (=no relapse/progressive disease and/or death of disease) **B.** Event but salvaged (=relapse/progressive disease but eventually complete remission or stable disease) **C.** Died of disease.

Dx; initial diagnosis
 2Ct; 2nd chemotherapy course
 4Ct; 4th chemotherapy course
 1L; first line treatment
 2L; second line treatment
 End 3L; end of third line treatment
 1IT; first course of immunotherapy
 end IT; at the end of immunotherapy
 After MAT; after myeloablative therapy
 R; relapse

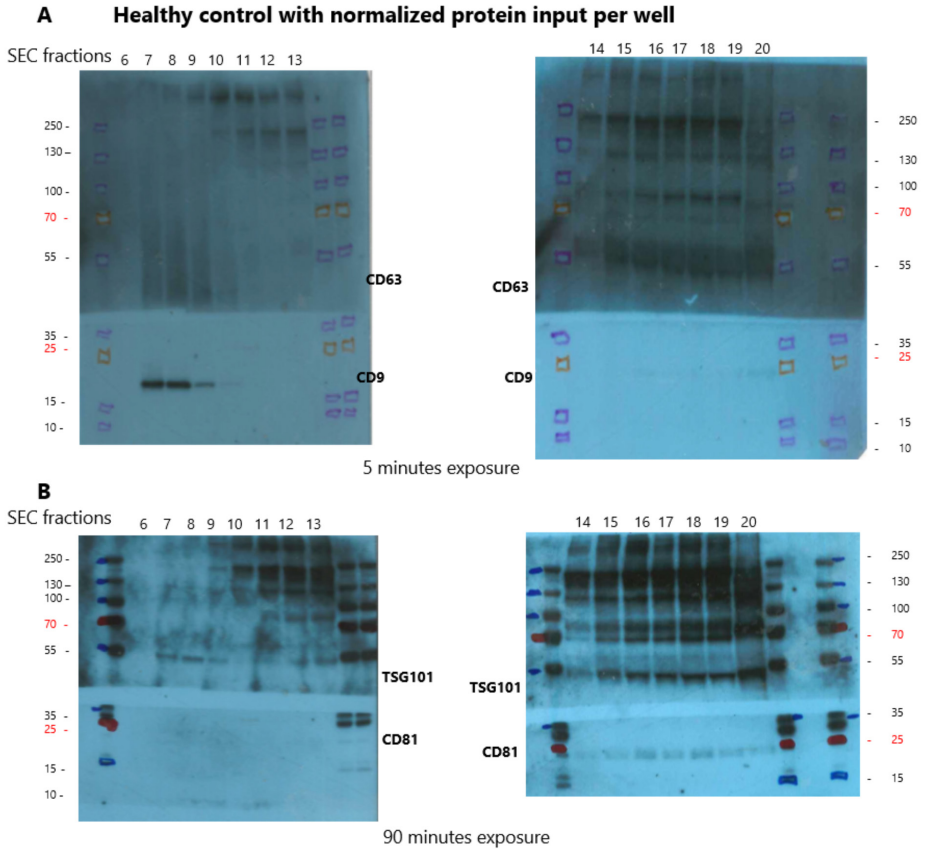


Supplemental figure 5. Western blot images from the size exclusion chromatography (SEC) fractions isolated from 500ul of plasma from 1 healthy control. **A.** The blots were cut and first stained with CD63 (a smear around 44-55kDa) and CD9 (a band around 24kDa). SEC fractions 7, 8 and 9 are positive for CD9. CD63 is not clearly present in this blot, much aspecific staining in the higher protein-rich SEC fractions. **B.** Below, the same blots stained for TSG101 (band around 46kDa) and CD81 (band around 25kDa). SEC fractions 7, 8 and 9 are positive for CD81. SEC fractions 11 and further seem positive for TSG101 but much aspecific binding in these protein-enriched fractions.

Please note that protein input was not normalized in this experiment.

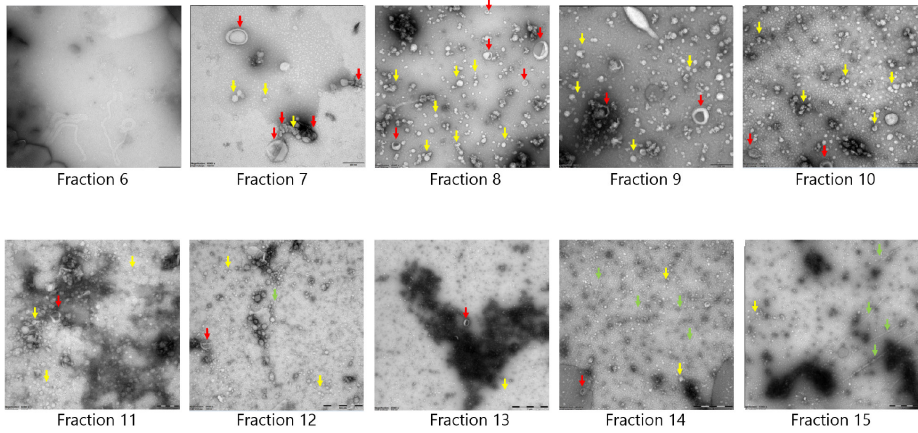


Supplemental figure 6. Western blot images from the size exclusion chromatography (SEC) fractions isolated from 500ul of plasma from 1 patient with metastatic neuroblastoma. **A.** The blots were cut and first stained with CD63 (a smear around 44-55kDa) and CD9 (a band around 24kDa). SEC fractions 7, 8, 9, 10, 11 and 12 are positive for CD9. CD63 is present as a smear especially in SEC fraction 8, and some aspecific staining in the higher protein-rich SEC fractions. **B.** Below, the same blots stained for TSG101 (band around 46kDa) and CD81 (band around 25kDa). SEC fractions 12 and higher are positive for CD81. SEC fractions 7, 8 and 9, and later from 12 upwards are positive for TSG101 but some aspecific binding in the higher SEC fractions is present as well in the high molecular weight area. Please note that protein input was not normalized in this experiment.



Supplemental figure 7. Western blot images from the size exclusion chromatography (SEC) fractions isolated from 500ul of plasma from a healthy control. **A.** The blots were cut and first stained with CD63 (a smear around 44-55kDa) and CD9 (a band around 24kDa). SEC fractions 7, 8 and 9 are positive for CD9. CD63 is present as a smear in SEC fractions 7, 8 and 9 and faintly in 10. A smear might be present in SEC fractions 16 and upwards, with also some aspecific staining in the high molecular weight area. **B.** Below, the same blots stained for TSG101 (band around 46kDa) and CD81 (band around 25kDa). SEC fractions 16 and higher are positive for CD81. SEC fractions 7, 8 and 9, and later from 12 upwards are positive for TSG101 but some aspecific binding is present in the higher SEC fractions in the high molecular weight area as well.

Please note that protein input was normalized per well.



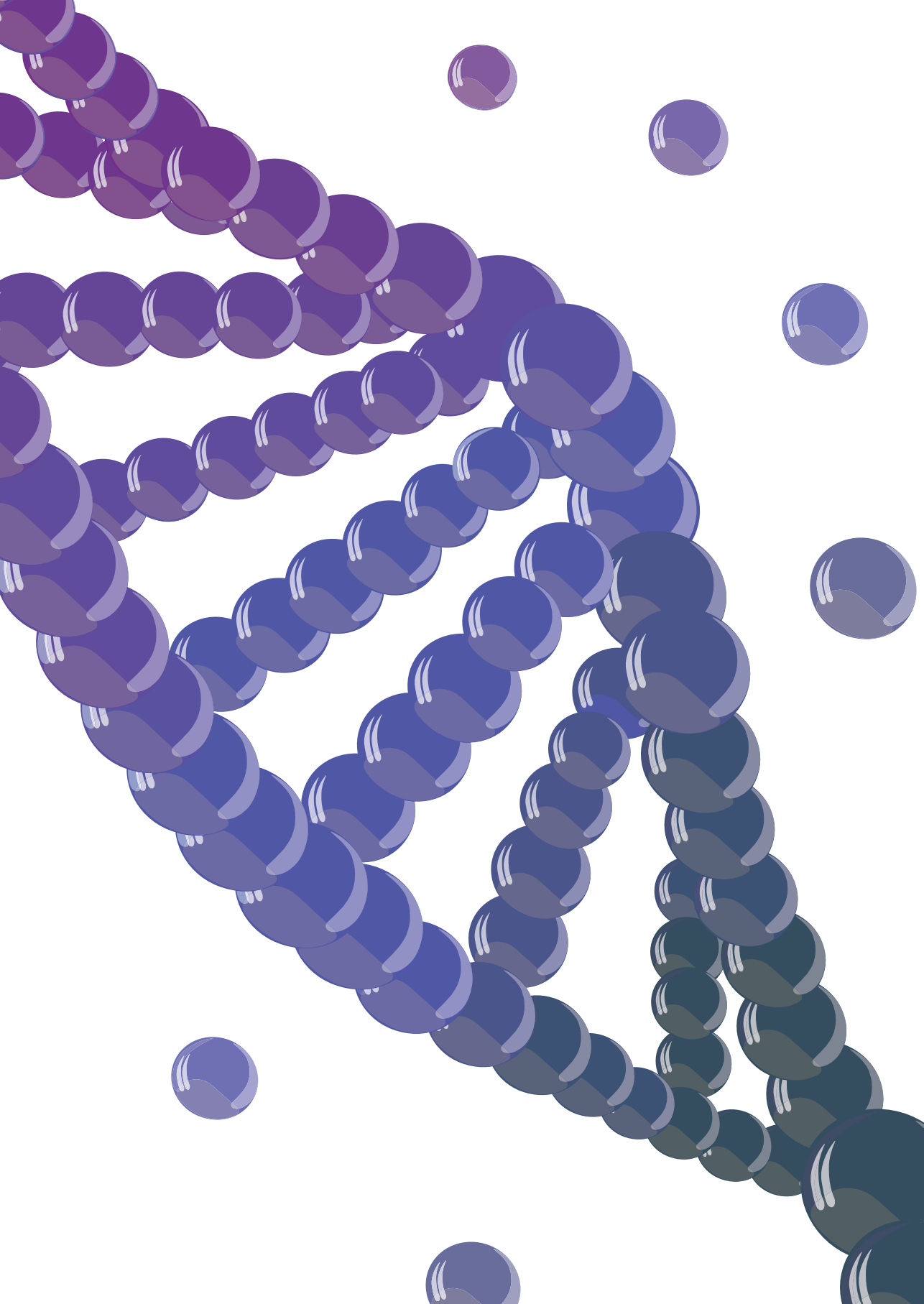
Supplemental Figure 8. Electron microscopy images of fractions (6 to 15) purified by size exclusion chromatography from 500ul of plasma from a patient with neuroblastoma. Red arrows indicate extracellular vesicles, yellow arrows lipoproteins and green arrows protein strands.

Supplemental Table 11. Results of the RNA-based ddPCR assays (both neuroblastoma-specific and cell cycle panels) and DNA-based ddPCR (*RASSF1A-M* and *ACTB*) on 200ul of SEC fractions isolated from 500ul of plasma.

	RNA										DNA				
	H2AFZ (copies/ml)	MCIM2 (copies/ml)	CDC6 (copies/ml)	ATAD2 (copies/ml)	DHFR (copies/ml)	EFZ1 (copies/ml)	GUSB (copies/ml)	B2M (copies/ml)	HPA1AB (copies/ml)	P.HOX2B (copies/ml)	CHRNA3 (copies/ml)	TH (copies/ml)	GUSB nbl (copies/ml)	RASSF1A (copies/ml)	ACTB (copies/ml)
F6	18.02074	0	0	0	2.21852	0	0	0	174.15	4.543044	0	0	0	0	264
F7	214.2802	18.32361	0	0	42.70461	10.67615	8.55086	2120.087	54.51653	0	0	0	8.556066	0	748
F8	121.905	20.97372	4.194744	2.210948	22.10948	22.10948	13.25055	1620.352	23.47239	2.150374	0	0	4.293177	352	2904
F9	62.16399	6.428407	0	0	13.932	2.316852	4.633905	530.0218	11.35761	0	0	0	10.82759	0	264
F10	23.09381	2.104944	0	0	12.56909	2.097372	0	212.0087	0	0	0	0	2.120087	352	4092
F11	47.24766	6.163396	0	4.066024	81.77479	0	0	287.7261	6.057392	0	0	0	2.062229	792	7084
F12	15.82494	2.256379	0	0	50.95781	0	2.210948	168.0926	15.14348	0	0	0	4.141742	132	968
NBL2196	F13	2.157946	2.157946	0	36.34435	4.543044	6.814566	67.38849	2.271522	0	0	0	2.0898	616	6072
F14	12.41765	2.067085	0	2.014083	44.3704	0	0	120.3907	2.271522	0	0	0	0	0	5324
F15	9.994697	0	0	0	96.1611	0	0	77.23175	0	2.04437	0	0	0	0	132
F16	2.0898	0	0	0	18.17218	0	0	31.04413	2.271522	0	0	0	0	0	2200
F17	2.029226	0	0	0	12.94768	2.157946	0	22.71522	0	0	0	0	0	0	8272
F18	1.930794	0	0	0	6.481409	0	0	30.28696	0	0	0	0	2.036798	0	4576
F19	0	2.014083	0	0	8.631784	0	0	17.415	4.543044	0	0	0	0	0	5324
F20	0	0	0	0	14.31059	0	0	29.52979	0	0	0	0	2.150374	0	1012
F6	28.99976	0	0	0	0	0	3.066555	393.7305	31.04413	0	0	0	4.573331	110	0
F7	689.0283	85.56066	14.31059	19.08078	156.735	23.32096	36.04148	6579.842	408.874	0	0	0	25.59248	1188	3212
F8	787.461	46.41477	8.101762	27.18255	159.0065	35.88718	29.30263	5678.805	401.3022	0	0	0	27.56113	2684	9284
F9	264.2537	23.62383	7.87461	4.111455	109.0331	16.43068	12.34194	1567.35	106.7615	0	0	0	10.90331	3696	9020
F10	123.4194	8.253197	0	0	156.735	10.75187	0	840.4631	60.57392	0	0	0	0	7876	25080
F11	35.81433	8.404631	0	2.067085	49.5949	0	0	179.4502	8.328914	0	0	0	0	14520	48400
F12	14.31059	0	0	0	113.5761	0	4.202316	124.9337	26.50109	0	0	0	0	24200	87120
NBL2187	F13	14.76489	4.209887	0	180.2074	0	0	74.20305	6.057392	0	0	0	0	24640	80960
F14	8.253197	0	0	4.30832	276.3685	0	0	67.38849	6.814566	0	0	0	0	34320	100320
F15	33.31566	1.961081	0	0	551.2227	0	0	65.87414	10.60044	0	0	0	0	8668	32120
F16	8.101762	2.021655	0	0	320.2846	0	0	44.67327	9.086088	0	0	0	0	18920	65560
F17	0	0	0	0	106.0044	0	0	25.74392	2.271522	0	0	0	0	33880	116160
F18	8.404631	2.097372	0	0	135.5341	0	0	25.74392	4.543044	0	0	0	2.112515	32560	99000
F19	10.82759	0	0	0	111.3046	0	0	12.11478	0	0	0	0	0	30360	121440
F20	3.967592	0	0	0	69.50857	0	1.930794	8.328914	2.271522	0	0	0	0	26840	97240







Chapter 9

Discussion and future directions

Part I: Liquid biopsies for patients with rhabdomyosarcoma

In **Part I** of this thesis, we mainly focus on liquid biopsies for patients with rhabdomyosarcoma. The overarching question was if liquid biopsy analysis in this group of patients is of additional value to current clinical practice. We hypothesized that liquid biopsies could be more sensitive than conventional analysis of bone marrow (BM) for disseminated disease. Furthermore, we speculated that detection of molecular disease in blood and BM might represent a novel prognostic entity by itself.

RNA-based approaches: historic and current findings

The groundwork for liquid biopsy analysis was laid out thirty years ago, when Galili *et al.* and Davis *et al.* reported on the presence of a fusion between *PAX3* and *FOXO1*, and *PAX7* and *FOXO1* respectively in alveolar rhabdomyosarcoma tumors.(1,2) These fusion genes formed the first targets used in liquid biopsy samples from patients. Detection of disseminated disease in blood and bone marrow (BM) by reverse transcriptase PCR (RT-PCR) was published for the first time by Kelly *et al.* in 1996.(3) These results inspired further efforts on the use of PCR for the detection of rhabdomyosarcoma-specific RNA markers in blood and bone marrow during the early 2000's. These studies widened the scope, including all subtypes of rhabdomyosarcoma, increasing the number of transcripts analyzed and investigating the association of PCR results with clinical outcome. Concurrently, the technique of RT-PCR evolved further over the years, integrating a real-time quantifying step of the targets, designated RT-qPCR (reverse transcriptase quantitative PCR).

In summary, these studies demonstrated that presence of rhabdomyosarcoma-specific transcripts in blood and/or BM at diagnosis was associated to poor clinical outcome and that detection of these transcripts in bone marrow could be of added value to conventional histology for the detection of BM metastasis.(4–6) However, the number of patients analyzed in these studies were rather small, ranging from 5 to 48.

These studies were at the origin of our study on the RNA panel for BM and blood analysis. Our findings in **Chapter 2** with an extended RNA panel containing 11 markers in a large cohort of 99 patients confirmed the previous results for increased sensitivity of BM metastasis detection through RT-qPCR instead of immunohistochemistry, and poor clinical outcome for patients with RNA-positivity in blood and/or BM at diagnosis. Survival of RNA-positive patients was significantly lower than RNA-negative patients (5-year event-free survival 35.5% vs 88%, and 5-year overall survival 54.8% vs 93.7%, $p < 0.001$). In our cohort, the 3 markers *MYOG*, *MYOD1*, and *PAX3/7-FOXO1* were most often positive. Positivity of multiple

markers was not associated to adverse clinical outcome. Of the novel markers, only *CDH11* was occasionally positive on its own and positivity was associated to poor clinical outcome.

Improving treatment stratification with a rhabdomyosarcoma-specific RNA panel

It remains to be investigated why RNA positivity at diagnosis is associated to poor clinical outcome. Does RNA-positivity reflect disseminated tumor cells and therefore more aggressive and advanced disease? This could explain why RNA-positivity in patients with supposedly localized disease results in a decreased disease-free and overall survival since these patients do not receive treatment according to the metastatic disease protocol. The finding that BM involvement as determined by conventional immunohistochemistry is associated with poor clinical outcome was already reported by Oberlin et al and Bailey et al.(7,8) Our data and data from previous studies underline that BM positivity by RT-qPCR alone is associated to poor outcome. In our cohort of 99 patients, 6 of 14 (42.9%) patients with localized disease and RNA positivity suffered from relapse and 3 eventually died, compared to five events in the 58 (8.6%) patients with localized disease without RNA panel positivity. These findings demonstrate that RT-qPCR of BM is a more sensitive technique for the detection of disseminated disease than conventional immunohistochemistry.

Moreover, in our cohort the subset of patients who were diagnosed with metastatic disease through conventional diagnostics and received the corresponding treatment, RNA-positivity especially in blood and/or BM at diagnosis still resulted in a significant decrease of event-free survival. This finding could suggest that presence of disseminated rhabdomyosarcoma-specific transcripts might originate from more aggressive disease and that these patients deserve even more intense therapy. Considering the recent developments and initiatives in the field of rhabdomyosarcoma, this could result in more targeted therapies, given in frontline. (9–11) Many preclinical trials have studied drugs affecting the activation of kinases and downstream pathways, or cell cycle regulation and apoptosis induction.(12) Another much sought after approach is inhibition of the PAX3/7-FOXO1 fusion product. Until now, this has been unsuccessful.(12) Clinical application of targeted therapies in pediatric oncology are still limited to small patient numbers and mostly relapsed tumors. This is illustrated by Langenberg *et al.* for different types of pediatric tumors including 5 patients with relapsed rhabdomyosarcoma and a case report on a single patient with refractory rhabdomyosarcoma by Acanda de la Rocha *et al.* (13,14) Personalized therapies included inhibitors of CDK4/6, PARP and FGFR4. (14)

Response monitoring for rhabdomyosarcoma with the RNA panel

Two important clinical challenges are identifying patients with poor response to first line treatment and (early) relapse detection. Considering the application of RT-qPCR in blood and BM for response monitoring, previous studies analyzed small numbers of inconsistently sampled blood and BM samples.(4–6,15). However, the results suggested that persisting RNA-positivity or (re)-emerging RNA-positivity is associated to poor clinical outcome. In **Chapter 2**, we analyzed serial samples from 20 patients. For blood samples, only one patient had a positive blood sample after 3 cycles of frontline therapy and once more shortly before death due to progressive disease. Three out of 10 blood samples at relapse were positive. BM was available at relapse for 5 patients and was positive for only 1 patient. All the other 41 blood samples collected during first line treatment and 34 samples during follow-up were negative. Notably, blood and BM samples drawn shortly before diagnosis of relapse were lacking.

As stated before, a lack of standardized sampling during first line treatment and follow-up is an important limitation. Comparison to the previous cohorts from the early 2000's is further complicated by difference in the frequency of BM sampling after initial diagnosis, with a tendency towards a higher number of BM sampling within these historical cohorts than within current treatment protocols. Another variable is the sensitivity and specificity of the *MYOD1* assay. We updated the design of the *MYOD1* assay to be fully specific for the transcript, since we found that the previously published design also amplified genomic DNA. This potentially false positive signal might be one explanation for the proportionately more positive follow up samples in the cohorts from Sartori *et al.*, Gallego *et al.* and Krskova *et al.*

Finally, clonal evolution of the tumor cells during treatment could result in distinct gene expression which would require a different combination of genes in the RNA panel. Data on gene expression in relapsed tumors were not available for our cohort but considering the increase in genetic data from pediatric refractory and recurrent tumors that is currently being generated,(14,16–18) we expect that in the future these gene expression data can advise a modified RNA panel for recurrence monitoring. Potentially, this modified panel would also be more suited to use for treatment response monitoring during frontline treatment.

RNA panel in rhabdomyosarcoma: future directions

During a follow-up liquid biopsy add-on study within the European paediatric Soft tissue sarcoma Study Group (EpSSG) multi-center clinical trial for Frontline and Relapsed Rhabdomyosarcoma (FaR RMS), which will include a larger number

of patients, we plan to validate our findings on the added value for treatment stratification by the RNA panel for blood and BM at diagnosis, and the possible increase of sensitivity of RT-qPCR in BM to conventional immunohistochemistry. Furthermore, by standardized sampling of blood and BM during first line treatment and follow-up, we want to investigate the potential for response monitoring by the RNA panel in serial PB and BM samples, possibly with a modified RNA panel. Finally, we will study whether the novel markers have an added value, apart from the traditional *MYOD1*, *MYOG* and the fusion genes. If not, it would be more efficient to continue with a selection of the markers, probably thus consisting of *MYOG*, *MYOD1*, *PAX-FOXO* and *CDH11*.

Liquid biopsies in rhabdomyosarcoma: different approaches for cell-free DNA analysis

We also explored several DNA-based approaches for the detection of tumor-derived cell-free DNA (cfDNA) from plasma, also in relation to clinical features. Plasma represents a very attractive source for biomarkers, since it is sampled less invasively than BM. Furthermore, the genetic landscape of rhabdomyosarcoma tumors offers a myriad of potential targets.

We were one of the first to analyze cfDNA in a large cohort of 57 well-characterized patients with rhabdomyosarcoma, as presented in **Chapter 4**. The finding that total cfDNA levels at diagnosis were not significantly higher in the patients with more aggressive disease (e.g. larger tumor size, alveolar subtype or metastatic disease) was in agreement with what we found in **Chapter 5** and as previously published by Klega *et al.* for 7 patients with alveolar rhabdomyosarcoma.(19) This is in contrast with what was found in neuroblastoma. In 2 reports from the same research group on cfDNA from plasma from patients with neuroblastoma, they demonstrated that the total level of cfDNA was higher in patients with a higher tumor burden at diagnosis and in patients with relapse.(20,21) In these studies, total cfDNA was quantified using qPCR. Wang *et al.* compared levels of total cfDNA in 79 patients at initial diagnosis of neuroblastoma to 79 patients with stable disease almost 2 years after diagnosis and found a higher level of cfDNA in newly diagnosed patients (265.80 ng/ml \pm 139.08 vs 23.70 ng/ml \pm 23.90).(20) Furthermore, they also demonstrated that patients with metastatic disease and larger tumor size had higher cfDNA levels (respectively 1465.5 vs 113.6 ng/mL and 861.8 vs 296.0 ng/ml).(20) Su *et al.* measured total cfDNA levels in 116 patients every 3 months from the start of maintenance therapy, and at relapse. Thirty-six of the 116 patients suffered from relapse and the median total cfDNA concentration at relapse was significantly higher than in patients without relapse (29.34 ng/ml vs 10.32 ng/ml).(22) Moreover, on average half a month before

clinical evidence of relapse, the cfDNA concentration rose above 29 ng/ml.(22) These differences in findings for rhabdomyosarcoma and neuroblastoma illustrate that the dynamics of total cfDNA can vary in different tumor entities and that findings from one tumor type cannot simply be extrapolated to other tumor types.

In **Chapter 4** we analyzed the methylation profile of circulating tumor cfDNA from 26 diagnostic plasma samples from patients with rhabdomyosarcoma using cell-free reduced representation bisulphite sequencing (cfRRBS), as published in the study by van Paemel *et al.*(23) The discovery that in more than 90% of the samples a rhabdomyosarcoma-specific profile was detected and that in 20/26 (77%) the methylation profile aligned with the correct tumor subtype, demonstrated how robust this technique is. This underlines the potential of cfRRBS to assist in the initial diagnostic workflow, especially if a tumor biopsy is not possible and a diagnosis is essential to start effective treatment as soon as possible. A next step might be to explore the potential of cfRRBS as a technique to detect tumor-derived cfDNA during treatment, as a marker for residual disease. However, since we observed that the levels of tumor-derived cfDNA are low during treatment, it must be determined whether cfRRBS would be sensitive enough.

Detection of copy number aberrations (CNA) in cfDNA during or after therapy can also be used to study disease response in liquid biopsies. Shallow whole genome sequencing is mostly used for detection of CNA, but these can also be detected by cfRRBS.(23) In **Chapter 4**, we applied copy number profiling to diagnostic plasma of 30 patients, resulting in 16 samples with CNA. CNA were mostly detected in plasma of patients with metastatic disease. It would be interesting to explore the potential of CNA detection in follow-up samples further, however the sensitivity in relation to low levels of tumor-derived cfDNA could be limited.

Patient-specific droplet digital PCR assays

The fusion gene breakpoints are well suited for patient-specific droplet digital (ddPCR) assays. We present a concise approach to determine the patient-specific fusion breakpoint, based on targeted locus amplification (TLA) as discussed in **Chapter 6**. An alternative approach to obtain the patient-specific fusion breakpoint is a next generation sequencing (NGS) panel targeting the rhabdomyosarcoma-specific fusion partners (e.g., *PAX3*, *PAX7* and *FOXO1*), as we present in **Chapter 5**. Both TLA and NGS approaches can result in design of a patient-specific assay within weeks after initial diagnosis. Our results, and other studies,(19,24) have shown that these breakpoints remain stable throughout the entire course of the disease. This makes fusion breakpoint assays well suited for implementation in clinical practice for response

monitoring. For fusion-negative tumors, several options remain. These tumors have been shown to contain at least 1 single nucleotide variation (SNV) in 80% of cases, as well as structural chromosomal variations, with amplifications or deletions.(25,26) As we have shown in **Chapters 3, 4, 5, and 6**, all these genetic aberrations can be used for patient-specific droplet digital (ddPCR) assays. However, this requires quite an extensive sequencing effort of the tumor at primary diagnosis. Furthermore, studies comparing genetic aberration in primary and relapsed tumors are lacking, but these are crucial for information on the stability of specific SNVs during the course of the disease. Currently, analysis through whole exome sequencing, methylation profiling and RNA sequencing of the primary tumor is standard of care at the Princess Máxima Center and is also often offered in relapsed tumors, with the goal of identifying targets for precision medicine. Similar initiatives have been launched internationally, so we expect that these data will become available within the coming years and can inform selection of liquid biopsy targets at the initial diagnosis.

Hypermethylated RASSF1A as a target for ddPCR

The most compelling finding described in **Chapters 3 and 4**, is on the detection of the hypermethylated tumor suppressor gene *RASSF1A* (*RASSF1A-M*) in plasma. *RASSF1A* is a tumor suppressor gene that is often hypermethylated in many tumors, both adult and pediatric, as shown in an impressive number of reports during the last two decades.(27–49) We found that *RASSF1A-M* positivity in plasma at diagnosis was associated with poor clinical outcome, especially in patients testing positive for *RASSF1A-M* and for the RNA panel in the matching cellular fraction. The limited number of patients did not allow for extensive multivariate analyses on the additional value of both molecular techniques to current treatment stratification. This is especially important since there seemed to be a tendency for double positivity in patients with metastatic disease. It is crucial to investigate the value of these liquid biopsy-based analyses further for their complementary value in a larger cohort of patients, which we will within the FaR RMS liquid biopsy add-on study. It is interesting to hypothesize whether the presence of hypermethylation of *RASSF1A* is a characteristic of more aggressive disease in rhabdomyosarcoma. This would also require analysis of the primary tumor itself. Within the previously mentioned FaR RMS add-on, we strive towards analysis of matched tumor and plasma, also including methylation.

Towards implementation of liquid biopsies in the treatment of rhabdomyosarcoma

Considering the results presented in this thesis and in literature on the potential of liquid biopsies in rhabdomyosarcoma, the next step is incorporation of liquid biopsies in standard diagnostics. This requires dedicated validation studies consisting

of well-timed samples to also evaluate added value for response monitoring and relapse surveillance. Implementation of liquid biopsies in large international clinical trials is therefore essential. Apart from the liquid biopsy add-on within the FaR RMS trial, collaboration with the Northern American Children Oncology Group (COG) and the German Cooperative Weichteilsarkom Studiengruppe (CWS) would speed up this process and thereby presumably implementation in clinical practice of liquid biopsies. An important challenge in these collaborations are the distinct molecular platforms applied to analyze cfDNA and RNA from liquid biopsies across the different laboratories. This is often presented as hampering reproducibility, which results in slowing down of validation in independent cohorts. However, this supposed limitation might represent an opportunity. If laboratories would collaborate to validate each other's findings through their respective molecular platforms, this would underline the robustness of a finding.

Ultimately, the question is whether it would matter if tumor-derived cfDNA or RNA is detected by a targeted PCR or a sequencing platform? Within the EpSSG, we are now working on projects to validate the different molecular platforms of the collaborating laboratories and comparing their sensitivity, using so-called 'round robin sendings' which consist of well-characterized synthetic reference samples. Hopefully this effort will result in a more standardized and collaborative infrastructure for rhabdomyosarcoma liquid biopsies studies in Europe.

Part II: Novel biomarkers from plasma

Extracellular vesicles in pediatric solid tumors

In **Part II**, we explored novel sources of biomarkers from liquid biopsies. In the last decade, publications on extracellular vesicles (EV) have increased exponentially. These particles are very intriguing for their diagnostic potential and for their function in health and disease. Since it has been shown that EV are involved in all hallmarks of cancer, ranging from cell proliferation to preparation of the metastatic niche and the induction of therapy resistance, further research could result in novel therapeutic modalities.^(50–55) However, the methods for EV isolation and subsequent analysis are extremely heterogeneous and result in diverse outcomes regarding data on EV characterization and content analysis, as we illustrate in the review in **Chapter 7**. EV-based studies validating previous results in large patient cohorts are absent, which keeps EV-based biomarker research from reaching clinical practice. A structured approach to EV isolation and analysis has already been advocated by the International Society for Extracellular Vesicles (ISEV), culminating

in the MISEV (Minimal Information required for Studies of Extracellular Vesicles) guidelines.(56,57) However, these are mostly intended for *in vitro* studies and for clinical samples collected from adults. As we also argue in **Chapter 7**, the field of pediatric oncology faces more challenges considering the low patient numbers and limited sample volumes. As illustrated in **Chapter 8**, the analysis of EV from pediatric patients cannot comply with an extensive quantification and characterization of EV from all patients, as well as all subsequent analyses. We could only perform a limited number of experiments for EV characterization due to low sample volumes. It is worth considering a pediatric-only initiative, similar to the MISEV guidelines, which specifies the minimal requirements for EV characterization and analysis of pediatric samples within studies. Pediatric EV research on clinical samples might benefit from a dichotomy within studies, one part focusing on a (limited) number of experiments for the quantification and characterization of the EV from the chosen enrichment method, as to confirm EV presence and characteristics; and a second part dedicated to the development and validation of EV-based markers in the clinical patient samples. This second part would also need to focus on feasibility within a clinical setting. For example, in **Chapter 8** we concluded that enrichment of EV did not result in a concentration of the targets. Follow up research for these specific targets would not need to involve EV enrichment, which would save time and means. In general, implementation of biomarkers in clinical practice would benefit from critical assessment of the techniques and platforms employed, and from studies reproducing findings and validating these in independent cohorts. Collaboration on an international level is crucial if liquid biopsy-based techniques are to reach the bedside, especially for pediatric oncology.

Analysis of cell-free RNA from plasma

Chapter 8 offers an illustration of the challenges arising in the analysis of the cell-free plasma compartment. We performed an explorative study of cell-free RNA (cfRNA) from plasma from patients with neuroblastoma and the association of cfRNA to EV. To use the limited sample volumes efficiently, we employed a multiplexed ddPCR for cfRNA analysis. Pre-analytical conditions were suboptimal in this project due to platelet contamination of the plasma. Platelets contain RNA, and can by themselves form a biomarkers source, as is shown for adult malignancies by the group of Wurdinger.(58–61) However, when focusing on cell-free RNA, the presence of platelet-derived RNA affects RNA analysis. We attempted to reduce this effect by devising a correction formula, but this remains suboptimal and limits reproducibility.

Due to a lack of literature on the pediatric cell-free transcriptome, the choice of RNA markers, including reference genes, was based on our experience in the analysis

of the cellular compartment of blood for the neuroblastoma-specific markers. Pragmatically, we chose two reference genes that we already used for RT-qPCR analysis in the cellular compartment of blood, *GUSB* and *B2M*. However, an unbiased approach using sequencing of plasma-derived cfRNA, similar to the study in adults including healthy controls by Larson *et al.*,⁽⁶²⁾ would result in a more comprehensive perspective on the plasma transcriptome. Notably, since the gene expression in cfRNA from pediatric plasma is probably very variable, reflecting the dynamics of a growing and developing child, this would require analysis of gene expression in plasma from differently aged children. Ultimately, a comparison of the cell-free transcriptome between age and gender-matched healthy children and children with different types of disease, e.g., malignancies, infectious and inflammatory diseases, would give the best overview. Rightfully, ethical dilemmas are raised if research in children is concerned and sampling healthy children for research that they do not directly benefit from is controversial. One way to overcome this hurdle, is the use of rest material from otherwise healthy children that undergo small surgical procedures or present in the emergency department. If thought out well enough, this effort could result in a cell-free atlas of the different plasma-derived particles, including the different types of RNA, proteomics and cfDNA, further elaborating on the different (epi-)genetic characteristics of these DNA fragments. Within the Princess Máxima Center, we are collaborating with different pediatric initiatives to set up the infrastructure to collect rest material of different body fluids, including blood, urine, and cerebro-spinal fluid.

Novel biomarkers for pediatric oncology: way forward

Research into novel biomarkers from plasma for application in pediatric oncology is very appealing but should also focus on cost-effectiveness and lead to a workflow suited for clinical practice. Although it is ethically challenging, studies into the characterization of the cell-free plasma compartment of healthy children are an essential starting point for further studies into clinical application of plasma-based biomarkers. This would also create the foundation for biomarker development for early detection of malignancy in patients with tumor predisposition syndromes.

Concluding remarks

This thesis demonstrates that liquid biopsy-based analysis is immensely versatile and can improve current diagnostic modalities in pediatric solid tumors, especially rhabdomyosarcoma. It intends to form a steppingstone towards the incorporation of liquid biopsy analyses in clinical practice. This goal requires further international collaboration and a shared vision that also focuses on clinical application as well as on the development of novel analytical techniques. Ultimately, the aim remains

improving the survival of children with pediatric rhabdomyosarcoma while maintaining a good quality of life. Liquid biopsies have shown their potential and should proceed from bench to bedside.



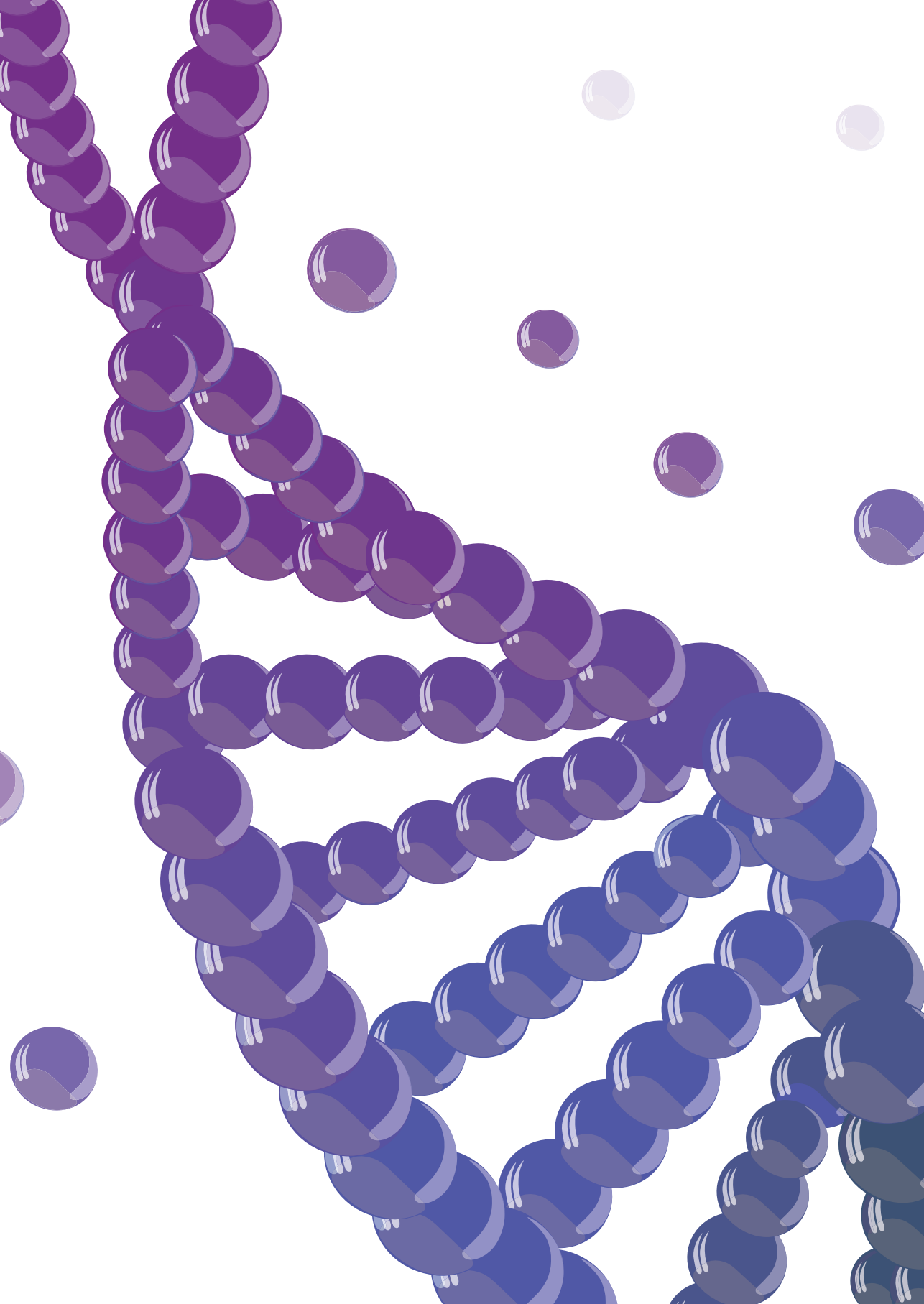
References

1. Galili N, Davis RJ, Fredericks WJ, Mukhopadhyay S, Rauscher FJ, Emanuel BS, et al. Fusion of a fork head domain gene to PAX3 in the solid tumour alveolar rhabdomyosarcoma. *Nat Genet.* 1993 Nov 1;5(3):230–5.
2. Davis RJ, D’Cruz CM, Lovell MA, Biegel JA, Barr FG. Fusion of PAX7 to FKHR by the variant t(1;13) (p36;q14) translocation in alveolar rhabdomyosarcoma. *Cancer Res.* 1994 Jun 1;54(11):2869–72.
3. Kelly KM, Womer RB, Barr FG. Minimal disease detection in patients with alveolar rhabdomyosarcoma using a reverse transcriptase-polymerase chain reaction method. *Cancer.* 1996 Sep 15;78(6):1320–7.
4. Sartori F, Alaggio R, Zanazzo G, Garaventa A, Di Cataldo A, Carli M, et al. Results of a prospective minimal disseminated disease study in human rhabdomyosarcoma using three different molecular markers. *Cancer: Interdisciplinary International Journal of the American Cancer Society.* 2006;106(8):1766–75.
5. Michelagnoli MP, Burchill SA, Cullinane C, Selby PJ, Lewis IJ. Myogenin—a more specific target for RT-PCR detection of rhabdomyosarcoma than MyoD1. *Med Pediatr Oncol* [Internet]. 2003;40(1):1–8. Available from: <https://www.ncbi.nlm.nih.gov/pubmed/12426678>
6. Gallego S, Llorca A, Roma J, Sabado C, Gros L, de Toledo JS. Detection of bone marrow micrometastasis and microcirculating disease in rhabdomyosarcoma by a real-time RT-PCR assay. *J Cancer Res Clin Oncol* [Internet]. 2006;132(6):356–62. Available from: <https://www.ncbi.nlm.nih.gov/pubmed/16435141>
7. Oberlin O, Rey A, Lyden E, Bisogno G, Stevens MC, Meyer WH, et al. Prognostic factors in metastatic rhabdomyosarcomas: results of a pooled analysis from United States and European cooperative groups. *J Clin Oncol* [Internet]. 2008;26(14):2384–9. Available from: <https://www.ncbi.nlm.nih.gov/pubmed/18467730>
8. Bailey KA, Wexler LH. Pediatric rhabdomyosarcoma with bone marrow metastasis. *Pediatr Blood Cancer* [Internet]. 2020;67(5):e28219. Available from: <https://www.ncbi.nlm.nih.gov/pubmed/32100935>
9. Schoot RA, Chisholm JC, Casanova M, Minard-Colin V, Georger B, Cameron AL, et al. Metastatic Rhabdomyosarcoma: Results of the European *Paediatric* Soft Tissue Sarcoma Study Group MTS 2008 Study and Pooled Analysis With the Concurrent BERNIE Study. *Journal of Clinical Oncology.* 2022 Nov 10;40(32):3730–40.
10. Chisholm JC, Merks JHM, Casanova M, Bisogno G, Orbach D, Gentet JC, et al. Open-label, multicentre, randomised, phase II study of the EpSSG and the ITCC evaluating the addition of bevacizumab to chemotherapy in childhood and adolescent patients with metastatic soft tissue sarcoma (the BERNIE study). *Eur J Cancer* [Internet]. 2017;83:177–84. Available from: <https://www.ncbi.nlm.nih.gov/pubmed/28738258>
11. Grünewald TG, Alonso M, Avnet S, Banito A, Burdach S, Cidre-Aranaz F, et al. Sarcoma treatment in the era of molecular medicine. *EMBO Mol Med.* 2020 Nov 6;12(11).
12. van Erp AEM, Versleijen-Jonkers YMH, van der Graaf WTA, Fleuren EDG. Targeted Therapy-based Combination Treatment in Rhabdomyosarcoma. *Mol Cancer Ther.* 2018 Jul 1;17(7):1365–80.
13. Acanda De La Rocha AM, Fader M, Coats ER, Espinal PS, Berrios V, Saghira C, et al. Clinical Utility of Functional Precision Medicine in the Management of Recurrent/Relapsed Childhood Rhabdomyosarcoma. *JCO Precis Oncol.* 2021 Nov;(5):1659–65.
14. Langenberg KPS, Meister MT, Bakhuizen JJ, Boer JM, van Eijkelenburg NKA, Hulleman E, et al. Implementation of paediatric precision oncology into clinical practice: The Individualized Therapies for Children with cancer program ‘iTHER’. *Eur J Cancer.* 2022 Nov;175:311–25.

15. Krsková L, Mrhalová M, Hilská I, Sumerauer D, Drahokoupilová E, Múdry P, et al. Detection and clinical significance of bone marrow involvement in patients with rhabdomyosarcoma. *Virchows Archiv*. 2010;456(5):463–72.
16. van Tilburg CM, Pfaff E, Pajtler KW, Langenberg KPS, Fiesel P, Jones BC, et al. The Pediatric Precision Oncology INFORM Registry: Clinical Outcome and Benefit for Patients with Very High-Evidence Targets. *Cancer Discov*. 2021 Nov 1;11(11):2764–79.
17. Berlanga P, Pierron G, Lacroix L, Chicard M, Adam de Beaumais T, Marchais A, et al. The European MAPPYACTS Trial: Precision Medicine Program in Pediatric and Adolescent Patients with Recurrent Malignancies. *Cancer Discov*. 2022 May 2;12(5):1266–81.
18. Jones DTW, Banito A, Grünewald TGP, Haber M, Jäger N, Kool M, et al. Molecular characteristics and therapeutic vulnerabilities across paediatric solid tumours. *Nat Rev Cancer*. 2019 Aug 12;19(8):420–38.
19. Klega K, Imamovic-Tuco A, Ha G, Clapp AN, Meyer S, Ward A, et al. Detection of Somatic Structural Variants Enables Quantification and Characterization of Circulating Tumor DNA in Children With Solid Tumors. *JCO Precis Oncol* [Internet]. 2018;2018. Available from: <https://www.ncbi.nlm.nih.gov/pubmed/30027144>
20. Wang X, Wang L, Su Y, Yue Z, Xing T, Zhao W, et al. Plasma cell-free DNA quantification is highly correlated to tumor burden in children with neuroblastoma. *Cancer Med*. 2018 Jul 14;7(7):3022–30.
21. Su Y, Wang L, Jiang C, Yue Z, Fan H, Hong H, et al. Increased plasma concentration of cell-free DNA precedes disease recurrence in children with high-risk neuroblastoma. *BMC Cancer*. 2020 Dec 6;20(1):102.
22. Su Y, Wang L, Jiang C, Yue Z, Fan H, Hong H, et al. Increased plasma concentration of cell-free DNA precedes disease recurrence in children with high-risk neuroblastoma. *BMC Cancer*. 2020;20(1):102.
23. Paemel R Van, Koker A De, Vandeputte C, Van L, Lammens T, Laureys G, et al. Minimally invasive classification of paediatric solid tumours using reduced representation bisulphite sequencing of cell-free DNA : a proof-of-principle study. *Epigenetics* [Internet]. 2020;00(00):1–13. Available from: <https://doi.org/10.1080/15592294.2020.1790950>
24. Eguchi-Ishimae M, Tezuka M, Koikeguchi T, Nagai K, Moritani K, Yonezawa S, et al. Early detection of the PAX3-FOXO1 fusion gene in circulating tumor-derived DNA in a case of alveolar rhabdomyosarcoma. *Genes Chromosomes Cancer* [Internet]. 2019;58(8):521–9. Available from: <https://www.ncbi.nlm.nih.gov/pubmed/30739374>
25. Seki M, Nishimura R, Yoshida K, Shimamura T, Shiraishi Y, Sato Y, et al. Integrated genetic and epigenetic analysis defines novel molecular subgroups in rhabdomyosarcoma. *Nat Commun* [Internet]. 2015;6:7557. Available from: <https://www.ncbi.nlm.nih.gov/pubmed/26138366>
26. Hettmer S, Linardic CM, Kelsey A, Rudzinski ER, Vokuhl C, Selfe J, et al. Molecular testing of rhabdomyosarcoma in clinical trials to improve risk stratification and outcome: A consensus view from European paediatric Soft tissue sarcoma Study Group, Children's Oncology Group and Cooperative Weichteilsarkom-Studiengruppe. *Eur J Cancer*. 2022 Sep;172:367–86.
27. Donninger H, Schmidt ML, Mezzanotte J, Barnoud T, Clark GJ. Ras signaling through RASSF proteins. *Semin Cell Dev Biol* [Internet]. 2016;58:86–95. Available from: <https://dx.doi.org/10.1016/j.semcdb.2016.06.007>
28. Volodko N, Salla M, Zare A, Abulghasem EA, Vincent K, Benesch MGK, et al. RASSF1A site-specific methylation hotspots in cancer and correlation with RASSF1C and MOAP-1. *Cancers (Basel)*. 2016;8(6).
29. Malpeli G, Amato E, Dandrea M, Fumagalli C, Debattisti V, Boninsegna L, et al. Methylation-associated down-regulation of RASSF1A and up-regulation of RASSF1C in pancreatic endocrine tumors. *BMC Cancer*. 2011/08/16. 2011;11:351.

30. Bin Y, Ding Y, Xiao W, Liao A. RASSF1A: A promising target for the diagnosis and treatment of cancer. *Clinica Chimica Acta* [Internet]. 2020;504(January):98–108. Available from: <https://doi.org/10.1016/j.cca.2020.01.014>
31. Vos MD, Ellis CA, Bell A, Birrer MJ, Clark GJ. Ras uses the novel tumor suppressor RASSF1 as an effector to mediate apoptosis. *J Biol Chem*. 2000/09/22. 2000;275(46):35669–72.
32. Dubois F, Bergot E, Zalczman G, Levallet G. RASSF1A, puppeteer of cellular homeostasis, fights tumorigenesis, and metastasis-an updated review. *Cell Death Dis*. 2019/12/06. 2019;10(12):928.
33. Levallet G, Creveuil C, Bekaert L, Peres E, Planchard G, Lecot-Cotigny S, et al. Promoter Hypermethylation of Genes Encoding for RASSF/Hippo Pathway Members Reveals Specific Alteration Pattern in Diffuse Gliomas. *J Mol Diagn* [Internet]. 2019/05/06. 2019;21(4):695–704. Available from: <https://www.ncbi.nlm.nih.gov/pubmed/31055025>
34. Donninger H, Vos MD, Clark GJ. The RASSF1A tumor suppressor. *J Cell Sci*. 2007/09/20. 2007;120(Pt 18):3163–72.
35. Lim S, Yang MH, Park JH, Nojima T, Hashimoto H, Unni KK, et al. Inactivation of the RASSF1A in osteosarcoma. *Oncol Rep* [Internet]. 2003;10(4):897–901. Available from: <https://www.ncbi.nlm.nih.gov/pubmed/12792742>
36. Hesson LB, Cooper WN, Latif F. The role of RASSF1A methylation in cancer. *Dis Markers*. 2007;23(1–2):73–87.
37. Wong IHN, Chan J, Wong J, Tam PKH. Ubiquitous Aberrant RASSF1A Promoter Methylation in Childhood Neoplasia. *Clinical Cancer Research*. 2004;10(3):994–1002.
38. Tian Y, Hou Y, Zhou X, Cheng H, Zhou R. Tumor suppressor RASSF1A promoter: p53 binding and methylation. *PLoS One*. 2011/03/03. 2011;6(2):e17017.
39. Schmidt ML, Hobbing KR, Donninger H, Clark GJ. RASSF1A Deficiency Enhances RAS-Driven Lung Tumorigenesis. *Cancer Res* [Internet]. 2018;78(10):2614–23. Available from: <https://dx.doi.org/10.1158/0008-5472.can-17-2466>
40. Grawenda AM, O’Neill E. Clinical utility of RASSF1A methylation in human malignancies. *Br J Cancer* [Internet]. 2015;113(3):372–81. Available from: <https://www.ncbi.nlm.nih.gov/pubmed/26158424>
41. Malpeli G, Innamorati G, Decimo I, Bencivenga M, Nwabo Kamdje AH, Perris R, et al. Methylation Dynamics of RASSF1A and Its Impact on Cancer. *Cancers (Basel)*. 2019/07/22. 2019;11(7).
42. Lázcoz P, Muñoz J, Nistal M, Pestaña Á, Encío I, Castresana JS. Frequent promoter hypermethylation of RASSF1A and CASP8 in neuroblastoma. *BMC Cancer*. 2006;6:1–10.
43. Honda S, Miyagi H, Suzuki H, Minato M, Haruta M, Kaneko Y, et al. RASSF1A methylation indicates a poor prognosis in hepatoblastoma patients. *Pediatr Surg Int* [Internet]. 2013;29(11):1147–52. Available from: <https://www.ncbi.nlm.nih.gov/pubmed/23989600>
44. Avigad S, Shukla S, Naumov I, Cohen IJ, Ash S, Meller I, et al. Aberrant methylation and reduced expression of RASSF1A in Ewing sarcoma. *Pediatr Blood Cancer*. 2009/07/29. 2009;53(6):1023–8.
45. Fu L, Zhang S. RASSF1A promotes apoptosis and suppresses the proliferation of ovarian cancer cells. *Int J Mol Med* [Internet]. 2014;33(5):1153–60. Available from: <https://dx.doi.org/10.3892/ijmm.2014.1671>
46. Xu G, Zhou X, Xing J, Xiao Y, Jin B, Sun L, et al. Identification of RASSF1A promoter hypermethylation as a biomarker for hepatocellular carcinoma. *Cancer Cell Int* [Internet]. 2020/12/10. 2020;20(1):547. Available from: <https://www.ncbi.nlm.nih.gov/pubmed/33292241>
47. Astuti D, Agathangelou A, Honorio S, Dallol A, Martinsson T, Kogner P, et al. RASSF1A promoter region CpG island hypermethylation in pheochromocytomas and neuroblastoma tumours. *Oncogene* [Internet]. 2001;20(51):7573–7. Available from: <https://www.ncbi.nlm.nih.gov/pubmed/11709729>

48. van Zogchel LMJ, van Wezel EM, van Wijk J, Stutterheim J, Bruins WSC, Zappeij-Kannegieter L, et al. Hypermethylated RASSF1A as Circulating Tumor DNA Marker for Disease Monitoring in Neuroblastoma. *JCO Precis Oncol* [Internet]. 2020;4. Available from: <https://www.ncbi.nlm.nih.gov/pubmed/32923888>
49. Misawa A, Tanaka S, Yagyu S, Tsuchiya K, Iehara T, Sugimoto T, et al. RASSF1A hypermethylation in pretreatment serum DNA of neuroblastoma patients: a prognostic marker. *Br J Cancer* [Internet]. 2009;100(2):399–404. Available from: <https://www.ncbi.nlm.nih.gov/pubmed/19165202>
50. Becker A, Thakur BK, Weiss JM, Kim HS, Peinado H, Lyden D. Extracellular Vesicles in Cancer: Cell-to-Cell Mediators of Metastasis. *Cancer Cell* [Internet]. 2016;30(6):836–48. Available from: <https://www.ncbi.nlm.nih.gov/pubmed/27960084>
51. Peinado H, Zhang H, Matei IR, Costa-Silva B, Hoshino A, Rodrigues G, et al. Pre-metastatic niches: organ-specific homes for metastases. *Nat Rev Cancer*. 2017 May 17;17(5):302–17.
52. Tamura T, Yoshioka Y, Sakamoto S, Ichikawa T, Ochiya T. Extracellular Vesicles in Bone Metastasis: Key Players in the Tumor Microenvironment and Promising Therapeutic Targets. *Int J Mol Sci* [Internet]. 2020;21(18). Available from: <https://www.ncbi.nlm.nih.gov/pubmed/32932657>
53. Xavier CPR, Caires HR, Barbosa MAG, Bergantim R, Guimaraes JE, Vasconcelos MH. The Role of Extracellular Vesicles in the Hallmarks of Cancer and Drug Resistance. *Cells* [Internet]. 2020;9(5). Available from: <https://www.ncbi.nlm.nih.gov/pubmed/32384712>
54. Hanahan D, Weinberg RA. Hallmarks of cancer: the next generation. *Cell* [Internet]. 2011;144(5):646–74. Available from: <https://www.ncbi.nlm.nih.gov/pubmed/21376230>
55. Hanahan D, Weinberg RA. The hallmarks of cancer. *Cell* [Internet]. 2000;100(1):57–70. Available from: <https://www.ncbi.nlm.nih.gov/pubmed/10647931>
56. Thery C, Witwer KW, Aikawa E, Alcaraz MJ, Anderson JD, Andriantsitohaina R, et al. Minimal information for studies of extracellular vesicles 2018 (MISEV2018): a position statement of the International Society for Extracellular Vesicles and update of the MISEV2014 guidelines. *J Extracell Vesicles* [Internet]. 2018;7(1):1535750. Available from: <https://www.ncbi.nlm.nih.gov/pubmed/30637094>
57. Lotvall J, Hill AF, Hochberg F, Buzas EI, di Vizio D, Gardiner C, et al. Minimal experimental requirements for definition of extracellular vesicles and their functions: a position statement from the International Society for Extracellular Vesicles. *J Extracell Vesicles* [Internet]. 2014;3:26913. Available from: <https://www.ncbi.nlm.nih.gov/pubmed/25536934>
58. Wurdinger T, In 't Veld SGJG, Best MG. Platelet RNA as Pan-Tumor Biomarker for Cancer Detection. *Cancer Res* [Internet]. 2020 Apr 1;80(7):1371–3. Available from: <https://aacrjournals.org/cancerres/article/80/7/1371/647760/Platelet-RNA-as-Pan-Tumor-Biomarker-for-Cancer>
59. Best MG, Vancura A, Wurdinger T. Platelet RNA as a circulating biomarker trove for cancer diagnostics. *Journal of Thrombosis and Haemostasis*. 2017 Jul;15(7):1295–306.
60. Best MG, Wesseling P, Wurdinger T. Tumor-Educated Platelets as a Noninvasive Biomarker Source for Cancer Detection and Progression Monitoring. *Cancer Res*. 2018 Jul 1;78(13):3407–12.
61. Best MG, Sol N, In 't Veld SGJG, Vancura A, Muller M, Niemeijer ALN, et al. Swarm Intelligence-Enhanced Detection of Non-Small-Cell Lung Cancer Using Tumor-Educated Platelets. *Cancer Cell*. 2017 Aug;32(2):238–252.e9.
62. Larson MH, Pan W, Kim HJ, Mauntz RE, Stuart SM, Pimentel M, et al. A comprehensive characterization of the cell-free transcriptome reveals tissue- and subtype-specific biomarkers for cancer detection. *Nat Commun*. 2021 Apr 21;12(1):2357.



Appendices

English summary

Nederlandse samenvatting

Curriculum Vitae

Acknowledgements

English summary

In **Part I** of this thesis, the main focus was on liquid biopsies in patients with rhabdomyosarcoma. We reported on the first prospective collection of blood and bone marrow samples from Dutch patients treated for rhabdomyosarcoma in **Chapter 2**. We describe the development of a rhabdomyosarcoma-specific RNA panel for the use in multiplex real-time quantitative PCR (RT-qPCR) assays. To eliminate false positivity due to background expression in healthy blood and bone marrow cells, we established a threshold for positivity of our 11-marker panel in healthy hematopoietic cells. Subsequently, we proceeded to measuring the samples from 99 patients and demonstrate that presence of rhabdomyosarcoma-specific mRNA in blood and/or bone marrow at diagnosis is associated to poor prognosis.

The tumor suppressor gene *RASSF1A* has been shown to be silenced by hypermethylation in many tumors, adult as well as pediatric. In **Chapter 3**, we describe in detail how we designed a specific droplet digital (ddPCR) assay for the detection of hypermethylated *RASSF1A* (*RASSF1A-M*) in cell-free DNA (cfDNA) from plasma and cerebro-spinal fluid (CSF). We demonstrated its potential as a cfDNA marker at diagnosis in plasma of patients with neuroblastoma, renal tumors, rhabdomyosarcoma, and Hodgkin lymphoma, and in CSF of patients with medulloblastoma. Furthermore, *RASSF1A-M* levels reflected tumor burden in patients with neuroblastoma, decreasing in response to therapy and increasing at relapse or progressive disease.

We explored the feasibility of different approaches for the analysis of cfDNA from patients with rhabdomyosarcoma in **Chapter 4**, by methylation profiling (cell-free reduced representation bisulphite sequencing (cfRRBS), copy number aberration (CNA) analysis, and *RASSF1A-M* ddPCR. We show that cfRRBS can sensitively detect tumor-derived cfDNA as well as CNA at diagnosis. An important finding in this chapter is that the presence of *RASSF1A-M* in plasma at diagnosis is associated with poor clinical outcome, especially for patients with metastatic disease. This association was even more apparent in patients that were positive for both *RASSF1A-M* in plasma and for the RNA panel in the matching cellular fraction. On the contrary, patients that were negative for both techniques did remarkably well, even the patients with metastatic disease.

In **Chapter 5**, we present an example of successful international collaboration for the analysis of longitudinal cfDNA samples from patients with rhabdomyosarcoma. First, a rhabdomyosarcoma patient-derived xenograft (PDX) model in mice was established, which demonstrated that presence of human, tumor-derived cfDNA in mouse plasma

correlated to tumor burden. For pediatric patients with rhabdomyosarcoma, we then analyzed tumor samples for patient-specific genetic aberrations, yielding mutations, specific gene amplifications and patient-specific genomic sequences of PAX-FOXO translocations. We used these aberrations to design patient-specific ddPCR assays for diagnostic and follow-up cfDNA samples, resulting in a positive signal in more than 75% of patients at diagnosis and confirmation that presence of tumor-derived cfDNA during follow-up reflected treatment response. Moreover, whole exome sequencing (WES) of cfDNA at diagnosis in a subset of samples with sufficient cfDNA input, detected tumor-derived aberrations in 7/7 samples. We concluded that tumor-derived cfDNA can be detected by both ddPCR and WES at diagnosis and that its presence can be used to monitor treatment response.

The potential of patient-specific ddPCR assays was further explored in different types of pediatric solid tumors in **Chapter 6**. This chapter illustrated that apart from fusion genes, regions with copy number aberrations can be employed for the design of patient-specific ddPCR assays. We present a workflow for the design of these assays using targeted locus amplification (TLA) on DNA from tumor-derived organoids or formalin-fixed paraffin-embedded (FFPE) tumor material in collaboration with Cergentis. We then proceeded to measure these patient-specific targets in cfDNA from diagnostic and follow-up samples from patients with neuroblastoma, rhabdomyosarcoma, and Ewing sarcoma. These targets were present in all diagnostic and relapse plasma samples. In neuroblastoma, the levels of the targets reflected tumor burden, with a decrease in patients with a good response to treatment and an increase in relapsed disease. In rhabdomyosarcoma and Ewing sarcoma, all sequential samples were negative, but well-timed samples, e.g., at progressive disease or relapse, were lacking.

In **part II**, we explored extracellular vesicles (EV) as novel cell-free markers from plasma. We first reviewed the studies on EV-derived biomarkers in different pediatric solid tumors in **Chapter 7**. We used a published scoring tool (EV-METRIC) and our own in-house PedEV score to grade studies for their in vitro/in vivo validation and reproducibility. After a systematic literature review, studies on desmoplastic small round cell tumors (DSRCT), neuroblastoma, hepatoblastoma, rhabdomyosarcoma, osteosarcoma and Ewing sarcoma were included. Ultimately, we concluded that implementation of EV-derived biomarkers in clinical practice is hampered by a lack of reproducibility in methodology and a scarcity of validation in clinically relevant cohorts.



In **Chapter 8** we studied the feasibility of cell-free RNA (cfRNA) analysis from plasma of patients with neuroblastoma by ddPCR, and the association of cfRNA and cfDNA to EV. For this purpose, we developed several multiplex ddPCR assays, including neuroblastoma-specific mRNA markers (*PHOX2B*, *CHRNA3* and *TH*) and introduced a novel cell cycle panel, consisting of genes involved in cell proliferation: *CDC6*, *ATAD2*, *E2F1*, *H2AFZ*, *DHFR* and *MCM2*. We tested these markers on a cohort of 40 neuroblastoma patients, with localized and metastatic disease, and studied the location of cfRNA and cfDNA in relation to EV. The EV were isolated using size exclusion chromatography (SEC) which leads to separation of particles based on size. Applying SEC to plasma results in different SEC fractions, with larger particles, including EV, eluting in earlier fractions ('EV-enriched' fractions) and smaller particles eluting later, containing smaller particles which are mostly proteins ('protein-enriched' fractions). Along the way, we encountered challenges arising from platelet contamination in the plasma for which we introduced correction formulas based on baseline expression of the cell cycle genes in healthy platelets. Finally, we observed that neuroblastoma-specific genes were only present in cfRNA from patients with metastatic disease and that *DHFR* had a higher expression in these patients, compared to patients with localized disease and healthy controls. Most cfRNA markers were concentrated in EV-enriched SEC fractions of plasma, whereas cfDNA was more prevalent in the protein-enriched SEC fractions.

Nederlandse samenvatting

In **Deel 1** van deze thesis richten we ons op het gebruik van vloeibare biopsieën in patiënten met rhabdomyosarcoom. Wij verzamelden bloed en beenmerg van 99 Nederlandse patiënten. In **Hoofdstuk 2** beschrijven wij de ontwikkeling van een panel bestaande uit 11 genen om rhabdomyosarcoom RNA te detecteren in bloed en beenmerg van patiënten. Om zeker te zijn dat we geen vals-positief signaal detecteerden, hebben we eerst het achtergrond signaal van deze genen vastgesteld in gezond bloed en beenmerg. Daarna hebben we bloed en beenmergcellen van patiënten met rhabdomyosarcoom, allemaal verzameld voordat behandeling was gestart, ook getest met dit panel. Toen bleek dat patiënten bij wie dit RNA aanwezig was in bloed of beenmerg, een aanzienlijk kortere ziektevrije overleving hadden, deze patiënten kregen sneller een terugval en hadden ook een grotere kans om te overlijden aan de ziekte.

In veel tumoren is het tumor suppressor gen *RASSF1A* gehypermethyleerd waardoor het niet meer tot expressie komt. Dit zorgt ervoor dat kankercellen onbeperkt kunnen delen en de tumor groeit. We beschrijven in **Hoofdstuk 3** hoe we een droplet digital PCR (ddPCR) hebben gemaakt om gehypermethyleerd *RASSF1A* (*RASSF1A-M*) op te sporen in het celvrije DNA (cfDNA) uit plasma en hersenvocht (liquor). We laten zien dat deze ddPCR succesvol *RASSF1A-M* kan aantonen in cfDNA uit plasma van patiënten met neuroblastoom, niertumoren, rhabdomyosarcoom en Hodgkin lymfoom en ook in de liquor van patiënten met een medulloblastoom, een type hersentumor.

In **Hoofdstuk 4** onderzoeken we verder de mogelijkheid voor analyse van cfDNA uit plasma van patiënten met rhabdomyosarcoom bij diagnose. We laten zien dat dit mogelijk is door te kijken naar het gehele genoom met betrekking tot het aantal kopieën van een bepaald gen (copy number aberration, CNA). In totaal hadden 16/30 samples CNAs. We hebben ook de methylatieprofielen van het cfDNA geanalyseerd. Hiermee kon in 20/24 het correcte rhabdomyosarcoom profiel worden aangetoond. Met de *RASSF1A-M* ddPCR analyseerden we 57 diagnostische cfDNA samples waarvan er 21 positief testten. Hiermee toonden we aan dat patiënten waar *RASSF1A-M* aanwezig was in plasma bij diagnose, een verminderde ziektevrije en absolute overleving hadden, vooral als deze patiënten ook positief waren voor rhabdomyosarcoom-specifiek mRNA in bloed of beenmerg (zoals onderzocht in **Hoofdstuk 2**). Dit was het duidelijkste te zien in patiënten met metastases: patiënten die positief testten voor het RNA panel en *RASSF1A-M* hadden een slechte overleving, terwijl patiënten die negatief waren voor beide testen een hele goede uitkomst hadden.

Binnen een internationale samenwerking onderzochten we de mogelijkheid voor het opsporen van patiënt-specifieke genetische afwijkingen in het cfDNA uit bloed van patiënten met rhabdomyosarcoom. Dit laten we zien in **Hoofdstuk 5**. Eerst keken we in muizen die een menselijk rhabdomyosarcoom ingespoten hadden gekregen of we menselijk DNA konden terugvinden in het bloed. Dit was inderdaad mogelijk en de hoeveelheid cfDNA kwam overeen met de grootte van de tumor bij de muizen. Hierna analyseerden we tumor materiaal van kinderen met een rhabdomyosarcoom om genetische afwijkingen op te sporen, waarbij we mutaties, CNA en breukpunten van het PAX-FOXO fusiegen vonden. Deze informatie gebruikten we om voor iedere patiënt persoonlijke ddPCR tests te ontwikkelen om cfDNA in plasma op te sporen. Hiermee vonden we bij meer dan 75% van de patiënten een tumor-specifiek signaal in het plasma bij diagnose en bleek dat de aanwezigheid van dit signaal tijdens therapie overeenkwam met behandelrespons. In een klein deel van de patiënten waarbij er genoeg cfDNA was, keken we ook in detail naar het hele DNA door whole exome sequencing (WES). Bij 7/7 van de cfDNA samples die we met WES analyseerden, vonden we afwijkingen die van de tumor afkomstig waren. We concludeerden hieruit dat ddPCR en WES allebei geschikt zijn om de aanwezigheid van rhabdomyosarcoom DNA aan te tonen in cfDNA uit plasma, en dat de aanwezigheid van dit signaal gebruikt kan worden om het effect van de behandeling te monitoren.

In **Hoofdstuk 6** hebben we verder gewerkt aan op maat gemaakte ddPCR tests voor kinderen met neuroblastoom, rhabdomyosarcoom en Ewing sarcoom. We hebben ontdekt dat niet alleen de specifieke breukpunten van fusiegenen hier geschikt voor zijn, maar dat ook regio's met CNA gebruikt kunnen worden om een patiënt-specifieke ddPCR te ontwikkelen. De specifieke DNA sequenties hebben we binnen dit project met hulp van het bedrijf Cergentis vastgesteld, door gebruik te maken van hun 'targeted locus amplification' (TLA) techniek die kan worden toegepast op vers tumor materiaal of cellen gekweekt daaruit, maar ook op formaline gefixeerd, paraffine ingebed (FFPE) materiaal. Met de patiënt-specifieke tests hebben we een tumor signaal aangetoond in al het plasma dat bij diagnose was afgenomen. Bij neuroblastoom zagen we dat de aanwezigheid van dit signaal ook het beloop van de ziekte volgde, het verdween als de behandeling succesvol was en verscheen weer bij een terugval. Bij de patiënten met rhabdomyosarcoom en Ewing sarcoom zagen we dit patroon niet, maar mogelijk dat de afwezigheid van samples die op cruciale momenten waren afgenomen daar een rol in speelde.

In **Deel 2** van deze thesis onderzochten we nieuwe celvrije markers uit plasma. We zetten de literatuur over het gebruik van extracellulaire vesikels (EV) als markers bij kinderen met verschillende soorten solide tumoren op een rij in **Hoofdstuk 7**. We

beoordeelden of de methodologie in deze studies goed te reproduceren was en of er een klinische en/of in vitro validatie was verricht. Dit deden we met behulp van de reeds gepubliceerde EV-METRIC score en onze eigen PedEV score. We includeerden studies over desmoplastisch small round cell tumoren (DSRCT), neuroblastoom, hepatoblastoom, osteosarcoom, rhabdomyosarcoom en Ewing sarcoom. Op basis van de literatuur concludeerden we dat biomarkers uit EV voornamelijk niet kunnen worden toegepast in de kliniek omdat in de meeste studies de methode niet gedetailleerd genoeg is beschreven, waardoor studies niet goed te reproduceren waren. Bovendien ontbrak vaak validatie in klinische cohorten.

In **Hoofdstuk 8** onderzochten we of het mogelijk is om celvrij RNA (cfRNA) te onderzoeken met de ddPCR in plasma van kinderen met neuroblastoom en of cfRNA geassocieerd is met EV. Hiervoor ontwikkelden we 2 soorten panels: een panel met genen die hoog tot expressie komen in neuroblastoom tumoren (*PHOX2B*, *CHRNA3* en *TH*) en een panel met genen die betrokken zijn bij de regulatie van de celdeling (*CDC6*, *ATAD2*, *DHFR*, *E2F1*, *MCM2*, *H2AFZ*). Eerder onderzoek heeft namelijk aangetoond dat dit soort genen ontregeld zijn in kankercellen, met name in neuroblastoom. We ontdekten dat neuroblastoom-specifieke genen alleen aanwezig waren in het cfRNA van patiënten met uitgezaaide ziekte. Daarnaast zagen we dat *DHFR*, verhoogd was bij dezelfde patiënten. We isoleerden EV met 'size exclusion chromatography' (SEC) uit plasma. Hierbij worden deeltjes uit plasma van elkaar gescheiden op basis van grootte, door ze door een kolom te laten druppelen wat leidt tot 'fracties' van het plasma. De grote deeltjes, waar de EV onder vallen, lopen sneller door de kolom heen en worden geconcentreerd in de eerdere fracties, de EV-verrijkte fracties. De latere fracties bevatten de kleinere deeltjes en daarom vooral eiwitten, de eiwit-verrijkte fracties. Wij ontdekten dat in plasma van patiënten met neuroblastoom de EV-verrijkte fracties vooral de cfRNA markers bevatten, en dat de eiwit-verrijkte fracties vooral het cfDNA bevatten.





Curriculum Vitae

Nathalie Saskia Marguerite Lak was born in Paris, France, on the 17th of April 1985. After only a few weeks, she moved back to The Hague with her parents where she spent her early childhood. When she was 6 years old, her family relocated to Bonn, Germany, where she visited a French primary school. In 1996, they moved back to The Hague where she attended Gymnasium Sorghvliet.

After graduation and a year in Spain to study the language, she started her medical studies at the University of Utrecht. During these years, she performed research at the lab of dr. Stephane Hatem at INSERM in Paris, and with dr. Marije Bartels at the lab of prof. Paul Coffey at the Wilhelmina Children's Hospital in Utrecht. After graduating as a medical doctor, she first worked in the pediatrics department of the Meander Medical Center in Amersfoort and at the Wilhelmina Children's Hospital. Nathalie was accepted as a resident for the pediatrics program at the Wilhelmina Children's Hospital in 2012. In 2018, she paused her pediatric training to join a PhD program in the group of dr. Lieve Tytgat and prof. Ellen van der Schoot, on *Liquid biopsies in pediatric rhabdomyosarcoma*. Within this project, she investigated the potential of both RNA and DNA-based assays in blood and bone marrow to improve risk stratification in patients with pediatric rhabdomyosarcoma. Her study on the development and validation of a rhabdomyosarcoma-specific RNA panel won her the SIOP Young Investigator Award in 2020. She joined the European Pediatric Soft tissue sarcoma Study Group (EpSSG) and became an active member of the EpSSG Biology spin-off group which focuses on liquid biopsies. She set-up collaborations with several groups, amongst them the groups of prof. Marca Wauben, Veterinary Institute, Utrecht University and Kendra Maass, Hopp Children's Tumor Center (KiTZ) and German Cancer Research Center (DKFZ), Heidelberg, Germany.

After finishing her pediatrics training, she started as a fellow in Pediatric Oncology at the Princess Máxima Center in Utrecht in 2023, combining clinical work with research. Her research revolves around liquid biopsies, with the ultimate aim to bring the findings of this thesis to daily clinical practice for patients with pediatric rhabdomyosarcoma. Furthermore, she is working on implementation of liquid biopsies for patients with central nervous system tumors at the Princess Máxima Center.

At home, Nathalie has 2 daughters, Violet and Aster, a husband, Juliaan, and her pets Lucy the labradoodle and Yoyo the cat. In her scarce spare time she likes to meet up with friends, read and go for a run.



Acknowledgements

Bij het ontstaan van dit proefschrift heb ik veel steun gehad van veel mensen waar ik erg dankbaar voor ben. Ik ga proberen jullie allemaal aan bod te laten komen, maar ik vrees dat het onmogelijk is om niemand te vergeten. Mijn oprechte excuses mocht je jezelf hier verwachten, maar toch niet zien staan.

Allereerst de **patiënten en ouders**: zonder jullie vertrouwen had dit proefschrift niet bestaan. Ik hoop dat de uitkomsten uit dit onderzoek uiteindelijk (en binnen niet al te lange tijd!) kunnen bijdragen aan verdere verbetering van kwaliteit van leven en overleving.

Lieve, ontzettend veel dank voor je steun tijdens dit hele proces. Het is indrukwekkend om te zien hoe jij kliniek en onderzoek combineert terwijl je ook nog een fijn mens blijft. Alle gesprekken die we ondanks onmogelijke agenda's hebben over alle belangrijke dingen in het leven (familie, patiënten, onderzoek ...). Je bent een voorbeeld voor me en ik hoop dat we nog lang samen blijven werken.

Janine, heel veel dank dat je het hebt aangedurfd me aan te nemen voor dit project. Ik bewonder hoe je vervolgens bij iedere stap mee hebt gedacht, terwijl je inmiddels bij de hemato-oncologie was blijven hangen. Het blijft een bizar idee dat ik iets meer dan 6 jaar geleden nog niets eens wist wat liquid biopsies precies waren. Dat is me inmiddels wel enigszins duidelijk geworden.

Ellen, vanaf het begin ben ik onder de indruk van je kennis en ervaring. Jij kan in één blik de fout in een experiment zien of een onjuiste aanname in een artikel doorzien. Ik hoop dat er in de loop van de jaren een klein sprankje van jouw genialiteit op mij is afgestraald. Heel veel dank voor je begeleiding en ik hoop dat ik in de toekomst nog steeds 'wilde ideeën' met jou kan blijven bespreken, zodat jij me kan helpen ze echt geniaal te maken.

Max, veel dank voor de steun bij het afronden van het manuscript en bij mijn traject om kinderoncoloog te worden. Het is een geruststellende gedachte dat jij de liquid biopsies een warm hart toedraagt, nu de rest van de wereld nog.

Beste **beoordelingscommissie**, veel dank dat jullie de tijd nemen om mijn proefschrift te beoordelen. Ik kijk uit naar de verdediging zodat we verder over liquid biopsies kunnen filosoferen.

Lieke, veel dank dat jij me vanaf het begin aan het handje hebt meegenomen naar al die enge PCR apparaten en me hebt geïntroduceerd in de wonderde wereld van de ddPCR. Gelukkig raken we nooit uitgepraat, van nieuwe ontwikkelingen binnen de ddPCR tot waanzinnige kindergeneeskunde avonturen. Heel fijn dat je mijn paranimf wilt zijn!

Mirthe, herinner je je nog de eerste dag van geneeskunde dat we elkaar voor het eerst ontmoetten? Inmiddels al 20 jaar geleden (!). We lopen dus al een tijdje mee in elkaars leven. Wat een toeval dat we ook nog een fascinatie voor het moleculaire en kwaadaardige delen... Daarom ben ik vereerd dat je mijn paranimf wilt zijn!

Lily, jij hebt me alles geleerd wat ik van RNA isolatie moet weten en ook hoe ik een zalm zelf moet roken. Alles met hetzelfde enthousiasme. Sorry dat mijn enthousiasme er steeds weer toe leidde dat we belachelijk vroeg op maandagochtend gingen pipetteren.

Ahmad, jij bent de rustige kracht achter al het rondvliegende enthousiasme. Dank voor je geduld en je hulp als mijn gebrek aan scheikundige kennis te schrijnend werd. (C=M/V toch?)

Nina, jouw vastberadenheid en veelzijdigheid vind ik jaloersmakend. De afgelopen jaren heb ik je zoveel (nieuwe) skills zien oppakken: marathon lopen, Stilla ddPCR, skiën, schrijven van meerdere boeken (Compendium ddPCR binnenkort?). Ik heb het vermoeden dat jouw veelzijdigheid nog veel groter is.

Sanquin: zoveel mensen hebben mij in de loop van de jaren geholpen met alle praktische en moleculaire zaken. Heel veel dank voor jullie geduld en steun. Vooral **Marion K., Aicha, Anita, Herbert, Carlijn V. en Masja**. En daarnaast natuurlijk iedereen bij **IHE, Immuuncytologie en Moleculair Platform!**

The sarcoma crew at thePrincess Maxima: **Hans M.**, thank you for your support. It is great to be able to fall back on your tremendous knowledge and experience in rhabdomyosarcoma. **Reineke, Roelof, Rutger, Lianne, Stephanie and Annemarie**: it is great working with you, in research, clinic and on our karaoke skills.

'**Sarcoma meeting-crew**' we started out with a small group in 2018 but it is now a thriving group of sarcoma-fanatics. Specifically I would like to thank **Michael, Frank, Jeff, Marian G. K., Laura H.-J. and Claudia** for sharing experiences and the great discussions. **Marta F.**, thank you very much for your statistical support.



'ddPCR-expert team' Pieter, Roy, Wim, Mieke, Rogier, Astrid van H, Nelleke: onze wekelijkse meetings op donderdag waren (en zijn) iets om naar uit te kijken. Het is heerlijk om ervaringen te delen en vragen te kunnen stellen aan een groep mensen die echt begrijpt wat je aan het doen bent en net zo geniet van eindeloos over ddPCR details te praten.

Tytgat group, aka Totally Tytgat with Astrid B, Arjan, Atia, Carlijn K, Carolina, Caro, Ilse, Julia, Leron, Lotte, Marieke, Thomas, Reno, Yvette, Zeinab, Nicky and of course Maaïke: I think everyone is (or should be) jealous of us. We belong to a very lucky group of people to have such funny, helpful and 'gezellige' colleagues. I hope to continue working with you guys for many years to come!

Michelle, je begon ooit als een 'appendix' bij de Tytgat groep, maar bent inmiddels uitgegroeid tot een belangrijke vriendin. Veel dank voor je steun gedurende dit hele traject en ik kijk uit naar nog vele decennia vreemde verhalen uit de kindergeneeskunde delen en bierproeverijen!

Veel dank aan de studenten die mij hebben geholpen, variërend van pipetteren tot literatuur screenen en klinische data bij elkaar schrapen: **Lotte, Elvera, Sarah en Fleur.**

Staf van de solide tumoren en verpleegkundig specialisten in het Máxima: dank voor de steun en heel fijn om te zien dat liquid biopsies steeds meer gaan leven. Hopelijk snel echt te gebruiken in de kliniek!

'RMS database meeting'-groep: in de loop van de jaren hebben veel mensen hier hun steentje aan bijgedragen, en dan denk ik specifiek aan **Jaap, Ellen en Carin.** Ergens in een parallel universum is er vast een RMS database die daadwerkelijk online is! Op naar die dimensie!

Molenaar groep: thank you very much for letting me, as a 'non-NBL' person join the discussions, especially **Jan, Marlinde, Kim, Emmy and Judith.**

At the veterinary institute in Utrecht: I am very grateful for the wonderful collaboration with great discussions on EV and cfrRNA with **Marca, Estefania, Anne, Anneloes and Alain.** Alain, also great to have you on my reading committee.

Of course, **Agustin, Armagan and Cees** from Enschede, thank you very much for our collaborations on EV.

Collaborators abroad: many thanks to the team in Ghent, with **Bram, Ruben, Charlotte, Jill, Lotte** and of course **Katleen**, thank you very much for being on my reading committee.

In the UK: **Janet, Olivia, Ajla, Susanne and Supriti**, thank you for the great collaboration through the years, and looking forward to hopefully further projects in the future.

In Paris: the team at Institut Curie with **Gudrun, Yasmine and Matthieu**, many thanks for the nice collaboration.

And of course everybody from the **EpSSG Biology group: Beat, Willemijn, Michaela and everyone else!** I look forward to further collaboration in the future.

Kindergeneeskunde in het Wilhelmina Kinderziekenhuis: veel dank aan heel veel mensen, maar specifiek aan **Edward N.** en **Joost F.** Jullie steun aan mijn bedrijfstechnisch onaantrekkelijke plan om tijdens mijn opleiding tot kinderarts een full-time PhD project te gaan doen, was ongelooflijk. Dat ik daardoor nog wat langer als 'eeuwige AIOS' mocht rondlopen was mooi meegenomen.

Lieve vrienden en vriendinnen, heel veel dank voor jullie geduld en steun! Hopelijk maakt dit feest alles een beetje goed :D.

Julie, veel dank voor je steun in de vorm van gezelligheid, entertainment voor de kinderen en je kookkunsten tijdens het ontstaan van dit proefschrift. **Ron,** dank voor je interesse in dit onderwerp.

Pap, doctor is misschien niet zo hoog in hiërarchie als de paus, maar ik denk toch dat ik niet zo ver was gekomen zonder jouw hulp. **Mam,** wie had gedacht dat je toch gelijk zou krijgen dat ik eigenlijk van binnen een echte onderzoeker ben. Je hebt nooit mee mogen maken dat ik onderzoek ging doen, maar ik denk dat je er ontzettend van had genoten dat je ook hierover gelijk had. Ik mis je.

Juliaan, deze promotie was niet mogelijk geweest zonder jouw steun om het huis met al zijn bewoners en huisraad draaiende te houden. Dan te bedenken dat fulltime onderzoek doen ooit aantrekkelijk leek omdat ik dan meer thuis zou kunnen zijn. Dat is toch geheel onverwacht helemaal uit de hand gelopen. **Violet en Aster,** kijk ik heb echt een boek geschreven! Veel dank voor jullie geduld als ik me weer eens verschanste achter mijn laptop of naar het buitenland moest voor een congres. En ik vrees dat dat geduld nog nodig zal zijn, dus op naar het volgende avontuur met z'n vieren! Ik hou van jullie!



